

**6**

Alzbeta Sapietova - Milan Saga - Alexandr Shimanovsky  
Milan Sapieta

**MOBILITY OF MULTIBODY SYSTEMS  
IN TERMS OF THEIR INCORRECTNESS**

---

**13**

Milan Saga - Milan Vasko - Peter Kopas  
Lenka Jakubovicova

**NUMERICAL ALGORITHM FOR BEAM  
RESIDUAL STRESS IDENTIFICATION**

---

**19**

Marian Handrik - Milan Vasko - Peter Kopas  
Milan Saga

**EFFECTIVE FINITE ELEMENT SOLUTION  
AND POST-PROCESSING FOR WIDE LOAD  
SPECTRUM**

---

**27**

Juraj Gerlici - Tomas Lack - Jozef Harusinec  
**DEVELOPMENT OF TEST STAND  
PROTOTYPE FOR RAIL VEHICLES BRAKE  
COMPONENTS TESTING**

---

**33**

Tomas Lack - Juraj Gerlici  
**WHEEL/RAIL TANGENTIAL CONTACT  
STRESS EVALUATION BY MEANS  
OF THE MODIFIED STRIP METHOD**

---

**40**

Peter Zvolensky - Vladimir Stuchly - Juraj Grecnik  
Roman Poprocky  
**EVOLUTION OF MAINTENANCE SYSTEMS  
OF PASSENGER AND FREIGHT WAGONS  
FROM THE ECM CERTIFICATION  
POINT OF VIEW**

---

**48**

Michal Holubcik - Jozef Jandacka  
**MATHEMATICAL MODEL FOR  
PREDICTION OF BIOMASS ASH MELTING  
TEMPERATURE USING ADDITIVES**

---

**54**

Andrej Kapjor - Jozef Huzvar - Branislav Ftorek  
Martin Vantuch

**CRITERION EQUATIONS OF HEAT  
TRANSFER FOR „N“ HORIZONTAL PIPES  
ONE ABOVE ANOTHER AT NATURAL  
CONVECTION IN LINEAR METHOD  
OF APPROXIMATION**

---

**62**

Radovan Nosek - Stanislav Gavlas - Richard Lenhard  
Veroslav Sedlak - Havard Mollerhagen Arvesen

**CONDENSER OPTIMIZATION  
OF HEAT PIPE**

---

**67**

Lubos Kucera - Tomas Gajdosik - Jan Bucala  
**THE VIBRODIAGNOSTICS OF DAMAGED  
GEARS OF PLANETARY GEARBOXES**

---

**74**

Robert Kohar - Slavomir Hreck  
**DYNAMIC ANALYSIS OF A ROLLING  
BEARING CAGE WITH RESPECT TO THE  
ELASTIC PROPERTIES OF THE CAGE  
FOR THE AXIAL AND RADIAL  
LOAD CASES**

---

**82**

Michal Petru - Josef Broncek - Petr Lepsik  
Ondrej Novak

**EXPERIMENTAL AND NUMERICAL  
ANALYSIS OF CRACK PROPAGATION IN  
LIGHT COMPOSITE MATERIALS UNDER  
DYNAMIC FRACTURING**

---

**90**

Jozef Pilec - Michal Derbas - Miroslav Janota  
Mario Kosut

**STUDYING THE IMPLEMENTATION  
OF POTENTIOMETRIC METHODS FOR  
THE DETECTION OF CRACKS  
IN RENOVATION OF FORGING TOOLS**

---

**96**

Dana Stancekova - Jan Semcer - Jozef Holubjak  
Mario Drbul

**MACHINABILITY OF NANO-STRUCTURED  
BIOMATERIALS FOR DENTAL IMPLANTS**

---

**101**

Branislav Micieta - Vladimira Binasova - Michal Haluska  
**THE APPROACHES OF ADVANCED  
INDUSTRIAL ENGINEERING IN NEXT  
GENERATION MANUFACTURING  
SYSTEMS**

---

**106**

Martin Krajcovic - Gabriela Gabajova - Branislav Micieta  
**ORDER PICKING USING AUGMENTED  
REALITY**

---

**112**

Branislav Micieta - Martin Gaso - Martin Krajcovic  
**INNOVATION PERFORMANCE  
OF ORGANIZATION**

---

**119**

Dana Bolibruchova - Lukas Richtarech  
Wladyslaw Orlowicz  
**POSSIBILITIES OF ELIMINATING  
THE HIGHER AMOUNT OF IRON  
IN SECONDARY AISi7Mg0.3 ALLOY  
BY CHROME**

---

**124**

Peter Fabian - Peter Jankejech - Martina Kyselova  
**SIMULATION OF ROUNDNESS,  
HARDNESS AND MICROSTRUCTURE  
OF BEARING RINGS WITH THIN CROSS  
SECTIONS BY USING SYSWELD**

---

**130**

Radoslav Konar - Marek Patek - Milos Mician  
**EXPERIMENTAL MEASUREMENTS  
AND NUMERICAL SIMULATION  
OF BRIDGE CONSTRUCTION WELDING  
AT LOW TEMPERATURES**

---

**136**

Ivana Pobocikova - Zuzana Sedliackova - Jan Simon  
**STATISTICAL ANALYSIS OF WIND SPEED  
DATA BASED ON WEIBULL  
AND RAYLEIGH DISTRIBUTION**

---

**142**

Daniel Riecky - Milan Zmindak - Zoran Pelagic  
**NUMERICAL FINITE ELEMENT METHOD  
HOMOGENIZATION OF COMPOSITE  
MATERIALS REINFORCED WITH FIBERS**

---

**148**

Darina Kumicakova - Zdenek Konecny  
**APPROACH TO THE PROBLEM  
OF BIO-INSPIRED ROBOTIC GRIPPER  
DESIGNING**

---

**154**

Juraj Uricek - Tibor Galbavy - Vladimir Bulej  
Peter Durec  
**THE CALCULATION OF INVERSE  
KINEMATICS FOR 6DOF SERIAL ROBOT**

---

**161**

Andrej Czan - Michal Sajgalik - Anton Martikan  
Jozef Mrazik  
**OBSERVATION OF DYNAMIC PROCESSES  
IN CUTTING ZONE WHEN MACHINING  
NICKEL ALLOYS**

---

**169**

Jerzy Jozwik - Ivan Kuric - Leszek Semotiuk  
**LASER INTERFEROMETER DIAGNOSTICS  
OF CNC MACHINE TOOLS**

---

**176**

Nadezda Cubonova - Ivan Kuric  
**DATA STRUCTURES IMPLEMENTATION  
OF THE PROTOCOL STEP-NC AT CNC  
MACHINES PROGRAMMING**

---

**184**

Michal Lukac - Frantisek Brumercik  
Leszek Krzywonos - Pawel Drozdziel  
**TENSION MECHANISM DYNAMIC  
ANALYSIS**

---

**189**

Filip Pastorek - Miroslav Omasta - Lenka Bukovinova  
Pavel Dolezal - Branislav Hadzima  
**BIODEGRADATION PROPERTIES  
OF AZ31 MAGNESIUM ALLOY COATED  
BY DICALCIUM PHOSPHATE DIHYDRATE**

---

**194**

Tatiana Liptakova - Monika Halamova - Ayman Alaskari  
Martin Lovisek - Maxim Puchnin  
**CORROSION PROPERTIES OF VARIOUS  
COPPER PIPES JOINTS**

---

# COMMUNICATIONS

---

**200**

Jaroslav Dubec - Miroslav Neslusan - Anna Micietova  
Maria Cillikova  
**INFLUENCE OF TOOL-WORKPIECE  
INTERFACE ON SURFACE INTEGRITY  
AFTER TURNING**

---

**206**

Luboslav Dulina - Miroslava Bartanusova  
**ERGONOMICS IN PRACTICE AND  
ITS INFLUENCE ON EMPLOYEES'  
PERFORMANCE**

---





*Ladies and Gentlemen, dear Readers,*

*Theoretical and experimental solutions of technical problems using advanced approaches and modern computational and measuring engineering are nowadays the only way to obtain new knowledge in all fields of science and technology.*

*This issue of the journal "Communications" presents original results of scientific activities of personnel of the Faculty of Mechanical Engineering in its research priority areas such as mechanics and design of machines, material and industrial engineering, automation, energy technology and renewable resources, progressive engineering technologies.*

*The publications are results of activities within the framework of national and transnational research projects as well as projects supported by structural funds.*

*Milan Saga*

# MOBILITY OF MULTIBODY SYSTEMS IN TERMS OF THEIR INCORRECTNESS

The paper presents examples of incorrectness from the point of view of body and Multibody System (MBS) kinematics. This incorrectness should be kept in mind when modeling Virtual Prototypes (VP) of MBS. During the analysis or synthesis of MBS it is necessary to correctly determine the degree of freedom (DOF) of mechanisms in order to properly design the mechanism. The basic relation for the DOF computation does not include parameters such as special dimensions of links or their mutual configuration and geometric constraints. In many cases, these issues require individual approach, i.e. by analyzing the properties of incorrect MBS to identify the causes of their incorrectness and apply the computation method to the actual mobility. The paper contains samples to illustrate a particular topic.

**Keywords:** MBS, singularity, degrees of freedom, actual mobility, incorrect MBS, kinematics.

## 1. Introduction

The structure and modeling of MBS is a starting and highly important component of theoretical fundamentals. It covers ways of creating kinematic chains, their topology and depiction, classification of geometric constraints and search for a number of freedom (movability), etc.

The DOF of a mechanical system with holonomic geometric constraints is a minimal number of necessary generalized coordinates required to define the system configuration. The DOF has practical use but it must be kept in mind that it has its own limitations. For the modeling of a mechanical system it is necessary to introduce simplifying hypotheses for its computation within the framework of analysis [1]. These hypotheses may cause a significant difference between the model and actual behavior of the mechanism. There is, for instance, a large class of mechanisms (referred to as overconstrained mechanisms) whose mobility is the function of precise dimensions of their parts, chosen geometric constraints or configuration [2, 3 and 4]. Moreover, under certain (singular) configurations, due to a sudden DOF variation, numerical results of particular software may be unreliable unless appropriate precautions are taken [5, 6 and 7]. The paper presents some chosen samples of MBS focusing on the computation of incorrectness, which means that DOF is computed according to the commonly used relation not in compliance with the real situation.

## 2. The basic concepts

### 2.1 Mobility

The mobility  $n$  of MBS is the number of prescribed position coordinates of input driving links required to uniquely determine the position of output driven links [8]. If the actual mobility  $n_s$  is identical to the theoretical mobility  $n$ , i.e.  $n_s = n$ , then we can say that MBS is correct. In the correct MBS, each geometric constraint of class  $t$  takes just  $t$  degrees of freedom of movement. Position and mobility of bodies in the correct MBS is determined according to the Grubler criterion:

$$n = n_v(u - 1) - \sum_{t=1}^{n_v-1} t \cdot S_t, \tag{1}$$

which satisfies the condition:

$$n = n_s, \tag{2}$$

where  $u$  is a total number of links in the MBS, frame included,  $n_v(u - 1)$  is the mobility of a group of free bodies,  $\sum_{t=1}^{n_v-1} t \cdot S_t$  are removed degrees of freedom between pairs of links of the MBS.

The below mentioned relation provides correctness between pairs of links of the MBS:

$$S_t = \sum_{v=2}^{v_m} S_{tv} (v - 1), \tag{3}$$

\* <sup>1</sup>Alzbeta Sapietova, <sup>1</sup>Milan Saga, <sup>2</sup>Alexandr Shimanovsky, <sup>1</sup>Milan Sapieta

<sup>1</sup>Department of Applied Mechanics, Faculty of Engineering, University of Zilina, Slovakia, E-mail: alzbeta.sapietova@fstroj.uniza.sk

<sup>2</sup>Department of Technical Physics and Engineering Mechanics, Belarusian State University of Transport, Belarus

where  $s_t$  is a number of joints of class  $t$  of all pairs linked in the MBS,  $n_v(u-1)$  is a number of joints of class  $t$  connecting number  $v$  of links,  $v$  is a number of bodies linked in  $s_t$  bodies,  $v_m$  is a maximum number of bodies in joints of class  $t$  in the MBS.

The MBS is considered incorrect if its actual mobility  $n_s$  differs from the theoretical mobility  $n$  determined according to equation 1; then it holds:

$$n_s \neq n. \tag{4}$$

All the reasons which cause this condition in MBS are referred to as *singularities*. Equation 1 does not reflect the real mobility in its entirety for each MBS because it does not contain information either about proportions (dimensions) or about mutual position (configurations) of links and geometrical joints [8].

If  $n_n$  is used to denote the number of unremoved DOF, the incorrect MBS will have the actual mobility when DOF computed in compliance with the Grübler criterion and the unremoved DOF are summed up:

$$n_s = n + n_n. \tag{5}$$

Theoretical mobility  $n$  of an incorrect MBS may be zero. It can indicate a configuration of links in the MBS or, in the case of negative indication, it can point to an indefinite, unclear structure which still might be real [8]. In spite of it the actual mobility can be  $n_s \geq 1$ . It is due to already mentioned configuration of links and geometric constraints as well as special dimensions.

### 2.2 Locked MBS - four bar mechanism

From the point of view of mobility of bodies and MBS, jam is a situation when the body has one degree of freedom and yet it cannot move. It is caused by the geometry of the body, by mutual configuration of links in the MBS and by force effects [9, 10 and 11]. If redundant constraints in the MBS become inconsistent with other constraints (due to manufacturing differences in length or links or deviation from geometric constraint position), the MBS may jam [8]. There is a four-bar in Fig. 1.

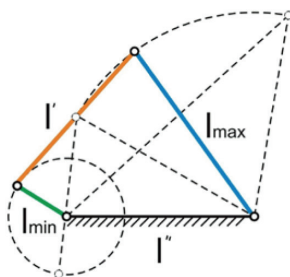


Fig. 1 Kinematic scheme of a four-bar mechanism

If we want the links of a four-bar mechanism in Fig. 1 to perform a rotational motion of  $360^\circ$ , i.e. to function as a crank mechanism, the following relation must hold:

$$l_{min} + l_{max} = l' + l'', \tag{6}$$

where  $l_{min}$  and  $l_{max}$  are lengths of the shortest and the longest link. Then  $l'$  and  $l''$  are lengths of the other links. Depending on which of the links is fixed, a crank mechanism, crank-rocker mechanism or rocker mechanism are formed.

### 2.3 Instantaneous and permanent singular state of MBS

- Instantaneous singular state occurs when the links of MBS can displace with *infinitely small values* of position coordinates (Fig. 2a).
- Permanent singular state occurs when the links of MBS can displace with *finite values* of position coordinates (Fig. 2b).

Fig. 2a shows a MBS whose links are in a horizontal position and loaded with forces. We get a matrix of system A from the set of static analysis equations. The solvability of the linear system of equation is based on the condition that the system has only one solution if the determinant of the matrix system A is different from zero. From the suggested solution it follows that determinant of the system  $D=0$ . Then, in the case of configuration of links in Fig. 2a the infinitely small displacement of point A occurs in the horizontal direction. The intersection of the tangents of trajectories of point A from individual links is in infinity. This leads to the virtual displacement in the direction of the tangent resulting into a singular state of MBS. It should be noted that infinitely large forces theoretically arise in the links. In fact, due to clearance in the pins the position of the links changes; but even so, axial forces are very large [12 and 13].

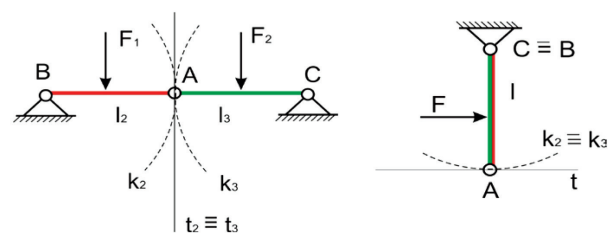


Fig. 2 Three members MBS a) virtual displacement of point A, b) final displacement of point A

The computation of the DOF according to Grübler:  $n=3$ .  $(3-1) \cdot 2 \cdot 3 = 0$ . But there is actually a virtual-rotation of links in the system, i.e.  $n_s=1$ .

$$D = \begin{vmatrix} 1 & 0 & -1 & 0 & 0 & 0 \\ 0 & 1 & 0 & 1 & 0 & 0 \\ 0 & 0 & 0 & l_2 & 0 & 0 \\ 0 & 0 & 1 & 0 & -1 & 0 \\ 0 & 0 & 0 & -1 & 0 & 1 \\ 0 & 0 & 0 & l_3 & 0 & 0 \end{vmatrix} = 1 \cdot (-1)^2.$$

$$\begin{vmatrix} 1 & 0 & 1 & 0 & 0 \\ 0 & 0 & l_2 & 0 & 0 \\ 0 & 1 & 0 & -1 & 0 \\ 0 & 0 & -1 & 0 & 1 \\ 0 & 0 & l_3 & 0 & 0 \end{vmatrix} = 1 \cdot (-1)^2 \cdot \begin{vmatrix} 0 & l_2 & 0 & 0 \\ 1 & 0 & -1 & 0 \\ 0 & -1 & 0 & 1 \\ 0 & l_3 & 0 & 0 \end{vmatrix} = 1 \cdot (-1)^3.$$

$$\begin{vmatrix} l_2 & 0 & 0 \\ -1 & 0 & 1 \\ l_3 & 0 & 0 \end{vmatrix} = 0$$

In Fig. 2b, the links are so oriented that the trajectories of their common point A are identical. In this case, there is a final-rotation of links and the system behaves like a pendulum. The solution of DOF and systems of linear equations is identical to the system in Fig. 2a. In this case a singular mode also occurs because  $n \neq n_s$ .

### 3. Incorrect MBS with passive joints (Overconstrained MBS)

The incorrect MBS is also such a system that contains geometric constraints which do not affect its mobility. This means that if we remove the elements of joints or the entire joint and the mobility of the output link does not change, the joint is totally or partially passive [4].

*Total passivity* - geometric constraint is from kinematic point of view totally passive and then redundant when after its removal, the actual mobility  $n_s$  of MBS does not change. Then, it holds that the number of unremoved DOF is equal to the class of constraints  $n_n = t$ . Parameter t is the number of DOF which the constrain removes. Then it holds:

$$n \leq 0 \text{ and } n_s \geq 1. \tag{7}$$

*Partial passivity* - geometric constraint of a class t is partially passive if it holds that the number of DOF removed by the MBS is smaller than its class, i.e.  $n_o < t$  [8].

An example of a totally passive bond is one rotational constraint (from two) to attach casement 2 (Fig. 3). The task is to analyze and compute the mobility of casement attached to the frame with two spatial rotational joints (Fig. 3).

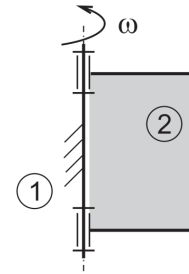


Fig. 3 Kinematic scheme of link with excess joint

We count the DOF according to equation (1):

$$n = n_v(u - 1) - \sum_{i=1}^{n_v-1} t_i \cdot s_i = 6 \cdot (2 - 1) - 5 \cdot 2 = -4,$$

where  $s_i = 2_{s2}(2 - 1) = 2$ .

Spatial rotational constraint removes 5 DOF. Since, it is excess (redundant), the number of unremoved DOF expresses just the number of DOF which this constraint should remove and it is:  $n_n = t = 5$ .

The actual number of DOF of the casement is:

$$n_5 = n + n_n = -4 + 5 = 1,$$

$$n \neq n_5.$$

If we remove the redundant constraint of the body in this example, then the calculation of mobility is according to (1):

$$n = n_v(u - 1) - \sum_{i=1}^{n_v-1} t_i \cdot s_i = 6 \cdot (2 - 1) - 5 \cdot 1 = 1.$$

It should also be said that one rotational joint is totally passive in terms of kinematic excess (redundancy). Its task is to achieve favorable conditions for mutual loading of bodies. The casement has always only one DOF regardless of the number of joints attached to the rotating frame. Geometric constraint is totally passive and in geometric terms redundant when, after its removal, the actual mobility  $s_i$  does not change.

### 4. Incorrect MBS with redundant links

If a link or group of links can be removed and the mobility of output link does not change, the link (group of links) is in excess (redundant) in terms of kinematics, therefore, we remove it before computing the mobility of MBS.

An example of MBS with redundant links is a five-bar system whose links are two and two parallel attached with rotary geometric constraints (Fig. 4).

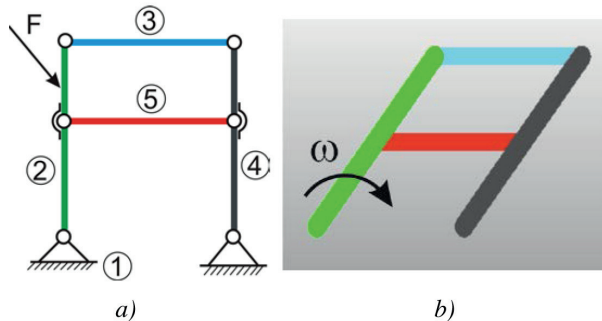


Fig. 4 Kinematic scheme of MBS with excess link

The computation of the DOF will be done as in the previous examples. The number of DOF according to Grubler:

$$n = n_v(u - 1) - \sum_{i=1}^{n_v-1} t_i S_i = 3.(5 - 1) - 2.6 = 0,$$

$$n = 0 \neq n_s = 1.$$

After the removal of excess link 5 or 3, we obtain:

$$n = n_v(u - 1) - \sum_{i=1}^{n_v-1} t_i S_i = 3.(4 - 1) - 2.4 = 1.$$

It should also be said that the cause of system mobility is configuration of its links, and the fact is that the links are two plus two parallel links. It is sufficient that one of the links is not parallel and the system will become shape determinate.

### 5. Redundant local mobility

Redundant local mobility is a passive redundant kinematic input which has no influence on the total mobility of the output link of the system.

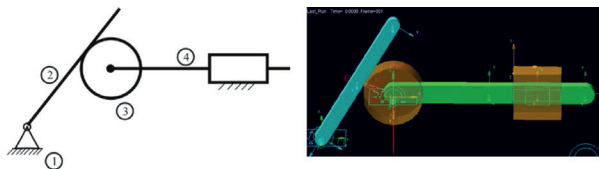


Fig. 5 Kinematic scheme of MBS with excess local mobility

$$n = n_v(u - 1) - \sum_{i=1}^{n_v-1} t_i S_i = 3.(4 - 1) - 2.3 - 1.1 = 2$$

If link 4 becomes the frame, link 3 can rotate. From this and also from the computation it follows that the MBS in Fig. 5 has two generalized coordinates. It should be noted that if we investigate the trajectory of an arbitrary point of the working member 2, it does not change even if the input acts on member 3, i.e. the only driving member will be member 4.

### 6. Freudenstein's criterion of MBS mobility

To solve MBS mobility which may be both correct and also incorrect, it is possible to use Freudenstein's mobility criterion of planar MBS with global coordinates of the position. It has the form:

$$n_{sF} = m - h_m, \tag{8}$$

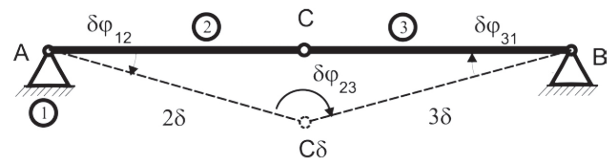


Fig. 6 VMS with marked virtual rotations of links 2 and 3

where  $n_{sF}$  is an actual number of DOF of the MBS according to Freudenstein,  $m$  is a total number of global coordinates,  $h_m$  is rank of the Jacobi matrix. Solution of mobility of a planar three-bar system of links (Fig. 6) [2] is presented below.

From the kinematic solution we obtain a matrix velocity loop equation for the given system:

$$\begin{bmatrix} -h_2 \sin \varphi_{12} & -h_3 \sin \varphi_{31} \\ -h_2 \cos \varphi_{12} & h_3 \cos \varphi_{31} \end{bmatrix} \begin{bmatrix} \dot{\varphi}_{12} \\ \dot{\varphi}_{31} \end{bmatrix} = \begin{bmatrix} 0 \\ 0 \end{bmatrix}, \tag{9}$$

then Jacobi matrix:

$$\gamma_{dm} = \begin{bmatrix} -h_2 \sin \varphi_{12} & -h_3 \sin \varphi_{31} \\ -h_2 \cos \varphi_{12} & h_3 \cos \varphi_{31} \end{bmatrix}. \tag{10}$$

For angles  $\varphi_{12}$  and  $\varphi_{31}$  following holds:

$$\varphi_{12} = \varphi_{31} = 0 \text{ and } \varphi_{31} = 0 \Rightarrow \gamma_{dm} = \begin{bmatrix} 0 & 0 \\ -h_2 & h_3 \end{bmatrix}$$

with  $\gamma_{dm} = 0$ , and  $h_m = 1$ ,

then, mobility MBS according to (8):

$$n_F = m - h_m = 2 - 1 = 1.$$

Mutual position (lengths, angles) of links and constraint elements allows to links 2 and 3 virtual rotation of  $\delta \varphi_{12}$  and  $\delta \varphi_{31}$ .

According to Grübler  $n=0$  and according to Freudenstein  $n=n_{sF}=1$ , a virtual displacement (rotation) occurs. If  $\det \gamma_{dm}=0$ , then the MBS with incorrect mutual position is in the singular state.

### 7. Location and mobility of MBS with rolling constraints

From the point of view of reaction effects in rolling constraint the following holds: if we do not consider passive resistance, this

constraint is of class  $t=2$ . Rolling constraint has both normal and tangential component of the reaction. It can be said that we have 2 constraint conditions in the kinematic model:

1. Tangential point with the frame is also pole P of relative mobility.
  2. The relative velocity at point P is zero.
- So, in terms of kinematics  $t=2$ .

Rolling constraints can be closed and opened in terms of configuration and shape links. Links may be separated when the constraint is opened. When it is closed, the links cannot be separated.

### 7.1 Closed rolling constraint

Links have the analogue relative position as in the previous solutions (planar three-bar system of bodies) in the constraint with a rolling closed circular shape. They are in a permanent singular mutual position. The constraint is partially passive and has 1 unremoved DOF  $n_n=1$  (Fig. 7).

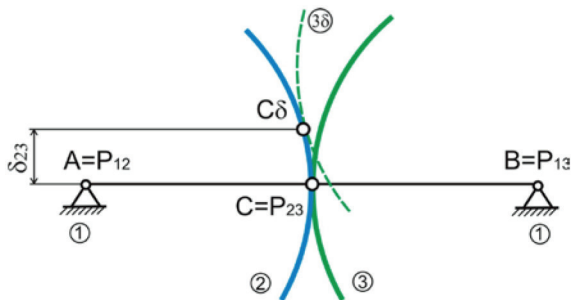


Fig. 7 MBS with rolling closed constraint

An example of the closed constraint is transmission gear. Fig. 8 presents a kinematic scheme of MBS for a switch point machine designed to handle switch points, switch diamonds, and derailleurs belonging to the equipment for railway operation.

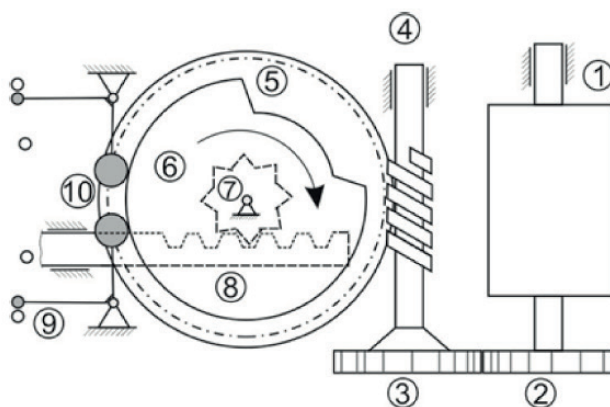


Fig. 8 MBS with mark virtual rotation of links 2 and 3

Computation of DOF according to Grubler:

$$n = n_v(u - 1) - \sum_{t=1}^{n_v-1} t \cdot S_1 =$$

$$n_v(u - 1) - \sum_{t=1}^{n_v-1} t \cdot S_1 = 3 \cdot (5 - 1) - 2 \cdot 7 = -2.$$

MBS has 3 types of gear and each of them has one unremoved DOF; then it follows that  $n_n=3$ .

The actual DOF of MBS for switch point machines are:

$$n_s = n + n_n = -2 + 3 = 1.$$

### 7.2 Opened rolling constraint - Incorrectness in terms of structural analysis.

The opened rolling constraint differs from the closed rolling constraint - in the former, separation of contacting surfaces of bodies may occur. The cause of incorrectness may be dimension and shape of tangential links [11].

In Fig. 9, there is the MBS with open rolling constraint, i.e. a cylinder in a plane. Link 3 is attached to the pin of cylinder 2. To clearly identify the position of the system it is necessary to know the location of the cylinder  $p_{13}$ , which is the function of rotations of cylinder  $\phi_{12}$ , and  $\phi_{13}$  which is an independent rotation of link 3 towards the frame. This system has 2 DOF. The structural scheme shows that links 1 and 2 are in contact through the rolling constraint, links 2 and 3 are in contact through rotational constraint, and link 3 is not in a direct contact with the frame. The structural scheme (topological model) of MBS does not contain any information about dimensions and mutual configuration of links.



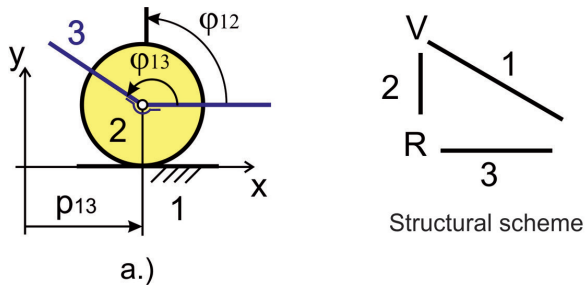


Fig. 9 MBS with open rolling constraint

Computation according to Grubler shows the actual DOF, but in this case it is incorrectness in terms of structural analysis:

$$n = n_v(u - 1) - \sum_{i=1}^{n_v-1} t_i S_i = 3.(3 - 1) - 2.2 = 2,$$

$$n_s = n + n_n = 2 + 0 = 2.$$

Parameter  $c$  is the total number of local coordinates - neighboring (dependent as well as independent) tangential to bodies; i.e. coordinates indicating the relative position (velocity, acceleration) between indicating the relative position (velocity, acceleration) 1, 2 and 2, 3, then  $c=2$ . Parameter  $m$  is the total number of global coordinates, i.e. coordinates between 1, 2 and 1, 3, then  $m=2$ .

We need to enter one more global coordinate in order to determine unambiguously the position of the system. It follows that we need 3 joint equations  $m_s=3$ , reflecting the fact that a shape of tangential links is crucial for open roller joints.

Incorrectness in terms of structural analysis:

$$c = 2, m = 2 \neq m_s = 3,$$

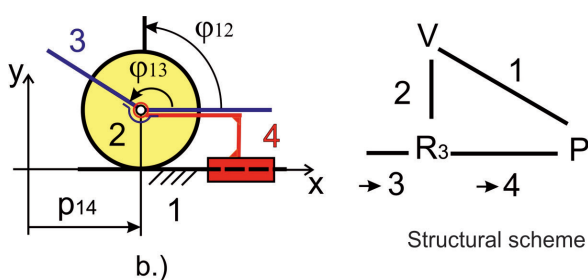


Fig. 10 Closed rolling constraint compensated by inserting binary link

$$n = n_v(u - 1) - \sum_{i=1}^{n_v-1} t_i S_i = 3.(4 - 1) - 2.(2_{22}(2 - 1) + 1_{23}(3 - 1))2 = 1,$$

$$n_s = n + n_n = 1 + 1 = 2.$$

Incorrectness of the open rolling constraint is compensated as we insert a fictional link to the system, which will replace the missing geometric constraint.

This particular incorrectness is compensated by inserting binary link 4. The centers of osculating circles of links were achieved. Thus the open rolling constraint is transformed to closed, which is permanently partially passive and the structural analysis will be correct (Fig. 10).

### 8. Conclusion

Practical importance of solution of the above mentioned issues lies in the determination of the number of independent degrees in the mechanism to determine a prescribed motion of the output link. This type of analysis can be preliminarily carried out by means of simple equations requiring only the knowledge of the number of links, the number of constraints and nature of their classes. However, they may fail during providing the correct answer.

Here, it is important to realize that it is necessary to orient oneself in basic knowledge which will allow us to:

- recognize and identify the critical configuration of a mechanism,
- compute the DOF of an overconstrained mechanism,
- identify passive or redundant DOF,
- identify the numerical effects due to the DOF variation.

Finally, it can be stated that causes of MBS incorrectness are identified based on analysis of properties of incorrect MBS and computational methods for actual mobility can be applied.

### Acknowledgement

The part of the results of this work has been supported by VEGA grant No. 1/1259/12.

### References

[1] ARNOLD, M., SCHIEHLEN, W.: Simulation Techniques for Applied Dynamics, *CISM Courses and Lectures*, vol. 507, Italy : Springer Wien : New York, 2008, 313 p., ISBN 978-3-211-89547-4.

[2] FREUDENSTEIN, F., ALIZADE, R.: *On the Degree of Freedom of Mechanisms with Variable General Constraint*, Proc. of Fourth World Congress on the Theory of Machines and Mechanisms, Newcastle upon Tyne, 1975, vol. I, 51-56.

- [3] PENNESTRI, E., CAVACECE, M., VITA, L.: *On the Computation of Degrees-of-freedom: A Didactic Perspective*, ASME Paper DETC, 2005, 2005-84109, 1-9.
- [4] SAGA, M., ZMINDAK, M., DEKYS, V., SAPIETOVA, A., SEGLA, S.: *Selected Methods of Analysis and Synthesis of Mechanical Systems*, VTS: University of Zilina, 2009, 360 p., ISBN 978-80-89276-17-2.
- [5] KOPAS, P., VASKO, M., HANDRIK, M.: Computational Modeling of the Microplasticization State in the Nodular Cast Iron, *Applied Mechanics and Materials*, 2014, vol. 474, 285-290, ISSN 16609336.
- [6] VASKO, M., GURAN, A., JAKUBOVICOVA, L., KOPAS, P.: Determination the Contact Stress Depending on the Load Rate of the NU220 Roller Bearing, *Communications - Scientific Letters of the University of Zilina*, vol. 15, No. 2, 2013, 88-94, ISSN 13354205.
- [7] SAPIETOVA, A., SAPIETA, M., HYBEN, B.: Sensitivity Analysis Application for Multibody System Synthesis, *Applied Mechanics and Materials*, vol. 420, 2013, 68-73, Online available since 2013/Sep/27 at [www.scientific.net](http://www.scientific.net) © (2013) Trans Tech Publications, Switzerland doi:10.4028/www.scientific.net/AMM.420.68 ISSN 1660-9336.
- [8] PALCAK, F.: *Theory of Mechanisms (in Slovak)*, 2<sup>nd</sup> ed., Bratislava : ES SVST, 1993. 166 p., ISBN 80-227-0531-4.
- [9] STANCEKOVA, D., SEMCER, J., DERBAS, M., KURNAVA, T.: Methods of Measuring of Residual Stresses and Evaluation of Residual State of Functional Surfaces by x-ray Diffractometric Methods, *J. Manufacturing Technology*, vol. 13, No. 4, December 2013, 547-552, ISSN 1213-2489.
- [10] CZAN, A., TILLOVA, E., SEMCER, J., PILC, J.: Surface and Subsurface Residual Stresses after Machining and their Analysis by x-ray Diffraction, *Communications - Scientific Letters of the University of Zilina*, vol. 15, No. 2, 2013, 69-76. ISSN 1335-4205.
- [11] KUCERA, L., GAJDOSIK, T.: *The Vibrodiagnostic of Gears*, Proc. of 54<sup>th</sup> Intern. Conference of Machine Design Departments, September, 2013, Hejnice - Liberec : Technical university, 2013. ISBN 978-80-7372-986-8, 93-98.
- [12] KUCERA, L., LUKAC, M., JURAK, L., BRUMERCIK, F.: Hydromechanical Automatic Transmission, *Communications - Scientific Letters of the University of Zilina*, vol. 11, No. 2, 2009, 33-35, ISSN 1335-4205.
- [13] LACK, T., GERLICI, J.: *Modified Strip Method Utilization for Wheel/Rail Contact Stress Evaluation*. 9<sup>th</sup> Intern. Conference on Contact Mechanics and Wear of Rail/wheel Systems (CM 2012), August, 2012, Chengdu : Southwest Jiaotong University, 2012, 87-89.

Milan Saga - Milan Vasko - Peter Kopas - Lenka Jakubovicova \*

## NUMERICAL ALGORITHM FOR BEAM RESIDUAL STRESS IDENTIFICATION

*The goal of the paper is the numerical study of the original hysteresis computational material models and their application in beam's bending theory. The paper presents the chosen differential material models and approaches based on step by step solution respecting the elastic and plastic conditions. In the centre of authors' interest is the numerical method study of the plastic zones identification or study of residual stresses distribution in the beam's cross-section. The results obtained from new MATLAB's programs are compared with FEM models in ADINA.*

**Keywords:** Stress identification and distribution, plastic zones, elastic-plastic analysis, MATLAB, ADINA, FEM analysis.

### 1. Introduction

Numerical simulation of the construction materials elastic-plastic behaviour is an important part of the various scientific works and studies today. A non-linear behaviour of the material does not mean the complete loss of bearing; it leads to the modification of some mechanical properties and to the stress redistribution in the structure caused by the plastic zones formation. In the case of simulation of the object behaviour under the loading exceeding the yield stress there are several problem types [1, 2, 3, 4, 5 and 6]:

- definition of the applicable elastic-plastic mathematical model,
- knowledge about material "constants" used in the model,
- choice of applicable computing tool or method (FEM, etc.),
- possibility to verify the computed values with the experiment,
- other specific problems (temperature influence, etc.).

The paper target will be to present the chosen mathematical models for the numerical solving of the beam elastic-plastic behaviour with the consequent plasticized zones identification in the cross-section area and residual stresses distribution. Continuous and discontinuous model analysis will be performed on a numerical example and compared with the FEM model in ADINA. The main goal of the structure state elastic-plastic analysis is to determine the stress, strain and boundaries between the elastic and plastic zone. This is true for the structure exposed to outer forces during the whole loading distribution [7]. There are two main theories of the elastic-plastic analysis; plastic flow theory and plastic strain theory.

Plastic flow theory assumes that the stress and strain state depends on the load history. This leads to the incremental problem solving, i.e. step by step. Loading will gradually grow with the step of  $\Delta F$  and for each load increment it is needed to evaluate the strain and stress state in particular areas. The method then evaluates if these areas have been plasticized. This theory simulates the real behaviour in a better way but it is more time consuming [8 and 9].

Plastic strain theory is based on the idea that the loading itself does not depend on the trajectory and, therefore, it is not necessary to track the stress history. The problem can be solved by loading the structure by whole force  $F$  without any increments. The results are obtained by the analysis of the given nonlinear differential system. The theory is currently used very rarely; it is applicable just for the small range of materials, slow and monotonic loading and for simple problems with very small deformation speed [5].

### 2. Algorithms proposition

#### 2.1 Proposed model No. 1

A new numerical approach will be presented; this approach allows analyzing the stress level throughout the whole cross-section area in the case of its plasticization [10 and 11]. The process is based on stress vector increment calculation  $\Delta\sigma(t)$  which defines discrete distribution of the stress increment in the

\* Milan Saga, Milan Vasko, Peter Kopas, Lenka Jakubovicova  
Department of Applied Mechanics, Faculty of Mechanical Engineering, University of Zilina, Slovakia  
E-mail: milan.saga@fstroj.uniza.sk

cross-section area. This increment will be added to the existing stress in the beam [5].

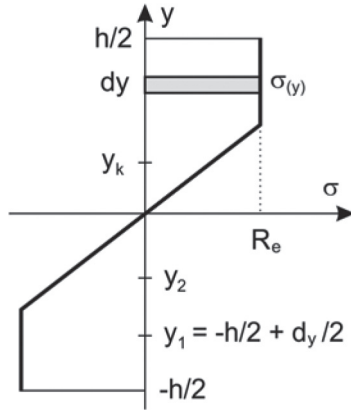


Fig. 1 Correction of the vector  $\sigma_L^{i+1}(t)$

The basic iterative equation for the calculation is

$$\sigma_L^{i+1}(t) = \sigma^i(t) + \Delta\sigma_L^i(t), \quad (1)$$

where  $i$  represents the iteration step,  $\sigma_L^{i+1}(t)$  is vector describing the quasi-linear stress distribution on which the correction must be applied,  $\sigma^i(t)$  is the stress in the cross-section,  $\Delta\sigma_L^i(t)$  is vector of the stress increments depending on loading values (internal values in the beam - bending moment  $Mo$ , axial force  $N$ ). The next step is the correction of the vector  $\sigma_L^{i+1}(t)$  in accordance with Fig. 1, i.e.

$$\begin{aligned} \sigma_k^{i+1}(t) &= \sigma_{Lk}^{i+1}(t) \text{ if } |\sigma_{Lk}^{i+1}(t)| < R_e, \\ \sigma_k^{i+1}(t) &= R_e \cdot \text{sgn}(\sigma_{Lk}^{i+1}(t)) \text{ if } |\sigma_{Lk}^{i+1}(t)| > R_e. \end{aligned} \quad (2)$$

The vector of the stress increments depending on loading values is described by

$$\Delta\sigma_L^i(t) = \Delta\sigma_{LN}^i(t) + \Delta\sigma_{LM}^i(t), \quad (3)$$

where  $\Delta\sigma_{LM}^i(t)$  is the vector of the stress increments depending on bending moment and  $\Delta\sigma_{LN}^i(t)$  is vector of the stress increments depending on the axial force. These increments can be obtained like

$$\Delta\sigma_{LN}^i(t) = \frac{1}{S} \cdot \Delta F^i(t), \quad (4)$$

$$\Delta\sigma_{LM}^i(t) = \frac{\Delta Mo_z^i(t)}{J_z} \cdot y, \quad (5)$$

where  $J_z$  is quadratic cross-section moment to the axis of  $z$ ,  $S$  is cross-section area of the beam,  $\Delta F^i(t)$  is vector of the difference between the loading force and the force calculated from the stress distribution in the beam cross-section.

$y = [y_1, y_2, \dots, y_k, \dots, y_n]^T$  is the discrete vector of the beam's

height coordinates  $\langle (-h + dy)/2; (h - dy)/2 \rangle$  and  $\Delta Mo_z$  is the difference between the loading moment and the moment calculated from the stress distribution in the beam cross-section (with constant width  $b$ )

$$\Delta Mo_{zp}^i(t) = Mo_{zd}(t) - Mo_{zp}^i(t). \quad (6)$$

The  $Mo_{zd}(t)$  is the loading bending moment to the axis of  $z$  and  $Mo_{zp}^i(t)$  is the moment really transferred by the beam, calculated as

$$Mo_z^i(t) = \int_S \sigma^i(t) \cdot y \cdot dS = \sum_{j=1}^n [\sigma_j^i(t) \cdot y_j] \cdot dy \cdot b. \quad (7)$$

After the substitution of equations (6) and (7) into eq. (5), the result equation will be

$$\Delta\sigma_{LM}^i(t) = \left\{ Mo_{zd}(t) - \sum_{j=1}^n [\sigma_j^i(t) \cdot y_j] \cdot dy \cdot b \right\} \cdot \frac{1}{J_z} \cdot y. \quad (8)$$

The  $\Delta F^i(t)$  is vector of variation between the loading force and the axial force calculated from the stress distribution

$$\Delta F^i(t) = [F_z(t) - F_p^i(t)] \cdot E_{nx1}, \quad (9)$$

where  $F_z(t)$  is the loading force,  $E_{nx1}$  is unit vector and  $F_p^i(t)$  is the axial force calculated from the stress distribution

$$F_p^i(t) = \int_S \sigma^i(y, t) \cdot dS = \sum_{j=1}^n [\sigma_j^i(t)] \cdot dy \cdot b. \quad (10)$$

After the substitution of equations (9) and (10) into eq. (4), it can be obtained

$$\Delta\sigma_{LN}^i = \left\{ F_z(t) - \sum_{j=1}^n [\sigma_j^i(t)] \cdot dy \cdot b \right\} \cdot \frac{1}{S} \cdot E_{nx1}, \quad (11)$$

and after the substitution of equations (8) and (11) into eq. (3) is

$$\begin{aligned} \Delta\sigma_L^i(t) &= \left\{ F_z(t) - \sum_{j=1}^n [\sigma_j^i(t)] \cdot dy \cdot b \right\} \cdot \frac{1}{S} \cdot E_{nx1} + \\ &\left\{ Mo_{zd}(t) - \sum_{j=1}^n [\sigma_j^i(t) \cdot y_j] \cdot dy \cdot b \right\} \cdot \frac{1}{J_z} \cdot y. \end{aligned} \quad (12)$$

After the substitution of equation (3) into (1)

$$\begin{aligned} \Delta\sigma_L^{i+1}(t) &= \left\{ F_z(t) - \sum_{j=1}^n [\sigma_j^i(t)] \cdot dy \cdot b \right\} \cdot \frac{1}{S} \cdot E_{nx1} + \\ &\left\{ Mo_{zd}(t) - \sum_{j=1}^n [\sigma_j^i(t) \cdot y_j] \cdot dy \cdot b \right\} \cdot \frac{1}{J_z} \cdot y + \sigma_L^i(t). \end{aligned} \quad (13)$$

The time stress distribution is obtained by discrete step by step solution. Starting step appears from non-loaded state, in each next step loading grows and eq. (1) is solved as long as  $\|\sigma^{i+1} - \sigma^i\| \leq \epsilon$ , if  $\epsilon \rightarrow 0$ .

### 2.2 Proposed model No. 2

The stress distribution in the beam made from an ideal elastic-plastic material can be expressed using the continuous equation

$$\Delta\sigma(Mo) = \left(1 - \left|\frac{\sigma}{R_e}\right|^n\right) \cdot \Delta y \cdot \left[\frac{2 \cdot \sigma_L}{h} - \left(\frac{2 \cdot \sigma_L}{h} - \frac{2 \cdot R_e}{h \cdot \sqrt{2 \frac{R_e - \sigma_L}{R_e} + 1}}\right) \cdot \frac{\text{sgn}(\sigma_L - R_e) + 1}{2}\right], \quad (14)$$

where  $R_e$  is yield stress,  $\sigma_L$  is linear stress,  $M_o$  is the bending moment and  $W_o$  is the bending cross-section modulus. Equation (14) describes the stress distribution in the beam's cross-section depending on bending moment

$$Mo^{i+1}(t) = Mo^i(t) + \Delta Mo^i(t), \quad (15)$$

where  $i$  is iteration step and  $\Delta Mo$  is increment of the bending moment. The stress distribution in time is calculated by iteration equation

$$\sigma^{i+1}(t) = \sigma^i(t) + \Delta\sigma^i(t), \quad (16)$$

where  $\sigma$  is the stress vector in cross-section and  $\Delta\sigma$  is vector of the stress increments in the cross-section area,

$$\Delta\sigma^i(t) = \Delta\sigma_z^i(t) - \left[\Delta\sigma_z^i(t) - \Delta\sigma_o^i(t)\right] \cdot \frac{\text{sgn}[-Mo^i(t) \cdot \Delta Mo^i(t)] + 1}{2}, \quad (17)$$

where  $\Delta\sigma_z^i(t)$  is vector of the stress increments in the cross-section (under load) and  $\Delta\sigma_o^i(t)$  is vector of the stress increments in the cross-section (unloading). The  $\Delta\sigma_z^i(t)$  can be calculated like

$$\Delta\sigma_z^i(t) = \sigma[Mo^i(t) + \Delta Mo^i(t)] - \sigma[Mo^i(t)], \quad (18)$$

where  $\sigma[Mo^i(t) + \Delta Mo^i(t)]$  is the stress vector obtained from equation (7) at the moment  $Mo^i(t) + \Delta Mo^i(t)$  and  $\sigma[Mo^i(t)]$  is the stress vector obtained from equation (7) at the moment  $Mo^i(t)$ . And

$$\Delta\sigma_o^i(t) = \frac{\Delta Mo^i(t)}{J_z} \cdot y, \quad (19)$$

where  $\Delta Mo^i(t)$  is the moment increment. After the substitution, the vector of the stress in the cross-section in the  $i+1$  step will be

$$\sigma^{i+1} = \sigma^i + \Delta\sigma_z^i(t) - \left[\Delta\sigma_z^i(t) - \Delta\sigma_o^i(t)\right] \cdot \frac{\text{sgn}[-Mo^i(t) \cdot \Delta Mo^i(t)] + 1}{2}. \quad (20)$$

### 2.3 3D generalization

In the case of 3D geometrical problem, the calculation starts from the equation (1) and the next step is a correction of the vector  $\sigma_L^{i+1}(t)$  by

$$\begin{aligned} \sigma^{i+1}(t) &= \sigma_L^{i+1}(t) \text{ if } |\sigma_{Lk}^{i+1}(t)| < R_e, \\ \sigma^{i+1}(t) &= \sigma_L^{i+1}(t) - \Delta\sigma_L^i(t) \cdot (1 - \alpha) \text{ if } |\sigma_{Lk}^{i+1}(t)| > R_e. \end{aligned} \quad (21)$$

The vector of the stress increments depending on the loading parameters is described like

$$\Delta\sigma_L^i(t) = \Delta\sigma_{LN}^i(t) + \Delta\sigma_{LM_y}^i(t) + \Delta\sigma_{LM_z}^i(t), \quad (22)$$

where  $\Delta\sigma_{LM_y}^i(t)$  and  $\Delta\sigma_{LM_z}^i(t)$  are vectors of the stress increments from bending moments in  $y$  and  $z$  axes. The  $\Delta\sigma_{LN}^i(t)$  is vector of the stress increments depending on axial force, these increments can be obtained by equations

$$\Delta\sigma_{LN}^i(t) = \frac{1}{S} \cdot \Delta F^i(t), \quad (23)$$

$$\Delta\sigma_{LM_z}^i(t) = \frac{\Delta Mo_z^i(t)}{J_z} \cdot y, \quad (24)$$

$$\Delta\sigma_{LM_y}^i(t) = \frac{\Delta Mo_y^i(t)}{J_y} \cdot z, \quad (25)$$

where  $J_z$  and  $J_y$  are quadratic cross-section moments to the axis of  $z$  and  $y$ ,  $y$  and  $z$  are discrete vectors of the beam's height and width coordinates (Fig. 2).

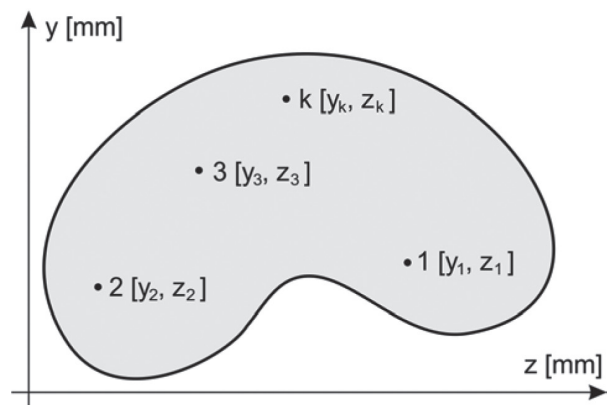


Fig. 2 The vector components

The  $\Delta Mo_z$  and  $\Delta Mo_y$  are differences between the loading moment and the moment calculated from the stress distribution in the beam cross-section,

$$\Delta Mo_z^i(t) = Mo_{zd}(t) - Mo_{zp}^i(t), \quad (26)$$

where  $MO_{zd}(t)$  is the loading bending moment to the axis of  $z$  and  $MO_{zp}^i(t)$  is moment really transferred by the beam, calculated as

$$MO_{zp}^i(t) = \int_S \sigma^i(t) \cdot y dS = \sum_{i=1}^n [\sigma_j^i(t) \cdot y_j] \cdot dy dz. \quad (27)$$

The result equation for calculating  $\Delta\sigma_{LMz}(t)$  will be

$$\Delta\sigma_{LMz}^i(t) = \left\{ MO_{zd}(t) - \sum_{i=1}^n [\sigma_j^i(t) \cdot y_j] \cdot dy dz \right\} \cdot \frac{1}{J_z} \cdot y. \quad (28)$$

In a similar way the equation for calculation  $\Delta\sigma_{LMy}(t)$  can be derived, i.e.

$$\Delta\sigma_{LMy}^i(t) = \left\{ MO_{yd}(t) - \sum_{i=1}^n [\sigma_j^i(t) \cdot z_j] \cdot dy dz \right\} \cdot \frac{1}{J_y} \cdot z \quad (29)$$

and

$$\Delta F^i(t) = [F_z(t) - F_p^i(t)] \cdot E_{(nx1)}, \quad (30)$$

where  $F_z(t)$  is loading force,  $F_p^i(t)$  is the axial force calculated from stress distribution

$$F_p^i(t) = \int_S \sigma^i(y, t) \cdot dS = \sum_{j=1}^n [\sigma_j^i(t)] \cdot dy dz. \quad (31)$$

After the substitution of equations (31) and (30) into eq. (23), following equation can be obtained

$$\Delta\sigma_{LN}^i = \left\{ F_z(t) - \sum_{j=1}^n [\sigma_j^i(t)] \cdot dy dz \right\} \cdot \frac{1}{S} \cdot E_{(nx1)}. \quad (32)$$

Time stress distribution is obtained by discrete step by step solution. Starting step appears from non-loaded state, in each next step loading grows and eq. (20) is solved as long as  $\|\sigma^{i+1} - \sigma^i\| \leq \varepsilon$ , if  $\varepsilon \rightarrow 0$ .

### 3. Numerical study

A model of beam with bilinear material and proposed computational model No.1 (Fig. 3) was implemented in MATLAB and compared with the more detailed FEM model created and analyzed in ADINA [12 and 13]. The beam was fixed at its one end and loaded at the other end.

The material parameters were: Young's modulus  $E = 2.1 \cdot 10^5$  MPa, yield stress  $R_e = 100$  MPa and the hardening coefficient  $\alpha = 0.1$ .

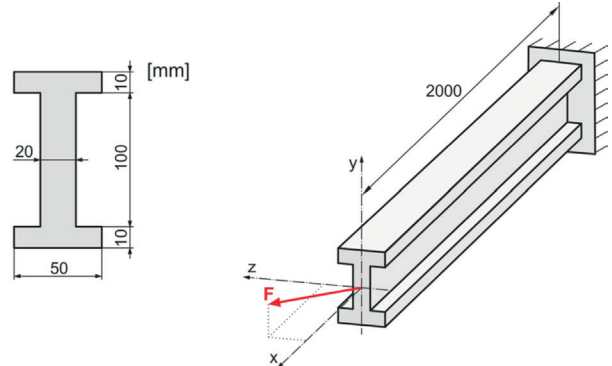


Fig. 3 Analyzed model dimensions

The forces distribution in the  $x$ ,  $y$  and  $z$  axes are shown in Figs. 4 and 5.

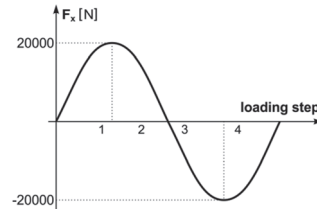


Fig. 4 Axial force behaviour

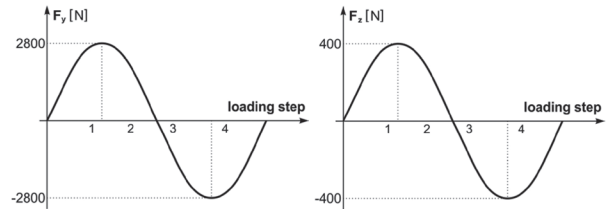


Fig. 5 Forces behaviour in the  $y$  and  $z$  axes

Comparison of maximum and minimum normal stresses in the particular loading steps is shown in Table 1. The stresses distribution monitored in the particular loading steps is shown in Figs. 6 to 9.

Comparison of maximum and minimum normal stresses Table 1

Loading step	$\sigma$	$\sigma$ [MPa]	$\sigma$ [MPa]
		(Proposed model No.1 MATLAB)	(FEM software ADINA)
1	$\sigma$ max	113.67	107.5
	$\sigma$ min	-116.4	-106.0
2	$\sigma$ max	23.8	20.4
	$\sigma$ min	-26.3	-31.6
3	$\sigma$ max	122.76	121.5
	$\sigma$ min	-123.52	-127.1
4	$\sigma$ max	16.833	23.3
	$\sigma$ min	-17.18	-14.7

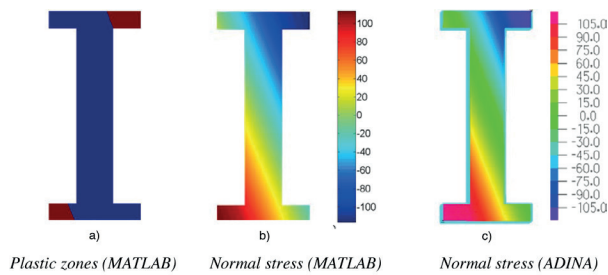


Fig. 6 Comparison of normal stress distribution at 1<sup>st</sup> loading step

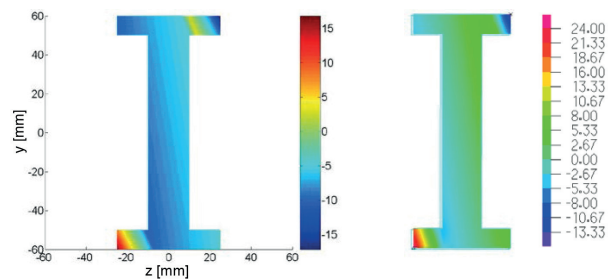


Fig. 9 Normal stress distribution at the 4<sup>th</sup> loading step

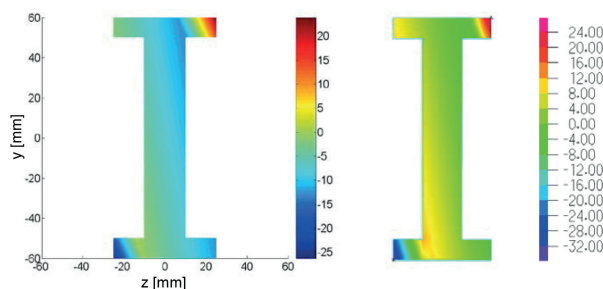


Fig. 7 Comparison of normal stress distribution at the 2<sup>nd</sup> loading step

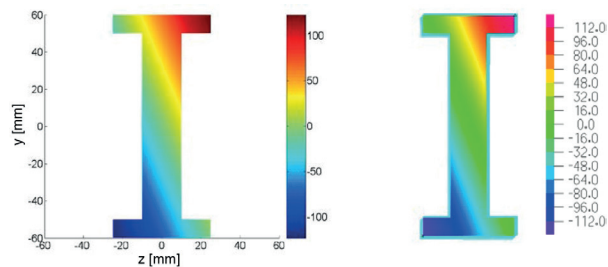


Fig. 8 Normal stress distribution at the 3<sup>rd</sup> loading step

## 5. Conclusion

The paper goal has been to present the study of new numerical approaches for plastic zones identification and residual stresses distribution in the cross-section area of the beams stressed above yield strength. The reason why this study was realized is to determine the stresses during the solution of the elastic-plastic structures state modelled by the beam finite elements.

According the authors' opinion, the graphical presentation of the residual stress distribution in the beam cross-section after application of the higher number of cycles can be important information from the view of the bearing capacity and reliability of the analyzed objects.

## Acknowledgement

This work has been supported by VEGA grant 1/0234/13.

This contribution is the result of the project implementation: Development of optimum technology for the analysis of limit states of structural elements in contact, ITMS code 26220220118, supported by the Research & Development Operational Programme funded by the ERDF.



Európska únia  
Európsky fond regionálneho rozvoja



We support research activities in Slovakia /  
The project is co-financed by the European Union.



## References

- [1] CZAN, A., TILLOVA, E., SEMCER, J., PILC, J.: Surface and Subsurface Residual Stresses after Machining and their Analysis by x-ray Diffraction. *Communications - Scientific Letters of University of Zilina*, vol. 15, No. 2, 2013, 69-76, ISSN 1335-4205.
- [2] EDWARDS, S. K., MCKEE, R. B., Jr.: *Fundamentals of Mechanical Component Design*. USA, 1991.
- [3] KOMPIS, V., NOVAK, P., HANDRIK, M.: Finite Displacements in Reciprocity-based FE Formulation. *Computer Assisted Mechanics and Engineering Sciences*, vol. 9, No. 4, 2002, 469-480, ISSN 1232-308X.
- [4] KUCERA, L., GAJDOSIK, T.: *The Vibrodiagnostic of Gears*. Proc. of 54<sup>th</sup> Intern. conference of machine design departments, September, 2013, Hejnice - Liberec : Technical university, 93-98, ISBN 978-80-7372-986-8.
- [5] SAGA, M., VASKO, M.: Stress Sensitivity Analysis of the Beam and Shell Finite Elements. *Communications - Scientific Letters of the University of Zilina*, vol. 11, No. 2, 2009, 5-12, ISSN 1335-4205.

- [6] STANCEKOVA, D., SEMCER, J., DERBAS, M., KURNAVA, T.: Methods of Measuring of Residual Stresses and Evaluation of Residual State of Functional Surfaces by x-ray Diffractometric Methods. *Manufacturing Technology*, vol. 13, No. 4, 2013, 547-552, ISSN 1213-2489.
- [7] VAVRO, J.: *Optimization of the Design of Cross-sectional Quantities in Transport Machines and Equipment*. Studia i materialy, Zelena Hora, 1998, 186-194.
- [8] KRAJNAK, J., GREGA, R.: Comparison of Three Different Gases and their Influence on Dynamic Properties One-bellow and Two-bellows Flexible Pneumatic Coupling. *Zeszyty naukowe Politechniki Slaskiej: Transport*, No. 81, 2013, 79-84, ISSN 0209-3324.
- [9] LACK, T., GERLICI, J.: *Modified Strip Method Utilization for Wheel/rail Contact Stress Evaluation*. 9<sup>th</sup> Intern. Conference on Contact Mechanics and Wear of Rail/wheel Systems (CM 2012), August 2012, Chengdu: Southwest Jiaotong University, 2012, 87-89.
- [10] KUCERA, L., LUKAC, M., JURAK, L., BRUMERCIK, F.: Hydromechanical Automatic Transmission. *Communications - Scientific Letters of the University of Zilina*, vol. 11, No. 2, 2009, 33-35, ISSN 1335-4205.
- [11] VASKO, A.: Analysis of the Factors Influencing Microstructure and Mechanical Properties of Austempered Ductile Iron. *Communications - Scientific Letters of the University of Zilina*, vol. 11, No. 4, 2009, 43-47, ISSN 1335-4205.
- [12] SAPIETOVA, A., SAPIETA, M., HYBEN, B.: Sensitivity Analysis Application for Multibody System Synthesis. *Applied Mechanics and Materials*, vol. 420, 2013, 68-73, ISSN 1660-9336.
- [13] ZMINDAK, M., NOVAK, P., DEKYS, V., PELAGIC, Z.: Finite Element Thermo-Mechanical Transient Analysis of Concrete Structure. *Procedia Engineering*, vol. 65, 2013, 224-229, Elsevier, ISSN 1877-7058.

Marian Handrik - Milan Vasko - Peter Kopas - Milan Saga \*

## EFFECTIVE FINITE ELEMENT SOLUTION AND POST-PROCESSING FOR WIDE LOAD SPECTRUM

*This paper presents a computational algorithm allowing the efficient use of high-performance computing resources to solve nonlinear problems of continuum mechanics using FEM. The algorithm is suitable for solving static problems and tasks of estimating lifetime of structures in cases where the load is defined by the load spectrum. The complexity of the problem increases significantly in the case of nonlinear problems. The principle of the stress superposition cannot be used in that case. For each loading mode a separate FE analysis must be made.*

*A quick and efficient procedure for evaluating the results of mentioned analysis for the static calculation as well as for the estimated life calculation is also presented in this paper. In the presented examples the contact of bodies is used as a source of nonlinearity. The size, shape or position of the contact area is not possible to estimate in contact of bodies. These types of problems are thus highly nonlinear. Programs for the presented algorithms are processed in the program package OCTAVE and calculations using FEM are made in the software ADINA.*

**Keywords:** FEM, static analysis, lifetime, spectrum of load, contact of bodies, state of stress, stress tensor, finite element mesh, ADINA, OCTAVE.

### 1. Introduction

Finite element method (FEM) is most commonly used in continuum mechanics for the analysis of stress state. Together with the increasing computing power, the complexity of the tasks also increases. The preparation of necessary matrices and their solution takes currently from several minutes to several tens of hours. The fact is that the user is willing to accept such a solution time and is ready to lower requirements for the accuracy to speed up the solution.

For static tasks solution it is mostly necessary to analyze stress state for a relatively small number of load spectrum (about tens of load states – lines of the load spectrum). This load spectrum is defined by a small group of phenomena which cause extreme loads during operation. Degree of safety against yield strength and strength limit of the used material is checked in the analysis. The aim of the static analysis is to ensure the operational safety and to prevent the sudden loss of the construction utility properties (change in shape, brittle fracture, etc.) [1].

Solving the estimated life of the structure requires an analysis of the state of stress for the given load spectrum which has a relatively low number of loads (force, moment, pressure) and a relatively high number of loading states. Such a load spectrum is usually defined by the time course of the dynamic load and it may have the character of accidental load.

Methods for reducing the number of load steps are often used to solve this kind of load spectrum. The final load spectrum may still contain tens to thousands of different loading states [2, 3, 4 and 5].

The main criterion for the establishment of an efficient algorithm for solving the above mentioned tasks is the relationship between the load and the resulting state of stress. This relationship can be linear or nonlinear.

### 2. Algorithm for linear relationship between load and state of stress

The principle of stress superposition can be used to speed up analysis of the state of stress in the case of linear relationship. Algorithm based on the principle of stress superposition is defined as follows:

1. Determine the number of individual loads (forces, moments, pressures). Only one single load is always considered.
2. FE analysis is performed for each individual load. The load size is modified so that the load will be unitary. The absolute size of all the loads shall be taken into account for normalization of loads. The unitary load is chosen in multiples of basic units.

\* Marian Handrik, Milan Vasko, Peter Kopas, Milan Saga

Department of Applied Mechanics, Faculty of Mechanical Engineering, University of Zilina, Slovakia

E-mail: marian.handrik@fstroj.uniza.sk

3. Analysis of the stress state for all types of loads and listing of the stress tensor components for all nodes of finite element mesh.
4. Calculation of the stress state for individual load cases (lines of the spectrum of load). The stress tensor is multiplied by a load coefficient at each point of the finite element mesh for the relevant unitary load. The individual components of stress tensors are then summed together because in the calculation all loads for the corresponding load state shall be included.
5. The processing of the analysis results for individual lines of the load spectrum, determination of the static safety level and calculating the estimated life of the structure.

It is necessary to implement  $N$  independent analyses of the state of stress if the  $N$  individual loads (forces, moments, and pressures) are defined in the spectrum. Arrays of stress tensors are subsequently written to the files. For each load a single file is obtained. This file contains six columns ( $\sigma_{xx}, \sigma_{yy}, \sigma_{zz}, \sigma_{xy}, \sigma_{xz}, \sigma_{yz}$ ) and the number of rows corresponds to the number of nodes in finite element mesh. These files are read and used for calculation of the stress state (using the method of stress superposition [6]).

In general, analysis of the stress state using the FEM is significantly more time consuming than reading the arrays of stress tensors and their multiplication and addition. The proposed algorithm allows a significant reduction in the time required for analysis of an entire spectrum of loads. The procedure can be easily parallelized in the phase of stress state analysis by FEM. Individual analyses may be solved on separate computers [7].

### 3. Algorithm for nonlinear relationship between load and state of stress

The principle of superposition of stress cannot be used in nonlinear relationship between the load and the resultant array tensors of stress at nodes of finite element mesh. A suitable example of such a nonlinear relationship is the contact of bodies. Contact of bodies is highly nonlinear problem with regard to the previously unknown size, shape or position of the contact area. For the solution of the contact analysis the significantly higher number of steps in nonlinear analysis is needed than for solving geometric and material nonlinearities.

The contact of bodies between several parts of the structure is defined in the example below. The bolts with a defined preload are used in this example. In the first step of the contact problem solution (time  $t = 0$ ) it is necessary to eliminate the initial penetrations of the contact bodies. The initial preload in the bolts needs to be solved at the same time.

Powerful computing resources in the form of a cluster enable parallelization of the computing algorithms. The cluster has 46 computational nodes (each computational node has 12 cores and 48 gigabytes of RAM). The algorithm for solution of nonlinear problems with the contact of bodies is as follows:

1. Preparation of the model and generating files needed for the analysis of a contact at time  $t = 0$ . Saving the model with finite element mesh in a binary form. The initial penetrations of the contacts of bodies are eliminated in this introductory calculation. Next, the shortening of bolts is calculated to apply the prescribed force acting in them. Analysis of the stress state is solved for the unitary loads at time  $t = 1$ . This analysis is needed for the next restart of the analysis at the same time. A separate time function is defined for each load.
2. Generating input files for individual calculations corresponding to different load states. Stored model is loaded in a binary form with the finite element mesh in the phase of generating. Restart of the analysis is defined for time  $t = 1$ . Time functions for individual loads are adjusted to correspond to the actual loads for individual load states.
3. The inclusion of tasks to the queue for middleware TORQUE which manages the calculations on the grid. Files needed to calculate the individual tasks are generated. Analysis of the state of stress by FEM is made. Analysis of the results and listing the individual components of stress tensor at all nodes of finite element mesh is made.
4. Checking if all tasks from the queue of managing system on the grid are processed. The monitoring of the completion of all tasks is performed periodically and the continuation is possible only after completion of all the tasks.
5. The processing of the analysis results for individual lines of the load spectrum, determination of the static safety level and calculating the prediction of lifetime of the structure.

### 4. Analysis of the results of static task for the spectrum of load

State of stress in the structure is most often evaluated for static analysis. Analysis of the results consists of creating the graphs of stress area distribution where points with increased values of stress are evaluated. The position of these points and corresponding numeric value are determined in this evaluation. The evaluation must be made for all analyzed states of load; therefore, it must be performed across the whole spectrum of load. Then, it is necessary to make the resulting evaluation of the state of stress.

Points of stress concentration may be located in several areas of the construction and results may correspond to various loading states. Therefore, each load state has its own graphical outputs where stress concentrations are to be displayed and located. This procedure becomes time consuming with a greater number of loading states. Its difficulty is based mainly on mutual comparison of the points and values of stress (and corresponding numeric arrays) on different graphs.

Both above mentioned algorithms for the analysis of stress state are designed to allow the use of cluster parallelization. The

results of the state of stress analysis for individual load cases are stored in a text file and they are ready for further processing. The algorithm for processing the results of static analysis in which the resulting state of stress and equivalent stress according to the required criteria (von Mises, Tresca) at each point of finite element mesh is evaluated as follows:

1. Processing of the results of analyses for individual load cases. The stress tensor for individual nodes of the finite element mesh is written to a separate file. All equivalent stresses determined in accordance with required criteria will be recorded into the second separate file. Maximum of 6 values can be written into one file. If necessary, several files with the results must be created (these files can be created immediately after analysis of the state of stress). Within the cluster solution, parallelization of the algorithm for stress state analysis is used.
2. The program package OCTAVE reads saved files in successive steps corresponding to the different states of load. The

maximum values for individual components of the stress tensor from previous loading states and those from current evaluation are compared. The serial number of the load state which caused the maximum value of the corresponding element of the stress tensor is also saved.

3. The results of the required criteria for evaluation of the equivalent stresses are processed. The serial number of the load state which caused the given state of stress is saved too.
4. Generating an input file for post-processing. It allows viewing the cumulative results and creation of graphical outputs from these results.

Equivalent stresses must always be evaluated for the individual states of load. The realization is most suitable in the program for the analysis of stress state using FEM - in our case - software ADINA. The equivalent stresses cannot be calculated from the cumulative stress tensor. This stress tensor contains the maximum values of stresses of the entire spectrum of loads. The individual

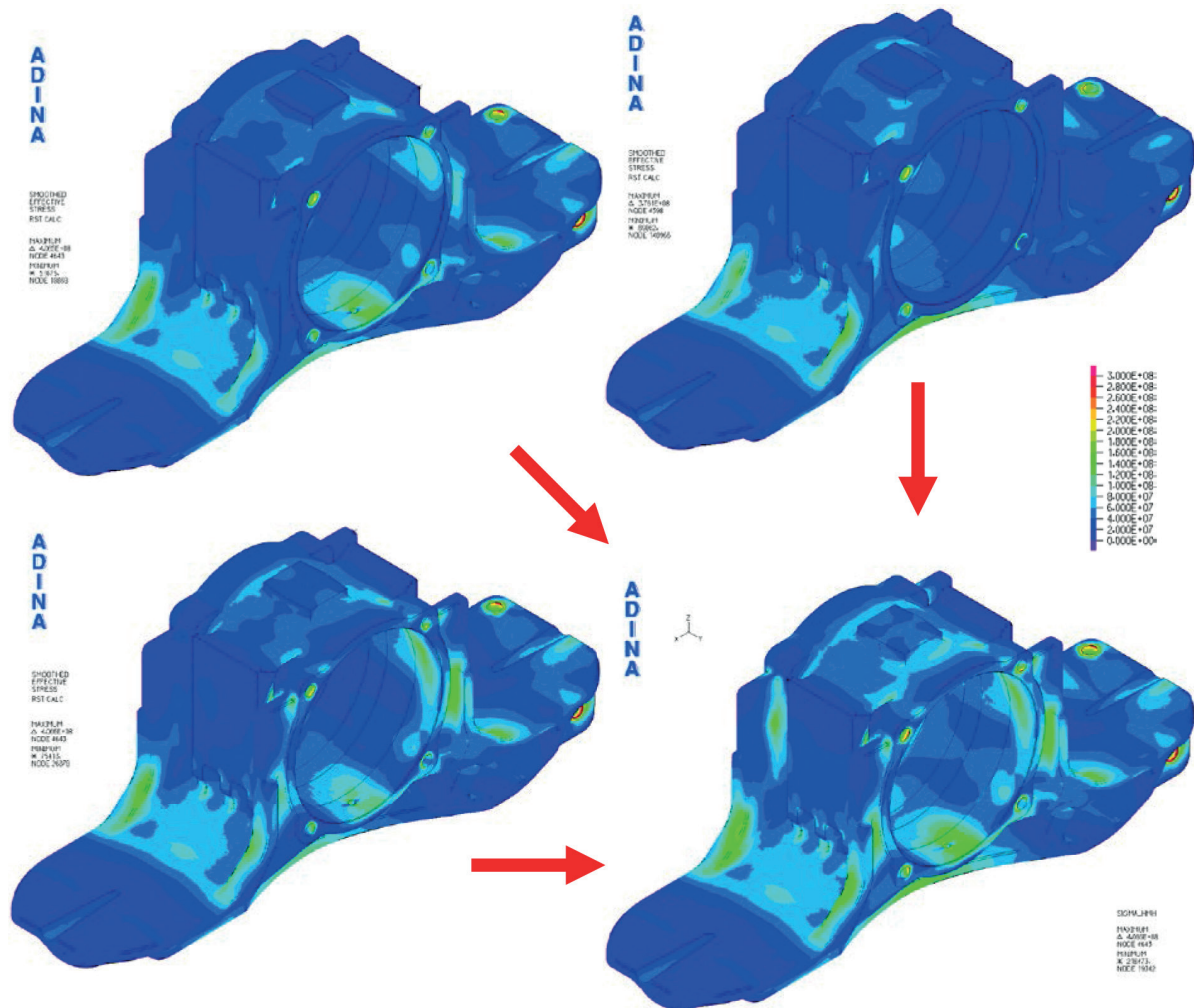


Fig. 1 Cumulative effective stress distribution results [Pa]

tensor components may, however, correspond to the different load cases [8].

The above mentioned processing of the state of stress analysis for the individual load cases allows a simplified evaluation of the results for the entire load spectrum. The maximum values of the corresponding stress tensor component or equivalent stress processed for the entire load spectrum can be displayed in one figure (Fig. 1). Registered serial number of the load state that achieved a maximum value of the relevant component of stress tensor or the equivalent stress allows a simple graphic representation of the corresponding state. The practical experience with this procedure for the model about the size of 1.2 million nodes shows that the reading and processing of one load state with two sets of results takes approximately 80 seconds.

## 5. The review of methods for the fatigue life evaluation of structural elements

Most of the criteria for the calculation of fatigue life used to estimate the life of the structure use knowledge of the stress state or knowledge of the deformation in the structure. The methodologies based on the evaluation of the extreme state of load are used to calculate the fatigue life of machine parts. In the first case, they evaluate the mode which causes maximum stress or strain [5 and 9]. In the second case cumulative criteria are used where each state of load contributes to the total damage. Using referred methodologies with regard to their specific state of load it is possible to predict the number of cycles to fracture  $N_f$  [10 and 11].

Input for the analysis of the fatigue life is the geometry, load and material properties of components or structures. Strength and fatigue properties (Wohler or Manson-Coffin curve) of the material are most commonly determined from the database or from the experiment. Loads can be obtained by experiment, analytical calculation, by estimation or based on the use of numerical methods. Based on these data it is possible to calculate the local stresses [12 and 13]. In the first case, the input for the analysis of lifetime is the file with a set of stresses for each load state and the file containing the corresponding loading process. In the second case, the file contains stresses for each load state and the number of load cases corresponds to the number of eigenvalue shapes of the flexible element used in the calculation. Loading history is analogously assigned to each mode. The output of the analysis is the lifetime calculation for each node of components or structure [14].

The main methods for predicting the fatigue life of the structures are based on:

- the nominal stresses,
- the local elastic stresses,
- the local elastic-plastic stresses and deformations,
- the fracture mechanics.

The S-N (Stress-Life) method and NSA (Nominal Stress Analysis) method belong to lifetime estimation methods which are based on the nominal stresses. Determination of fatigue life based on the S-N curve is inaccurate especially in low cycle fatigue. It is the oldest method which can be used for a wide range of applications. The method provides an extensive database and its use is appropriate for the high cycle fatigue. The NSA method uses the relationship between the size of the nominal stress of cycles and the number of cycles to failure. The method uses correction of medium stress according to Goodman or Gerbera.

The LESA (Local Elastic Stress Analysis) method belongs to lifetime estimation methods which are based on the local elastic stress. The method uses the relationship between the size of the local elastic stress of cycles and the number of cycles to failure. This method is a modification of the NSA method. The method is particularly useful in high cycle fatigue and uses the same corrections of medium stress as the NSA method.

The  $\epsilon$ -N (Strain-Life) method and LPSA (Local Plastic Strains and Stress) method belong to lifetime estimation methods based on the local elastic-plastic stresses and deformations. The LPSA method is based on the testing of the material in the context of local deformation according to cycles in order to initiate macroscopic cracks. This approach allows the analysis of elastic-plastic deformation at the critical points. The method uses (in uniaxial stress) mostly values of the stresses and strains identified on the basis of elastic calculation. The method subsequently makes the elastic-plastic correction according to the most common methods of Neubert, Mertens-Dittmann or Seeger-Best. Methods of SWT (Smith, Watson, Topper) or Morrow most frequently used for medium stress corrections. The values of the local elastic-plastic stresses and strains can also be determined using a nonlinear elastic-plastic calculation. In this case it is necessary to make a separate calculation for each local maximum of the load. This is time consuming and puts considerable demands on the computing power.

The FMA (Fracture Mechanics Analysis) method belongs to lifetime estimation methods that are based on fracture mechanics. The linear-elastic fracture mechanics analysis most often uses the Paris rule for predicting the crack extension. The size of crack increase and stress intensity factor at the end of the crack is brought into relationship. The method is mostly used in the aerospace industry for the calculation of the allowable damage (Damage-Tolerant). The calculation allows reliable monitoring of the crack of a certain size. This approach enables monitoring of crack growth in each step – cycle after cycle.

In addition to these most commonly used methods of fatigue life evaluation, there are also other methods for calculating the number of cycles to failure of machine parts [15]. This group of methods includes the following methods – Vibration Fatigue Analysis, Biaxial Fatigue Analysis, Multiaxial Fatigue Analysis, Global Multiaxial Fatigue (Safety Factor Analysis, Dang Van, McDiarmid, Crack Initiation Life Analysis, SWT-

Bannantine, Fatemi-Socie, Wang-Brown, Normal Strain, Shear Strain), Local Multiaxial Fatigue (Crack Initiation Life Analysis, Mróz-Garud, Wang-Brown criterion, Multiaxial Elasto-plastic Neuber Correction), Welds Fatigue Analysis and Temperature Dependent Fatigue etc.

**6. Analysis of the results for the dynamic load spectrum and lifetime rating of the structure with respect to the Smith’s diagram**

Evaluation of fatigue life based on a state of stress evaluation in the construction with respect to the Smith diagram determines if the state of stress is in the stress scope which causes a critical accumulation of fatigue damage. For the lifetime evaluation of the structure with respect to the Smith diagram, the value of average stress and amplitude of the stress range is necessary to know [4, 5 and 9].

Algorithm for lifetime evaluation of the structure with respect to the Smith diagram has the following form:

1. The first analysis of the results is made in post-processing of the FEM software ADINA; the principal stress  $\sigma_1$  and directional angles of the first principal stress are calculated. The results are written to a text file. Equivalent stresses according to the von Mises method will also be written to the file.
2. The second analysis of the results is made in post-processing of the FEM software ADINA; the individual components of stress tensor are displayed. Both analyses of results are made one after the other within the results loading in post-processing.
3. Files containing the principal stress  $\sigma_1$  and directional angles of the first principal stress are sequentially loaded in the program package OCTAVE [16]. After loading the first principal stress for one load state, the result is compared with the maximum value in the previous states. The maximum value of the first principal stress, its directional vectors and the serial number of the load state will be found. The maximum tensile stress ( $\sigma_{max}$ ) of the entire spectrum of the dynamic load on each point of finite element mesh is determined in this step (Fig. 2).
4. The stress tensor for individual load states is sequentially loaded after the determination of the maximum first principal stress and its direction. The stress tensor is projected into the direction of the main stress according to the equation

$$p = T_{\sigma} \cdot n = \begin{bmatrix} \sigma_x & \tau_{xy} & \tau_{xz} \\ \tau_{yx} & \sigma_y & \tau_{yz} \\ \tau_{zx} & \tau_{zy} & \sigma_z \end{bmatrix} \cdot \begin{Bmatrix} \cos(\alpha) \\ \cos(\beta) \\ \cos(\gamma) \end{Bmatrix} \quad (1)$$

From the entire spectrum of the load the minimum value of the stresses in the direction of the maximum principal

stress is found. In this step, the minimum tensile stress ( $\sigma_{min}$ ) or maximum pressure stress of the entire spectrum of the dynamic load is determined (Fig. 3).

5. The values of average stress and amplitude of the stress range are determined from values  $\sigma_{min}$  and  $\sigma_{max}$  as follows (Fig. 4 and 5):

$$\sigma_m = \frac{\sigma_{max} + \sigma_{min}}{2} \text{ and } \sigma_a = \frac{\sigma_{max} - \sigma_{min}}{2} \quad (2)$$

6. Evaluation of the degree of safety against the fatigue damage of the structure with respect to the Smith’s diagram (Fig. 6) is carried out as follows - for the real value of average stress determined by the relation in point 5 - the maximum allowable value of the stress amplitude ( $\sigma_{aLIM}$ ) is subtracted in the Smith’s diagram. The safety coefficients are subsequently determined according to the relation (Fig. 7 and 8)

$$k = \frac{\sigma_{aLIM}}{\sigma_a} \quad (3)$$

7. The processing of equivalent stresses according to von Mises method is identical to the static loading mode.
8. The input for the post-processing is generated. The file allows display of the cumulative results and creation of their graphical outputs.

The principal stresses calculation is made within the post-processing in the program ADINA. This procedure is faster than the calculation in the program OCTAVE. Both post-processing steps in 1<sup>st</sup> and 2<sup>nd</sup> point of the above mentioned algorithm are performed during one loading of results files into the program ADINA. This part can be repeated in a parallel mode immediately after the analysis of stress state.

The practical experience with this procedure (for the model about the size of 1.2 million nodes) shows that the reading and processing of one load state with two sets of results takes approximately 250 seconds.

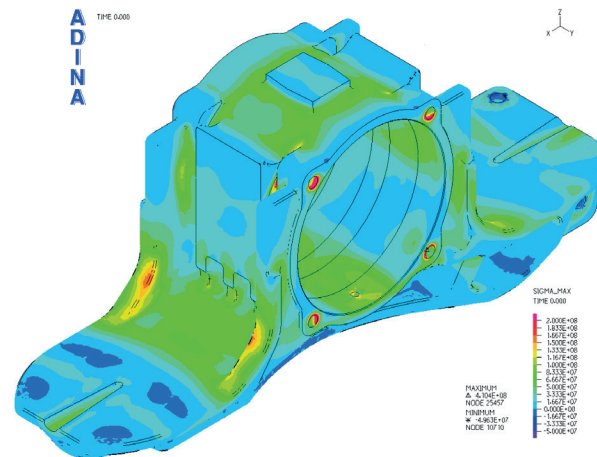


Fig. 2 The maximum tensile stress  $\sigma_{max}$  [Pa]

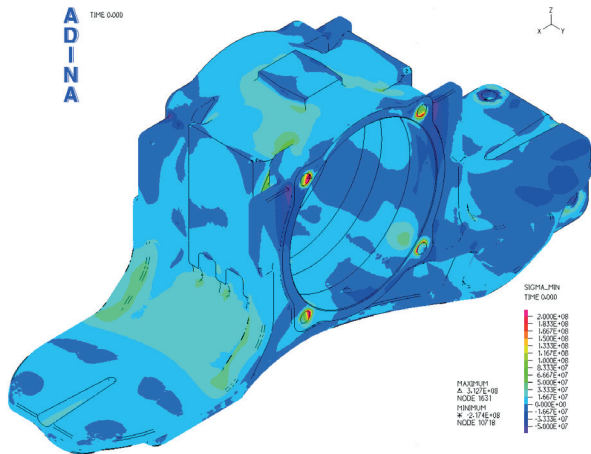


Fig. 3 The minimum tensile stress  $\sigma_{min}$  [Pa]

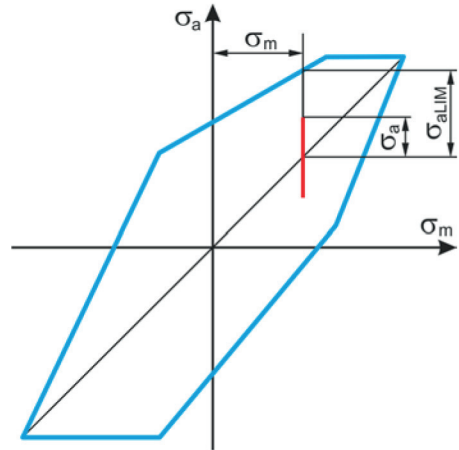


Fig. 6 Smith's diagram

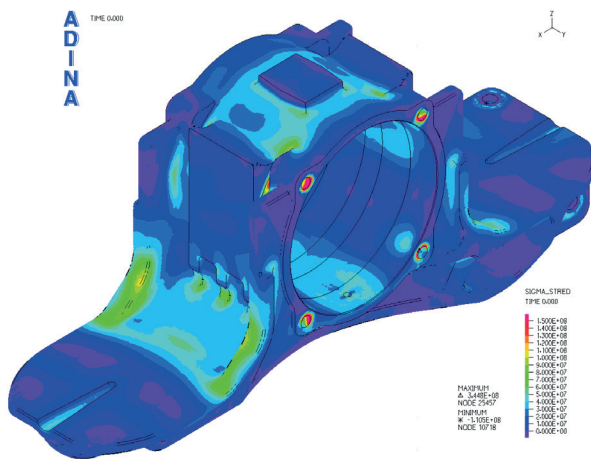


Fig. 4 The average stress  $\sigma_m$  [Pa]

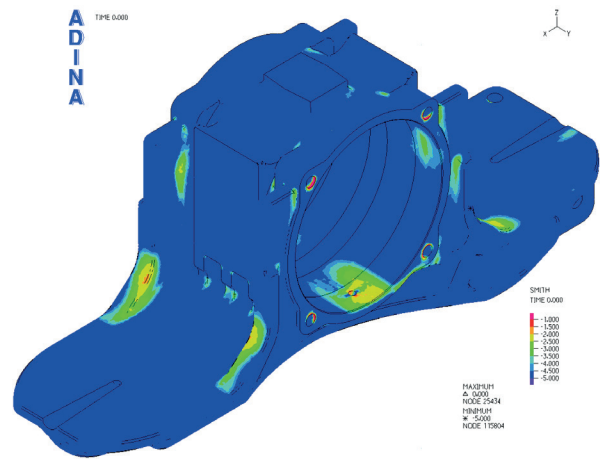


Fig. 7 Smith's safety factor

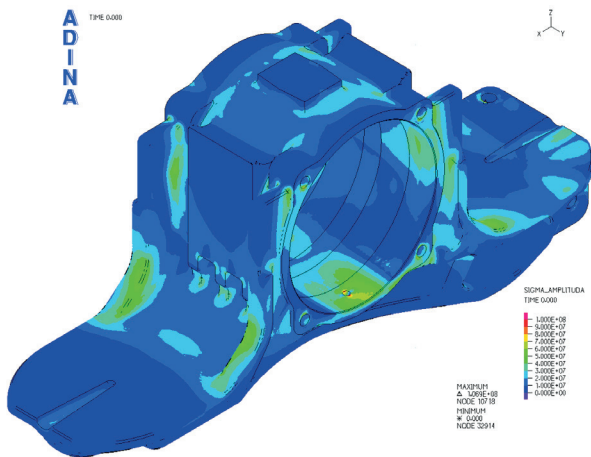


Fig. 5 The amplitude of the stress range  $\sigma_a$  [Pa]



Fig. 8 Static safety factor

## 7. Conclusion

Computer processing of the stress state analyses using FEM can significantly simplify and speed up the process. Manual processing of the results for the spectrum of load is difficult in terms of time and user. The above proposed algorithms process the results of the analysis to the cumulative form. The subsequent analysis of cumulative results becomes significantly simpler. The cumulative results are then displayed on a relatively small number of figures.

Another significant factor is that the results processing is independent of the user and can be performed in the user's absence. It is possible to process the results of analysis for the static spectrum of load of more than 1000 different modes during 24 hours. For the dynamic spectrum of load it is possible to process more than 350 different modes during 24 hours. In our presented example, one analysis of the stress state for a static or dynamic load mode (with considering the contact of bodies) takes approximately 4.5 hours.

Created algorithms, their implementation and use of powerful cluster computing resources allow efficient solving of the problems of the state of stress analysis or the life estimation of structures. Algorithms are applicable to the problems of contact (for static and dynamic spectrum of load) with a relatively large number of loading states in a short time (4-5 days including the processing of analyses results).

## Acknowledgements

*This contribution is the result of the project implementation: Development of optimum technology for the analysis of limit states of structural elements in contact, ITMS code 26220220118, supported by the Research & Development Operational Programme funded by the ERDF.*



Agentúra  
Ministerstva školstva, vedy, výskumu a športu SR  
pre štrukturálne fondy EÚ



*We support research activities in Slovakia /  
The project is co-financed by the European Union.*

## References

- [1] SAPIETOVA, A., SAPIETA, M., HYBEN, B.: Sensitivity Analysis Application for Multibody System Synthesis. *Applied Mechanics and Materials*, vol. 420, 2013, 68-73, ISSN 1660-9336.
- [2] BATHE, K.J.: *Finite Element Procedures*. Prentice Hall, 1996.
- [3] DEKYS, V., BRONCEK, J.: Measuring Strain of the Lattice Towers. *Communications - Scientific Letters of the University of Zilina*, vol. 14, No. 3, 2012, 39-42, ISSN 1335-4205.
- [4] MURIN, J.: *Finite Element Method for Truss and Frame Structures (in Slovak)*. Bratislava: STU Bratislava, 1999, 130 p., ISBN 80-227-1287-6.
- [5] SAGA, M., KOPAS, P., VASKO, M.: Some Computational Aspects of Vehicle Shell Frames Optimization Subjected to Fatigue Life. *Communications - Scientific Letters of the University of Zilina*, vol. 12, No. 4, 2010, 73-79, ISSN 1335-4205.
- [6] SAGA, M., VASKO, M., KOPAS, P.: *Strength of Materials - Selected Methods and Applications (in Slovak)*. VTS: University of Zilina, 2011, 400 p., ISBN 978-80-89276-34-9.
- [7] ZMINDAK, M., RIECKY, D.: Meshless Modelling of Laminate Mindlin Plates under Dynamic Loads. *Communications - Scientific Letters of the University of Zilina*, vol. 14, No. 3, 2012, 24-31, ISSN 1335-4205.
- [8] *ADINA - Theory and Modelling Guide, Volume I* [help manual]. Watertown, 2010.
- [9] RUZICKA, M.: *Methods for the Fatigue Life Evaluating (in Czech)*. CVUT: Praha, 1999.
- [10] KOPAS, P., SAGA, M., UHRICIK, M.: Contribution to Multiaxial Damage Calculation using FEM. *Applied Mechanics and Materials*, vol. 420, 2013, 318-224, ISSN 1660-9336.
- [11] TREBUNA, F., BIGOS, P., JURICA, V., RITOK, J.: Possibility of Identifying the Residual Life of Machines and Equipment by Experimental Methods in Mechanics (in Slovak). *Strojárstvo*, Zilina, No. 2, 2000, 57-63.
- [12] LEITNER, B.: Discrete optimization of the rail vehicle frame weight with respect to fatigue damage cumulation process. *Transport means 2013*, proceedings of the 17<sup>th</sup> international conference, October 24-25, 2013, Kaunas University of Technology, Lithuania, 17-20, ISSN 1822-296X.
- [13] VASKO, A.: Analysis of the Factors Influencing Microstructure and Mechanical Properties of Austempered Ductile Iron. *Communications - Scientific Letters of the University of Zilina*, vol. 11, No. 4, 2009, 43-47, ISSN 1335-4205.
- [14] BIGOS, P., KUBIN, K., KULKA, J., MANTIC, M., BURAK, J., PUSKAR, M., TANYASI, O., FALTINOVA, E.: *Computational and Experimental Methods for Increasing Efficiency and Life Examination of Structures for Selected Power Drives and Transport Equipment (in Slovak)*. TU Kosice, 2010, 215 p., ISBN 978-80-553-0522-6.

- [15] KOPAS, P., SAGA, M.: In-phase Multiaxial Fatigue Experimental Analysis of Welded Cylindrical 6063-T66 Aluminium Alloy Specimens. *Manufacturing Technology*, vol.13, No. 1, 2013, 59-64, ISSN 1213-2489.
- [16] *OCTAVE manual* [help manual], [www.octave.org](http://www.octave.org).

Juraj Gerlici - Tomas Lack - Jozef Harusinec \*

## DEVELOPMENT OF TEST STAND PROTOTYPE FOR RAIL VEHICLES BRAKE COMPONENTS TESTING

*The paper deals with the new RAILBCOT test stand building reasons explanation. A project features definition is described. There is possible to perform the railway wheel tread profiles wear research under the rail vehicle in operation conditions simulation. This simulation is possible to execute on the test bench. An important feature of the research is the equivalent conicity change analysis. The paper outlines the stand operation principles a main structure components design and components parameters specification, the tests control, data acquisition and data assessment.*

**Keywords:** Wheel/rail contact, test stand, equivalent conicity, brake blocks testing.

### 1. Introduction

Reduction of noise due to rolling contact of wheel and rail for freight cars is one of the principal tasks to be solved by the European railways. Experts of railways companies, industry and universities were engaged during the last about ten years in searching for technical solutions. An important noise reduction of freight cars can be achieved by replacing the cast iron brake shoes by composite brake shoes. Doing that, two directions have been taken into consideration. This is due to the fact that at that time most composite brake shoes friction coefficients were far away from the friction coefficient of the cast iron brake shoes. Applying such friction materials on existing vehicles would cause the change of braking forces acting on the wheels. These types of brake shoes (K-block) show a friction coefficient which is higher than the coefficient of cast iron. Consequently, the application of the "silent" composite brake blocks of type K affords the adaptation of the braking system of the vehicle, which is costly. For these reasons, the application of K-brake block was proposed for newly built vehicles. For the existing vehicles, solutions having the same friction coefficient as the cast iron brake shoes were requested (LL-Brake blocks). In this case, we can avoid to the modification of the braking equipment of existing freight cars.

### 2. Tests of brake components

For the development of the braking system on the basis of composite brake blocks a lot of research in different areas was carried out:

- Tests on test rigs to improve the friction characteristics under dry, wet and hot conditions including stop braking and braking in severe downhill conditions.
- Tests to inhibit negative influences on the shunting circuits in railway lines.
- Tests under heavy winter conditions to avoid exceeding braking distances of trains due to the influence of snow.
- Thermo mechanical test to avoid high residual stresses in the wheel rigs and important plastic lateral deformations of the wheels.
- Tests to avoid material inclusions into the brake shoes.
- In line test to prove the braking power.
- Downhill test under severe load conditions.
- Test to prove the whole system behaviour under real service conditions including all the seasons (winter, summer, etc.)
- Fuse tests (behaviour under failures in the braking system, handbrake not released, etc.)

As it can be seen from the above, a lot of tests had to be carried out. They were partly based on a long experience, especially based on the application of cast iron brake shoes. Some of them had to be newly developed due to the different behaviour of composite brake shoes in comparison to cast iron brake blocks (for example, winter tests, tests concerning the shunting behaviour, fuse tests). With growing experience it was possible to develop tests on test rigs instead of expensive tests on lines. During the service tests it was observed that under certain conditions and configurations an unfavourable wear concerning especially the treads of the wheels arose. As a consequence, high equivalent conicities were reached partly after short inservice time. As these parameters concern

\* Juraj Gerlici, Tomas Lack, Jozef Harusinec

Department of Transport and Handling Machines, Faculty of Mechanical Engineering, University of Zilina, Slovakia  
E-mail: juraj.gerlici@fstroj.uniza.sk

dynamic vehicle behaviour it is completely understood only by experts of running dynamics.

### 3. Equivalent conicity

What is equivalent conicity? The wheel and the rail have a particular surface geometry in their contact area. In a first approximation the wheel can be described as a cone rolling on a pointed edge. Conicity describes the angle (tangent) of this cone. Equivalent conicity is a measure comparing real geometries with this theoretical model. This makes it possible to compare different wheel geometries in terms of running behaviour [1, 2 and 3].

Importance of equivalent conicity: In order to sustain a good running behaviour of the vehicle on the track, to prevent wheel, rail and track damage and, in the worst case, the risk of a derailment the equivalent conicity must remain within given limits. The geometry of the wheel profile is designed in such a way that during operation, equivalent conicity does not exceed these limits due to wheel wear. The values are defined in EN 14363, stating that equivalent conicity in service may not deviate more than 50% or a maximum of 0.05 from original values.

Different behaviour of cast-iron brake blocks and composite brake blocks (Fig.1): Cast iron brake blocks adapt their contact geometry to the wheel so that there is no influence on the equivalent conicity of the wheels. This is not the case with composite brake blocks. Here, the brake blocks influence the geometry of the wheel profile and, therefore, also equivalent conicity. Therefore, a new element is introduced into the wheel - rail system. It is important that the new system is at least equal to the old one with respect to the wheel/rail contact conditions (compare Fig. 1).

LL-brake block homologation: In the operational tests of LL-blocks the equivalent conicity was not measured systematically with the exception of Switzerland. Here, it was shown that the equivalent conicity values increased too rapidly. If this proves to be the case in other situations, a monitoring system would be required and wheels would have to be re-profiled more often than with cast-iron brake blocks. This would increase the life-cycle-costs, which runs counter to the idea of having a low cost retrofitting possibility.

What are possible reasons for the increase in equivalent conicity? A UIC study showed that the increase in equivalent conicity is probably due to the geometry of the friction surface of the brake block. There are guidelines on the geometry of brake blocks; however it is unclear how they emerged. It is likely that the contact geometry of the brake block has not been adapted to the geometry of the wheel profile.

Possible approach: The issue of equivalent conicity can be approached in two ways:

*Determine if higher deviations from original equivalent conicity are possible:* This work would define a new limit value for equivalent conicity. Added to this approach a system for monitoring equivalent conicity during operation must be developed and implemented.

*Determine if changes in brake block geometry can reduce high increases in equivalent conicity.* The change of geometries during operation must be studied and new brake block geometry must be developed and tested. Ideally, brake block geometry is chosen in such a way that there is no influence on the equivalent conicity of the wheel during operation.

*Determine if brake shoes can be developed with properties similar to cast iron brake shoes concerning wheel wear.*

**Opportunities:**

Pursuing the suggested steps gives an opportunity to homologate an economically satisfying LL-brake block because wheel wear questions may be solved.

Insights from this work will also help design an optimal K-block which may reduce observed high wheel wear that is observed in certain cases, thus reducing life cycle costs.

Having optimal brake block wear improves the wheel wear which, in turn, optimises rail wear: Finding an optimal solution reduces costs both in operations and in infrastructure.

Influence on regular homologation: This work can be done in parallel to the regular homologation and can be considered to be an economic optimisation. It is suggested, however, that operational tests include measurements of equivalent conicity.

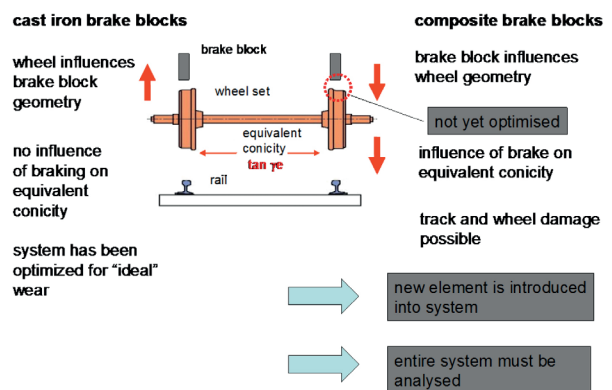


Fig. 1 Wheel wear and equivalent conicity for cast-iron brake blocks and for composite brake blocks

The problems concerning wear on wheels and wear on brake blocks have been found out during service tests. As service tests are very costly and time consuming, there exists a need to perform the tests on a test rig in the future. For these reasons the University of Zilina proposes a research project with the scope of optimization of the interaction between brake shoes and wheels.

#### 4. RAILBCOT - Rail vehicles brake parts test stand

The Railway vehicles brake components test stand RAILBCOT, [4] (see Figs. 2 and 3) is the facility where the core consists of an electromotor position 1 with the power of 440 kW. The motor power is led via a transmission (position 2 - conical gearbox) UNIMEC500 to the discs of rotational rails position 3. The railway wheelset (position 5) is via a cable stayed transmission (position 6) pressed to these discs with the force of 225.000N. The wheelset is integrated into the movable frame (position 4) that enables rotating of wheelset about the angle of attack and the lateral movement in the acceptable limits.

During the facility design and conception specification was badly needed to resolve several functional nodes. They are necessary for simulation of the wheelsets drive ability in true railway operation.

Such nodes are:

- change of track gauge possibility,
- change of strike angle possibility,
- lateral forces loading solution,
- axle loading solution.

#### 5. RAILBCOT - operation principle

Electromotor (1) will transmit the torque through gearbox (2) which has one input and three output shafts and rotate the rotating rails (3).

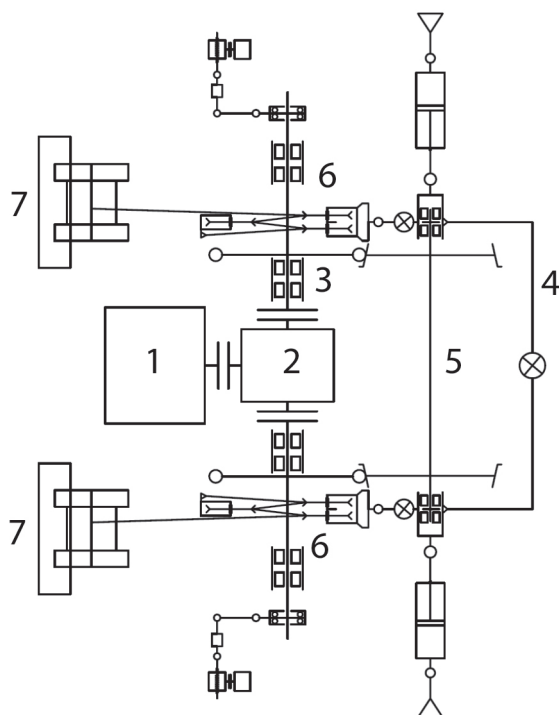


Fig. 2 Schema of the test stand functionality top view

These rotating rails are mounted in bearing housings which are connected with the frame. The supporting frame (4) will hang on two hinges. Rear hinge is of a more simple design and its duty is to hold the support frame in the requested position. Four locomotive brake units are implemented in the support frame. Axle boxes are mounted on the wheelsets (5), they are attached with screw binding to the support frame. A pneumatic cylinder creates the necessary axial force. The front hinge is attached with a tilting lever of the wheelset.

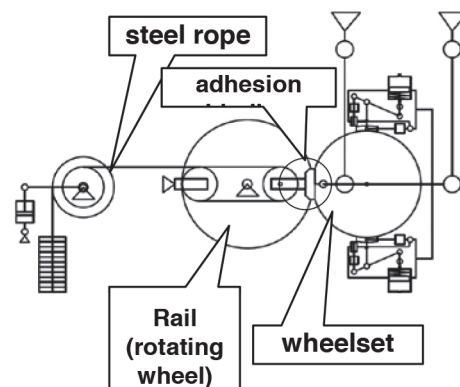


Fig. 3 Schema of the test stand functionality - side view

A force sensor is placed on pull rod which measures the longitudinal forces arising during braking. The adapter is attached to the bearing box in which is a force sensor that is connected to the rope fairlead (6). A vertical wheel force is evoked by weights (7) and each wheel is loaded with one weight. For simulation of the vehicle running arc track the rotating rails are moving in a lateral direction for max. 16mm. For this change the rotating rail mechanism of transverse displacement is used. This simulates a track gauge change when vehicles are passing the arc. The test bench is placed on two bases.

Scheme of the brake test stand RAILBCOT consists from electromotor, gearbox, rotating rails, brake units, rear hinge, front hinge, support frame, railway wheelset, base, weight units).

Wheel is braked with two locomotive brake units (four units per wheelset). The test stand will be not included into the UIC brake stands branch but ride stands branch. The utilization of the stand, operation and scientific investigation direction is different from Flywheel test stand UIC.

#### 6. Test stand model

Three dimensional model of test stand was created in CATIA system. In Fig. 4 is a central executive part of the device. The left side represents the driving part and constitutes the rail the right side (separated by dash dot line) represents a vehicle and constitutes a bogie with railway wheelset.

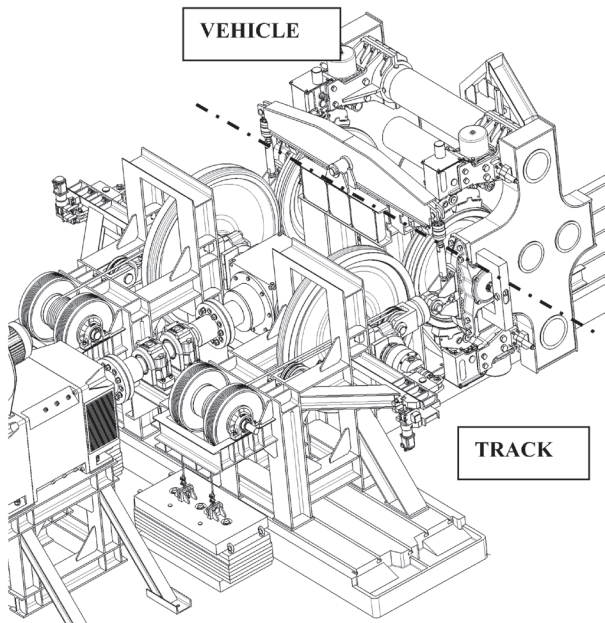


Fig. 4 3D projection of the test stand model

Test stand model-side view is depicted in Fig. 5, test stand model-front view is in Fig. 6 and test stand model-front view in Fig. 7.

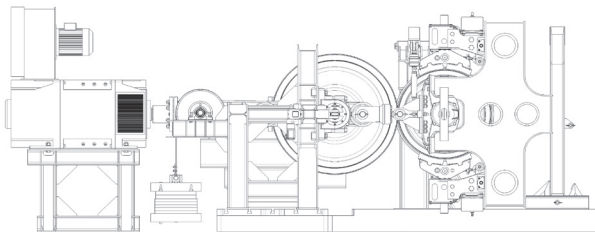


Fig. 5 Test stand model- side view

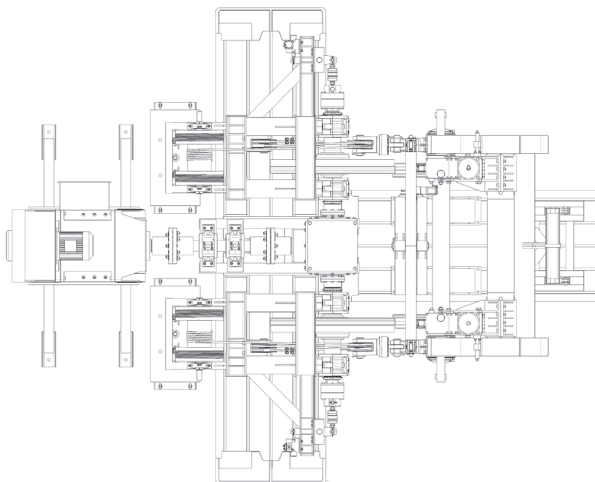


Fig. 6 Test stand model- top view

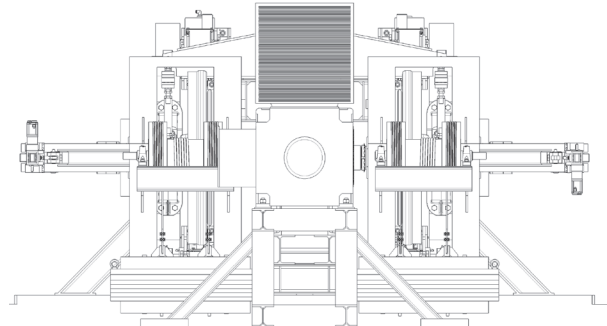


Fig. 7 Test stand model-front view

The test stand is in its basic version equipped with force sensors (2x wheel forces, 2x forces in the ride direction, 2x frame lateral forces, 4x normal brake forces a 4x tangential brake forces) as well as the wheel revolution sensors and sensors of rail discs. The ground of technical support of data acquisition and data processing are two stations HBM MGC Plus. In the following figures: Fig. 8 is the photo of the PRORAIL test stand - part RAIL and in Fig. 9: PRORAIL test stand facility - part BOGIE.



Fig. 8 PRORAIL test stand - part RAIL

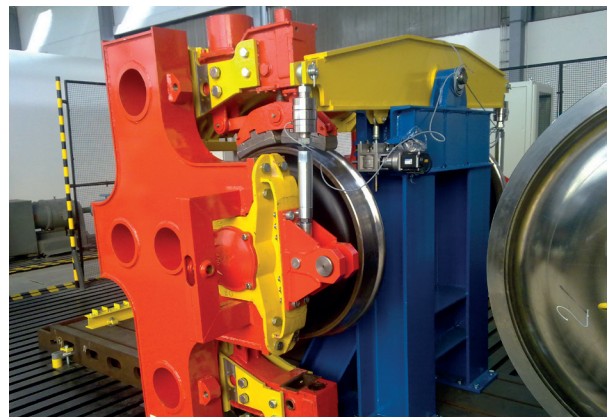


Fig. 9 PRORAIL test stand facility - part BOGIE



Fig. 10 Parameters tuning



Fig. 11 Rails tread measurement with MiniProf device

Data acquisition (Figs. 10 and 11), data processing and data assessment is performed by means of the “application development environment” written by us and all the test stand control will be guaranteed by this software solution.

## 7. Conclusions

The article deals with the motivation to solve the issue of development, building and utilization of a brand new original test

stand. The aim is to create the sophisticated tool for scientific research of railway wheels running tread modification due to wear under simulated operational loads in laboratory conditions. Such tool is the test stand named “RAILBCOT - RAIL Vehicles Brake COmponents Test Stand”, that we are building under ITMS Code 26220220011 project that is mainly based on the support of Research and Development Operational Program financed by European Fund for Regional Development. The principle design, functional demands on device and building of the frames, 3D model building, structural analysis execution, working drawing generation for device part production are results of work of the University working research team. The complete measure chain specification, data acquisition, data assessment and loading running - breaking collection specification are results of the same team.

The project implementation is aimed not only at the solution of one separated, even though very topical and important issue (wheel tread wear). It enables to create presuppositions for performance of new projects aimed at the study of wear wheel/rail in contact, new wheel or rail profiles development [2, 3, 5 and 6] wheel/rail couple adhesion phenomena, friction conditions of wheel tread / brake block, analysis of wear of rotating members of test stand, temperature and thermal fields spreading, initiation and disposition of stress fields in test specimens (wheelsets, surface stresses in wheels rims, and wheels bodies), wheel unroundness analysis [7], noise transmission and so on. All tests will be supported by the possibility of active input into the realistic, operational loads of railway wheelset. This test stand offers the possibility of composite materials brake blocks testing [8 and 9], as well as the wheel axles quality evaluating [10, 11 and 12]. The new testing device may be an excellent base tool for international scientific and research cooperation.

## Acknowledgements

This paper was created during the processing of the project “RAILBCOT - RAIL Vehicles Brake COmponents Test Stand”, ITMS Code 26220220011 based on the support of Research and Development Operational Program financed by European Fund for Regional Development. The work was also supported by the Scientific Grant Agency of the Ministry of Education of the Slovak Republic and the Slovak Academy of Sciences in project No. 1/0347/12: “Railway wheel tread profile wear research under the rail vehicle in operation conditions simulation on the test bench.”, project No. 1/0383/12: “The rail vehicle running properties research with the help of a computer simulation.” and the project No. APVV-0842-11: “Equivalent railway operation load simulator on the roller rig”.

**References**

- [1] GERLICI, J., LACK, T.: Railway Wheel and Rail Head Profiles Development Based on the Geometric Characteristics Shapes. *Wear*, vol. 271, No. 1-2, 2011, 246-258.
- [2] GERLICI, J., LACK, T.: *Railway Wheel Profile Development Based on the Geometric Characteristics Shapes*, Proc. of Contact mechanics and wear of rail/wheel systems, Firenze: AB EDITORE, 2009, 961-967.
- [3] GERLICI, J., LACK, T.: Contact Geometry Influence on the Rail / Wheel Surface Stress Distribution, *Procedia Engineering*, vol. 2, No. 1, 2010, 2249-2257.
- [4] GERLICI, J., LACK, T., HARUSINEC, J., MULLER, R., DOLEZEL, P.: *RAILBCOT Rail Vehicles Brake Components Test Stand*, Proc. of PRORAIL 2011, Scientific and Technical Society at the University of Zilina, 2011, 233-241.
- [5] LACK, T., GERLICI, J., DOLEZEL, P.: *Analysis of the Wheelset/Rails Interaction on the Roller Rig by Means of Computer Simulation*, Proc. of PRORAIL 2011, Scientific and Technical Society at the University of Zilina, 2011, 229-242.
- [6] GERLICI, J., LACK, T.: Iterative Method for Railway Wheel Profile Design, *Communications - Scientific Letters of the University of Zilina*, vol. 11, No. 2, 2009, 49-56.
- [7] GERLICI, J., LACK, T.: *Rail Roughness and Railway Wheel Unroundness Analysis*, Proc. of XVIII konferencja naukowa - pojazdy szynowe : Katowice-Ustron, 2008, 308-318.
- [8] KALINCAK, D., REZNICEK, R.: *New Brake Materials in Railway Operation*. Proc. of BulTrans-2013: anniversary scientific conference on aeronautics, automotive and railway engineering and technologies: Sofia: Izdatelstvo na Techniceskija Universitet, 2013, 91-94.
- [9] HRINAK, J., NOVY, F., REZNICEK, R., KALINCAK, D.: Comparison of the Properties of Composite Organic Railway Brake Blocks of Type K with Cast Iron Brake Block P10. *Logistyka*, Nr. 3, 2012, CD-ROM, 815-823.
- [10] NOVOSAD, M., FAJKOS, R., REHA, B., REZNICEK, R.: Fatigue Tests of Railway Axles. *Procedia Engineering*, No. 1, 2010, 2259-2268.
- [11] REZNICEK, R., NOVOSAD, M., REHA, B.: Fatigue Strength of Railway Axles. *Materials Engineering*, vol. 16, No. 3a, 2009, 46-49.
- [12] VASKO, M., LEITNER, B., SAGA, M.: Computational Fatigue Damage Prediction of the Lorry Frames under Random Excitation. *Communications - Scientific Letters of the University of Zilina*. vol. 12, No. 4, 2010, 62-67.

Tomas Lack - Juraj Gerlici \*

## WHEEL/RAIL TANGENTIAL CONTACT STRESS EVALUATION BY MEANS OF THE MODIFIED STRIP METHOD

*The article deals with the way of calculating tangential stresses over non-elliptical contact patch where Kalker's simplified method FASTSIM can be used advantageously. This method named FASTSTRIP is adapted for non-elliptical contact area calculated by means of the Strip method. This method is almost as quick as FASTSIM and the results are similar to the CONTACT results. This method may be useful for rail vehicles in track dynamics computation.*

**Keywords:** FASTSIM, FASTSTRIP, modified Strip method, wheel/rail contact, contact tangential stress evaluation, optimized computation procedure.

### 1. Introduction

The rail /wheel contact relations for purposes of rail vehicles dynamics are often calculated by means of Hertz method [1] and Kalker's simplified method applied in the program code FASTSIM [2]. Kalker's variation method [3] used to be considered as an etalon for contact patch and contact stress between railway wheel and rail calculation. Normal stresses and contact patches areas are assessed with the program code NORM [3], tangential stresses and tangential forces with the program code TANG [3]. The computation with Kalker's variation method takes longer time than the computation with the simplified method. This is the reason why the variation method is not widely used for rail vehicles dynamics computation and the simplified method is preferred for this purpose. The results gained with the simplified method are partially different (but acceptable) from the results gained with the variation method. The most significant difference consists in the contact area shape and size calculated in program FASTSIM that always presupposes to be elliptical. The Strip method procedures [4] give more opportunities to solve the contact with respect to non-elliptical contact patch. Our aim is to create the calculation procedure of "FASTSIM" type - we can name it "FASTSTRIP" for calculation of stresses over a non-elliptical contact area. We derived the procedures for fast non-elliptical contact patch calculation [5] as a presupposition of tangential forces computation. The resultant values of our brand new procedure presented in this article are closer to calculation results achieved by Kalker's variation method [3], while the computation speed is similar to the computation speed

of FASTSIM [2]. The authors' initial remarks on the wheel/rail tangential contact stress evaluation by means of the modified Strip method can be found in [6] and first article in [7].

### 2. Prerequisites

To begin with, we calculate the moduli of shear elasticity for wheel and rail materials [3]:

$$G_1 = \frac{E_1}{2 \cdot (1 + \nu_1)}, G_2 = \frac{E_2}{2 \cdot (1 + \nu_2)},$$

$$G_{12} = \frac{2}{\frac{1}{G_1} + \frac{1}{G_2}} \quad (1)$$

where:

$G_1, G_2$  - moduli of shear elasticity,

$E_1, E_2$  - moduli of elasticity,

$\nu_1, \nu_2$  - Poisson's ratios,

The contact area assembled from strips and normal stress above the strips is calculated with the Strip method.

The output parameters from the Strip method that come into the modified procedure are:

$N$  - number of strips,

$y_i$  - centre of  $i$ -th strip coordinate,.

$y_d$  - half-length of the strips,

$x_{di}$  - half-length of the  $i$ -th strip,

$p_{oi}$  - normal stress in the middle of  $i$ -th strip,

$A_{NS}$  - area of all strips.

\* Tomas Lack, Juraj Gerlici

Department of Transport and Handling Machines, Faculty of Mechanical Engineering, University of Zilina, Slovakia

E-mail: tomas.lack@fstroj.uniza.sk

We used the modified "FASTSTRIP" method for the tangential stresses computation. Figure 1 shows the program dialog with graphical output of results.

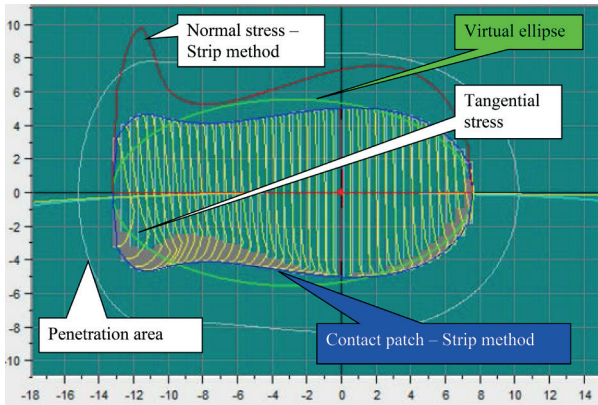


Fig. 1 Plot of AreaNORM and AreaFASTSTRIP against wheelset treads profiles lateral movement

We use this method for computation of the stresses in the non-elliptical contact patch area. Before the computation, it is needed to compute or find out the virtual ellipse parameters:

Slips  $s_x, s_y$  and spin  $\psi$  are calculated from the geometrical relations.

For constants  $C_{11}, C_{22}, C_{23}$  determination, the imaginary elliptical contact patch with the  $b$  semi-axis:

$$b = \frac{y_N - y_1}{2} + y_d \quad (2)$$

the  $a$  semi-axis:

$$a = \frac{A_{NS}}{\pi \cdot b} \quad (3)$$

and with the ellipse centre coordinate  $y_0$ :

$$y_0 = \frac{y_1 + y_N}{2} \quad (4)$$

will be used.

For the semi axes proportion the following relation is valid:

$$D = \frac{b}{a}. \quad (5)$$

We will set  $C_{11}, C_{22}, C_{23}$  constants for the given  $D$  parameter and  $\mu$  friction coefficient.

For  $C_1, C_2, C_3$  constants the following relations are valid:

$$C_1 = \frac{9}{32} \cdot C_{11}, C_2 = \frac{9}{32} \cdot C_{22}, C_3 = \frac{3\sqrt{D}}{\pi} \cdot C_{23} \quad (6)$$

We determine the number of splitting up the strips in the longitudinal direction:

$$n_x = \text{Int}(8 \cdot a) \quad (7)$$

The tangential forces  $T_x, T_y$  and the spin moment  $M_z$  are set to be zero at the beginning.

### 3. Mathematical computational algorithm

The mathematical computational algorithm is schematically depicted in the flow chart in Fig. 2.

#### 3.1 Calculation at the i-th strip (A):

For the i-th strip position the coordinate in the imaginary ellipse area is as follows:

$$y_{ei} = \frac{y_i}{b} \quad (8)$$

and for its width the following holds:

$$y_{ed} = \frac{2 \cdot y_d}{b}. \quad (9)$$

For tangential maximum stress the relation mentioned below holds:

$$T_0 = \mu \cdot p_{0i}, \quad (10)$$

where:

$\mu$  is the friction coefficient.

We will calculate the following constants:

$$C = \frac{G_{12}}{T_0}, U_x = C \cdot C_1 \cdot s_x, U_y = C \cdot C_2 \cdot s_y, \quad (11)$$

$$F_x = C \cdot C_3 \cdot b \cdot \psi, F_y = C \cdot C_3 \cdot a \cdot \psi$$

For the half-length of the strip the following relation holds:

$$a_{ei} = \frac{x_{di}}{a}. \quad (12)$$

For a calculating step we have:

$$\delta_x = \frac{a_{ei}}{n_x} \quad (13)$$

and for the area element:

$$A_e = y_{ed} \cdot \delta_x \quad (14)$$

For the strip slip in the  $x$ -axis direction we have:

$$s_{xi} = U_x - F_x \cdot y_{ei}. \quad (15)$$

### 3.2 Calculation over the length of i-th strip (B):

The  $p_x, p_y$  tangential stresses are set to be zero at the beginning of the calculation over the strip length.

The  $x_e$  coordinate is being changed in interval

$$\left\langle a_{ei} - \frac{\delta_x}{2}, -a_{ei} + \frac{\delta_x}{2} \right\rangle \text{ with a step of } \delta_x.$$

For the current slip in the  $y$  direction following holds:

$$s_{yi} = U_y + F_y \cdot \frac{(a_{ei} + x_e)}{2}. \quad (16)$$

For tangential stresses over the area element with coordinates  $(x_e, y_{ei})$  following relation holds:

$$p_x = p_x - s_{xi} \cdot (a_{ei} - x_e), p_y = p_y - s_{yi} \cdot (a_{ei} - x_e) \quad (17)$$

Then the stress amplitude and maximum feasible amplitude ratio will be calculated

$$p = \frac{\sqrt{p_x^2 + p_y^2}}{a_{ei} - x_e}. \quad (18)$$

If  $p > 1$ , then:

$$p_x = \frac{p_x}{p}, p_y = \frac{p_y}{p}. \quad (19)$$

We will calculate the  $T_{ex}, T_{ey}$  tangential forces and  $M_{ez}$  spin moment for an area element.

$$\begin{aligned} T_{ex} &= p_x \cdot A_e, T_{ey} = p_y \cdot A_e, \\ m_{ez} &= (p_x \cdot y_{ei} - p_y \cdot x_e) \cdot A_e \end{aligned} \quad (20)$$

These forces and spin moment are added to  $T_x, T_y$  forces and  $M_z$  spin moment:

$$T_x = T_x + T_{ex}, T_y = T_y + T_{ey}, M_z = M_z + M_{ez} \quad (21)$$

Having completed the calculation over all the strips, the  $T_x, T_y$  forces and the  $M_z$  spin moment will be divided by the  $T_z = \frac{\pi}{2}$  constant.

$$T_x = \frac{T_x}{T_z}, T_y = \frac{T_y}{T_z}, M_z = \frac{M_z}{T_z}. \quad (22)$$

To obtain true values of  $T_x, T_y$  and  $M_z$  spin moment, the values calculated from (22) have to be multiplied by the constant  $T$ :

$$T = N \cdot \mu, \quad (23)$$

$$T_x = T_x \cdot N \cdot \mu, T_y = T_y \cdot N \cdot \mu, M_z = M_z \cdot N \cdot \mu \quad (24)$$

where:

$\mu$  is a friction coefficient,

$N$  is a normal force.

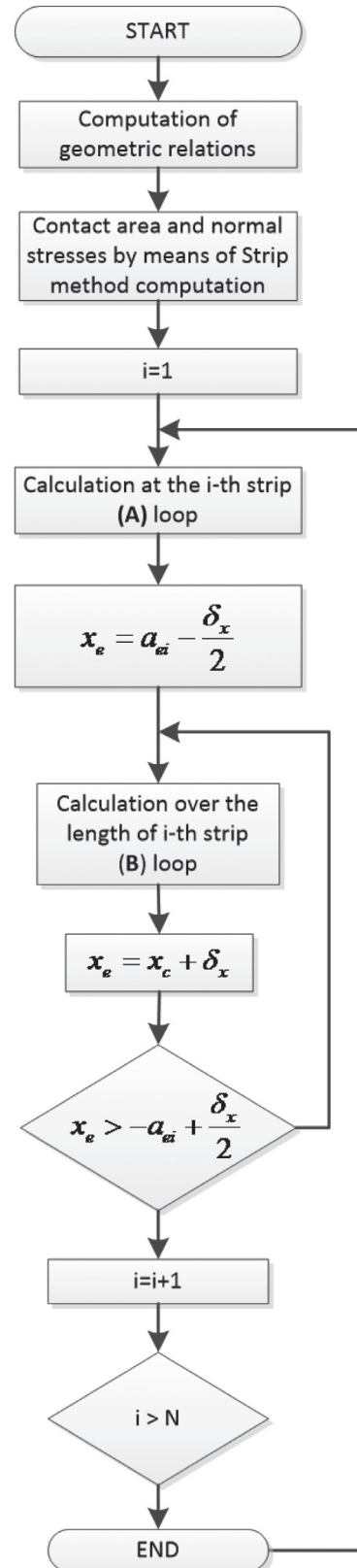


Fig. 2 Flow chart of the procedure

#### 4. Results and validation

We analyzed the contact patch area, contact stress between the wheel equipped by S1002 tread profile and UIC60 rail head profile inclined by 1:40. The lateral shift is in interval of (cca -5mm to 5mm).

##### 4.1 Input parameters

The wheel force is  $Q = 100.000N$ . We used our fast strip method [5] for the computation of contact patches and contact stresses and we compared our results with the results obtained by Kalker's Contact-NORM method [3].

In Table 1 are summarized input parameters:  $y_w$  [mm] is lateral shift of wheels profiles over the rail heads profiles,  $F_n$  [N] is a normal force,  $\tan(\text{Gama})$  is the value of Tangent Gamma function that is the contact area angle tangent in the contact point.  $\text{Gama}$  [rad] is the same angle expressed in radians.  $S_x$  and  $S_y$  are the slips (creepages in x and y directions) and  $\Phi$  is expressed in [rad/mm]. The difference with the FASTSIM

method is that the computation is executed along the strip separately, regardless of the strip size - whether it is smaller or longer than the virtual ellipse border.

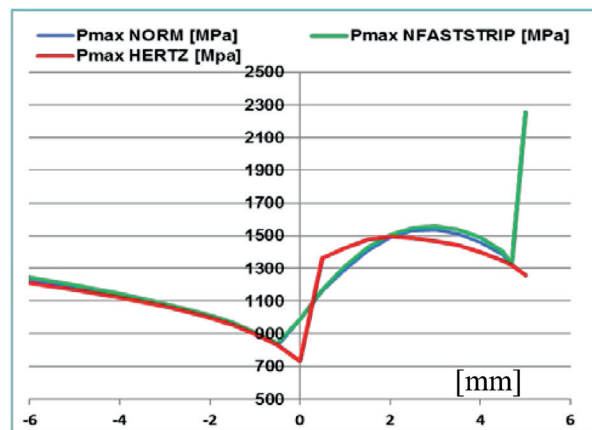


Fig. 3 Plot of  $P_{max}$  CONTACT-NORM,  $P_{max}$  NFASTSTRIP and  $P_{max}$  HERTZ against wheelset treads profiles lateral movement

Contact input parameters

Table 1

$y_w$	$F_n$ [N]	$\tan(\text{Gama})$	$\text{Gama}$ [rad]	$S_x$ [-]	$S_y$ [-]	$\Phi$ [rad/mm]
-5	100004	-0.008948	-0.00894776	0.001645	0	0.000019
-4	100004.7	-0.009655	-0.00965470	0.001295	0	0.000021
-3	100006.0	-0.010960	-0.01095956	0.001054	0	0.000024
-2.5	100007.1	-0.011927	-0.01192643	0.000953	0	0.000026
-2	100008.6	-0.013144	-0.01314324	0.000859	0	0.000029
-1.5	100010.9	-0.014776	-0.01477492	0.000773	0	0.000032
-1	100014.2	-0.016839	-0.01683741	0.000684	0	0.000037
-0.5	100019.5	-0.019748	-0.01974543	0.000595	0	0.000043
0	100029.0	-0.024072	-0.02406735	0.000000	0	0.000052
0.5	100222.8	-0.066581	-0.06648288	-0.000595	0	0.000145
1	100249.4	-0.070613	-0.07049599	-0.000684	0	0.000153
1.5	100282.8	-0.075148	-0.07500702	-0.000773	0	0.000163
2	100317.3	-0.079742	-0.07957362	-0.000859	0	0.000173
2.5	100360.8	-0.084998	-0.08479419	-0.000953	0	0.000184
3	100411.8	-0.090812	-0.09056359	-0.001054	0	0.000197
3.5	100472.2	-0.097318	-0.09701251	-0.001166	0	0.000210
4	100550.2	-0.105034	-0.10465029	-0.001295	0	0.000227
4.5	100652.9	-0.114436	-0.11394035	-0.001449	0	0.000247
4.7	100703.2	-0.118818	-0.11826354	-0.001519	0	0.000256
5	100799.7	-0.126724	-0.12605211	-0.001645	0	0.000273

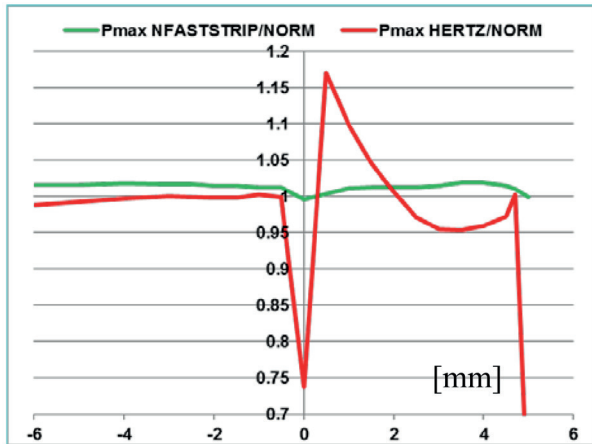


Fig. 4 Plot of  $P_{max}$  NFASTSTRIP/NORM and  $P_{max}$  HERTZ / NORM [-] proportional comparison of evaluated quantities

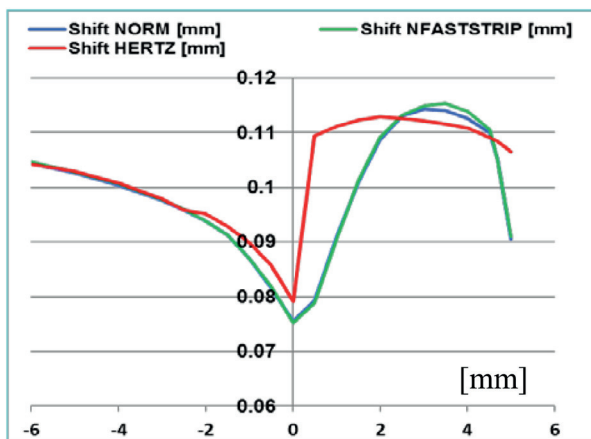


Fig. 5 Plot of Shift NORM, Shift FASTSTRIP and Shift HERTZ against wheelset tread profiles lateral movement

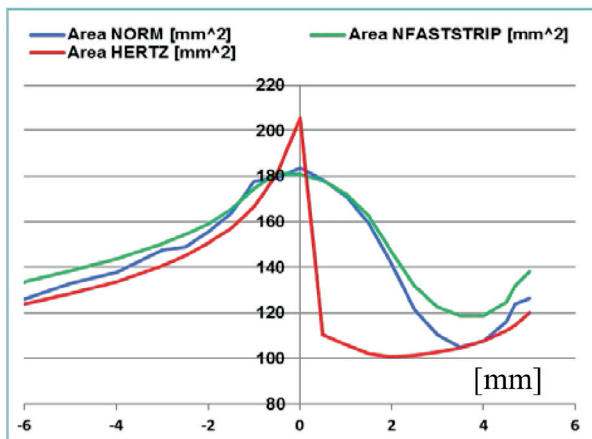


Fig. 6 Plot of Area NORM, Area FASTSTRIP and Area HERTZ against wheelset tread profiles lateral movement

#### 4.2 Results of tangential stresses calculation

Tangential stresses,  $T_x$ ,  $T_y$  forces and  $M_z$  moment for separate strips are computed by means of the  $T_x$ ,  $T_y$  and  $M_z$  computed by "CONTACT-TANG", "FASTSIM" and "FASTSTRIP" methods for the purpose of comparison.

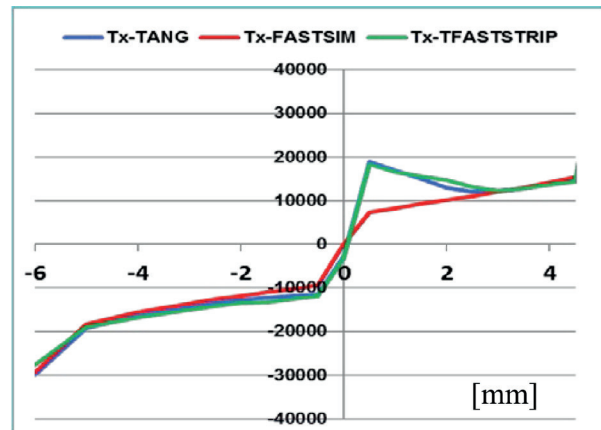


Fig. 7 Plot of  $T_x$  [N] against wheelset tread profiles lateral movement

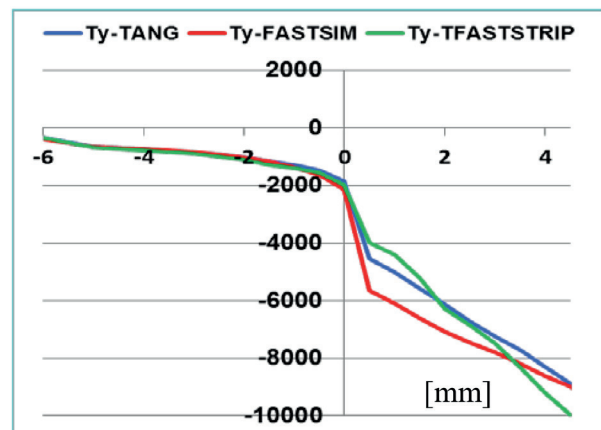


Fig. 8 Plot of  $T_y$  [N] against wheelset tread profiles lateral movement

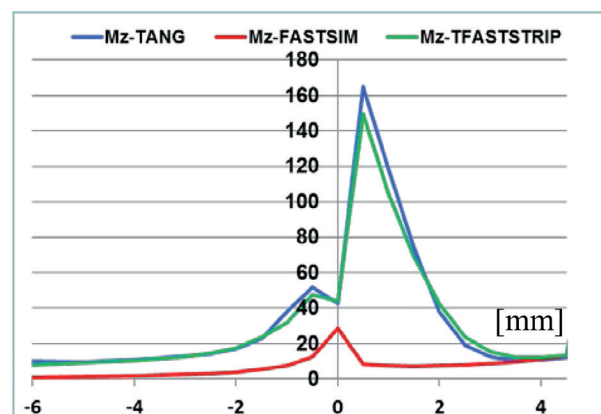


Fig. 9 Plot of  $M_z$  [N.m] against wheelset tread profiles lateral movement

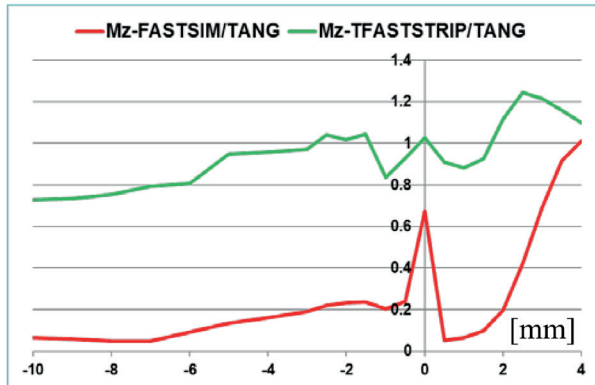


Fig. 10 Plot of  $M_z$  [N.m] - Proportional comparison of evaluated quantity

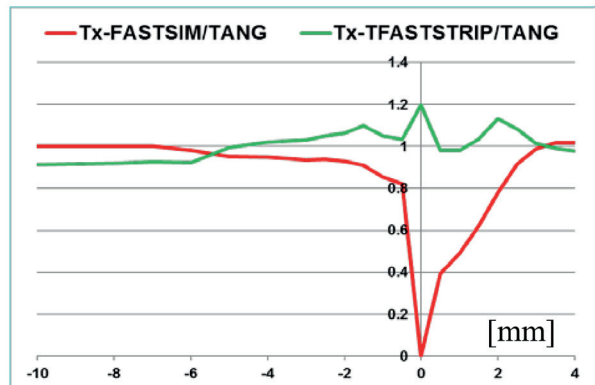


Fig. 11 Plot of  $T_x$  [N] - Proportional comparison

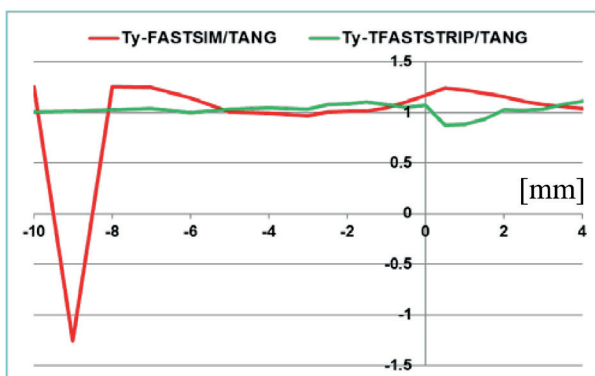


Fig. 12 Plot of  $T_y$  [N] - Proportional comparison of evaluated quantity

### 5. Conclusions

Our aim is to create the calculation procedure of "FASTSIM" type. We named this procedure for calculation of stresses over non-elliptical contact area "FASTSTRIP". The result values are closer to the results achieved by Kalker's variation method results and the computation speed is similar to the computation speed of FASTSIM. This method is adapted for a non-elliptical contact area calculated by means of the Strip method [5]. This method utilizes the FASTSIM theory [2] as a calculation engine for tangential stress assessment. The calculation procedure is outlined in Fig. 2 in which a flowchart with two program loops is illustrated. These loops are in detail described in the part "Mathematical model". Results and validation follow. In Table 1 are some input parameters, Figs. 3, 4, 5 and 6 compare the results gained by means of NORM [3] and our calculation procedure [5] shift, area and pmax. They express the reality that the ground input parameters for tangential forces calculations are mutually very close.

Figures 7, 8, 9 and 10 give results of tangential stresses calculation for input parameters. The curves of dependencies ( $T_x$ ,  $T_y$ ,  $M_z$ ) calculated with TANG [3] and FASTSTRIP are shown in graphs. For better resolution are these curves shown in Figs. 11 and 12 as comparative proportional curves. The meaning or importance of the procedure FASTSTRIP for us or anybody who writes his/her own code is in the fact that this procedure can be implemented into the code for computation of rail vehicles dynamics offering the advantage of fast computations. Of course, the field may be analysed from other points of view [8, 9 and 10] where multi-software platforms are presented. The field of wheel /rail contact task is very close to the computational analysis of contact stress distribution in the case of mutual slewing of roller bearing rings [11 and 12], or from the more sophisticated field [13, 14 and 15].

### Acknowledgement

The work was supported by the Scientific Grant Agency of the Ministry of Education of the Slovak Republic and the Slovak Academy of Sciences in project No. 1/1098/11: "Stress Distribution in a Braked Railway Wheel". No. 1/0347/12: "Railway wheel tread profile wear research under the rail vehicle in operation conditions simulation on the test bench", project No. 1/0383/12: "The rail vehicle running properties research with the help of a computer simulation." and the project No. APVV-0842-11: "Equivalent railway operation load simulator on the roller rig".

Research-Educational Center of Rail Vehicles (VVCKV)

## References

- [1] JOHNSON, K. L.: *Contact Mechanics*. Cambridge university press Cambridge, p. 510. 1987.
- [2] KALKER, J. J. *A Fast Algorithm for Simplified Theory of Rolling Contact*. Vehicle systems dynamics, 11, 1982, 1-13.
- [3] KALKER, J. J.: *Three-dimensional Elastic Bodies in Rolling Contact*. Kluwer academic publishers: Dordrecht, 1990.
- [4] KNOTHE, K., HUNG, L.-T.: *Ermittlung der Normalspannungs-Verteilung beim Kontakt von Rad und Schiene*. Forsch. Ing.-Wes. 49, 1983, 79-83, 1983.
- [5] LACK, T., GERLICI, J.: *Modified Strip Method Utilisation for Wheel / rail Contact Stress Evaluation*. 9<sup>th</sup> intern. conference on contact mechanics and wear of rail/ wheel systems (CM2012) : Southwest Jiaotong University, 2012. Presented in Chengdu, 2012.
- [6] LACK, T., GERLICI, J.: *Wheel/rail Contact Stress Evaluation by Means of the Modified Strip Method*. Communications - Scientific Letters of the University of Zilina, vol. 15, No. 3, 2013, 126-132. ISSN 1335-4205.
- [7] LACK, T., GERLICI, J.: *Tangential Stresses for Non-elliptical Contact Patch Computation by Means of Modified FASTIM Method*. Intern. Association of Vehicles Systems Dynamics (IAVSD) 2013 : 23<sup>rd</sup> intern. symposium on dynamics of vehicles on roads and tracks, August 2013, Qingdao: Chengdu: Southwest Jiaotong University, 2013. USB key, [6] p.
- [8] SAPIETOVA, A., SAGA, M., NOVAK, P.: *Multi-software Platform for Solving of Multibody Systems Synthesis*, Communications - Scientific Letters of the University of Zilina, vol. 14, No. 3, 2012, 43-48. ISSN 1335-4205.
- [9] LEITNER, B.: *The software tool for mechanical structures dynamic systems identification*. Transport means 2011. Proceedings of the 15th international conference : October 20-21, 2011, Kaunas University of Technology, Lithuania. - ISSN 1822-296X. - Kaunas: Kaunas University of Technology, 2011. - S. 38-41.
- [10] BEDNAR, R. SAGA, M., VASKO, M.: *Effectivity Analysis of Chosen Numerical Methods for Solution of Mechanical Systems with Uncertain Parameters*. Communications - Scientific Letters of the University of Zilina, vol. 13, No. 4, 2011, 40-45. ISSN 1335-4205.
- [11] JAKUBOVICOVA, L., SAGA, M.: *Computational Analysis of Contact Stress Distribution in the Case of Mutual Slewing of Roller Bearing Rings*. Applied Mechanics and Materials, 2014.
- [12] JAKUBOVICOVA, L., SAGA, M., VASKO, M.: *Impact Analysis of Mutual Rotation of Roller Bearing Rings on the Process of Contact Stresses in Rolling Elements*. Manufacturing Technology, 2013.
- [13] ZMINDAK, M., RIECKY, D., SOUKUP, J.: *Failure of Composites with Short Fibres*. Communications - Scientific Letters of the University of Zilina, vol. 12, No. 4, 2010, 33-39. ISSN 13354205.
- [14] ZMINDAK, M., NOVAK, P.: *Particle Interactions in Composites Reinforced by Fibre and Spherical Inclusions*. Communications - Scientific Letters of the University of Zilina, vol. 11, No. 2, 2009, 13-18, ISSN 1335-4205.
- [15] LEITNER, B.: *Optimization of Dynamic Strength Dimension of Machine Frame by MATLAB*. Transport Means - Proc. of the Intern. Conference 2012, Pages 104-107, 16<sup>th</sup> Intern. Conference Transport Means 2012; Kaunas; October 2012.

Peter Zvolensky - Vladimir Stuchly - Juraj Grecik - Roman Poprocky \*

## EVOLUTION OF MAINTENANCE SYSTEMS OF PASSENGER AND FREIGHT WAGONS FROM THE ECM CERTIFICATION POINT OF VIEW

*RCM and ECM are abbreviations seemingly the same though the meaning is different. However, they have a lot in common as both are aimed at increased reliability of operation and minimising risk. RCM stands for Reliability Centred Maintenance and ECM stands for Entity in Charge of Maintenance, thus maintenance is the common term for both. Indeed, maintenance is a key for increased safety and reduced risk. The paper presents basic principles and theory behind the RCM – an advanced maintenance concept with its origin in aviation and consequently applied in industries connected with high level of risk, such as power generation, etc. The ECM certification is a new approach for assessment of how railway vehicle operators are managing the risks connected with operation of the rolling stock. Entities, either owners or keepers of the rolling stock, are those who are responsible for the technical condition guaranteeing safety of railway traffic. There is common European methodology (requirements) for assessing the competence of ECMs based on EC Regulation No. 445/2011. Behind this methodology are efforts to minimise risks of freight train operation and prevent serious accidents resulting from improper maintenance and insufficient technical state. In line with these efforts is our proposal for implementation of RCM in railway vehicle maintenance.*

**Keywords:** Railway wagon, maintenance, risk, RCM, FMEA, ECM certification.

### 1. Introduction

Quality, safety and environment - these words stand for the basic requirements for any industrial and service activity, railway transport not excluding. There are few words that always go together - reliability, safety, risk, which characterise any system functioning. There are many factors influencing the reliability - the fundamental is so called inherent reliability - built in the product (system, machine) by its design and manufacture. Yet there are many more factors influencing the reliability of a system during its life (operation), among which perhaps the most important is maintenance. Inherent reliability is recognised even in maintenance terminology standard [1], which also recognises failure criticality as combination of failure consequence severity and its frequency (probability of occurrence). This is just for illustration that importance of risks is emphasised even in basic terminology standards.

Of course, problems of risk require much more than a basic definition. There are many methods dealing with risks analysis and their mitigation. In machine operation and maintenance risks are always connected with failures. In traditional maintenance approach the requirements for maintenance of each component were determined in accordance with its actual or

assumed technical characteristics, without considering its failure consequences. The resulting maintenance schedules were used to all similar objects without considering the different consequences coming from different operational contexts.

Wherever possible, new approaches should be searched for that would synthesise new findings into a form so that it would be possible to evaluate and implement those approaches having the best value for functioning of physical objects and the whole organisation (company). Philosophy that provides such a framework is called Reliability Centred Maintenance (RCM) [2]. RCM uses analytical methods of a-priori reliability, especially:

1. Fault Tree Analysis (FTA),
2. Reliability Block Diagram (RBD),
3. Failure Mode and Effect Analysis (FMEA),
4. Root Cause Failure Analysis (RCFA).

These methods in broader context contribute also to Fault Prevention, Fault Forecasting, Fault Removal, and Fault Tolerance.

The area of fault forecasting is decisive from the maintenance system proposal point of view. RCM is a strong method in defining failure consequences (in fact it is recognition that the only reason for doing any form of preventive maintenance is not in preventing occurrence of failure themselves but in avoiding

\* Peter Zvolensky, Vladimir Stuchly, Juraj Grecik, Roman Poprocky

Department of Transport and Handling Machines, Faculty of Mechanical Engineering, University of Zilina, Slovakia

E-mail: peter.zvolensky@fstroj.uniza.sk

or at least in minimising **failure consequences**). However, for determination of intervals to maintenance action (maintenance tasks schedule) it is necessary to utilise the reliability methods.

## 2. Maintenance of railway wagons

### 2.1 Current state of railway personal wagons maintenance system

Similarly to manufacture, the maintenance system (maintenance types and maintenance strategies) of railway wagons has been evolving within the years.

In Table 1 is an example of maintenance cycle of selected types of railway passenger wagons after the 5<sup>th</sup> change that has been introduced since the 1<sup>st</sup> April, 2001. The railway wagons are divided into maintenance groups according to the “repair” types. Corresponding repair levels, mileages (distance run between maintenance interventions) and maintenance cycles are given in Table 1.

In the current organisation of preventive maintenance of railway vehicles at the Slovak Railway Company (ZSSK) according to the valid maintenance regulations the *main decision criterion* is so called *mileage* (in km) and for certain types of wagons also *time periods*. This approach is based on relatively

long evolution and, in principle, by tradition at implementation of planned-preventive maintenance system.

Process of monitoring, preparing and delivering vehicles into maintenance (at different maintenance levels) has its characteristic steps and individual elements, which in modern maintenance concepts, and in particular with regards to costs priority, do not always mean economically suitable conditions of predetermined maintenance itself.

1. The typical characteristics of currently performed maintenance of passenger vehicles are [4]:
2. Elaborated performance standards, especially at higher maintenance levels.
3. Technological routine and periodicity of maintenance actions.
4. Specialisation of workplaces and technological procedures at higher maintenance levels.
5. High routine in monitoring of simple indicators for delivery into maintenance.
6. Maintenance is not performed in accordance with real technical conditions of a railway vehicle and differentially.
7. Operational utilisation (conditions) is not considered at railway wagons.
8. Often uselessly vast disassembly of important structural units significantly worsen their overall functional stability and negatively influence the vehicles reliability.

Regulation V66 – Maintenance groups for selected types of wagons [3]

Table 1

Maint. group	Wagon type	Repair level	Mileage (km)
1a	Salon wagons – RIC regime	R1 - 12 months R2 - 48 months R3 R4	50 000 200 000 400 000 800 000
Nw (R4) R1 R1R1R2 R1 R1R1R3 R1 R1R1R2 R1 R1R1 R4			
3 b	Other wagons (except for wagons of group 1 and 2) – inland regime for InterCity trains	R1 - 6 months R2 - 36 months R3 R4	110 000 440 000 1 320 000 3 960 000
Nw (R4) R1R1R1 R2 R1R1R1 R2 R1R1R1 R3 R1R1R1 R2 R1R1R1 R2 R1R1R1 R3 etc.			
4	Four axle wagons of inland regime with speed over 120 km/h (except for wagons of group 1, 2 and 3)	R1 - 6 months R2 - 48 months R3 R4	100 000 300 000 900 000 1 800 000
Nw (R4) R1R1 R2 R1R1 R2 R1R1 R3 R1R1 R2 R1R1 R2 R1R1 R4			

Legend: Nw – New Wagon  
R1, R2, R3, R4 – Revisions (maintenance/repair level of 1 – 4)

9. Fixed work of "hard" planned maintenance actions may result in ineffective labour costs and overheads.
10. Insufficient personal responsibility of workers for maintenance quality and, consequently, for technical condition of a railway vehicle.
11. In current financial situation at ZSSK, there is danger of not fulfilling the periodicity of maintenance actions given by regulations which deteriorates current technical condition of railway vehicles.

## 2.2 Current state of railway freight wagons maintenance system

In Slovakia, a generally accepted maintenance system for freight wagons is so called SUNV (Maintenance System of Freight Wagons; in Slovak: Systém údržby nákladných vozňov) based on the former Regulation V67 [5]. ZSSK Cargo and other freight wagons operators have the system of freight wagons periodic maintenance based on time considering a specific design of a freight wagon type.

The fundamental terms of the maintenance system are as follows:

1. "Medium repair N2.1, N2.2, N2.3, N4" - lower type of preventive periodic maintenance with due terms of 2 or 4 years. The basic scope of maintenance tasks is given in chapter 5 of the regulation. The main task is inspection and function test of components and functional subassemblies of freight wagons.
2. "Revision repair N8" - the top level of preventive maintenance with due term of 8 years. The basic scope of maintenance tasks is given in chapter 5 of the regulation. The main task is revision and/or replacement of components and assemblies. There must always be a protocol issued on the regular technical check.
3. "Extended due term of periodic repair +3M" - extended operational period by 3 months after due term based on the technical inspection. This can be done only on approval of wagon's ECM (entity in charge of maintenance).
4. "Regular technical check" - technical check carried out in compliance with law. The main purpose is the check of actual technical state and assessment of technical condition before return to operation. Protocol on the technical check can be issued only by a competent person.
5. "Safety inspection" - technical inspection is carried out in the scope given in chapter 5 on freight wagons with 6 months delay after medium or revision repair due term or on wagons deposited more than 12 month for the purpose of transport into maintenance workshop or physical disposal.

From the analysis of forms, technology and consequences of current maintenance of railway wagons in Slovakia it can

be concluded that keeping the current state is not realistic and economically probably unsustainable. That is why a system change aimed at rationalisation and improved maintenance effectiveness is necessary. Change of maintenance systems of railway vehicles must be based on their increased availability at more effective maintenance costs. Proposed transformation change is aimed at transition from current predetermined maintenance to predictive (reliability centred - condition based) maintenance.

## 3. Utilisation of theory of reliability

For utilisation of reliability characteristics in the maintenance of railway vehicles, the following questions should be answered:

1. How can the reliability characteristics be determined?
2. Is there a reason for their determination?
3. Is it reasonable to analyse elements or whole systems?
4. Which reliability characteristics are the most important for maintenance? And are some of them meaningful?
5. How, when, where and in what extent should the reliability characteristics be determined?
6. How can the calculations of reliability characteristics help in creation of maintenance systems?

Reliability of the already operated railway vehicles (because these are the most important for maintenance) was built-in during their design and manufacture phase (inherent reliability). Maintenance itself cannot increase these built-in reliability properties (but can *preserve* them).

Creation of maintenance system (based on the reliability theory) can be divided into the following steps:

1. Determination of reliability characteristics (by mathematical-statistical methods).
2. Determination of optimum periods (intervals) of operation of components until the planned maintenance action. It is based on element's reliability and costs for planned (preventive) and unplanned (corrective) maintenance.
3. Creation of maintenance system. It is based on determined times (intervals) between maintenance for elements and costs of maintenance [6].

### 3.1 Statistic and parametric reliability of elements

In the reliability theory we look at failures in a mathematical-statistical way as random phenomena because we are not able to reliably determine in advance the moment of occurrence of a failure and its extent because of complexity of phenomena related to the failure. Reliability analyses are carried out especially in the phase of concept definition, in the phase of designing and development and in the phase of utilisation (operation and maintenance) on different levels of structure breakdown for

evaluation and estimation of reliability parameters of an item (element or system).

**Stochastic reliability models** can be determined from the detailed knowledge of behaviour of a given set of objects in operation. **They must provide generalisation** of obtained findings also on other similar items that were not directly subject of investigation.

Implementation of statistical methods needs the following subsystems:

1. System of information collection on operational reliability;
2. System of selection, use and primary analysis of evaluated sample of objects;
3. System of quantification of reliability indicators (parameters) of elements of objects;
4. System of quantification of object's reliability as a system;
5. System of consequent technical analysis and implementation of obtained knowledge in operation, maintenance etc.

The most suitable theoretical model that optimally characterises reliability of engineering products is a *Weibull model* in particular because in its generality it covers virtually most of possible function courses of random quantities of items reliability [7] and [8]. Weibull distribution function (three-parameter) is expressed by equation:

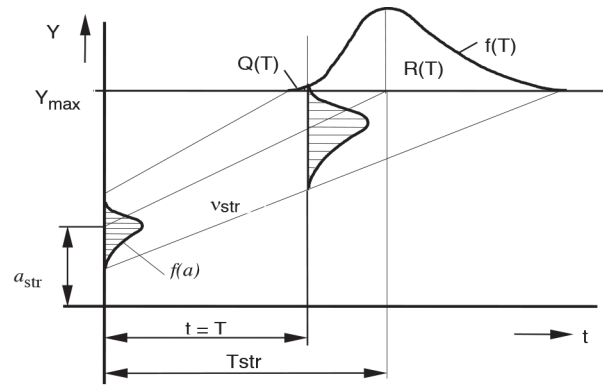
$$F(t) = 1 - e^{-\left(\frac{t-c}{a}\right)^b}, \text{ for } t > 0 \quad (1)$$

where:  $a > 0$  is a scale parameter,  $b > 0$  is a shape parameter,  $c$  is a location parameter

On this basis 5 fundamental reliability parameters (indicators) are defined: failure probability  $Q(t)$ , reliability probability  $R(t)$ , probability failure density  $f(t)$ , failure rate  $\lambda(t)$ , mean operation time to failure  $T_{str}$ . In Fig. 1 failure density and failure rate are illustrated.

*Indicators of parametric reliability* are the same as for statistic reliability and can be calculated in accordance with the selected model of parameter change. For calculations of indicators of parametric reliability it is necessary to determine equation of

parameter change with initial value and a velocity of its change using a suitable method (Fig. 2).



$$Y(T) = a_{str} + k \cdot t$$

$$R(T) = 0.5 + \Phi\left(\frac{Y_{max} - a_{str} - v \cdot T}{\sigma_a}\right)$$

where  $\Phi$  is Laplace function

Fig. 2 Model of gradual failure formation (generalised) and calculation of reliability  $R(T)$

#### 4. Optimisation model of maintenance intervals

Time, or mileage, to repair can be determined for components reliability. To ensure required reliability level, planned preventive maintenance actions are carried out after a predetermined mileage  $L$  (km). For simplifying the mathematical model we assume that the duration of maintenance action is short compared to up-time (operation without failures).

Because of carrying out the maintenance, operation time of components will have a cut distribution  $f(l)$  with mean value  $L_{str}$ . Value  $L_{str}$  depends on the degree of cut, that is, the value of selected interval between maintenance  $L$ .

Probability of failure of a component during the interval  $L$  (km), which is the probability of corrective (unplanned) maintenance of the component, is

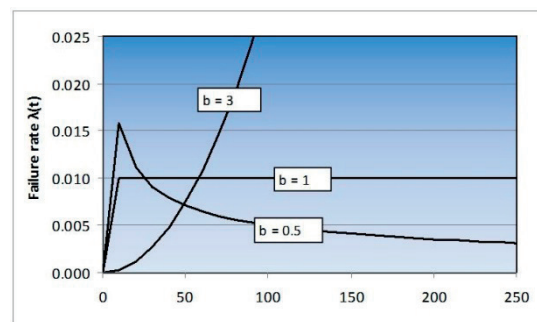
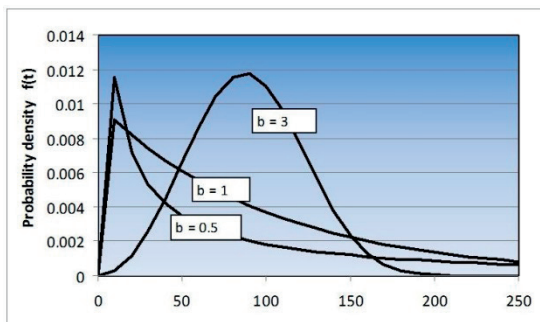


Fig. 1 Reliability parameters for Weibull distribution function for different  $b$

$$Q(L) = \int_0^L f(l)dl \tag{2}$$

The probability that a component is working without failure during  $L$  (km) and will be replaced (or restored) in planned maintenance is

$$R(L) = 1 - Q(L) = 1 - \int_0^L f(l)dl \tag{3}$$

The task of determination of optimum interval between maintenance works leads to determination of such interval  $L$  between planned (preventive) maintenance in which the total costs for keeping objects up-state will be minimum.

We will determine overall costs connected with restoring failed components of  $i$ -th subsystem during the interval  $L'$  (km); for this we will use the designation:

$C_N$  - mean value of  $i$ -th subsystem in corrective maintenance costs (besides direct costs for repair, the production and other induced losses should be included);

$C_p$  - mean value of costs of component of  $i$ -th subsystem in preventive maintenance.

Maintenance costs for intervals  $L'$  (km) will be calculated using the formula for calculation of  $M$ , that is the mean value of costs for restoring one component of  $i$ -th subsystem for the interval  $Lstr$  (km) in the ratio of costs for preventive and corrective maintenance:

$$M = \frac{\int_0^{\infty} R(l) \cdot dl}{\int_0^L R(l) \cdot dl} \cdot [1 - (1 - p) \cdot R(L)] \tag{4}$$

where:  $p = C_p / C_N$  - ratio of costs for preventive and corrective maintenance. Condition  $C_p \leq C_N$  is assumed; then value of  $p$  is within the interval  $0 < p \leq 1$ .

From (4) it concludes that  $M$  is a function of selected interval between maintenance  $L$  and depends on the type and parameters of probability distribution function and also on ratio of costs  $p$ . For analysis of solution of function  $M$  it is necessary to find analytical expression for various types (most commonly used) of failure probability distribution functions.

For Weibull distribution:

$$M = \frac{\Gamma\left(1 + \frac{1}{b}\right) \cdot [1 - (1 - p) \cdot e^{-\vartheta^b}]}{\int_0^{\frac{L}{a}} e^{-\vartheta^b} \cdot d\vartheta_e} \tag{5}$$

For analysis of the formula (5) we use a graphic interpretation of  $M = f(\vartheta_e, p, b)$  in Fig. 3 for  $b = 3.43$  and for various values of  $p$ . Optimum interval for maintenance can be found at the minimum of the function  $M$ .

we obtain the value of optimum mileage (in km) multiplying  $M$  by  $a$  (scale parameter of Weibull distribution).

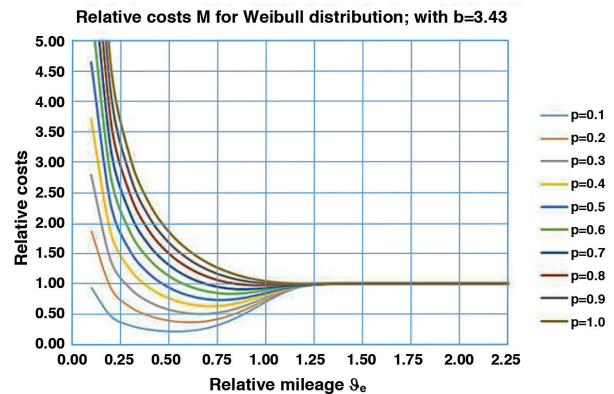


Fig. 3 Graph of relative costs  $M$  for Weibull probability distribution with shape parameter  $b = 3.43$

### 5. Reliability Centred Maintenance and ECM

Because of inaccessibility of the data from operation of railway vehicles it is not possible to fully use the methods of a posteriori reliability for determination of maintenance tasks.

Both maintenance regulations for railway wagons follow the conventional maintenance systems. RCM method takes into consideration failure consequences and CONSEQUENCES are evaluated as RISK.

Complex definition of RCM is: “Process used to determine what must be done to ensure that any physical asset continues to do whatever its users want it to do in its present operating context” [2]. When evaluating consequences one of the decisive categories is RISK.

The railway undertakings or the infrastructure managers should ensure, through their safety management system, the control of all risks related to their activity, including the use of contractors. To this purpose, a railway undertaking should rely on contractual arrangements involving entities in charge of maintenance for all wagons it operates. This could be a contract between the railway undertaking and the entity in charge of maintenance or a chain of contracts involving other parties, such as the keeper. These contracts should be consistent with the procedures outlined by a railway undertaking or an infrastructure manager in its safety management system, including for the exchange of information [9].

Risk assessment is a structured approach to assess risks associated with the maintenance of freight wagons, including those directly arising from operational processes and the activities of other organisations or persons, and to identify the appropriate risk control measures.

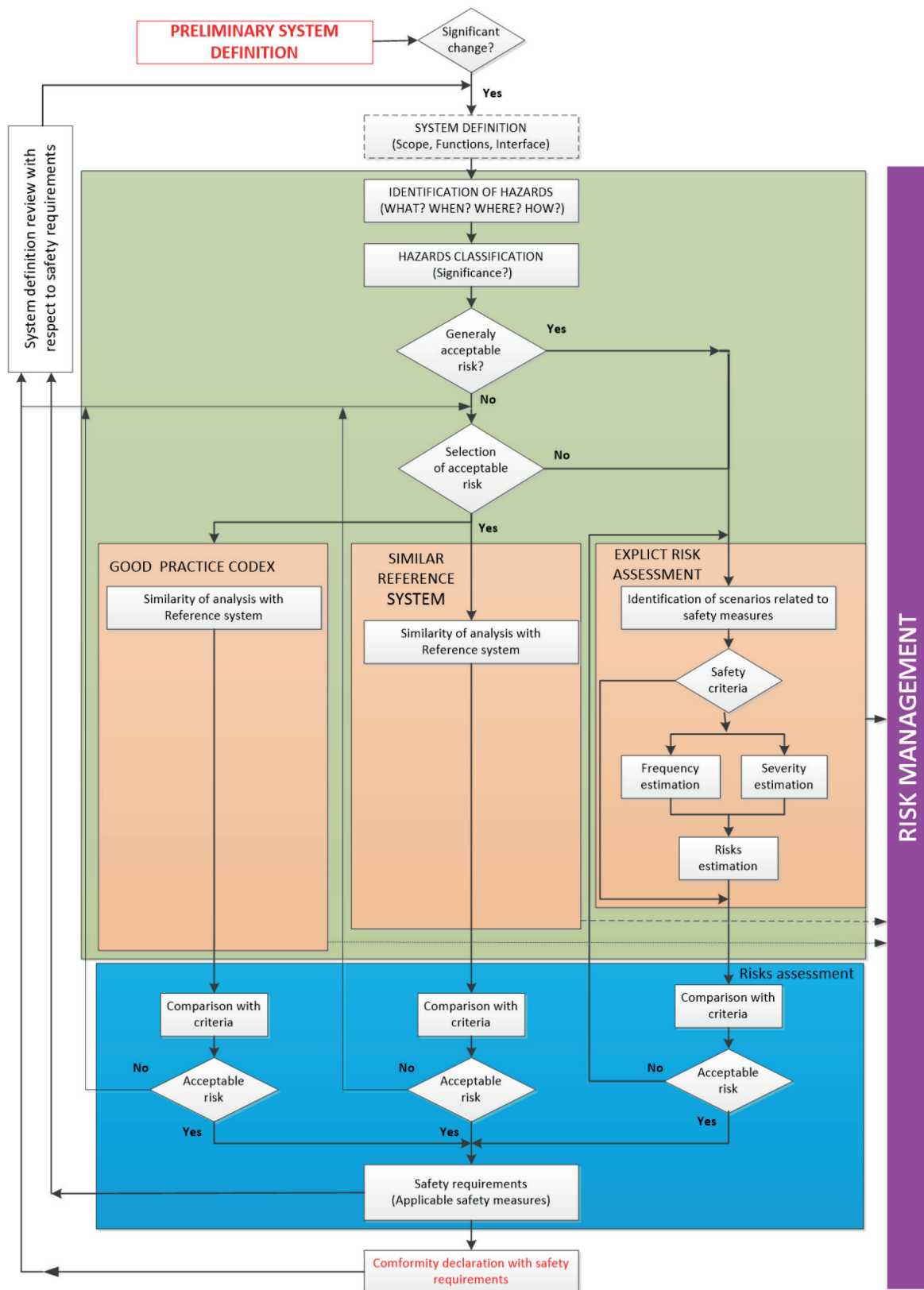


Fig. 4 System of risk assessment (adapted from [10])

Complex process of risk assessment is shown in Fig. 4. This process can be applied in general as well as for risk assessment of freight wagons [10].

The organisation must have procedures for:

1. analysing risks relevant to the extent of operations carried out by the organisation, including the risks arising from defects and construction non-conformities or malfunctions throughout the lifecycle;
2. evaluating the risks referred to in point (a);
3. developing and putting in place risk control measures.

The organisation must have a procedure to regularly collect, monitor and analyse relevant safety data, including:

1. the performance of relevant processes;
2. the results of processes (including all contracted services and products);
3. the effectiveness of risk control arrangements;
4. information on experience, malfunctions, defects and repairs arising from day-to-day operation and maintenance.

For solutions within RCM, a FMEA method (Failure Mode and Effect Analysis (FMEA) is used, which in RCM is formalised as RCM information and RCM decision form.

The FMEA is a systematic set of actions carried out with the purpose to:

1. identify and evaluate possible failure of a product/process and consequences of this failure,
2. determine measures that would reduce probability of creation (occurrence) of possible failure,

3. document the whole process.

It completes the process of definition of what the design or process for customer's satisfaction should fulfil.

The FMEA method represents a team work aimed at definition of possible failure modes and their consequences. Based on experience it is said that by this method it is possible to reveal 70 - 90% of failures. Base and purpose of FMEA is to exclude, or to acceptable level reduce failures of production processes and products during their utilisation by minimising the risk number  $R$ . Risk number  $R$  is given by multiplication of failure occurrence probability ranking  $Z$ , severity of failure consequences  $V$  and probability of preventive failure detection  $D$ :

$$R = Z * V * D \tag{6}$$

At the Department of Transport and Handling machines we have been using FMEA process supported by software tool IQ RM PRO 6. Structured risks of a freight wagon created by this program are shown in Fig. 5.

## 6. Conclusions

Trends to minimise risk in railway operation are among the most important topics in Europe. European commission through its regulation Commission Regulation (EU) No 445/2011 intends to improve safety of railway, especially freight transport

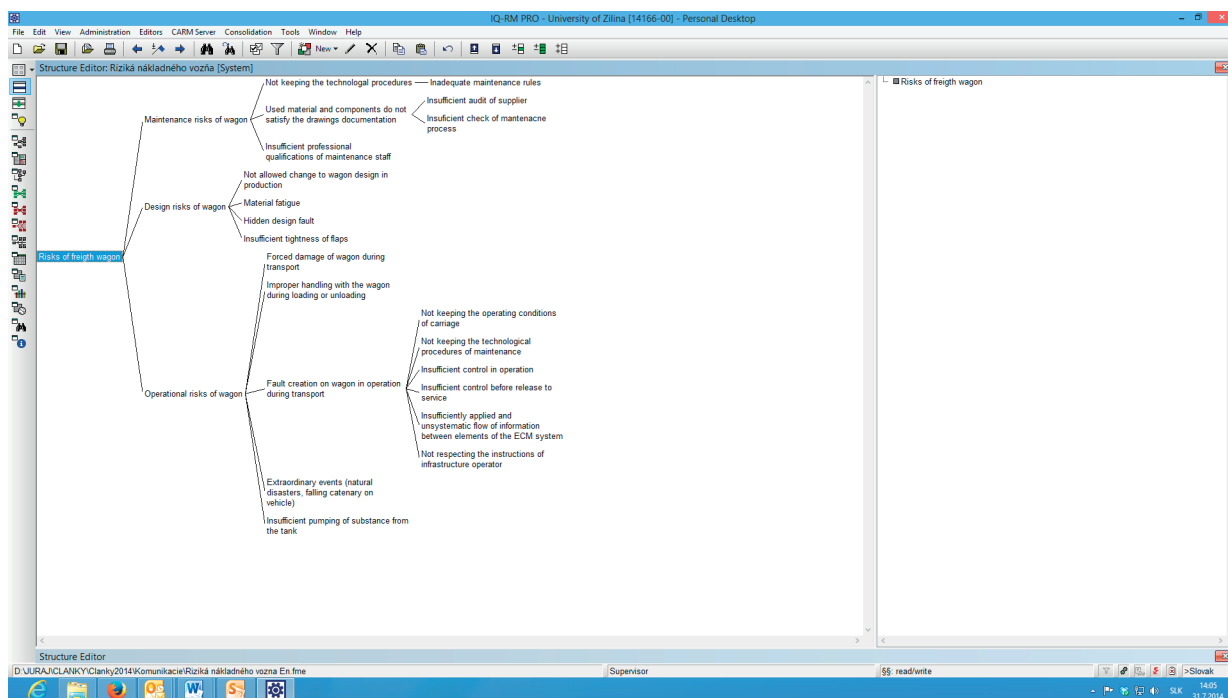


Fig. 5 Risks of a freight wagon (example)

by creating system of certified ECMs (Entities in Charge of Maintenance) that are fully responsible for performing all maintenance functions properly. The Department of Transport and Handling Machines, University of Zilina, was recognised as an ECM certification body. It has audited and certified most of the railway freight wagons operators in Slovakia. Generally, it can be concluded that the certification process forced the rolling stock maintenance operators to review their approach to risks and to start new thinking of risk management.

Theoretical methods of risks assessment presented in the paper are base and tool for analysis in real practice and consequent improvement of operational safety of freight wagons. Freight wagons operators have to realise the importance of safe operation, though demanding more efforts, costs and enhancements in maintenance, but this should be balanced by reduced number of accidents. Consequences of accidents in railway freight transport are mostly very costly and their prevention is worth searching for improvements.

## References

- [1] STN EN 13306: *Maintenance - Terminology (in Slovak)*, 2010.
- [2] MOUBRAY, J.: *Reliability-centered Maintenance*, Industrial Press Inc : New York 1997, ISBN 0-8311-3078-4.
- [3] ZSSK V 66: *Railway Wagons Maintenance Regulation (in Czech)*, Praha : NADAS, 1976 (applicable from 1.7.1976 - modified 19.6.2001).
- [4] STUCHLY, V., GRENCIK, J.: *Proposed Implementation of RCM Method for Maintenance of Bogies of Railway Passenger Wagon*, EuroMaintenance 2012, Belgrade, May, 2012, 87-96. ISBN 978-86-89141-00-9, CD-ROM.
- [5] Kol.: *Railway Wagons Maintenance Regulation (in Slovak)*, version 2.0, ZSSK Cargo Slovakia: Bratislava, 2011.
- [6] STUCHLY, V., GRENCIK, J.: *Calculation of Preventive Maintenance Tasks using RCM Method*, EuroMaintenance 2010 Conference, May 2010, Fiera di Verona, 207- 209.
- [7] STUCHLY, V., POPROCKY, R.: *Maintainance Machine and Devices - 1<sup>st</sup> ed. (in Slovak)*, Zilinska univerzita : Vysokoskolske ucebnice, 2014, ISBN 978-80-554-0845-3.
- [8] ABERNETHY, R. B.: *The New Weibull Handbook, Fifth Edition (Reliability & Statistical Analysis for Prediction Life, Safety, Survivability, Risk, Cost a Warranty Claims - Waloddi Weibull)*. Published and distributed by Dr. Robert B. Abernethy, 536 Oyster Road, North Palm Beach, Florida 33408-4328, 2004, ISBN-10 0-9653062-3-2.
- [9] Commission Regulation (EU) No. 445/2011 of 10 May 2011 on a system of certification of entities in charge of maintenance for freight wagons and amending Regulation (EC) No. 653/2007.
- [10] ERA/GUI/02-2008/SAF, Version: 1.1: Collection of Examples of Risk Assessments and of Some Possible Tools Supporting the CSM Regulation, ERA, Valenciennes Cedex, France, 06.01.2009, <http://www.era.europa.eu>.

Michal Holubcik - Jozef Jandacka \*

---

## MATHEMATICAL MODEL FOR PREDICTION OF BIOMASS ASH MELTING TEMPERATURE USING ADDITIVES

*Some types of biomass ash have low ash melting temperature which can result in various problems in combustion processes. Ash slags and sinters can avoid heat transfer in heat exchangers, which can also cause corrosion of heat transfer surfaces. One of the ways of burning fuels with low ash melting temperature is to use additives. Ash melting temperature can be determined in a laboratory on the basis of standard STN ISO 540. Meltability of ash is characterized by the physical state of ash occurring during the heating process under well-defined conditions in the furnace. Experimental determination of ash melting temperature is quite expensive. In this work a prediction method of ash melting temperature is described. The mathematical model uses multiple linear regression where input parameters are the known chemical composition of fuel ash and used additive converted to an amount of SiO<sub>2</sub>, CaO, K<sub>2</sub>O, MgO and Al<sub>2</sub>O<sub>3</sub>. The mathematical model is relatively accurate with real ash melting temperatures and reaches accuracy about of 90% compared with ash melting temperatures obtained by STN ISO 540 method in a laboratory.*

**Keywords:** Ash melting temperature, biomass ash, additives, prediction.

### 1. Introduction

Biomass is continuously gaining interest as a sustainable energy resource that is available in many forms and can be obtained from different sources [1]. With further development, utilization of bioenergy can be expanded to meet the increasing energy demands, reduce the carbon dioxide emissions and global warming, with the benefit of urban and rural wastes disposal [2]. Currently, biomass combustion still remains the dominant technology for heat and power production [3].

The use of biomass may be connected with problems and limitations. One of these is ash from biofuel which may cause various problems during combustion processes in heating devices [4].

#### 1.1. Ash related problems during biomass combustion

Biomass consists of combustible substance, ash and water [5]. Combustible substance is the part of fuel which releases heat by oxidation, i.e., energy is chemically bound in fuel [6]. Ballast of fuel consisting of ash and water is an undesirable proportion of the fuel [7].

Fuel ash is a result of the reaction of minerals presented in biomass. Minerals and other different substances which form ash got into biomass during growth. Ash is a solid residue resulting from the perfect laboratory combustion of fuel. It is composed

of minerals that are present in the fuel. In published works [3], [8] and [9] it was found out that silicon, aluminum and iron reach the highest concentration of diversity to make up the ash biomass. Chemically, the ash from biomass is mainly composed of a mixture of oxides of inorganic elements K<sub>2</sub>O, Na<sub>2</sub>O, CaO, MgO, Fe<sub>2</sub>O<sub>3</sub>, Al<sub>2</sub>O<sub>3</sub>, SiO<sub>2</sub>, P<sub>2</sub>O<sub>5</sub> [10]. Amount of ash depends on combustion conditions [11]. The presence of ash forming elements of biomass is the result of chemical processes, intake of minerals from the soil and method of biomass transportation. Some of these elements are necessary for plant growth [12]. Constituent parts of ash biomass are divided into macronutrients (potassium, calcium, magnesium, phosphorus and sulphur) and micronutrients (iron, manganese and chlorine). Silicon, aluminum and sodium are essential for plant growth [13].

Ash in biofuel can avoid heat transfer in heat exchangers, which can cause corrosion of heat transfer surfaces. When using biofuels it is necessary to monitor content of potassium, sodium, sulfur, chlorine and their compounds because during burning they create a molten phase in which the ash particles become sticky and adhere to the heat exchange surface [14]. During combustion of certain types of plant biomass, such as straw, whole plant cereals and hay, the temperature in the combustion chamber ranges from 800 to 900 °C, which exceeds the melting temperature of these fuels. They are, therefore regarded as technically complicated combustible fuels [12]. Maintaining the temperature in the combustion chamber under the ash melting temperature

---

\* Michal Holubcik, Jozef Jandacka

Department of Power Engineering, Faculty of Mechanical Engineering, University of Zilina, Slovakia

E-mail: michal.holubcik@fstroj.uniza.sk

(AMT) and avoiding the formation of sinter deposits and slags is quite a complex task. Nevertheless, it is possible to control the combustion temperature at least within certain limits so that the formation of sediments and sinters is significantly limited [15]. Sometimes it is not possible to do constructional modifications. Then, a possible solution to the low AMT of biomass may be the use of additives to the fuel during its production or before its combustion. Additives change the chemical composition of ash, which causes the change in AMT.

## 1.2. The aim of the article

The article deals with the chemical composition of biomass ash changed by the use of various additives and with their influence on AMT. In the next part of the article a method for the prediction of biomass AMT is proposed. The input parameters are weights and chemical compositions of potential biofuel and additive.

## 2. Use of additives to increase biomass ash melting temperature

### 2.1. Materials

3 different types of basic biofuels were used:

- Spruce wood - relative humidity is 10%, calorific value is 16,47 MJ.kg<sup>-1</sup>. Chemical composition: 49.84% C, 6.03% H<sub>2</sub>, 43.2% O<sub>2</sub>, 0.12% N<sub>2</sub>, 0.01% S, 0.005% Cl.
- Miscanthus giganteus - relative humidity is 10%, calorific value is 15,72 MJ.kg<sup>-1</sup>. Chemical composition: 46.66% C, 5,84% H<sub>2</sub>, 41.7% O<sub>2</sub>, 0.74% N<sub>2</sub>, 0.15% S, 0.22% Cl.
- Wheat straw - relative humidity is 12%, calorific value is 15,12 MJ.kg<sup>-1</sup>. Chemical composition: 45.64% C, 5.96% H<sub>2</sub>, 42.4% O<sub>2</sub>, 0.73% N<sub>2</sub>, 0.082% S, 0.19% Cl.

Calorific value of biofuels samples was determined by tests with using of calorimeter LECO AC 500. Chemical compositions of samples were determined in external accredited laboratory. Values of chemical composition are reported for water - free combustible part of samples.

### 2.1. Used additives

An additive is a substance (ingredient) added to some material (product) in order to improve some of its properties [5]. In practice, it usually happens that when some characteristics are improved, some deficiencies begin to appear. It is, therefore necessary to analyze the effects of each used ingredient on fuel properties. In compliance with the recommendations in [16], 6 types of additives were used:

- Kaolin - is a white or light-colored unpaved sedimentary rock, formed mostly by decomposition of rocks rich in feldspar. The main ingredient is clayey mineral kaolinite - Si<sub>2</sub>Al<sub>2</sub>O<sub>5</sub>(OH)<sub>4</sub> which makes up 80% of its capacity.
- Talc - is a white mineral composed of hydrated magnesium silicate with the chemical formula H<sub>2</sub>Mg<sub>3</sub>(SiO<sub>3</sub>)<sub>4</sub> or Mg<sub>3</sub>Si<sub>4</sub>O<sub>10</sub>(OH)<sub>2</sub>.
- Limestone - or calcium oxide (CaO) is a white, caustic, alkaline crystalline solid at room temperature [17].
- Lime - is a sedimentary rock composed largely of the minerals calcite and aragonite which are different crystal forms of calcium carbonate (CaCO<sub>3</sub>).
- Dolomite - is a carbonate mineral composed of calcium magnesium carbonate CaMg(CO<sub>3</sub>)<sub>2</sub>. The term is also used to describe the sedimentary carbonate rock dolostone.
- Bentonite - is an absorbent aluminum phyllosilicate, essentially impure clay consisting mostly of montmorillonite. There are different types of bentonite, each named after the respective dominant element, such as potassium (K), sodium (Na), calcium (Ca), and aluminum (Al). For the purpose of this paper Al - bentonite was used.

### 2.1. Methodology of sample preparation

Pelletizing was chosen to provide good distribution of additive in biofuel. Pellets production is a complex process in which the starting material must meet certain conditions [18]. It cannot contain undesirable objects. The biggest size of sawdust fraction must be smaller than a diameter of holes in the matrix of pellet mill [19]. The humidity of input material should be around 15%. Manufactured pellets must be cooled and stored properly.

In the laboratory of the University of Zilina an experimental device for pelletizing has been designed and implemented. The device consists of an input material tank (in which biomass for production of pellets is delivered), a crusher (which crushes material to fractions of size max. 4mm in accordance with the recommendations in [3]), a crushed material tank (where the crushed material is temporarily stored), a dryer (where wet material is dried for optimal humidity), a mixing machine with capacity of 50 dm<sup>3</sup> (where dried material is mixed with water to relative humidity of about 15 - 20% in accordance with the recommendation in [11] and an additive in amount of 2%), a pellet mill with capacity of 70 - 100 kg.h<sup>-1</sup> (where the material prepared from biomass is pressed to pellets), a cooler and a duster with fan (final product - pellets are cooled to room temperature and dusted), and a produced pellets tank (where pellets are temporarily stored before packing).

18 samples of pellets with 2% addition of various additives from 3 different biomass fuels and 3 samples without additives were made- reference samples (wood pellets, miscanthus pellets and straw pellets).

### 3. Methods of experiments

The AMTs and chemical compositions of ash for selected samples were experimentally determined on the basis of results in [3].

#### 3.1. Ash melting temperature

AMT of produced samples was determined on the basis of standard STN ISO 540. Meltability of ash is characterized by the physical state of the ash occurring during the heating process under well-defined conditions in the furnace [20]. The following temperatures were monitored during the melting of ash:

1. Shrinkage temperature (ST) - is the temperature at which first symptoms of rounded edges or the edges of the test specimen occur due to melting.
2. Deformation temperature (DT) - is the temperature at which the edges of the test specimen are completely rounded, without changing the amount.
3. Hemisphere temperature (HT) - is the temperature at which the test specimen creates a hemisphere, the amount of which is equal to about half the base.
4. Flow temperature (FT) - is the temperature at which the ash spreads on a base to such a layer whose amount is approximately one third of the test specimen at the melting temperature.

Resulting value of AMT was determined by averaging 2 AMT measurements for each sample.

#### 3.2. Chemical composition of ash

Chemical compositions of ash were determined using inductively coupled plasma with atomic emission spectroscopy (ICP-AES) in an off-campus laboratory. The sample was melted to meet the required elements. The ICP-AES analysis requires adhibition of elements to be analyzed in argon plasma induced by high frequency where the temperature ranges from 8000 to 10000 °C. The sample in aerosol form was put into the plasma where it was excited. Each excited particle of an element emits a characteristic spectrum of light (qualitative analysis) which is captured by the optical system of the spectrometer and further processed electronically. The intensity of the emitted radiation is directly proportional to the amount of this element in the sample (quantitative analysis). Amounts of silicon dioxide (SiO<sub>2</sub>), calcium oxide (CaO), magnesium oxide (MgO), aluminium oxide (Al<sub>2</sub>O<sub>3</sub>) and potassium oxide (K<sub>2</sub>O) were determined.

Resulting value of SiO<sub>2</sub>, CaO, MgO, Al<sub>2</sub>O<sub>3</sub> and K<sub>2</sub>O amount was determined by averaging 2 measurements for each sample.

### 4. Results of experiments

Table 1 shows average values of AMTs and amounts of SiO<sub>2</sub>, CaO, MgO, Al<sub>2</sub>O<sub>3</sub> and K<sub>2</sub>O.

The results in Table 1 show that addition of some additives can change chemical composition of ash and increase AMT. The increase of AMT can help reduce problems with ash sintering during combustion of some types of biofuels.

Average values of AMTs and amounts of SiO<sub>2</sub>, CaO, MgO, Al<sub>2</sub>O<sub>3</sub> and K<sub>2</sub>O

Table 1

Sample	ST [°C]	DT [°C]	HT [°C]	FT [°C]	SiO <sub>2</sub> [%]	CaO [%]	MgO [%]	Al <sub>2</sub> O <sub>3</sub> [%]	K <sub>2</sub> O [%]
Wood (reference)	1170	1212	1219	1231	49.5	19.84	4.0	5.67	7.76
Wood + kaolin	1283	1302	1324	1416	29.84	9.47	1.59	20.41	3.2
Wood + talc	1258	1310	1355	1458	25.76	8.74	16.82	2.58	2.82
Wood + lime	1302	1362	1416	1482	8.19	67.3	5.22	2.25	2.36
Wood + limestone	1318	1354	1424	1517	8.59	49.91	5.44	2.32	2.94
Wood + dolomite	1361	1452	1560	1638	8.37	38.13	18.35	2.08	3.25
Wood + bentonite	1129	1157	1187	1377	42.26	9.65	4.89	13.13	3.49
Miscanthus (reference)	940	980	1170	1190	54.4	4.7	2.72	0.22	20.37
Miscanthus + kaolin	1187	1215	1238	1319	33.79	9.25	1.85	19.81	8.36
Miscanthus + lime	1171	1231	1240	1268	17.34	14.88	3.87	0.25	4.95
Miscanthus + dolomite	1131	1189	1218	1250	21.38	11.8	8.23	0.31	6.05
Straw (reference)	915	941	1111	1226	64.3	5.4	1.8	0.3	17.0
Straw + kaolin	1146	1227	1261	1337	47.18	5.78	2.31	21.34	10.76
Straw + lime	1193	1223	1240	1280	38.93	18.51	4.56	0.42	9.41
Straw + dolomite	1111	1133	1165	1235	38.32	10.5	7.94	0.51	10.19
Straw + bentonite	1003	1142	1217	1318	43.76	5.60	3.67	11.74	8.59

The highest AMT of spruce wood was achieved by adding 2% of dolomite where ST was higher by 16.3%, DT higher by 19.8%, HT higher by 27.9% and HT higher by 33.1% in comparison with the reference sample. The addition of kaolin had the most positive impact on the AMT of miscanthus giganteus or wheat straw; the AMT increased on average by 15.9% or by 18.6%, in comparison with the reference sample.

In terms of chemical composition of biomass samples it can generally be argued that the higher amount of CaO and MgO at the expense of the lower amount of SiO<sub>2</sub> and, mainly, of K<sub>2</sub>O (probably the most negative compound in terms of AMT), increases the AMT of some types of biofuels.

### 5. Mathematical model for prediction of biomass ash melting temperature using additives

To obtain a correlation for calculating biomass AMT, the proposed mathematical model uses a multiple linear regression [3] which examines the relationship between several variables. It was necessary to choose the method of least squares to minimize the sum of squares of residues. The proposed mathematical model was inspired by works [16], [21], [22] and [23].

Inlet values are weight contents of SiO<sub>2</sub>, CaO, K<sub>2</sub>O, MgO and Al<sub>2</sub>O<sub>3</sub> in a basic biofuel (for example, spruce wood) and weight contents of SiO<sub>2</sub>, CaO, K<sub>2</sub>O, MgO and Al<sub>2</sub>O<sub>3</sub> in an added additive (for example, dolomite). Weight contents of compounds in biofuel with additive are calculated:

$$m_{SiO_2} = m_{fuel} \cdot A_d \cdot \%SiO_2 + m_{adit} \cdot \%_{adit} SiO_2 \quad (1)$$

$$m_{CaO} = m_{fuel} \cdot A_d \cdot \%CaO + m_{adit} \cdot \%_{adit} CaO \quad (2)$$

$$m_{K_2O} = m_{fuel} \cdot A_d \cdot \%K_2O + m_{adit} \cdot \%_{adit} K_2O \quad (3)$$

$$m_{MgO} = m_{fuel} \cdot A_d \cdot \%MgO + m_{adit} \cdot \%_{adit} MgO \quad (4)$$

$$m_{Al_2O_3} = m_{fuel} \cdot A_d \cdot \%Al_2O_3 + m_{adit} \cdot \%_{adit} Al_2O_3 \quad (5)$$

where  $m_{fuel}$  [g] is the weight of biofuel,  $A_d$  [%] is the ash content in biofuel (in accordance with STN EN 14775),  $\%(SiO_2, CaO, K_2O, MgO, Al_2O_3)$  [%] is the amount of SiO<sub>2</sub>, CaO, K<sub>2</sub>O, MgO, Al<sub>2</sub>O<sub>3</sub> in biofuel ash,  $m_{adit}$  [g] is the amount of used additive,  $\%_{adit}(SiO_2, CaO, K_2O, MgO, Al_2O_3)$  [%] is the amount of SiO<sub>2</sub>, CaO, K<sub>2</sub>O, MgO, Al<sub>2</sub>O<sub>3</sub> in used additive.

To increase the accuracy of the mathematic model the following 3 factors were created:

Dolomite index ( $D_{IXm}$ ) - determines the weight proportion of dolomitic compounds (CaO and MgO) to the sum of the amounts of SiO<sub>2</sub>, CaO, K<sub>2</sub>O, MgO and Al<sub>2</sub>O<sub>3</sub> in biomass ash

$$D_{IXm} = \frac{m_{CaO} + m_{MgO}}{m_{SiO_2} + m_{CaO} + m_{K_2O} + m_{MgO} + m_{Al_2O_3}} \quad (6)$$

Factor CMK - the ratio of the sum of CaO and MgO weight content to K<sub>2</sub>O weight content in biomass ash

$$f_{CMKm} = \frac{m_{CaO} + m_{MgO}}{m_{K_2O}} \quad (7)$$

Factor PH - the ratio of the weight sum of basic (CaO, K<sub>2</sub>O, MgO) and acidic (SiO<sub>2</sub>, Al<sub>2</sub>O<sub>3</sub>) compounds in biomass ash

$$f_{PHm} = \frac{m_{CaO} + m_{K_2O} + m_{MgO}}{m_{SiO_2} + m_{Al_2O_3}} \quad (8)$$

The equation for AMT (ST, DT, HT, FT) prediction under reducing atmosphere is:

$$t = b_0 + b_1 \cdot m_{SiO_2} + b_2 \cdot m_{CaO} + b_3 \cdot m_{K_2O} + b_4 \cdot m_{MgO} + b_5 \cdot m_{Al_2O_3} + b_6 \cdot D_{IXm} + b_7 \cdot f_{CMKm} + b_8 \cdot f_{PHm} \quad (9)$$

Constant  $b_0$  [°C], the regression coefficients  $b_1 - b_8$  [°C], standard deviation  $\sigma$  and correlation index R for prediction of AMT of ST, DT, HT and FT are illustrated in Table 2.

Regression coefficients for prediction of AMT

Table 2

Coef.	Indication.	Variables	DT	ST	HT
$b_0$	constant	1093.191937	1099.834412	1128.7016	1194.585516
$b_1$	$m_{SiO_2}$	-3.081022249	1.329223672	1.49702109	10.10272854
$b_2$	$m_{CaO}$	6.65923753	3.406691792	-6.680170818	-11.02965381
$b_3$	$m_{K_2O}$	-14.91887671	-25.57010491	-5.184487742	-32.62187073
$b_4$	$m_{MgO}$	0.579373798	-1.277753798	-4.628135914	-2.346833511
$b_5$	$m_{Al_2O_3}$	12.62898213	13.44301574	7.58442836	5.377643061
$b_6$	$D_{IXm}$	385.3944151	488.614852	379.7246862	238.4313286
$b_7$	$f_{CMKm}$	-1.420007209	-2.563995809	2.022658794	7.698079425
$b_8$	$f_{PHm}$	-22.44450524	-15.34711914	10.89210758	19.24253498
$\sigma$ [°C]		58.83	53.13	55.87	69.30
R		0.915	0.934	0.905	0.882

Calculated values of ash melting temperatures obtained using the equation (9) together with the correlation coefficients in Table 2 are very accurate because the standard deviation  $\sigma$  of all biomass ash melting temperatures is lower than 70 °C, which is below the limit value of the reproducibility of the experiment (STN ISO 540). High accuracy of the mathematic model confirms high levels of correlation index R exceeding the value of 0.9, except for one temperature (HT determination, R = 0.882). In comparison with a similar mathematical model in [22] the proposed mathematical model for AMT prediction is very accurate.

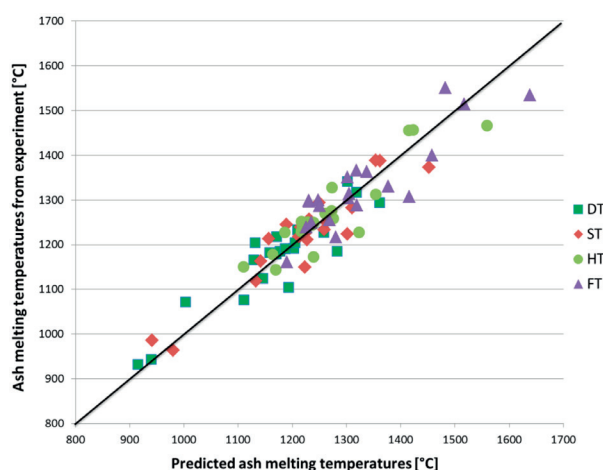


Fig. 1 Comparison of AMT from experiment and predicted AMT

The high accuracy of the model is also confirmed by Fig. 1 which compares the real values of biomass AMT gathered from experimental measurements with those obtained from the mathematical model.

## 6. Conclusion

The use of additives can be a highly interesting and effective way how to solve problems arising from combustion of biofuels with low ash melting temperature. Based on the above mentioned results we can argue that the addition of dolomite and kaolin increased most significantly the AMT of tested biofuels. It was caused by the change in chemical composition of biofuel ash. Empirical equations in the proposed mathematical model were derived from the AMT values gathered in reducing atmosphere. The mathematic model can be used with a small standard deviation for various types of biofuels with various ash chemical compositions. It can also be used for prediction of AMT biomass with addition of various types of additives with known chemical composition. The proposed mathematical model can help to choose a suitable additive for combustion of problematic biomass in practice.

## Acknowledgement

This work is supported by the financial assistance of the project APVV-0458-11.

## References

- [1] WANG, L., HUSTAD, J., SKREIBERG, O., SKJEVRAK, G., GRONLI, M.: A Critical Review on Additives to Reduce Ash Related Operation Problems in Biomass Combustion Applications, *Energy Procedia*, vol. 20, 2012, 20-29.
- [2] BUCZYNSKI, R., WEBER, R., SZLEK, A., NOSEK, R.: Time-dependent Combustion of Solid Fuels in a Fixed-bed: Measurements and Mathematical Modeling, *Energy and Fuels*, 26, 8, 2012, 4767-4774.
- [3] HOLUBCIK, M.: *Possibilities of Increasing Ash Melting Temperature from Biomass (in Slovak)*, PhD thesis, University of Zilina, 2013.
- [4] LABAJ, J., PATSCH, M., BARTA D.: *Combustion of Alternative Fuels*, Proc. of TRANSCOM 2009, University of Zilina, 2009, 67-76.
- [5] SOOS, L., KOLEJAK, M., URBAN, F.: *Biomass - Renewable Energy Source (in Slovak)*, Vert: Bratislava, 2012.
- [6] PILAT, P., PATSCH, M., MALCHO, M.: Solar Heat Utilization for Adsorption Cooling Device, *EPJ Web of Conferences*, vol. 25, 2012.
- [7] URBAN, F., KUCAK, L., BEREZNAI, J., PULMANN, M., TYHANYI, J.: Influence of the Mixing Grid Position on the Coolant Flow at the Outflow Part of the Nuclear Reactor Fuel Assembly Physical Model and Validation of CFD Model, *Communications - Scientific Letters of the University of Zilina*, vol. 14, No. 4a, 42-46. ISSN 1335-4205.
- [8] WERKELIN, J., SKRIFVAR, B., HUPA, M.: Ash-Forming Elements in Four Scandinavian Wood Species, *Biomass And Bioenergy*, vol. 29, No. 6, 2005, 451-466.
- [9] BOSTROM, D.: Slagging Characteristics during Combustion of Corn Stovers with and without Kaolin and Calcite. *Energy and Fuels*, 22, (Compendex), 2008, 3465-3470.
- [10] HUZVAR, J., KAPJOR, A.: *Micro-cogeneration incl. the Conversion of Chemical Energy of Biomass to Electric Energy and the Low Potential Heat*, Proc. of AIP Conference, vol. 1337, 2011, 40-42.

- [11] RIMAR, M., KUNA, S.: Comparison of Methods of Wood Chip Moisture Evaluation, *Advanced Materials Research*, vol. 724-725, 222-225.
- [12] ZEVENHOVEN, M.: *Ash-Forming Matter, Biomass Fuels*. Abo/Turku: Faculty of Chemical Engineering: Abo Akademi University, 2001, 88 p.
- [13] ORZECZOWSKI, T., ORMAN, L. J.: Thermovision Inspection of Air Polluting Emitters, *Pollution Engineering*, vol. 38, 7, 22-25, 2006.
- [14] VITAZEK, I., VITAZKOVA, B., PLOTH, J.: Production of Gas Emissions from Biomass Heat Source. *Engineering Mechanics*, vol. 20, 2013, No. 3/4, 289-298. ISSN 1805-4633.
- [15] NEMEC, P., MALCHO, M., SMITKA, M., MATUSOV, J.: Performance Parameters of a Closed Loop Thermosyphon, *Communications - Scientific Letters of the University of Zilina*, vol. 14, No. 4a, 53-57.
- [16] LIORANTE, M. J. F., AROCAS, P. D., NEBOT, L. G., GARCIA, J. E. C., The Effect of the Addition of Chemical Materials on the Sintering of Biomass Ash. *Fuel*, 87, 12 2008, 2651-2658.
- [17] LELOVICS, H., LIPTAKOVA, T.: Time and Mixing Technique-dependent Changes in Bone Cement SmartSet (R) HV, *Acta of Bioengineering and Biomechanics*, vol. 12, No. 4, 63-67, 2010.
- [18] CERNECKY, J., NEUPAUEROVA, A., JANOSKO, I., SOLDAN, M.: *Environmental Technology (in Slovak)*, Technicka univerzita: Zvolen, 274 p., 2010.
- [19] TAUS, P., TAUSOVA, M.: Economic Analysis of FV Power Plants According Installed Performance, *Acta Montanistica Slovaca*, vol. 14, No. 1, 2009
- [20] HORAK, J., JANKOVSKA, Z., STRAKA, F., BURYAN, P., KUBESA, P., HOPAN, F., KRPEC, K.: Problems of Determination of Characteristic Temperatures of Biomass Ash Fusibility (in Czech), *Chemické listy*, vol. 107, No. 6, 2013, 502-509. ISSN 0009-2770.
- [21] SEGGIANI, M.: Empirical Correlations of the Ash Fusion Temperatures and Temperature of Critical Viscosity for Coal and Biomass Ashes, *Fuel*, vol. 78, 1999, 1121-1125
- [22] LIORANTE, M. J. F., GARCIA, J. E. C.: Comparing Methods for Predicting the Sintering of Biomass Ash in Combustion, *Fuel*, 84, 2005, 1893-1900
- [23] NEMEC, P., CAJA, A., MALCHO, M.: Mathematical Model for Heat Transfer Limitations of Heat Pipe, *Mathematical and Computer Modelling*, vol. 57, No. 1-2, 2013, 126-136.

Andrej Kapjor - Jozef Huzvar - Branislav Ftorek - Martin Vantuch \*

## CRITERION EQUATIONS OF HEAT TRANSFER FOR „N“ HORIZONTAL PIPES ONE ABOVE ANOTHER AT NATURAL CONVECTION IN LINEAR METHOD OF APPROXIMATION

*The aim of the analysis of heat and fluxional pipe fields "n" pipes one above another at natural convection is the creation of criterion equation on the basis of which the heat output of heat transfer from pipe oriented areas one above another with given spacing could be quantified. For creating criteria-relation and calculating the Nusselt number for „n“ tubes one above the other were used computational data from Ansys-Fluent software and criterion equations for a single tube. Based on the heat transfer analysis of a single horizontal tube will be used criterial equation for calculating the Nusselt number according to Morgan. For themselves derive criteria equations data evaluated were calculated and adjusted for mathematical processing of results. Formation criterion equations was based on approximation of planar curves prepared from adjusted modeled data by using CFD. In calculating was used the least squares approximation method.*

**Keywords:** Convection, heat transfer, thermal temperature, criterial equation, natural convection.

### 1. Introduction

On the basis of this comparison where equalities were gained [1 and 2] in calculated and modelled results, models were created in the programme Ansys-Fluent for "n" horizontal pipes one above another.

Data from this program and famous criterion equation for one pipe were used to create criterion relation to calculate Nusselt number [3 and 4] for "n" pipes one above another. A criterion relation for calculating Nusselt number according to Morgan [5 and 6] will be used on the basis of analyses of heat transfer of one horizontal pipe.

To deduce criterion relation, calculated data were evaluated and modified for mathematical processing of results. The creation of criterion equation came out from the approximation of a space curve formed from modified modelled data with the help of CFD. The least squares fitting method was used. A linear model of criterion equation for "n" pipes one above another was created.

### 2. Simulations

The aim of analysis of temperature and stream fields of "n" pipes one above another at natural convection is to create a criterion equation on the basis of which a heat output of heat transfer from pipe oriented areas above each other with

given spacing could be quantified. At present a sum of criterion equations exists for simple geometrical shapes of individual oriented geometrical areas but the criterion equation which would consider interaction of fluxional field generated by free convection from multiple oriented areas is not mentioned in standardly accessible technical literature and other magazine publications. Creation of criterion equation for calculation of heat output is significant for quantification of heat outputs calculations of geometrically more complicated heat transfer areas in engineering practice and, furthermore, for optimization of processes such as schemes of pipe heat bodies and many other applications in technical practice that are related to heat transfer by free convection [7, 8 and 9].

The process of finding a new criterion equation for above mentioned geometries was carried out on the basis of numerical experiment by simulation of heat transfer for various thermokinetic and geometrical parameters of pipe alignment one above another. Some simulations were verified by measuring the output of real pipe system in a specialized thermostatic chamber. Used numeric model of CFD method was validated in this way.

Simulations of ten pipes one above another with the diameter of 27mm at a wall temperature 30°C, 45°C, 60°C, 75°C, 90°C, 105°C and at a surrounding temperature 20°C were carried out in order to put together criterion relation for "n" pipes one above another at natural convection on the basis of calculations in the programme Ansys - Fluent, Fig. 1. Heat output of pipe

\* <sup>1</sup>Andrej Kapjor, <sup>1</sup>Jozef Huzvar, <sup>2</sup>Branislav Ftorek, <sup>1</sup>Martin Vantuch

<sup>1</sup>Department of Power Engineering, Faculty of Mechanical Engineering, University of Zilina, Slovakia

<sup>2</sup>Department of Applied Mathematics, Faculty of Mechanical Engineering, University of Zilina, Slovakia

E-mail: andrej.kapjor@fstroj.uniza.sk

system with this diameter was measured also in the thermostatic chamber.

The modelling of heat transport from ten horizontal pipes in the programme Ansys 13 - Workbench was carried out in the analysis system Fluid Flow (Fluent) [10].

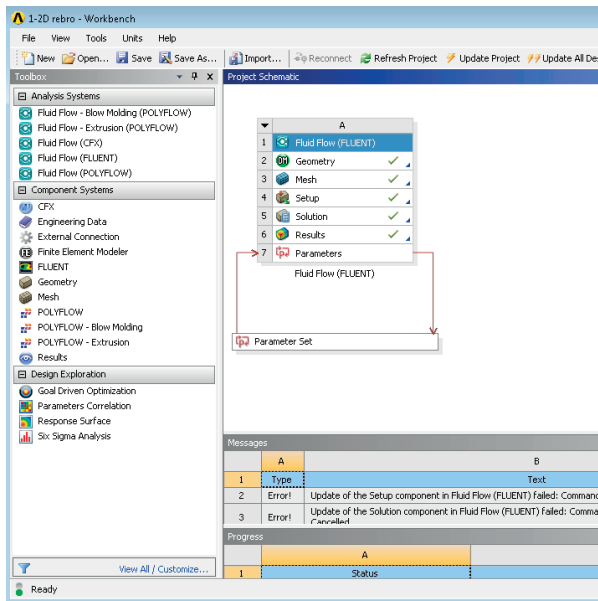


Fig. 1 The basic scheme of calculation

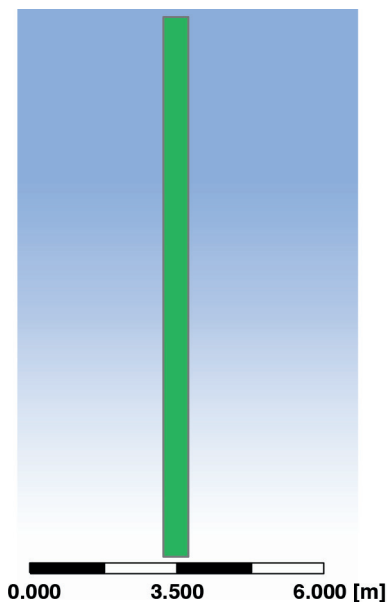


Fig. 2 The geometry of ten pipes one above another and its surrounding

Figure 1 shows a basic scheme of the way of analyzing the heat transfer by natural convection from ten horizontal pipes in the air. Primarily, it would be necessary to create a geometry of ten horizontal pipes together with the surrounding of pipes (a model

of placing system of pipes into nondimensional space) to visualize temperature fields as well as to calculate output characteristics. To simplify calculations and due to the geometry of pipes, a 2-D model of heat transport calculation from horizontal pipe with given parameter for spacing of ten horizontal pipes could be used Fig. 2.

In the next step a computing grid with higher density around pipes was created in the subsystem of the programme Ansys in order to receive better accuracy of calculations of output characteristics of natural convection of horizontal pipes - Fig. 2. After the creation computing mesh with higher density of meshing around the tubes [Fig. 3] the model was imported into computing module Fluent where 2-D calculation model was chosen [11 and 12].

Similar boundary conditions for calculation were entered in the programme Fluent:

- unsteady model (because of instability of streaming),
- laminar model of streaming (results from the calculation of Rayleigh number of similarity theory where the critical value for laminar streaming is  $Ra_{krit} = 10^9$ ),
- temperature of pipe 's walls - given as parameter,
- limiting control area for natural convection analysis was entered as "pressure outlet" with given temperature of 20°C, which means  $T_{\infty} = 20^{\circ}C$ ,
- gravity acceleration  $9.81m.s^{-2}$ ,
- Boussinesq model for calculation of air density, which is useful for natural convection (according to the Fluent publication),
- under-relaxation factors except for energy and pressure, they decreased by half (according to the Fluent publication).

A nonstationary model was selected (unsteady model) which is suitable for calculation of a free convection from more complicated shapes of heat exchange areas [13 and 14].

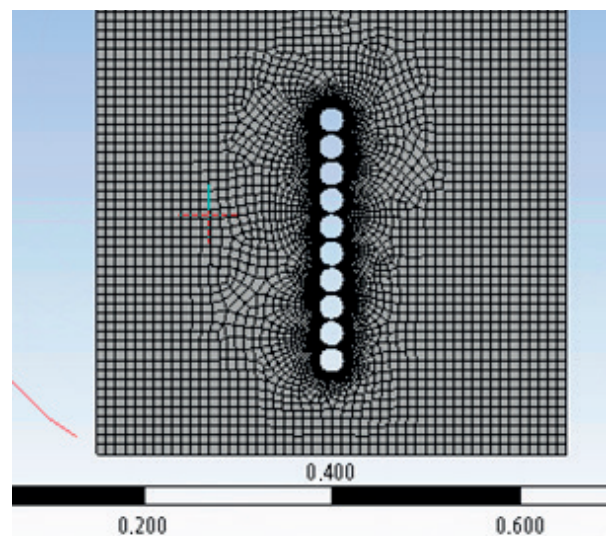


Fig. 3 Computing grid vertical plate and its surrounding

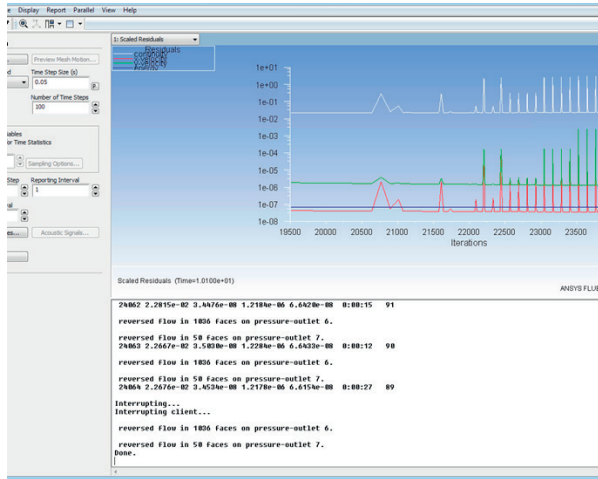


Fig. 4 Process of computing in programme Ansys-Fluent

### 3. Criterion relation

Calculation of heat output (Fig. 4) was carried out after entering boundary conditions and after configuration of parameters for parametric analysis where eighteen spacings "S" in vertical direction were stated. When pipe's wall temperature was entered in the programme Fluent as another parameter, automatically another column was generated in which it was possible to change temperature values. When selecting the "Update all design point", the programme automatically recounts all the entered calculation values and writes defined outgoing parameters from the Fluent code into another column. In this case a heat output was used as outgoing parameter. Such analyses were carried out for more temperatures, namely, for wall temperatures 30°C, 45°C, 60°C, 75°C, 90°C and 105°C. Heat outputs of ten horizontal pipes at these temperatures are shown in Table 1 and in graph 1 where except for spacing a new parameter for calculating the output S/D was given. The pictures show reciprocal interaction of individual pipes where at minimum spacing (for the dimensionless parameter S/D = 1) the pack of pipes behaved similarly to a vertical panel. After following increase of S/D the interaction was expressed not only at increasing heat output Fig. 5, but also at creating temperature fields and at stream character. As also seen in these pictures Figs. 6 - 11 the streaming process at lower parameters S/D is relatively stable, stationary, where a fine waving occurs only at the end of the reach of the air [15].

Heat outputs of ten horizontal pipes at a surrounding temperature 20°C and pipe's wall temperatures 30-105°C Table 1

S/D	30°C Q [W]	45°C Q [W]	60°C Q [W]	75°C Q [W]	90°C Q [W]	105°C Q [W]
1.05	24.85	82.89	154.57	236.19	325.90	422.60
1.4	31.10	104.23	195.98	301.18	417.07	542.27
1.5	32.77	109.62	205.81	316.77	439.31	572.34
1.75	36.16	121.58	227.12	350.48	485.04	630.22
2	39.28	133.23	248.62	382.10	527.49	684.03
2.5	45.85	159.93	293.44	457.82	621.90	805.44
3	51.24	176.65	350.63	518.94	727.33	937.22
3.5	54.87	192.42	363.47	561.12	764.37	974.49
4	58.95	210.29	403.87	618.16	848.46	1089.57
4.5	58.81	202.40	384.76	585.91	795.60	1015.09
5	63.77	224.60	432.04	655.66	900.33	1165.18
7.5	62.18	231.60	449.60	671.39	923.33	1192.95
10	58.46	240.45	464.92	716.46	983.14	1284.73
15	52.40	212.25	464.09	727.93	1025.62	1361.48
20	51.25	16.91	397.70	715.66	1010.09	1306.05
25	50.17	158.99	299.56	562.64	932.84	1281.74
30	50.11	158.30	287.23	434.69	625.30	839.26
35	50.05	158.28	287.22	434.50	600.12	838.00

By further increase of S/D the heat transfer at natural convection intensifies by reciprocal influencing of individual pipes. Furthermore, streaming gets nonstationary on upper pipes that are the most influenced ones. By further increase of S/D the reciprocal interaction of pipes is being decreased which causes decreasing of heat output at natural convection till such S/D ratio is achieved where pipes are not being influenced at all and no other change of heat output at natural convection occurs. As evident from these analyses and from Fig. 5, it is possible to divide the process of heat transport at natural convection from "n" pipes in four output areas. The area one is characterized by huge increase of heat output at natural convection.

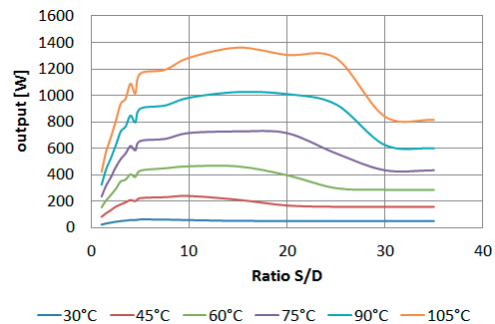


Fig. 5 Heat outputs of ten horizontal pipes at a surrounding temperature 20°C and pipe's wall temperatures 30-105°C

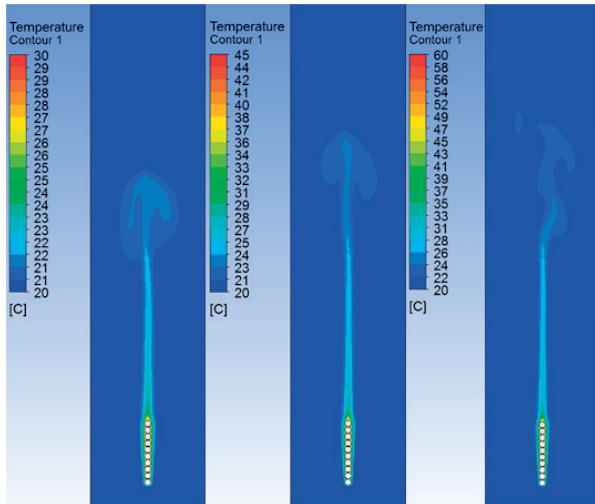


Fig. 6 Temperature fields of ten horizontal pipes with the diameter 27 mm, with given ratio  $S/D$  1.05 and surrounding temperature  $20^{\circ}\text{C}$

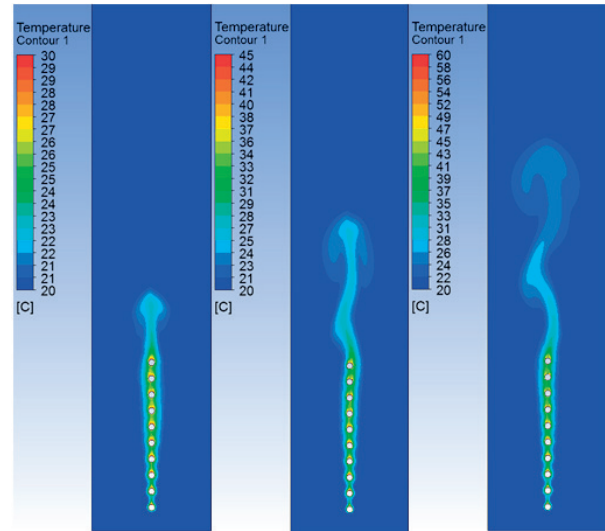


Fig. 8 Temperature fields of ten horizontal pipes with the diameter 27 mm, with given ratio  $S/D$  2.5 and surrounding temperature  $20^{\circ}\text{C}$

An insignificant increase is present in area two. In area three decreasing of heat output occurs because of the influence of interaction decrease. Area four is characterized by constant heat output which means that individual pipes are not being influenced. The pipe's wall temperature and the surrounding temperature have a very big influence on a clear definition of borders of these four areas which will be defined by non-dimensional temperature  $T^{\infty}/T_s$  when searching for a suitable criterion relation.

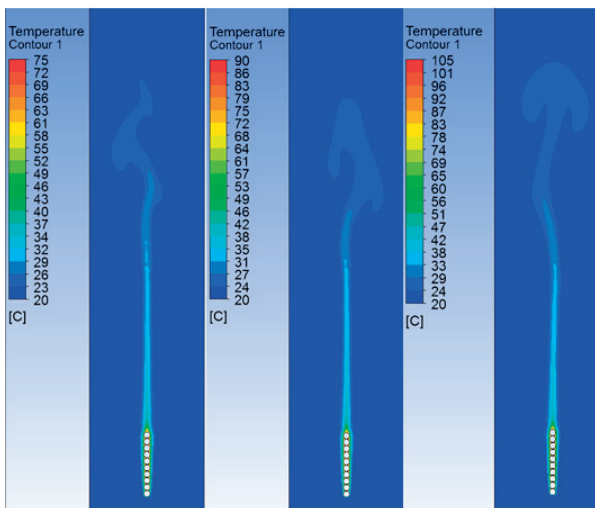


Fig. 7 Temperature fields of ten horizontal pipes with the diameter 27 mm, with given ratio  $S/D$  1.05 and surrounding temperature  $20^{\circ}\text{C}$

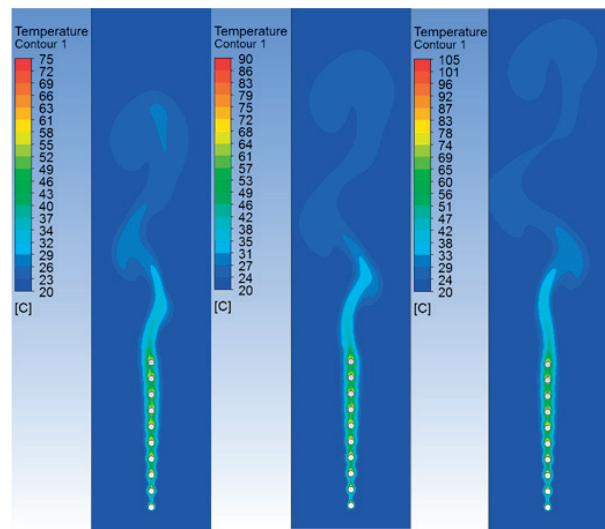


Fig. 9 Temperature fields of ten horizontal pipes with the diameter 27 mm, with given ratio  $S/D$  2.5 and surrounding temperature  $20^{\circ}\text{C}$

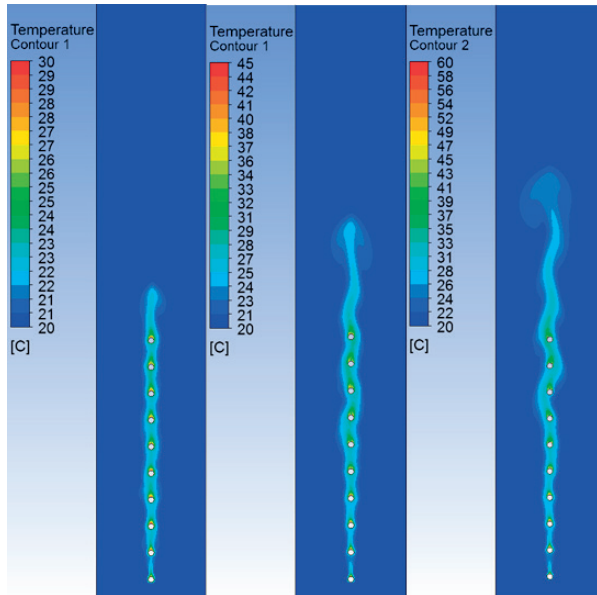


Fig. 10 Temperature fields of ten horizontal pipes with the diameter 27 mm, with given ratio S/D 4.5 and surrounding temperature 20°C

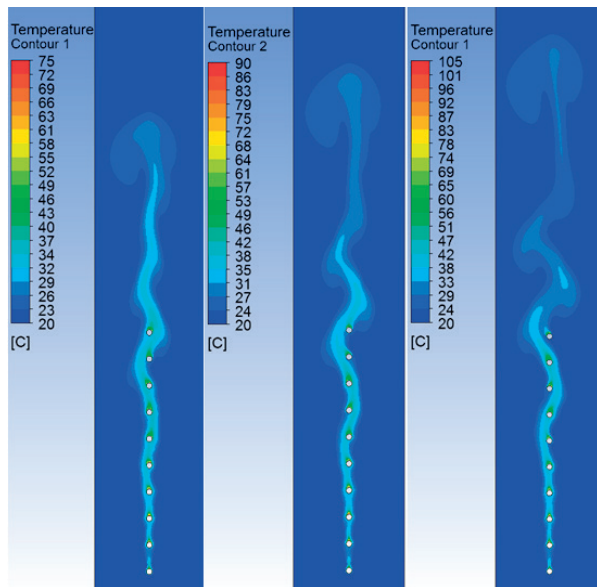


Fig. 11 Temperature fields of ten horizontal pipes with the diameter 27 mm, with given ratio S/D 4.5 and surrounding temperature 20°C

A criterion relation for calculating Nusselt number according to Morgan will be used on the basis of heat transfer analyses of one horizontal pipe:

$$\overline{Nu}_d = \frac{\overline{\alpha} d}{\lambda} = CRa_d^n [1] \quad (1)$$

Multiple article C and exponent n

Table 2

Ra <sub>d</sub>	C	n
10 <sup>-10</sup> -10 <sup>-2</sup>	0.675	0.058
10 <sup>-2</sup> -10 <sup>2</sup>	1.02	0.148
10 <sup>2</sup> -10 <sup>4</sup>	0.85	0.188
10 <sup>4</sup> -10 <sup>7</sup>	0.48	0.25
10 <sup>7</sup> -10 <sup>12</sup>	0.125	0.333

Table 2 shows C and n exponent in Ra changes. It is necessary to evaluate calculated data or to modify them for mathematical processing of results to be able to deduce criterion relation. More variants for creation of given equation were analysed while analysing and processing data in order to put together criterion equation. As mentioned above the heat output at natural convection from "n" horizontal pipes depends on ratio S/D (non-dimensional spacing) as well as on T<sup>∞</sup>/T<sub>s</sub>. This implies that the searched functional dependency will have a shape of functional dependency of space area. Fig. 12 shows functional dependencies of Nusselt number of pipe bundle which was calculated from general relation for calculating Nu number

$$\overline{Nu}_{D_{zv}} = \frac{\alpha L}{\lambda} [1] \quad (2)$$

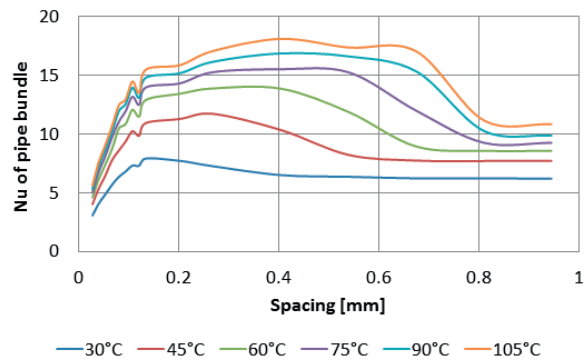


Fig. 12 Process of ratio Nu depending on spacing, pipe's wall temperature 30°C-105°C and surrounding temperature 20°C

As it is necessary to find the dependency of Nusselt number of "n" horizontal pipes one above another ( $Nu_{D_{zv}} = Nu_d * f(S/D, T^\infty/T_s)$ ) the data were calculated and Fig. 13 was created. As seen in the graph it would be very difficult to create a functional dependency for such an area and created functional dependency would show a significant mistake. For that reason it was necessary to bring some physical dependency into this problem. By dividing of  $Nu_{D_{zv}}$  by conjunction of  $Nu_d$  (Nu of one pipe), using parameter S/D and parameter T<sup>∞</sup>/T<sub>s</sub> we got data from which Fig. 14 and 3-D graph of space area were created. It is evident from these graphs that the functional dependency has an exponential character. On

the basis of these analyses the final criterion equation will be as follows:

$$\overline{Nu_{D_{zv}}} = Nu_d \cdot \frac{S}{D} \cdot \frac{T_\infty}{T_s} \cdot f\left(\frac{S}{D}, \frac{T_\infty}{T_s}\right) \quad (3)$$

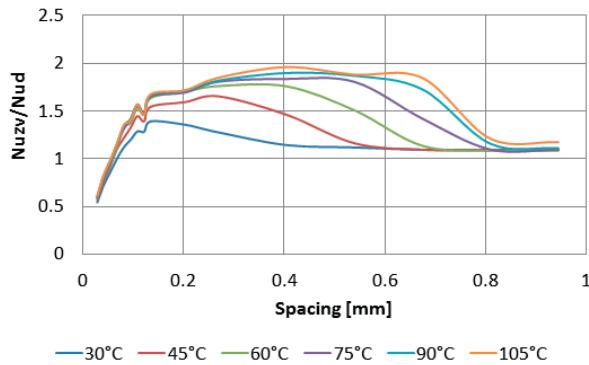


Fig. 13 Process of ratio  $Nu_{zv}/Nu_d$  depending on spacing, pipe's wall temperature 30°C-105°C and surrounding temperature 20°C

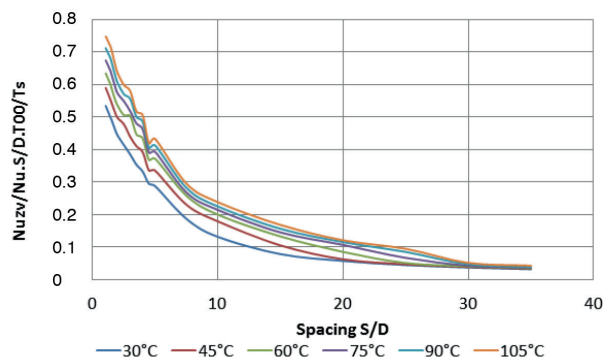


Fig. 14 Process of ratio  $Nu_{zv}/(Nu_d \cdot S/D \cdot T_\infty/T_s)$  depending on  $S/D$ , pipe's wall temperature 30°C-105°C and surrounding temperature 20°C

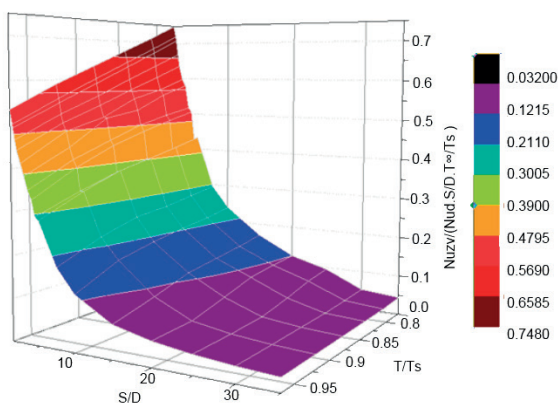


Fig. 15 Process of ratio  $Nu_{zv}/(Nu_d \cdot S/D \cdot T_\infty/T_s)$  depending on  $S/D$  a  $T_\infty/T_s$

Creation of criterion equation comes out from previous analysis of data and their following processing which results in the conclusion that the final criterion equation will be as follows

$$\overline{Nu_{D_{zv}}} = Nu_d \cdot \frac{S}{D} \cdot \frac{T_\infty}{T_s} \cdot f\left(\frac{S}{D}, \frac{T_\infty}{T_s}\right)$$

We demand that the final curve or area is continuous and as well as possible approximated points of empiric polygon which is given by calculated data. This approximation is necessary for defining the process of an event for any argument value and it is used for quantification of physical-technical relations. While creating criterion equation at approximation, we will use the least squares method for the function of two variables

$$f\left(\frac{S}{D}, \frac{T_\infty}{T_s}\right)$$

To create functional dependency it is necessary to choose approximate basis functions which highly influence the correctness of results. For the function of two variables in general a higher number of elements is necessary than for the function of one variable. As the result of these facts we see big equation systems at approximation of the function with two variables and the question of solution stability regarding round-off errors can be brought to the forefront. For the approximation of the area as seen in Fig. 15, we used three methods namely a linear model, non-linear model and interpolation approach - using cubic splines.

Linear model:

This model was proved good for the interval  $\frac{S}{D}$ , which is divided in four parts where we chose for basic functions the conjunction of powers  $\left(\frac{T_\infty}{T_s}\right)^\alpha \cdot \left(\frac{S}{D}\right)^\beta$ ,  $\alpha + \beta \leq 3$ . This means that the final polynomial of two variables was of a third degree and the number of basic functions was  $n=10$ . A good compromise was gained between the simplicity of basis functions and the total degree of polynomial. A low degree of polynomial suppresses the inclination of polynomial approximation to parasitic oscillations and this would completely devalue the results. The relative error of this polynomial model to enter data was in given intervals up to 8% which can be considered as a very good result [16]. Constants of the equation for each interval are shown in Tables 3, 4, 5 and 6.

The approximation equation is as follows

$$f\left(\frac{T_\infty}{T_s}, \frac{S}{D}\right) = c_1 + c_2x + c_3y + c_4x^2 + c_5xy + c_6y^2 + c_7x^3 + c_8x^2y + c_9xy^2 + c_{10}y^3 \quad (4)$$

where we identify

$$x = \frac{T_\infty}{T_s}, y = \frac{S}{D} \quad (5)$$

Constants of the equation  $2 \frac{S}{D} \in < 1.05; 5 >$  Table 3

c1	c2	c3	c4	c5
6.4978	-17.0293	-0.6537	17.8059	1.0878
c6	c7	c8	c9	c10
0.0173	-6.6608	-0.5758	0.0042	-0.0017

Constants of the equation  $2 \frac{S}{D} \in < 5; 15 >$  Table 4

c1	c2	c3	c4	c5
8.7138	-26.6054	-0.2258	31.6232	0.0074
c6	c7	c8	c9	c10
0.0176	-12.985	0.0594	-0.0043	-0.0004

Constants of the equation  $2 \frac{S}{D} \in < 15; 25 >$  Table 5

c1	c2	c3	c4	c5
18.8068	32.406	-4.3318	-32.772	-0.4562
c6	c7	c8	c9	c10
0.2303	10.4933	0.2714	0	-0.0038

Constants of the equation  $2 \frac{S}{D} \in < 25; 35 >$  Table 6

c1	c2	c3	c4	c5
24.8859	-9.2346	-2.1961	1.2677	0.4729
c6	c7	c8	c9	c10
0.0662	1.1953	-0.1222	0.004	-0.0007

Relevant calculations of this linear polynomial model are carried out in the Matlab.

References

[1] INCROPERA, F. P., DEWITT, D. P., BERGMAN, T. L., LAVINE, A.: *Fundamentals of Heat and Mass Transfer*. 6<sup>th</sup> ed. John Wiley, New York, 2007.

[2] MORAN, M. J., SHAPIRO, H. N., MUNSON, B. R., DEWITT, D. P.: *Introduction of Thermal Systems Engineering: Thermodynamics, Fluid Mechanics and Heat Transfer*. John Wiley&Sons, Inc, 2003, ISBN 0-471-20490-0.

[3] PILAT, P., PATSCH, M., MALCHO, M.: *Solar Heat Utilization for Adsorption Cooling Device*. Conference on Experimental Fluid Mechanics (EFM) Jicin, November, 2011.

[4] JAKUBSKY, M., LENHARD, R., VANTUCH, M., MALCHO, M.: *Borehole Model for Simulation Transport Geothermal Heat with Heat Pipe System and with Forced Circulation of Heat Carrier*. Conference on Experimental Fluid Mechanics, EFM 2011, Jicin.

[5] LENHARD, R., JAKUBSKY, M., MALCHO M., JANDACKA, J.: Analysis of Transmission Phenomena in Low-potential Heat Transport by Heat Pipes in the Deep-borehole Simulator. *Communications - Scientific Letters of the University of Zilina*, vol. 14, No. 3, 2012, 10-16.

[6] BRESTOVIC, T., JASMINSKA, N.: Software Support Development for Numerical Solution of ANSYS CFX. *Acta Mechanica et Automatica*, vol. 17, No. 4, 2013, 215-221. ISSN 1898-4088.

The final criterion equation for Nusselt number of "n" pipes one above another will be as follows:

$$\overline{Nu}_{D_{2v}} = Nu_d \cdot \frac{S}{D} \cdot \frac{T_\infty}{T_s} \cdot (c_1 + c_2x + c_3y + c_4x^2 + c_5xy + c_6y^2 + c_7x^3 + c_8x^2y + c_9xy^2 + c_{10}y^3) \quad (6)$$

Where x is  $\frac{T_\infty}{T_s}$  and y is  $\frac{S}{D}$ .

4. Conclusion

The article deals with the topic of heat transfer from oriented heat exchange areas in relation to creating a criterion equation for "n" horizontal pipes one above another. On the basis of this comparison where equalities were gained in calculated and modelled results, models were created in the programme Ansys-Fluent for "n" horizontal pipes one above another.

As mentioned above the heat output at natural convection from "n" horizontal pipes depends on ratio S/D (non-dimensional spacing) as well as on  $T_\infty/T_s$ . In creating the criterion equation was used in approximation the least squares method. To create functional dependency it was necessary to choose suitable basic functions which highly influence the correctness of results.

In the near future we want to simplify these equations and check their functionality in all extensity. For this verification we proposed a new measurement and evaluation state in a thermostatic chamber where will be every pipe made from electric spiral. These spirals will be separately connected to a DC source of electrical power.

Acknowledgement

The research is supported by the European Regional Development Fund and the Slovak state budget for the project "Research Centre of University of Zilina", ITMS 26220220183.

- [7] CARNOGURSKA, M., PRIHODA, M., BRESTOVIC, T.: Modelling of Nitrogen Oxides Formation Applying Dimensional Analysis. *Chemical and Process Engineering - Inzynieria Chemiczna i Procesowa*, vol. 32, No. 3, September 2011. ISSN: 02086425.
- [8] DURCANSKY, P., LENHARD, R., JANDACKA, J.: *Heat Exchanger Design for Hot Air Ericsson-Brayton Piston Engine*. AIP Conference Proc. of 11<sup>th</sup> Intern. Conference of Numerical Analysis and Applied Mathematics, ICNAAM 2013, Rhodes, 2013.
- [9] JANDACKA, J., HOLUBCIK, M., PAPUCIK, S., NOSEK, R.: Combustion of Pellets from Wheat Straw. *Acta Montanistica Slovaca*, vol. 17, No. 4, 2012, 283-289.
- [10] JANDACKA, J., PAPUCIK, S., DEKYS, V., MELICHER, R.: An Analysis of Air Flow at Various Spacing of Fans on a Physical Model of a Road Tunnel, *Communications - Scientific Letters of the University of Zilina*, vol. 10, No. 3, 2008, 40-44.
- [11] PRIHODA, J., ZUBIK, P., SULC, J., SEDLAR, M.: Experimental and Numerical Modelling of Turbulent Flow Over an Inclined Backward-facing Step in an Open Channel, *Communications - Scientific Letters of the University of Zilina*, No. 4A, 2012.
- [12] CARNOGURSKA, M., PRIHODA, M., BRESTOVIC, T.: Modelling of Nitrogen Oxides Formation Applying Dimensional Analysis. *Chemical and Process Engineering - Inzynieria Chemiczna i Procesowa*, vol. 32, No. 3, September 2011. ISSN: 02086425.
- [13] NEMEC, P., CAJA, A., MALCHO, M.: *Mathematical Model for Heat Transfer Limitations of Heat Pipe*. *Mathematical and Computer Modelling*, vol. 57, No. 1-2, January 2013, 126-136
- [14] LENHARD, R., GAVLAS, S., MALCHO, M.: *Numerical Simulation of Borehole Model which Utilizes Low-potential Geothermal Heat*. *EPI Web of Conferences*. Conference on Experimental Fluid Mechanics, EFM 2011, Jicin, November 2011.
- [15] SAGA, M., KOPAS, P., VASKO, M.: Some Computational Aspects of Vehicle Shell Frames Optimization Subjected to Fatigue Life. *Communications - Scientific Letters of the University of Zilina*, vol. 12, No. 4, 2010, 73-79.
- [16] JANDACKA, J., PAPUCIK, S., DEKYS, V., MELICHER, R.: An Analysis of Air Flow at Various Spacing of Fans on a Physical Model of a Road Tunnel, *Communications - Scientific Letters of the University of Zilina*, vol. 10, No. 3, 2008, 40-44

## CONDENSER OPTIMIZATION OF HEAT PIPE

Construction of heat exchanger assembly has important role for efficient operation of energy systems. Within this assembly a heat pipe is utilized for heat transfer. The condensation part of the heat pipe is situated on top of the heating zone. The device placed in the heating zone is condenser which is used for efficient heat transfer from one medium to another. The thermal oil is used as cooling medium in the condenser. This paper analyzes the effect of different operation conditions of thermal oil to thermal performance. From the collected results it is obvious that the larger mass flow and higher temperature cause better thermal performance and lower pressure drop.

**Keywords:** Condenser, heat pipe, efficiency.

### 1. Introduction

Heat pipes can be used to enhance the amount of heat transfer. Since heat transmitted through a heat pipe is based on phase change, it can be pointed out that using a heat pipe with similar dimensions of a solid metal pipe, larger amounts of heat transfer will be obtained [1]. Due to the two-phase characteristics, the heat pipe is ideal for transferring heat over long distances with a very small temperature drop and for creating a nearly isothermal surface for temperature stabilization. As the working fluid operates in a thermodynamic saturated state, heat is transported using the latent heat of vaporization instead of sensible heat or conduction where the heat pipe then operates in a nearly isothermal condition [2 and 3].

Their application is wide and can be used, for example, in energy conservation, such as heat recovery in hot exhaust gas system, and for use in domestic and industrial applications. Solar heating is also another example for the application of heat pipes [4 and 5]. For example, a heat pipe solar collector is widely used nowadays [6 and 7].

Optimization of condenser plays important role in efficient operation of the system. In order to improve the performance of condenser it is required to elaborate thermal analysis for different mass flows and temperatures. In this article different power of condenser in regard to various mass flows and the temperatures on the heat pipe of condenser are investigated.

### 2. Condenser design

In this section, the heat power and pressure drop of condenser are calculated. The investigated system consists of the condenser (see Fig. 1). Condenser is placed on the heating zone of heat pipe and is used for efficient heat transfer from one medium to another. The water is used as a working fluid in the heat pipe and in the condenser is used thermal oil as cooling medium which is pumped through the connection (see Fig. 1).

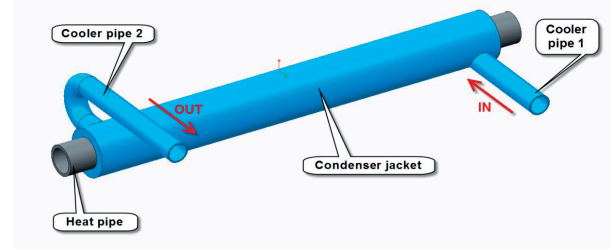


Fig. 1 Heat pipe condenser

The main objective of this work was to identify the pressure build-up in the condenser (dP), the outlet temperature of the thermal oil ( $T_{out}$ ) and the output effect (quantity kW added to the thermal oil).

This task was done for the different temperatures on the heat pipe 100°C -150°C -200°C -250°C -300°C (the temperature was constant over the whole surface), with flow 10-20-30-40 g/s of thermal oil, with the fixed inlet temperature of 80°C. The aim of

\* <sup>1</sup>Radovan Nosek, <sup>1</sup>Stanislav Gavlas, <sup>1</sup>Richard Lenhard, <sup>2</sup>Veroslav Sedlak, <sup>2</sup>Havard Mollerhagen Arvesen  
<sup>1</sup>Department of Power Engineering, Faculty of Mechanical Engineering, University of Zilina, Slovakia  
<sup>2</sup>Goodtech Recovery Technology AS, Norway  
 E-mail: radovan.nosek@fstroj.uniza.sk

the task is to design stationary simulation of the heat exchanger to cool the condenser of the heat pipe.

### 3. CFD Modelling

Computer modelling reduces the total effort required in the experiment design and data acquisition. Numerical simulation of this case was used in order to predict fluid flow, heat transfer and pressure over the condenser.

#### Physical model

The 3D model of a heat exchanger was created based on the drawings and subsequently was modified to be able to use simulations in finite volume. Calculated model consists of a heated finned tube, jacket and oil (see Fig. 2).

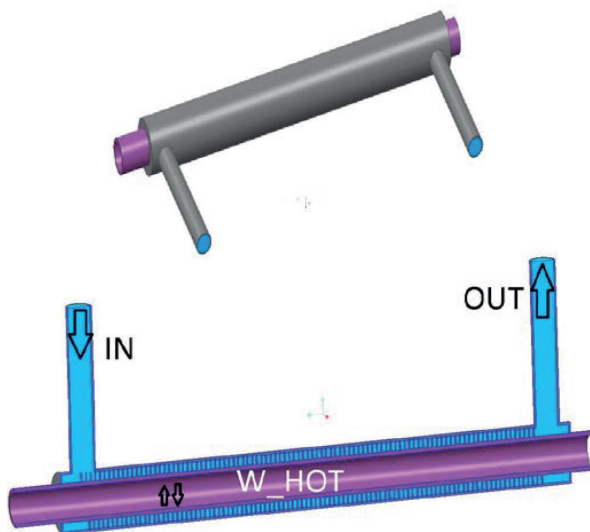


Fig. 2 Heat pipe condenser- cross section

Thermal oil is pumped in through the connection and then it spins around the heat pipe via the three parallel tracks before it comes out again through the second connection.

The most important part of the work was the determination of the detailed boundary conditions. In Table 1 are boundary conditions that were set at the inlet of condenser.

#### Boundary conditions

Name	Type	Set parameters		
		Mass flow (kg.s <sup>-1</sup> )	Temperature (°C)	Turbulence (%)
IN	Mass-flow-inlet	0.01 - 0.04	80	10
OUT	Pressure-outlet	-	-	10
Surface of the heat pipe	Wall	-	100 - 300	-

### 4. Analysis of results

In this section are presented results of numerical solution for the heat pipe condenser. In Fig. 3 is shown a position of the line where the output temperatures were calculated. This line is situated in the middle of distance between the jacket and heat pipe. In this point average values of temperature and pressure were calculated.

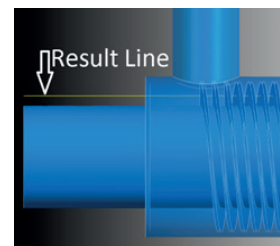


Fig. 3 Position of the result line

#### Results of case No. 1:

- Numerical simulations for mass flow of thermal oil 0.01 kg.s<sup>-1</sup>;
- Temperature on the heat pipe was set as follows: 100°C - 150°C - 200°C - 250°C - 300°C.

In Table 2 are presented results of five different simulations for following parameters:

- Output temperature of the thermal oil (Tout)
- Heat power of the condenser (Q)
- Differential pressure over the condenser (dP)

Case 1

Table 2

Parameter	Mass flow	Tin		dP
	kg.s <sup>-1</sup>	80	°C	
0.01	0.01	80	°C	
Units	T - Heat Pipe	Tout	Q	dP
	°C	°C	W	Pa
1	100	97	386	6718
2	150	140	1371	4972
3	200	182	2455	4043
4	250	224	3633	3282
5	300	266	4920	2658

The purpose of this section is to evaluate effect of different temperatures on the heat pipe to the output temperature of the thermal oil. Figure 4 shows the dependence of temperatures on the length of the condenser.

Table 1

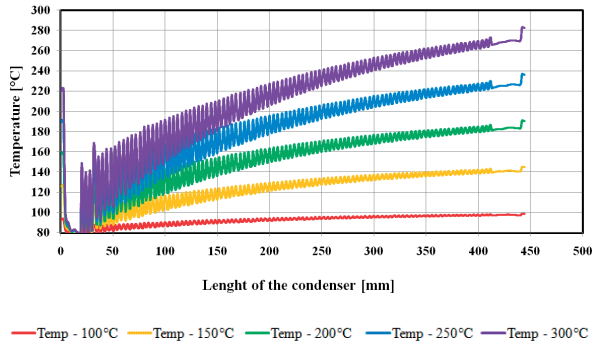


Fig. 4 Temperature dependence over the length of the condenser - Mass flow  $0.01 \text{ kg.s}^{-1}$

Results of case No. 2:

- Numerical simulations for mass flow of thermal oil  $0.02 \text{ kg.s}^{-1}$ ;
- Temperature on the heat pipe was set as follows:  $100^\circ\text{C}$  -  $150^\circ\text{C}$  -  $200^\circ\text{C}$  -  $250^\circ\text{C}$  -  $300^\circ\text{C}$ .

Table 3 presents results of numerical simulations for the condenser.

Case 2

Table 3

Mass flow		Tin		
<b>0.02</b>	$\text{kg.s}^{-1}$	80	$^\circ\text{C}$	
Parameter	T - Heat Pipe	Tout	Q	dP
Units	$^\circ\text{C}$	$^\circ\text{C}$	W	Pa
1	100	93	591	17189
2	150	127	2134	14061
3	200	161	3797	11820
4	250	194	5609	9893
5	300	229	7526	8492

This section presents distribution of temperature on the length of the condenser with flow  $0.02 \text{ kg.s}^{-1}$  of thermal oil.

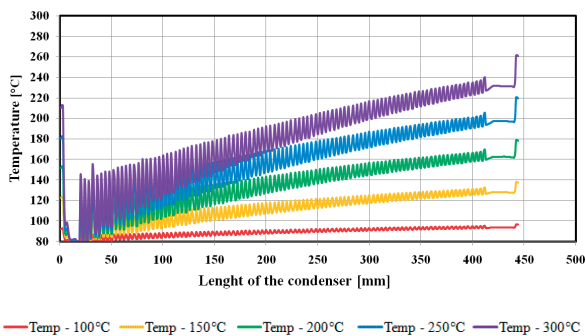


Fig. 5 Temperature dependence over the length of the condenser - Mass flow  $0.02 \text{ kg.s}^{-1}$

Figure 5 compares the predicted effect of temperature on the heat pipe to the output temperature at the condenser.

Results of case No. 3:

- Numerical simulations for mass flow of thermal oil  $0.03 \text{ kg.s}^{-1}$ .
- Temperature on the heat pipe was set as follows:  $100^\circ\text{C}$  -  $150^\circ\text{C}$  -  $200^\circ\text{C}$  -  $250^\circ\text{C}$  -  $300^\circ\text{C}$ .

Table 4 presents results of numerical simulations for the condenser.

Case 3

Table 4

Mass flow		Tin		
<b>0.03</b>	$\text{kg.s}^{-1}$	80	$^\circ\text{C}$	
Parameter	T - Heat Pipe	Tout	Q	dP
Units	$^\circ\text{C}$	$^\circ\text{C}$	W	Pa
1	100	91	732	30483
2	150	119	2655	25725
3	200	148	4723	21476
4	250	177	6917	18576
5	300	205	9232	16243

This section presents distribution of temperature on the length of the condenser with flow  $0.03 \text{ kg.s}^{-1}$  of thermal oil.

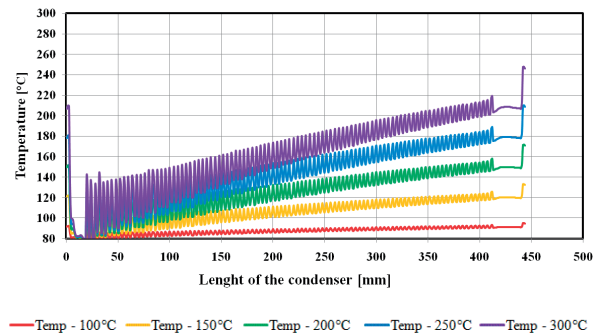


Fig. 6 Temperature dependence over the length of the condenser - Mass flow  $0.03 \text{ kg.s}^{-1}$

The purple curve (temperature on the heat pipe -  $300^\circ\text{C}$ ) presents the maximum difference between temperature at the inlet and outlet (Fig. 6).

Results of case No. 4:

- Numerical simulations for mass flow of thermal oil  $0.04 \text{ kg.s}^{-1}$ .
- Temperature on the heat pipe was set as follows:  $100^\circ\text{C}$  -  $150^\circ\text{C}$  -  $200^\circ\text{C}$  -  $250^\circ\text{C}$  -  $300^\circ\text{C}$ .

Table 5 presents results of numerical simulations for the condenser.

Case 4

Table 5

Mass flow		Tin		Parameter	T - Heat Pipe	Tout	Q	dP
0.04	kg.s <sup>-1</sup>	80	°C					
Units	°C	°C	W	Pa				
1	100	90	847	45112				
2	150	114	3066	38492				
3	200	139	5435	32396				
4	250	164	7906	28600				
5	300	188	10509	25440				

This section presents distribution of temperature on the length of the condenser with flow 0.04 kg.s<sup>-1</sup> of thermal oil.

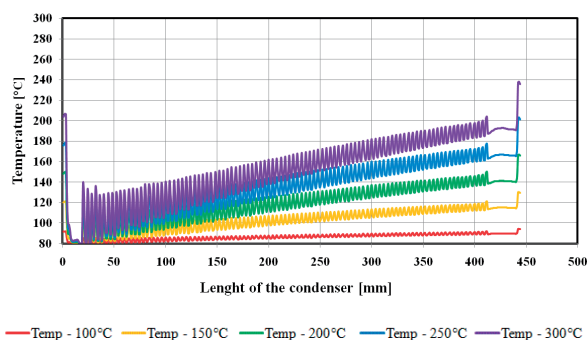


Fig. 7 Temperature dependence over the length of the condenser - Mass flow 0.04 kg.s<sup>-1</sup>

The purple curve (temperature on the heat pipe - 300°C) presents the highest difference between temperature at the inlet and outlet (Fig. 7). In this case the highest heat power of condenser was also calculated.

### 5. Summary

The aim of this work was to analyse the pressure build-up in the condenser and thermal power of the condenser for different temperatures on the heat pipe. Figures 8 and 9 show the dependence of the thermal power and the pressure differences of condenser for different flows.

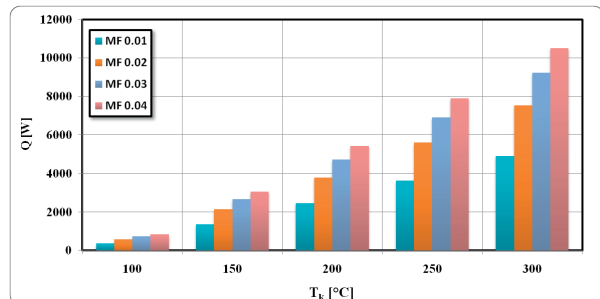


Fig. 8 Thermal power of condenser for different Mass flows (MF)

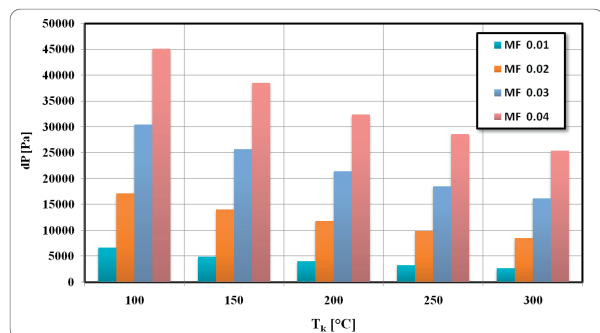


Fig. 9 Differential pressure over the condenser for different Mass flows (MF)

### 6. Conclusion

Calculated data were compared and following conclusions were reached. The highest thermal power of condenser was observed in case No. 4 (mass flow 0.04 kg.s<sup>-1</sup> and temperature on the heat pipe 300°C). The lowest differential pressure over the condenser was noticed in case No. 1 (mass flow 0.01 kg.s<sup>-1</sup> and temperature on the heat pipe 300°C)

In the case of differential pressure the pressure drop is observed with the increase of temperature. When the flow of thermal oil increases, the condenser reaches higher heat performance. This effect can be very well observed when the temperature on the heat pipe is 300 °C. At a flow rate 0.01 kg.s<sup>-1</sup> only half of heat power is achieved in comparison with the flow 0.04 kg.s<sup>-1</sup>.

### Acknowledgements

This work is supported by the financial assistance of the company Goodtech Recovery Technology AS.

This article is supported by the financial assistance of the project VEGA No. 1/1353/12.

The research is supported by European regional development fund and Slovak state budget by the project Research centre of University of Zilina, ITMS 26220220183.

**References**

- [1] JEBRAIL, F. F., ANDREWS, M. J.: *Energy Research*, 21, 101-112, (1998).
- [2] HOLUBCIK, M., HUZVAR, J., JANDACKA J.: *Combined Production of Heat and Electricity with Use of Micro Cogeneration*, IN-TECH 2011 - proc. of intern. conference on innovative technologies, Bratislava, Slovakia. - [S.l.]: Jan Kudlacek, 2011. ISBN 978-80-904502-6-4. - S. 200-202.
- [3] HUZVAR, J., KAPJOR, A.: *Micro-cogeneration Incl. the Conversion of Chemical Energy of Biomass to Electric Energy and the Low Potential Heat*, vol. 1337, 2011, 40-42, 4<sup>th</sup> Global Conference on Power Control and Optimization, Sarawak.
- [4] LENHARD, R., MALCHO, M.: Numerical Simulation Device for the Transport of Geothermal Heat with Forced Circulation of Media. *Mathematical and Computer Modelling*, vol. 57, No. 1-2, 111-125, 2013, ISSN 0895-7177.
- [5] NEMEC P., CAJA A., MALCHO M.: Mathematical Model for Heat Transfer Limitations of Heat Pipe, *Mathematical and Computer Modelling*, vol. 57, 1-2, 2013, 126-136.
- [6] PILAT, P., PATSCH, M., MALCHO, M.: *Solar Heat Utilization for Adsorption Cooling Device*, vol. 25, Article No. 01074, Conference on Experimental Fluid Mechanics, EFM 2011, Jicin, 2012.
- [7] SCHMALHOFER, J., FAGHRI, A.: *Heat Mass Transfer*, 36, 201-212, 1993.

Lubos Kucera - Tomas Gajdosik - Jan Bucala \*

## THE VIBRODIAGNOSTICS OF DAMAGED GEARS OF PLANETARY GEARBOXES

*This article deals with description of a diagnostic device used at the Department of Design and Machine Elements at the University of Zilina which has been built in order to measure, diagnose and evaluate gearbox faults by vibrodiagnostics. The article describes methods and damage creation process for tested gearboxes. Evaluation of different faults is also processed in this article as well as description of comparative measurements between real and artificially created pitting. Comparison of all measured data with SPM methods is also included.*

**Keywords:** Vibrodiagnostics, frequency, spectrum, damage.

### 1. Introduction

The Vibrodiagnostics is considered to be one of most progressive maintenance methods. It offers possibilities to diagnose status and conditions of devices while they are fully operational [1]. The testing device has been constructed at the Department of Design and Machine Elements in order to measure and evaluate faults of components by analysing frequency spectra of gearboxes (Fig. 1). Laboratory research primarily aims at diagnostics of damaged gears of planetary gearboxes.

The testing device consists of one 15 kW electromotor controlled by a phase shifter, two planetary gearboxes type A2000 mounted in series and also one dynamometer. Components

are coupled together by cardan shafts. The testing device is supplemented with noncontact sensors HBM T10F for RMP and torque measurement. Gearbox A 2000 is a planetary gearbox with two planetary gearings with involute spur gears [2].

The diagnostic apparatus was purchased from SKF and it contains six acceleration sensors with sensitivity of 100 mV/g, on-line diagnostic unit type IMx-S and one PC equipped with @plitude analyst software. Both frequency analysis and envelope method for signal processing are used to determine gearbox faults.

Gearbox A2000 was tested for fault response at  $1470 \pm 10$  RPM. Input shaft can rotate both clockwise and anticlockwise according to current needs.

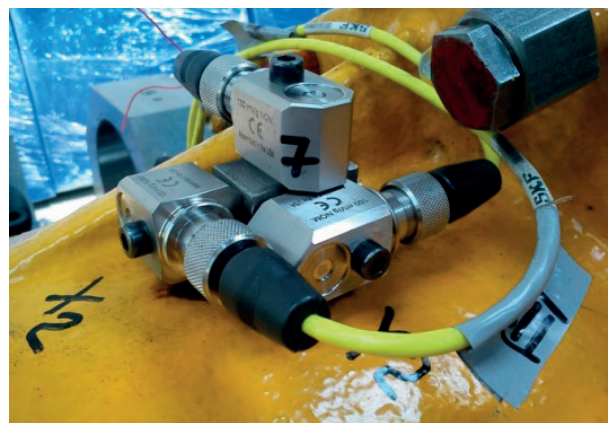


Fig. 1 The testing device used at the Department of Design and Machine Elements for diagnostics of planetary gearboxes' faults (left) and placement of vibration sensors (right)

\* Lubos Kucera, Tomas Gajdosik, Jan Bucala

Department of Design and Machine Elements, Faculty of Mechanical Engineering, University of Zilina, Slovakia  
E-mail: lubos.kucera@fstroj.uniza.sk

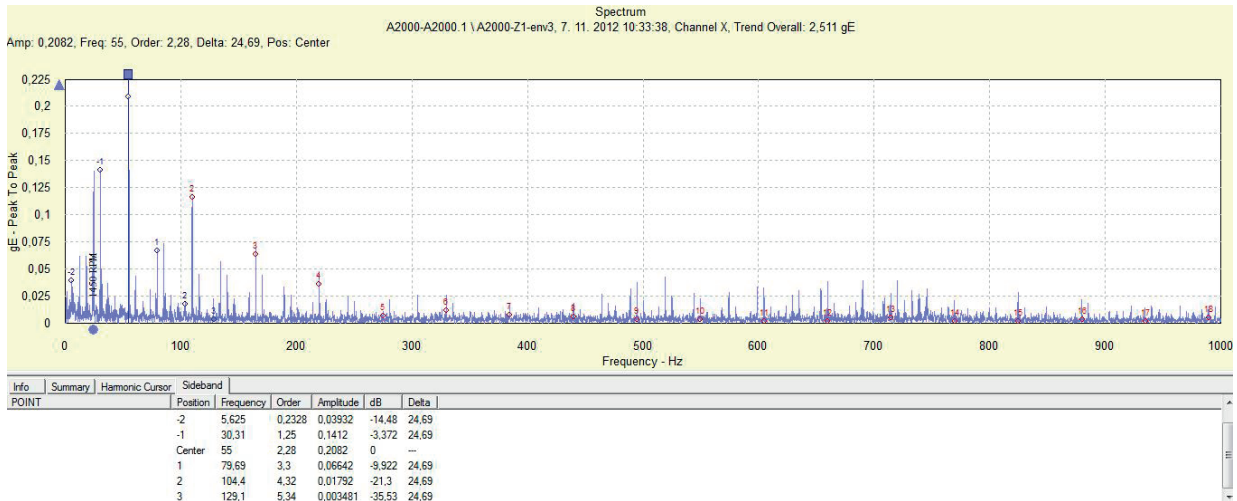


Fig. 2 The frequency spectrum of enveloped accelerations filter 3 for tooth of the sun gear damaged by the notch on its face area

Preliminary measurements of undamaged gearboxes needed to be done first in order to indicate key frequencies in spectrum of undamaged gearbox. Some components of gearboxes were artificially damaged later.

## 2. Measurements of gears with teeth damaged by pitting

The sun gear of the first planetary gearing was first to be damaged. First type of damage is represented by the notch on face area of one tooth. This damage was done with assumption of significant response within frequency spectrum. The damage can be seen in vibrations velocity spectrum by analysing sideband of gear mesh frequency of the first planetary gearing, because first amplitudes significantly surpassed magnitude of gear mesh frequency. Its effect was even more significant in enveloped

accelerations spectrum filter 3 (Fig. 2). Frequency 55 Hz of damaged sun gear dominated throughout spectrum and its harmonic frequencies showed up (marked as red). Sideband was created around gear frequency with the delta equal to RPM frequency 24.69 Hz of damaged gear (marked as blue). Sideband can be clearly seen in vicinity of its harmonic frequency [3].

Small pitting was created on the opposite side of already damaged tooth after first fault simulated by the notch was evaluated. This type of fault showed similar effect when compared to tooth damaged by the notch in vibrations velocity spectrum, however amplitudes of sideband were not as significant. Fault effect in enveloped accelerations spectrum filter 3 also showed similar results as before and once again amplitude of the gear frequency of the damaged gear was significant, but values were lower when compared to those of tooth damaged by single notch [4] - [7]. Its harmonic frequencies were not as significant; however 2<sup>nd</sup>, 3<sup>rd</sup> and 4<sup>th</sup> harmonic frequency is clearly visible.

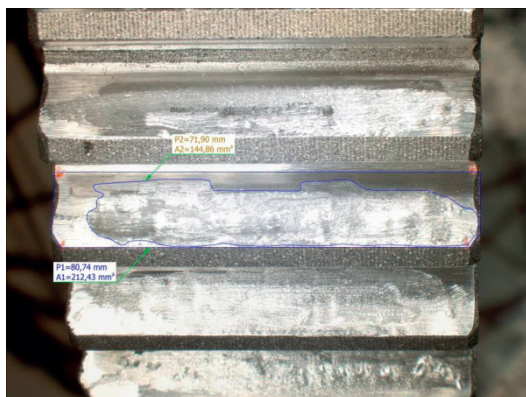


Fig. 3 Sun gear of planetary gearing damaged by artificially created pitting (left) and sun gear damaged by real pitting (right)

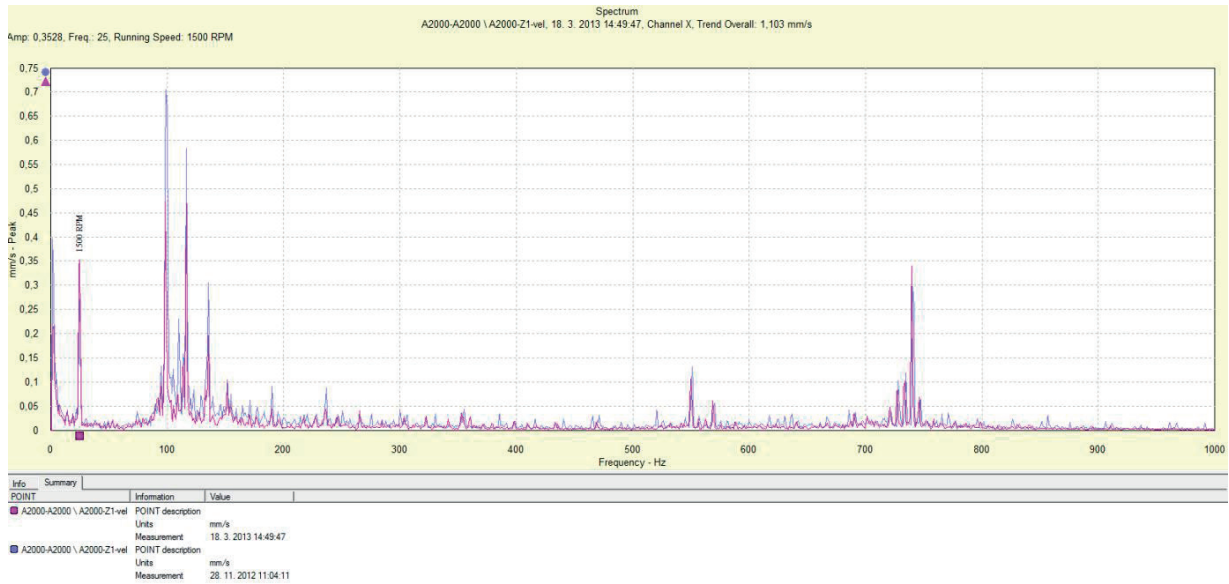


Fig. 4 The comparison of frequency spectra of gearbox with sun gear damaged by artificially created pitting on half of gear's teeth (blue) and sun gear damaged by real pitting (violet)

Pitting was created on every single tooth of the sun gear as experiments continued. Significant change occurred in vibrations velocity spectrum where one more sideband appeared with the delta equal to gear mesh frequency of damaged gear alongside regular gear mesh frequency of first planetary gearing. 2<sup>nd</sup> and 3<sup>rd</sup> harmonic frequency of gear mesh frequency also showed up (Fig. 4). Fault effect in enveloped accelerations spectrum filter 3 was similar to previous faults. Values of amplitude however increased greatly and amplitude of gear mesh frequency of the gear damaged by pitting on every tooth rose by 2100% when compared to the gear damaged by pitting only on one tooth.

In order to compare all measured data, another experiment with artificially created pitting on half of gear's teeth (on the same face

area as damaged by the notch) took place (Fig. 3 left). Artificially damaged sun gear was replaced by another sun gear damaged by real pitting on half of gear's teeth (Fig. 3 right). After both spectra were measured and frequency spectra were compared, we came to the conclusion that artificially created pitting has very similar effect when compared to real pitting (Fig. 4). This comparison confirmed that measured data match reality and test method was suitable for this application as well [8] and [9].

Vibrations velocity frequency spectra with different pitting affected area of the sun gear of the first planetary gearing can be seen in Fig. 5. The upper part of spectra represents only one tooth damaged by pitting, middle part corresponds to all teeth damaged by pitting and lower part represents the gear damaged on half

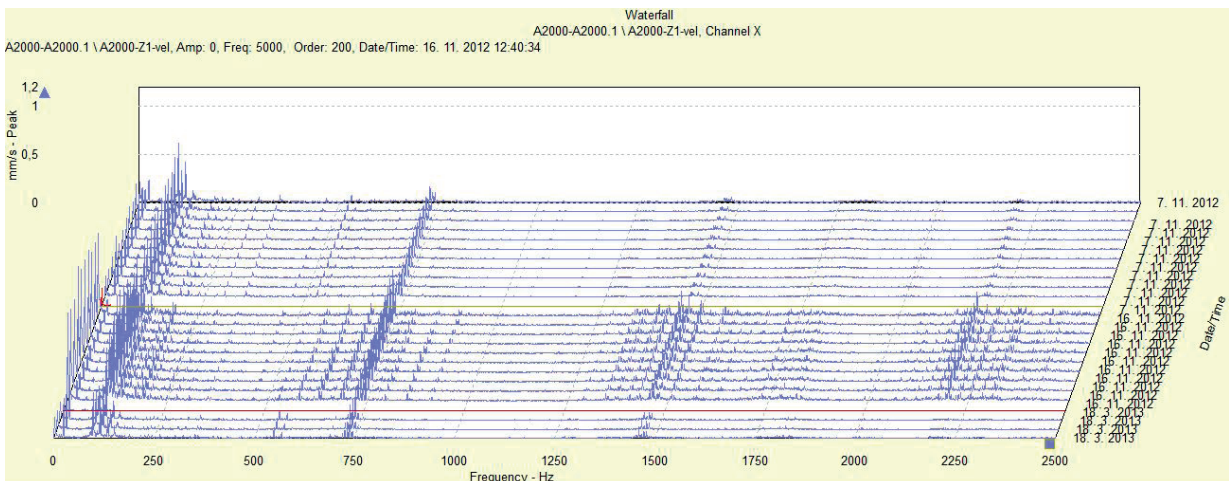


Fig. 5 Frequency spectrum of velocity of vibrations with differently damaged sun gears of first planetary gearing by pitting

of its teeth by real pitting. Straight lines between measurements reflect time when the testing device was offline.

### 3. Measurements of gears with teeth damaged by breaking

Another phase involved sun gear with one tooth partially broken and later with whole missing tooth. Measurements were made on gears which were previously damaged by pitting on half of their teeth (Fig. 6).

There was no significant change in vibrations velocity spectrum (Fig. 7) compared to the sun gear damaged by pitting on half of its teeth [10]. Enveloped accelerations spectrum filter 3 - from 5 Hz to 1kHz (Fig. 8) also had similar characteristic compared to same sun gear with no missing teeth, but amplitude

of gear mesh frequency and its harmonic frequencies had higher values compared to pitting damaged sun gear.

### 4. Comparative measurements of two different methods

Comparative measurements were made in cooperation with vibrodiagnostic specialists from SPM Instrument s.r.o. SPM HD and SPM Spectrum methods were used to examine current status of the gearbox. The gearbox was damaged by missing tooth and pitting on the sun gear and notch type damage was made on the satellite gear.

Frequency spectrum measured by SPM HD method is shown in Fig. 9. Teeth frequency of damaged gear (54.976 Hz) and its harmonic frequencies within spectrum are marked by numbers. Figure 10 contains data measured by enveloped accelerations method filter 3 where teeth frequency (55 Hz) and its harmonic frequencies of damaged gear are also marked by numbers. Spectra



Fig. 6 Sun gear with one missing tooth

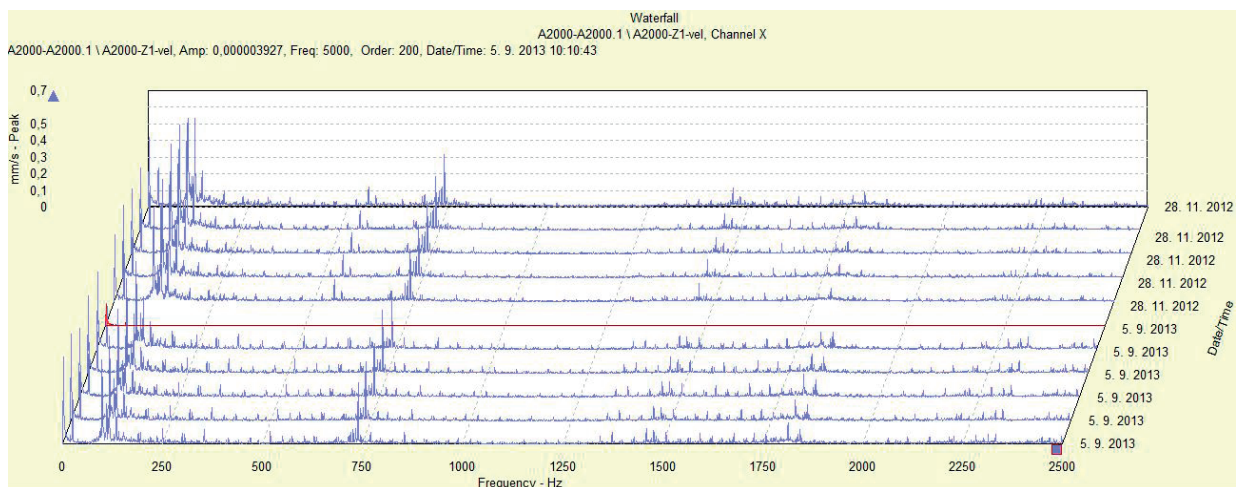


Fig. 7 The comparison of frequency spectra of vibrations for pitting created on half of teeth of sun gear (upper part) and for gear damaged by same pitting with one missing tooth (lower part)

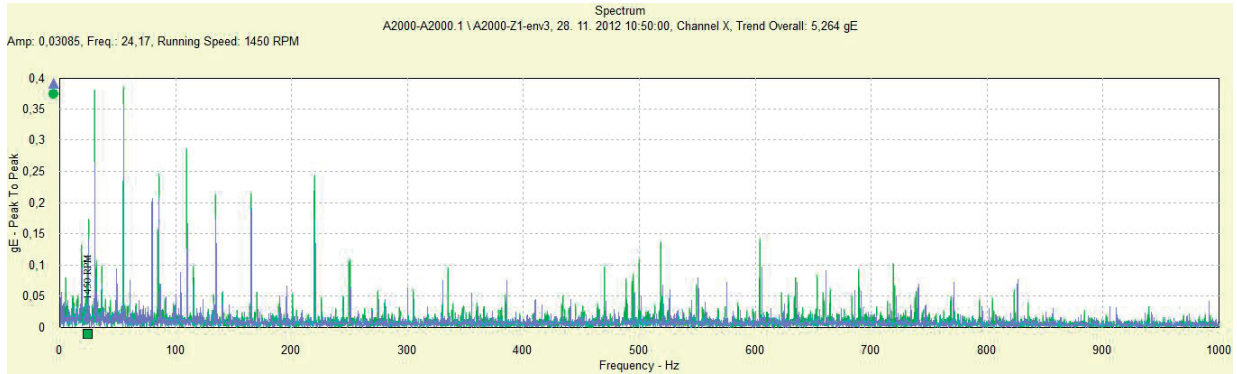


Fig. 8 The comparison of frequency spectra of enveloped acceleration filter 3 for pitting created on half of teeth of sun gear (blue) and for gear damaged by same pitting with one missing tooth (green)

in both figures are very similar with small difference of amplitude magnitude for 6<sup>th</sup>, 7<sup>th</sup> and 8<sup>th</sup> harmonic frequency because these harmonic frequencies have much lower amplitudes with enveloped accelerations method.

Vibrations velocity frequency spectrum obtained by SPM Spectrum method can be seen in Fig. 11. Spectrum's shape is very similar to SKF methods in direct comparison (Fig. 12), difference

is in amplitude magnitudes. Spectra in both figures highlighted amplitudes of sideband with the spacing of teeth frequency of damaged sun gear (55 Hz) and amplitude of sideband of gear mesh frequency of the first planetary gearing which has high value of amplitude dominating through whole spectrum.

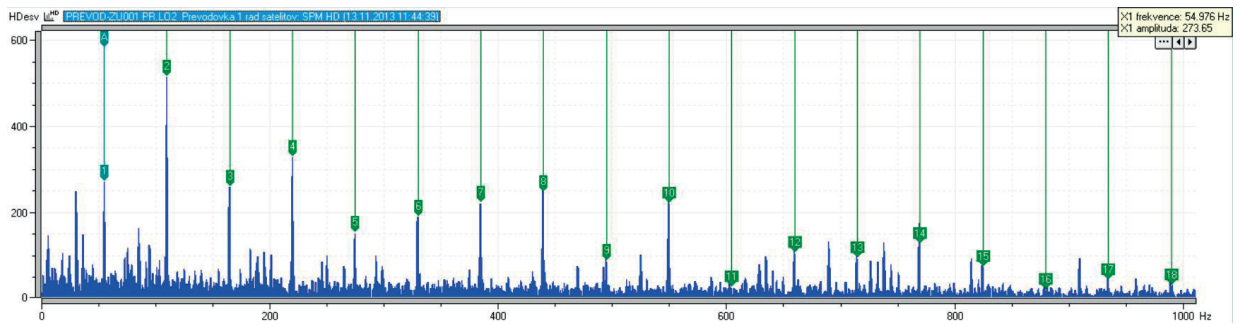


Fig. 9 Frequency spectrum measured by SPM HD method

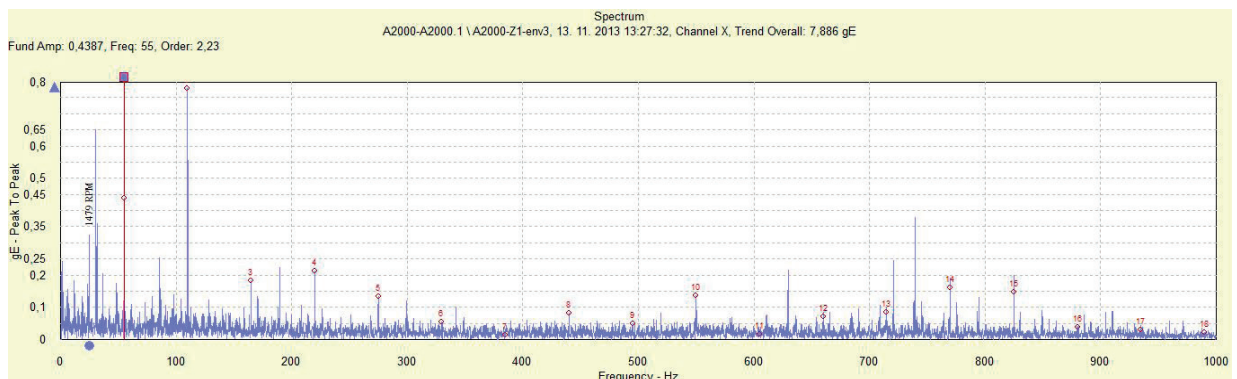


Fig. 10 Frequency spectrum measured by enveloped accelerations method (SKF)

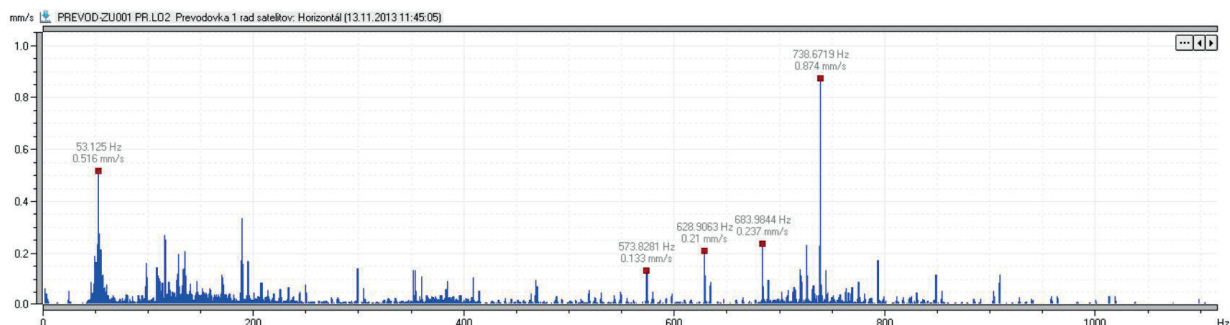


Fig. 11 Frequency spectrum of vibrations velocity measured by SPM Spectrum method

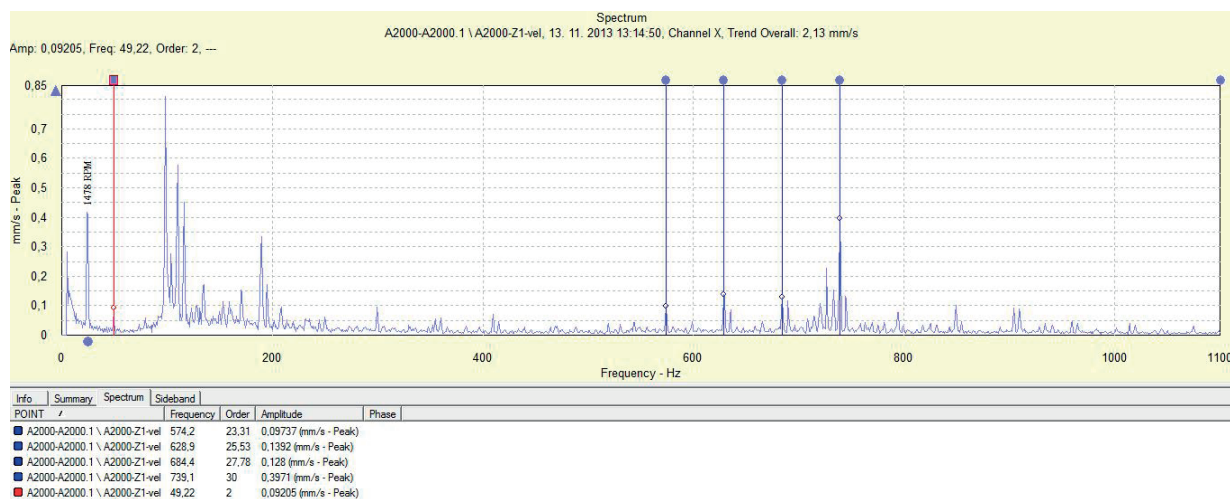


Fig. 12 Frequency spectrum of vibrations velocity measured by SKF diagnostic methods

It is necessary to mention that influence of damaged planet gear has not been detected either in vibrations velocity spectrum or in enveloped accelerations spectrum [11], [12] and [13].

### 5. Conclusion

Measurements we made so far clearly show artificially developed faults of the sun gear in high frequency vibrations velocity spectrum and enveloped accelerations spectrum for given

gearbox correspond to vibration responses of faults developed under real conditions for same gearbox and, therefore, confirm used methods of measurements. Similarity of SKF and SPM methods was proved by comparing both results. Effects of faults are also similar although technology for signal processing differs significantly between these two methods.

This article was created with support of Slovak Research and Development Agency (SRDA) based on agreement No. SUSPP-001409 and under project No. APVV 087-10: "Intelligent diagnostic systems of gearboxes and their components".

### References

- [1] PRODAJ, J.: *Applications and Diagnosis of Selected Nodes of Stationary and Mobile Gear System (in Slovak)*, Dissertation thesis, Zilina, 2012.
- [2] GAJDOSIK, T., BUCALA, J., KOVALICEK, M.: *Vibrodiagnostic of Gearboxes*, Proc. of intern. conference Transcom 2013, Zilina, 2013.
- [3] KUCERA, L., GAJDOSIK, T.: *The Vibrodiagnostic of Gears*, 54<sup>th</sup> Intern. conference of machine design departments, September 2013, Hejnice: Liberec: Technical university, 93-98, 2013. ISBN 978-80-7372-986-8.

- [4] SAPIETA, M., STEVKA, O., DEKYS, V.: Localization Luders Band in Infrared Spectrum, *Applied Mechanics and Materials*, vol. 420, 2013, 194-201, ISSN 1660-9336.
- [5] DEKYS, V., DVOULETY, O.: A Contribution to the Condition Monitoring of Fans, *Zeszyty naukowe Politechniki Slaskiej: Transport*, z. 76, No. 1865, 2012, 49-56. ISSN 0209-3324.
- [6] DEKYS, V., SAGA, M., ZMINDAK, M.: *Damage Detection Based on Dynamic Measurements*, New methods of damage and failure analysis of structural parts, September, 2012, Ostrava: Technicka univerzita, 41-49, ISBN 978-80-248-2802-2.
- [7] VASKO, M., SAGA, M., DEKYS, V.: *Contribution to Numerical Analysis of Uncertain Mechanical Systems Using Probability and Possibility Theory*, Advances in mechanisms design, Proc. of TMM 2012, Dordrecht: Springer Science+Business Media, ISBN 978-94-007-5124-8, (Mechanisms and machine science, vol. 8, 263-269. ISSN 2211-0984).
- [8] KOPAS, P., SAGA, M., UHRICIK, M.: Contribution to Multiaxial Damage Calculation Using FEM, *Applied Mechanics and Materials*, vol. 420, 2013, 318-324. ISSN 1660-9336.
- [9] NEMECEK, M., DEJL, Z.: *Geometric Calculations of the Chamfered Tip and the Protuberance Undercut of a Tooth Profile* (Conference Paper), ASME 2011 Intern. Design Engineering Technical Conferences on Computers and Information in Engineering Conference, IDETC/CIE 2011, Washington: DC, August 2011; Code 91020.
- [10] NEMECEK, M.: *Problems with the Design of Internal Gearing with Extreme Parameters* (Conference Paper), 2007, Proc. of the ASME International Design Engineering Technical Conferences and Computers and Information in Engineering Conference, DETC2007, vol. 7, 2008, 199-206, 10<sup>th</sup> Intern. Power Transmission and Gearing Conference, presented at 2007 ASME International Design Engineering Technical Conferences and Computers and Information in Engineering Conference, IDETC/CIE2007; Las Vegas, NV, September 2007, Code 72172.
- [11] KOHAR, R., HRCEK, S.: *Dynamic Analysis of Rolling Bearings with Elastic Cage*, Proc. of 54<sup>th</sup> intern. Conference of Machine Design Departments, 211-216, September 2013, Hejnice: Liberec: Technical university, 2013. ISBN 978-80-7372-986-8.
- [12] KOHAR, R., HRCEK, S., MEDVECKY, S.: Usage of Dynamic Analysis to Determine Force Interactions between Components of Rolling Bearings, *Communications - Scientific Letters of the University of Zilina*, vol. 14, No. 3, 2012, 62-67. ISSN 1335-4205.
- [13] HRCEK, S., KOHAR, R., MEDVECKY, S.: Determination of the Maximum Roller bearing Load with Regards to Durability thereof using FEM Analysis, *Communications - Scientific Letters of the University of Zilina*, vol. 14, No. 3, 2012, 55-61. ISSN 1335-4205.

Robert Kohar - Slavomir Hreck \*

## DYNAMIC ANALYSIS OF A ROLLING BEARING CAGE WITH RESPECT TO THE ELASTIC PROPERTIES OF THE CAGE FOR THE AXIAL AND RADIAL LOAD CASES

*The aim of this paper is to detail the creation of a large tapered roller bearing model with flexible body cages in the Adams program suite for subsequent dynamic analysis and to obtain information about kinematic and dynamic relationships of steel and plastic cages under various operating conditions. The bearing model was made to closely resemble its real-life counterpart, which allows us to estimate load conditions, dynamic conditions of individual bearing parts and interactions between them.*

**Keywords:** Rolling bearing, flexible body, cage, Adams, dynamic.

### 1. Introduction

This article details the creation of a virtual bearing model allowing the analysis of individual bearing components under dynamic behavior. Although inner and outer bearing rings and rollers are defined as solid materials, the bearing cage models also take into account elastic properties thereof. Chapter 2 details the creation of the said models. Two models of tapered roller bearings will be considered: one with steel cage and the other with plastic cage.

### 2. Creation of "Flexible body" cage models

Dynamic simulations of the tapered roller bearing were performed in the MSC.Adams system. Model creation along with definition of material properties, contact parameters, geometric and kinematic boundary conditions is detailed in [1] and [2]. A Modal Neutral File (MNF) file was necessary to take into account flexible properties. The said file contains important information pertaining to inertial and flexible model properties, including information necessary to integrate the flexible model within the virtual prototype in MSC.Adams program [3] and [4].

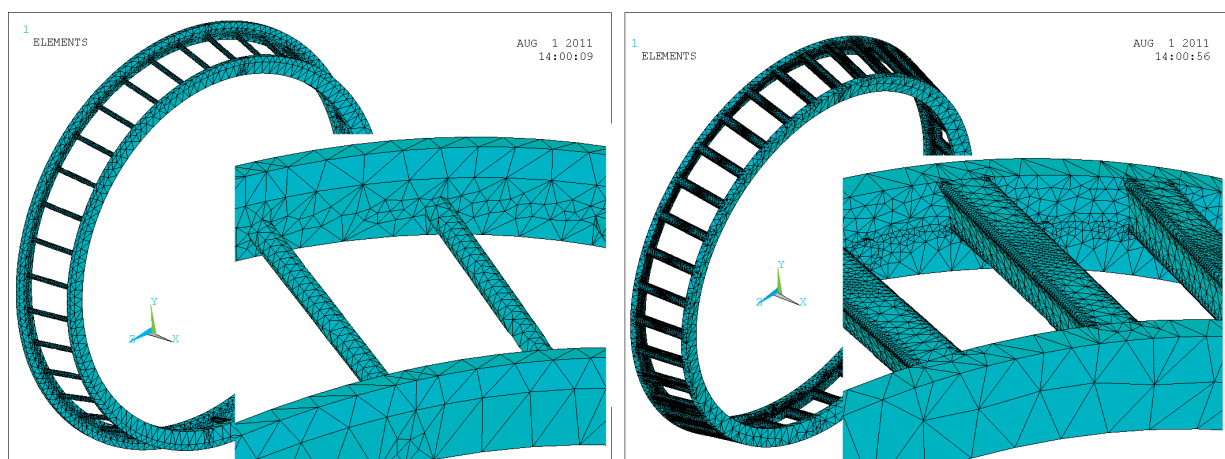


Fig. 1 Finite-element mesh of steel (left) and plastic (right) cage in Ansys program

\* Robert Kohar, Slavomir Hreck

Department of Design and Machine Elements, Faculty of Mechanical Engineering, University of Zilina, Slovakia

E-mail: robert.kohar@fstroj.uniza.sk

The actual MNF file can be created in various FE programs such as Nastran, Ansys or Abaqus [5], [6] and [7].

The flexible cage model was created in FE software Ansys which contains a built-in macro for this purpose. The first step consisted of finite-element mesh creation along with the definition of material properties (Fig. 1, Table 1) [8] and [9].

Material properties of steel and plastic cage Table 1

	Density [kg. mm <sup>-3</sup> ]	Young modulus [MPa]	Poisson constant [-]	Element type	Number of elements
Steel cage	7.85.10 <sup>-6</sup>	2.02.10 <sup>5</sup>	0.29	Solid 187	39105
Plastic cage	1.1.10 <sup>-6</sup>	3000	0.42	Solid 187	259694

After generation of the finite-element mesh and material definition a macro is executed, creating the MNF file which requires the following user input: System of Model Units, Eigenmodes, Element Results, Shell Element Result Output Control, Filename, Solve and create export file to ADAMS.

MNF file analysis and further modification thereof is possible using the MD Adams/Flex Toolkit. The "MNF-MNF Optimizer"

was used to analyze and reduce the complexity of the cage models by removing Internal Solid Element Geometry. An alternative approach is to apply the Mesh Coarsening Algorithm, resulting in reduced element counts and increased calculation speed. However, the mentioned approach also modifies node coordinates, which would invalidate load simulations obtained by dynamic simulations for further analysis in FE programs and was thus not used [10].

The next step after applying the above process consists of integration of "flex body" within MSC.Adams/View modeler. Figure 2 shows the flexible model integration algorithm within the dynamic simulation.

Dynamic simulation results - axial load force  $F_a=518kN$  with rotational speed  $n=15.5rPM$

Dynamic simulation results with axial load force and rotational speed  $n = 15.5 rPM$  represent force interactions between individual bearing parts, movement of bearing cage center of gravity and angular velocity thereof.

Figure 3 shows a comparison of load distribution of individual rollers with theoretical calculations based on [11] and [12], wherein element load  $Q_{max} = 56568 N$ . Results of the dynamic simulation were obtained in time  $t = 10$  seconds.

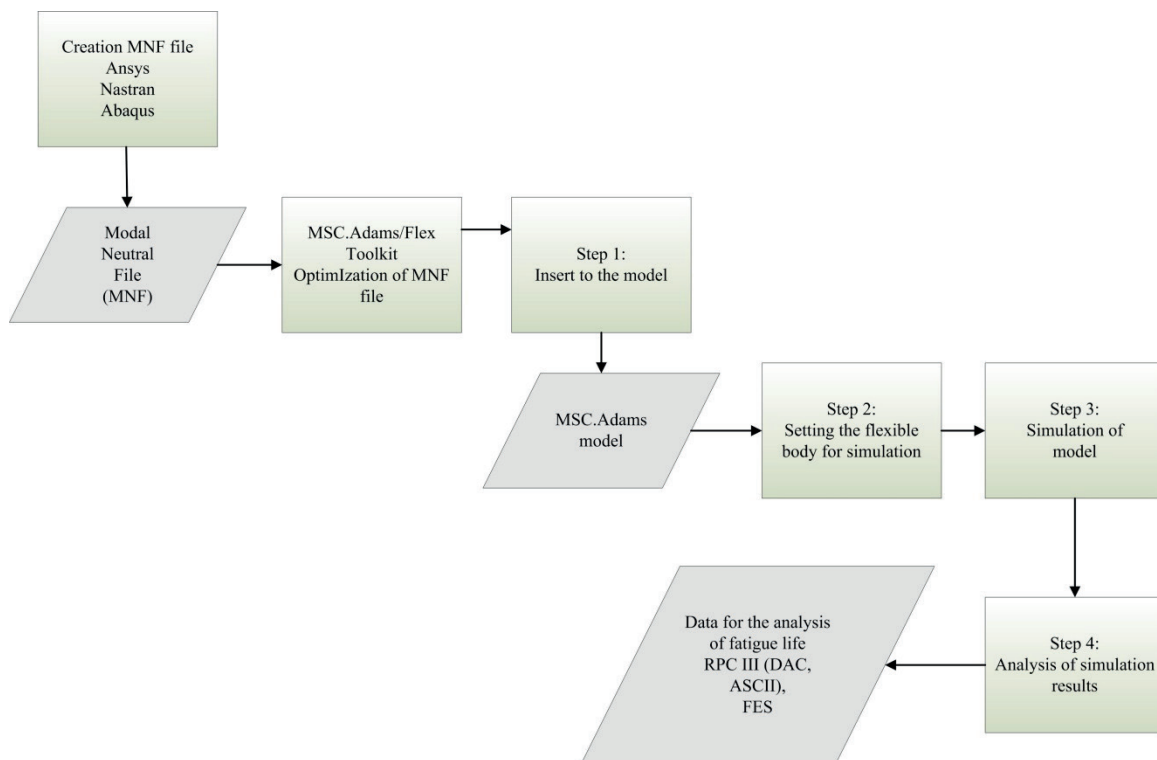


Fig. 2 "Flexible body" integration algorithm within the dynamic simulation

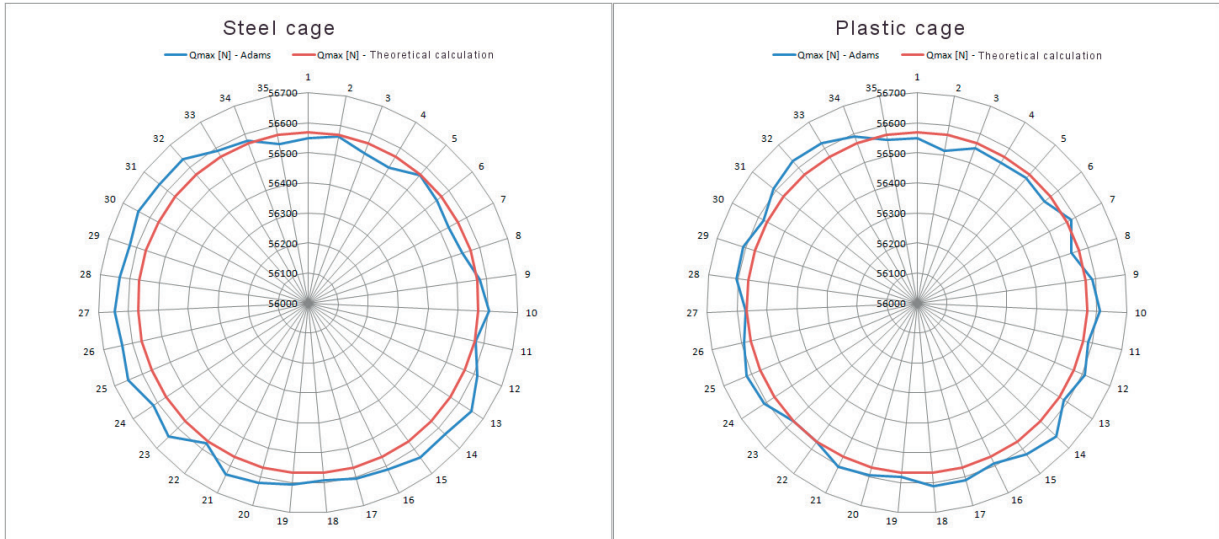


Fig. 3 Load distribution of individual elements compared with theoretical calculations

Figure 4 shows forces between roller and cage, roller and inner ring and angular velocity of this roller. Maximum force between steel cage and rollers was observed during interaction of the cage with roller n.22 and is equal to 686 N (Fig. 4 up, green line). Also shown is the force between inner ring and roller n. 22 (red line) which varied between 54023 N and 58593 N. The blue line displays angular velocity of roller n. 22 and varies between 484°/s and 495°/s.

Maximum force between plastic cage and rollers was observed during interaction of the cage with roller n. 24 and is equal to 301N (Fig. 4 down, green line). Also shown is the force between inner ring and roller n. 24 (red line) which varied between 54273 N and 58571 N. The blue line displays angular velocity of roller n. 24 and varies between 485°/s and 494°/s, similar to the velocity observed for the steel cage.

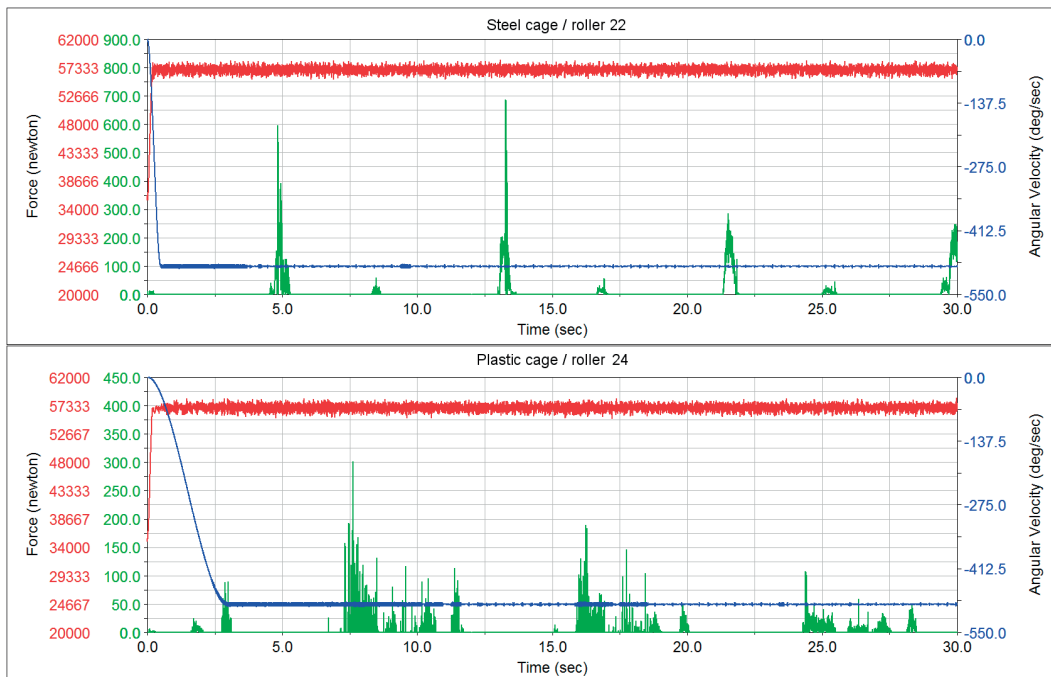


Fig. 4 Force interaction between inner ring and rollers (red lines), force interaction between cage and rollers (green lines) and angular velocity of rollers.

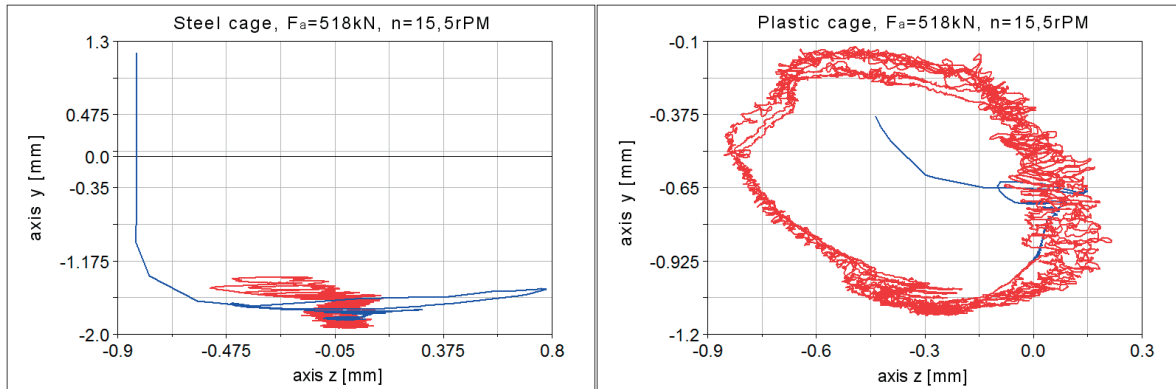


Fig. 5 Movement of center of gravity of steel cage (left side) and plastic cage (right side) in the y-z plane under axial load

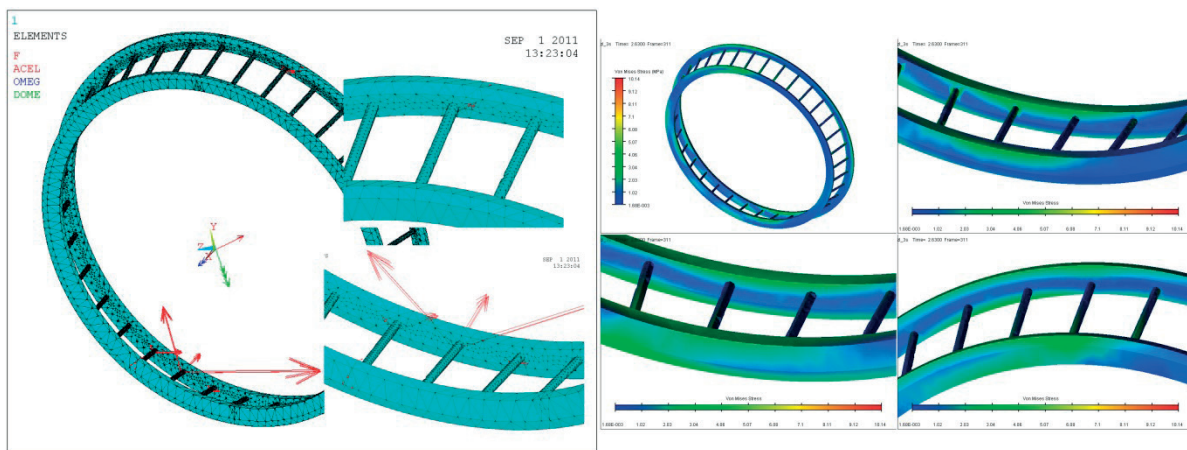


Fig. 6 Force interaction between steel cage and rollers (left side) and maximum von Mises stress of steel cage

Figure 5 shows the center of gravity location in the y-z plane of steel and plastic cage. Fig. 6 shows force interaction between inner ring and rollers and the von Mises stress of steel cage and Fig. 7 shows force interaction between inner ring and rollers and the von Mises stress of plastic cage.

Analysis of dynamic simulation results shows the steel cage is in contact with rollers in lower and upper parts of the bearing, with forces in the upper bearing parts reaching up to 700N at cage guides and 100N at lower parts, also at cage guides. Maximum von Mises stress of 10 MPa was recorded in time  $t = 2.63$  s (Fig. 6).

Dynamic simulation of plastic cage bearing shows similar results to those presented above. The plastic cage is in contact with rollers in lower and upper parts of the bearing. Forces in the lower part of the bearing reach up to 300N at cage guides and up to 50N at upper parts of the bearing cage guide surfaces. Maximum von Mises stress of 0.6 MPa was recorded in time  $t = 16.8$  s (Fig. 7).

Dynamic simulation results - radial load force  $F_r=4500kN$  with rotational speed  $n=15.5$  rpm

Similar to axial load force, we calculated force interactions between individual bearing parts, movement of bearing cage and angular velocity thereof when subjected to radial force.

Figure 8 shows a comparison of load distribution of individual rollers with theoretical calculations based on [3], wherein element load  $Q_{max} = 56499$  N. Results of the dynamic simulation were obtained in time  $t = 10$  seconds.

Figure 9 shows force between roller and cage, roller and inner ring and angular velocity of the roller. Also shown is the force between inner ring and roller n. 13 (red line). Maximum force between steel cage and rollers was observed for roller n. 13 and is equal to 800N (green line). The analysis also showed that highest load rates are present at rollers 10 to 14 during start-up time (2-5 seconds) and are equal to 800N. During subsequent simulation time, the cage was in contact with rollers only when the rollers were off-loaded and maximum force value was equal to 500N. Angular speed was constant ( $489^\circ/s$ ) under applied roller load and lowered under roller load in the 20000N to 70000N range, achieving a minimum value of  $435^\circ/s$  (blue curve).

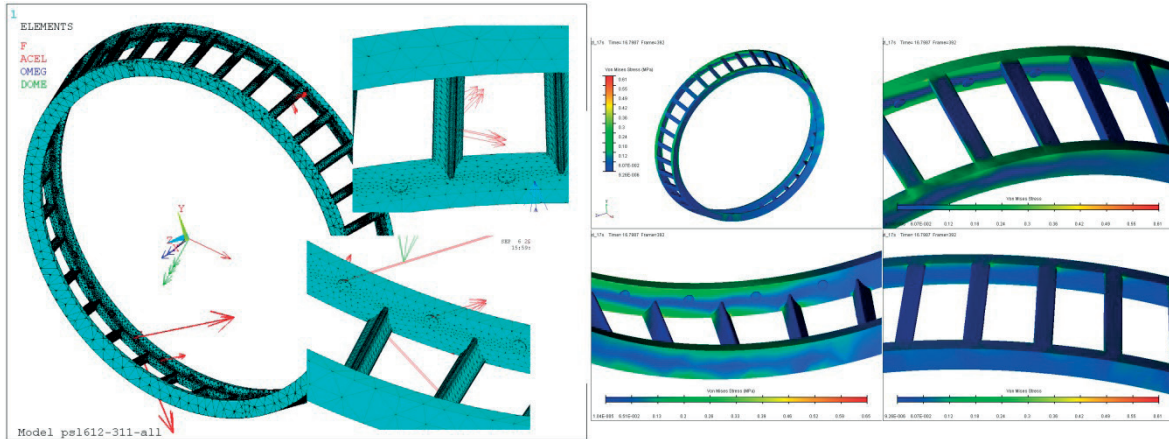


Fig. 7 Force interaction between plastic cage and rollers (left side) and maximum von Mises stress of plastic cage

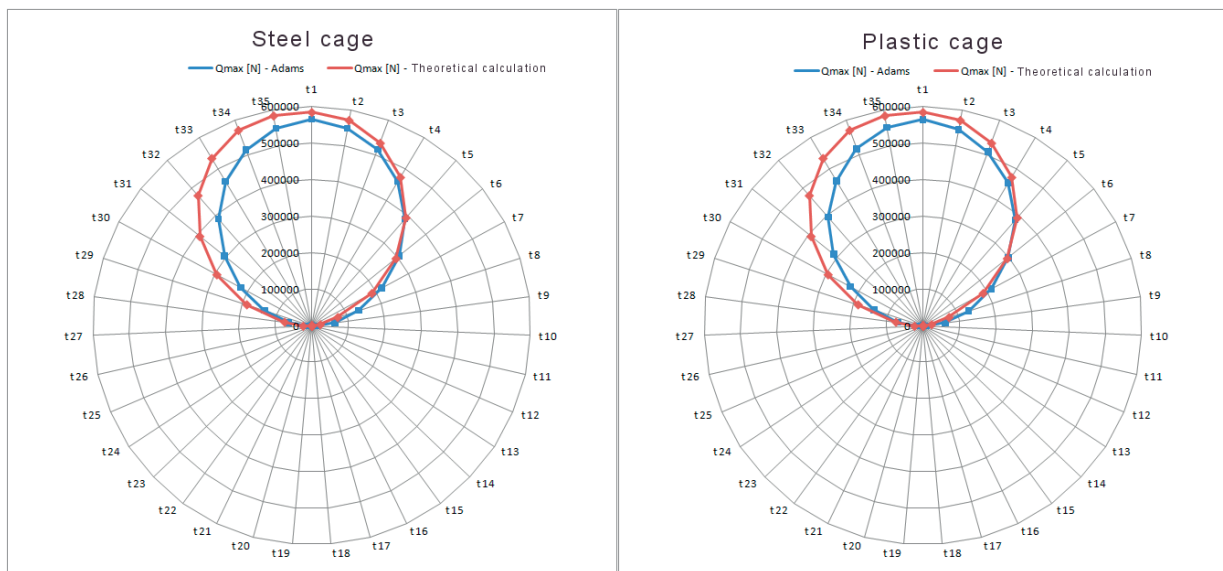


Fig. 8 Load distribution of individual elements compared with theoretical calculations

Figure 9 down shows force between inner ring and roller n. 14 (red line) for bearing with plastic cage. Maximum force between the plastic cage and rollers was observed for roller n.14 and is equal to 691N (green line). Similar to the steel cage, highest load rates were present at rollers 10 to 14 during start-up time (2-5 seconds) and are equal to 700 N. When compared to the steel cage, the rollers were in contact not only in the off-load phase (force equal to 150 N) but also during the load phase, with the force equal to 400 N. Angular speed was constant (489°/s) under applied roller load and, similar to the steel cage, lowered under roller load in the 20000N to 70000N range, achieving a minimum value of 260°/s (blue curve) and zero values under load.

Figure 10 shows the center of gravity location in the y-z plane of steel and plastic cage, Fig. 11 shows force interaction between inner ring and rollers and the von Mises stress of steel cage and

Fig. 12 shows force interaction between inner ring and rollers and the von Mises stress of plastic cage.

Analysis of dynamic simulation results shows the steel cage is in contact with rollers in lower and upper parts of the bearing, with forces in the upper bearing parts reaching up to 800N at cage guides and 500N at lower parts, also at cage guides. Maximum von Mises stress of 14.5 MPa was recorded in time  $t = 3.5$  s (Fig. 11).

Dynamic simulation of plastic cage bearing shows similar results to those presented above. The plastic cage is in contact with rollers in lower and upper parts of the bearing. Forces in the lower part of the bearing reach up to 150N at cage guides and up to 400N at upper parts of the bearing cage guide surfaces. Maximum von Mises stress of 1.5 MPa was recorded in time  $t = 9$  s (Fig. 12).

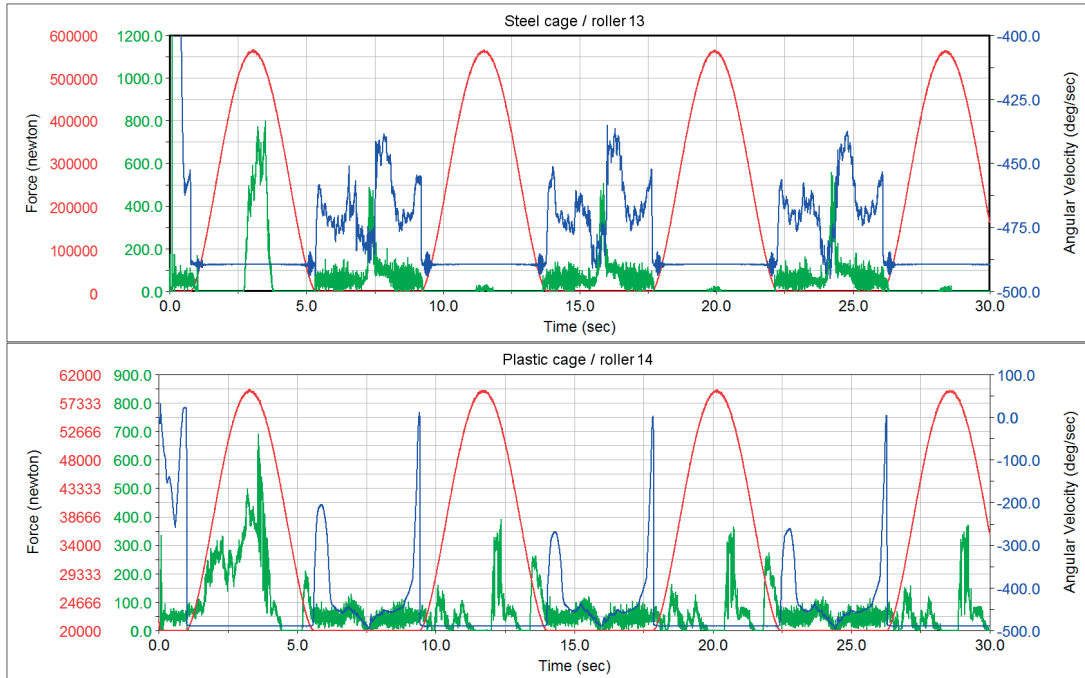


Fig. 9 Force interaction between inner ring and rollers (red lines), force interaction between cage and rollers (green lines), angular velocity of rollers (blue line)

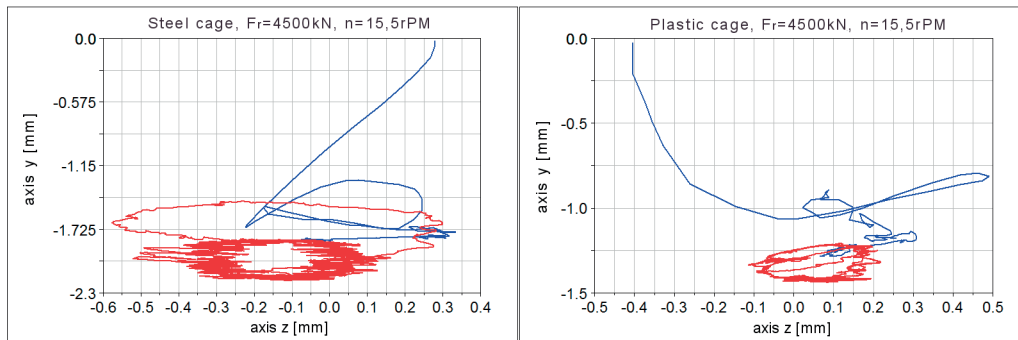


Fig. 10 Movement of center of gravity of steel cage (left side) and plastic cage (right side) in the y-z plane under axial load

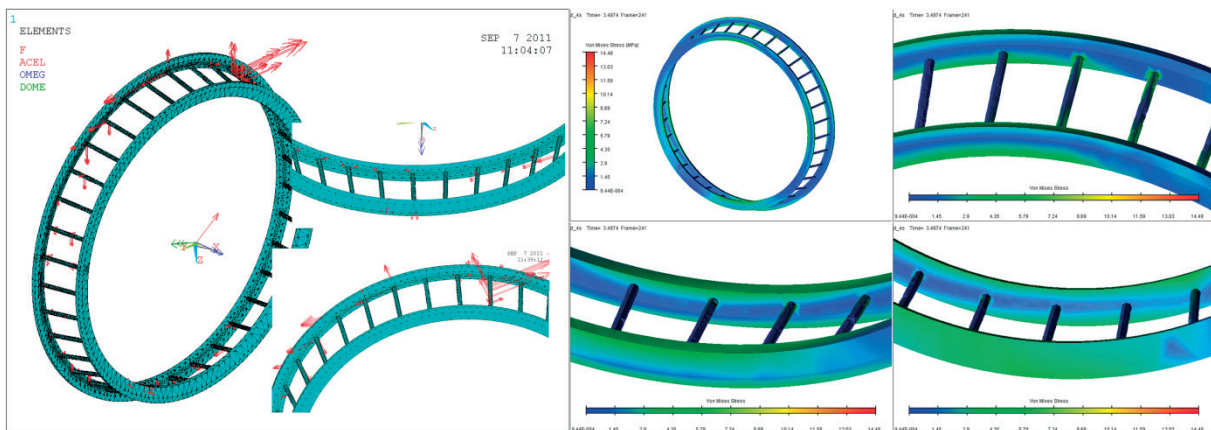


Fig. 11 Force interaction between steel cage and rollers (left side) and maximum von Mises stress of steel cage

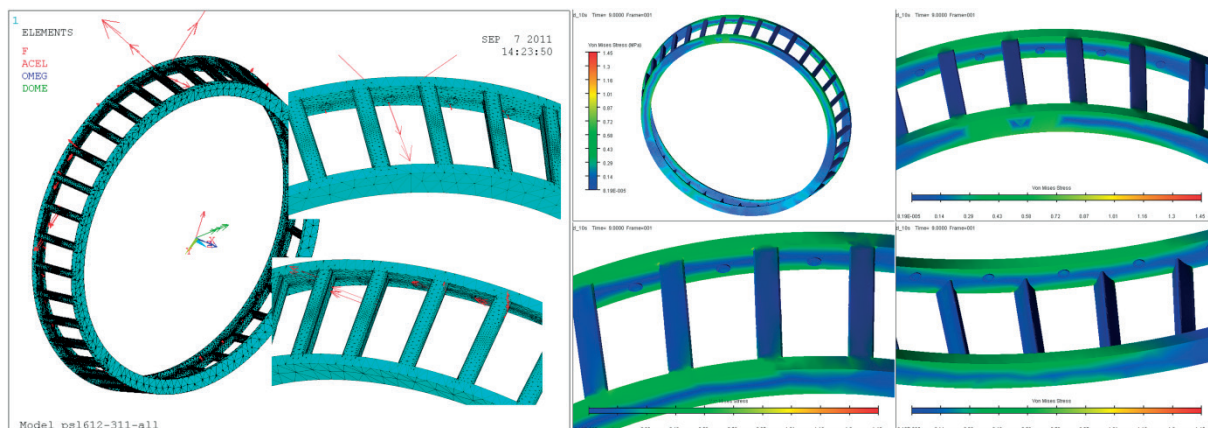


Fig. 12 Force interaction between plastic cage and rollers (left side) and maximum von Mises stress of plastic cage

## 5. Conclusion

The aim of this article was to detail with the creation of a tapered roller bearing model in the Adams software suite to be used for further dynamic analysis and to obtain information about individual parts during the simulation process taking into account the properties of the steel and plastic bearing cage for different load cases.

For axial load, dynamic analysis results show increased load variation of individual elements in steel cage when compared to the plastic cage, with a difference of 0.5% for minimum load for axial load. Minimal differences were observed under maximum loading conditions. Angular velocities of both analyzed cages shared similar waveforms. Analysis also shows that forces generated by interaction of rollers and plastic cage were 56% lower when compared to the steel cage. Likewise, the overall plastic cage stress was an order of magnitude lower compared to the steel cage. The center of gravity of the plastic cage varied by 0.4-0.5 mm in all three axes when compared to the steel cage.

When applying radial force, we discovered that using plastic cage, the loading of rollers on offloaded side is lower when

compared to steel cage. However, on the loaded side, the loading of rollers was higher when using a plastic cage. The analysis of the angular speeds rollers was found that at the time of loading, for both cages angular velocity does not change, the constant size of about  $489^{\circ}.s^{-1}$ . Difference occurred at a time to reduce the load rollers when a steel cage changes randomly in the range of  $436^{\circ}.s^{-1}$  to  $494^{\circ}.s^{-1}$ . For a plastic cage, the course of the angular velocity was smoother, but compared to a steel cage, the rate decreased significantly and varied from  $490^{\circ}.s^{-1}$  to  $0^{\circ}.s^{-1}$ . It was also found that the interaction force between the steel cage and the rollers occurred only at times of reduced loading rollers and it reached to 500N, which was 20% higher load than with a plastic cage. Plastic cage was received into contact throughout the course of the simulation, and the unloading rollers maximum load value amounted to 150N, the increase of load rollers, load increased to 400N. Variations in the rotation center of gravity for plastic cage were lower in all three axes as compared with a steel cage of 0.1 to 0.5 millimeters as opposed to the axial load.

The performed analyses have shown that the steel cage is more appropriate for axial loads, whereas the plastic cage is more suited for radial loads.

## References

- [1] KOHAR, R., MEDVECKY, S., HRCEK, S.: Usage of Dynamic Analysis to Determine Force Interactions between Components of Rolling Bearings with Different Rotation Speed. *Machine Design*, vol. 4, No. 3, 2012, 145-150, ISSN 1821-1259.
- [2] RADEK, N., SLADEK, A., BRONCEK, J., BILSKA, I., SZCZOTOK, A.: Electrospark Alloying of Carbon Steel with WC-Co-Al<sub>2</sub>O<sub>3</sub>: deposition technique and coating properties, *Advanced Materials Research*, vol. 874, 2014, 101-106, ISSN 1022-6680, © (2014) Trans Tech Publications, Switzerland, doi:10.4028/www.scientific.net/AMR. 874.
- [3] BRONCEK, J., DZIMKO, M., HADZIMA, B., TAKEICHI, J.: *Acta Metallurgica Slovaca*, vol. 20, No. 1, 97-104, 2014. DOI 10.12776/ams.v20i1.273.

- [4] KUCERA, L., LUKAC, M., JURAK, L., BRUMERCIK, F.: Hydromechanical Automatic Transmission, *Communications - Scientific Letters of the University of Zilina*, vol. 11, No. 2, 2009, 33-35.
- [5] BRUMERCIK, F., KOCUR, R., PAZICAN, M., LUKAC, M.: Differential Hydro-mechanical Transmissions with Hydrostatic Units, *Communications - Scientific Letters of the University of Zilina*, vol. 7, No. 1, 2005, 49-53.
- [6] DEKYS, V., BRONCEK, J.: Measuring Strain of the Lattice Towers, *Communications - Scientific Letters of the University of Zilina*, vol. 14, No. 3, 2012, 39-42.
- [7] BRONCEK, J., DZIMKO, M., HADZIMA, B., TAKEICHI, Y.: Experimental Investigations of Aluminium Alloys, 2024, T3 Form in Terms of Tribocorrosion Characteristics, *Communications - Scientific Letters of the University of Zilina*, vol. 20, No. 1, 2014, 97-104.
- [8] SOARES, D. JR., SLADEK, V., SLADEK, J., ZMINDAK, M., MEDVECKY, S.: Porous Media Analysis by Modified MLPG Formulations, *Computers, Materials and Continua*, vol. 27, No. 2, 2012, 101-126.
- [9] GREGOR, M., MEDVECKY, S.: Zilina University Concept of Digital Factory, *Communications - Scientific Letters of the University of Zilina*, vol. 10, No. 2, 2008, 60-66.
- [10] MD Adams 2011 Online Help.
- [11] HARRIS, T. A., KOTZALAS, M. N.: *Essential Concepts of Bearing Technology*, 5<sup>th</sup> edition, 2007.
- [12] FROHLICH, J.: *Bearing Applications with Rolling Bearing*, (in Slovak), Nakladatelství technické literatury : Praha, 1980.

Michal Petru – Josef Bronceck – Petr Lepsik – Ondrej Novak \*

## EXPERIMENTAL AND NUMERICAL ANALYSIS OF CRACK PROPAGATION IN LIGHT COMPOSITE MATERIALS UNDER DYNAMIC FRACTURING

*Research and analysis of mechanical properties including crack propagation in a light composite material is currently very important because composite structures are gradually becoming an alternative material that allows a significant reduction in the weight of car parts. This leads to an increase in efficiency in transport vehicles. This article describes experimental as well as model analysis of damage to composite textiles during dynamic fracturing. The obtained information provides an approach to the complex problem of crack propagation in composite textiles intended for use in car seats. This is especially important from the point of view of safety, because during an accident a significant overload of the human body occurs and its kinetic energy can cause deformation of a breach in the composite textile. Therefore, identifying the direction of crack propagation is very important for the safety of passengers. Experimental studies have demonstrated that a dynamic breach is caused by the significant deformation of the tested sample. The distribution and direction of crack propagation in the sample was studied using a FEM model, based on the Griffith-Irwin criterion with nonlinear orthotropic properties of the composite textile.*

**Keywords:** Light composite material, crack, FEM model, Irwin factor.

### 1. Introduction

The current trends and efforts in the development of components and systems, especially for vehicles, include their innovation leading to weight reduction. The main parameters of structural optimization are primarily dynamic and static strength and durability. They influence the mechanical properties (materials of construction, geometrical dimensions, shape), technological factors (quality, surface properties, nicks, welds and joints), loading conditions (load, climatic conditions, temperature, corrosion) and vibration [1]. Weight reduction is also very important. For this purpose light, energy-saving and recyclable materials that have the same or better parameters than standard materials are used. New composite structures have become the subject of interest. The optimal directional arrangements of fibres and the type and amount of the matrix for a given load have yet to be defined for these structures. Therefore, the research is focused on testing and analysis of alternative textile materials that are currently being used for the production of the frame constructions of car seats. The safety wall elements of the current seat design are preserved and the supporting metal or spring construction of the seat and backrest is replaced by an alternative low-weight composite textile reinforcement [2 and 3]. The problem lies mainly in the

fact that this structural modification leads to a reduction in the weight of the seat frame construction, but the risk of deformation of the textile during an accident increases. The weight and body constitution directly affect the interaction of the seat, especially during impact [4 and 5]. A dynamic impact could lead to a break in alternative textiles which can be damaged. The main objective of this paper was to perform an experimental analysis and to construct a simulation model describing the distribution of the limit state and the rate of crack propagation in a hyper elastic composite with textile reinforcement. The crack occurs in the loaded material in the anchor points on the frame. Degradation may also occur due to the creep properties of the material. This can be caused by long-term acting forces (random loading by the human body, pre-stress of textile). It is very difficult to describe the course, direction and initiation of cracks in the composite textile and they are practically immeasurable. The rate of crack propagation and the characteristic force-elongation dependence can be experimentally determined using the Aramis measuring system, but it is not possible to describe the distribution of stress intensity, e.g. by the direction of the principal stress tensor. It is possible to a certain extent to describe the stress intensity using FEM model simulation based on mathematical theories that use Griffith-Irwin criteria.

\* <sup>1</sup>Michal Petru, <sup>2</sup>Josef Bronceck, <sup>3</sup>Petr Lepsik, <sup>4</sup>Ondrej Novak

<sup>1</sup>The Institute for Nanomaterials, Advanced Technologies and Innovation, Technical University of Liberec, Czech Republic

<sup>2</sup>Department of Design and Mechanical Elements, Faculty of Mechanical Engineering, University of Zilina, Slovakia

<sup>3</sup>Department of Design of Machine Elements and Mechanisms, Faculty of Mechanical Engineering, Technical University of Liberec, Czech Republic

<sup>4</sup>Department of Nonwovens and Nanofibrous materials, Faculty of Textile Engineering, Technical University of Liberec, Czech Republic

E-mail: michal.petru@tul.cz

**2. Materials and methods**

**2.1 Experimental measurements**

Test samples of a hyper elastic composite reinforcement consist of two different layers - woven with orthotropic properties and a hyper elastic coating. A combination of these structures causes changes in the mechanical properties - especially changes to the viscoelastic and hyper elastic parameters. The physical properties of the tested samples are given in Table 1. Testing equipment for the drop test with an impact velocity of  $8 \text{ m}\cdot\text{s}^{-1}$

was built for the experiment. The equipment comprises jaws for mounting the composite textile sample, sensors for acceleration, displacement, force and the Aramis system. This system uses two high speed cameras for stereoscopic visualization. The layout of the experiment is illustrated in Fig. 1 and the time course of the dynamically loaded composite textile is shown in Fig. 2. The obtained data were evaluated using the DEWESoft 7.0 software. The dimensions of the composite textile sample were  $150 \times 150 \times 1.3 \text{ mm}$ .

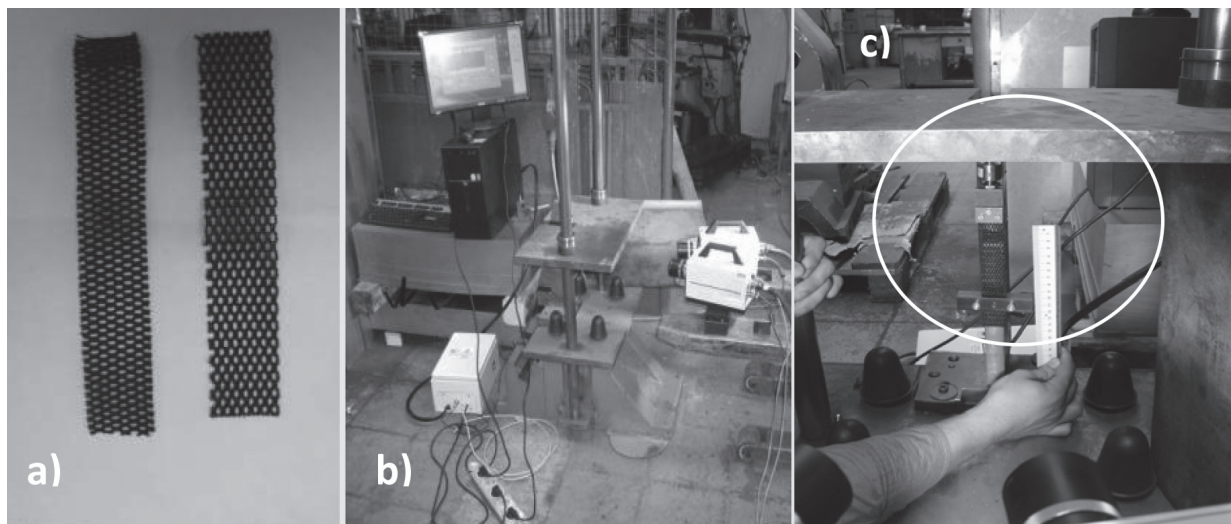


*Fig. 1 Experimental measurement of a dynamically loaded sample: a) composite textile - longitudinal and transverse direction, b) arrangement of the experimental device, c) close up of sample placement*

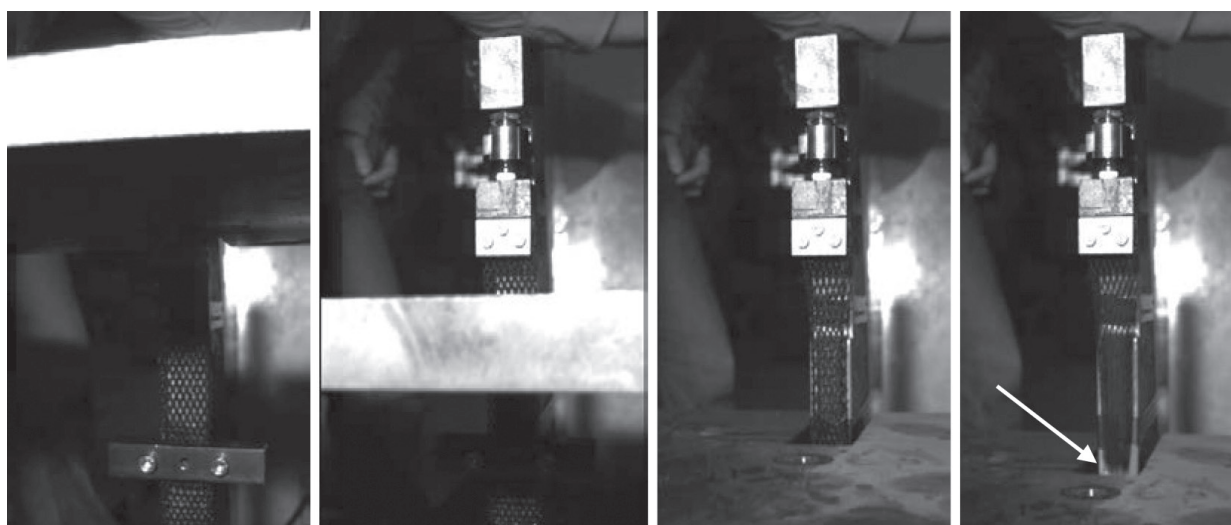


*Fig. 2 The time course of dynamically loaded composite textile: Time (0-60 ms)*

Mechanical properties of samples compressed to 50% deformation

Table 1

Specific properties	Value	Unit
Density	1052	kg.m <sup>3</sup>
Strain at yield	1800	MPa
Tensile creep modulus (0.5% 1000 hrs.)	1100	MPa
Modulus of elasticity	112	MPa
Ultimate bending strength	2700	MPa
Tensile strength	33	MPa
Fatigue limit under alternating bending stress (10e+7 cycles)	0.24-0.4	min
The coefficient of sliding friction compared to steel in a dry environment	1.7	J.g <sup>-1</sup> .K
Specific heat capacity	235	°C
Tensile creep modulus (0.5% 1000 hrs.)	1050-1250	kg.m <sup>3</sup>

### 2.2 Mathematic theory of cracks

Integral parameters of the crack will be introduced to describe the crack propagation and its instability. These parameters will then be compared with the experimentally identified critical values. The Irwin factor  $K$  [6, 7 and 8] can be used for this purpose. It is based on energy of stress intensity where the zone of stress intensity factor (1-2) and the field of shifts in nonlinear behaviour in the crack are used. The Irwin factor can be used to describe the crack in the isotropic and anisotropic materials. The sample of the hyper elastic orthotropic reinforcement has properties that are different in machine direction as well as cross direction [2 and 3], but during dynamic tearing they have a similar course which can be described by the multiplying with a constant. This may be due to the fact that such a structure under dynamic failure is significantly stiffer. In this case a volume strain occurs, which is manifested by a deformation of the plastic. The application of Irwin factor distribution on the tested sample is shown in (Fig. 3).

$$\sigma_{ij}(r, \Psi) = (r^{-1/2}) \cdot [K_I f(\Psi) + K_{II} g_{ij}(\Psi)] \quad (1)$$

$$u_i(r, \Psi) = \left(\frac{r^{-1/2}}{G}\right) \cdot [K_I F_i(\Psi) + K_{II} G_i(\Psi)] \quad (2)$$

where  $\sigma_{ij}$  is the Cauchy tensor of stress,  $u_i$  is the vector of translation,  $r, \Psi$  are separated variables which describe the assumed direction of crack propagation (the assumption is  $0 < \Psi < \pi/2$ ,  $a$  is a half length of crack edge (flaw) in a material,  $r/a$  is a dimensionless parameter expressing the ratio of separated variables  $r$ , which describe the assumed direction of the crack propagation and  $a$  is a half length of crack edge (flaw)

in a material,  $K_I, K_{II}$  is the determined factor of stress intensity,  $f_{ij}, g_{ij}$  are nonzero functions of stress related to intensity factors  $K_I, K_{II}$ ,  $G$  is a shear modulus of elasticity,  $F_i, G_i$  are nonzero functions describing the field of translations related to intensity factors  $K_I, K_{II}$ ,  $t_{crack}$  is the time of crack propagation,  $t_{mit}$  is the time of crack initiation ( $t_{crack} > t > t_{mit} > t_0$ ),  $t_0$  is the time (limit state) before crack initiation.

The types of stress intensity factor  $K_i$  respond to the crack course as follows:

- I. type - critical normal stress  $\sigma_{22}$  in axis  $X_2$  ( $K_I$  for  $t : t_0 < t_{mit}$ ),
- II. type - critical shear stress  $\sigma_{12}$  in a plane  $X_1 X_2$  ( $K_{II}$  for  $t_{mit} : t < t_{crack}$ ).

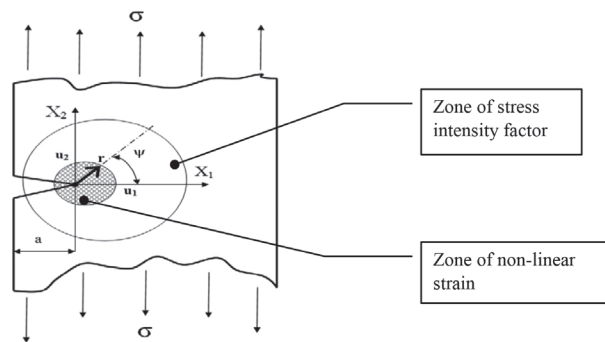


Fig. 3 Crack study with character description of the stress intensity due to the Irwin factor

The initiation of the crack in the sample  $t_{mit} \geq t > t_0$  is characterized by stress intensity  $K_I$  and nonzero harmonic stress functions  $f_{ij}$ . It can be described by the following equations 3-5.

$$f_{11}(\Psi) = \frac{1}{\sqrt{2\pi}} \cos \frac{\Psi}{2} \left(1 - \sin \frac{\Psi}{2} \sin \frac{3\Psi}{2}\right), \quad (3)$$

for  $t \geq t_{mit} > t_0$

$$f_{22}(\Psi) = \frac{1}{\sqrt{2\pi}} \cos \frac{\Psi}{2} \left(1 - \sin \frac{\Psi}{2} \sin \frac{3\Psi}{2}\right), \quad (4)$$

for  $t \geq t_{mit} > t_0$

$$f_{12}(\Psi) = \frac{1}{\sqrt{2\pi}} \cos \frac{\Psi}{2} \sin \frac{\Psi}{2} \sin \frac{3\Psi}{2}, \quad (5)$$

for  $t \geq t_{mit} > t_0$

Then the field of translations is described by the following function  $F_i$  obtained from equations 6 - 7.

$$F_1(\Psi) = \frac{1}{\sqrt{2\pi}} \cos \frac{\Psi}{2} \left(1 - 2\mu_1 + \sin^2 \frac{\Psi}{2}\right), \quad (6)$$

for  $t \geq t_{mit} > t_0$

$$F_2(\Psi) = \frac{1}{\sqrt{2\pi}} \sin \frac{\Psi}{2} \left( 2 - 2\mu_2 + \cos^2 \frac{\Psi}{2} \right), \quad (7)$$

for  $t \geq t_{init} > t_0$

where  $\mu_i$  is the Poisson ratio in longitudinal and transverse directions <sub>1,2</sub>.

The propagation of the crack in the sample follows  $t_{crack} > t > t_{init}$  and it is characterized by the stress intensity  $K_{II}$  and nonzero harmonic stress functions  $g_{ij}$  (8 - 10).

$$g_{11}(\Psi) = -\frac{1}{\sqrt{2\pi}} \sin \frac{\Psi}{2} \left( 2 + \cos \frac{\Psi}{2} \cos \frac{3\Psi}{2} \right), \quad (8)$$

for  $t_{crack} \geq t > t_{init}$

$$g_{22}(\Psi) = -\frac{1}{\sqrt{2\pi}} \sin \frac{\Psi}{2} \cos \frac{\Psi}{2} \cos \frac{3\Psi}{2}, \quad (9)$$

for  $t_{crack} \geq t > t_{init}$

$$g_{12}(\Psi) = -\frac{1}{\sqrt{2\pi}} \cos \frac{\Psi}{2} \left( 1 - \sin \frac{\Psi}{2} \sin \frac{3\Psi}{2} \right), \quad (10)$$

for  $t_{crack} \geq t > t_{init}$

Then, the field of translations is described by the following functions  $G_i$  obtained from equations 11 - 12.

$$G_1(\Psi) = \frac{1}{\sqrt{2\pi}} \sin \frac{\Psi}{2} \left( 2 - 2\mu_1 + \cos^2 \frac{\Psi}{2} \right), \quad (11)$$

for  $t_{crack} \geq t > t_{init}$

$$G_2(\Psi) = \frac{1}{\sqrt{2\pi}} \cos \frac{\Psi}{2} \left( -1 - 2\mu_2 + \sin^2 \frac{\Psi}{2} \right), \quad (12)$$

for  $t_{crack} \geq t > t_{init}$

### 2.3 FEM model of crack propagation in composite textiles

The FEM model gives not only a description of translation fields and velocity of crack propagation but also stress intensity [7, 9 and 10]. For a calculation of factors  $K_I, K_{II}$  Cauchy stress  $\sigma_{ij}$  ( $\sigma_{11}, \sigma_{22}, \sigma_{12}$ ) and variables  $r, \Psi$  from the FEM simulation are used. Then,  $K_I, K_{II}$  can be expressed by equation (1). The FEM model was created using PAM-CRASH software which can be used for nonlinear mechanical properties of anisotropic materials (hyper elastic, visco-elastic, etc.) [2 and 3]. The principle of the calculation in PAM CRASH is based on an explicit method where the time step of the calculation is solved using central differences. An explicit method allows the solution of shock wave distribution [11]. The advantage of the explicit solution compared to an implicit solution is not only the possibility to study dynamic phenomena but also in its significantly shorter calculation (Figs. 4 and 5). For such

complex nonlinear processes as the study of cracks in composite textiles the calculation of an explicit algorithm, which is described by equation (13), has a higher stability than an implicit algorithm, which is described by equation (14). Compared to an implicit solution the explicit solution does not need to calculate the inverse stiffness matrix [12, 13 and 14].

Timing diagram for the displacement, velocity and acceleration of the movement equation:  $m\ddot{x} + kx = f(t)$

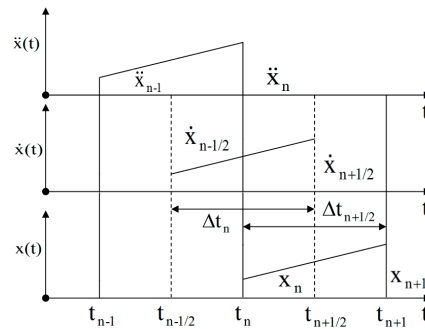


Fig. 4 Explicit solutions

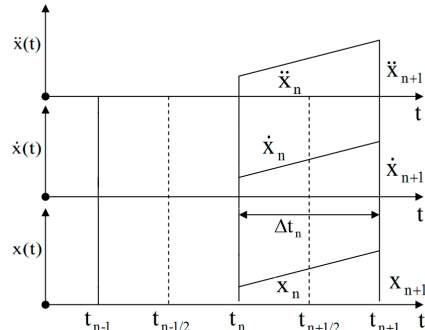


Fig. 5 Implicit solutions

$$x_{n+1} = (m/\Delta t_{n+1}^2 + x)^{-1} \cdot (f_{n+1} - m/\Delta t_{n+1} (2x_n - x_{n-1})) \rightarrow m\ddot{x}_n + kx_n = f_n \quad (13)$$

where the known values are displacement  $x_n$  in time  $t_n$  and velocity  $\dot{x}_{n-1/2}$  in time  $t_n$ . Search values are displacement  $x_{n+1}$  in time  $t_{n+1}$  and velocity  $\dot{x}_{n+1/2}$  in time  $t_{n+1/2}$ .

$$x_{n+1} = x_n + \Delta t_{n+1/2} \rightarrow m\ddot{x}_{n+1} + kx_{n+1} = f_{n+1} \quad (14)$$

where the known values are displacement  $x_n$  in time  $t_n$  and velocity  $\dot{x}_{n-1/2}$  in time  $t_{n+1/2}$ . Search values are displacement  $x_{n+1}$  in time  $t_{n+1}$  and velocity  $\dot{x}_{n+1/2}$  in time  $t_{n+1/2}$ .

It is also possible to study the crack propagation. "Material 150 - Layered Membrane Element" was selected for the material

Data required for creating the FEM model

Table 2

Model	Material model	Density [kg.m-3]	Initial module E [MPa]			Shear modulus G [MPa]		
			Fibres in MD	Fibres in CD	Matrix	Fibres in MD	Fibres in CD	Matrix
Composite textile	150	1052.8	1100	1300	90	450.8	532.8	30.2

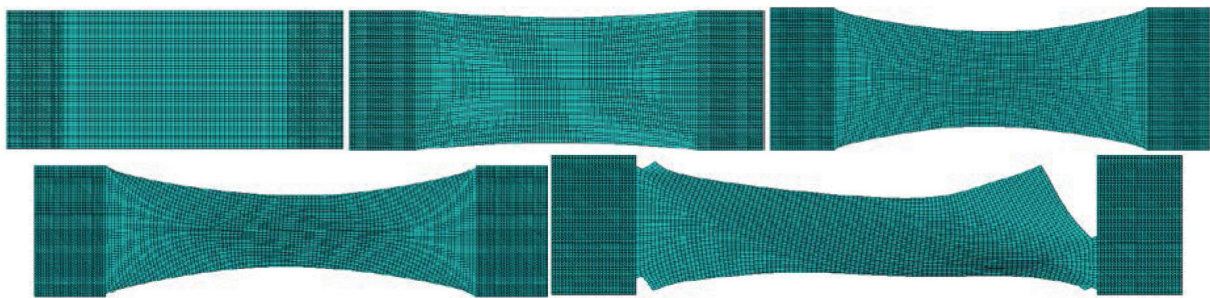


Fig. 6 FEM model of composite textile for studying cracks

model of the composite textile. This model uses 2D membrane elements. It can simulate different mechanical properties of composite textiles in MD (Machine Direction) and CD (Cross Direction) because it allows the material properties for three different layers to be defined including the fibre orientation [2 and 3]. The input parameters of the material model are shown in Table 2. The finite element method mesh (Fig. 6) was created to describe the stress intensity, velocity of crack propagation and especially for the stability of the calculation [6, 8 and 14].

### 3. Results and discussion

The resulting courses of stress intensity factors  $K_I$ ,  $K_{II}$  depending on the ratio  $r/a$ , are shown in Fig. 7 and the parametric dependence is shown in Fig. 8. A significant difference of stress intensity factors  $K_I$  and  $K_{II}$  for ductile failure is explained in [6 - 8]. Comparing the experimental values with the FEM model, the deviation of model was determined as being 9% (Fig. 9). The size, direction, and visualization of the main crack stress tensor, from which the time-course  $\Psi$  can be determined is shown in Figs. 10 and 11. The maximum value of the principal stress was located at the nodal point of the critical damage of the textile and it reached a value of 17.44 MPa. The vectors of velocity and direction of momentum during crack propagation are shown in Figs. 12 and 13. The velocity of crack propagation in the textile may be influenced by the individual components of the material, the directional orientation of the fibres that affect the orthotropy, and friction between the fibres. However, the friction is very difficult to measure [15 - 19].

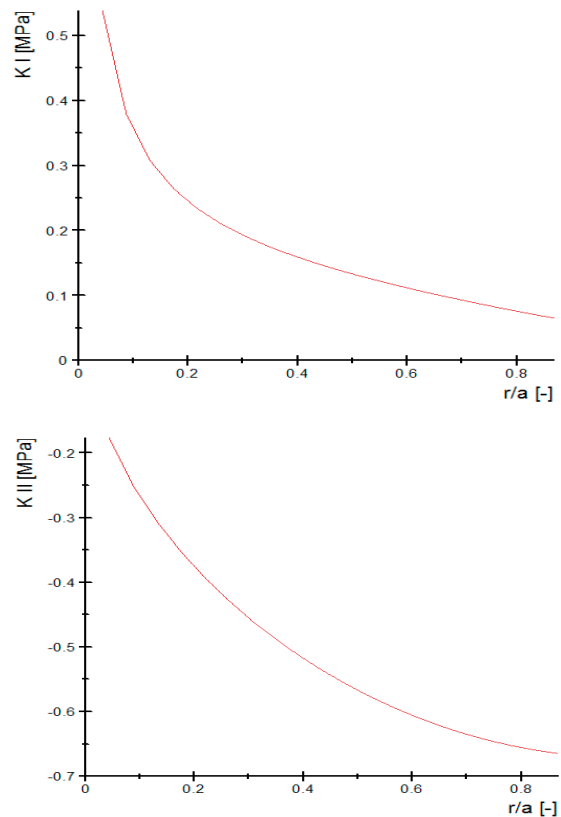


Fig. 7 The dependence of the stress intensity factor  $K_I$ ,  $K_{II}$  on rate  $r/a$

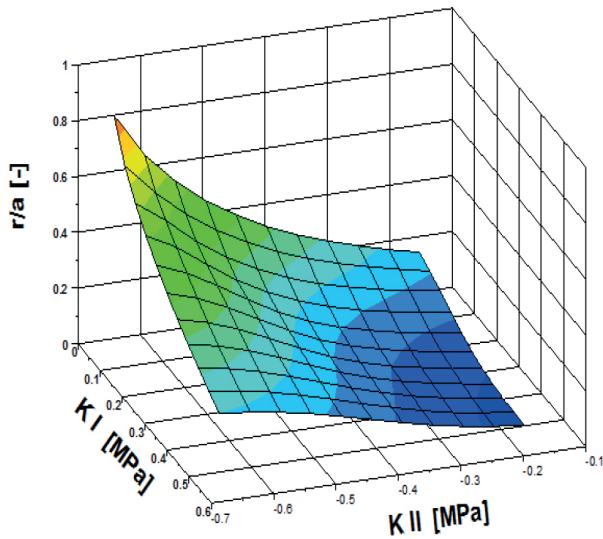


Fig. 8 Parametric dependence  $K_I$ ,  $K_{II}$  on rate  $r/a$

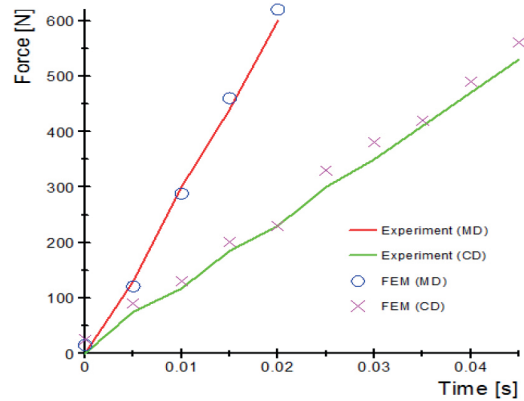


Fig. 9 Comparison of FEM results with the experiment

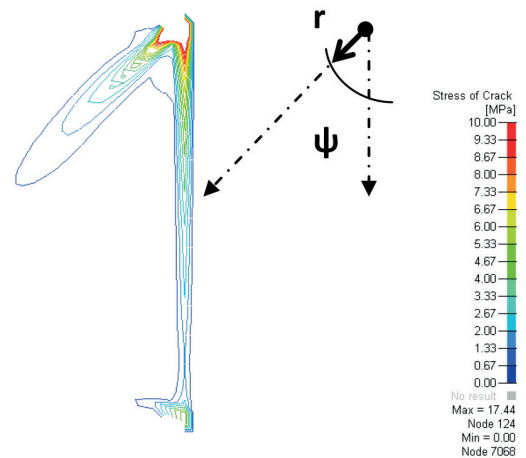
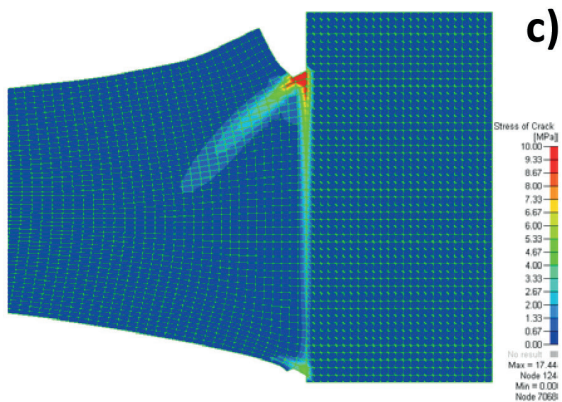
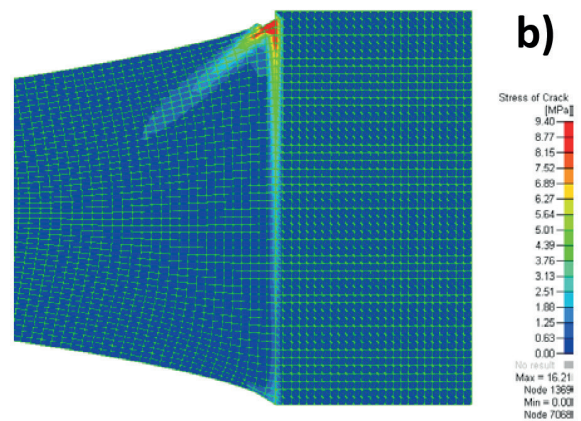
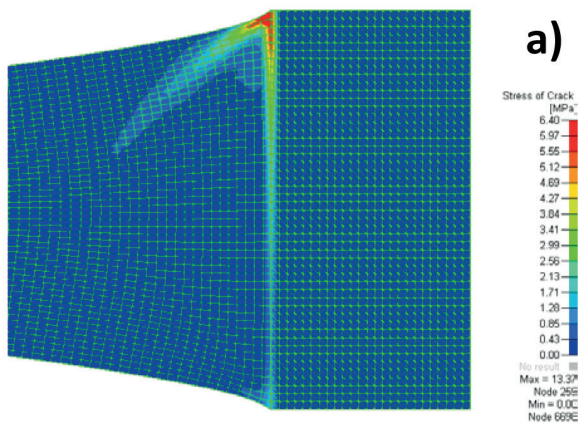


Fig. 10 Stress intensity in the crack: a) Limit state ( $t_{init} > t > t_0$ );  
 b) crack initiation ( $t_{crack} > t > t_{init}$ );  
 c) crack propagation ( $t = t_{crack}$ )

Fig. 11 Distribution of stress intensity: determination of variables  $r$ ,  $\psi$

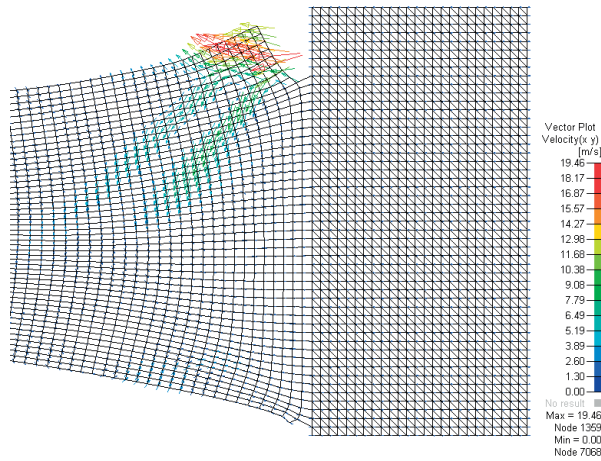


Fig. 12 Vectors of crack velocity propagation in a composite textile

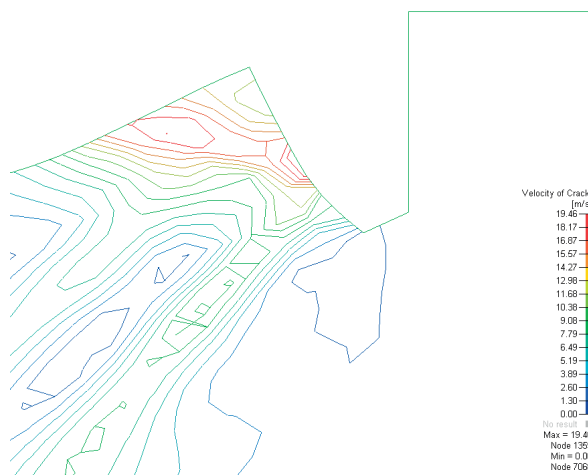


Fig. 13 Distribution of velocity fields in the crack

#### 4. Conclusion

This article deals with the description and modelling of crack propagation in a sample of hyper elastic composite textile which could be used as a reinforcing material in car seats. The distribution and intensity of stress in the crack can be described using the Irwin factor based on a continuum where only the crack is solved. The FEM model had significantly nonlinear properties with parameters which are taken from the experiment. The model showed the distribution, initiation and also propagation velocity of the crack in the textile. The model can be used to determine the approximate values of the stress intensity factor in the crack. Thus, the FEM model can help with the study of cracks during fast loading such as during a car accident and it simplifies the optimization process of the material design of different car parts.

#### Acknowledgements

The research reported in this paper was supported in part by the Project OP VaVpI Centre for Nanomaterials, Advanced Technologies and Innovation CZ.1.05/2.1.00/01.0005 and the results of this project LO1201 were obtained through co-funding from the Ministry of Education, Youth and Sports as part of targeted support from the “Narodni program udrzitelnosti I” programme and the project “Development of Research Teams of R&D Projects at the Technical University of Liberec” CZ.1.07/2.3.00/30.0024 and the CREATex project (CZ.1.07/2.2.00/28.0321) which has been financed by the European Social Fund and The Ministry of Education, Youth and Sports of the Czech Republic. This work was supported by the ESF operational programme “Education for Competitiveness” in the Czech Republic in the framework of the project “Support of engineering of excellent research and development teams at the Technical University of Liberec” No. CZ.1.07/2.3.00/30.0065.

#### References

- [1] SUH, N. P.: *Complexity: Theory and Applications (Mit-Pappalardo Series in Mechanical Engineering)*, Oxford, 2005.
- [2] PETRU, M., NOVAK, O., LUFINKA, A.: *Study and Analysis of Transmissibility of Car Seat with Non Polyurethane Material*, Proc. of 50<sup>th</sup> Annual Conference on Experimental Stress Analysis, EAN, Tabor, June 2012, 321-326.
- [3] PETRU, M., NOVAK, O.: *Testing and Simulation of Viscoelastic Reinforcement Applied into Car Seat Construction*, *ACC Journal*, No. 17, No. A, Natural Sciences and Technology, 80-88, 2011.
- [4] RAGAN, R., KERNOZEK, T. W., BIDAR, M., MATHESON, J. W.: *Seat Interface Pressures on Various Thicknesses of Foam Wheelchair Cushions: A Finite Modeling Approach*, *Archives of Physical Medicine and Rehabilitation*, vol. 83, 872-875, 2002.
- [5] DUFFY, V. G.: *Handbook of Digital Human Modeling - Research for Applied Ergonomics and Human Factors Engineering*, Purdue University: Indiana, No. ER564X, 2008.
- [6] BITTNER, Z., SEJNOHA, J.: *Numerical Methods in Structural Mechanics*, Pitman Monographs and Surveys in Pure and Applied Mathematics, Thomas Telford Publications: London, 1996.
- [7] TADA, H., PARIS, C.P., IRWIN G.R.: *The Stress Analysis of Cracks Handbook*, 3<sup>rd</sup> ed., Asme Digital Library, 2000.
- [8] CRISFIELD, M. A.: *Non-linear Finite Element Analysis Solids and Structures*, John Wiley & Sons, 1991.

- [9] KOHAR, R., HRCEK, S., MEDVECKY, S.: Determination of the Maximum Roller Bearing Load with Regards to Durability there of Using Fem Analysis, *Communications - Scientific Letters of the University of Zilina*, vol. 14, No. 3, 2012, 55-61.
- [10] HRCEK, S., KOHAR, R., MEDVECKY, S.: Usage of Dynamic Analysis to Determine Force Interactions between Components of Rolling Bearings, *Communications - Scientific Letters of the University of Zilina*, vol. 14, No. 3, 2012, 62-67.
- [11] PETRU, M., NOVAK, O., HERAK, D., SIMANJUNTAK, S.: Finite Element Method Model of the Mechanical behaviour of Jatropha Curcas L. Seed under Compression Loading, *Biosystems Engineering*, vol. 111, No. 4, 412-421, 2012.
- [12] PETRU, M., NOVAK, O., LEPSIK, P.: Analysis and Measurement of the Charge Intensity of the Selected Electrospinning Electrodes, *Applied Mechanics and Materials*, vol. 486, 217-222, 2014.
- [13] PETRU, M., NOVAK, O., SEVCIK, L., LEPSIK, P.: Numerical and Experimental Research of Design Optimization of Baths for the Production of Nanofibers by the Electrospinning, *Applied Mechanics and Materials*, vol. 486, 157-162, 2014.
- [14] NOELS, L., STAINIER, L., PONTHOT, J. P.: Combined Implicit/explicit Time-integration Algorithms for the Numerical Simulation of Sheet Metal Forming, *J. of Computational and Applied Mathematics*, vol. 168, 1-2, 331-339, 2004.
- [15] BRONCEK, J., DZIMKO, M., HADZIMA, B., TAKEICHI, J.: Experimental Investigations of Aluminium Alloys 2024-t 3 Form in Terms of Tribocorrosion Characteristics, *Acta Metallurgica Slovaca*, vol. 20, 1, 97-104, 2014.
- [16] SAGA, M., DUDINSKY, M., PECHAC, P.: Optimization of Thin Shell Structures using FSD Algorithms, *Communications - Scientific Letters of the University of Zilina*, vol. 14, No. 3, 2012, 32-38.
- [17] DEKYS, M., BRONCEK, J.: Measuring Strain of the Lattice Towers, *Communications - Scientific Letters of the University of Zilina*, vol. 14, No. 3, 2012, 39-42.
- [18] HRCEK, S., KRAUS, V., KOHAR, R., MEDVECKY, S., LEHOCKY, P.: Construction of a Bearing Testing Apparatus to Assess Lifetime of Large-scale Bearings, *Communications - Scientific Letters of the University of Zilina*, vol. 11, No. 2, 57-64, 2009.
- [19] HERAK, D., KABUTEY, A., PETRU, M., HRABE, P., LEPSIK, P., SIMANJUNTAK, S.: Relaxation Behaviour of Jatropha Curcas L. Bulk Seeds under Compression Loading, *Biosystems Engineering*, vol. 125, 2014, 17-23.

Jozef Pilc - Michal Derbas - Miroslav Janota - Mario Kosut \*

## STUDYING THE IMPLEMENTATION OF POTENTIOMETRIC METHODS FOR THE DETECTION OF CRACKS IN RENOVATION OF FORGING TOOLS

Mass production using forging tools leads to an enormous increase in the consumption of forging tools and the need for rapid and flexible tool renovations. A major shortcoming in the renovations is the failure to identify cracks propagating from the surface towards the core of the basic components. Forging tools made from special tool steels are highly cost-intensive. The main cost component is the price of the material, heat treatment and other chemical-heat treatment surfaces. This is the main reason why it is necessary to think about renovation at the design stage, in case of the need for repairs. An important factor in the renovation process is the optimal choice of technology to restore the mechanical and physical properties of tools at an acceptable price, of course. The main issue in the choice of the optimal technology is heat treatment to achieve a high hardness and surface of the die, which is nitrided to ensure wear resistance. This article deals with the application of non-destructive detection technology when considering the size of die forging defects that arise in the process of forming.

**Keywords:** Forging tools, renovations, potentiometric methods, crack detection.

### 1. Introduction

Forging is one of the most economical manufacturing methods for making parts from steel and non-ferrous metals. Its advantages in comparison to other methods are: significant savings in materials, higher production rate, better grain structure and better surface quality. The materials from which forging tools are made must comply with the high demands of the mechanical, physical and chemical aspects of high strength, toughness and hardness. The technical and technological process depends on these requirements, which directly affect the cost of the individual components and their competitiveness [1]. The impact of satisfying these demands is that the tool will have a longer shelf life, and thus there will be less downtime for replacement and repair. In this way, we can make better use of production machinery and equipment. Generally, when machining materials with more difficult machinability and high hardness, we use methods with non-cutting technologies that achieve high productivity, flexibility and excellent functional properties [2 and 3].

Heat distribution and temperature fluctuations on the surfaces of forging tools cause plastic deformation, and the influence of thermo-mechanical stress leads to thermal fatigue and the formation of surface cracks. These defects significantly affect the quality of finished forgings and forging die life itself. To capture and track these defects there are several procedures, whether destructive or non-destructive methods, for the detection

of cracks within. As regards forging dies, the solution is to use non-destructive methods that do not disturb the shape and surface components [4 and 5].

For mass production, die forging is used (Fig. 1), whereby the principle is that the heated material takes on the final shape of the die cavity with one or more strokes. This can ensure a more accurate shape than with free forging. The accuracy of the surface can be significantly improved by further finishing operations such as calibration, and to achieve a high quality surface, which would not require further machining. Die forging makes it possible to achieve a major reduction of material and fibres reflecting the contour of die forging, which has a positive effect on the mechanical properties of the material [6 and 7].

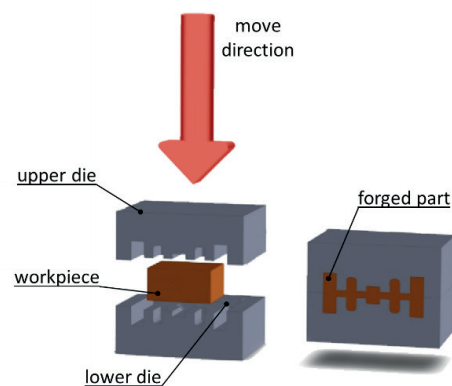


Fig. 1 The principle of die forging

\* Jozef Pilc, Michal Derbas, Miroslav Janota, Mario Kosut

Department of Machining and Manufacturing Technology, Faculty of Mechanical Engineering, University of Zilina, Slovakia

E-mail: jozef.pilc@fstroj.uniza.sk

The workpiece is inserted into the lower die. By action of energy, the shaping machine moves one part of the die against the other while the starting material fills the cavity. By fully grasping, the die cavity is filled and transformed into the desired shape. The procedure for filling a cavity influences the speed of deformation, which depends on the type of machine. The effect of impact hammers causes more rapid creep in the direction of shock and the force of the press results in better filling of the cavities in a direction perpendicular to the acting force. These differences in filling the die cavity influence the choice of the type of moulding machines and choice of forging operations for the part [7 and 8].

## 2. Cracks and their growth in the forging tool

The formation of fatigue cracks is explained by various models. One of the basic models takes the idea of formation of intrusions and extrusions with recurring shear in one or two shear systems. The relative motion of individual shear belts allows deepening of the intrusion and crack formation. If the loaded body has construction, metallurgical or technological notches, the first phase of crack growth will not arise [9 and 10]. By gradual cyclic stresses, the crack penetrates to the depth of the body, after which the crack deviates perpendicularly to the direction of principal stress. The length of the crack, which corresponds to the transition from the first phase to the second phase of crack growth, depends on the material and amplitude size of the stress loading [11 and 12].

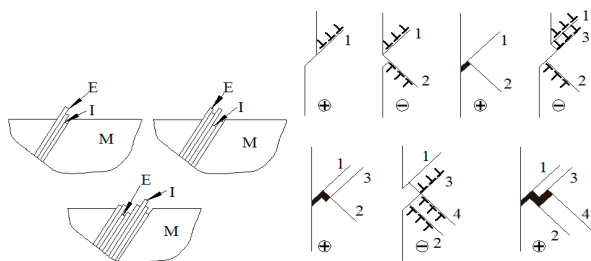


Fig. 2 Formation of micro-crack by formation of intrusions (I) and extrusions (E) in one- and two-shear systems (Neuman's model)

The forging process leads to mechanical stress that causes wear on the shape of the die (Fig. 2) and also fatigue fracture which reduces the required quality of the finished forgings. Therefore, after a fixed life, the forging die is removed from the forging process and sent for repair or renovation. Cracks can occur using the wrong modes of production. Poor cooling of cast or forged parts, overheating during grinding, or excessive tension during the manufacturing process are common causes of cracks. Cracks (Fig. 3) are defined as a narrow gap, where the length along the surface is at least ten times greater than their depth in

the material, and a visual example of the forging tools is shown in Fig. 4. In addition, the width of the fracture is very small, at least ten times less than the depth. The bottom of the fracture is mostly sharp, causing sharp notches in the material. Due to mechanical stress, especially when changing or alternating loads, there is a sharp notch at the bottom of the tension that can cause enlargement of cracks [14, 15 and 16].

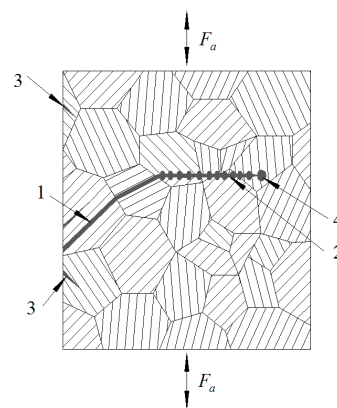


Fig. 3 Scheme of growth of fatigue crack 1 - first phase, 2 - second phase, 3 - non-effective cracks, 4 - plastic zone of the crack [13]

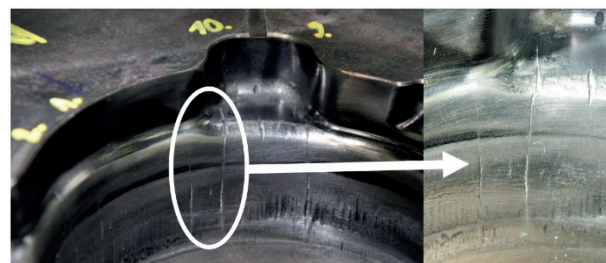


Fig. 4 Wear of die forging



Fig. 5 Fatigue cracks on the functional surface of die forging

It is therefore very important to always pay close attention to the crack. Early detection and assessment of cracks is essential. This is especially true for surface cracks. In most cases the exposed parts, such as auto parts, experience the biggest stress generated on the surface of parts. It is also important to note that not every flaw will damage components (Fig. 5). The laws of

crack mechanics indicate that some cracks can be tolerated. This depends on many factors and it is sometimes hard to decide on the use of standard methods or non-destructive material testing [17, 18 and 19].

### 3. Renovation of die forging

Renovation is a special case of repair where the repaired object is a machine component. It is work to renew machine parts whose functional properties are damaged. Renovation is a set of activities carried out in order to restore the operational status of components and their life. It is a repair in which the worn parts are restored to their geometric shape, original size, and functional and mechanical properties in accordance with drawings and technical specifications. Renovation may be seen as a repair sub-sector, which contributes to reducing the cost of restoration and operation of machinery, but it can also be seen as a special case of recycling materials, which, moreover, reduces the demand for raw materials and energy resources [20, 21 and 22].

Before renovation, it is necessary to map the extent of tool wear and the inferred extent of renovations and the required technology. Range is determined with respect to the size of the fracture surface that needs to be removed by the machining surface until the outer surfaces show no signs of defects. This process is usually performed by visual observation of the surface using optical devices which can find the largest size defects generated in the forging process, which are preventing efficient use. Since control is exercised subjectively by a worker who often cannot assess the degree of wear, not least the size of the fracture, the process is repeated until all defects are removed. It often happens that the extent of wear is destructive for the die, which is can be detected by only a few controls and subsequent surface treatment. From an economic point of view, the time required for renovation and extension of the life, causes costs to rise. Sometimes it is necessary to completely remove the forging dies for the renovation process due to excessive wear and damage. This process is well run and widely used in practice, and, therefore, seeks to simplify and intensify the technology of renovations [23, 24 and 25].

For this purpose, there are various methods involving surveys of defects in materials and products using either destructive or non-destructive detection technology, which is able to assess the extent of wear and thus indicate more options for the renovation. The best approach to renovation, and also a non-destructive method, is defectoscopy, due to its ability to change the status of the sample for future use (Fig. 6) [1].

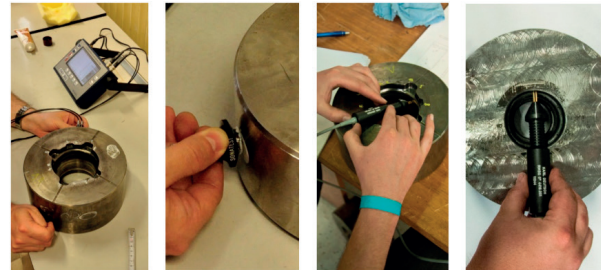


Fig. 6 The process of examining cracks by the potentiometric method with RMG 4015 device

### 4. Crack mapping by potentiometric defectoscopy

The principle of the potentiometric method is shown in Fig. 7. Electric current (with intensity  $I$ ) is supplied to the examined sample via electrodes  $E_1$  and  $E_2$ . Voltage electrodes  $N_1$  and  $N_2$  measure the potential  $U_0$  in the surface layer at a distance  $l_0$  [26].

$$U_0 = R \cdot I = \frac{\rho \cdot l_0}{S} \cdot I$$

where  $R$  - resistance between  $N_1$  a  $N_2$ ,  $\rho$  - resistivity of material,  $S$  - cross-sectional area of material

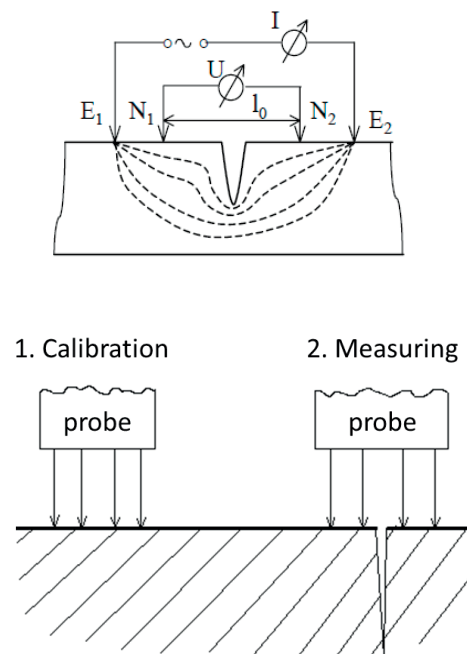


Fig. 7 Principle (left) and process (right) of measuring [26]

For good functioning of this process, four electrodes are necessary: two for electric current and two for voltage. For the most accurate measurements, the voltage electrodes must be between the electrodes for electric current. All the tips of the

electrodes are sprung, therefore contact pressure is exerted by the tip on the surface. Due to this fact, reliable contact is ensured also on uneven surfaces [2 and 27].

Measurement of crack depth is usually a comparative measurement. Comparison between the decrease of voltage on the intact surface and the surface with the crack identifies the depth of the crack. One advantage of the potentiometric method is that the width of the crack has no effect on the measured values, if this crack is narrower than the distance between electrodes [2 and 28].

**5. Experimental results and discussion**

For crack depth detection the potentiometric device RMG 4015 was used. The examined sample is a forging die with recesses and a cylindrical course of inner cavity (Fig. 8). This forging die performs a die forging with recesses and a cylindrical inner cavity.

As seen in Fig. 9, the measured values of the depth of cracks, the maximum depth of the crack is located at the edge of the die. The course of the crack is significantly different from the other measured cracks, which are much shorter and are found mainly in the vicinity of the internal curvature of the die cavity. This crack presents a particular risk because the next time the die is used there could be further spread and deepening of the cracks, which could lead to exclusion of forging die and the inability to undertake further renovations.

In crack No. 1, the first five crack depth measurements were carried out at the top of the forging die, therefore, the depth of

measurement data has the value 0. The measurement was carried out towards the edge of the external die to the die cavity inner edge.

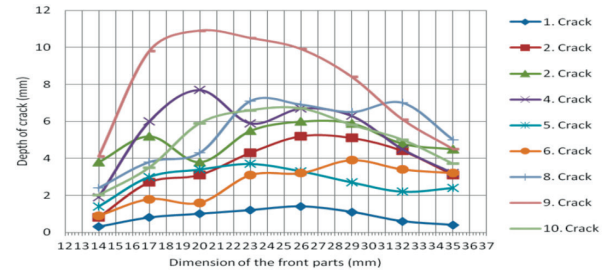


Fig. 9 Graphical representation of cracks in the forging die

From the graphic course (Fig. 9) you can see that the depth of cracks increases to a maximum and after this peak begins to fall. It is also possible to see that the cracks on the die are of different depths. Measuring the cracks using the RMG 4015 device was quick and smooth, making it possible to demonstrate the practical use of the machine in engineering practice.

**6. Conclusion**

High thermo-mechanical loading on the working surface of forging tools causes thermal fatigue and the formation of surface cracks, affecting the quality of final products and the operating life of the forging die. For monitoring of these defects, there are some procedures and methods for crack mapping, both destructive and non-destructive.

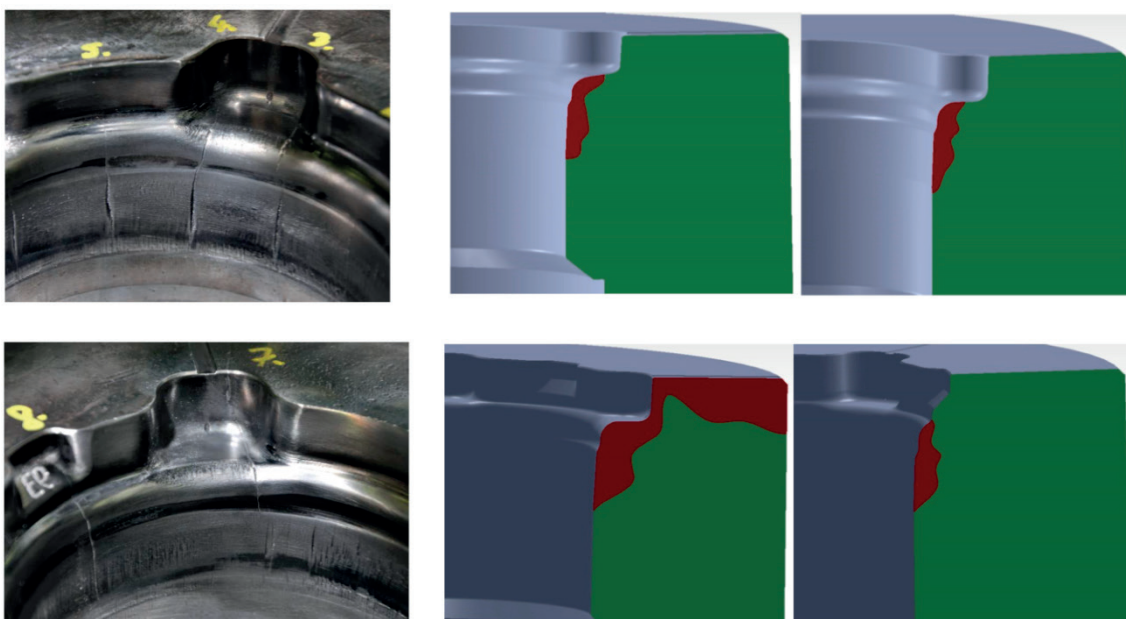


Fig. 8 Detail and course of selected cracks on forging die

When examining the progression of cracks, the potentiometric device can detect the crack on the surface and measure its depth without destructive invasion. This device can map the crack profile, and find its origin and the direction of its progress. It can be used and applied for complicated surface profiles and cavities of parts when examining surface defects. The measurement has some limitations: the surface of the sample must be clean without any dirt and the sample must be conductive.

The potentiometric method can be applied when renovating forging tools, and for renovation generally, for example, in the area of the renovation of cutting punches where it is necessary

to determine the surface defects which inhibit their use. The device can be used in the rationalization of renovation, where it is necessary to restore the functional properties of all machine parts affected by very significant wear.

#### Acknowledgements

The article was funded by the project with the University of Zilina OPVaV-2009/2.2/04-SORO No. 26220220101 "Intelligent system for nondestructive technologies on evaluation for the functional properties of components of X-ray diffraction".

#### References

- [1] DERBAS, M., CZAN, A.: *Renovating Intensification of Machining Nitride Layers of Tools for Volume Forming*, TRANSCOM 2011: 9<sup>th</sup> European conference of young research and scientific workers, June, 2011, University of Zilina. ISBN 978-80-554-0374-8. - S. 57-60.
- [2] VASILKO, K., PILC, J.: New Technological Knowledge of the Rotary Turning Tool, *J. Manufacturing Technology*, vol. 13, No. 4, December 2013, 571-575, ISSN: 1213-2489
- [3] MICHALIK, P., ZAJAC, J., HATALA, M.: Programming CNC Machines using Computer-aided Manufacturing Software, *Advanced Science Letters*, vol. 19, No 2, 2013, 369-373, ISSN: 19366612
- [4] SAJGALIK, M., CZAN, A.: Studying of Processes in Cutting Zone by Non-destructive Methods, *Technological Engineering*, vol. 8, No. 2, University of Zilina, 2011
- [5] CEP, R., JANASEK A., PETRU J., CEPOVA L., CZAN A., VALICEK J.: Hard Machinable Machining of Cobalt-based Superalloy. *Manufacturing Technology XIII/13*, 2013, 226-231, UJEP: Usti n. Labem. ISSN 1213-2489
- [6] MORAVEC, J., BOHUSOVA, Z.: *Technology of Forming (in Slovak)*, EDIS University of Zilina, 2010, 570 p., ISBN 978-80-554-0200-0
- [7] ZELENY, J.: *Manufacturing of Dies and Molds (in Czech)*. MM prumyslove spektrum SPECIAL, April 2001
- [8] MOHYLA, P., TOMCIK, P., BENES, L., HLAVATY, I.: Effect of Post-welding Heat Treatment on Secondary Hardening of Welded Joints of Cr-Mo-v Steel. *Metal Science and Heat Treatment*, 53 (7-8), 374-378. ISSN: 0026-0673
- [9] CZAN, A., TILLOVA, E., SEMCER, J., PILC, J.: Surface and Subsurface Residual Stresses after Machining and their Analysis by x-ray Diffraction. *Communications - Scientific Letters of the University of Zilina*, vol. 15, No. 2, 2013, 69-76. ISSN 1335-4205
- [10] HOLESOVSKY, F., NAPRSTKOVA, N., NOVAK, M.: GICS for Grinding Process Optimization. *Manufacturing Technology*, XII/12, 2012, 22-26, UJEP : Usti n. Labem, ISSN 1213-2489
- [11] DEUTSCH, V., PLATTE, M.: *Crack Depth Gauging with the Potential Probe Method*, Castell Publication Inc.: Wuppertal, 2003, 34 p., ISBN 3-934 255-17-5
- [12] SAPIETOVA, A., SAGA, M., NOVAK, P.: Multi-software Platform for Solving of Multibody Systems Synthesis, *Communications - Scientific Letters of the University of Zilina*, vol. 14, No. 3, 2012, 43-48, ISSN 1335-4205
- [13] PALCEK, P., HADZIMA, B., CHALUPOVA, M.: *Material Characteristics (in Slovak)*, EDIS: University of Zilina, 2004, 163 p., ISBN 80-8070-240-3
- [14] ZMINDAK, M., RIECKY, D.: Meshless Modelling of Laminate Mindlin Plates under Dynamic Loads Synthesis, *Communications - Scientific Letters of the University of Zilina*, vol. 14, No. 3, 2012, 24-31, ISSN 1335-4205
- [15] NOVAKOVA, J., PETRKOVSKA, L., BRYCHTA, J., STANCEKOVA, D.: Influence of Cutting Parameters on Integrity Surface at High Speed Cutting. Transactions of the VSB-Technical University of Ostrava. *Mechanical Series*, vol. LV, No. 1, 2009, 203-209, Ostrava: VSB - TUO
- [16] CEP, R., OCENASOVA, L., NOVAKOVA, J., PETRKOVSKA, L., CZAN, A., STANCEKOVA, D.: *Interrupted Machining Tests of Ceramic Cutting Tools*, Proc. of TMT 2009, October 2009, Hammamet, vol. 13, No. 1, 733-736, ISSN 1840-4944
- [17] STANCEKOVA, D., SEMCER, J., DERBAS, M., KURNAVA, T.: Methods of Measuring of Residual Stresses and Evaluation of Residual State of Functional Surfaces by x-ray Diffractometric Methods, *J. Manufacturing Technology*, vol. 13, No. 4, December 2013, 547-552, ISSN: 1213-2489

- [18] PANDA, A., DUPLAK, J., VOROBEL, T., JURKO, J., FABIAN, S.: Study of the Surface Material AISI 304 usable for Actuator after the Process of Turning, *Applied Mechanics and Materials*, vol. 460, 2014, 107-114, ISSN: 1660-9336
- [19] PILC, J., MICIETOVA, A., SALAJ, J., CILLIKOVA, M.: The Influence of the Selected Aspects in Planing Operations by using Auto-rotation Tool, *Transactions of Famena*, vol. 29, No. 2, 2005, 55-60, ISSN: 1333-1124
- [20] PARKER, D.: *Remanufacturing in the UK, A Significant Contributor to Sustainable Development*, Aylesbury: UK Oakdene Hollins, 245, 2003
- [21] NESLUSAN, M., CZAN, A., ZURPEL, U.: Analysis of the Heat Distribution when Grinding of a VT 9 Titanium Alloy and its Relation to Residual Tresses, *Strojnicki vestnik - J. of Mechanical Engineering*, vol. 48, No. 10, 557-564, 2002, ISSN 0039-2480
- [22] NAPRSTKOVA, N., HOLESOVSKY, F.: *Admeasurement of Grinding Wheel Loss at FPTM*. 24<sup>th</sup> Intern. colloquium Advanced manufacturing and repair technologies in vehicle industry, 159-164, 2007. ISBN 978-80-7194-962-6
- [23] CZAN, A., SAJGALIK, M., HOLUBJAK, J., KOURIL, K.: Studying of Cutting Zone when Finishing Titanium Alloy by Application of Multifunction Measuring System, *Manufacturing Technology*, vol. 13, No. 4, 2013, 428-431, ISSN: 1213-2489
- [24] CEP, R., KOURIL, K., MRKVICA, I., JANASEK, I., PROCHAZKA, J.: Testing of Kyocera Tools in Conditions of Interrupted Cut (in Czech). *Strojirenska technologie*, vol. XV, No. 3, 2010, 51-58, ISSN 1211-4162
- [25] LUKOVICS, I., BILEK, O., HOLEMY, S.: Application of Sintered Corundum in Manufacturing of Tools (in Czech), *Strojirenska technologie*, XV, No. 3, 2010, 27-34, ISSN 1211-4162
- [26] BALOG, J., CHOVANEC, A., KIANICOVA, M.: *Technical Diagnostics (in Slovak)*, GC Tech: Trencin, 2002, 115 p., ISBN 80-88914-66-3
- [27] CEP, R., JANASEK, A., CEPOVA, L., PETRU, J., HLAVATY, I., CAR, Z., HATALA, M.: Experimental Testing of Exchangeable Cutting Inserts Cutting Ability. *Tehnicki Vjesnik*, 20 (1), 2013, 21-26. ISSN: 1330-3651
- [28] KOPEC, B.: *Non-destructive Testing of Materials and Constructions (in Czech)*, 2008, CERM: Praha.

Dana Stancekova - Jan Semcer - Jozef Holubjak - Mario Drbul \*

## MACHINABILITY OF NANO-STRUCTURED BIOMATERIALS FOR DENTAL IMPLANTS

*High quality materials are characterized by increased wear resistance, high strength and hardness, abrasive wear resistance, heat and creep resistance. Due to these properties some materials are considered as hard to machine. This group of materials includes biocompatible materials used for manufacturing implants from commercially pure titanium TiGr2, TiGr5, nano-structured commercially pure titanium nTi and volume-formed titanium alloy TiNbTa. Materials were tested by milling operations with different cutting parameters and force of cutting monitoring.*

**Keywords:** Biocompatible material, nano-structured titanium, machining.

### 1. Introduction

Biomaterial is a material used in medicine for manufacturing implants, tools and parts for medical devices which are intended to be in physical contact with living tissue. Research and development of both metallic and non-metallic biomaterials enables advances in the field of medicine and especially brings great benefit to those who need it. Problems occur in the life-time of implants, which can be a few years, due to their low chemical conductivity and low stiffness. Therefore, current research is focused on bioinert materials, bioactive materials and materials that are able to be absorbed [1 and 2].

Attempts to mechanically fix artificial teeth in living tissue were first made by the ancient Egyptians around the year 2000 BC, according to Tvrdon [3], and his literary records mention stone-made implants dating from the period before Columbus. At that time, the inhabitants of South America experimented with the replacement of missing teeth using hand-made ivory substitutes or alternatively wooden substitutes.

According to Selingerová [4], the oldest methods of tooth substitution include injecting gold needles into bone tissue as performed by the ancient Chinese. She likewise states that denture development was first recorded in the 18th century. The initial human efforts to replace missing teeth with teeth from another donor were unsuccessful, and had an extremely low success rate. This changed in 1809 with Maggiolo's implant made of gold.

In 1886, Edmund was the first in the United States to test the implantation of a platinum plate into the jaw followed by deployment of a porcelain crown. In 1930 brothers Alvin and

Moses Stock came up with a thread-shaped implant and used Vitallium as a biocompatible Cr-Co-Mo alloy. Certain types of implants used today are still cast from Vitallium. A few years later, the Italian Formigini started a new era of dental implantology by using bioinert tantalum as the implant material. In 1948, a new type of implant, the subperiosteal implant, was developed. The creator was Swedish dentist Gustav Dahl. Independently of Dahl, in 1967 the first razor titanium implant was introduced by New York dentist Leonard I. Linkowom. Rapid expansion of razor implants (Fig. 1) into the practice reached a peak at the end of the 1960s and early 1970s [4].

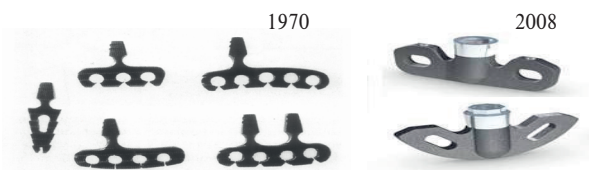


Fig. 1 Blade implant in 1970 and now [4]

So far the most significant breakthrough in the field of dental implantology is the work of Professor Per-Ingvar Branemark. His beginnings date back to 1952 when he discovered the principle of osseointegration, the integration of an implant into bone tissue. According to Simunek [5], Branemark later became the founder of modern dental implantology. He experimented with cylindrical implants made of pure titanium, which showed long-term results.

Currently, dental implants manufactured from commercially pure titanium and titanium alloys do not meet all the needed requirements, so new materials are under development, such as nano-structured titanium which is produced by extrusion of the

\* Dana Stancekova, Jan Semcer, Jozef Holubjak, Mario Drbul

Department of Applied Mechanics, Faculty of Mechanical Engineering, University of Zilina, Slovakia  
E-mail: dana.stancekova@fstroj.uniza.sk

material through a tube with constant diameter, i.e., the use of ECAP technology. Volume-formed TiNbTa alloys are often used too.

## 2. Design of dental implants

Commonly used conventional materials are currently being replaced by materials with better mechanical properties. This group of materials includes high chromium steels, cobalt and nickel alloys, titanium and titanium alloys. Titanium and titanium alloys belong to the group of materials that are hard to machine owing to their good chemical and physical properties like high strength, high corrosion resistance, low specific weight and high temperature wear resistance, along with low thermal conductivity which has a negative influence on the machining process [6, 7 and 8].

Commercially pure titanium, unlike titanium alloys, doesn't have the strength required to endure higher force loads and is primarily used for surface coatings and dental implants [9].

The advantage of titanium-based materials is that they are absolutely tasteless and can be a good alternative choice for patients with an allergy or toxic reaction to various dental alloys. Titanium corrosion behaviour is recommended for dental applications [10 and 11]. Moreover, titanium alloys are increasingly used for dental implants these days.

The final chemical composition of nano-structured titanium depends on the initial chemical composition of the titanium at the beginning of the forming process, for example ECAP, where the structure of the formed material is transformed as a result of grain size reduction and thus modification to the mechanical properties. Therefore, these nano-structured materials are characterised by unique mechanical properties that have positive effects on biocompatibility and still maintain the required chemical purity, (Fig. 2) [12, 13 and 14].

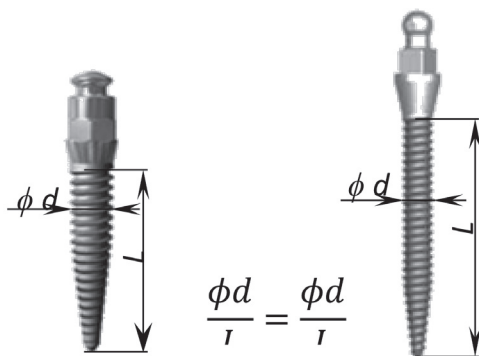


Fig 2 Nano-structured titanium

The most important property is its strength. The strength of nano-structured titanium nTi is 3.6 times greater than the strength

indicated in standards for commercially pure titanium cpTiGr 2. This value is represented by ultimate strength Rm which is not final and with gradually improving manufacturing technologies the Rm of nTi is now almost four times higher than cpTi, as well as having a lower modulus of elasticity. Titanium has the greatest values of Rm and density in comparison to Ti alloys or Ni-Co-Cr-Mo alloys. The chemical composition corresponds to the quality of Gr 4, containing 99% titanium and is free from the potential of the organism having an allergic reaction to other elements [15 and 16].

## 3. Material and experiment conditions

Experimental measurements were performed on materials: commercially pure titanium Ti Grade 2 (Fig. 3a), Ti Grade 5 (Fig. 3c) which is considered as an alloy, commercially pure volume-formed titanium (Fig. 3b) and titanium alloy TiNbTa (Fig. 3d) modified by volume-forming technology. The main mechanical properties and hardness are shown in Table 1.

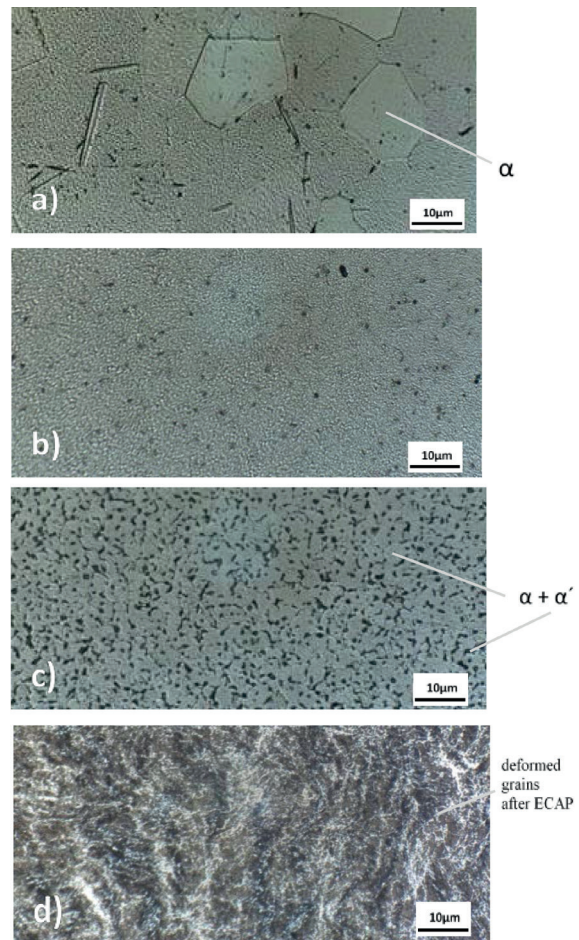


Fig. 3 Microstructure of machined materials: a) nTi, b) TiGr2, c) TiGr5, d) TiNbTa - etch Kroll

Main mechanical properties and hardness of machined materials

Machined material	Rm (MPa)	Rp0.2 (MPa)	A5 (%)	HV10
TiGr2	min. 345	275 - 450	20	146
TiGr5	min. 895	min. 828	10	314
nTi	1 240	1 200	12	336
TiNbTa	917	859	10,9	233

Table 1

Samples were prepared from these materials and then tested on a CNC machining centre HURCO WMX 30t. The experiment was focused on monitoring cutting forces relative to cutting parameters in the milling operation. Cutting conditions were chosen according to functional dependencies: cutting speed  $v_c = 20 \div 40 \text{ m}\cdot\text{min}^{-1}$ , feed  $f_z = 0.02 \div 0.06$ , depth of cut  $a_p = 0.3 \div 0.5 \text{ mm}$ . In the experiment a monolithic endmill with diameter 4 mm was used (Fig. 4). This is a sintered carbide milling tool with four cutting edges with TiAlN coating.



Fig. 4 The monolithic endmill

#### 4. Experiment

In milling, the cross-section of the chip varies, which leads to significant modification of the cutting forces during the process. The value of the cutting forces also depends on the number of cutting edges and the sum of the lengths of the cutting edges currently in work. The total force of cutting is the sum of the elemental forces caused by individual cutting edges. The cutting forces caused by the mill-tooth on the machined material can be imagined as two forces (see Fig. 5): tangential force  $F_c$  and radial force  $F_f$  which points out of the centre of the circle at the location of the largest chip cross-section [13, 17 and 18].

The result of these forces is  $F_A$  with the same orientation as the vector of main cutting speed  $v_c$  and is called the active force. If the mill has oblique or helical teeth, there is an additional force  $F_p$  in the axial direction. The sum of  $F_p$  and  $F_A$  results in the total force of cutting  $F$  [13 and 19].

To measure the components of cutting forces during milling, as well as the axial force and torque during drilling, a four-component piezoelectric dynamometer KISTLER type 9273 was used.

The values recorded by the dynamometer were subsequently processed using DASY Lab software and used to construct the graphical dependencies of cutting forces and time which served as the core for the creation of structural equations describing the effect of cutting parameters on cutting force components (Tables 2 and 3).

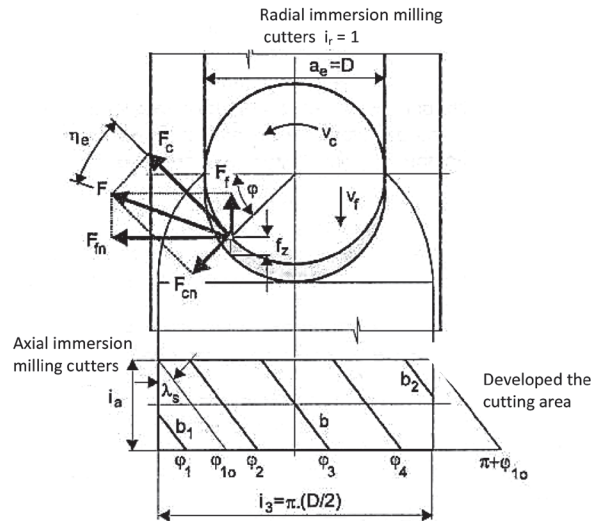


Fig. 5 Decomposition of force of cutting in helical milling [13]

Structural equations of  $F_c$  and  $F_f$  determined from the experiment

Table 2

	$F_{fn}$	$F_f$
<b>TiGr2</b>	$F_c = 12.64 \cdot v_c^{1.28} \cdot f^{0.9} \cdot a_p^{0.49}$	$F_f = 6.97 \cdot v_c^{1.4} \cdot f^{0.62} \cdot a_p^{1.46}$
<b>R<sup>2</sup></b>	0.89	0.88
<b>nTi</b>	$F_c = 1005.63 \cdot v_c^{0.18} \cdot f^{0.88} \cdot a_p^{1.07}$	$F_f = 1958.75 \cdot v_c^{-0.28} \cdot f^{0.76} \cdot a_p^{1.24}$
<b>R<sup>2</sup></b>	0.96	0.92
<b>TiGr5</b>	$F_c = 795.32 \cdot v_c^{0.17} \cdot f^{0.94} \cdot a_p^{0.84}$	$F_f = 74.74 \cdot v_c^{0.64} \cdot f^{0.88} \cdot a_p^{0.91}$
<b>R<sup>2</sup></b>	0.94	0.92
<b>TiNbTa</b>	$F_c = 127.33 \cdot v_c^{0.82} \cdot f^{1.03} \cdot a_p^{0.95}$	$F_f = 175.30 \cdot v_c^{0.28} \cdot f^{0.57} \cdot a_p^{1.36}$
<b>R<sup>2</sup></b>	0.91	0.9

Structural equations of  $F_p$  and  $F$  determined from the experiment

Table 3

	$F_p$	$F$
<b>TiGr2</b>	$F_p = 1.05 \cdot v_c^{1.95} \cdot f^{1.1} \cdot a_p^{0.94}$	$F = 14.85 \cdot v_c^{1.34} \cdot f^{0.84} \cdot a_p^{0.77}$
<b>R<sup>2</sup></b>	0.9	0.87
<b>nTi</b>	$F_p = 178.25 \cdot v_c^{0.28} \cdot f^{0.77} \cdot a_p^{1.46}$	$F = 1498.75 \cdot v_c^{0.09} \cdot f^{0.85} \cdot a_p^{1.1}$
<b>R<sup>2</sup></b>	0.93	0.97
<b>TiGr5</b>	$F_p = 2114.31 \cdot v_c^{-0.11} \cdot f^{1.14} \cdot a_p^{1.41}$	$F = 738.09 \cdot v_c^{0.28} \cdot f^{0.94} \cdot a_p^{0.93}$
<b>R<sup>2</sup></b>	0.92	0.97
<b>TiNbTa</b>	$F_p = 8.47 \cdot v_c^{1.27} \cdot f^{0.93} \cdot a_p^{1.8}$	$F = 191.39 \cdot v_c^{0.63} \cdot f^{0.88} \cdot a_p^{1.04}$
<b>R<sup>2</sup></b>	0.87	0.95

The structural equations formed a core for the creation of a complete 3D visual display of four-dimensional functionality (Figs. 6 - 9).

From the output values of the total force of cutting  $F$ , it can be stated that the lowest values of total static force  $F$  were

achieved with titanium alloy TiNbTa, and the highest values were achieved with nano-structured titanium Grade 4. From the results it can be observed that with the chosen moderate cutting speed  $v_c = 30 \text{ m}\cdot\text{min}^{-1}$ , moderate feed  $f_z = 0.04 \text{ mm}$  and low cutting depth  $a_p = 0.1 \text{ mm}$  the lowest values of total static and dynamic force of cutting  $F$  can be achieved. With the chosen moderate cutting speed  $v_c = 30 \text{ m}\cdot\text{min}^{-1}$ , moderate feed  $f_z = 0.04 \text{ mm}$  and high cutting

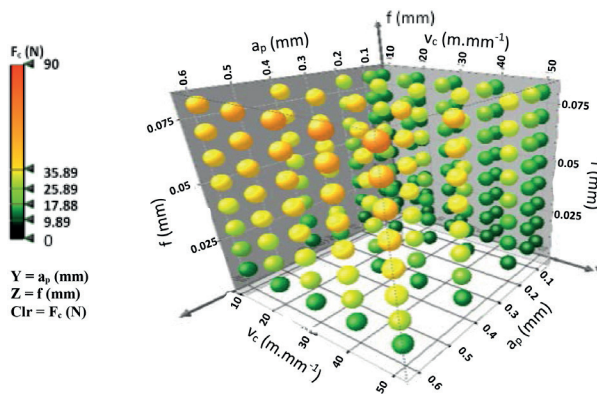


Fig. 6 Cutting force component when applying estimated cutting parameters for TiGr2

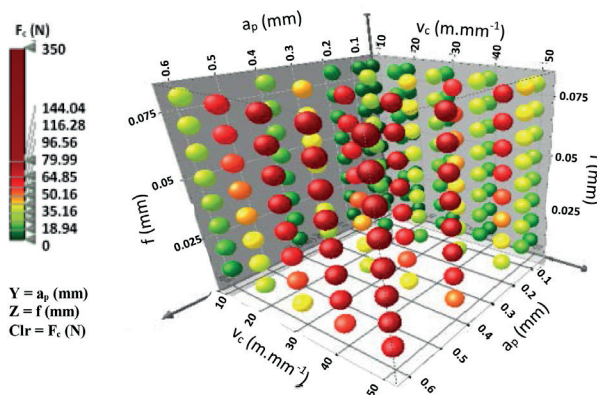


Fig. 7 Cutting force component when applying estimated cutting parameters for nTi

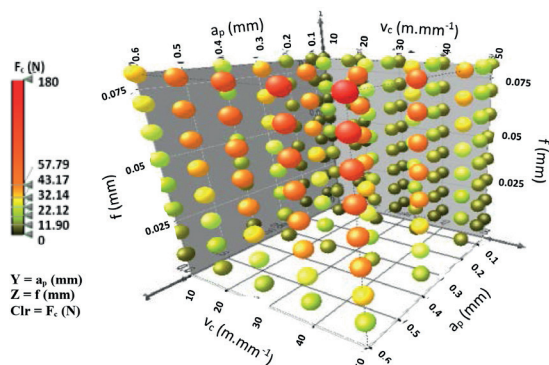


Fig. 8 Cutting force component when applying estimated cutting parameters for TiGr5

depth  $a_p = 0.5 \text{ mm}$  the highest values of total static and dynamic force of cutting  $F$  can be achieved.

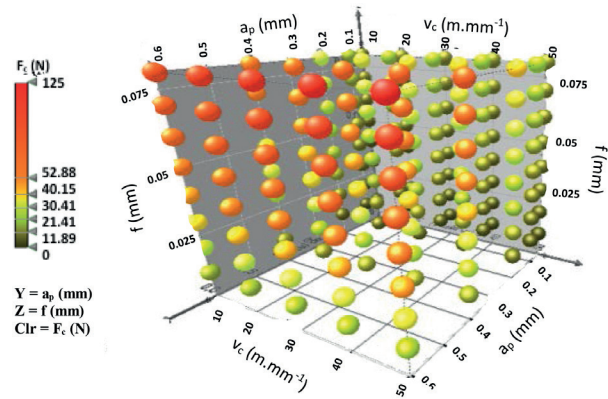


Fig. 9 Cutting force component when applying estimated cutting parameters for TiNbTa

### 5. Conclusion

Based on the analysed results of experimental tests performed on these titanium materials, technically pure titanium and its alloys behave very differently in the cutting process compared to conventional metallic materials.

The main task of the experiment was to obtain information from the machining process about the behaviour of new materials introduced into the field of dental medicine for the production of extremely thin dental implants, with emphasis on their practical use. The experiment aimed to examine the dynamic power ratios and measuring components of cutting force during milling, especially where static variables were monitored.

The facts referred to in this article provide valuable knowledge of machining titanium and titanium alloys, which can contribute to the choice of the appropriate cutting conditions for machining these materials, considering the process intensification. The correct choice of cutting conditions may reduce the static and dynamic load of the machine-tool-workpiece-jig system, and thereby it is possible to increase the performance and operational characteristics of the products and to reduce production costs. These results serve as a support for solving problems in the manufacturing of dental implants as well as in other industries using titanium-based biomaterials.

### Acknowledgement

The article was funded by the University of Zilina project OPVaV-2009/2.2/04-SORO number (2622020101) - "Intelligent system for nondestructive technologies on evaluation for the functional properties of components of X-ray diffraction" and grant project VEGA 1/0773/12 - "Implementation of technical ceramic material research to increase the innovation of hybrid products".

## References

- [1] CZAN, A., STANCEKOVA, D., MRAZOVA, M., SEMCER, J.: *Conditions of Hardmachining Materials Machinability usable in Biomedicine*, Intern. working conference: Total Quality Management - Advanced and Intelli-Genapproaches, with Second Special Conference: Manufuture in Serbia 2011, ISBN 978-86-7083-727-0
- [2] SEMCER, J., MRAZOVA, M., PILC, J.: Biocompatible Materials and their Ways of Machinin, *Technological Engineering*, 2010, 45-46, ISSN 1336-5967
- [3] TVRDON, M. et al.: *Prosthetic Stomatologia (in Slovak)*, Bratislava : Svornost, 2006, 581 p., ISBN 80-969524-4-7
- [4] SELINGEROVA, S.: *Development of dental implants (in Czech)*, Bachelor thesis, VUT Brno : Fakulta strojniho inzenyrstvi : Ustav mechaniky telies mechatroniky a biomechaniky, 2009
- [5] SIMUNEK, A. et al.: *Dental Implantolog (in Czech)*, Hradec Kralove: Stomatologicka klinika FN a LFUK, 2008, 296 p., ISBN 978-80-87009-30-9
- [6] CZAN, A., TILLOVA, E., SEMCER, J., PILC, J.: Surface and Subsurface Residual Stresses after Machining and their Analysis by x-ray Diffraction, *Communications - Scientific Letters of the University of Zilina*, No. 2, 69-76, 2013, ISSN 1335-4205
- [7] CEP, R., JANASEK A., PETRU J., CEPOVA L., CZAN A., VALICEK J.: Hard Machinable Machining of Cobalt-based Superalloy, *Manufacturing Technology*, XIII/13, 2013, 226-231, UJEP : Usti n. Labem, ISSN 1213-2489
- [8] NAPRSTKOVA, N., HOLESOVSKY, F.: *Admeasurement of Grinding Wheel Loss at FPTM*, 24<sup>th</sup> intern. colloquium Advanced manufacturing and repair technologies in vehicle industry, 2007, 159-164, ISBN 978-80-7194-962-6.
- [9] HOLESOVSKY, F., NAPRSTKOVA, N., NOVAK, M.: GICS for Grinding Process Optimization. *Manufacturing Technology*, XII/12, 2012, 22-26, UJEP: Usti n. Labem, ISSN 1213-2489.
- [11] SKUBLOVA, L., SKORIK, V., MRAZIKOVA, R., HADZIMA, B: Corrosion Resistance of Ti6al4v Titanium Alloy with Modified Surfaces. *Communications - Scientific Letters of the University of Zilina*, No. 4, 2010, 80-84, ISSN 1335-4205
- [12] CEP, R., JANASEK, A., CEPOVA, L., PETRU, J., HLAVATY, I., CAR, Z., HATALA, M.: Experimental Testing of Exchangeable Cutting Inserts Cutting Ability. *Tehnicki Vjesnik*, 20 (1), 2013, 21-26, ISSN: 1330-3651
- [13] NOVAKOVA, J., PETRKOVSKA, L., BRYCHTA, J., STANCEKOVA, D.: Influence of Cutting Parameters on Integrity Surface at High Speed Cutting. Transactions of the VSB - Technical University of Ostrava. *Mechanical Series*, vol. LV, No. 1, 2009, 203-209, Ostrava: VSB - TUO
- [14] SAPIETOVA, A., SAGA, M., NOVAK, P.: Multi-software Platform for Solving of Multibody Systems Synthesis, *Communications - Scientific Letters of the University of Zilina*, vol. 14, No. 3, 43-48, 2012, ISSN 1335-4205
- [15] LITVAJ, I., PONISCIAKOVA, O., STANCEKOVA, D., DRBUL, M.: *Knowledge Processes and their Implementation in Small Transport Companies*, 17<sup>th</sup> intern. conference Transport Means 2013, Kaunas, October 2013, Code 102486, 153-156, ISSN: 1822-296X
- [16] CZAN, A., SAJGALIK, M., HOLUBJAK, J., KOURIL, K.: Studying of Cutting Zone when Finishing Titanium Alloy by Application of Multifunction Measuring System, *Manufacturing Technology*, vol. 13, No. 4, December 2013, 428-431, ISSN: 1213-2489
- [17] PILC, J., MICIETOVA, A., SALAJ, J., CILLIKOVA, M.: The Influence of the Selected Aspects in Planing Operations by using Auto-rotation Tool, *Transactions of Famena*, vol. 29, No. 2, 2005, 55-60, ISSN: 1333-1124
- [18] VASILKO, K., PILC, J.: New Technological Knowledge of the Rotary Turning Tool, *J. Manufacturing Technology*, vol. 13, No. 4, December 2013, 571-575, ISSN: 1213-2489
- [19] KRAJCOVIC, M., BULEJ, V., SAPIETOVA, A., KURIC, I.: Intelligent Manufacturing Systems in Concept of Digital Factory. *Communications - Scientific Letters of the University of Zilina*, No. 2, 2012, ISSN 1335-4205
- [20] CUBONOVA, N.: Post-processing of CL Data in CAD/CAM System Edgcam using the Constructor of Post-processors, *Manufacturing Technology : J. for Science, Research and Production*, vol. 13, No. 2, 2013, 158-164, ISSN 1213-2489.

Branislav Micieta - Vladimira Binasova - Michal Haluska \*

## THE APPROACHES OF ADVANCED INDUSTRIAL ENGINEERING IN NEXT GENERATION MANUFACTURING SYSTEMS

*The article deals with new approaches to the development trends in the advanced industrial engineering in manufacturing systems. The authors emphasize the need for integration of advanced industrial engineering in next generation manufacturing systems, which responds to new trends of production, innovation and advanced technology. This integration represents a sustainable development so that humanization of work is increased, more effective use of natural and energy resources are achieved and production costs are reduced. Trends in the products manufacturing must meet both industrial engineering as well as production management. The development trends in the industrial engineering in manufacturing organizations must use methods and tools of advanced industrial engineering to achieve competitiveness. The third part of this article deals with specification of these approaches in next generation manufacturing systems.*

**Keywords:** Advanced industrial engineering, development trends, manufacturing system, intelligent agent, autonomous control.

### 1. Introduction

Advanced industrial engineering (AIE) must be able to use the opportunities of information technology and scientific methods of industrial engineering. Currently, enterprises are unable to adapt to rapidly changing market and to increasing demand requirements, therefore, we focused on clarifying the possibilities for further development of today's modern techniques of AIE. Industrial Engineering will be recognized as the leading profession whose practitioners plan, design, implement, and manage integrated production and service delivery systems that assure performance, reliability, maintainability, schedule adherence and cost control. These systems may be socio-technical in nature, and will integrate people, information, material, equipment, processes, and energy throughout the life cycle of the product, service, or program. The profession will adopt as its goals profitability, effectiveness, efficiency, adaptability, responsiveness, quality and the continuous improvement of products and services throughout their life cycle [1]. The humanities and social sciences (including economics), computer science, basic science, management science, highly developed communications skills along with physical, behavioral, mathematical, statistical, organizational, and ethical concepts will be used to achieve these ends. Both definitions are clearly aligned with the engineering profession as a whole. The key ingredients that make IE unique in both definitions concern the human and organizational perspectives as bodies of knowledge to be used in developing the desired systems. In this paper, we

analyze the advanced industrial engineering in next generation manufacturing systems. The paper is organized as follows: Section 1 discusses the advanced industrial engineering. Section 2 introduces the holistic production system. Section 3 presents results of integration of advanced industrial engineering to the next generation manufacturing companies and future work. Section 4 gives conclusions.

### 2. Advanced industrial engineering

Advanced industrial engineering (AIE) is based on the standard industrial engineering and pursues a goal to change companies by using new methods and approaches. It deals with the implementation of these systems and the approaches to manufacturing [2].

The significant way in advanced industrial engineering is:

1. The first such a significant way that can be expected in advanced industrial engineering is the development of information and communication technologies that will continue to influence all engineering disciplines, including the education of industrial engineers [3].
2. The second direction is to combine the artificial intelligence (AI) with robotics to create a space for the development of adaptive manufacturing, intelligent devices, and for the development of intelligent manufacturing systems [4].

\* Branislav Micieta, Vladimira Binasova, Michal Haluska

Department of Industrial Engineering, Faculty of Mechanical Engineering, University of Zilina, Slovakia  
E-mail: branislav.micieta@fstroj.uniza.sk

3. AIE will more and more move into consulting and service area at the expense of traditional production (research and development services, services related to the use of information and communication technology, management consulting, services related to enterprise management) [5].
4. Significant development of virtual reality and digital factory and their integration into design applications and make process of optimization in laboratory conditions and the following implementation in an industrial environment very fast. This is a major competitive advantage [6].
5. Another change or direction which is to be expected and advised to AIE problems is a question of a new form of cooperation. They should use the knowledge of supply chain management in virtual enterprises. Get in the virtual factory knowledge of all partners to work together in future production [7].
6. It will require a synergy of networking to create added value.
7. In the future, industrial engineering will use more techniques of operations research with advanced base of PC models for production and service problem analysis [8].
8. With the expansion of e-business, companies will need more advanced and accurate techniques for predicting the outputs. These techniques are based on computer simulation [9].
9. Modern IE must be able to use the opportunities of information technology and scientific methods of IE. It must be able to work with the principles of the new Taylorism - human knowledge base and its manufacturing expertise. We also realize a new paradigm of development of industrial engineering.
10. The integration of man and his knowledge base in manufacturing processes.

That's the premise of its success in the future. New directions in relation to the technology platform that is being developed in Europe are the basis for the development of advanced industrial engineering. The idea of advanced industrial engineering was well developed by the German professor Westkamper. Advanced industrial engineering is focused mainly on subgroups: industrial networks, adaptive production and digital engineering. They form the core of the changes through which the European Union intends to increase its competitiveness [10].

Decisive role of the rapid adaptation of production depends on the production variability and reduced time for outsourcing. Requirement for adaptive production requires a high degree of control complexity composed into the company network.

Innovative organizational performance is contingent upon the development of its innovative potential. The significant problem in the organization is the question on how to identify it and subsequently quantify it.

In general, the potential characterizes the extent of opportunities of the object under examination which are available to achieve the desired effect. We understand the desired effect as

a transformation from the existing state (IS) to the target state (WILL BE).

In relation to the need for creating and commercializing innovation it is necessary to distinguish:

1. **Innovative potential of the product.** Products and services are marketable products of human labor which must be capable of fulfilling the requirements of a potential customer. That is why the first natural object of examination is the product.
2. **Innovative potential of people.** People are carriers of the ability to invent, develop and implement new products. Therefore, the human (humanity) is another object of the study.
3. **Innovative potential of the organization.** For creating innovation and its commercialization, it is necessary to obtain tangible and intangible resources. Usually the working environment of the organization is the environment that allows you to connect the innovative potential of individuals and working groups with innovation potential of knowledge networks.

In the following sections differences of innovative potential of the product, innovative potential of people forming those innovations and innovation potential of the organization are highlighted.

### 3. The holistic production systems

The systems approach is based on the view that managers should focus on the role that each part of an organization plays in the whole organization rather than dealing separately with each part. It takes into account the different needs of various functional management areas, such as production, marketing and finance. For example, the marketing department might want to be able to sell a large variety of products, while the production unit would prefer to have long production runs of a few items, and financial managers might be mainly concerned with keeping costs as low as possible [11]. This interaction requires a high degree of communication and the breaking down of barriers between the various departments and functions of an organization. The emphasis is on management awareness of:

*Subsystems* - the individual parts that make up the whole organization, for example a unit, department, company or industry.

*Synergy* - emphasizes the interrelationships between all the parts of an organization; thus reflecting the concept that the whole is greater than the sum of its parts. This suggests that departments and units in a business are more productive when they work together than when they operate separately.

*Open and closed systems* - reflect the extent to which an organization interacts with its environment. Companies providing services to the public will normally be open systems, while those working within a larger organization, such as component part manufacturers, will be more closed.

*Boundaries* - in a closed system will tend to be more rigid than those in an open system where boundaries with the outside environments are constantly changing.

*Flows* - of information, materials and human energy which move through a system and are transformed in the process into goods and services.

The organization must always be ready for the future, look for technological trends which are perspective to include to their policies, early prepared for the development and production in order to minimize time needed for introducing the product to market and to allow customer to start using it at the right time [12]. The goal of the holistic production system is especially high added value, competitive ability and creative innovation and share knowledge in manufacturing organizations [13].

#### 4. Integration of advanced industrial engineering to the next generation manufacturing companies

Importance is placed on the ability to adjust quickly to the new production of existing requirements and the turbulent states which may be internal or external. The aim of the system is to maintain its competitiveness in the market through the production of sufficient quantities of low-cost, high products quality that meet customer demand. Due to the fact it is necessary for future generations manufacturing companies to be able to autonomously react to generating changes.

Enterprises need to have an integrated telecommunications network and information technology through which they can transmit the necessary information and dates within the organization [14]. Customers require specific and innovative products which can have adverse effects on the environment (Fig. 1).

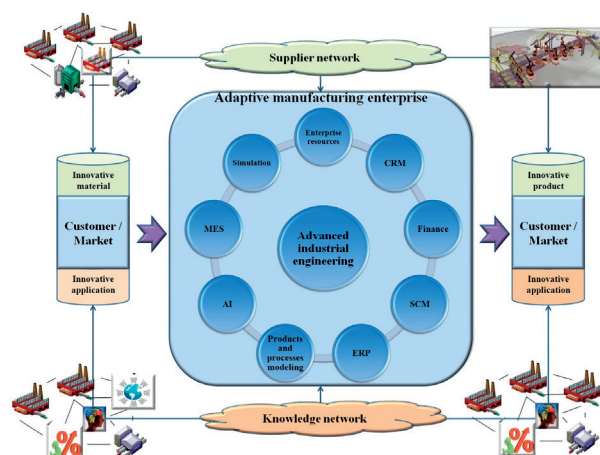


Fig. 1 Network architecture of future manufacturing enterprises

For the development of new product platforms it is necessary to ensure mutual cooperation with partner companies to provide the necessary knowledge to develop new products and solutions on base of sharing experience [15 and 16]. At the same time the intention is to develop advanced materials and new approach to analysis. Simultaneously, the customer must specify requirements through the communication interface over which the enterprise will obtain documents on draft products:

- Implementation of unique information technology.
- Reliable modeling, monitoring and simulation of manufacturing processes.
- Reliable detection of abnormalities.
- The sustainability of production.
- Fast reconfiguration depending on the external environment.

The development of sophisticated information technology and intelligent control of business processes is the key to the humanization of human labor. The trend will accelerate depending on the production environment. In production it is necessary to use a number of information technologies with support of digital engineering (control systems), modeling and monitoring systems. In view of turbulent external environments it requires a high complexity of supply chain management which affects the development of software platforms for enterprise resource planning, management of finances and time efficiency performance of the contracts.

#### 4.1 Digital manufacturing

The turbulent market and global competition affect the requirement for shorting the innovation cycle. Many enterprises tasks are generated as a result of these aspects and growing of complexity within the network cooperation. Disposition of product models allow more simultaneous realization of product development and manufacturing [17]. Consequently, the time which is required to construct models will be shortened and simulation will provide the desired results for the optimum adjustment of production processes.

Digital manufacturing (Fig. 2) provides effective support to business process in manufacturing companies. New product development and meeting deadlines of orders forms an essential application area of supporting tools for digital production.

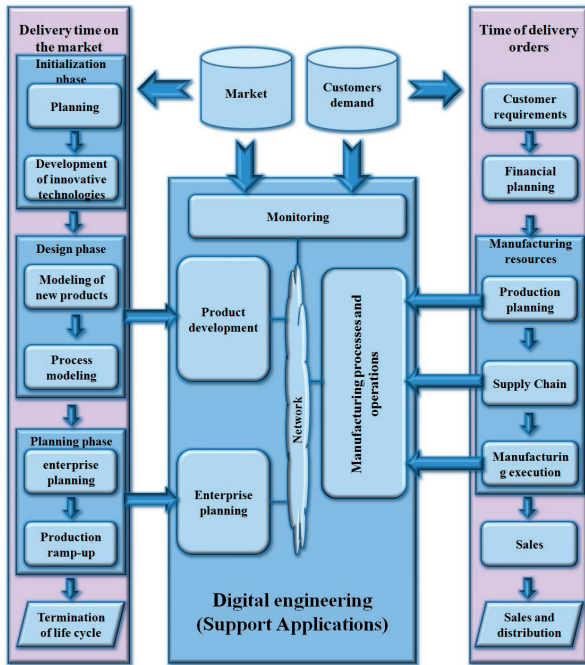


Fig. 2 Digital manufacturing in enterprise processes

4.2 Integration of artificial intelligence

Artificial intelligence that ensures autonomous tasks directionally through the agent communication should be integrated into an enterprise system. Individual agents can transmit tasks and in the frame of interactive activities conduct evaluation activities. Mutual communication is based on priority rules for the realization the current transformational needs of the

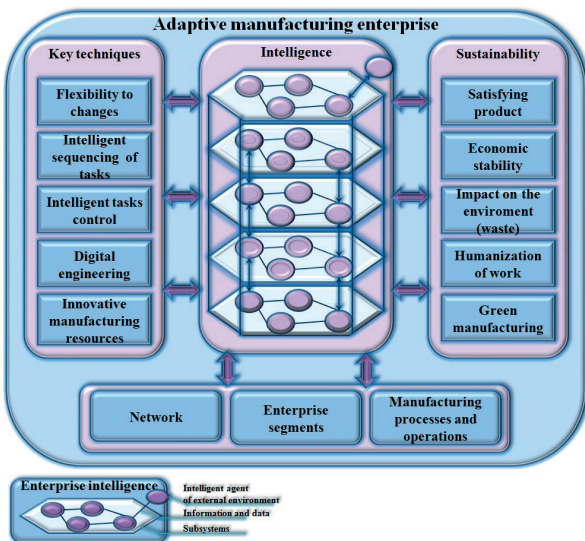


Fig. 3 The integration of artificial intelligence into enterprise infrastructure

defined roles in meeting the corporate goals. The key technology is needed to build an adaptable manufacturing enterprise with embedded intelligence. This technology is represented by the agent communication infrastructure.

Intelligent control mechanism should ensure the transfer of data and information which subsequently perform analytical procedures, evaluation action and remedial activities (Fig. 3). The aim of the integrated control system is the sustainability of the production company in a competitive environment which includes the prerequisites.

4.3 An intelligent learning mechanism

The mechanism is designed to educate the manufacturing facility for the purpose of autonomous operation (Fig. 4). The emphasis is on acquiring knowledge from external and internal environment which is necessary for optimizing the design of products, manufacturing processes, operations and production plan [18]. Output parameters are monitored by the sensory disposition which converts the signals into actual data values and initializes activity of detection mechanism to detect abnormalities through a simulation model. The increasing complexity of system architecture may result in adverse effects on the autonomous control system tasks and system reliability. In view of the fact that manufacturing or assembly system must be equipped with reconfigurability which provides quick configuration of maintenance system and switches generating variants by switching generating tasks depending on the need of production of a particular family of work pieces and subassemblies parts by adding or removing functional elements.

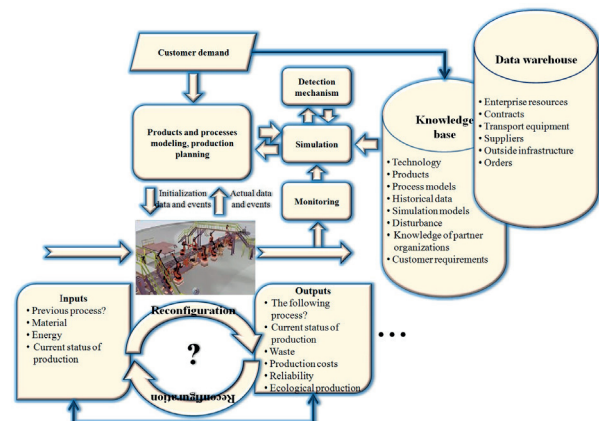


Fig. 4 Intelligent learning mechanism of manufacturing resources

The purpose of the reconfiguration is to change system functionality and ensure the scalability of production capacity. Based on rapid response to changing requirements and the actual behaviour of the manufacturing system, machines (handling

units) can be independently added, removed, modified and converted by the reconfiguration of system. The system with given ability may increase life of production and should offer a cost effective solution in the long term.

## 5. Conclusions

Transferring this holistic view of a production plant leads to main partial systems that have to be considered: product design, process planning (with interlinked machines and personnel controlled through production management), energy model

(the technical building services and the building shell). Having in mind the integrated process model, all involved input and output flow result in a complex control system with dynamic interdependencies between these subsystems via different internal and external influencing variables. Advanced industrial engineering cannot function without the excellence industrial engineers. As a result of the competitive struggle it is necessary for existing enterprises to adapt rapidly and flexibly to the changing requirements of the current market environment. In view of the fact it is necessary to rebuild the thought architecture of today's manufacturing companies.

## References

- [1] GREGOR, M., MEDVECKY, S.: Zilina University Concept of Digital Factory. *Communications - Scientific Letters of the University of Zilina*, vol. 10, No. 2, 2008, 60-66, ISSN 1335-4205
- [2] KRAJCOVIC, M. et al.: Intelligent Manufacturing Systems in Concept of Digital Factory. *Communications - Scientific Letters of the University of Zilina*, vol. 15, No. 2, 2013, 77-87, ISSN 1335-4205, 2013
- [3] GASO, M., TUREKOVA, H.: *Management of Innovation Projects (in Slovak)*, InvEnt 2009, Zilina: SLCP, ISBN 978-80-89333-07-3
- [4] DULINA, L., BARTANUSOVA, M.: *Ergonomics and Preventive Medicine in Companies in Slovak Republic and the EU. Ergonomics 2013*, Zagreb: Croatian Ergonomics Society, 2013, 81-86, ISSN 1848-9699
- [5] MICIETA, B., TUREKOVA, H.: *Innovation Management (in Slovak)*, Zilina: Georg, 2010, ISBN 978-80-89478-02-6
- [6] MAGVASI, P., GREGOR, M.: *Advanced Industrial Engineering and Quality of Industrial Enterprises. Kvalita produkcie od kvality k zodpovednosti a inováciám*, Kosice: Technicka univerzita, 2013, 38-42, ISBN 978-80-553-1466-2
- [7] RAKYTA, M., BUBENIK, P.: The Economic Crisis, the Time to Develop New Approaches towards Technological Development (in Slovak), *Technika: casopis o priemysle, vede a technike*, vol. 8, No. 5, 2010, 50-51, ISSN 1337-0022
- [8] STASZEWSKA, J., BARGLIK, J.: *Considerations on the Cluster Concept as a Tool to Improve the Efficiency of the Logistics Process (in Polish)*, Politechnika Slaska, 2008.
- [9] KOHAR, R., HRCEK, S.: *Dynamic Analysis of Rolling Bearings with Elastic Cage*, 54<sup>th</sup> intern. conference of Machine design departments, Hejnice, September, 2013, ISBN 978-80-7372-986-8, p. 211-216
- [10] GEYER, A.: *The Challenge of Sustainable Manufacturing*. IPTS, 2010
- [11] SLAMKOVA, E. DULINA, L., TABAKOVA, M.: *Ergonomy in the Industry (in Slovak)*, Zilina: Georg, 2010. ISBN 978-80-89401-09-3.
- [12] MICIETOVA, A., CILLIKOVA, M.: *Technology - Cutting (in Slovak)*, Zilinska univerzita, 2009, 486 p., ISBN 978-80-554-0010-5.
- [13] MICIETOVA, A., CILLIKOVA, M., SALAJ, J.: *Influence of Some Selected Factors on Surface Quality when Cutting by Plasma and Laser Beam, J. of Machine Manufacturing: Design and Manufacturing*, vol. 49, No. E3-E5, 2009, 104-106, ISSN 0016-8580
- [14] COLISEUM, B., WAYNE, F.: *Revisiting System Paradigms from the Viewpoint of Manufacturing Sustainability*, ISSN 2071-1050, 2011, 1323-1340.
- [15] SU, J.: *Component-based Intelligent Control Architecture for Reconfigurable Manufacturing Systems*, Virginia, 2007.
- [16] VYATKIN, V.: *Function Blocks for Embedded and Distributed Control Systems Design*, New Zealand: ISA, 2011, ISBN 978-1-936007-93-6.
- [17] MAVRIKIOS, D., PAPAKOSTAS, N.: *Digital Manufacturing: History, Perspectives, and Outlook*, 2008
- [18] BOTTI, V., GIRET, A.: *A Multi-agent Methodology for Holonic Manufacturing Systems*, London, 2008. ISBN 978-1-84800-309-5.

Martin Krajcovic - Gabriela Gabajova - Branislav Micieta \*

## ORDER PICKING USING AUGMENTED REALITY

*This article examines the problem of application of augmented reality in terms of picking goods in static systems with the deployment of a man (systems „goods to man“). Article describes a comprehensive methodology for the use of augmented reality in the process of picking starting from the preparation of input data, through optimizing the movement of workers in the warehouse, to actual worker navigation using augmented reality. The problem was solved on the authors' workplace and the proposed solution has been verified in the experimental workplace built under the concept of ZIMS (Zilina Intelligent Manufacturing System) which is developed at the University of Zilina in cooperation with the Central European Institute of Technology (CEIT).*

**Keywords:** Augmented reality, order picking, pick-by-vision, Unifey Design.

### 1. Paperless picking systems

Picking process creates in the logistics chain an irreplaceable role associated with the preparation and processing of orders. With increasing pressure on the quality and timeliness of deliveries, and the increasing number and diversity of picking items, also new forms of organization are developed and new technologies are applied to the picking process [1].

The traditional approach is based on picking goods according to the documents. This principle is advantageous mainly in terms of its simplicity, financial cost and relative flexibility to change volumes of picking process. On the other hand, the need for repeated reading and checking the data in the documents leads to significant time losses and higher error rates due to human error.

Therefore, in practice, we should start to apply paperless picking systems. The advantage of these systems is mainly in replacing the traditional paper documents by picking orders electronically, which allows, in combination with other technologies, to simplify, accelerate and improve the process of searching items into the picking order. An example of such a method of picking is called "Pick-by" systems.

Types of "pick-by" systems are [1]:

1. **System Pick-by-light** (Pick-to-Light): This system is based on storage places equipped with special light panels which contain the lights indicating the storage location from which the goods need to be picked. The navigation system Pick-by-light is also used in reverse action, i.e. when saving assortment of items in the correct storage position. Then we talk about the so-called Put-to-light system. The system Pick-by-light

is not suitable for large warehouses where there are large distances between picking items.

2. **System Pick-by-voice:** The picker is equipped with a headset (headphones + microphone) ensuring two-way communication between the picker and control system and portable terminal which is used for storing and radio transmission of information between the picker and control system. The system includes a radio transmission of information and voice recognition software. The picker receives from the control system gradually in the optimal sequence information necessary for picking individual order lines. After removing the item, the picker reports back to the managing systems the number of taken items, also confirms the completion of the processing line orders. The system Pick-by-voice puts higher demands on worker's concentration (only voice information) and is not suitable for noisy operations.
3. **System Pick-to-belt:** Items are in the required quantity collected from a store and placed on the conveyor which transports them automatically to a packaging workplace.

In addition to above mentioned basic types of "pick-by" systems, manufacturers of storage and handling equipment also offer other types of paperless picking systems such as: e-pick, pick-to-tote, pick-to-bucket, etc., which further modify and develop the fundamental principles of mentioned "pick-by" systems.

Among the new, progressive types of "pick-by" systems is currently classifiable the picking system known as Pick-by-vision [2] which represents the use of augmented reality for navigation worker during picking and which is currently the subject of intense research in terms of the technological solutions and suitability of its application in industrial practice.

\* Martin Krajcovic, Gabriela Gabajova, Branislav Micieta

Department of Industrial Engineering, Faculty of Mechanical Engineering, University of Zilina, Slovakia

E-mail: martin.krajcovic@fstroj.uniza.sk

## 2. Augmented reality technology

Augmented Reality (AR - Augmented Reality) is one of the fast growing sectors of virtual reality. The basis of augmented reality is the ability to combine elements of the real and virtual worlds into a single view. Augmented reality is a technology supported by human visual perception. With appropriate combination of real and virtual objects it is possible to provide large amount of additional information. The condition is to preserve the link with the user and real environment [3].

In contrast to virtual reality, which is all modeled by computer, augmented reality does not replace the real world, but only adds selected virtual elements or objects into the real environment. The view can be realized through the monitor and the camera or using HMD (Head Mounted Display), i.e. equipment placed on the head [4].

In practice there are two basic types of systems for augmented reality [5]:

1. Systems using position sensors and transparent display: position sensor sends information about the position and direction of the user's perspective, the scene generator based on this information displays virtual objects located in the user's field of vision. Subsequently, virtual objects are projected on semi-transparent mirror through which the user sees the real scene.
2. Capturing real camera image for the registration of markers that indicate the position of virtual objects: a video camera captures the real scene and sends it to the computer, the software on the computer is looking for the marker. If the marker is found, the software identifies the type of tags, calculates the camera position to the marker and assigns to the marker image of the virtual object and then draws on display the resulting image of scenes – the real scene added by the virtual objects.

## 3. The application of augmented reality in picking process

The proposed methodology for augmented reality applications in the process of picking the goods consists of the following basic steps (Fig. 1):

1. Preparation and processing of input data;
2. Proposal of the optimal picking route;
3. Proposal for navigation system using AR;
4. Selection of software and hardware resources;
5. Transformation of picking routes into the process map (workflow) in software for augmented reality;
6. Realization of picking process.

A more detailed description of each step of the methodology is presented in the following chapters of this article.

### 3.1 Base of input data

To be able to pick items from warehouse by order using augmented reality, it is necessary to know some basic input data and information. A basic resource for obtaining input data is warehouse management system (WMS - Warehouse management system). Required information for picking is [6]:

1. Information about the item itself: name of the item, code (catalog number), the available quantity, the number of items on stock position, type of items (food, chemical product, etc.), specific handling (weight, shape, dimensions, etc.).
2. Information about the location of items, warehouse map: name of the center, name of the department, room, mark of rack or other device where the item is stored.
3. Other information that may be useful for warehouseman: information about the supplier (name, address, etc.), information about the income items (date, time, quantity, etc.), specific information about the items (time of consumption in food products, specific conditions for handling with chemical products, etc.), etc.

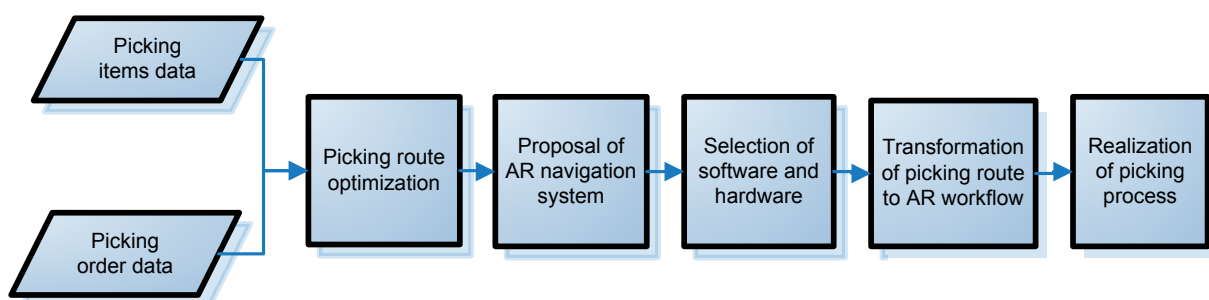


Fig. 1 The methodology of using augmented reality in the process of picking

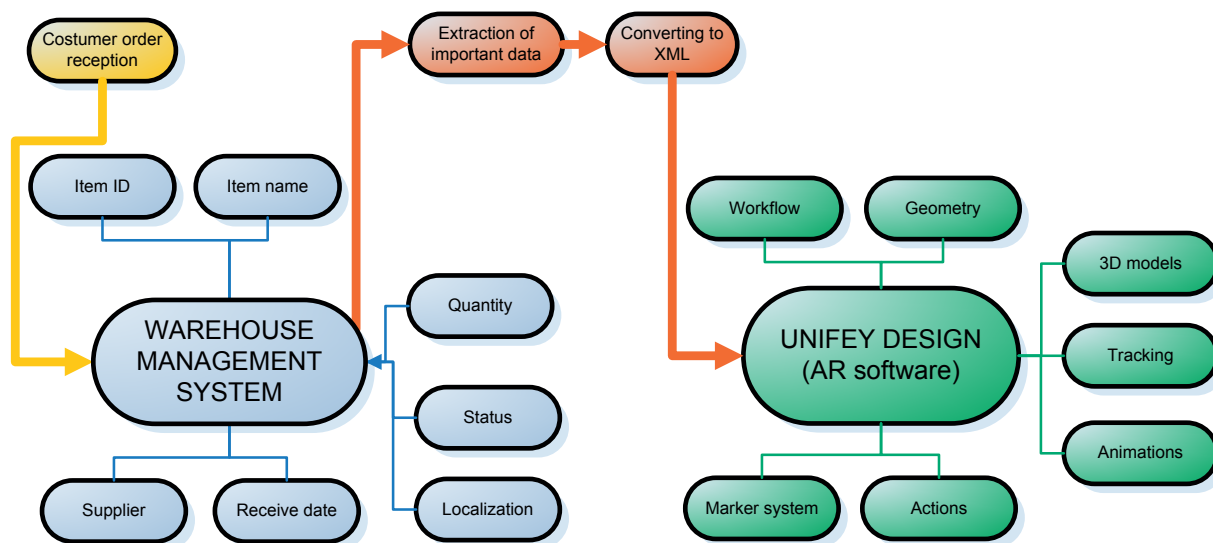


Fig. 2 Interconnection of WMS with AR

One of the basic conditions for interconnection the AR system with WMS is the ability to extract information from the package which contains information system, only those, which are further input to software support for augmented reality [7]. This information must be exported to a format that the software for augmented reality could use as input for workflow and other actions. One possible solution is export to the XML (extensible markup language) format which is currently used as a standard for data exchange between applications.

Interconnection of information system with the software solution for augmented reality is shown in Fig. 2 and can be summarized into the following steps:

1. Finding the required data in WMS - the item name, item code, location in the store, the available number, specifications, etc.,
2. Export data from WMS in a compatible format (.xml),
3. Import data in .xml format to the software for augmented reality,
4. Creating a scenario using AR tools - location of markers, position of displayed information, animation, motion, rotation, control of objects, etc.

### 3.2 Proposal of the optimal picking route

The process of picking path optimization includes the following steps:

1. Identifying the position of picking items in the warehouse (warehouse address position),
2. Assigning coordinates of storage position of each storage unit which includes searched item, determine the coordinates of the reference or zero point - the beginning of the coordinate system),

3. Route optimization of collection of items by selected algorithm,
4. Sorting picking items by the proposed route.

Choosing the most appropriate routes for workers' movement in the warehouse during the picking largely depends on the use of appropriate methods. The most appropriate method seems to be the Traveling Salesman Problem (TSP) [8]. For solution of TSP we use various methods. In the view of the nature of the task and the restriction that the picking worker must move only along the aisles between the rows of shelves, the Nearest neighbor heuristic method (resp. Greedy algorithm) was chosen, which provides satisfactory results at low computational complexity of the algorithm. When applying the nearest neighbor method to the conditions for optimizing the picking route, the route always begins in a nodal point which represents the starting and final position of the process of picking.

### 3.3 Proposal of navigation system using AR

The main task of augmented reality in the process of picking items is to navigate the worker in the warehouse in such a way that the worker moves by the shortest route designated in the previous step and also, this system provides the worker with basic information necessary for elimination of errors in the picking process (designation of the correct item for picking, determination of correct amount of removed items).

When designing a suitable navigation system with the support of AR, we can build on existing variants of tracking systems used in AR [9]: marker tracking system, 3D extensible tracking systems, 2D markerless tracking system, 3D markerless tracking

system, geolocation tracking systems, gyroscopic tracking systems, combination of individual tracking systems.

In the case of the navigation system in the process of picking, the marker appears as the optimal tracking system that is based on the use of special signs (markers) in the real scene, which are used to determine the position of the worker and also for identification of virtual object which has to be added to the real scene. Marker tracking system works according to the principle 2 described in Chapter 2.

The main reasons for the selection of marker tracking system [10]:

1. easy way to navigate,
2. wide support from software solutions,
3. low cost,
4. wide range of generating markers.

For navigation during the picking process, following method of displaying information (Fig. 3) was chosen:

Položka	Ks
Telo vidlice	1
Hlava vidlice	1
Púzdro	1
Kolík fázový	4
Zaist'ovacia matica	1

a) picking order



b) navigation symbols

Fig. 3 The basic elements of the navigation system with the support of AR

*The table presenting the order* - contains items which have to be picked. In the beginning all lines of table are marked in red. After picking a particular item, its name will change from red to green.

*Yellow arrow* - yellow arrow is a directional arrow that indicates the direction of the nearest location of items in a row for picking. By following the directional arrow operator is passively navigated to the item.

*Green arrow* - green arrow shows to the specific storage position from which the item has to be picked.

*Numerical information* - number located above the box represents the number of items which have to be picked from a particular type of stored items.

Move for picking the next item in the list is done after checking the previous item has already been collected. Next step is displayed after pushing the confirmation button.

### 3.4 Selection of software and hardware resources

For navigation through markers and displaying navigation elements described in Chapter 3.3 following software and hardware are necessary:

- Software solution - software Unifeye Design from Metaio is designed for displaying virtual information using augmented reality. It is also suitable for use in the process of navigation, it allows the generation of markers and includes Workflow tool which can create a scenario of displaying virtual objects and how to control virtual objects in real space.
- Hardware solution:
  - portable computer which contains the Windows operating system and, at least, 3 USB ports and also allows the VGA connection to Vuzix glasses for augmented reality.
  - VUZIX glasses for augmented reality.
  - handcart to store computer and picking items.

### 3.5 Transformation of picking route into a scenario of workflow for AR

An essential part of applications of augmented reality into the picking process is the creation of a scenario. The scenario defines how virtual elements added in the real scene will behave (display and control objects in space and time). Chosen software solution Unifeye Design has its own tool for creating scenarios - Workflow tool [11]. Workflow allows you to create a scenario by organizing individual blocks and creating links between them (Fig. 4). The resulting scenario from Workflow tool is saved as XML code.

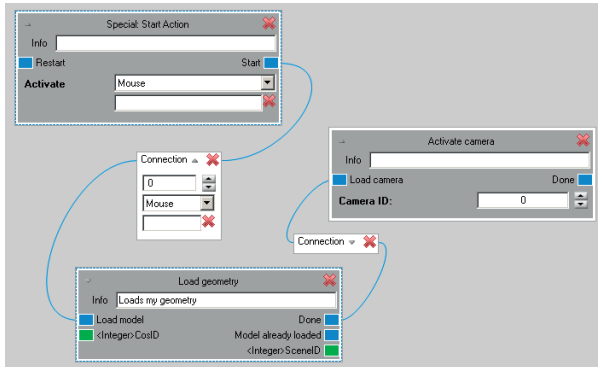


Fig. 4 Example of part of scenario created using Workflow

Basic activities that can be assigned to each block are divided into the following groups:

- Camera - work with camera, camera work, its activation, calibration and settings.
- Geometry - work with displayed objects such as animation, rotation, scale, visibility, timing, loading and removing the object.
- Interaction - interaction of virtual objects (e.g., motion control or object rotation).
- Monitoring - allows you to stop the current monitoring and load the new configuration tracking.
- Special functions - these blocks allow the switch to full-screen mode, synchronization, insert music background, and more.

The scenario of picking process is always based on specific order picking which is transformed into an optimal picking route. This implies the ranking of picking items and also the position of each item in the warehouse which determines at each step of the picking process kinds of navigation symbols which are assigned to the markers.

**3.6 Implementation of picking process with AR**

The process of picking using augmented reality runs as follows (Fig. 5):

1. In the first step the worker takes:
  - the box for picked items
  - the truck where the computer and the box are placed,
  - glasses for AR (iWear Vuzix VR920) which is connected to the computer.
2. After loading the picking order the worker can see the table which is placed on marker. The table contains a list of picked items arranged in the right sequence. All items are marked in red color, progressively, as they are picked the color changes from red to green.
3. After the confirmation with the button on the keyboard, the yellow directional arrow appears to navigate the worker

which direction he needs to move. The directional arrows are shown from two sides, from the left and the right side of rack, for worker's better orientation. In addition to the yellow direction arrows the worker can see a green arrow pointing to the box from which items need to be picked and number of pieces shown by numerical information.

4. After taking the item and confirmation the worker can see the table again where the first line changes from red to green (because it has already been picked).
5. After confirmation the system again displays arrows and navigates the worker to the nearest point of picking - to the next item in the order list.
6. This process is repeated until the last item is picked.

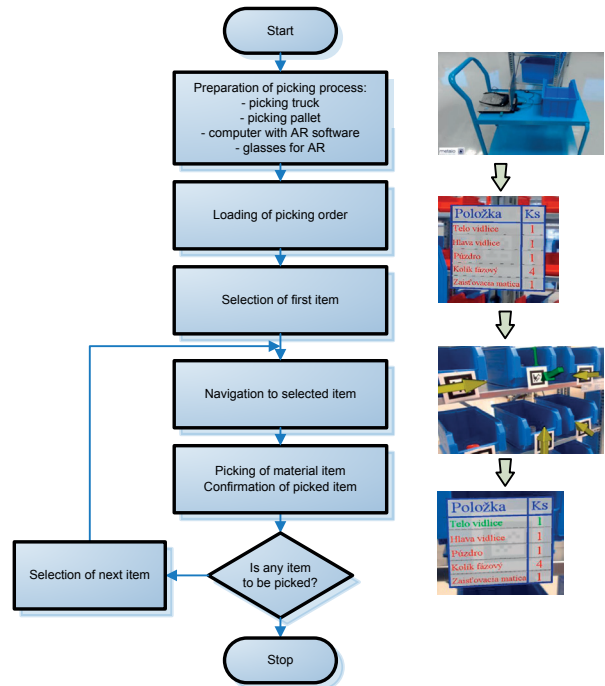


Fig. 5 Implementation of the picking process using augmented reality

**4. Conclusion**

Picking process with the support of augmented reality helps to short the time of finding and identification of items, it reduces cognition burden of workers in the process of selection, it reduces picking errors, increases flexibility, reliability and productivity and ultimately, it reduces logistics costs for picking process [12]. Described picking system is suitable for customized environment characterized by permanent change of storage places of items. This methodology of picking with the support of AR. was verified by the experimental workplace, which was built in within the concept ZIMS (Zilina Intelligent Manufacturing System) [13]. The problem of AR applications in the processes of picking

requires further research especially in terms of closer integration of AR and WMS systems, increasing comfort of hardware components (wireless glasses, mobile terminal) and the possibility

of linking the picking system with automatic identification systems (barcodes, RFID).

## References

- [1] KRAJCOVIC, M.: Paperless systems of order picking in practice (in Slovak). *Produktivita a inovacie*, No. 1, 2006, ISSN 1335-5961
- [2] SCHWERDTFEGGER, B. at al.: Pick-by-Vision: *A First Stress Test*. 8<sup>th</sup> IEEE intern. symposium on mixed and augmented reality, 2009. Orlando : Florida, 115 - 124, ISBN 978-1-4244-5390-0
- [3] BRUNO, F., CARUSO, F., DE NAPOLI, L., MUZZUPAPPA, M.: Visualization of Industrial Engineering Data in Augmented Reality. *J. of visualization*. ISSN 1343-8875, vol. 9, No. 3, 319-329, 2006.
- [4] GASO, M., SMUTNA, M.: *The Relations of Input Quantities for Creation of Stereoscopic Record*. Transcom 2011. 9<sup>th</sup> European conference of young research and scientific workers, 2011, University of Zilina, ISBN 978-80-554-0370-0, 59-62.
- [5] MIRANDOVA, G., GABAJ, I., GRZNAR, P.: *Use of Augmented Reality in Visual Management*. Industrial engineering moves the world - InvEnt, University of Zilina, 2012, ISBN 978-80-554-0542-1, 112-115.
- [6] SLAMKOVA, E., DULINA, I., TABAKOVA, M.: *Ergonomics in Industry (in Slovak)* - 1<sup>st</sup> ed., Zilina: Georg, 2010, 262 p., ISBN 978-80-89401-09-3.
- [7] REIF, R. et al.: *Pick-by-Vision Comes on Age: Evaluation of an Augmented Reality Supported Picking System in a Real Storage Environment*. 6<sup>th</sup> intern. conference on computer graphics, Virtual Reality, Visualisation and Interaction in Africa (Afrigraph 2009), 2009.
- [8] BRAU, H. et al.: *Gestaltung von augmented reality applikationen für kommissionieraufgaben*. L. Urbas and C. Steffens, editors, Zustandserkennung und Systemgestaltung Bd. 19. VDI-Verlag, 2005.
- [9] KALL, F., GABAJ, I.: *Design of Assembly Workstations Supported with Smart Technologies*. CO-MAT-TECH 2012. 20<sup>th</sup> intern. Scientific conference, 2012, Trnava: Alumnipress, ISBN 978-80-8096-180-0, 493-501.
- [10] DULINA, L., BARTANUSOVA, M.: *Ergonomics and Preventive Medicine in Companies in Slovak Republic and the EU*. Ergonomics 2013, Zagreb: Croatian Ergonomics Society, 2013, 81-86, ISSN 1848-9699.
- [11] FURMANN, R., STEFANIK, A.: *Progressive Solutions Supporting Manufacturing and Logistics Systems Design Developed by CEIT SK, s.r.o. (in Slovak)*. Produktivita a inovacie, Zilinska univerzita: Ustav konkurencieschopnosti a inovacii, vol. 2, No. 2, 2011, 3-5 ISSN 1335-5961.
- [12] HNAT, J.: *Virtual Factory Framework*. Industrial Engineering Moves the World - InvEnt 2012, University of Zilina, 2012, 56-59, ISBN 978-80-554-0542-1.
- [13] KRAJCOVIC, M. et al.: Intelligent Manufacturing Systems in Concept of Digital Factory. *Communications - Scientific Letters of the University of Zilina*, vol. 15, No. 2, 2013, Zilina, 77-87, ISSN 1335-4205.

Branislav Micieta - Martin Gaso - Martin Krajcovic \*

## INNOVATION PERFORMANCE OF ORGANIZATION

*Globalization has confirmed that the competitive ability of organizations is conditioned by the successful development of innovations. Innovation management and development of innovative potential of organizations are becoming a scientific problem, since the existing approaches in this area do not have satisfactory results. The paper presents a new approach to enhancing innovation performance of the organization that is built on a systematic examination of possible innovation potential of the organization and purposeful creation of a suitable innovative environment in the organization.*

**Keywords:** Innovative potential, innovation performance, market, organization, innovation.

### 1. Introduction

Quality of decision-making depends on the degree of knowledge of causal relations. Deciding on new products, services as well as the development and implementation of new systems is associated with the uncertainty and risk. It may be minimized if we can correctly estimate the consequences and affect the causes of controlled processes. However, this requires the design and use of scientific method for the systematic examination of causation and purposeful search, quantification and increasing the innovation potential in the organization. Only then we can expect a successful commercialization of innovation and success with the customer.

On the one hand, the system identification and quantification of the innovation potential of the organization and, on the other hand, creating an appropriate (innovative) environment in the organization is needed for the successful implementation of this process. We need the environment that will systematically create conditions for the generation, development and commercialization of innovations.

### 2. Innovative potential in the organization

Innovative organizational performance is contingent upon the development of its innovative potential. The significant problem in the organization is the question on how to identify it and subsequently quantify it.

In general, the potential characterizes the extent of opportunities of the object under examination which are available to achieve the desired effect. We understand the desired effect as a transformation from the existing state (IS) to the target

state (WILL BE). In relation to the need for creating and commercializing innovation it is necessary to distinguish:

1. **Innovative potential of the product.** Products and services are marketable products of human labor, which must be capable of fulfilling the requirements of a potential customer. That is why the first natural object of examination is the product.
2. **Innovative potential of people.** Carriers of the ability to invent, develop and implement new products are people. Therefore, another object of the study is a human (humanity).
3. **Innovative potential of the organization.** For creating innovation and its commercialization, it is necessary to obtain tangible and intangible resources. Usually the working environment of the organization is the environment that allows you to connect the innovative potential of individuals and working groups with innovation potential of knowledge networks.

In the following sections are highlighted differences of innovative potential of the product, innovative potential of people forming those innovations and innovation potential of the organization.

#### A. Innovative potential of the product

Global markets require targeted creating of specific products. We are asking how the offered product suits the specific environment (customer) and what is expected of the product to succeed. Just to answer these questions, the innovative potential of the product ( $IP_{PR}$ ) must be examined. From a systemic perspective, it is important to opt for such methodologies that continuously assess the potential because it is a newly created tradable product, economically efficient, environmentally

\* Branislav Micieta, Martin Gaso, Martin Krajcovic

Department of Industrial Engineering, Faculty of Mechanical Engineering, University of Zilina, Slovakia  
E-mail: kpi@fstroj.uniza.sk

friendly, ready to be produced, corresponding to the legislation and acceptable for people. In connection to this, it is needed to parametrize these conditions for success.

During the innovation projects, innovator must maximize the innovation potential of the product offered by maximizing the following parameters: marketability ( $p_1$ ), economic efficiency ( $p_2$ ), environmental friendliness ( $p_3$ ), technology ( $p_4$ ), legislation ( $p_5$ ), and culturalism ( $p_6$ ).

$$\max IP_{PR} = \max f(p_1, p_2, p_3, p_4, p_5, p_6)$$

$$\text{while : } p_1 > 0 \wedge p_2 > 0 \wedge p_3 > 0 \wedge p_4 > 0 \wedge p_5 > 0 \wedge p_6 > 0$$

By setting the evaluation criteria for  $p_{1-6}$ , it is possible to guide the decision already in solving the subtasks of the innovative project.

Innovative potential of the product is the characteristics of the product, which through these parameters expresses its possible commercialization. Innovative potential of the product can be increased by aligning its parameters with the anticipated market requirements. The condition is that none of the product's parameters is in a direct violation of the anticipated market requirements.

As we see, we can assess the potential success of innovation through the key parameters that affect the global market. It is fundamentally a new view eliminating subjective quantification of the strengths and weaknesses of the product.

**a. Innovative potential of people**

Innovative potential of **people** (individuals, groups, humankind) refers to the possibility to invent, develop and implement a product that succeeds with customers. The need to invent is associated with creativity. Creativity means a set of characteristics that gives humans the ability to create a new product or a new process due to changes in human consciousness. Knowledge of the development of creativity allows for the results of scientific investigations in the field of psychology, medicine and management. Knowledge, that every creative individual is a carrier of innovation potential, is essential for studying the innovation potential of people. Innovative potential of an individual can be expressed as a function of three parameters  $i_{1-3}$ .

$$IP_1 = f(i_1, i_2, i_3)$$

$$\text{while: } i_1 > 0 \wedge i_2 > 0 \wedge i_3 > 0$$

where:

$IP_1$  innovative potential of individual,

- $i_1$  motivation of the individual, his ability and willingness to cooperate, his personal interest for achieving the objective, courage and desire or need to create something new,
- $i_2$  explicit and tacit knowledge of the individual,
- $i_3$  working environment.

Innovative potential of defined group of people is formed by contributions of cooperating individuals. It can be expressed through the innovative potential of individual group members.

$$IP_{PE} = f(IP_{11}, IP_{12}, \dots, IP_{1n})$$

where:

$IP_{PE}$  innovative potential of people

$IP_{ix}$  innovative potential of x-th individual,

n number of group members.

Stimulating element in maximizing the above parameters is the effective cooperation. Innovative potential of an individual lies mainly in its openness to adopt new knowledge and willingness to cooperate. Individual is the fountain of good ideas, but needs colleagues for his development and implementation of ideas.

By introducing appropriate forms of work organization (e.g. teamwork) we can achieve even greater increase in the synergistic effect of using the innovative potential of individuals.

**b. Innovative potential of organization**

To provide standard operation of the organization requires considerable effort and resources. However, if the organization has to develop, it is necessary to purposefully implement the development activities. To create and maintain an innovative organization is possible if significant support will be given to the use of existing innovative potential of individuals and groups. This means providing information, material and financial resources necessary to achieve the objectives set in relation to the use of the innovative potential of people.

Innovative potential of the organization is a function of all of its available resources. These resources can be divided into four basic groups, while the prerequisite for this process are sufficient funds. Innovative potential of organizations can be, therefore, expressed as follows:

$$IP_0 = f(r_1, r_2, r_3, r_4)$$

$$\text{while: } z_1 > 0 \wedge z_2 > 0 \wedge z_3 > 0 \wedge z_4 > 0$$

where:

$IP_0$  innovative potential of organization

$r_1$  people ( $IP_p$  - innovative potential of people),

- $r_2$  information (technology, licenses, patents, trade mark, trade secrets, know-how, codified knowledge,...),
- $r_3$  material (tangible assets, technical equipment, materials, energy, ...)
- $r_4$  funds

Innovation potential of **organization** refers to the ability of organization to coordinate the work of individuals, working groups and to develop links in the network of cooperating organizations in order to succeed with customers. To utilize the innovative potential of the organization it is also necessary to ensure the efficient organization and working environment [1].

Neither individual nor group or organization is able to exploit the potential of the knowledge contained in the global business environment by themselves. Wealth of the whole range of disciplines and knowledge potential hidden in the individual organizations cannot be used without networking and fellow innovators [2]. Networking and coordinated cooperation can strengthen the innovative potential of each of the organizations involved.

**c. Integrated innovative potential**

It is possible to present an integrated innovative potential through schematic representation of integration of the individual innovative potentials. (Fig. 1)

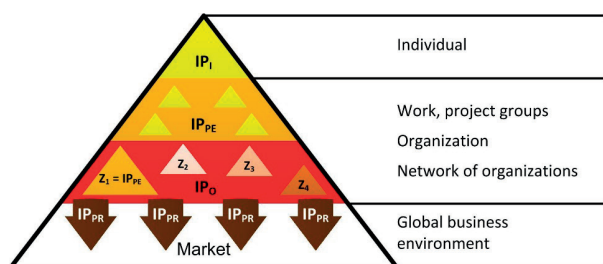


Fig.1. Integrated innovative potential

The individual plays a role of creativity bearer, generating good ideas ( $IP_i$ ). The implementation of the idea generally requires not only resources but also colleagues ( $IP_{PE}$ ). The organization enables efficient coordination of the work of individuals and groups, securing the necessary tangible and intangible resources ( $IP_o$ ) and active involvement in networks of organizations. The size of the innovation potential of the organization always depends both on the availability of creative individuals willing to cooperate, as well as their ability to actively participate in organization's networks. Given this mechanism, organizations create products based on the new innovation potential ( $IP_{PR}$ ) and place them on the market within the global business environment.

The pattern of activities (provided below), aimed at efficient use of innovation potentially hidden in people, shows how to purposefully increase innovative potential of the organization.

**3. Creating Innovative Climalite in Organization**

The success of innovations significantly affects innovative environment within the organization. The following findings are formulated as prerequisites and context that must be accepted by all workers engaged in innovation activities and in a process of creating a suitable environment.

At present, it is necessary to work with a large number of activities and knowledge when managing innovations. To better understand the interrelations that have to be accepted in creating innovative environment in the organization, the three dimensional model is designed (Fig. 2). In that model, the first dimension is dedicated to activities during the process of innovating (in relation to the second and third dimension). The process can be divided into the idea generation phase (a) and the solving of innovation projects phase (b). Several supporting activities are ongoing within these stages. The second dimension of the model focuses on activities related to the need to obtain the necessary resources in order to create innovations. These are the human, material (including financial) and information resources. The last and the most problematic dimension focuses on the four basic spheres in which a great potential for the development of innovative solutions is concentrated. The results of the analysis in the area of specific supporting activities (for new innovations) taking place in any organization which can be changed and adjusted have led us to the proposal of four basis spheres. These are:

- *Area of Thought* - where the philosophy and strategy reflecting the ways of thinking of those focused on future clearly belongs.
- *Area of Work (Execution)* - consisting especially of processes, work organization, methods and techniques utilized in the work processes.
- *Area of Behavior* - reflects the ability to develop the intellectual potential, and partnerships in a relatively open business environment.
- *Area of Learning by Experience* - representing the implementation of knowledge management.

This dimension allows us to specify activities performed by managers that affect thinking, working, behavior and the learning process of organization's employees.

The particular benefit this model offers is that it systemizes activities within the above-mentioned three dimensions. This allows creating specific working conditions required to increase the involvement of workers in innovating. Moreover, the model

provides a structure that can be continually updated, including in it new activities in the organizations.

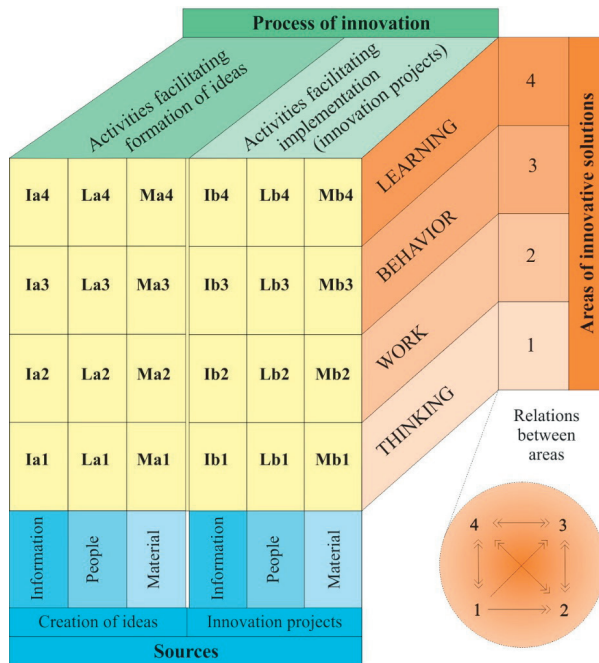


Fig. 2 Activities supporting innovation [3]

In the following sections, individual activities are interpreted, broken down according to the model presented in (Fig. 2) and key notes are formulated to their breakthrough. Their understanding plays a serious role in achieving successful innovative processes.

2.1 Innovative solutions in the area of thought

Thinking into the future is one of the pillars of innovation. The area of thought is deciding for the other area, bearing in mind that innovators need to especially master thinking in long term horizons.

a) Promoting stage of generation of ideas

Information (Ia1). Within this area senior management must present the meaning of innovation for the future, use the terminology in the area of innovation and find suitable information channel. It is a way to make the employees interested in engaging in development of something new. If people have a clear idea of what innovation is and how innovation can improve our competitiveness, their thinking will be tuned to capture the stimuli (signaling) changes in both internal and external environments.

Shared vision, understanding of how the company shall evolve through innovation, coupled with genuine support of

innovation will be reflected also in activities performed by the innovators. The correct information supports the courage to bear the risk of failure, courage necessary to build self-confidence, the hallmark of innovators.

People (Pa1). Emergence of new ideas can be encouraged when the people will not only be referred to as the most valuable resource of the company, but they will actually be treated as such. If employees acquire new skills and come up with ideas how to use them, it is up to the managers to support them in doing so. The question of motivation and remuneration of employees is also closely related to this topic.

Activities performed by the employees, associated with working with and using new knowledge can be supported also by organizational measures. Sharing knowledge and ideas requires certain psychological readiness to open behavior and willingness to hand over the results of one's work for the benefit of the entire organization.

Organizational and material resources (Ma1). Today, providing material resources and technical equipment for the workplace is usually not a problem [4]. The problem is their efficient use of innovators. A prerequisite for their proper use is that they will be integrated into the existing organizational structures in an organic manner.

If the organizational environment encourages innovation, allows flexible decisions, gives the time and space to study even seemingly unreasonable ideas, enables team work and encourages experimentation, then we can talk about an organizational environment inductive the inception and implementation of innovation [5].

b) Support of stage of delivering innovative projects

Information (Ib1). The manager deciding over initiation of an innovation project must be aware of the fact that:

- There must be a clear link between the innovative project to be implemented and the business strategy.
- He must have enough information on methodologies, techniques and procedures appropriate for the management of innovative projects.
- Addressing innovative projects requires also knowledge of metrics and methods of evaluation of project success.

People (Pb1). The philosophy of managing the company includes finding and utilizing qualified and creative people and involving them in the development of the organization. This approach practically manifests in the fact that company's teams receive flexible goals, offering the responsible people possibility to take decisions in how to solve them. When granted with this freedom, they feel confidence in their abilities and these can be strongly supported by the tools of the knowledge management.

The success of innovative projects may be supported by involving or acquiring workers from other fields or industries. The

necessary development of the organization's knowledge potential is also supported by the concept of so-called open innovations, the aim of which is to activate the best minds in the external environment in finding solutions to complex problems.

*Organizational and material resources (Mb1).* Here, the deciding factor is the way the executive managers think and emphasis on the acquisition and allocation of resources. If useful ideas are generated, which however are not applicable within the organization itself, then possibilities of how to use them within partner networks, sell them or protect by industrial patents should be sought.

The system of managing innovation projects must be flexible enough to allow implementation of both small (fast) and large (more time consuming) projects.

## 2.2 Innovative solutions in the area of work

In the area of work we are trying to answer the following question: What can be done now, in the present moment, so that in the future we can let something new appear or discover something new? The work is best organized when there are known and transparent processes. The level of business processes provides well-structured information, which can be used in the phase of generating ideas and also directly during implementation of the innovative projects.

### a) Promoting of stage generation of ideas

*Information (Ia2).* From the process-oriented point of view, the point here is to secure, preserve and distribute information obtained as well as related ideas that originated in the company. The ability to respond to the innovation stimuli coming from the environment and use them to benefit, requires the organization to have thought-through method of their transmission implemented. For innovators, information is a key resource. It is, therefore, appropriate to establish clear procedures, understandable to everyone in the organization, relating to:

- evaluation of new events and developments of products, technologies and markets,
- creation of knowledge databases,
- use of excellent ideas that do not fit into our business,
- involvement of all departments in the development of new products and processes,
- utilization of techniques for transfer of knowledge from other sectors.

*People (Pa2).* Preparing people to behave as innovators is among the most important processes and it should be strived to achieve involvement of as many employees as possible. For this reason it is desirable to complement the usual processes of training with activities encouraging the interest of employees in:

- systematic search for new ideas,
- improving relationships with our partners and customers,
- strong involvement in innovative processes.

*Organizational and material resources (Ma2).* To support the people in generating ideas, it is useful if they have contact with the surrounding environment. Important is to choose the right methods of technical support and appropriate processes of obtaining the necessary resources.

Generating ideas is not stimulated only by the supporting technology. It requires creating personal contacts, visiting scientific meetings, internships and other similar activities.

### b) Support of stage of delivering innovative projects

*Information (Ib2).* If we look at the proven methodologies of innovative project management, we can see that the quality of information obtained in the preparatory phase may decide over the success of the project. Consistent preparation of information and discipline in documenting this information always proves its value in the later phases of the project.

*People (Pb2).* The actual process of delivering an innovative project always depends on the cooperation of team members. The success of the project is significantly dependant on the conviction in the correctness of the procedure, the mutual confidence in abilities of other team members and agreement that the objective of the project is realistic [6].

Experience with innovation projects shows that it is particularly important that the project team himself is convinced that the objectives set are correct.

*Organizational and material resources (Mb2).* From the organizational point of view, it is important that processes conducive to efficient management of new product development from design to its marketing are in place. This requires a support of methodological expertise. Such methodological background can be provided by internal resources, or can be procured by hiring a specialized consulting firm.

## 2.3 Innovative solutions in the area of behavior

This section focuses on those activities which have not been emphasized in the preceding areas, although they are necessary preconditions for implementation of innovative solutions.

*Information (Ia3, Ib3).* To obtain information possibly leading to exceptional ideas, it is necessary to gain different viewpoints. The easiest way to do so is to use informal connections to people from other professional fields or industries. However, this approach also requires people equipped with knowledge and training in the skill of efficient communication. Similarly, every active link to the research and technological community can

generate ideas that are not only results of joint efforts, but also offer the possibility to achieve and deepen mutual respect.

*People (Pa3, Pb3).* Equipping the staff with proper knowledge for innovation is a key issue to address by managers in an innovative organization.

The development of intellectual potential can be achieved by specifically targeted education and training. To specify professional skills and qualification levels of already existing job functions, organizations establish standardized routine processes. The real problem is how to determine what knowledge will be needed in the future.

For that reason, the training of organization's managers should focus on skills of leadership and developing and supporting creativity within the organizations human resources.

*Organizational and material resources (Ma3, Mb3).* In addition to properly established organizational environment that allows creating and maintaining highly creative teams, sufficient attention needs to be given to remuneration. Even the most gifted and devoted employee is a human whose efforts, ideas and results achieved need to be appreciated.

All our knowledge about motivation will be useful to us, only if we try to understand what actually is for innovators most rewarding way to appreciate their accomplishments.

#### 2.4 Innovative solutions in the area of learning

Traversing the proposed model (Fig. 2), we have moved from the level where the basic direction is determined (area of thought), through processes to people and the behavior of innovators - and now we reach the area of learning by experience.

In general, we learn by studying the already available knowledge and performing experiments.

By solving problems, those involved themselves learn in the process and if they are capable of transmitting this experience to others - sharing knowledge takes place.

A part of this learning is a fundamental change or shift in thinking. By learning, people expand their capacity to create.

When in stages of generating ideas and delivering innovation projects, the focus should be on those activities that facilitate development of a learning enterprise.

*Information (Ia4, Ib4).* To gain ideas and overview, it is necessary to look further, beyond the borders of the given field or industry. We try to identify and understand the needs of our customers who can provide us with new insights and inputs for

what we are dealing with. Thus, we use the opportunity to learn also from our customers.

It is important to understand that by solving problems, we are also learning. Only then we have the reason to document the lessons learned and reuse them later. Then, we can capture what we have learnt so that it can be also utilized by others in the organization.

*People (Pa4, Pb4).* Members of the creative teams look for internal benefits in their work. The conviction in meaningfulness of what we do and the ability to look back at the process underwent, allows us to learn from our own experience and consider it a part of the experiments.

If we know that problems stimulate thought, we can consciously acquire habits of creative thinkers. These support our dispositions to utilize knowledge. Although each of us has the potential of creativity inherent, the development of it is tied to work - an active participation in the process of creating new things. Joint work and climate of mutual respect makes it possible to share ideas and enriching one another.

*Organizational and material resources (Ma4, Mb4).* In the present time we have the opportunity to solve problems and learn not only in the real environment of our organizations, but we can also benefit from virtual working environments [7]. This allows us the use fundamentally new way of exploring options of innovative solutions.

#### 4. Conclusion

Organizations are looking for opportunities to increase their efficiency and competitiveness in world markets. Innovations crucially contribute to this. But the problem is how to mobilize organization's performance to support the creation and commercialization of innovative solutions. This paper has focused on this area and presented a possible approach for evaluation of innovative potential of organizations and presented a three-dimensional model illustrating the complex linkages in the process of innovating.

The aim of the proposed model was to create a structure of the system supporting innovative environment that is necessary for successful innovation processes in the organization. To create innovative environment, we can certainly use more approaches and processes. The presented model was based on the study of the available innovation theories, presented experience from innovative practice and own knowledge verified in practice.

#### References

- [1] DULINA, L., BARTANUSOVA, M.: Ergonomics and Preventive Medicine in Companies in Slovak Republic and the EU, *Ergonomics* 2013, Zagreb : Croatian Ergonomics Society, 2013. 81-86, ISSN 1848-9699.

- [2] STASZEWSKA J.: *Marketing Companies (in Poland)*, Gliwice : Wydawnictwo Politechniki Slaskiej, 2008. p. 148, ISBN: 978-83-7335-525-5
- [3] MICIETA, B., TUREKOVA, H.: *Innovation Management: Support for Establishing Innovation (in Slovak)*, Zilina: GEORG, 2010, p. 184, ISBN 978-80-89478-02-6
- [4] MICIETOVA, A., CILLIKOVA, M.: *Technology - Machining (in Slovak)*, Zilina: Zilinska univerzita, 2009, p. 486, ISBN 978-80-554-0010-5.
- [5] GREGOR, M., MEDVECKY, S.: Zilina University Concept of Digital Factory. *Communications - Scientific Letters of the University of Zilina*, ISSN 1335-4205, 2008, vol. 10, No. 2, 60-66.
- [6] BINASOVA, V.: *Management of Manufacturing Organizations in Conditions of Economic Crisis (in Slovak)*, Advanced Industrial Engineering [CD-ROM]: Monograph of scientific seminar AIE realized at the Department of Industrial Engineering in 2011, 105-123, Zilina: CEIT, 2012, ISBN 978-80-970440-4-6-CD-ROM.
- [7] KRAJCOVIC, M. et al.: Intelligent Manufacturing Systems in Concept of Digital Factory, *Communications - Scientific Letters of the University of Zilina*, ISSN 1335-4205, 2013, vol. 15, No. 2, 77-87.

Dana Bolibruchova - Lukas Richtarech - Wladyslaw Orlowicz \*

## POSSIBILITIES OF ELIMINATING THE HIGHER AMOUNT OF IRON IN SECONDARY AlSi7Mg0.3 ALLOY BY CHROME

*This paper deals with influence on segregation of iron based phases by chrome. Iron is one of the most common impurities that could be found in Al-Si alloys. It is impossible to remove iron from melt by standard operations, but it is possible to eliminate its negative influence by addition of some other elements that affect the segregation of intermetallics in less harmful type. Realization of experiments and results of analysis show new perspective on solubility of iron based phases during melt preparation with higher iron content and influence of chrome as iron corrector of iron based phases. It could be concluded that higher amount of chrome causes the formation of sludge particles.*

**Keywords:** Secondary AlSi7Mg0.3 based alloys, iron phases, thermal analysis, iron correctors, AlCr20.

### 1. Introduction

Due to increasing requirements on the quality of castings, final fatigue properties and due to the pressure on price of final castings, it is necessary to search compromises in the casting production from secondary alloys with the presence of various impurities. A basis for initiating this work was lack of theoretical knowledge of using secondary Al-Si-Mg alloys with higher amount of iron and its appropriate and efficient elimination in production of demanding casting for automotive industry by serial conditions [1 - 3].

The increased content of iron in aluminium alloy has a consequent exclusion of intermetallic phases in various forms which affect the final quality and durability of castings. The adverse effect of iron on the final properties of the casting is that it greatly affects the mechanical properties [4 and 5].

Iron cannot be removed from melt by conventional procedures, but it is possible to eliminate the adverse effect by adding some elements which affect the exclusion of iron intermetallic phases in the less adverse form. The input to solve this problem was detection that in the literature are a number of elements (e.g. Mn, Cr, Ni, V, Zr, Co) which affect the exclusion of iron based phases, but their using in practice is neither widespread nor implemented [6].

Chrome occurs as impurity in commercially available master alloy, in the range from 5 to 50  $\mu\text{m}$ , provides strength at room temperature and slightly increases the ductility. The presence of Cr phases  $\text{Al}_{13}\text{Si}_4(\text{CrFe})_4$  and  $\text{Al}_2\text{Si}_8(\text{CrFe})_5$  can increase brittleness [7 - 9].

Using chrome, a similar effect on the exclusion of phases was observed as with manganese, but without a clearer microstructural explanation. The presence of chromium, together with iron and manganese can cause the exclusion of so-called "sludge" particles [10].

### 2. Experimental work

#### 2.1 Experimental notes

Experimental melts were executed at the Department of Technological Engineering, University of Zilina. Metal was melted in an electrical resistance furnace T15, controlled by PID regulator CAL 3200 in a graphite crucible treated by protective coating. Individual casts consisted of creating four samples poured at a temperature  $760 \pm 5$  °C. Melt was not refined and was without addition of a modifier or grain refiner. The only operations during melt preparation were stirring and oxide film removal from the melt surface. Melt was poured into a metal mold with minimal temperature of 100 °C.

AlSi7Mg0.3 cast alloy was used as an experimental material. The chemical composition of the used alloy is shown in Table 1. This alloy finds applications in automotive, aerospace and general engineering industries due to its excellent combination of properties such as good fluidity, low coefficient of thermal expansion, high strength-to-weight ratio and good corrosion resistance. This foundry alloys have excellent tensile and fatigue properties and also good corrosion resistance.

\* <sup>1</sup>Dana Bolibruchova, <sup>1</sup>Lukas Richtarech, <sup>2</sup>Wladyslaw Orlowicz

<sup>1</sup>Department of Technological Engineering, Faculty of Mechanical Engineering, University of Zilina, Slovakia

<sup>2</sup>Rzeszow University of Technology, Faculty of Mechanical Engineering and Aeronautics, Rzeszow, Poland

Email: lukas.richtarech@fstroj.uniza.sk

Chemical composition of AlSi7Mg0.3 cast alloy

Table 1

Elements	Si	Fe	Cu	Mn	Mg	Ni	Cr	Pb	Ti	Zn	Sb
[wt. %]	6.93	0.1204	0.0036	0.0037	0.3896	0.0042	0.0011	0.0033	0.1141	0.0083	0.0001

Chemical composition of AlSi7Mg0.3 cast alloy after addition of iron

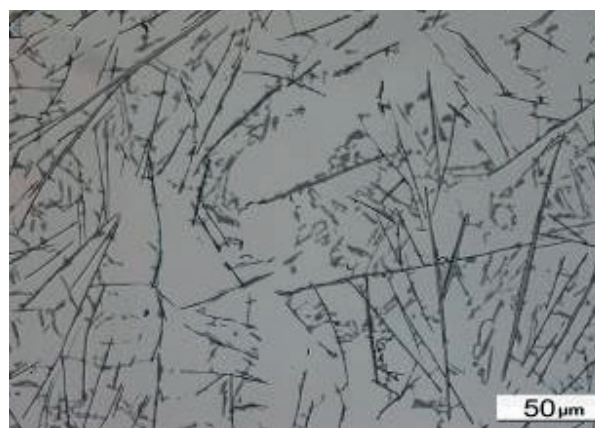
Table 2

Elements	Si	Fe	Cu	Mn	Mg	Ni	Cr	Pb	Ti	Zn	Sb
[wt. %]	6.49	1.280	0.053	0.092	0.349	0.034	0.087	0.006	0.113	0.027	< 0.0004

Certain amount of AlFe10 master alloy (deliberate “contamination”) was added to experimental alloy to increase the iron content. The main aim was to increase the iron content in alloy so that the amount would be close to the maximal allowed content by customer specification for automotive components made from secondary alloys AlSi7Mg0.3. The amount of AlFe10 added to the basic AlSi7Mg0.3 was 70000 ppm of the total batch. The chemical composition of alloy with a higher amount of iron is shown in Table 2.

Influence of the iron amount on the microstructure and shape of intermetallic phases was studied by the classic black - white contrast method. Sample preparation and execution of metallographic image was done in a standard way for the evaluation of intermetallic phases in aluminum alloys. Evaluated samples were etched by 20 ml of H<sub>2</sub>SO<sub>4</sub> + 100 ml of H<sub>2</sub>O. Images of alloy microstructures were obtained by the light microscope NEOPHOT 32. In Fig. 1 is shown microstructure of a sample from melt with a higher amount of iron. The structure consists of silicon eutectic, dendrites of α - phase excreted in the form of white units and black areas as iron based particles. The impact of the iron on iron based particles themselves is visible in the microstructure. The average length of these particles was approximately 37 μm.

To influence the segregation of iron based phases a master alloy AlCr20 was used. Different amounts of master alloy AlCr20 were added to the alloy with a higher amount of iron: 0.5 % (melt No. 2), 1 % (melt No. 3) and 1.5 % (melt No. 4). The chemical compositions of these melts are in Table 3.



Mag. 200 x and 500x, etching 20 ml H<sub>2</sub>SO<sub>4</sub> + 100 ml H<sub>2</sub>O  
 Fig. 1 Microstructure of alloy with higher amount of iron

Chemical composition of melts after addition of master alloy AlCr20  
 a) 0.5 % Cr

Table 3

Elements	Si	Fe	Cu	Mn	Mg	Ni	Cr	Pb	Ti	Zn	Sb
[wt. %]	6.41	1.737	0.054	0.128	0.330	0.080	0.289	0.006	0.111	0.027	< 0.0004

b) 1 % Cr

Elements	Si	Fe	Cu	Mn	Mg	Ni	Cr	Pb	Ti	Zn	Sb
[wt. %]	6.43	1.733	0.055	0.128	0.324	0.081	0.411	0.006	0.110	0.027	< 0.0004

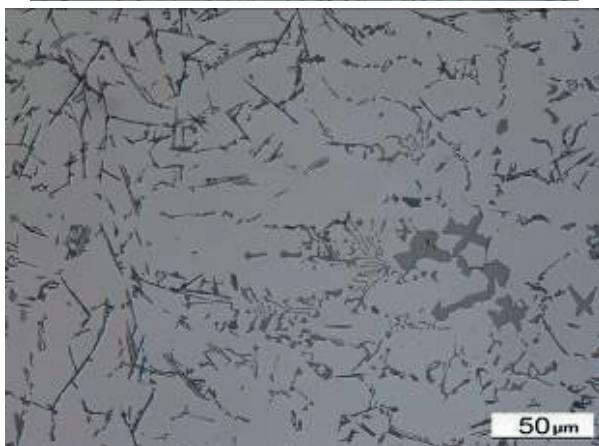
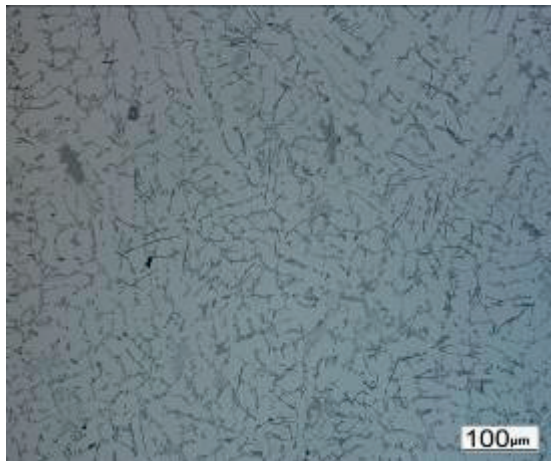
Chemical composition of melts after addition of master alloy AlCr20

Table 3

c) 1.5% Cr

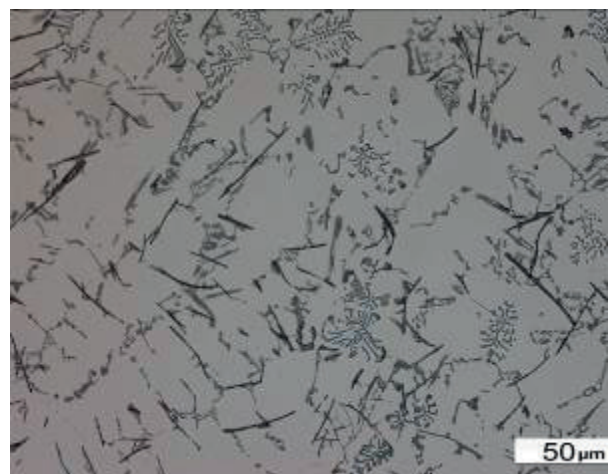
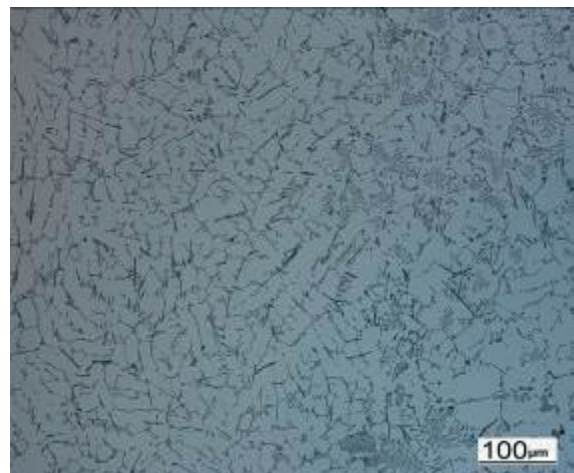
Elements	Si	Fe	Cu	Mn	Mg	Ni	Cr	Pb	Ti	Zn	Sb
[wt. %]	6.45	1.654	0.055	0.119	0.347	0.081	~0.472	0.006	0.109	0.027	< 0.0004

Taking a closer look at the chemical composition we can see an increasing amount of iron content with increasing amount of AlCr20 alloy. In all the cases there was an increase of iron content over 1% Fe which is the maximum allowable content for this type of alloy. With the increasing amount of iron, the iron based particles also changed. In Figs. 2, 3 and 4 are shown microstructures of samples from melts with a higher amount of iron and with addition of AlCr20.



Mag. 200 x and 500x, etching 20ml H<sub>2</sub>SO<sub>4</sub> + 100ml H<sub>2</sub>O

Fig. 2 Microstructure of alloy with 0.5% Cr



Mag. 200 x and 500x, etching 20ml H<sub>2</sub>SO<sub>4</sub> + 100ml H<sub>2</sub>O

Fig. 3 Microstructure of alloy with 1% Cr



Mag. 200 x and 500x, etching 20ml H<sub>2</sub>SO<sub>4</sub> + 100ml H<sub>2</sub>O

Fig. 4 Microstructure of alloy with 1.5% Cr

In the mentioned figures we can see the change of iron based particles and their length. With increasing amount of AlCr20 master alloy, the length of iron based particles decreased. In case of 0.5% Cr, the length of iron based particles was approximately 19.6 μm, in case of 1% Cr was approximately 11 μm and in case of 1.5% Cr was approximately 16.6 μm. It is also possible to see the presence of new particles which are not in shape of long thin needles.

Thermal analyses (Figs. 5, 6, 7 and 8) were recorded from all the melts. By evaluating the solidification curves it is impossible to see the exclusion of iron based phases, therefore, the first derivation of curves was made according to solidification time. In graphs we can be see the influence of different amounts of Cr in alloy and its influence on temperature of primary crystallization and also on temperature of eutectic reaction. In this area exclusion of iron based phases affected by chromium also occurs. To measure the solidification curves two thermocouples located in the sample mould were used; one at the wall and one at the centre. The use of the ΔT curve allows identification of minor precipitation events that evolve only a small amount of latent heat and are, therefore, otherwise difficult to see on the derivate curve.

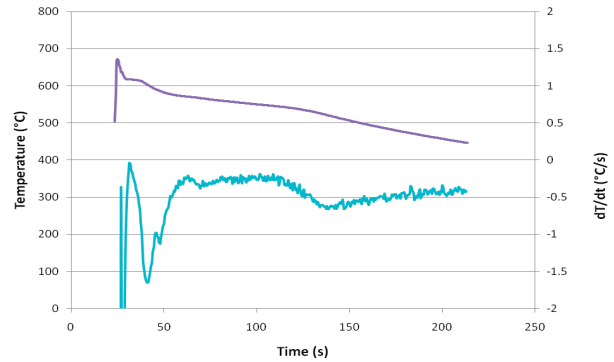


Fig. 5 Cooling curves graph of melting without addition of AlCr20

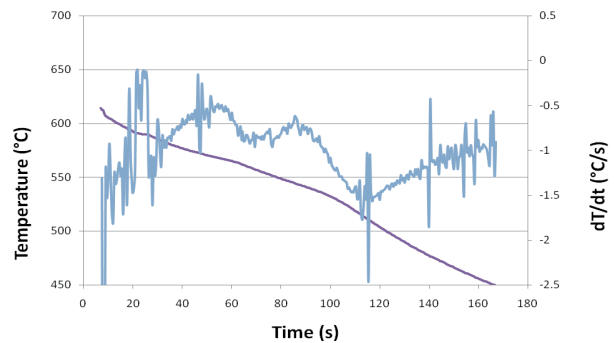


Fig. 6 Cooling curves graph of melting with 0.5 wt. % of AlCr20

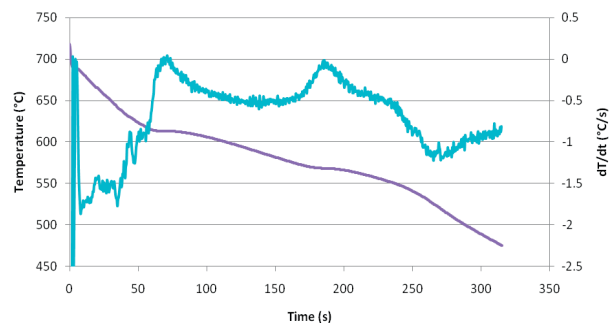


Fig. 7 Cooling curves graph of melting with 1 wt. % of AlCr20

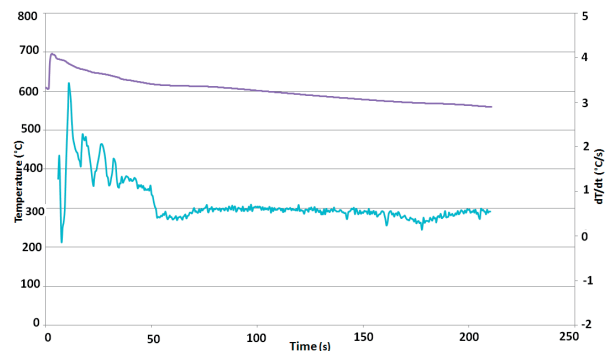


Fig. 8 Cooling curves graph of melting with 1.5 wt. % of AlCr20

For all the samples tensile strength and elongation were evaluated. The tensile test was performed on a tensile machine WDW - 20 in the laboratory of mechanical tests, University of Zilina at 22 °C. Results of tensile strength and elongation measurements are presented in Table 4.

Results of tensile strength and elongation before and after chrome addition

Table 4

Alloy	Tensile strength [MPa]	Elongation [%]
AlSi7Mg0.3	170	1 - 2
0 % Cr	167	0.93
0.5 % Cr	170	1.03
1 % Cr	173	1.26
1.5 % Cr	161	1.11

### 3. Conclusions

The goal of the article was to evaluate the effect of chrome in secondary alloy AlSi7Mg0.3. It is possible to conclude that high chrome content has detrimental influence on microstructure - occurrence of very thick and long iron based  $\beta$  ( $Al_3FeSi$ ). Presence of AlCr20 has also impact on the occurrence of other phases whose chemical composition will be examined by EDX analysis in further work. Addition of chrome increases tensile strength and decreases elongation; however, even higher amount of chrome decreases tensile strength. Therefore, we can say that chrome can be used as iron corrector in secondary aluminium alloys.

### Acknowledgment

*This work was created in the framework of the grant project VEGA č. 1/0363/13. The authors would like to thank the Grant Agency for support.*

### References

- [1] KAHLIFA W.: *Role Inclusions in the Precipitation of  $\alpha$ -aluminium and Fe-intermetallics in Aluminium Rich Corner of the Al-Si-Fe Ternary System*, 2003
- [2] HURTALOVA, L., TILLOVA, E.: Elimination of the Negative Effect of Fe-rich Intermetallic Phases in Secondary (recycled) Aluminium Cast Alloy. *Manufacturing Technology*, vol. 13, No. 1, 44-50, ISSN 1213-2489
- [3] BRUNA, M., KUCHARCIK, L.: Prediction of the Porosity of Al Alloys. *Manufacturing Technology*, vol. 13, No. 3, 2013, 296-302, ISSN 1213-2489
- [5] BOLIBRUCHOVA, D., RICHTARECH, L.: Effect of Adding Iron to the AlSi7Mg0.3 (EN AC 42 100, A356) Alloy. *Manufacturing Technology*, vol. 13, No. 3, 2013, 276-281, ISSN 1213-2489
- [6] BOLIBRUCHOVA, D., RICHTARECH, L.: Study of the Gas Content in Aluminium Alloys. *Manufacturing Technology*, vol. 13, No.1, 2013, 276-281, ISSN 1213-2489
- [7] BURSAK, M., BOKUVKA, O.: Influence of Technological Factors on Fatigue Properties of Steel Sheets. *Communications - Scientific Letters of the University of Zilina*, vol. 8, No. 4, 34-37, ISSN 1335-4205
- [8] PALCEK, P., HADZIMA, B., BOKUVKA, O., CHALUPOVA, M., NOVY, F.: Corrosion Resistance of Magnesium and its Alloys. *Communications - Scientific Letters of the University of Zilina*, vol. 5, No. 3, 2003, 21-22, ISSN 1335-4205
- [9] TAYLOR, J. A.: *The Effect of Iron in Al-Si Casting Alloys*. 35<sup>th</sup> Australian Foundry Institute National Conference, Adelaide, 2004, 148-157
- [10] TILLOVA, E., CHALUPOVA, M., HURTALOVA, L., DURNIKOVA, E.: Quality Control of Microstructure in Recycled Al-Si Cast Alloys. *Manufacturing Technology*, vol. 11, No. 11, 70-76.



Chemical composition of 100CrMnSi6-4 bearing steel

Table 1

C	Cr	Mn	Si	P	S	Ni	Mo
0.9-1.05	1.4-1.65	1-1.02	0.5-0.7	Max. 0.03	Max. 0.025	Max. 0.3	0-0.1

**2. Short description of the simulation software SYSWELD**

The SYSWELD software is designed to simulate and evaluate different methods of welding and heat treatment which works on the finite element method (FEM). The program can simulate volumetric and surface heat treatment and thermo-mechanical heat treatment (carburizing, nitriding and nitro-carburizing). The calculation of SYSWELD software is divided into two stages. The first stage contains thermo-metallurgical calculation and the second stage mechanical calculation. Thermo-metallurgical part analyses the calculation of non-stationary temperature fields, phase transformation, hardness structure or austenitic grain size. Mechanical analysis follows the thermo-metallurgical analysis and allows the calculation of waveforms of stress tensor components, the value of principal stresses, analysis of the spatial stress conditions according to the HMM theory and also Tresca analysis of shear stresses. Simulation (calculation) is based on measured data which form the internal database. These data are specific for each material, and depend on the chemical composition of the material [1, 6 and 7].

**3. Heat treatment parameters of the outer ring**

During the heat treatment of the outer ring the standardized parameters recommended by the manufacturer were used. These parameters were taken from the CCT diagram and tempering diagram for 100CrMnSi6-4 bearing steel.

Heating of the outer ring took place in the intermediate chamber furnace with protective atmosphere. Austenitizing temperature was carried out at 850° C for 20 minutes, but when moving the ring by belt elevator the temperature dropped to 10° C. As a quenching medium the quenching oil Marquench 875 was used. After completing the quenching process, the ring was put into the tempering furnace at a temperature of 190° C for about 120 minutes. These are the basic parameters that are needed for the SYSWELD software to make the simulation of the heat treatment. More detailed information is not necessary for the numerical simulation because the software can't take this information into account [1 and 7].

**4. Creating the 3D model for simulation**

For the simulation of heat treatment of the outer ring the input parameters of a real technological process were used. First, it was necessary to create a model that had a defined volume. The volume consists of grids that are important for simulation. It is, therefore, necessary to define the density of these grids. The higher the density is, the more accurate the calculation is, but also time-consuming. When the volume of the outer ring was finished the surface of the model had to be defined. The surface of the model also consists of grids for heat transfer simulation (Fig. 2). It is necessary to know what features or what part of the model (the ring) is the most important for the results. In this case it is the surface layer. Therefore, the density gratings in the surface layer must be greater than the whole volume of the outer ring (Fig. 3). The coating has a thickness of 0.1 mm and consists of five other layers. Other layers have a thickness of 0.5 mm. For the computer simulation of mechanical processes there is a need to define three points of the model. The first point is anchored in all three axes. The second point is anchored in two axes and the last in only one axis. Diagram of the model is shown in Fig. 4.

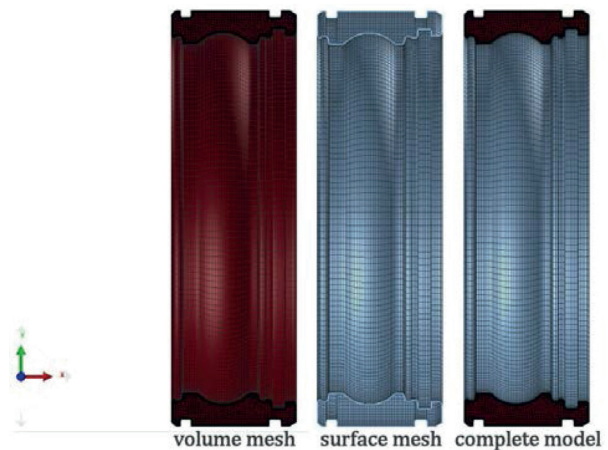


Fig. 2 3D model of the outer bearing ring

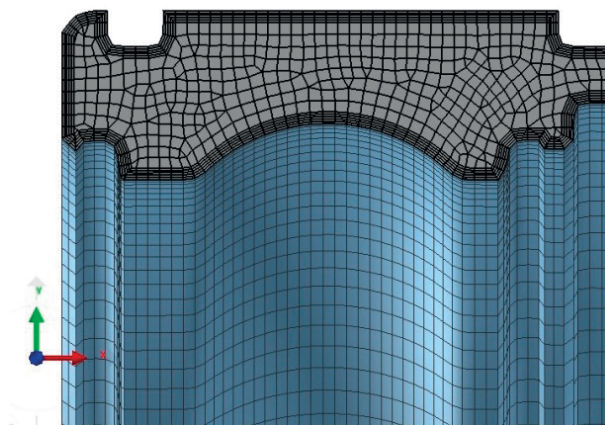


Fig. 3 Cross section of the outer ring and the representation of the surface layer



Fig. 4 Scheme of the outer ring in the SYSWELD software

After creating the model and selecting the material properties from the internal database, all input data were entered into the application HT (heat treatment) consultant which is part of the SYSWELD software. We focused on two parts of the computer simulation. First part consists of thermo-metallurgical analysis, the second part of mechanical. These two parts were selected because of the comparison of microstructure and hardness with the real measured values [8 and 9].

### 5. Results of the computer simulation

The most important results emerging from the heat treating simulation in SYSWELD is hardness, microstructure, deformation and residual stresses after quenching. From Fig. 5 it is obvious

that hardness has the same values in the whole volume of the outer ring. The average value of the simulated hardness was not higher than 58.8 HRC. Another output data from the simulation was the microstructure [10 and 11].

Figure 6 shows the microstructure which contains martensite and Fig. 7 residual austenite. Percentage representation of martensite and residual austenite is approximately 77% - 23%. The large presence of residual austenite is due to the fact that the outer ring was simulated after quenching. In the real process of thermal heat treatment the outer ring would undergo tempering and the share of residual austenite would tumble down. The output of stresses and deformations in numerical simulation is roundness of bearing rings which is a consequence of uneven distribution of stresses (Fig. 8) during the quenching of rings. Roundness in most cases can be removed by grinding, but when the roundness is very high, it is unable to remove it. Numerical simulation in this case shows relatively high roundness which can be a consequence of slots that are turned around the rings (Fig. 9). The value of roundness by numerical simulation is 93  $\mu\text{m}$ . All the results of numerical simulation represent non-tempered state because tempering can't be simulated by this software [12 and 13].

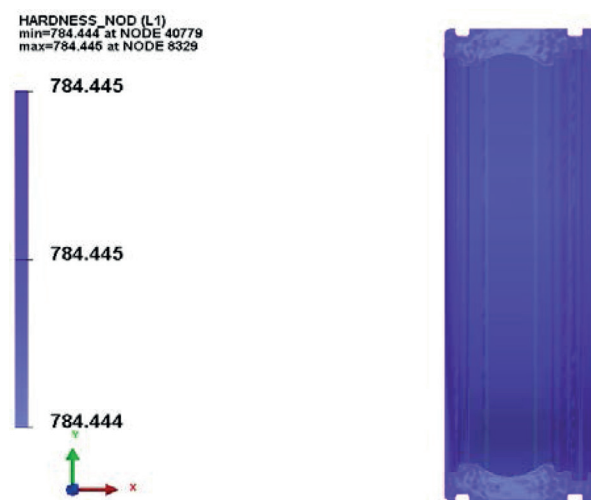


Fig. 5 The result of heat treating simulation focused on hardness

### 6. Real measured values of the outer ring

Hardness of the experimental ring was measured by the Rockwell and Vickers method on certified devices. The measurement procedure of Vickers method consists of placing stitches perpendicular to the axis of the ring. This measurement was repeated three times at random locations on the surface of the outer ring. The average value of hardness on the surface of the outer ring was 734 HV1/10. Rockwell hardness was measured on the front side of the ring. Its average value was not higher than 60 HRC. Microstructure of the ring was etched with

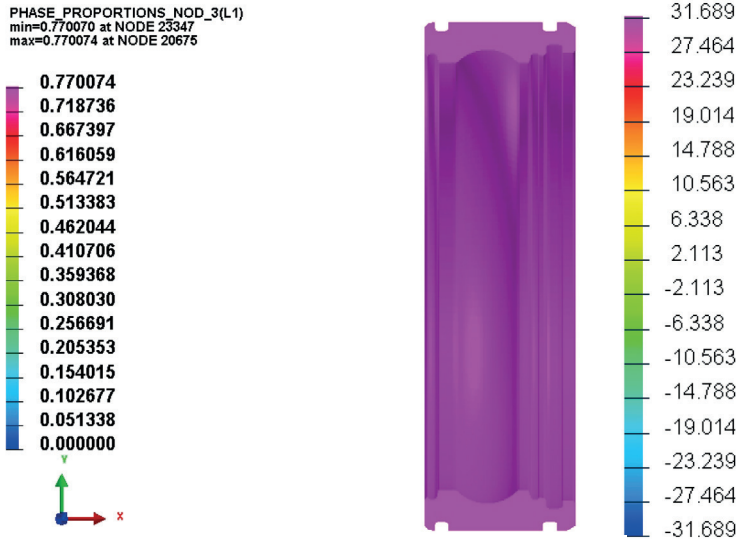


Fig. 6 Percentage representation of martensite in the microstructure

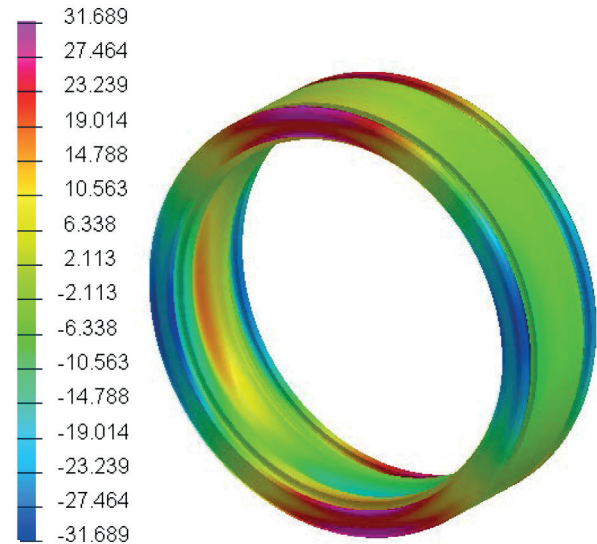


Fig. 8 Result of residual stress simulation

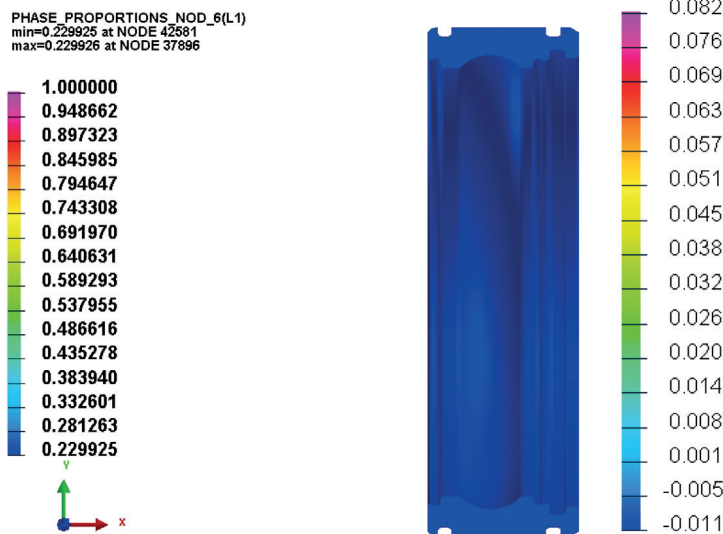


Fig. 7 Percentage representation of residual austenite in the microstructure

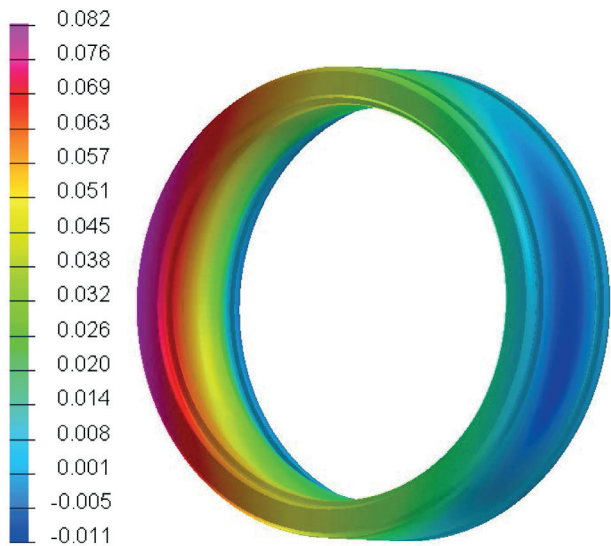


Fig. 9 Result of roundness simulation

picric acid and observed on a light microscope. Figure 11 shows the microstructure in which martensite forms the greater part and retained austenite the lower part. Carbides are uniformly distributed (white dots). Roundness of the outer ring was measured using a 3D measuring apparatus, in two perpendicular diameters in the same ring plane. Roundness values are shown in Fig. 10.

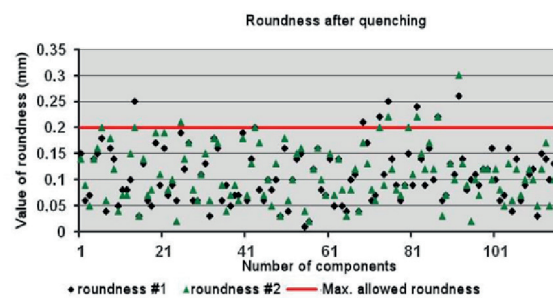


Fig. 10 Values of roundness

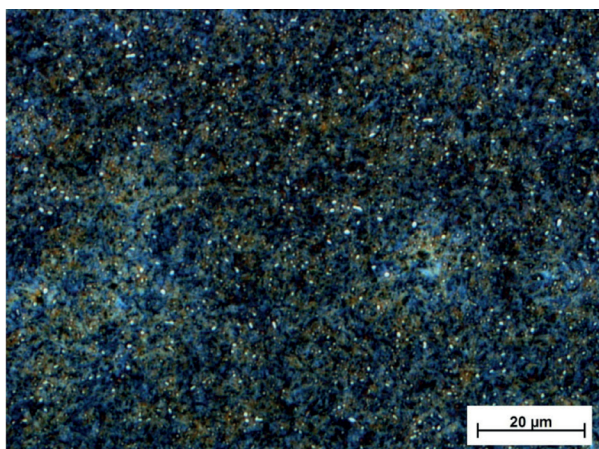


Fig. 11 The microstructure of the 100CrMnSi6-4 bearing steel,  
Magnification 1250x.

## 7. Conclusion

The aim of this experiment was to compare the results from simulation of heat treatment of the outer ring which was made

of material 100CrMnSi6 - 4 with the actual measured values. Roundness of the ring came to 93 $\mu$ m. The values of actually measured roundness were from 30 to 40  $\mu$ m. That means these values from real measurement were from 0.05 to 0.06 millimeters smaller than simulated. When comparing the microstructure and hardness of the true values, these simulated results are close to reality. It should be noted that the ring is not the final product of heat treatment because it has to be tempered to reduce distortion and residual austenite after hardening, together with a reduction of hardness. The measured values indicate that the calculation program SYSWELD can be used to simulate the heat treatment for the purpose of predicting the values such as hardness, microstructure and roundness in the process of cooling. The roundness may contain extreme values in some rings [14, 15 and 16].

## Acknowledgement

The work has been supported by the grant project APVV SK-PL\_0034-12: Research of Tribological Properties of Electrospark Deposited Coatings.

## References

- [1] KONAR, R., MICIAN, M.: Numerical Simulation of Residual Stresses and Distortions in butt Weld in Simulation Programme Sysweld. *Communications - Scientific Letters of the University of Zilina*, vol.14, No. 3, 2012, 49-54, ISSN 1335-4205
- [2] BREZNICAN, M., FABIAN, P., MESKO, J., DRBUL, M.: The Simulation of Influence of Quenching Temperature on Properties of Bearing Rings, *Manufacturing Technology: J. for Science, Research and Production*, vol. 13, No. 1, 2013, 20-25, ISSN 1213-2489
- [3] FABIAN, P., KECKOVA, E., BETAK, P.: *Metals Heat Treatment*, Zilina 2007, 113 p., ISBN 978-80-969592-7-3
- [4] KONAR, R., MICIAN, M., HOPKO, A.: Analysis of Boundary Conditions for the Simulation of Welding at the Repair of Gas Pipelines with Steel Sleeve, *Communications - Scientific Letters of the University of Zilina*, vol. 13, No. 4, 2011, 36-39, ISSN 1335-4205
- [5] TOTTEN, G.: *Steel Heat Treatment: Metallurgy and Technologies*, Boca Raton: Taylor & Francis Group LLC, 2006, 820 p., ISBN 978-0-8493-8455-4.
- [6] KANG, S. H., IM, Y. T.: Thermo-elasto-plastic Finite Elements Analysis of Quenching Process of Carbon Steel. *J. of Materials Processing Technology*, No. 192-193, 2007, 381 -390.
- [7] HAKAN GUR, C., PAN, J.: *Handbook of Thermal Process Modeling of Steels*, 2008, 342-380, Taylor & Francis Group LLC, Boca Raton.
- [8] PASTIRCAK, R., KRIVOS, E.: Effect of Opening Material Granularity on the Mould Properties and the Quality of Castings Made by Patternless Process Technology, *Manufacturing Technology: J. for Science, Research and Production*, vol. 13, No. 1, 2013, 92-97, ISSN 1213-2489.
- [9] PASTIRCAK, R., URGELA, D., KRIVOS, E.: Production of Castings by Patternless Process, *Archives of Foundry Engineering*, vol. 12, No. 1, 2012, 87-92, ISSN 1897-3310
- [10] BRONCEK, J., DZIMKO, M., HADZIMA, B., TAKEICHI, J.: *Acta Metallurgica Slovaca*, vol. 20, No. 1, 2014, 97-104, DOI 10.12776/ams.v20i1.273
- [11] PETRU, M., NOVAK, O., HERAK, D.: *Biosystems Engineering*, vol. 111, No. 4, 2012, 412 -421, DOI:10.1016/j.biosystemseng.2012.01.008

- [12] RADEK, N., SLADEK, A., BRONCEK, J., BILSKA, I., SZCZOTOK, A.: Electrospark Alloying of Carbon Steel with WC-Co-Al<sub>2</sub>O<sub>3</sub>: Deposition Technique and Coating Properties, *Advanced Materials Research*, vol. 874, 101-106, © (2014) Trans Tech Publications, Switzerland, doi:10.4028/www.scientific.net/AMR.874, ISSN 1022-6680
- [13] JANKURA, D., DRAGANOVSKA, D., BREZINOVA, J.: *Chemické listy*, vol. 105, No. 16, 2011, 542-545
- [14] PIETRAZSEK, J., GADEK-MOSZAK, N., RADEK, N.: *Studies in Computational Intelligence*, vol. 513, No. 1, 2014, 125-134, DOI:10.1007/978-3-319-01787-7\_12
- [15] TOMAS, M., DRAGANOVSKA, D., HUDAK, J., IZOL, P.: *Acta Metallurgica Slovaca*, vol. 20, No. 1, 2014, 105-114, DOI 10.12776/ams.v20i1.274
- [16] CZICHOS, H., HABIG, K. H.: *Tribologie - Handbuch*, Reibung und Verschleiss, VERLAG VIEWEG, 1992, 456 p.

Radoslav Konar - Marek Patek - Milos Mician \*

## EXPERIMENTAL MEASUREMENTS AND NUMERICAL SIMULATION OF BRIDGE CONSTRUCTION WELDING AT LOW TEMPERATURES

*This article describes experimental measurements and welding simulation by welding of bridge construction with thickness 30 mm. The welded bridge plate was made from steel S355. Welding was carried out at low ambient temperature. Welding parameters and temperature cycles were measured during welding. Deformations of welded construction were obtained using optical system TRITOP before and after welding process. Experimental results except for deformations were used as boundary conditions for FEM simulation in SYSWELD. Temperature cycles, angular deformations and residual stresses were computed. The values of computed and measured angular deformations are almost identical. It follows that SYSWELD is able to predict angular and linear deformation with a good accuracy.*

**Keywords:** Bridge construction, simulation of welding, SYSWELD.

### 1. Introduction

Welding is extensively used as a principal method of fabricating and assembling numerous metal products in shipbuilding, construction aviation, and automotive industries. One of the popular arc welding processes is manual metal arc welding (MMA) that has been applied in a wide range of plate thicknesses due to its ease and relatively high productivity. Welding is considered one of the most efficient, dependable, and economical means of fabrication to join metals permanently. However, distortion emerges as a result of the welding process which adversely affects the dimensional accuracy and esthetical value, which in turn can lead to expensive remedial work, which increases the overall fabrication costs [1]. Deformation in a welded part occurs due to non-uniform expansion and contraction of the weld metal and adjacent parent metals caused by complex temperature changes during the welding process. In addition, the deformation resulting from the welding process can also induce residual stress, which may significantly influence the structural performance of the welded structure [2].

Multipass butt is widely used in bridge construction. To minimize production cost, it is important to understand the distortion behaviour of multipass welding, which can be predicted by using simulation approach. The computational analysis can be used to achieve good welding quality and effective welding design in bridge construction [3 and 4].

### 2. Simulation system SYSWELD

SYSWELD integrates effects linked to metallurgical transformations in the thermal, mechanical and hydrogen diffusion analysis process. Simulation is broken down into a number of successive steps due to the modular aspect of the product. Figure 1 illustrates interaction between the various modules, with the two principle modules shown shaded. The electromagnetism module is used to compute current densities, and thus determine Joule effect power dissipation. Typical applications for this module include induction heating. It should also be noted that a powerful link has been developed between the thermo-metallurgical model and the electro-kinetic model, for simulation of processes such as spot-welding. The hydrogen diffusion computation module, with integration of trapping effects, is also of major interest for the study of cold cracking of steels following welding process [5].

Simulation is consequently conducted in a number of successive steps (with the results of one step forming input data for the following step):

- thermal and metallurgical computation (determination of thermal cycles and metallurgical phase proportions according to space and time),
- mechanical computation (stresses and residual strains),
- computation of hydrogen diffusion, integrating the effect of temperature, stresses and traps (reversible or irreversible) [6 and 7].

\* Radoslav Konar, Marek Patek, Milos Mician

Department of Technological Engineering, Faculty of Mechanical Engineering, University of Zilina, Slovakia  
E-mail: radoslav.konar@fstroj.uniza.sk

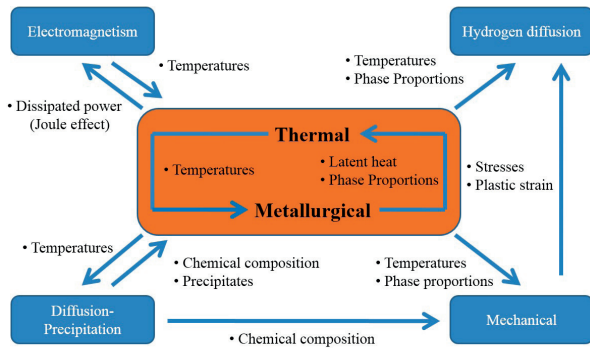


Fig. 1 General architecture of SYSWELD [8]

### 3. Experimental part

At the experimental part of article experimental measurement at the welding process and simulation of steel sheet with 30mm thickness welding at the low temperature are described. Experiment was focused to observe deformational influence of welding and thermal expansion of material to the welded part.

#### 3.1 Experimental sample

Experimental sample was made of steel S355J2G3 with chemical composition specified in Table 1.

The sample was composed of two parts with dimensions of 1320x450x30mm (Fig. 2). The sample was welded by asymmetrical double-V-groove weld according to WPS protocol.



Fig. 2 Experimental sample

Scheme of weld edge preparation is shown in Fig. 3. Experimental sample was after tacking exposed to influence of negative ambient temperatures. Exterior ambient temperature at winter season was used to achieve negative temperature of the

sample during welding process. Welded joint was made by MMA method (111 according to STN EN ISO 4063) at the ambient temperature about -10 °C. Made weld consists of 26 weld beads from which 11 were deposited in PE position and 15 in PA position (in terms of STN EN ISO 6947). The welding sequence of individual weld beads is shown in Fig. 3.

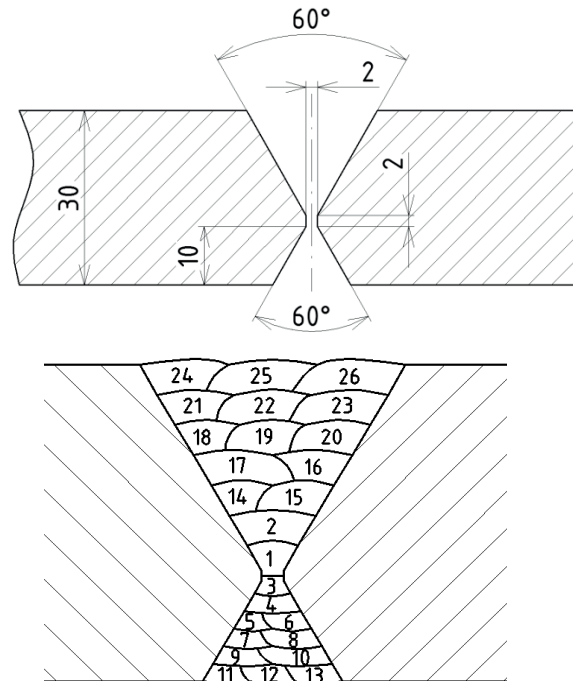


Fig. 3 Scheme of weld edge preparation (up) and welding sequence (down)

The sample was preheated by oxyacetylene flame to the temperature 180 °C before welding process and interpass temperature was maintained at temperature 300 °C during welding. Electrode CONARC 49 (E 46 3 B 32 H5 according to STN EN ISO 2560 standard) was used as filler material.

#### 3.2 Experimental measurements

Experimental measurements can be divided into two parts:

- measuring of welding parameters and thermal cycles during and after welding,
- measuring of displacement in chosen points due to welding influence - thermal expansivity of material caused by change of ambient temperature [9].

Chemical composition of steel S355

Table 1

Chemical composition of steel S 355 (%)												
C	Si	Mn	Cu	Al	Cr	Mo	Ni	V	Ti	Nb	P	S
0.166	0.375	1.440	0.017	0.044	0.050	0.004	0.034	0.049	0.003	0.003	0.018	0.005

Welding parameters and thermal cycles were measured by PC that allowed observed values on-line. Measuring system TRITOP was used to determine displacement of selected points [9].

### 3.2.1 Measuring and examination of thermal cycles

Thermal cycles were measured by 16 thermocouples. The points where the thermocouples were placed, allowed detailed time description of thermal fields near the weld during and after welding when the experimental sample was cooled (Fig. 4).

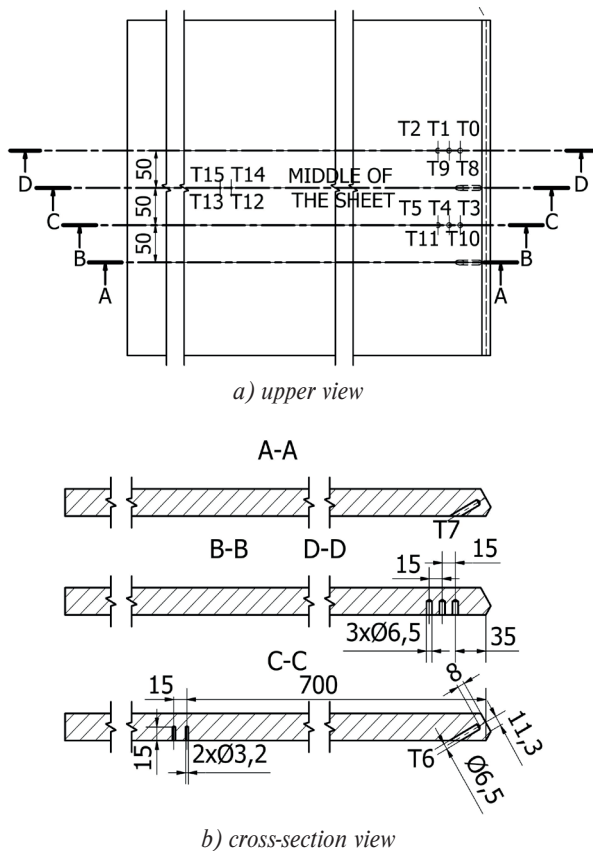


Fig. 4 Location of thermocouples on the welded plates

Thermal cycles recorded by thermocouples T0, T6, T10 (Fig. 5) were analysed to better comparing of thermal cycles obtained by experiment and simulation. Characteristic parameter  $T_{max}$  was determined for the first 4 beads. Maximal temperature  $T_{max}$  of the cycle is the most appropriate characteristic parameter of thermal cycle to verify the accuracy of the simulation (Table 3).

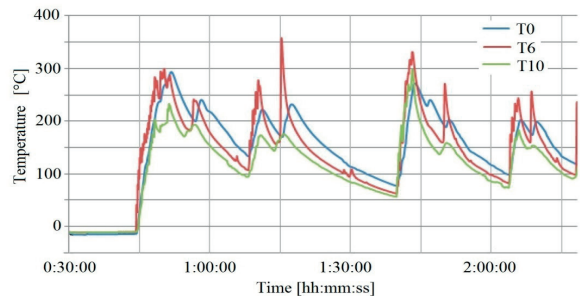


Fig. 5 Thermal cycles of thermocouples T0, T6 and T10 for the first 4 weld beads

Sample for macrostructural analysis was prepared from made weld. Macrostructural evaluation was in compliance with STN EN 1321 standard. Individual weld beads and their heat affected zones can be observed on macrostructural photography (Fig. 6). Macrostructural photography has also served as a background for macrostructure digitalization, which is important initial parameter of simulation.



Fig. 6 Macrophotography of welded joint, etch. 5% Nital

### 3.2.2 Measuring of displacement

Deformations of welded plates were measured by optical system TRITOP. This system measured displacement in properly chosen points. Displacement of points was measured 4 times. The first measurement (M1) was performed after tacking the sample in the manufacturing hall. The ambient temperature was about 20 °C. The sample was exposed to influence of negative ambient temperature after that measurement. When the sample temperature was steady in whole volume at about -10 °C, the second measurement (M2) was performed. Third measurement (M3) was performed after welding and stabilizing the temperature at about -10 °C. The last measurement (M4) was realized in the hall where ambient temperature was about 13 °C. Based on measurements of individual point displacements angular deformation of welded plates was analysed. Location and identification of analysed planes formed by three points are shown in Fig. 7.

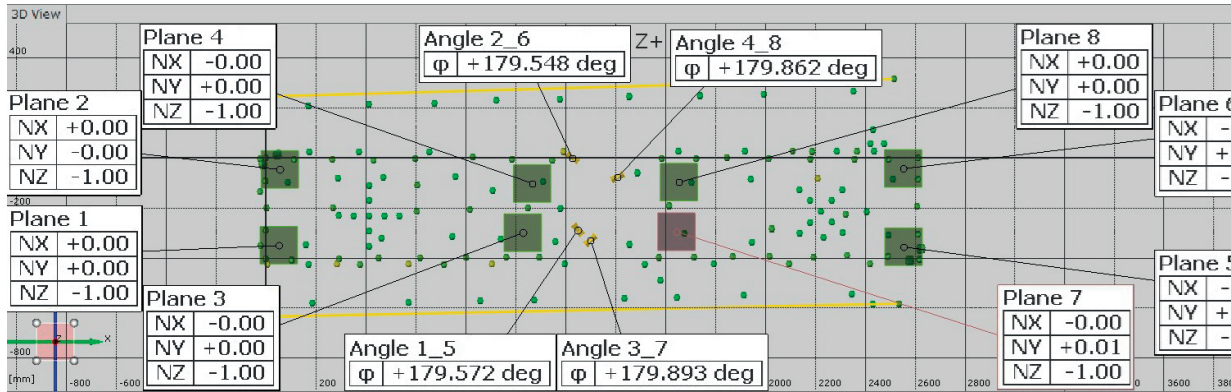


Fig. 7 Location of analysed planes and angles on welded plates

Angular deformation of sample were computed as the difference between the individual measurements (Table 2).

Angular changes between analysed planes Table 2

Angular change	Compared measures		
	M2 - M1	M3 - M2	M4 - M3
$\Delta\Phi_{1,5} (^{\circ})$	-0.046	-0.033	0.01
$\Delta\Phi_{2,6} (^{\circ})$	-0.095	0.027	0.01
$\Delta\Phi_{3,7} (^{\circ})$	0.051	0.027	-0.017
$\Delta\Phi_{4,8} (^{\circ})$	-	0.217	0.174

Maximal angular deformation of welded plates was detected between planes 4 and 8 with dimension 0.217°.

#### 4. Numerical simulation of welding at low temperatures

Based on experimental findings the numerical simulation in programme SYSWELD was processed and obtained results were verified with measured results after welding.

##### 4.1 Definition of initial parameters of simulation

Some simplifications were done at the numerical model because of wide dimensions of the real sample. Symmetrical 2D model was used for numerical simulation. Symmetrical axis of model is identical to the vertical axis of the weld. Digitized macrostructure was created in AutoCAD software and then was converted to FEM mesh (Fig. 8) in programme Visual MESH [10].

Material and physical properties were generated from SYSWELD database for material S355J2G3.

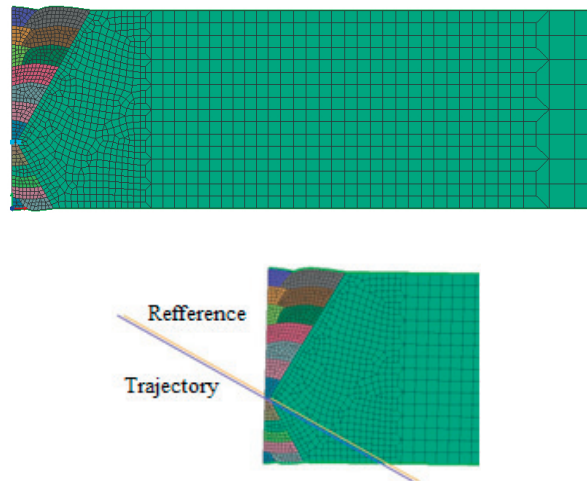


Fig 8 Finite element mesh of 2D model

2D Gaussian heat source was used for material preheating and Goldak's double-ellipsoidal heat source was used for simulation of welding. Parameters of heat source models were defined separately for preheating and for each weld beads. Welding process was simulated at ambient temperature -10°C. Heat exchange from material to atmosphere had to be modified. Heat flow coefficient for this purpose was  $q = 10 \text{ W.m}^{-2}$ .

##### 4.2 Thermal analysis results

The thermal analysis was computed after definition of initial parameters for welding. Simulation thermal fields of beads corresponded with real thermal fields of beads, which can be observed on macrophotography. Thermal cycles were generated at the same points as thermocouples were placed on the sample (Fig. 9). Maximal temperature  $T_{\text{max}}$  of three thermal cycles was determined for four weld beads from experimentally measured and simulated thermal cycles. Its values are in Table 3.

Parameter  $T_{max}$  of three thermal cycles for four weld beads

Table 3

$T_{max}$ (°C)	Weld bead											
	1			2			3			4		
	Thermocouple			Thermocouple			Thermocouple			Thermocouple		
	T0	T6	T10									
Simulation	255.3	469.4	255.0	168.5	343.2	168.0	164.7	259.3	164.2	166.5	261.3	165.8
Experiment	240.5	240.9	193.8	231.9	357.6	175.6	202.2	270.9	158.9	198.2	256.1	153.8

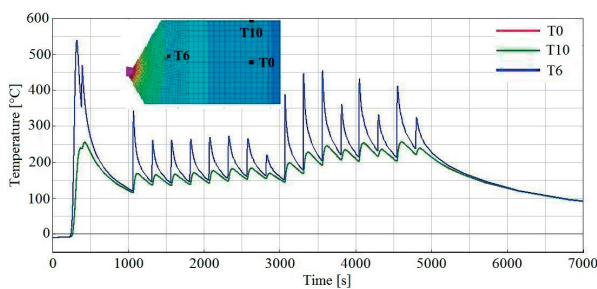


Fig. 9 Thermal cycles of simulated welding process

Values of parameter  $T_{max}$  obtained by simulation and experiment reached a good agreement. The maximal deviation between experiment and simulation was 18.4%.

### 4.3 Mechanical analysis results

Mechanical analysis of welding allows getting information about values and distribution of longitudinal, transversal, residual stresses by von Mises and deformation of weldments. Residual stresses by von Mises in weld construction computed in SYSWELD are shown in Fig. 10. The maximal value of residual stress in specific node was 1,018 MPa. This value is only approximate because it was calculated just for discrete node. Location of this maximal stress value was in the weld root.

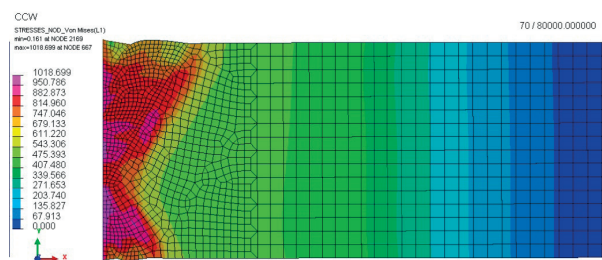


Fig. 10 Von Mises residual stresses of weld construction

To better compare measured and simulated welding deformations, angular deformation were computed. Computation of angular deformation was based on displacement in Z axis of chosen points and total length of metal sheet model (1,321 mm). Values of angular deformation after simulation of welding are listed in Table 4.

Angular deformation values obtained by simulation in 2D symmetrical model represent only half of real deformation value. Resulting value of angular deformation is 0.212° which is in good agreement with experimentally obtained deformation (0.217°).

### 5. Conclusion

This article describes experimental measurements and numerical simulation during welding of bridge construction at low temperatures. Results of thermal cycles and weld macrostructure were used as boundary conditions for the simulation in SYSWELD. Residual stresses and angular deformation were calculated. Calculated angular deformations were almost identical to the experimentally measured deformations by optical system

Angular deformations obtained by simulation

Table 4

Angular deformation									
Layer	1	2	3	4	5	6	7	8	
Bead	1	2	3	4	5	6	7	8	9
Deformation(°)	0.074	0.851	0.559	0.299	0.084	-0.095	-0.254	-0.382	-0.473
Layer	9	10	11		12		13		-
Bead	10	11	12	13	14	15	16	17	-
Deformation (°)	-0.478	-0.349	-0.217	-0.119	-0.063	0.019	0.036	0.106	-

TRITOP. The results of experiments and experiences can be concluded that the program SYSWELD is able to calculate deformations of welded construction within a tolerance of 10%.

#### Acknowledgement

This work has been supported by Scientific Grant Agency of Ministry of Education of the Slovak Republic, grant VEGA: 1/0547/11, KEGA: 039ZU-4/2011, and non-profit organization EkoFond project No. 561/PG04/2011.

#### References

- [1] FENG, Z.: *Processes and Mechanisms of Welding Residual Stress and Distortion*, CRC Press, USA, 2005, ISBN 978-0-8493-3467-2.
- [2] TOTTEN, G., HOWES, M., INOUE, T.: *Handbook of Residual Stress and Deformation of Steel*, AMS International, Materials Park, 2002, ISBN 0-87170-729-2.
- [3] KONAR, R., MICIAN, M.: Numerical Simulation of Residual Stresses and Distortions in Butt Weld in Simulation Programme SYSWELD, *Communications - Scientific Letters of the University of Zilina*, vol. 14, No. 3, 2012, 49-54, ISSN 1335-4205.
- [4] MORAVEC, J.: *Influence of Welding Parameters on Weld Pool's Geometry in Shielding Gas Welding*, Pollypress : Liberec, 2011, ISBN 978-80-7372-805-2.
- [5] MESKO, J. et al.: Shape of Heat Source in Simulation Program SYSWELD using Different Types of Gases and Welding Methods, *Strojirenska technologie*, 2011, No. 5, 6-11, ISSN 1211-4162.
- [6] BREZNICAN, M., et al.: The Simulation of Influence of Quenching Temperature on Properties of Bearing Rings, *Manufacturing Technology*, vol. 13, No. 1, 2013, 20-25, ISSN 1213-2489.
- [7] NOVAK, P., MESKO, J., ZMINDAK, M.: Finite Element Implementation of Multi-pass Fillet Weld with Phase Changes, *Manufacturing Technology*, 2011, vol. 13, No. 1, 79-85, ISSN 1213-2489.
- [8] KONAR, R., MICIAN, M., HOPKO, A.: Analysis of Boundary Conditions for the Simulation of Welding at the Repair of Gas Pipelines with Steel Sleeve, *Communications - Scientific Letters of the University of Zilina*, vol. 13, No. 4, 2011, 36-39, ISSN 1335-4205.
- [9] ZMINDAK, M., NOVAK, P., MESKO, J.: Numerical Simulation of Arc Welding Processes with Metallurgical Transformations, *Metalurgija*, vol. 49, No. 2, 2010, 595-599, ISSN 0543-5846.
- [10] SLADEK, A., et al.: The Roundness and Microstructure of Thin-wall Bearing Rings, *Manufacturing Technology*, vol. 12, No. 13, 2012, 237-241, ISSN 1213-2489.

Ivana Pobocikova - Zuzana Sedliackova - Jan Simon \*

## STATISTICAL ANALYSIS OF WIND SPEED DATA BASED ON WEIBULL AND RAYLEIGH DISTRIBUTION

*In this paper the wind speed data from Meteorological observatory Bratislava-Mlynska dolina were statistically analyzed. The data were analyzed based on Weibull and Rayleigh distribution. The distribution parameters were estimated using maximum likelihood method. The both distributions were compared for their performance using the coefficient of determination and the root mean square error. The results indicate that the better performance can be obtained by the Weibull distribution.*

**Keywords:** Wind speed data, Weibull distribution, Rayleigh distribution, maximum likelihood method, coefficient of determination, root mean square error.

### 1. Introduction

Global warming and environmental pollution become widely discussed issues within last decades. Current major energy sources have significant impact on ecosystems and should be replaced by alternative renewable sources of energy. Wind power plants are promising energy sources with minimal environmental impact and huge energetic potential. However, attention has to be paid to the optimal locality selection to maximize efficiency and reduce costs. Presented paper introduces the Weibull and Rayleigh distribution as the inventive tools in wind speed analyses as well as proposes a complex methodology recommended for evaluation of wind speed conditions in specific locality.

For the sake of this study the wind speed data from the Meteorological observatory Bratislava - Mlynska dolina were statistically analyzed. Processed data were collected during year 2009 in quasi-continuous regime by anemometer connected to electronic buffer. The main objective of presented paper is to propose better probability distribution functions for fitting the observed wind speed data and to establish methodology for wind conditions analyses. Based upon studies [1] - [14] we introduced the Weibull distribution and its special case Rayleigh distribution to approximate the measured wind speed data.

The maximum likelihood method was used to estimate the parameters of the distribution functions. The coefficient of determination ( $R^2$ ) and the root mean square error ( $RMSE$ ) were used to evaluate the fitting performance of the Weibull and Rayleigh distribution functions.

The Weibull distribution and its special case the Rayleigh distribution are commonly used and recommended probability distributions to describe the wind speed data. The probability density function of the Weibull distribution with parameters  $k > 0$  and  $c > 0$  is for  $v > 0$  given by

$$f(v) = \frac{k}{c^k} v^{k-1} \exp\left(-\left(\frac{v}{c}\right)^k\right), \quad (1)$$

where  $v$  is the wind speed,  $k$  is the dimensionless shape parameter and  $c$  is the scale parameter in units of the wind speed. The corresponding cumulative distribution function is given by

$$F(v) = 1 - \exp\left(-\left(\frac{v}{c}\right)^k\right), v > 0. \quad (2)$$

The Rayleigh distribution is a special case of the Weibull distribution where the shape parameter is set to  $k = 2$ . Consequently the probability density function of the Rayleigh distribution transforms as follows

$$f(v) = \frac{2v}{c^2} \exp\left(-\left(\frac{v}{c}\right)^2\right), v > 0. \quad (3)$$

### 2. Methods for estimating the parameters of the Weibull and Rayleigh distribution

There are several methods available in literature to estimate the Weibull and Rayleigh distribution parameters. In presented

\* Ivana Pobocikova, Zuzana Sedliackova, Jan Simon

Department of Applied Mathematics, Faculty of Mechanical Engineering, University of Zilina, Slovakia

E-mail: ivana.pobocikova@fstroj.uniza.sk

paper we chose the maximum likelihood method (see [3], [5] and [15]) for estimation of the shape parameter  $k$  and the scale parameter  $c$

$$\frac{1}{k} - \frac{\sum_{i=1}^n v_i^k \ln v_i}{\sum_{i=1}^n v_i^k} + \frac{1}{n} \sum_{i=1}^n \ln v_i = 0, \tag{4}$$

$$c = \left( \frac{1}{n} \sum_{i=1}^n v_i^k \right)^{1/k}, \tag{5}$$

where  $v_i, i = 1, 2, \dots, n$ , is the wind speed and  $n$  is the number of nonzero wind speeds. The shape parameter  $k$  was estimated by numerical solving of nonlinear equation (4). Newton method was employed to obtain numerical result. The scale parameter  $c$  was estimated by evaluating equation (5).

The maximum likelihood method estimate for the parameter  $c$  of the Rayleigh distribution can be solved explicitly by equation (6)

$$c = \left( \frac{1}{n} \sum_{i=1}^n v_i^2 \right)^{1/2}. \tag{6}$$

### 3. Descriptions of wind speed data

The wind speed data processed in presented paper were measured at the Meteorological observatory Bratislava - Mlynska dolina, situated in the campus of Faculty of mathematics, physics and informatics, Comenius University in Bratislava, within time frame January 2009 to December 2009. The wind speed and direction were measured continually by anemometer connected to the storage system. In order to remove accidental fluctuations continual data were hourly averaged and rounded to the nearest integer.

### 4. Statistical analysis of wind speed distributions

The wind speed data were generally divided into subsets with respect to the months and four seasons. Spring was considered to last from March to May. Summer lasts from June to August, autumn from September to November and winter from December to February. The monthly, yearly and seasonal average wind speeds  $\bar{v}$  and the standard deviations  $s_v$  were calculated by following equations

$$\bar{v} = \frac{1}{n} \sum_{i=1}^n v_i, \tag{7}$$

$$s_v = \sqrt{\frac{1}{n-1} \sum_{i=1}^n (v_i - \bar{v})^2}, \tag{8}$$

where  $v_i, i = 1, 2, \dots, n$ , is the averaged wind speed (month, year, season) and  $n$  is the number of records.

The estimates of the Weibull and Rayleigh distribution parameters were calculated using (4), (5) and (6) for each month, season and whole year, respectively.

The performance of the Weibull and Rayleigh distribution was evaluated by the coefficient of determination ( $R^2$ ) and the root mean square error ( $RMSE$ ). These parameters were calculated using equations (9) and (10)

$$R^2 = 1 - \frac{\sum_{i=1}^N (y_i - x_i)^2}{\sum_{i=1}^N (y_i - \bar{y})^2}, \tag{9}$$

$$RMSE = \sqrt{\frac{1}{N} \sum_{i=1}^N (y_i - x_i)^2}, \tag{10}$$

where  $N$  is the number of wind speed data,  $y_i$  is the  $i^{th}$  ordered observed wind speed data ( $y_1 \leq y_2 \leq \dots \leq y_N$ ),  $x_i$  is the  $i^{th}$  predicted data calculated using the Weibull or Rayleigh distribution, respectively,  $i=1, 2, \dots, N$ , and  $\bar{y}$  is average of values  $y_1, y_2, \dots, y_N$ .

The coefficient  $R^2$  ranges from 0 to 1. The higher value of  $R^2$  is better,  $R^2$  approaches 1 in an ideal case. The coefficient  $RMSE$  ranges from 0 to infinity. In this case lower value of  $RMSE$  is better, in an ideal case it approaches 0. Therefore, the most suitable wind speed distribution is selected according to higher value of  $R^2$  and lower value of  $RMSE$ .  $R^2$  and  $RMSE$  were calculated for each month, season and whole year.

### 5. Results and discussion

Table 1 shows the monthly and yearly descriptive statistics - average wind speeds, standard deviations, maximum, skewness, kurtosis and median. It has been shown that the yearly average wind speed is 10.485 km/h and the yearly standard deviation is 5.841 km/h. The monthly average wind speed varies between 8.272 and 13.617 km/h with maximum in March and minimum in September. The same goes for monthly standard deviation which reaches the highest value in March (7.525 km/h) and the lowest one in September (4.327 km/h). The monthly average wind speeds are shown in Fig. 1.

Table 2 shows the seasonal wind speed descriptive statistics. One can see that the highest value of the average wind speed is observed in the winter season 11.657 km/h and the lowest value in the summer season 9.380 km/h. The highest value of the standard deviation was calculated for the spring season 6.260 km/h and the lowest one in the summer season 4.917 km/h.

Table 3 shows the monthly and yearly estimates of the Weibull and Rayleigh distribution parameters and statistical analysis for the monthly and yearly wind speeds distributions. One can see that the yearly shape parameter  $k$  of the Weibull distribution is

Monthly and yearly wind speed descriptive statistics

Table 1

Months	Average wind speeds $\bar{v} (km/h)$	Standard deviation $s_v (km/h)$	Maximum $v_{max} (km/h)$	Skewness	Kurtosis	Median $\tilde{v} (km/h)$
Jan	11.013	5.545	29	0.233	-0.412	11
Feb	12.945	6.318	33	0.188	-0.324	13
Mar	13.617	7.525	38	0.533	-0.182	13
Apr	10.140	5.379	28	0.552	-0.219	9
May	10.298	4.910	25	0.336	-0.497	10
Jun	9.269	4.882	28	0.594	0.341	9
Jul	9.870	5.337	37	1.019	1.584	9
Aug	8.997	4.458	26	0.588	-0.037	9
Sep	8.272	4.327	24	0.556	0.063	8
Oct	9.784	6.260	30	0.799	-0.067	8
Nov	10.590	5.930	34	0.663	0.197	10
Dec	11.138	6.202	32	0.492	-0.108	11
Yearly	10.485	5.841	38	0.718	0.429	10

Seasonal wind speed descriptive statistics

Table 2

Seasons	Average wind speeds $\bar{v} (km/h)$	Standard deviation $s_v (km/h)$	Maximum $v_{max} (km/h)$	Skewness	Kurtosis	Median $\tilde{v} (km/h)$
Winter	11.657	6.081	33	0.338	-0.250	12
Spring	11.366	6.260	38	0.770	0.586	11
Summer	9.380	4.917	37	0.806	1.007	9
Autumn	9.551	5.657	34	0.819	0.415	9

Monthly and yearly estimates of the Weibull and Rayleigh distribution parameters and statistical analysis for wind speed distributions

Table 3

Months	Weibull distribution				Rayleigh distribution		
	$k$	$c (km/h)$	$R^2$	$RMSE$	$c (km/h)$	$R^2$	$RMSE$
Jan	2.083	12.423	0.70181	0.01392	12.329	0.70568	0.01380
Feb	2.148	14.598	0.72251	0.01190	14.413	0.70296	0.01231
Mar	1.883	15.362	0.84599	0.00745	15.568	0.82786	0.00788
Apr	1.999	11.493	0.91894	0.00745	11.493	0.91894	0.00745
May	2.233	11.644	0.92244	0.00736	11.415	0.91642	0.00764
Jun	2.174	10.810	0.93649	0.00772	10.631	0.94539	0.00716
Jul	1.952	11.155	0.95882	0.00603	11.219	0.95942	0.00598
Aug	2.142	10.178	0.93706	0.00821	10.040	0.93843	0.00812
Sep	2.002	9.336	0.90796	0.01012	9.334	0.90804	0.01012
Oct	1.629	10.986	0.88958	0.00844	11.628	0.69942	0.01393
Nov	1.877	11.976	0.94372	0.00592	12.152	0.92346	0.00690
Dec	1.979	12.866	0.86210	0.00859	12.895	0.85901	0.00868
Yearly	1.902	11.897	0.99027	0.00251	12.034	0.97921	0.00367

Seasonal estimates of the Weibull and Rayleigh distribution parameters and statistical analysis for wind speed distributions Table 4

Seasons	Weibull distribution				Rayleigh distribution		
	$k$	$c$ (km/h)	$R^2$	$RMSE$	$c$ (km/h)	$R^2$	$RMSE$
Winter	2.042	13.257	0.85497	0.00868	13.203	0.85634	0.00864
Spring	1.911	12.853	0.97799	0.00355	12.987	0.97070	0.00410
Summer	2.064	10.713	0.98038	0.00430	10.641	0.98071	0.00427
Autumn	1.768	10.770	0.97509	0.00431	11.110	0.92833	0.00732

1.902, while the yearly scale parameter  $c$  is 11.897 km/h. The yearly parameter  $c$  of the Rayleigh distribution is 12.034 km/h. The comparison of the yearly Weibull and Rayleigh probability density distributions with the observed yearly probability density distribution of the wind speed is illustrated in Fig. 2. The top points of the curves are the most frequent wind speeds for the compared distributions (Weibull: 8.037 km/h, Rayleigh: 8.509 km/h). Both of the theoretical curves of the probability density distributions match the observed data satisfactorily at well acceptable levels of  $R^2$  and  $RMSE$ .

Analyses show that the monthly shape parameter  $k$  of the Weibull distribution ranges from 1.629 to 2.233 and the monthly scale parameter  $c$  ranges from 9.336 to 15.362 km/h. The highest value of the parameter  $c$  was observed in March and the lowest one in September, which corresponds with observation well. The monthly parameter  $c$  of the Rayleigh distribution ranges from 9.334 to 15.568 km/h with maximum in March and minimum in September, thus corresponding to the monthly average wind speeds too.

The performance of the Weibull and Rayleigh distribution was evaluated by the coefficient of determination ( $R^2$ ) and the root mean square error ( $RMSE$ ). The value of  $R^2$  is 0.99027 for the Weibull distribution and 0.97921 for the Rayleigh distribution when applied to yearly wind speed data. The value of  $RMSE$  is 0.00251 for the Weibull distribution and 0.00367 for the Rayleigh distribution when applied to the same set of data. The yearly comparison shows that the Weibull distribution returns higher value of  $R^2$  and the smaller value of  $RMSE$ . This indicates that the Weibull distribution is slightly better choice for fitting the yearly wind speed data than the Rayleigh distribution.

For the monthly wind speed data the value of  $R^2$  ranges from 0.70181 to 0.95882 for the Weibull distribution and from 0.69942 to 0.95942 for the Rayleigh distribution. The  $RMSE$  ranges from 0.00592 to 0.01392 for the Weibull distribution and from 0.00598 to 0.01393 for the Rayleigh distribution. The month to month comparison shows that, in general, the Weibull distribution leads to the higher values of  $R^2$  and the smaller values of  $RMSE$  than the Rayleigh distribution. It holds true for 8 months of year 2009. It confirms that the Weibull distribution is slightly better for fitting the monthly wind speed data than the Rayleigh distribution. The values of  $R^2$  and  $RMSE$  obtained by fitting the monthly

probability density distributions derived from the observed data with the Weibull and Rayleigh probability density distributions are illustrated in Fig. 3.

Table 4 shows the seasonal estimates of the Weibull and Rayleigh distribution parameters and statistical analysis for seasonal wind speed. The comparison of seasonal Weibull and Rayleigh probability density distributions with the observed seasonal probability density distributions of the wind speed are illustrated in Fig. 4. In general, the value of the scale parameter  $c$  of the Weibull distribution is the highest in the winter season and the lowest in the summer season. Basically the same goes for the parameter  $c$  of the Rayleigh distribution. The seasonal value of the Weibull distribution parameter  $k$  ranges from 1.768 to 2.064. The value of the parameter  $c$  ranges from 10.713 to 13.257 km/h. The seasonal value of the Rayleigh distribution parameter  $c$  ranges from 10.641 to 13.203 km/h. The seasonal value of  $R^2$  ranges from 0.85497 to 0.98038 for the Weibull distribution while for the Rayleigh distribution ranges from 0.85634 to 0.98071. The value of  $RMSE$  ranges from 0.00355 to 0.00868 for the Weibull distribution while for the Rayleigh distribution ranges from 0.00410 to 0.00864.

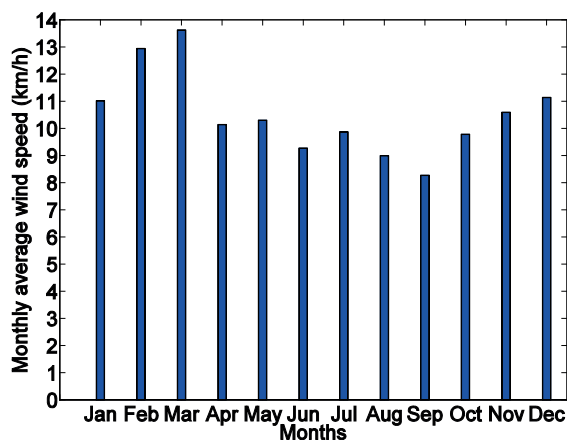


Fig. 1 Monthly average wind speeds

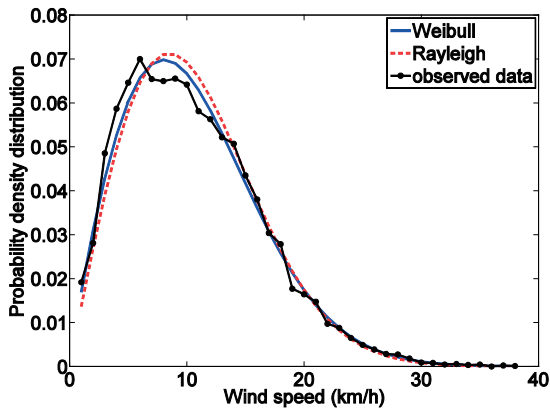


Fig. 2 Comparison of yearly Weibull and Rayleigh probability density distributions

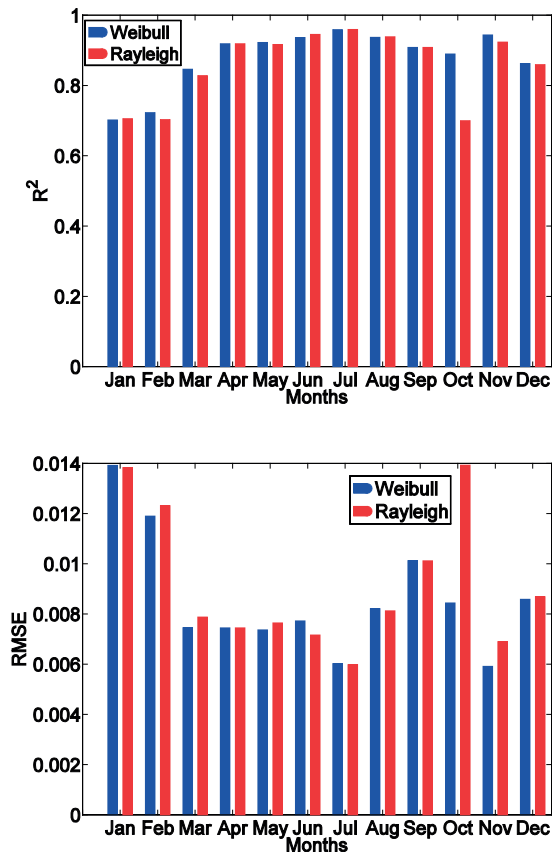


Fig. 3  $R^2$  and RMSE values obtained by fitting observed monthly probability density distributions with Weibull and Rayleigh probability density distributions

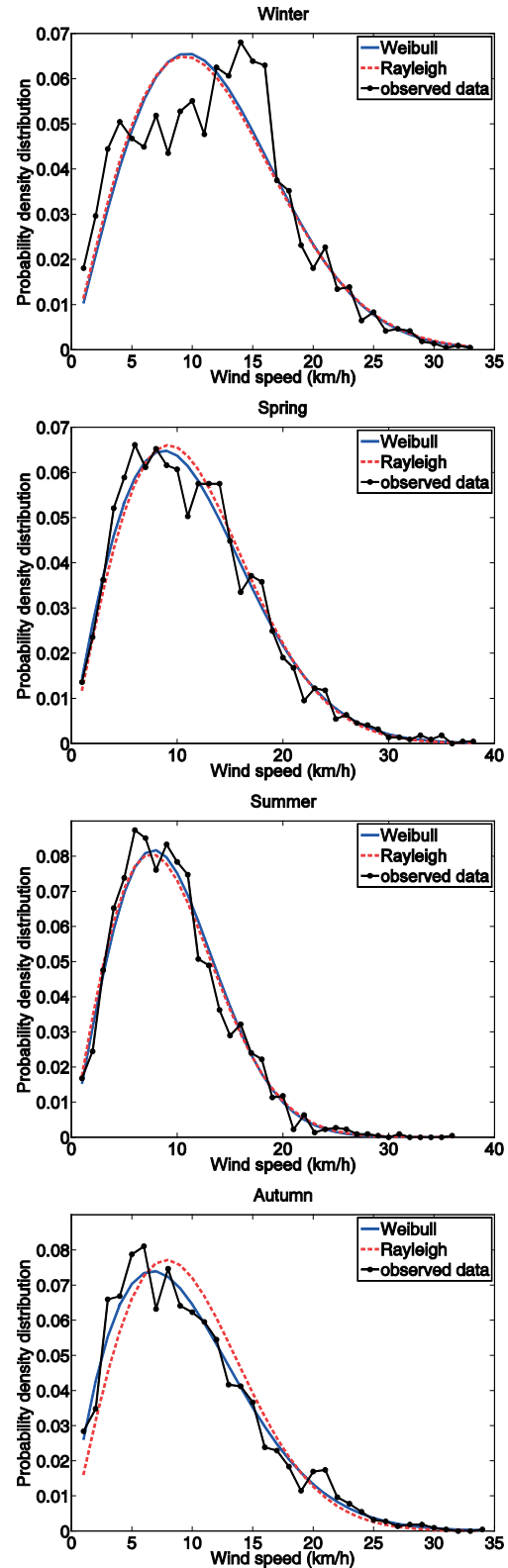


Fig. 4 Comparison of seasonal Weibull and Rayleigh probability density distributions

## 6. Concluding remarks

In this paper the wind speed data from Bratislava have been statistically analyzed using the Weibull and Rayleigh probability distributions. The probability distributions have been derived from the measured wind speed data for the year 2009. The monthly, yearly and seasonal Weibull and Rayleigh distribution parameters have been calculated. To evaluate the performance of the considered probability distributions the coefficient of determination and the root mean square error have been used. The following conclusions can be made.

The Weibull distribution has been found to be more suitable for fitting the wind speed data obtained in year 2009 in Bratislava than the Rayleigh distribution at the yearly base.

The Weibull distribution has been found to be more suitable for fitting the wind speed data in eight months than the Rayleigh distribution.

The Weibull distribution can be recommended for fitting the wind speed data at the seasonal base.

## Acknowledgement

This paper was supported by the Slovak Grant Agency VEGA through the projects No. 1/1245/12. The authors gratefully acknowledge the Meteorological observatory Mlynska dolina and Faculty of mathematics, physics and informatics for providing us with measured wind speed data.

## References

- [1] ALBUHAIRI, M. H.: A Statistical Analysis of Wind Speed Data and an Assesment of Wind Energy Potential in Taiz-Yemen. *Assiut University Bulletin for Environmental Research* 9(2), 21-33, 2006
- [2] AKDAG, S. A., DINLER, A.: A New Method to Estimate Weibull Parameters for Wind Energy Applications. *Energy Conversion and Management* 50, 1761-1766, 2009
- [3] CARTA, J. A., RAMIREZ, P., VELASQUEZ, S.: A Review of Wind Speed Probability Distributions Used in Wind Energy Analysis: Case Studies in the Canary Islands. *Renewable and Sustainable Energy Reviews* 13, 933-955, 2009
- [4] CELIK, A. N.: A Statistical Analysis of Wind Power Density Based on the Weibull and Rayleigh Models at the Southern Region of Turkey. *Renewable Energy* 29, 593-604, 2003
- [5] CONRADSEN, K., NIELSEN, L. B. PRAHM, L. P.: Review of Weibull Statistics for Estimation of Wind Speed Distributions. *J. of Climate and Applied Meteorology* 23, 1173-1183, 1994
- [6] DORVLO, A. S. S.: Estimating Wind Speed Distribution. *Energy Conversion and Management* 43, 2311-2318, 2002
- [7] FADARE, D. A.: A Statistical Analysis of Wind Energy Potential in Ibadan, Nigeria, Based on Weibull Distribution Function. *The Pacific J. of Science and Technology* 9 (1), 110-119, 2008
- [8] GUPTA, B. K.: Weibull Parameters for Annual and Monthly Wind Speed Distribution for Five Locations in India. *Solar Energy* 37 (6), 673-678, 1986
- [9] GOKCEK, M., BAYULKEN, A., BEKDEMIR, S.: Investigation of Wind Characteristics and Wind Energy Potential in Kirklareli, Turkey. *Renewable Energy* 32, 1739-1752, 2007
- [10] LUN, I. Y. F., LAM, J. C.: A Study of Weibull Parameters Using Long-term Wind Observation. *Renewable Energy* 20, 145-153, 2000
- [11] RAMIREZ, P., CARTA, J. A.: Influence of the Data Sampling Interval in the Estimation of Parameters of the Weibull Wind Speed Probability Density Distribution: a Case Study. *Energy Conversion and Management* 45, 2419-2438, 2005
- [12] SEGURO, J. V., LAMBERT, T. W.: Modern Estimation of the Parameters of the Weibull Speed Distribution for Wind Energy Analysis. *J. of Wind Engineering and Industrial Aerodynamics* 85, 75-84, 2000
- [13] ULGEN, K., HEPBASLI, A.: Determination of Weibull Parameters for Wind Energy Analysis of Izmir, Turkey. *Intern. J. of Energy Research* 26, 495-506, 2002
- [14] FERANEC, V.: Wind Engineering in the 21<sup>th</sup> Century. *Communications - Scientific Letters of the University of Zilina*, vol. 2, No. 4, 74-83, 2000
- [15] CHU, Y. K., KE, CH. J.: Computation Approaches for Parameter Estimation of Weibull Distribution. *Mathematical and Computational Applications*, vol. 17, No. 1, 39-47, 2012.

Daniel Riecky - Milan Zmindak - Zoran Pelagic \*

---

## NUMERICAL FINITE ELEMENT METHOD HOMOGENIZATION OF COMPOSITE MATERIALS REINFORCED WITH FIBERS

*The paper presents the micromechanical modelling of fiber-reinforced composites in order to determine elastic properties of the homogenized material. For this purpose implementation of homogenization theory was required and analyses were performed. The polymer matrix of three-dimensional representative volume element (RVE) of the composites is modelled by the finite element method (FEM). Software for homogenization of material properties uses direct homogenization method which is based on volume average of stresses in the RVE. Homogenization of composite plate is performed by linking MATLAB and ANSYS software. Calculated elastic properties of the homogenized material are given for epoxy matrix reinforced with carbon, fiberglass and kevlar fiber material.*

**Keywords:** Fiber-reinforced composites, Representative volume element, Finite element method.

### 1. Introduction

Modern materials are characterized by a wide spectrum of tailored mechanical, optical, magnetic, electronic, or thermomechanical properties. Using of laminated composites allows the designer to optimize material/structural systems which complicates their analysis. The prediction of the macroscopic stress-strain response of the composite material is related to the description of its complex microstructural behavior [1 and 2]. Some analytical and numerical techniques have been used for prediction and characterization of composite microstructure behavior [3]. Analytical methods provide reasonable prediction for relatively simple configurations of the phases. Complicated geometries, loading conditions and material properties often do not yield analytical solutions, due to complexity and number of equations. In this case, various numerical methods [4 - 7] are used for approximate solving, but they still make some simplifying assumptions about the microstructures of heterogeneous multiphase materials.

In homogenization process the original heterogeneous material is replaced by homogeneous material with the same mechanical properties. In other words, homogenization and averaging of properties and micro-fields of the material are considered as a homogeneous equivalent medium at the macro-level, and the effective properties of the medium are determined on the basis of the analysis of the microstructure, micro-geometry and properties of the materials.

There are various homogenization methods. Direct homogenization is based on the volume average of field variables, such as stress, strain and energy density. Effective properties can be calculated from effective properties definitions. The average and calculation of field variables can be performed numerically, for example, by finite element method (FEM) or boundary element method and geometry and microstructural properties can be generalized for real composite materials which do not have periodic structure distribution of the fibers in the matrix [8].

Indirect homogenization is based on the Eshelby solution of self-deformation for one inclusion in an infinite matrix - the equivalent inclusion method [9]. An alternative approach to direct and indirect homogenization is the variational method which can determine the upper and lower limits of the elasticity modulus [10].

A relatively new approach for homogenization of microstructures consists of mathematical homogenization based on a two-scale extension of the displacement field [11].

### 2. Methodology

The composite under consideration is constituted by continuous and parallel cylindrical fibers with equal radius and centers periodically spaced in a hexagonal and a squared array, as it appears in Fig. 1. We assumed an ideal cohesion between the fiber and the matrix. A procedure of homogenization

---

\* Daniel Riecky, Milan Zmindak, Zoran Pelagic

Department of Applied Mechanics, Faculty of Mechanical Engineering, University of Zilina, Slovakia  
E-mail: milan.zmindak@fstroj.uniza.sk

of material properties of composites using the method of representative volume element RVE was used. For the analysis of material properties an own software in MATLAB language was programmed and a part of the solution was carried out in ANSYS software. The RVE consists of volume elements SOLID45 (Fig. 2) and then it is loaded by unit strains in various directions. The effective lamina properties are obtained from the volume means of stress values obtained by loading of the RVE.

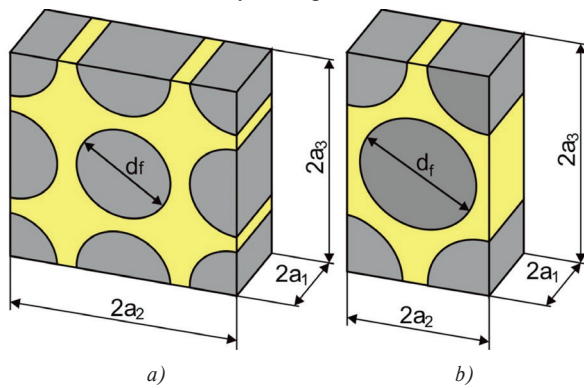


Fig. 1 Representative volume elements, a) square configuration, b) hexagonal configuration

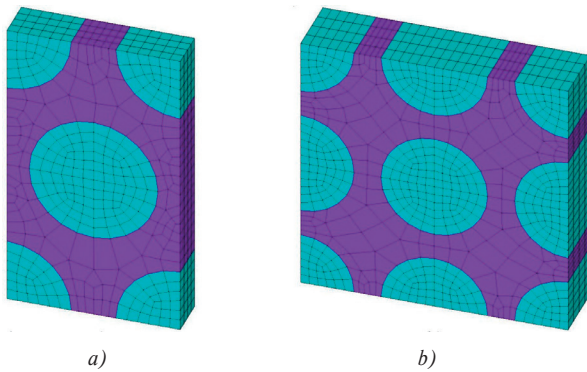


Fig. 2 The finite element mesh adopted in the computation, a) square configuration, b) hexagonal configuration

Homogenized lamina RVE consists of fibers and epoxy matrix. The fibers are from three material types: carbon, glass, polyaramide. Used carbon fibers have an industrial label T300 and M40J. The glass fiber label is EGlass and S2Glass. Polyaramide fibers have the label K49. Fiber material properties are listed in Table 1 and the matrix properties are listed in Table 2.

Fiber material properties

Table 1

	Fiber material		
	Carbon M40J	Fiberglass S2Glass	Kevlar K49
$E_f$ [GPa]	377	85.5	135.5
$F_{it}$ [GPa]	4.41	4.6	3.53
$\nu$	0.33	0.22	0.37
$\rho_m$ [kg/m <sup>3</sup> ]	1770	2490	1450
$d_f$ [μm]	5	10	10

Matrix material properties

Table 2

Matrix material	$E_m$ [GPa]	$F_{it}$ [MPa]	$\nu$	$\rho_f$ [kg/m <sup>3</sup> ]	$G_m$ [GPa]
Epoxy	3.45	70	0.3	85.5	1.33

where subscript “*f*” denotes fiber and “*m*” matrix, respectively and

$E$  - Young modulus                       $\nu$  - Poisson number

$G$  - Shear modulus                       $\rho$  - Density

$F_{it}$  - Longitudinal tensile strength     $d_f$  - fiber diameter

The RVE dimensions are calculated for the square fiber configuration - Fig. 1a, from the relations

$$a_2 = \sqrt{\frac{1}{4} \frac{\pi d_f^2}{V_f}}, a_3 = a_2, a_1 = 0.5 a_2 \quad (1)$$

and for a hexagonal fiber configuration the RVE dimensions are in Fig. 1b, from the relations

$$a_2 = \sqrt{\frac{1}{8} \frac{\pi d_f^2}{V_f \text{tg}(60^\circ)}}, a_3 = a_2 \text{tg}(60^\circ), a_1 = 0.5 a_2 \quad (2)$$

where  $a_i$  is the  $x$ -direction, in this case the fiber direction,  $a_2$  is the  $y$ -direction, orthogonal to the fiber direction,  $a_3$  is  $z$ -direction, transverse vertical to the fiber direction and  $V_f$  is fiber volume fraction.

Analysis of microstructure directly yields a transversely isotropic stiffness tensor

$$\begin{Bmatrix} \bar{\sigma}_{11} \\ \bar{\sigma}_{22} \\ \bar{\sigma}_{33} \\ \bar{\sigma}_{23} \\ \bar{\sigma}_{13} \\ \bar{\sigma}_{12} \end{Bmatrix} = \begin{bmatrix} C_{11} & C_{12} & C_{12} & 0 & 0 & 0 \\ C_{12} & C_{22} & C_{23} & 0 & 0 & 0 \\ C_{12} & C_{23} & C_{22} & 0 & 0 & 0 \\ 0 & 0 & 0 & 1/2(C_{22} - C_{23}) & 0 & 0 \\ 0 & 0 & 0 & 0 & C_{66} & 0 \\ 0 & 0 & 0 & 0 & 0 & C_{66} \end{bmatrix} \begin{Bmatrix} \bar{\epsilon}_{11} \\ \bar{\epsilon}_{22} \\ \bar{\epsilon}_{33} \\ \bar{\gamma}_{23} \\ \bar{\gamma}_{13} \\ \bar{\gamma}_{12} \end{Bmatrix} \quad (3)$$

where the 1-axis is aligned with the fiber direction and the overbar indicates the average computed over the volume RVE. The components of the tensor  $C$  are determined by solving three elastic models of RVE with parameters  $(a_1, a_2, a_3)$ , subjected to the boundary conditions on the following displacement components.

$$\begin{aligned}
 u_1(a_1, y, z) - u_1(-a_1, y, z) &= 2a_1 \epsilon_{i1}^0, \\
 -a_2 \leq y \leq a_2, \\
 -a_3 \leq z \leq a_3,
 \end{aligned} \tag{4}$$

$$\begin{aligned}
 u_1(x, a_2, z) - u_1(x, -a_2, z) &= 2a_2 \epsilon_{i2}^0, \\
 -a_1 \leq x \leq a_1, \\
 -a_3 \leq z \leq a_3,
 \end{aligned} \tag{5}$$

$$\begin{aligned}
 u_1(x, y, a_3) - u_1(x, y, -a_3) &= 2a_3 \epsilon_{i3}^0, \\
 -a_1 \leq x \leq a_1, \\
 -a_2 \leq y \leq a_2,
 \end{aligned} \tag{6}$$

For the homogeneous composite material, the relationship between average stress and strain is

$$\bar{\sigma}_\alpha = C_{\alpha\beta} \bar{\epsilon}_\beta \tag{7}$$

$\alpha, \beta = 1, \dots, 6$  is the contracted notation given in [12]. This implies that elements of the matrix  $C$  are determined by solution of six elastic RVE models in which boundary conditions (4-6) are applied for only one component of the strain  $\epsilon_{ij}^0$ . This component is different from zero for each of the six problems. Once the components of the transversely isotropic tensor  $C$  are known, the five elastic properties of the homogenized material can be computed by [13]:

$$\begin{aligned}
 E_1 &= C_{11} - 2C_{12}^2 / (C_{22} + C_{23}) \\
 \nu_{12} &= C_{12} / (C_{22} + C_{23}) \\
 E_2 &= (C_{11}(C_{22} + C_{23}) - 2C_{12}^2) / (C_{11}C_{22} - C_{12}^2) \\
 \nu_{23} &= (C_{11}C_{23} - C_{12}^2) / (C_{11}C_{22} - C_{12}^2) \\
 G_{12} &= C_{66}
 \end{aligned} \tag{8}$$

where  $E_i$  and  $E_2$  are longitudinal and transversal Young's moduli,  $\nu_{12}$  and  $\nu_{23}$  are longitudinal and transversal Poisson's ratios and  $G_{12}$  is the longitudinal shear modulus. The shear modulus  $G_{23}$  in the transversal plane can be obtained using classical relation between Young modulus  $E$  and shear modulus  $G$ , so

$$G_{23} = C_{44} = \frac{1}{2}(C_{22} - C_{23}) = \frac{E_2}{2(1 + \nu_{23})} \tag{9}$$

In order to evaluate the elastic matrix  $C$  of the composite, the RVE is subjected to an average strain  $\bar{\epsilon}_\beta$ . The unit strain applied on the boundary results in a complex state of stress in the RVE.

Then the volume average of the strain in the RVE equals to the applied strain

$$\bar{\epsilon}_{ij} = \frac{1}{V} \int_V \epsilon_{ij} dV = \epsilon_{ij}^0 \tag{10}$$

Then volume average of stress in RVE equals to required components of the elastic matrix as

$$C_{ij} = \bar{\sigma}_i = \frac{1}{V} \int_V \sigma_i dV \tag{11}$$

The coefficients in  $C$  are found by setting a different problem for each column of  $C$  and the components. Details of the procedure for calculation of the coefficients of the matrix  $C$  are given in [14].

### 3. Results

Homogenization of a composite plate is performed by linking MATLAB and ANSYS software. Homogenization of the material properties were done for fiber volume fractions  $V_f$  from the interval  $<0.2, 0.6>$ . The entire process is automated requires just entering a type of fibers, their arrangement and the step increment volume fraction. The finite element code ANSYS 11.0 is used to solve the problem described above. The matrix and fibers are modeled by linear elastic isoparametric brick elements with eight nodes and six faces (i.e. the ANSYS SOLID elements). FE mesh is symmetric with respect to the coordinate planes.

In Figs. 3 to 6 deformed shapes and contour plots of stresses for different strains applied to stretch the RVEs are described. The boundary conditions in the calculation of the sixth column of  $C$  are enforced by using coupling constraint equations (CE).

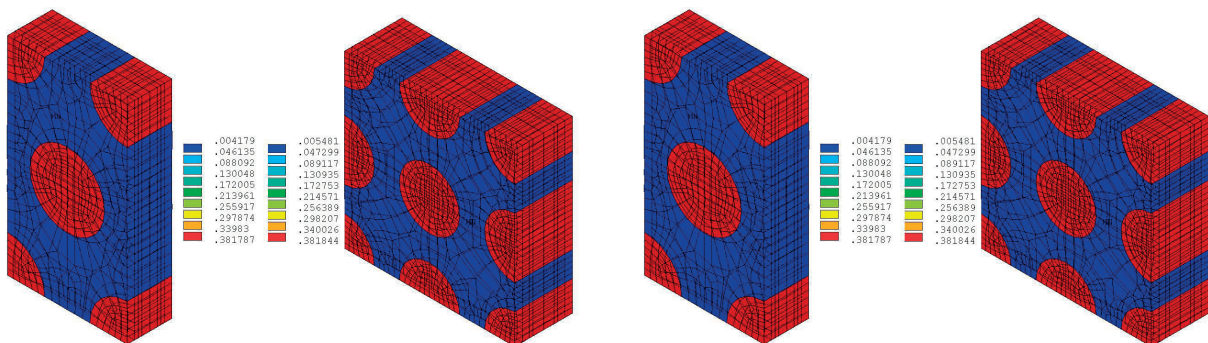


Fig. 3 Deformed shape and contour plot of stress  $\sigma_{11}$ ,  $\epsilon_1^0 = 1$ ,  $\epsilon_2^0 = \epsilon_3^0 = \gamma_4^0 = \gamma_5^0 = \gamma_6^0 = 0$

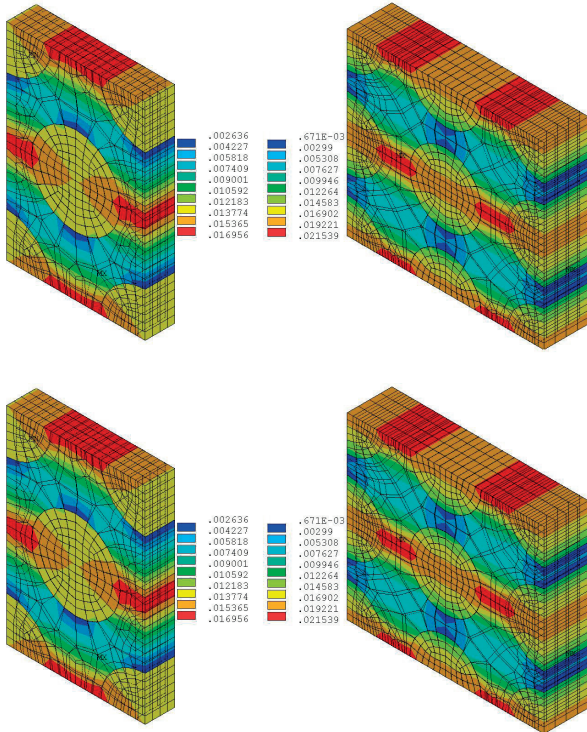


Fig. 4 Deformed shape and contour plot of stress  $\sigma_{22}$ ,  
 $\epsilon_2^0 = 1, \epsilon_1^0 = \epsilon_3^0 = \gamma_4^0 = \gamma_5^0 = \gamma_6^0 = 0$

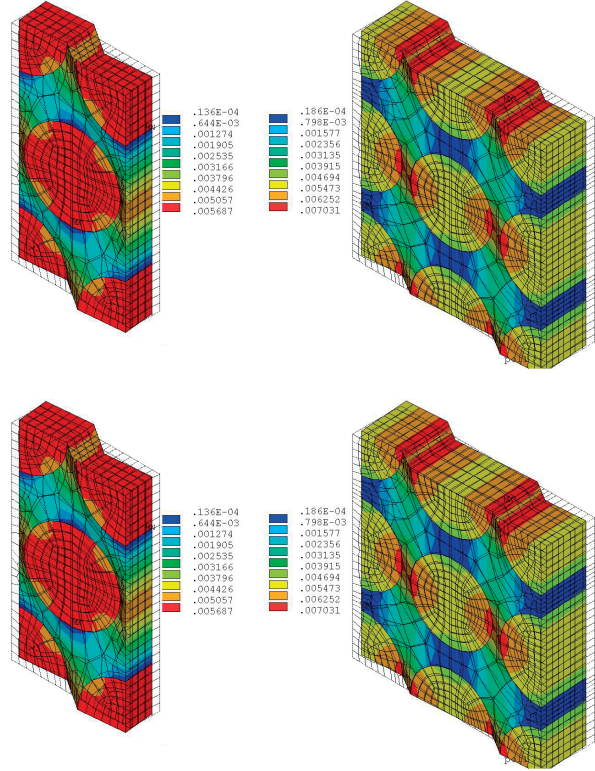


Fig. 6 Deformed shape and contour plot of stress  $\tau_{13}$ ,  
 $\gamma_6^0 = \epsilon_{12}^0 + \epsilon_{21}^0 = 1, \epsilon_1^0 = \epsilon_2^0 = \epsilon_3^0 = \gamma_4^0 = \gamma_5^0 = 0$

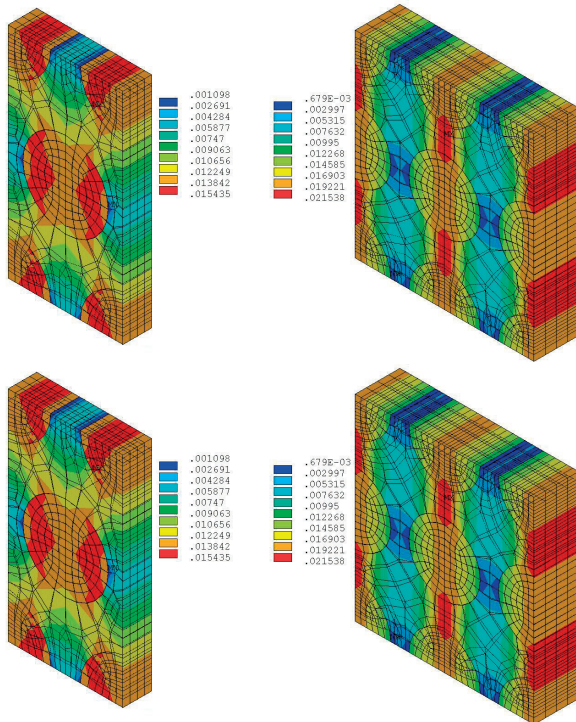


Fig. 5 Deformed shape and contour plot of stress  $\sigma_{33}$ ,  
 $\epsilon_3^0 = 1, \epsilon_1^0 = \epsilon_2^0 = \gamma_4^0 = \gamma_5^0 = \gamma_6^0 = 0$

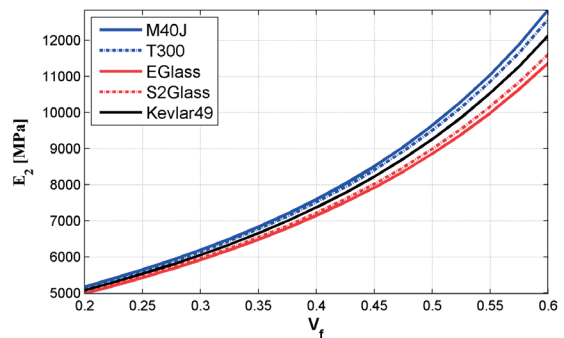
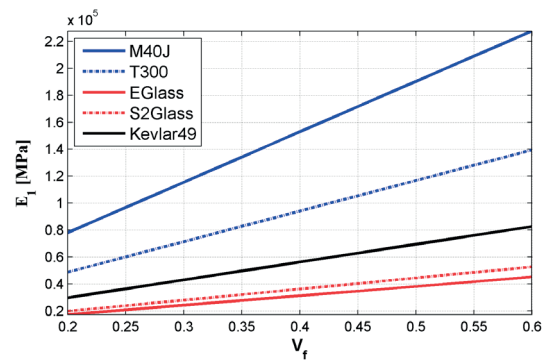


Fig. 7 Effective elastic constants  $E_1$  and  $E_2$  vs.  $V_f$

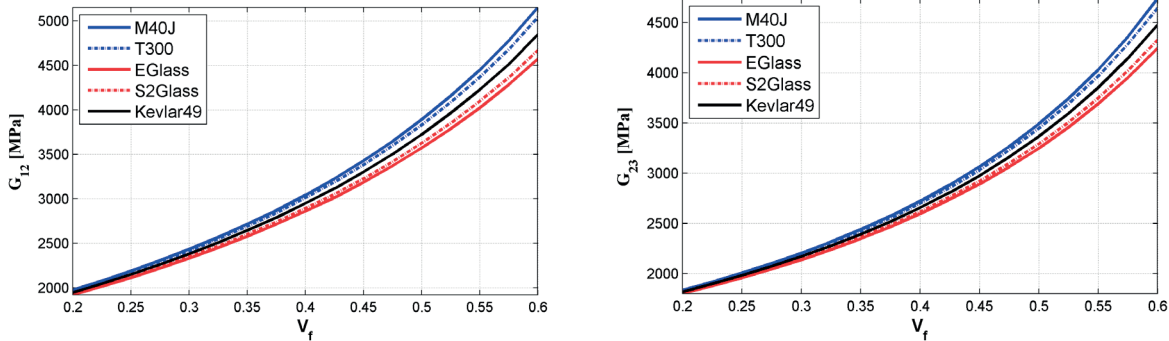


Fig. 8 Effective elastic constants  $G_{12}$  and  $G_{23}$  vs.  $V_f$

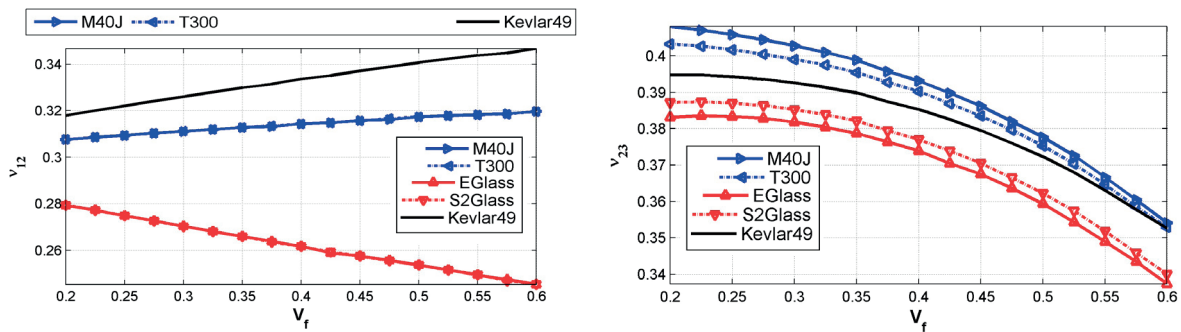


Fig. 9 Effective elastic constants  $\nu_{12}$  and  $\nu_{23}$  vs.  $V_f$

Calculated elastic properties of the composite with fiber volume fraction  $V_f = 0.6$

Table 3

$V_f = 0.6$	M40J		S2Glass		K49	
	h	s	h	s	h	s
$E_1$ [GPa]	227.58	227.58	52.683	52.687	82.683	82.685
$E_2$ [GPa]	12.831	16.71	11.607	14.334	12.121	15.301
$G_{12}$ [GPa]	5.15	5.53	4.67	4.94	4.844	5.155
$G_{23}$ [GPa]	4.737	6.967	4.3314	5.905	4.481	6.288
$\nu_{12}$	0.320	0.321	0.246	0.245	0.347	0.348
$\nu_{23}$	0.354	0.199	0.340	0.214	0.352	0.217

In Figs. 7 to 9 courses of the homogenized elastic material properties for hexagonal array computed using equations (8) are described. Calculated elastic properties of the homogenized material for  $V_f = 0.6$  are given in Table 3 where the indices “h” and “s” denote hexagonal array and square array, respectively.

#### 4. Conclusions

Accurate and efficient methods have been proposed within the framework of the displacement-based FEM for solving the unit cell homogenization (RVE) problem for periodic composites.

The modelling procedure is explained briefly in this paper. If one wishes to perform a parametric study, repeating this process on an interactive session, using the CAE graphical user interface (GUI) is very time consuming and prone to errors. Instead, it is possible to capture the ANSYS script generated by CAE during an interactive session and use it to automate the process.

#### Acknowledgement

The authors gratefully acknowledge support from the Slovak and Technology Assistance Agency registered under number APVV-0736-12, Slovak Grant Agency VEGA 1/1226/12.

## References

- [1] CAPORALE, A., LUCIANO, R., SACCO, E.: Micromechanical Analysis of Interfacial Debonding in Unidirectional Fiber-reinforced Composites, *Computers and Structures* 84, 2006, 2200-2211.
- [2] DEKYS, V., KOPAS, P., SAPIETA, M., STEVKA, O., A Detection of Deformation Mechanisms using Infrared Thermography and Acoustic Emission, *Applied Mechanics and Materials*, vol. 474, 2014, 315-320.
- [3] ZMINDAK, M., NOVAK, P.: Special Approach for Thermal Modelling Fibre-reinforced Composites with Larger Aspect Ratio, *Communications - Scientific Letters of the University of Zilina*, 4A/2012, 73-78.
- [4] SOARES, D. JR., SLADEK, J., SLADEK, V., ZMINDAK, M., MEDVECKY, S: Porous Media Analysis by Modified MLPG Formulations, *CMC: Computers, Materials & Continua*, vol. 27(2), 2012, 101-127.
- [5] LACK T., GERLICI J.: Wheel/rail Contact Stress Evaluation by Means of the Modified Strip Method, *Communications - Scientific Letters of the University of Zilina*, No. 3, 2013, 126-132.
- [6] BEDNAR, R., SAGA, M., VASKO, M.: Effectivity Analysis of Chosen Numerical Methods for Solution of Mechanical Systems with Uncertain Parameters. *Communications - Scientific Letters of the University of Zilina*, No. 4, 2013, 40-45.
- [7] V. KOMPIS, Z. MURCINKOVA: Thermal Properties of Short Fiber Composites Modeled by Meshless Method, *Advances in Materials Science and Engineering*, vol. 2014, Article ID 521030, 8 p., <http://dx.doi.org/10.1155/2014/521030>
- [8] POSPISIL, T.: Generating Non-periodic Microstructures of Fiber Composites. *Engineering Mechanics*, vol. 17, No. 5/6, 2010, 393-405.
- [9] ESHELBY, J. D.: *The Determination of Elastic Field of an Ellipsoidal Inclusion and Related Problems*, Proc. R. Soc. London, 1957, 276-396.
- [10] HASHIN, Z., SHTRIKMAN, S.: On Some Variational Principles in Anisotropic and Nonhomogeneous Elasticity, *J. Mech. Phys. Solids*, vol. 10, 1962, 335-342.
- [11] KOUZNETSOVA, V. G.: *Computational Homogenization for the Multi-scale Analysis of Multi-phase materials*, TU Eindhoven, 2012.
- [12] BARBERO, E. J.: *Finite Element Analysis of Composite Materials*, CRC Press : Boca Raton, 2007.
- [13] REDDY, J. N.: *Mechanics of Laminated Composite Plates and Shells: Theory and Analysis*, 2<sup>nd</sup> ed., CRC Press, 2004.
- [14] KORMANIKOVA, E., RIECKY, D., ZMINDAK, M.: *Strength of Composites with Short Fibers*. In: Eds, J. Murin: Computational Modelling and Advanced Simulations, Series: Computational Methods in Applied Sciences, vol. 24, 2011.

Darina Kumicakova - Zdenek Konecny \*

## APPROACH TO THE PROBLEM OF BIO-INSPIRED ROBOTIC GRIPPER DESIGNING

*The article with its content belongs to the field of bio-inspired robotics. This main focus is aimed at the problem of a specialised human-like robotic gripper designing. The article presents our approaches to solution of the chosen problems of multifunctional robotic grippers designing on the example of a proposed 3D model of three-fingered bio-robotic gripper. Attention is devoted to utilisation of CAD/CAE tools for exploring characteristics of the design using computer simulation.*

**Keywords:** Bio-inspired robots, object grasping, computer simulation, CAD/CAE, contact analyses.

### 1. Introduction

Biologically inspired robotic subsystems – robotic hands are becoming more and more popular not only as rehabilitation devices but also as the dextrous ones for human-like manipulation with objects. Namely, the three-fingered robotic grippers as a robot arm working tool can find application in industrial field too. Automated workplaces have often required utilising robots that are able to response to changes in product production flexibly. According to the flexibility required level it can be achieved by utilisation of a robot's multiple grasping end effector, a system of automated exchange of robotic grippers or a specialised biorobotic gripper that is able to grasp objects of different types similarly to human-like way. Kinematics, actuation and control of bio-robotic grippers are more complicated than it is in case of standard industrial grippers. Therefore, the development of these special robotic subsystems design requires a special approach and application of modern methods and means of computer simulation. The present research in the field of multifunctional robotic hands/grippers development is aimed at the problem of their virtual models grasping ability exploration [1] and [2]. Novelty in robotic hands/grippers designing requires creative and innovative approach.

A multifunctional – bio-robotic gripper is a special technical system. In general, the design methodology of this system involves algorithmised procedures of technical creative work most of all. Creative technical work deals with the solution of tasks with unknown resolution procedure [3] and [4]. TRIZ as one of the worldwide applied methods suitable for solution of this type of tasks, is based on logic, data and research, not intuition approach

to a problem solution. “TRIZ brings repeatability, predictability, and reliability to the problem-solving process with its structured and algorithmic approach”. It offers the means that support abilities of engineers to enhance their creativity. TRIZ is based on [5]:

- the regularities of objectively existing tendencies of the technical systems development,
- and principles for the technical contradictions overcoming.
- The procedure of TRIZ methodology application in process of technical system development consists of the next steps [6]:
- a preparatory stage (the choice of the object of innovation, specification of the project team, etc.),
- an information stage (a collection of all important information about innovated object, marketing, etc.),
- a function-cost analysis of innovated object – *FNA* (finding answers to the questions what (?) and why (?) should be improved in a technical system),
- an algorithmization of innovative solutions – *ARIZ* (specification and solution of technical and physical contradictions),
- a verification stage (choice and verification of the best solution),
- a stage of construction and the proposals testing with support of CAD/CAM/CAE.

Utilisation of simulation tools of appropriate CAD/CAE system enables to obtain information how the chosen kinematic parameters and construction influence the robotic hand ability to grasp different objects relatively fast and to optimize its constructional design for required result still before its prototype production [7].

\* <sup>1</sup>Darina Kumicakova, <sup>2</sup>Zdenek Konecny

<sup>1</sup>Department of Automation and Production Systems, Faculty of Mechanical Engineering, University of Zilina, Slovakia

<sup>2</sup>Department of Robotics, Faculty of Mechanical Engineering, VSB – Technical University of Ostrava Ostrava-Poruba, Czech Republic

E-mail: darina.kumicakova@fstroj.uniza.sk

The paper presents application of TRIZ methodology principles and utilisation of simulation tools of systems creo parametric and MSC ADAMS in the process of a 3D model of three-fingered bio-robotic gripper designing that was proposed for purposes of research possibilities of the object grasping stability evaluation by simulation in real time.

## 2. Description of the bio-robotic gripper design

The latest 3<sup>rd</sup> version of bio-robotic gripper's design consists of three identical fingers that are placed at the palm of lightened construction - see Fig. 1a. Two fingers (Finger1 and Finger 2) are mounted at the gripper's palm in opposite to Finger 3. Every finger has three joints and 4DOF (2+1+1). Movement of every finger is activated separately through a motion transmission system. Movement of proximal and medial links of every finger for the biorobotic gripper closing/opening is activated directly by tensile forces acting in bendable steel plaited wires - cables. Movement of each of these links is controlled by own pair of cables. Movement of distal links is activated indirectly through the rigid rods depending on the proximal links movement.

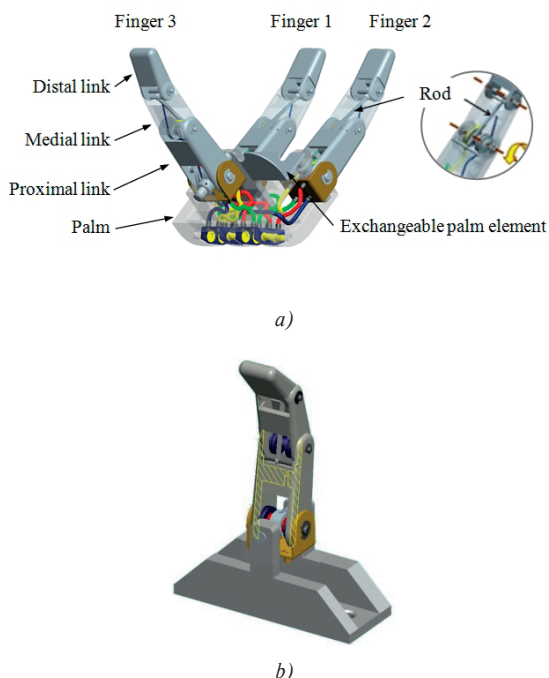


Fig. 1 Design of the 3<sup>rd</sup> version of bio-robotic gripper:  
a) 3D model (creo parametric 5);  
b) an innovated construction of the finger.

The new concept of bio-robotic gripper was created on the base of TRIZ methodology principles. Two parameters from 39 Features of Altshuller's Contradiction Matrix were chosen:

1. "35. Adaptability or versatility": This parameter represents a main requirement in the process of multifunctional robotic hands designing. But the solution of this one leads to the technical system complexity increase. It means that high requirements will be asked to specify the interaction among the technical system subsystems and their control too. Therefore, the second - worsening parameter was chosen:
2. "33. Ease of operation": the movements control.

Four principles (No.: "1.", "15.", "16." and "34.") were chosen on the base of analysis of TRIZ 40 principles [8] successfully applied to overcome the contradictions. The offered solutions have brought a new view at the bio-robotic gripper's finger construction. The new construction element was added to the finger's 1<sup>st</sup> joint (application of principle "1." Segmentation). Applications of the principles: "15. Dynamics", 16. Partial or excessive actions and "34. Discarding and recovering" have led to a change of cables guiding towards to the finger medial link and an elimination of pulleys as the source of redundant forces that acted between the finger's distal and medial links. This new concept of finger (Fig. 1b) was applied for creation of the bio-robotic gripper's 3<sup>rd</sup> construction.

## 3. Simulation model of bio-robotic gripper

The basic problem of the bio-robotic gripper's mechanism simulation resulted from a large number of both degrees of freedom and members of the kinematic chain whose movement must be controlled. The finger's mechanical structure represents an open kinematic chain for which the physical parameters and their boundary conditions were not precisely defined. Therefore, the principle of bionics and heuristic approach based on empiricism and analogy with human hands will be used for the motion simulation [9].

The first phase of the flexible components simulation was focused on computer modelling of plaited wires (cables) as the flexible elements which constitute the actuation and transformation mechanism of the bio-robotic gripper's propulsion subsystem. Two approaches were applied in this phase.

The idea of implementing the necessary simulations was to use Pro/Engineer WF5 and apply alternative approaches to modelling and simulation of mentioned cables [10]. We considered the cable as a 3D model with a constant length, resulting in the subsequent simulation procedures (chain method). Solution like this one represents the application of simulation based on object modelling features of the mechanism. The basic principle of testing was to simplify the real model to the theoretical one to eliminate many parameters and variables entering the process

that could affect the test results in ways previously unpredictable. The bendable wire was modelled as a linkage consisting of  $n$  cylindrical elements of constant length:

$$dl_1 = dl_2 = \dots = dl_n \quad (1)$$

Total length of the cable model is expressed as follows:

$$l = \sum_{i=1}^n dl_i \quad (2)$$

The cable model's base element - a cylinder of diameter 0.8mm was closed from the one side by convex cylindrical surface and from the second side by concave surface. These both surfaces create references to the building elements for the mutual interconnection between neighbouring elements in the chain. A trajectory of cable model was defined by the cable outlet (output) at the base, a rotating guide roller surface and point of its mounting to the proximal link. This trajectory was created in the model as "Sketch" associative curve changing its shape depending on the configuration of characteristic elements position during their mutual movement. The created simplified testing model is shown in Fig. 2. A previously considered actuator - artificial pneumatic muscle (PAM) is modelled in the proximal link motion transmission system too. The simulation model of PAM is connected with an output end of the cable model. The length and diameter of PAM were defined as parameters depending on a control parameter  $P$  (a pressure inside PAM). The PAM's length was changed during the simulation with subsequent change in control parameter  $P$  and by regeneration of the simulation model. It led to the cable tensing and rotational movement of the finger's proximal link execution.

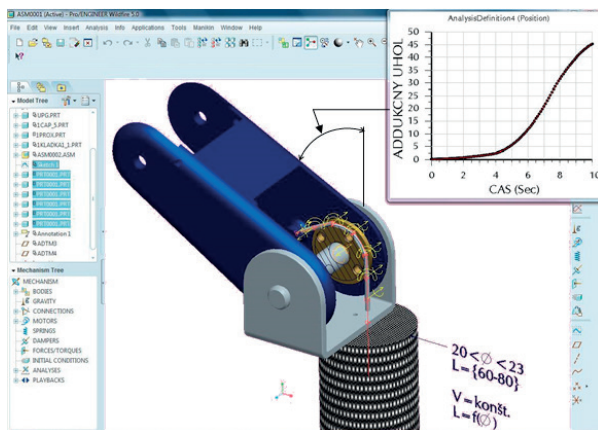


Fig. 2 Tested simulation model of the finger proximal link motion transmission system (3D model; creo parametric).

The results of the simulation experiments showed that [10]:

- the difficulty and time of simulation calculations increase in proportion to the increasing number of elements  $n$ . It could

be caused by non-optimized calculation algorithm system for a given application and hardware performance PC.

- a simulation based on variations of parameter  $P$  enables to obtain only discrete values (angular rotation and position).

The conclusion was that this approach to the motion transmission system model creation will not be suitable for exploration of the bio-robotic gripper grasping abilities by simulation in real time and will not be appropriate for the complex bio-robotic gripper mechanism creation.

The new testing simulation model was created in ADAMS/View [11]. A pulley mechanism was proposed for a transmission simulation model creation. The cable was modelled as "immaterial" element placed between two pulleys in tangential contact points. Kinematic dependency between movement of the cable model and pulleys was defined by *Rackpin Joint*. In this way the tensile force acting on the cable could be transformed to the pulley's torque and conversely too. The following assumptions were adopted too:

- Tendons (cables) are ideally rigid-bodies.
- Masses of tendons (cables) and pulleys are negligible.
- Friction between a tendon (cable) and a pulley is infinitely large - a pulley transmits the torque.
- Friction between a pulley and its pin is negligible.

Proposed testing model was validated with the help of ADAMS tool. Also a correct function of the testing model was verified by dynamic simulation. Obtained results showed a direct kinematic dependency between angular rotation of medial and distal links. The finger testing model could be utilized for the bio-robotic gripper virtual model creation. Further, the tasks of 3D contacts modelling for simulation of the bio-robotic gripper grasping ability in real time in MSC ADAMS 2012 were solved [12]. The simulation experiment of a cylindrical object grasping was executed. Measured parameters were: single tensile forces acting on the proximal and medial links cables (Table 1) and values of the cables displacements  $\Delta l$  - see Fig. 3.

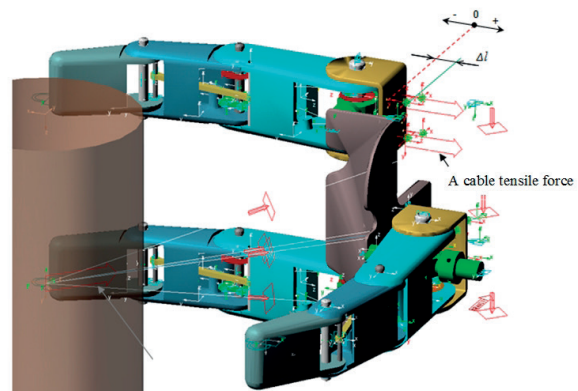


Fig. 3 Virtual model for object grasping simulation (MSC ADAMS 2012)

Values of measured tensile forces in moment of the object stable grasping

Table 1

Object: a cylinder	Closed bio-robotic gripper	Finger 1	Finger 2	Finger 3
		Tensile forces - $F_{max}$ (N)		
Material: wood; $\phi D = 60$ mm, $L = 110$ mm	Proximal link cable	2.877	2.877	5.764
	Medial link cable	3.609	3.609	7.209

Measured values of tensile forces for Fingers 1, 2 and 3 demonstrate a symmetrical configuration of forces on single fingers resulting from the steady state of forces acting at the grasped object in the moment of its stable grasping.

In addition, previously considered actuators - pneumatic artificial muscles were replaced by electric motors Maxon EC 20 including a simple transmission system (Fig. 4). The pulley (3) for fixation and reeling the cables was specially designed.

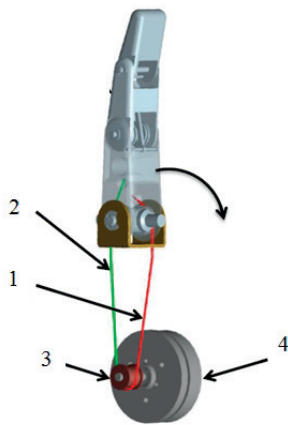


Fig. 4 Principle of a motion transmission system proposed for the proximal links movement: 1 - a cable activated on finger closing; 2 - a cable activated on finger opening; 3 - a pulley; 4 - Maxon EC 20.

#### 4. Analysis of an object grasping optimal conditions

Generally, the requirements to minimize forces or torques actuating on robotic gripper and also the reducing of mechanism whole mass at a minimum are important for a robotic gripper construction. These conditions are common also for a multifunctional bio-robotic gripper. An optimal value of transfer function ( $U/F$ ) is sought for an object grasping effective way. The transfer function is given as follows [13]:

$$\frac{U}{F} = f(d_1, d_2, d_3, \dots, d_n), \quad (3)$$

where:

$U$  - the value of grasping force (N),

$F$  - the value of actuating force of the mechanism actuating system (N),

$d_1, d_2, d_3, \dots, d_n$  - parameters defining the kinematic structure of a robotic gripper.

All known optimization methods are based on seeking the minimal value of a target function. The presented CAD/CAE systems are able to solve a complex optimization tasks too. They integrated the different FEM methods that open new possibilities of components and assemblies analyses [14]. Contact analyses don't require calculation of reactions of mechanism single joints for a lot of cases. The primary force (or torque) is applied on

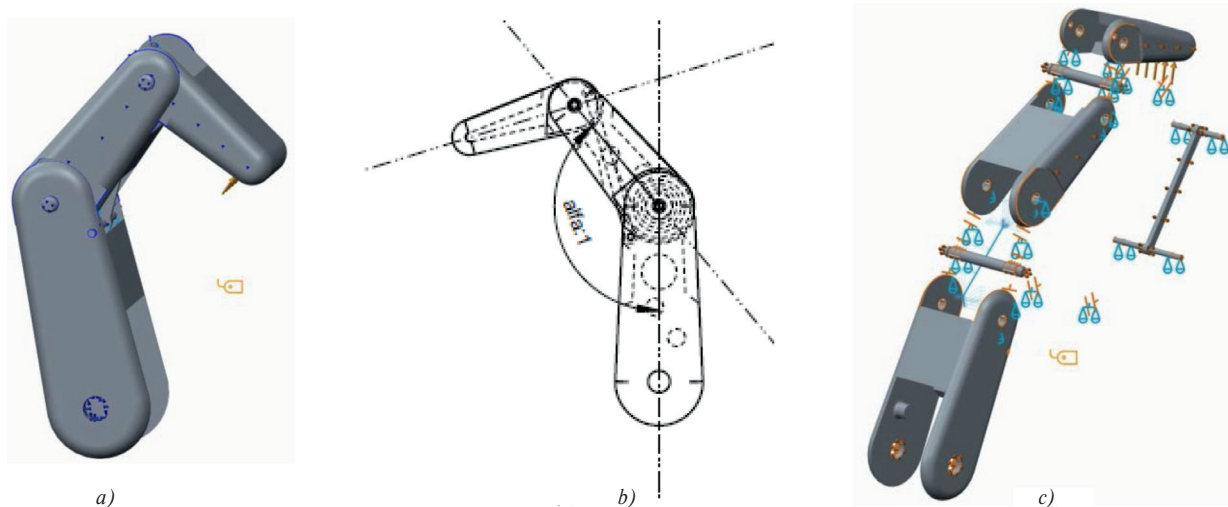


Fig. 5 Created computational model of the finger (creo 2): a) a simplified model; b) the specification of a parameter  $\alpha:1$ ; c) created contacts.

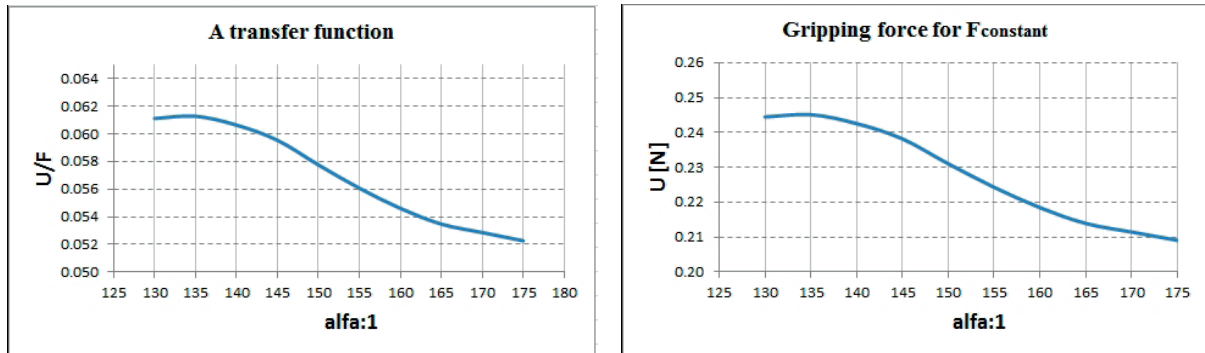


Fig. 6 Results of contact analyses (creo2)

mechanism and is analysed as a whole. Influence of responses is automatically reflected in deformations of the mechanism individual components. If the contact analyses of flexible parts are realized, the mechanism's redundancies have to be eliminated to obtain regular results of analyses [15]. A simplified computational model of the bio-robotic gripper's finger was used for the optimal transfer function seeking (Fig. 5a). The defined parameter *alfa:1* (Fig. 5b) is an angle between the finger's proximal and medial links. Contact analyses were performed for the angle that was changed from 130° to 175°. The contact model was also created (Fig. 5c).

Material properties of the computational model were defined on the base of mechanical properties of the manufactured finger prototype. Three phalanges and one pulley are manufactured from material ABS 400 by Rapid Prototyping method that is usually used for prototype parts production [16]. The remaining parts are manufactured from steel material. The cable was simulated by element of a *Beam* type that enables to obtain an axis force (actuating tensile force in the solved task) that was used for the transfer function calculation. The values of Table 1 were used for definition of the mechanism model loading. Results of the contact analyses show that parameter *alfa:1* = 135deg represents angle of an optimal grip of proximal and medial links (see Fig. 6).

Results of deformation analyses showed that influence of the gripping force *U* on the distal link is minimal (Figs. 6 and 7) - therefore, material ABS400 is possible to consider as isotropic material in this case.

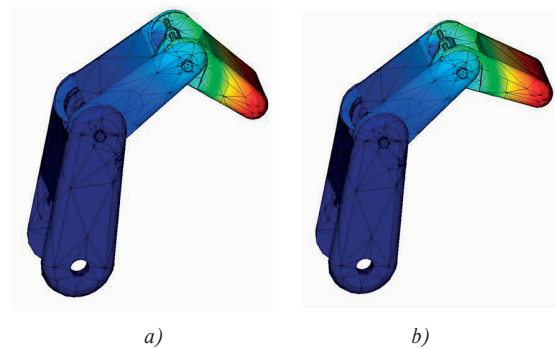


Fig. 7 Deformation of the finger model:  
 a) a model without deformation of distal link;  
 b) a deformed model.

## 5. Conclusions

The paper presents one of research trends in robotics that is partially solved at the Department of Automation and Production Systems and Department of Robotics. The article points out approaches that have been applied in: the innovation process of 3D model of three-finger bio-robotic gripper, creating the simulation environment for objects robotic grasping in real time and solving of problem of utilization contact analysis for seeking the optimal grip of finger links. The future tasks will be focused on improvement of the created simulation environment and optimization of the bio-robotic gripper design.

## References

- [1] PRATTICHIZZO, D., TRINKLE, J. C.: *Handbook of Robotics*, 28, Grasping, 2008, 671-700, Springer-Verlag Berlin Heidelberg. ISBN: 978-3-540-23957-4.
- [2] KURIC, I.: New Methods and Trends in Product Development and Process Planning, *Academic J. of Manufacturing Engineering. Editura Politehnica - Scientific Papers*, vol. 9, No. 1, 2011, 83-88, Cluj-Napoca. ISSN 1583-7904.

- [3] NAGY, S., R., LOBONTIU, M., KURIC, I., PETROVAN, A.: Innovative Development of One-Off and Small Series Products, *Applied mechanics and Materials*, vol. 371, 2013, 852-856. ISSN: 1662-7482.
- [4] LITVAJ, I., PONISCIAKOVA, O., STANCEKOVA, D., DRBUL, M.: *Knowledge Processes and their Implementation in Small Transport Companies*, 17<sup>th</sup> Intern. Conference on Transport Means 2013, Kaunas, October 2013, Code 102486, 153-156, ISSN: 1822-296X.
- [5] SKARUPA, J., MOSTYN, V.: *Methods and Means of Industrial and Service Robots Designing, 1<sup>st</sup> ed. (in Czech)*, Viena: Kosice 2002. 190 p., ISBN 80-88922-55-0.
- [6] TRIZ - IPA Slovakia - IPA Magazin - *Creation and solution of innovative tasks. (in Slovak)*: [cit. 2014-03-14], [online] <http://www.ipaslovakia.sk/sk/ipa-slovník/triz-tvorba-a-riesenie-inovacnych-zadani>.
- [7] CUBONOVA, N.: *Utilization of CAD/CAM System Pro/Engineer in Mechanical Engineering Industry*. Proc. of 15<sup>th</sup> intern. conference on manufacturing systems - ICMaS. Bucharest: Editura Academiei Romane, 2006, 445-448. ISSN 1842-3183.
- [8] <http://www.triz40.com/>
- [9] KUMICAKOVA, D., GORSKI, F., MILECKI, A., GRAJEWSKI, D.: Utilization of Advanced Simulation Methods for Solving of Assembly Processes Automation Partial Tasks. *Manufacturing Technology: J. for Science, Research and Production*, vol. 13, No. 4, 2013, 478-485. ISSN 1213-2489.
- [10] JAKUBCIK, M., KUMICAKOVA, D.: Computer Aided Design of Unconventional Robotic Gripper. *Intern. J. of Mechanics and Control*, vol. 13, No. 1, 2012, 29-34. ISSN 1590-8844.
- [11] KUMICAKOVA, D., JAKUBCIK, M.: *Advanced Methods for the Bio Robotic Gripper Grasping Ability Exploration*. Proc. of Intern. conference on innovative technologies IN-TECH 2013, Budapest, September 2013, 125-128, Rijeka: Faculty of Engineering University, ISBN 978-953-6326-88-4.
- [12] KUMICAKOVA, D., JAKUBCIK, M.: Specialised Robotic Hand Designing and Object Grasping Simulation. *Applied Mechanics and Materials*, vol. 282, 2013, 90-98. ISSN 1660-9336.
- [13] KONECNY, Z., KRYS, V.: *CAD III - Strength Analysis (in Czech)*, Multimedia educational text. VSB-TU Ostrava, 2007. 198 S. ISBN 978-80-248-1513-8.
- [14] SAPIETOVA, A., SAGA, M., NOVAK, P.: Multi-software Platform for Solving of Multibody Systems Synthesis, *Communication - Scientific Letters of the University of Zilina*, vol. 14, No. 3, 2012, Zilina, 43-48, ISSN 1335-4205.
- [15] KONECNY, Z.: *Designing of Service Robots Nods (in Czech)*. *Habilitation thesis*, VSB-TU Ostrava, 116 p., 2009.
- [16] NOVAKOVA-MARCINCINOVA, L., NOVAK-MARCINCIN, J., TOROK, J., BARNA, J.: Selected Experimental Tests of Materials used in Rapid Prototyping Area. *Manufacturing Technology: J. for Science, Research and Production*, vol. 13, No. 2, 2013, 220-226. ISSN 1213-2489.

Juraj Uricek - Tibor Galbavy - Vladimir Bulej - Peter Durec \*

## THE CALCULATION OF INVERSE KINEMATICS FOR 6DOF SERIAL ROBOT

*This article deals with the inverse kinematic model of robot devices which was implemented into the simulation software RoboSim designed at the Department of Automation and Production Systems – Faculty of Mechanical Engineering, University of Zilina. Concretely there is shown the technique how to develop the system of equations for serial kinematic mechanism with 6 degrees of freedom (DOFs). Further this software can be used as universal platform for simulation of mechanisms with serial, parallel as well as hybrid kinematic structure. This flexibility can be considered as a main advantage of the software RoboSim. Its specific feature is that there are used two different methods for calculation of inverse kinematics: heuristic and vector method as well. The versatility, openness and access to the source code create the predisposition for its deployment under the laboratory conditions for controlling of robotic devices developed in authors' workplace within the last few years.*

**Keywords:** Vector method, robot inverse kinematics, matrix equations.

### 1. Introduction

The main aim of this article is off-line programming of robotic systems as well as their computer simulation. It contains the basic information about the development process of universal software for simulation of automated workplaces equipped with one or more robots. This software is developed during last few years in authors' workplace and is called RoboSim. The article is focused on one specific part of its development, concretely on calculation of kinematic model for specified type of robots.

Kinematics is the study of possible motion and configuration of a mechanism and it is related to the geometry of solved system. To understand how the system will move in given circumstance requires knowledge of speed, forces, torque, inertia, energy, etc. We need to know the position and orientation of the last linkage or the end-effector in terms of robot joint variables. This method is called forward kinematics [1]. The basic idea is to find matrices corresponding to the motion of each joint. We can use rotation and transformation matrices for this task. Combining these matrices in the correct order will give us the basic transformation equations for the final linkage as a function of the joint variables [2]. The position and orientation of any point rigidly attached to the gripper can be found if the joint angles are known. Inverse kinematics tells us how to do it in a backward way. The angles for each joint are calculated separately which must be set when the given position and orientation of the gripper want to be reached.

This is one of the basic aims in robotics, since whenever we specify the motion of the robot's gripper we need to know the corresponding joint motion.

There are currently a number of programs used for simulation of robots and complete robotic workstations on the market. These programs are used for visualization, testing, debugging and repairing of programs for real robots. Debugging option is therefore very advantageous in pre-production stage because the standing time of robots or whole line can be reduced to a minimum. These programs also find their application in production planning and training of operators in the field of robotics.

Requirements for simulation programs are:

- simple operation,
- good quality results,
- low initial and total costs
- quality of interface (the ability to import / export existing data)
- correct selection of simulation tools,
- processing and evaluation of results,
- visualization and animation.

Simulation programs can be divided into two main categories - programs developed by manufacturers of industrial robots (ABB, Kuka, Fanuc, etc.) and systems developed by software producers.

\* Juraj Uricek, Tibor Galbavy, Vladimir Bulej, Peter Durec

Department of Automation and Production Systems, Faculty of Mechanical Engineering, University of Zilina, Slovakia

Email: juraj.uricek@fstroj.utc.sk

A specific feature of the software RoboSim is that there are used two different methods for calculation of inverse kinematics: heuristic and vector method as well. Vector method is applicable to only one type of kinematic structure (in our case just the serial robot with six degrees of freedom and rotation constraints) but it is very fast and accurate. On the other hand, heuristic method allows us to find a solution for more degrees of freedom than the number of known parameters. This method is especially useful when the robot moved fast from point to point when there is not needed very high precision of orientation (just high precision of position).

The versatility, openness and access to the source code created the predisposition for its deployment under the laboratory conditions for controlling of robotic devices developed in authors' workplace within the last few years. Some of them are based on parallel or hybrid kinematic structure and the simulation software can be used for creating and testing of control programs for these machines as well. Designed simulation software is based on modular principle what enable to modify the software according to our application (modules can be changed).

## 2. Basic transform equations within the robot workspace

The task is to formulate the robot with transform equations. These equations arise when the manipulated object as well as the robot is described with respect to the same reference system. In Fig. 1 is shown the automated cell based on robot which is described by *WRD-matrix* (world) within the global reference system. The robot end link is described by *UCS-matrix* and *T6-matrix* as well, while the end-effector is described by *GRP-matrix* (gripper) relatively to the robot's end link. All matrixes could be defined as dynamics, but only *T6-matrix* is controlled by inverse kinematics. At the opposite side in Fig. 1 is shown a manipulated object described by relative transformation *CONV-matrix* (conveyor), *OBJ-matrix* (object) and *PICK-matrix* (place where it is possible to catch the object).

Then, for the task "grasping the object by robot" we can mathematically formulate this equation [robot gripper coordinate system must be identified to the gripping (welding, touching, picking) position of a moveable object]:

$$WRD * UCS * T6 * GRP = WRD * CONV * OBJ * PICK \quad (1)$$

Then for the robot position we can write general equation:

$$T6 = CONV * OBJ * PICK * UCS^I * GRP^I \quad (2)$$

This is the basic procedure how it is possible to find *T6-matrix* for selected robot. Using inverse kinematics we can find unknown joint variables of the robot arm.

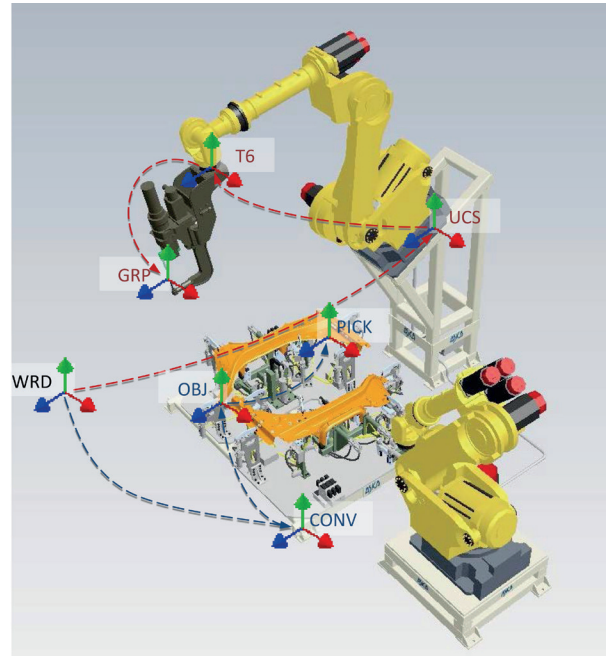


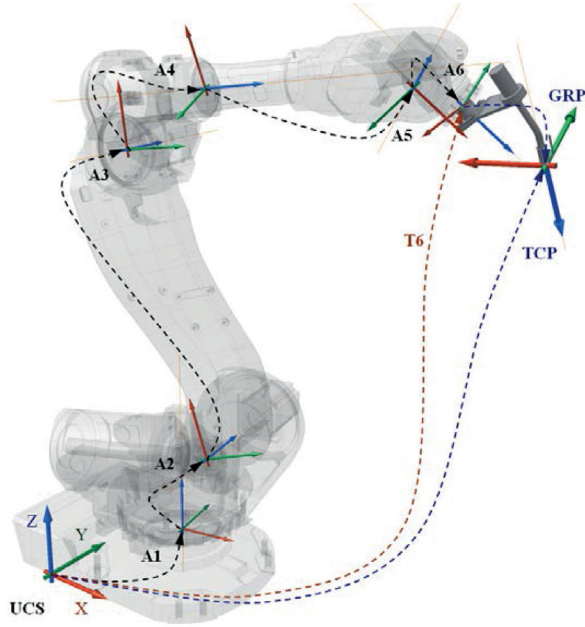
Fig. 1 Coordination system of working space and robots

## 3. General inverse kinematics calculation

Any robot can be taken as a group of links connected by joints. To each link of manipulator we can connect one coordinate system. Using homogeneous transformations, the relative position and orientation between the link coordinate matrixes can be described (Fig. 2). The *A-matrix* is a simple homogeneous transformation describing the relative displacement (translation and rotation) between the coordinate systems of two neighboring links. The *A1-matrix* describes the position and orientation (variable *U*) of the first link, *A2-matrix* the second link with respect to the first one. All *A-matrixes* can be composed of two other matrixes, *B-matrix* and *C-matrix*. The *B-matrix* represents translation and rotation to another link and the *C-matrix* represents only setup angle *U*. For a robot with six degrees of freedom, we can write:

$$T6 = A1 * A2 * A3 * A4 * A5 * A6 \quad (3)$$

$$A1=B1 * C1, \quad A2=B2 * C2 \quad \dots \quad A6=B6 * C6 \quad (4)$$



UCS - robot coordinate system, could be placed everywhere  
 WRD - basic world coordinate system (not shown)  
 TCP - position and orientation of end-effector relative to UCS  
 GRP - position and orientation of end-effector relative to T6  
 WRS - wrist center (orange axis)

Fig. 2 Kinematic structure and coordinate system of serial links

Then, we can write:

$$WRD * UCS * TCP = WRD * UCS * T6 * GRP \quad (5)$$

And after modification and substitution:

$$A1 * A2 * A3 * A4 * A5 * A6 = TCP * GRP^l \quad (6)$$

The  $T_6$ -matrix represents the desired position and orientation of the end-effector. The task is to find all values for joint variables inside  $A$ -matrixes. For standard manipulator it is supposed that the desired position and orientation of the final frame are given by:

$$T_6 = \begin{bmatrix} r_{11} & r_{12} & r_{13} & O_x \\ r_{21} & r_{22} & r_{23} & O_y \\ r_{31} & r_{32} & r_{33} & O_z \\ 0 & 0 & 0 & 1 \end{bmatrix} \quad (7)$$

For example, to find the corresponding joint variables  $U1, U2, U3, U4, U5$  and  $U6$  we must solve the following simultaneous set of nonlinear trigonometric equations:

$$r_{11} = c_1 [c_2 (c_4 c_5 c_6 - s_4 s_6) - s_2 s_5 c_6] - s_1 (s_4 c_5 c_6 + c_4 s_6) \quad (8)$$

$$r_{21} = s_1 [c_2 (c_4 c_5 c_6 - s_4 s_6) - s_2 s_5 c_6] - c_1 (s_4 c_5 c_6 + c_4 s_6) \quad (9)$$

$$r_{31} = -s_2 (c_4 c_5 c_6 - s_4 s_6) - c_2 s_5 s_6 \quad (10)$$

$$r_{12} = c_1 [-c_2 (c_4 c_5 c_6 + s_4 s_6) + s_2 s_5 c_6] - s_1 (-s_4 c_5 c_6 + c_4 s_6) \quad (11)$$

$$r_{22} = s_1 [-c_2 (c_4 c_5 c_6 + s_4 s_6) + s_2 s_5 c_6] - c_1 (-s_4 c_5 c_6 + c_4 s_6) \quad (12)$$

$$r_{32} = s_2 (c_4 c_5 c_6 + s_4 s_6) - c_2 s_5 s_6 \quad (13)$$

$$r_{13} = c_1 (c_2 c_4 s_5 + s_2 c_5) - s_1 s_4 s_5 \quad (14)$$

$$r_{23} = s_1 (c_2 c_4 s_5 + s_2 c_5) - c_1 s_4 s_5 \quad (15)$$

$$r_{33} = -s_2 c_4 s_5 + c_2 c_5 \quad (16)$$

$$O_x = c_1 s_2 d_3 - s_1 d_2 + d_6 (c_1 c_2 c_4 s_5 + c_1 c_5 s_2 - s_1 s_4 s_5) \quad (17)$$

$$O_y = s_1 s_2 d_3 - c_1 d_2 + d_6 (c_1 s_4 s_5 + c_2 c_4 s_1 s_5 - c_5 s_1 s_2) \quad (18)$$

$$O_z = c_2 d_3 + d_6 (c_2 c_5 - c_4 s_2 s_5) \quad (19)$$

These equations are too difficult to solve directly in a closed form. This is the case for most robot arms. Therefore, it is needed to develop efficient and systematic techniques that exploit the particular kinematic structure of the manipulator. Whereas the forward kinematics problem always has a unique solution that can be obtained simply by evaluating the forward equations, the inverse kinematics problem may or may not have a solution. Even if a solution exists, it may or may not be unique. Furthermore, because these forward kinematic equations are in general complicated nonlinear functions of the joint variables, the solutions may be difficult to obtain even when they exist.

Solving the inverse kinematics problem is most interesting in finding a closed form solution of the equations rather than a numerical solution.

Closed form solutions are preferable for two reasons:

- In certain applications, such as tracking a welding seam whose location is provided by a vision system, the inverse kinematic equations must be solved at a rapid rate, say every 20 milliseconds, and having closed form expressions rather than an iterative search is a practical necessity.

- The kinematic equations in general have multiple solutions. Having closed form solutions allows one to develop rules for choosing a particular solution among several.

The practical question whether the solution of inverse kinematics problem exists or not depends on engineering as well as mathematical considerations. For example, the motion of the revolute joints may be restricted to less than full 360 degrees of rotation so that not all mathematical solutions of the kinematic equations will correspond to physically realizable configurations of the manipulator.

#### 4. Kinematics decomposition

The position and orientation of a robot's end-effector are derived from the joint positions by means of a geometric model of the robot arm. For serial robots, the mapping from joint positions to end-effector pose is easy whereas the inverse mapping is more difficult [3]. Therefore, most industrial robots have special designs that reduce the complexity of the inverse mapping. The most popular designs involve a spherical wrist.

Although the general problem of inverse kinematics is quite difficult, it turns out that for manipulators having six joints (with the last three joints intersecting at a point) it is possible to decouple the inverse kinematics into two separate and simpler problems (Fig. 3). They are known as **inverse position kinematics**, and **inverse orientation kinematics**. For a six-DOFs manipulator with a spherical wrist, the inverse kinematics problem may be separated into two simpler problems, namely first finding the position of the intersection of the wrist axes, called the wrist center, and then finding the orientation of the wrist (matrix WRS).

$$WRS = \begin{bmatrix} R & P \\ 0 & 1 \end{bmatrix} \quad (20)$$

where  $P$  and  $R$  are the desired position and orientation of the tool frame, expressed with respect to the world coordinate system. For given  $P$  and  $R$  the inverse kinematics problem is to calculate parameters  $U1-U6$ . The important point of this assumption for the inverse kinematics is that the motion of the final three links about these axes will not change the position of WRS. The position of the wrist center is only a function of the first three joint variables ( $U1, U2$  and  $U3$ ). But orientation of the wrist center is a function of all joint variables ( $U1-U6$ ). This is the reason why it is preferable to find the position of wrist as first.

Next important step is defining coding system for position and orientation of end-effector. Here is the big variability. It is possible to use: a coding system based by *Euler angles, rotation Roll Pitch Yaw, Cardan angles* or many others [4]. The best way for robot programming is to use a coding system based on rotating of robot wrist center around axis  $Rz, Rx, Ry$  (exactly

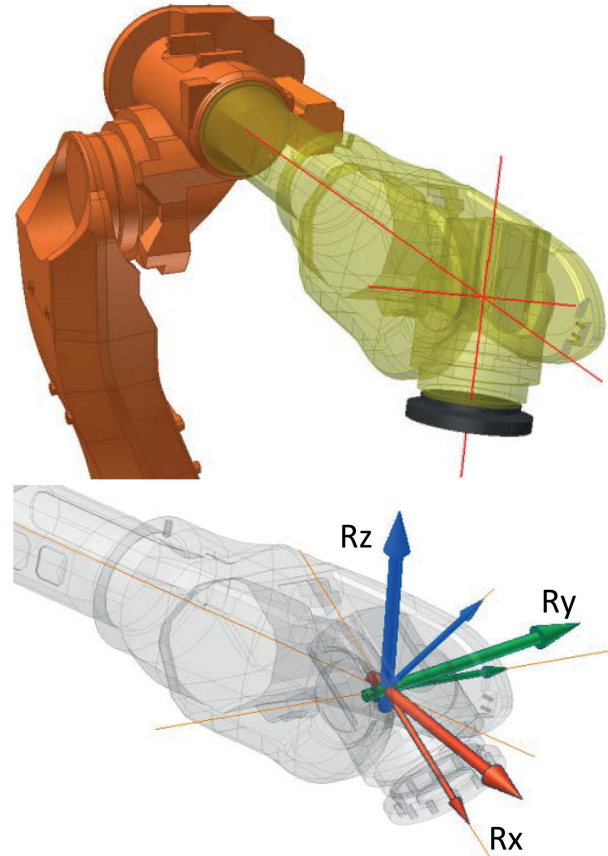


Fig. 3 The relative position of the wrist axis and coding system of wrist

in that order), where the direction of Z-axis is parallel with axis of the end-effector (direction of Y-axis goes left for right angle coding system). Finally, the coding system can be  $X, Y, Z, Rz, Rx, Ry$ , which is also user-friendly for robot programming. Coding system doesn't have any influence on calculation either for the controlling of robot. Coding system is important only for user comfort and for preventing errors and mistake.

#### 5. General equations for robot links

The first task for joint variables computing is finding position and orientation for the center point of wrist, then:

$$WRS = TCP * GRP^l * B6^l \quad (21)$$

Matrix of wrist has a form:

$$WRS = \begin{bmatrix} n_x & o_x & a_x & p_x \\ n_y & o_y & a_y & p_y \\ n_z & o_z & a_z & p_z \\ 0 & 0 & 0 & 1 \end{bmatrix} \quad (22)$$

Vector  $p$  is determined by the position of the wrist. Three unit vectors  $a, o, n$  describe the orientation of the gripper as follows:

- $a$  is the vector which defines the direction of closing up the wrist to the object
- $o$  vector called orientation, determines the orientation of the hand
- $n$  is the normal vector and is calculated as the vector product

Then, the position of wrist center is easy to find from  $WRS$  matrix:

$$P(p_x, p_y, p_z) \quad (23)$$

To find orientation it is good idea to put the position vector to zero because we know that the position doesn't have influence on orientation. Then:

$$WRS = R_z(U_z) \cdot R_y(U_y) \cdot R_x(U_x) \quad (24)$$

$$R_z(U_z)^{-1} \cdot WRS = R_y(U_y) \cdot R_x(U_x) \quad (25)$$

Having multiplied the matrix:

$$\begin{bmatrix} \cos U_z & -\sin U_z & 0 & 0 \\ \sin U_z & \cos U_z & 0 & 0 \\ 0 & 0 & 1 & 0 \\ 0 & 0 & 0 & 1 \end{bmatrix}^{-1} \cdot \begin{bmatrix} n_x & o_x & a_x & p_x \\ n_y & o_y & a_y & p_y \\ n_z & o_z & a_z & p_z \\ 0 & 0 & 0 & 1 \end{bmatrix} = \begin{bmatrix} 1 & 0 & 0 & 0 \\ 0 & \cos U_x & -\sin U_x & 0 \\ 0 & \sin U_x & \cos U_x & 0 \\ 0 & 0 & 0 & 1 \end{bmatrix} \cdot \begin{bmatrix} \cos U_y & 0 & \sin U_y & 0 \\ 0 & 1 & 0 & 0 \\ -\sin U_y & 0 & \cos U_y & 0 \\ 0 & 0 & 0 & 1 \end{bmatrix} \quad (26)$$

$$\begin{bmatrix} \cos U_z \cdot n_x + \sin U_z \cdot n_y & \cos U_z \cdot o_x + \sin U_z \cdot o_y \\ -\sin U_z \cdot n_x + \cos U_z \cdot n_y & -\sin U_z \cdot o_x + \cos U_z \cdot o_y \\ n_z & o_z \\ 0 & 0 \end{bmatrix} = \begin{bmatrix} \cos U_y \\ \sin U_x \cdot \sin U_y \\ -\cos U_x \cdot \sin U_y \\ 0 \end{bmatrix} \quad (27)$$

$$\begin{bmatrix} \cos U_z \cdot a_x + \sin U_z \cdot a_y & 0 \\ -\sin U_z \cdot a_x + \cos U_z \cdot a_y & 0 \\ a_z & 0 \\ 0 & 1 \end{bmatrix} = \begin{bmatrix} 0 & \sin U_y \\ \cos U_x & -\sin U_x \cdot \cos y \\ \sin U_x & \cos U_x \cdot \cos U_y \\ 0 & 0 & 1 \end{bmatrix}$$

Result of equation from matrix:

$$U_z = \arctg \frac{o_x}{o_y} \quad U_x = \arctg \frac{o_z}{-\sin U_z \cdot o_x + \cos U_z \cdot n_y}$$

$$U_y = \arctg \frac{\cos U_z \cdot a_x + \cos U_z \cdot a_y}{\cos U_z \cdot n_x + \cos U_z \cdot n_y} \quad (28)$$

It should be remembered that the calculated rotation angles are wrist angles ( $WRS$ -matrix) based on the original coordinate system ( $UCS$ -matrix). These angles will be needed later to calculate the real angles of the robot wrist  $U4, U5, U6$ . These angles are already affected by the position, not only the orientation of the wrist.

### 5.1 Inverse position

For the common kinematic arrangements, we can use a geometric approach to find the variables  $U1, U2, U3$  corresponding to the right center position of wrist. The complexity of the inverse kinematics increases with the number of nonzero link parameters in general. For most manipulators, many of the parameters of  $B$ -matrix and  $C$ -matrix are zero, or the angles included inside are  $0$  or  $\pm \pi/2$ , etc. In these cases especially a geometric approach is the simplest and most natural way.

For calculation of  $U1, U2, U3$  it is easy to define this angle from the robot triangle, known links length and known center of wrist  $P$  (Fig. 4).

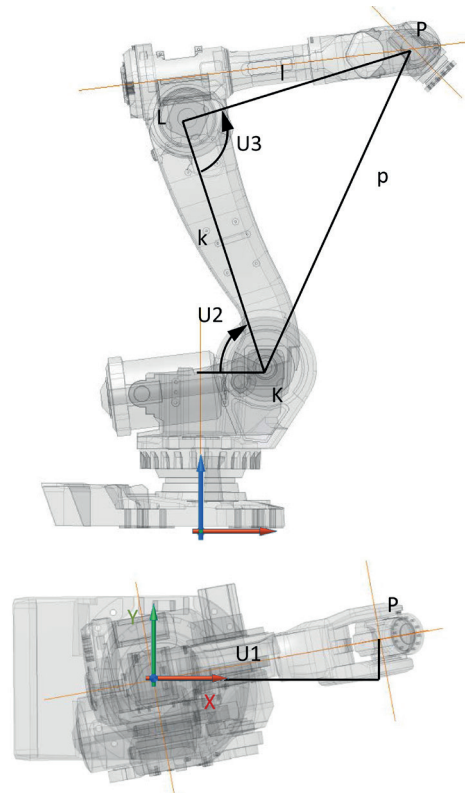


Fig. 4 Motion equation in a graphic form

The position of points is defined in the known matrix:

$$K[x,z] = B2[x,z] \quad (29)$$

$$P[x,z] = (WRS \cdot A1^{-1})[x,z] \quad (30)$$

Then, it is possible to write for rectangle lengths:

$$k = B3z \tag{31}$$

$$l = \sqrt{B4x^2 + (B4z + B5z)^2} \tag{32}$$

$$p = \sqrt{(Px - Kx)^2 + (Pz - Kz)^2} \tag{33}$$

For angle U3 and U2 from cosine theorem are valid:

$$U3 = \arccos\left(\frac{k^2 + l^2 - m^2}{2kl}\right) \tag{34}$$

$$U2 = 180 - \left(\arccos\left(\frac{k^2 - l^2 + m^2}{2km}\right)\right) - \left(\arcsin\frac{Pz - Kz}{m}\right) \tag{35}$$

And from top view for U1:

$$U1 = \arcsin\frac{Py}{Px} \tag{36}$$

### 5.2 Inverse orientation

The inverse orientation problem is now one of finding the values of the final three joint variables  $U4, U5, U6$  corresponding to a given orientation with respect to the dimensions (all *B-matrixes*) and set-up of frame (join  $U1, U2, U3$ ). For a spherical wrist, this can be interpreted as the problem of finding a set of  $Rz, Rx, Ry$  angles corresponding to a given rotation matrix  $R$ . Recall that equation shows that the rotation matrix obtained for the spherical wrist has the same form as the rotation matrix for the  $Rz, Rx, Ry$  transformation given in the previous chapter.

For last joint angles ( $U4, U5$  and  $U6$ ) it is necessary to define differential matrix *DIF* like a difference between angles at the end of *T5-matrix* and requested set up angles  $Rz, Rx, Ry$ :

$$DIF = WRS * T5^l$$

Also matrix *DIF* has a known form and it is possible to use the analogously mathematical principle like for finding angles from matrix *WRS*, then:

$$DIF = \begin{bmatrix} n_x & o_x & a_x & p_x \\ n_y & o_y & a_y & p_y \\ n_z & o_z & a_z & p_z \\ 0 & 0 & 0 & 1 \end{bmatrix} \tag{37}$$

And for finding angles  $U4, U5, U6$  are valid:

$$U4 = \arctg\frac{o_x}{o_y} \tag{38}$$

$$U5 = \arctg\frac{o_z}{-\sin U4 \cdot o_x + \cos U4 \cdot o_y}$$

$$U6 = \arctg\frac{\cos U4 \cdot a_x + \cos U4 \cdot a_y}{\cos U4 \cdot n_x + \cos U4 \cdot n_y}$$

Now we have all unknown variable  $U1-U6$  like a function of TCP coordinate ( $X, Y, Z, Rz, Rx, Ry$ ).

### 6. Conclusion

Industrial robots have a distinct set of capabilities that allows them to perform in industrial environments while also distinguishing them from other specialized robots. Manufacturing companies are seeking ways to ramp up production in a flexible way, as European economies start to recover from the recession [5]. One option is to use industrial robots, which are now more cost-effective both to purchase and to implement [6 and 7], thanks largely to programming software that is more engineer-friendly.

One of the basic tasks which need to be solved in robotics is so-called inverse kinematics. The vector method of inverse kinematics may not use Denavit-Hartenberg coordinates placement rule for links [8] but it is advantageous in terms of automated building transformation equations. This method is used most frequently for real time continuous path control due to easy programming as well as very fast calculation of results. It is, however, necessary to treat certain position programmatically links of mechanism when triangles and associated trigonometric equation, generate calculation errors.

Nowadays the investigation of system properties based on activity simulation in its virtual model belongs to the commonly used scientific methods for solving any technical problems. Simulation has substantial economic gains. Its usage can reduce pre-production stages. Thanks to that it can help us to examine several alternative solutions, find the optimal one as well as to avoid possible collisions.

The main aim of this article is original and special software *RoboSim* developed at authors' workplace which enables the simulation of automated manufacturing systems equipped with one or more robots. There is described more detailed one specific part of its development process - design of the mathematical model used for motion simulation of robots. Output equations are used for calculation of all joint coordinates which are necessary for motion control of robot devices. They make it possible to carry out collision detection between the robot and its environment in real time as well. Proposed software is based on a modular principle, which allows the system continuously to innovate and extend according to our requirements. The versatility, openness and access to the source code created the predisposition for its deployment under the laboratory conditions. The software development will continue in next period.

**References**

- [1] SKARUPA, J., MOSTYN, B.: *Theory of Industrial Robots (in Czech)*. Viena : Kosice, 2000, ISBN 80-88922-35-6, p. 146
- [2] LUNG-WEN, T: *Robot Analysis: The Mechanics of Serial and Parallel Manipulators*. Interscience, 1999, 520 p., ISBN 04-7132-593-7.
- [3] POPPEOVA, V., et al: *Design of Anti-collision System for Robotics*. Intern. Proc. of Computer Science and Information Technology: Mechanical Engineering, Robotics and Aerospace - ICMERA 2011, Singapore: IACSIT Press, editor: Jiang Xiaolan, vol. 4, 298-302, ISSN 2010-460X.
- [4] BULEJ, V., POPPEOVA, V., et al: *Actual State of Development in Field of Parallel Kinematic Structures and Mobile Robots at the Department of Automation and Production Systems in Zilina (in Slovak)*. Technological forum 2011, 93-101, Praha, ISBN 978-80-01-04852-8.
- [5] BULEJ, V., STOIANOVICI, G.-V., POPPEOVA, V.: *Material Flow Improvement in Automated Assembly Lines Using Lean Logistics*. Annals of DAAAM for 2011 & Proc. of 22<sup>nd</sup> intern. DAAAM Symposium, Vienna : DAAAM International, 2011, editor: B. Katalinic, vol. 22, No. 1, 253-254, ISSN 1726-9679.
- [6] KURIC, I.: *New Methods and Trends in Product Development and Process Planning*. *Academic J. of Manufacturing Engineering. Editura Politehnica: Scientific Papers*, vol. 9, No. 1, 2011, Cluj-Napoca, 83-88. ISSN 1583-7904
- [7] SAGA M., HANDRIK M., KOPAS P.: *Contribution to Computer Simulation of Induction Bending of Large Diameter Pipes*. *Meturgija (Metallurgy)*, vol. 49, No. 2, 2010, 498-502, ISSN 0543-5846.
- [8] SAPIETOVA, A., SAGA, M., NOVAK, P.: *Multi-software Platform for Solving of Multibody Systems Synthesis*. *Communications - Scientific Letters of the University of Zilina*, vol. 14, No. 3, 2012, Zilina, pp. 43-48, ISSN 1335-4205.

Andrej Czan - Michal Sajgalik - Anton Martikan - Jozef Mrazik \*

## OBSERVATION OF DYNAMIC PROCESSES IN CUTTING ZONE WHEN MACHINING NICKEL ALLOYS

*Process models of super alloys and included finite element modelling simulations are important for optimizing the metal cutting process, allowing industry to make parts faster, better, and at less cost. Innovative measurement methods of the process can be used to improve and verify the accuracy of these models. With these methods, there are many sources of error when using empirical or exact methods such as infrared radiation thermography to measure the temperature distribution of the tool, workpiece, and chip during metal cutting. Furthermore, metal cutting presents unique measurement challenges due to factors such as the high magnification required, high surface speeds and deformations, micro-blackbody effects, changing emissivity, and primary, secondary and tertiary deformations. As part of an ongoing effort to improve our understanding of the uncertainties associated with these measurement methods, multi-measurement sets of experiments were performed. One set explored how accurately the surface temperature of the cutting tool reflects the internal temperature. This was accomplished by measuring the temperature using a thermal camera in the cutting zone. The second set provided high-speed scanning of dynamic processes such as formation of elastic and plastic deformation. For this measurement, a high-speed scanning system was applied, with a macro conversion lens for monitoring micro-structural changes in deformation areas. The next set applied was necessary for recording dynamic processes by the implementation of a piezoelectric measurement device for monitoring cutting forces. The outputs from this multi-measuring system are the basis for verification of theoretical knowledge from this field and elimination of the uncertainties that arise with computational simulation systems.*

**Keywords:** Nickel alloys, cutting zone, multifunction measuring system, high-speed imaging, infrared thermography.

### 1. Introduction

Cutting process analytical modelling allows us to understand the basic principles of the metal cutting phenomena while reducing the dependence on empiricisms by avoiding a large amount of time-consuming experiments. What is more important, it enables the evaluation of the main process factors such as force of cutting and aids in its prediction, which is required for the optimal execution of the machining operation. Many analytical models have been developed to date which can determine the relations between the variables involved in the cutting process. It is generally accepted that the cutting process in the course of metal machining is restricted to the area in front of the tool cutting edge due to intensive local shear deformation of the machined material [1 and 2].

Most of the current analytical models describe the cutting process as a simple two-dimensional model named orthogonal cutting. However, most cutting operations are actually three-dimensional and can be properly described using an oblique cutting model where the cutting edge is inclined at an angle of obliquity,  $\lambda$ , consistent with the primary motion course of the

workpiece. Nevertheless, the simplified orthogonal model is generally used as a good demonstration of the oblique model. Figure 1 illustrates the orthogonal and oblique cutting models. In Fig. 1c, the workpiece, initially moving at speed  $v$ , goes through a plastic shearing strain and that leads to a chip streaming at speed  $v_c$  after passing a certain shear area exemplified by the shear plane AB. Due to its importance as a measure of the energy efficiency of the cutting process, the shear plane orientation,  $\phi$ , is essential to analytical models for the development of the cutting process [3 and 4]. In addition to the stress at the cutting area, the orientation of the shear plane affects the kinematics of the machining process too. Merchant [5] designed the most simple and widely used model to determine the shear plane angle. He constituted a mathematical concept for describing force relationships in the cutting process.

\* Andrej Czan, Michal Sajgalik, Anton Martikan, Jozef Mrazik

Department of Machining and Manufacturing Technology, Faculty of Mechanical Engineering, University of Zilina, Slovakia  
E-mail: andrej.czan@fstroj.uniza.sk

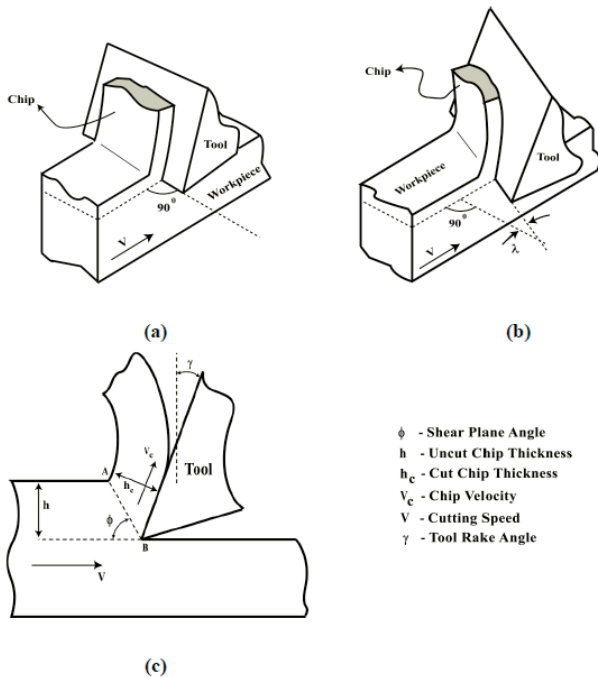


Fig. 1 a) Orthogonal cutting model; b) Oblique cutting model; c) General 2D representation of the cutting process with the variables of the cutting process [6]

Another premise of Merchant's force of cutting model is that the whole shearing action is restricted to a single plane of deformation. Lee and Shaffer [7] chose another approach and modelled the cutting process based on the plasticity theory. Lee and Shaffer's model expects that plastic deformation spreads over the defined shear zone represented by  $\Delta ABC$ . There is uniform stress presumed within the shear zone without work hardening effects. The complete shearing action is expected to occur along parallel lines of slip within the shear zone. Lee and Shaffer's model also presumes that the maximum shear stress is orientated in the same direction as the shear plane AC.

Zorev [8] pointed out incongruities of both the single shear plane and homogeneous stress slip-line theoretical models. He concluded that both models are limited in their premises; the slip-line model does not consider the real aspect of work hardening (and thus no stress gradient) during machining, while the single shear plane model ignores the enormous velocity deceleration of the work material from speed  $v$  to speed  $v_c$ . Zorev designed a shear plane model shown in Fig. 2 a) which describes the shear zone by a series of distinct shear planes, each defined by continuously varying shear stress values and velocity gradients. A simplified version of this model is shown in Fig. 2 b) and presents the shear zone as series of straight shear planes each with a different shear angle.

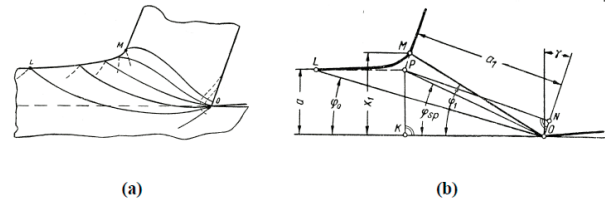


Fig. 2 a) Zorev's curved slip line model, b) The simplified version of the curved slip line model (Zorev, 1966)

Palmer and Oxley [9] experimentally studied the cutting process using a cinematography technique. Their results validated the multi-shear plane theory. They also concluded that tool-chip contact occurs some distance away from the tool tip, resulting in a kinematic dead zone at the tool tip. It was incorrectly assumed that no further plastic deformation occurs as the chip contacts the tool face and the secondary deformation observed is larger due to elastic chip flattening at this point. As proven conclusively from the later experimental work of Wallace and Boothroyd [6], the chip continues to undergo plastic deformation via shear upon contact with the tool rake face. A similar theory was included in Zorev's [8] work on predicting the shear zone area.

Thus, two major deformation zones called the Primary Deformation Zone (PDZ) and Secondary Deformation Zone (SDZ) can be identified in the metal cutting process. The second occurs because of shear due to the contact friction conditions between the chip and the tool rake face. Based on experimental observations, Roth and Oxley [10] developed a slip-line field model using velocity-dependent material flow lines that definitively identify the PDZ and SDZ. Based on the latter set of slip-line field models, the orthogonal cutting process can be presented as shown in Fig. 3. Depending on the subject matter under consideration, both single shear plane models and slip-line models have been used alternatively by researchers to study the cutting process [11]. Aside from the seminal work already mentioned, several excellent analytical models characterizing cutting mechanics are available. A list of analytical models is presented by Shaw [3] and will not be mentioned here for brevity.

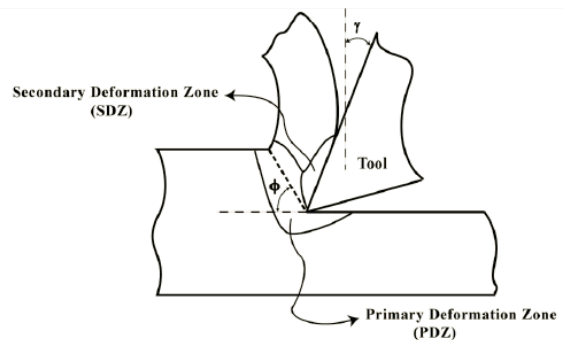


Fig. 3 Orthogonal schema showing primary and secondary deformation zones

## 2. Multifunction measuring system

The modelling system FEM is an important tool for rationalization of the metal cutting process, allowing industry to make parts faster, better, and at less cost but mainly ensuring the functional characteristics [12 and 13]. Innovative measurement methods of the process using thermal systems, high-speed scanning of dynamic processes and influence can be used to improve and verify the accuracy of these models. Four goals of manufacturing-related research at the Department of Machining and Manufacturing are: to develop and improve measurement techniques, to develop an understanding of the uncertainties involved with performing such measurements, to compare models of machining with thermal and visible spectrum images to verify the models, and to share this understanding with the machining community [14 and 15].

The formation of individual deformation zones is shown in Fig. 4, which shows a schematic of a typical image of an orthogonal cutting process. The relative motion between a cutting tool and a workpiece causes material to be removed from the workpiece. This removed material is referred to as a formation chip. Most of the deformation of the workpiece material occurs within a thin area called the shear zone [16 and 17].

Two of the many types of chips are called continuous and segmented. A continuous chip is a long ribbon of relatively uniformly deformed material. By contrast, a segmented chip has alternating zones of low and high shear strain. A zone of low strain in a segmented chip is called a segment. The zones of high strain between the segments are mechanically weak, so the long ribbons of material tend to break into short pieces [18]. These short pieces are more manageable than a continuous chip. Even when segmented chips do not break completely, there is generally a partial gap between the segments. The shear zone is somewhat stationary when continuous chips are formed, but often travels along with the chips when the chips are segmented. We will call the area surrounding the shear zone the face of the chip. The shear zone has a higher temperature than the face. For segmented chips, the shear zone generally also has a higher emissivity than the face [19 and 20].

The system used for measuring and observation processes in the cutting zone consists of a high-speed imaging camcorder, thermo-vision system and dynamometer for measurement of the cutting forces. Besides these sub-devices, there is a laboratory cold light for lighting the studied area and a computer for synchronizing all the measured data. This multi-axis measuring system (Fig. 4) was designed for the universal lathe SUI-40, but the construction of the stand guarantees some universality of the measuring system for other types of machines.

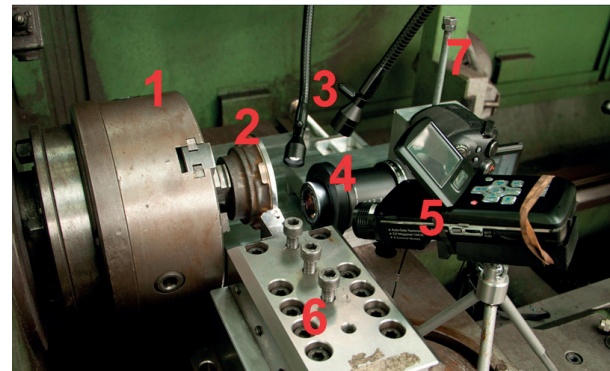


Fig. 4 Multifunction measuring system, 1 - chuck; 2 - sample; 3 - cold light; 4 - high-speed imaging camcorder, 5 - thermo-vision system; 6 - dynamometer with tool; 7 - macro-stand

Dynamical monitoring of the cutting process can be provided by the high-speed imaging camcorder, which ensures high-speed imaging in all experiments, with an imaging frequency of 1000fps. For detailed study, a super-macro lens Raynox MSN-202 with 20x magnification was used. Based on this optical system, we can capture an area of 4mm x 3mm.

The actual heat distribution can be monitored by the thermo-vision system which captures the thermal field in the cutting zone and heat distribution when machining. This compact camera allows us to measure temperatures up to 1200°C with a tolerance of  $\pm 2^\circ\text{C}$ . Special optics with deflected lens allows us to place the camera outside of the perpendicular on the scanned object [14].

The piezoelectric 3-component dynamometer can capture fast dynamic force relations measured as cutting forces with high-speed scanning up to  $1 \times 10^5 \text{ Hz}$ . All the applied measuring devices are integrated on a macro-stand (Fig. 5). For correct mounting and manipulation, the macro-stand was designed with mounting on the lathe support in order to ensure the simultaneous motion of the camera and cutting tool.

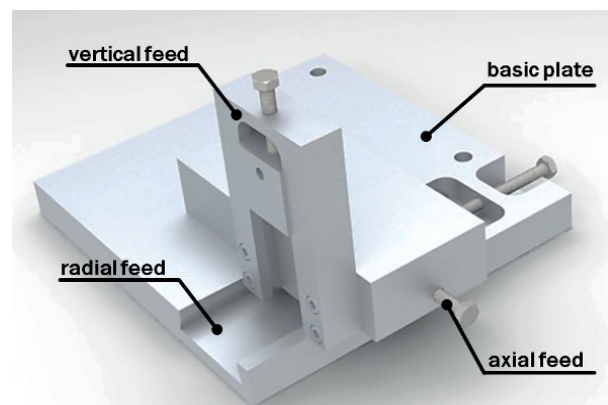


Fig. 5 Macro-stand with triaxial feed for mounting of high-speed imaging camcorder which provides simultaneous movement of the cutting tool and camcorder

Nickel alloys are popular materials due to their high heat and creep resistance. Due to their specific properties, they are used in the aerospace industry. Due to their mechanical and chemical properties, they are included among the hard-machined materials. Because this material is characterized as having a combination of strength, toughness and hardness, it is necessary to choose specific cutting conditions [21 and 22]. These were chosen from the real cutting conditions used in practice and they are shown in the caption of Fig. 6. All experiments were performed without coolant because this would prevent the scanning by the high-speed thermo-graphic camera [23 and 24].

To prevent the influence of bound-cutting by the cutting edge effect, the technology of free-cut turning was chosen. The free cutting approach ensures as much as possible of the area of the cutting zone and also ensures that the chips depart in the opposite direction of action from that of the cutting tool [25 and 26].

### 3. Evaluation of the experiments

Measurements of cutting forces were conducted in various cutting conditions. As we can see, the cutting force  $F_f$  increased with the increasing feed and, conversely, cutting force  $F_c$  decreased with increasing cutting speed (Fig. 6). It can be deduced from the measured data that the behaviour of nickel alloy Monel 400 is similar to the machining austenite of steel, but with a higher ratio of cutting forces considering the mechanical properties of this alloy.

From the monitoring of the dynamic course of the cutting forces, we can say that the cutting process is created by frequent accumulation of material as the built-up edge. The built-up edge has considerable influence on the cutting geometry, which causes the high dynamization of the cutting process.

Methods of examining and monitoring the cutting zone are developing with available technologies that are applicable for the monitoring and capturing of processes during the cutting

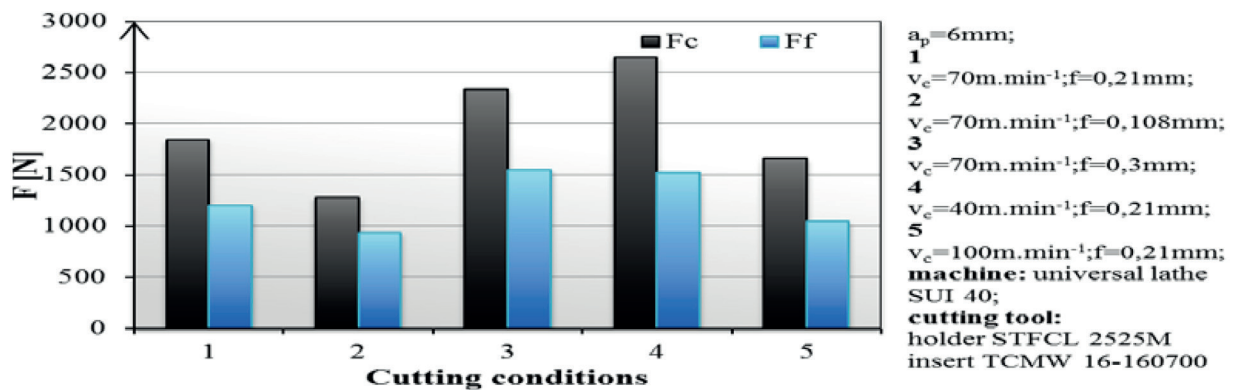


Fig. 6 Static values of cutting forces in various cutting conditions

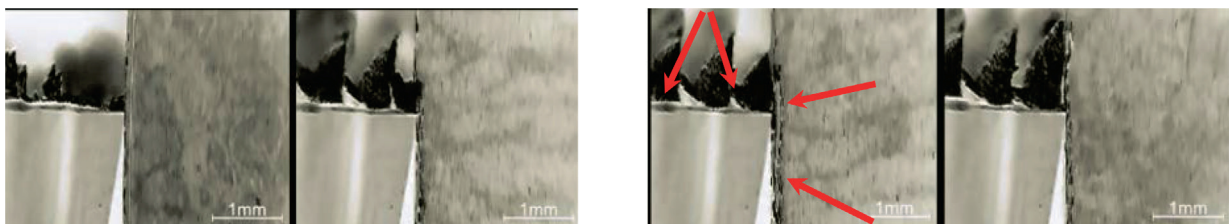


Fig. 7 Cutting process with continuous cut and minimal cutting speed  $v_c = 40 \text{ m}\cdot\text{min}^{-1}$  and feed  $0.21\text{mm}$ , rise of elementary chip and deformation areas of plastic and elastic deformation

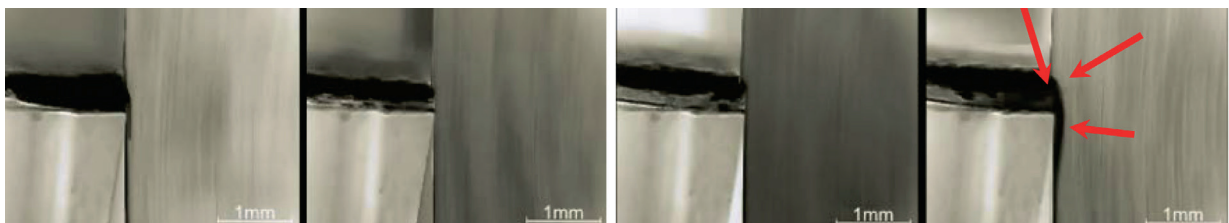


Fig. 8 Cutting process with continuous cut and maximal cutting speed  $v_c = 100 \text{ m}\cdot\text{min}^{-1}$  and feed  $0.21\text{mm}$ , formation of continuous ribbon chip and deformation areas of plastic and elastic deformation

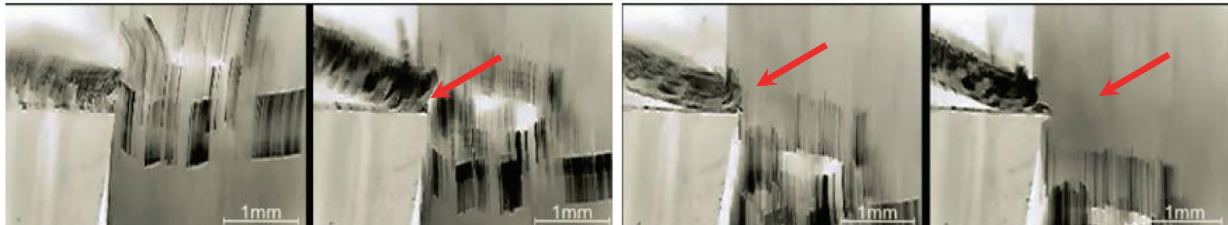


Fig. 9 Cutting process with continuous cut and maximal cutting speed  $v_c = 100 \text{ m}\cdot\text{min}^{-1}$  and feed  $0.21 \text{ mm}$ , formation of continuous ribbon chip and deformation areas of plastic and elastic deformation

process [27]. The most common possibilities include research of deformation processes based on finished changes after the end of the cutting process, such as examining metallographic samples from the cutting zone, acquired by the immediate interruption of the cutting process, etc. [28 and 29]. This research reached sufficient and complete conclusions about the processes in the cutting zone, but in a static concept after the finished process. Therefore, it was necessary to find new innovative technologies for idealized physico-mathematical models as the previous experimental outcomes provide information about finished processes only [30 and 31]. It is necessary to record deformation processes in the form of a high-speed video and image sequences from which the creation, shape of chips and deformations in the cutting zone when machining can be evaluated, and these can be made from monitoring the cutting zone by a high-speed imaging camcorder [32 and 33].

In the high-speed video records, it is possible to see the formation of deformation processes depending on the cutting conditions. At low cutting speeds, the formation of elementary chips occurs, giving rise to high dynamic shocks which load and cyclically fatigue the cutting edge up to destruction (Fig. 7).

At the higher cutting speeds, the formation of continuous ribbon chip occurs, which has a different character of influence on the cutting edge where thermal effects outweigh the dynamic shocks and cyclic loadings (Fig. 8).

In the last picture (of Fig. 8) of the measuring system, the primary and tertiary area and their influence on the machined surface can be seen. This surface has the effect of pooling the high stress loadings which act negatively on the functional properties of parts.

By application of the notch, there was simulation of discontinuous cut in which the monitoring of the cutting process before and after tensioning of the technological system was important. Cutting conditions were identical to the conditions of the continuous cut. In this experiment, there is formation of the same chip which has an identical character to that in the previous experiment. The cutting edge of the cutting tool is exposed to temperature mainly and dynamic shock and cyclic loadings (Fig. 9).

In each picture of the measuring system, relaxation of the technological system (tool - workpiece) can be seen with the transition to the tensioning of the technological system. These

images show the formation of deformation processes, and are thus a suitable basis for new simulation and mathematical models.

The data obtained from the individual processes during the experiments have a direct relationship with each other because they were obtained simultaneously in a single machining process. In this case they provide especially a waveform record of the cutting forces, the time course of development of the temperature field, and visual records of the deformation phenomena during the machining process. The measured data were then processed on a computer into video clips that show how individual phenomena are associated with each other in the cutting zone (Fig. 10).

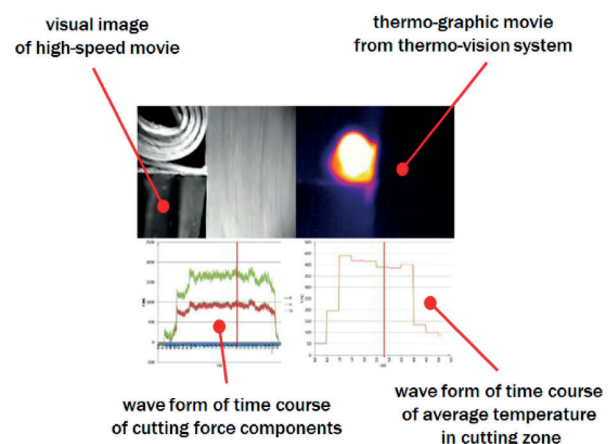
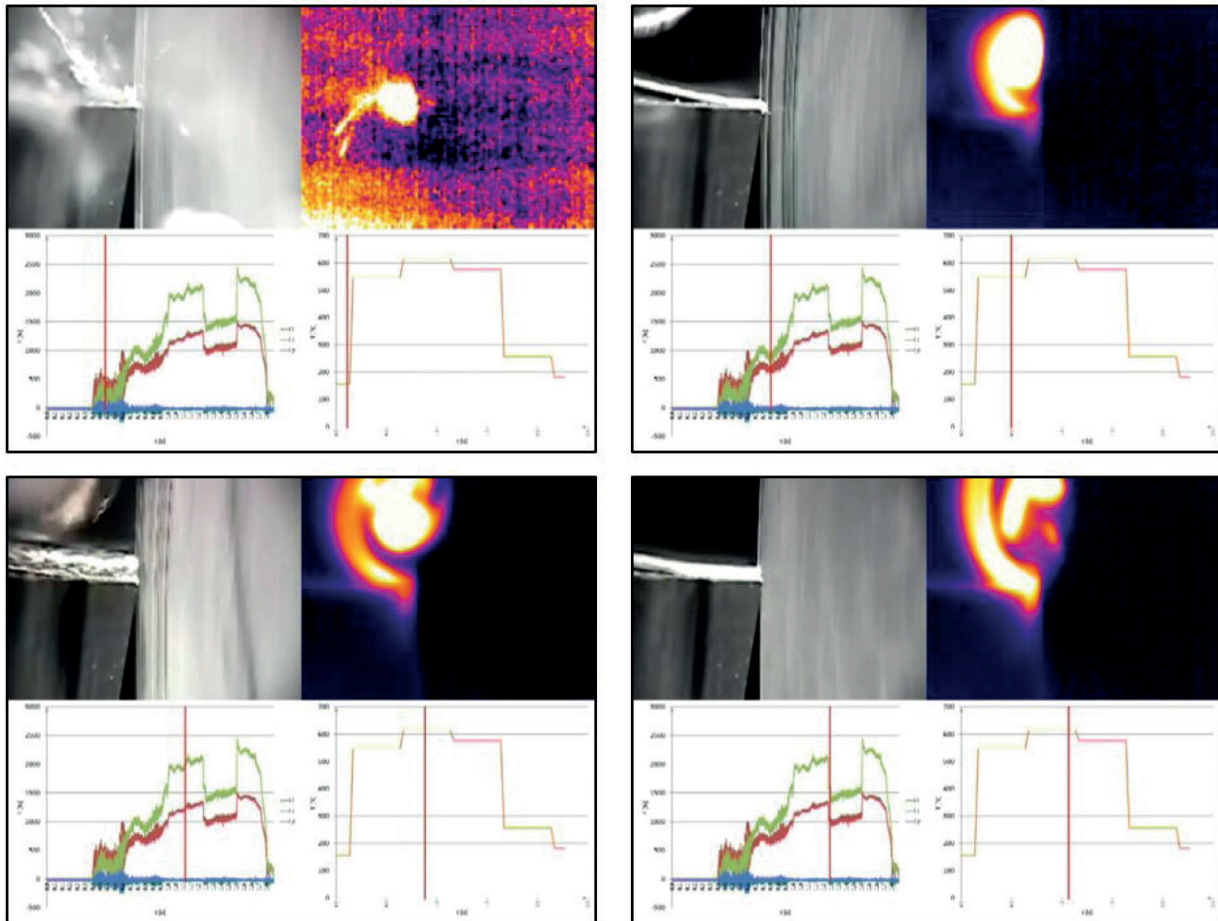


Fig. 10 Deployment of monitored processes in the video output of multifunctional measuring system [11]

Sequential frames from multi-parametric output are shown schematically: In the upper left corner is a visual record from the high-speed camera. In the top right corner is a thermo-graph or the thermo-graphic time course of the thermo-vision system (this is slowed down for the high-speed camera frame rate). Below the video output is the waveform of the components of the cutting force on the left and the graphic time course of the development of the average temperature in the cutting zone.

During the turning of the nickel alloy Monel 400, the phenomenon occurs that the primary contact of the tool and machined material is highly loaded with the pressure of transition from forming to the cutting process. In the first frame (Fig. 11), it is possible to see the formation of elementary chips after



cutting conditions: continuous cutting;  $v_c=70\text{m}\cdot\text{min}^{-1}$ ;  $f=0,21\text{mm}$ ;  $a_p=6\text{m}$ ; machine: univ. lathe SUI-40; cutting tool: holder STFCL 2525M, insert TCMW 16-160700

Fig. 11 Selected frames from video output of the multifunction measuring system

the intrusion of the cutting tool into the action, and after the stabilization of the cutting process, flat spiral chips were created.

The microstructure and mechanical properties of the materials caused a built-up edge to form almost throughout the cutting process. The components of cutting force during the formation of the built-up edge and its subsequent “holding on” to the front face of the cutting tool grew very high. After being picked, the cutting forces decreased sharply. With the new creation of a built-up edge, the whole process was repeated. This iterative cycle resulted in a specific shape of waveform of the components of the cutting force. In the third frame of Fig. 11 the built-up edge and increased components of the cutting force can be seen. The last frame of Fig. 11 captures the moment immediately after the built-up edge is picked.

#### 4. Conclusions

The multifunction measuring system designed for the monitoring of processes in the cutting zone allows observation of the deformations, temperature field, forming and shape of chip directly in the course of the cutting process, without interruption. We can evaluate the measured data in the specific dependences which exist between them.

The forces which act in the process change depending on the cutting conditions, structure and mechanical properties of the machined material.

The deformation processes which are in the cutting zone during machining take place at high speed. Under normal observation with the naked eye or by microscope only, these processes are not identifiable. Detailed observation is possible using the high-speed imaging camcorder. In this way, we can

observe not only the deformation processes but also the creation and formation of chips.

With the multifunction measuring system, we can better intensify the machining process, cutting conditions and so improve the product quality. We can also reduce the cost, because this system allows simultaneous measuring. Based on the observations of the deformation processes in the cutting zone, as

well as the creation and formation of chips, we can also optimize the shape of the cutting inserts.

#### Acknowledgements

This article was funded by the University of Zilina project OPVaV-2009/2.2/04-SORO number (26220220101) - "Intelligent system for nondestructive technologies on evaluation for the functional properties of components of X-ray diffraction".

#### References

- [1] CEP, R., OCENASOVA, L., NOVAKOVA, J., PETRKOVSKA, L., CZAN, A., STANCEKOVA, D.: *Interrupted Machining Tests of Ceramic Cutting Tools*, Proc. of TMT 2009, October 2009, Hammamet, vol. 13, No. 1, 733-736, ISSN 1840-4944.
- [2] NOVAKOVA, J., PETRKOVSKA, L., BRYCHTA, J., STANCEKOVA, D.: Influence of Cutting Parameters on Integrity Surface at High Speed Cutting. Transactions of the VSB - Technical University of Ostrava, *Mechanical Series*, vol. LV., No. 1, 2009, 203-209.
- [3] SHAW, M. C.: *Metal Cutting Principles*, 2<sup>nd</sup> Edition, 2005, Oxford University Press.
- [4] LUKOVICS, I., BILEK, O., HOLEMY, S.: Application of Sintered Corundum by Manufacturing of Tools (in Czech), *Strojirenska technologie*, vol. XV, No. 3, 2010, 27-34, ISSN 1211-4162.
- [5] MERCHANT, M. E.: Basic Mechanics of the Metal Cutting Process, *J. of Applied Mechanics*, V11, 168-175, 1944.
- [6] BOOTHROYD, G., KNIGHT, W. A.: *Fundamentals of Machining and Machine Tools*, 3<sup>rd</sup> ed., CRC Press, 2006.
- [7] LEE, E. H., SHAFFER, B. W.: Theory of Plasticity Applied to a Problem of Machining, *J. of Applied Mechanics*, V18, 1951, 405-413.
- [8] ZOREV, N.N.: *Metal Cutting Mechanics*, Pergamon Press, 1966.
- [9] PALMER, W. B., OXLEY, P. L. B.: *Mechanics of Orthogonal Machining*, Proc. of the Institution of Mechanical Engineers, V173, No. 24, 623-654, 1959.
- [10] ROTH, R. N. AND OXLEY, P. L. B.: A Slip Line Field Analysis for Orthogonal Machining Based on Experimental Flow Fields, *J. of Mechanical Engineering Science*, V14, 1972, 85-97.
- [11] CEP, R., JANASEK A., PETRU J., CEPOVA L., CZAN A., VALICEK J.: Hard Machinable Machining of Cobalt-based Superalloy. *Manufacturing Technology XIII/13*, 2013, 226-231, UJEP : Usti n. Labem, ISSN 1213-2489.
- [12] SAPIETOVA, A., SAGA, M., NOVAK, P.: Multi-software Platform for Solving of Multibody Systems Synthesis, *Communications - Scientific Letters of the University of Zilina*, vol. 14, No. 3, 43-48, 2012, ISSN 1335-4205.
- [13] MOHYLA, P., TOMCIK, P., BENES, L., HLAVATY, I.: Effect of Post-welding Heat Treatment on Secondary Hardening of Welded Joints of Cr-Mo-v Steel. *Metal Science and Heat Treatment 53 (7-8)*, 2011, 374-378, ISSN: 0026-0673.
- [14] SAJGALIK, M., CZAN, A.: Studying of Processes in Cutting Zone by Non-destructive Methods, *Technological Engineering*, vol. 8, No. 2, University of Zilina, 2011.
- [15] ZMINDAK, M., RIECKY, D.: Meshless Modelling of Laminate Mindlin Plates under Dynamic Loads Synthesis, *Communications - Scientific Letters of the University of Zilina*, vol. 14, No. 3, 2012, 24-31, ISSN 1335-4205.
- [16] PANDA, A., DUPLAK, J., VOROBEL, T., JURKO, J., FABIAN, S.: Study of the Surface Material AISI 304 usable for Actuator after the Process of Turning, *Applied Mechanics and Materials*, vol. 460, 2014, 107-114, ISSN: 1660-9336.
- [17] CZAN, A., TILLOVA, E., SEMCER, J., PILC, J.: Surface and Subsurface Residual Stresses after Machining and their Analysis by x-ray Diffraction. *Communications - Scientific Letters of the University of Zilina*, vol. 15, No. 2, 2013, 69-76. ISSN 1335-4205
- [18] NAPRSTKOVA, N., HOLESOVSKY, F.: *Admeasurement of Grinding Wheel Loss at FPTM*. 24<sup>th</sup> Intern. Colloquium (Advanced manufacturing and repair technologies in vehicle industry), 159-164, 2007, ISBN 978-80-7194-962-6.
- [19] VASILKO, K., PILC, J.: New Technological Knowledge of the Rotary Turning Tool, *J. Manufacturing Technology*, vol. 13, No. 4, 571-575, December 2013, ISSN: 1213-2489.
- [20] MICHALIK, P., ZAJAC, J., HATALA, M.: Programming CNC Machines using Computer-aided Manufacturing Software, *Advanced Science Letters*, vol. 19, No. 2, 369-373, February 2013, ISSN: 19366612.
- [21] NESLUSAN, M., CZAN, A., ZURPEL, U.: Analysis of the Heat Distribution when Grinding of a VT 9 Titanium Alloy and its Relation to Residual Tresses, *Strojnicki vestnik - J. of Mechanical Engineering*, vol. 48, No. 10, 557-564, 2002, ISSN 0039-2480.
- [22] MRKVICA, I., JANOS, M., SYSEL, P.: *Contribution to Milling of Materials on Ni Base*. *Applied Mechanics and Materials*, 217-219, 2012, 2056-2059. ISSN: 1660-9336

- [23] ZEBALA, W., SLODKI, B., STRUZIKIEWICZ, G.: Productivity and Reliability Improvement in Turning Inconel 718 Alloy - Case study, *J. Eksploatacja i Niezawodność*, vol. 15, No. 4, 421-426, 2013, ISSN: 1507-2711.
- [24] WHITENTON, E.P., et al. in: *High-speed Dual Spectrum Imaging for the Measurement of Metal Cutting Temperatures*, Manufacturing Engineering Laboratory, NIST, Gaithersburg, 2010.
- [25] PILC, J., MICIETOVA, A., SALAJ, J., CILLIKOVA, M.: The Influence of the Selected Aspects in Planing Operations by using Auto-rotation Tool, *Transactions of Famena*, vol. 29, No. 2, 55-60, 2005, ISSN: 1333-1124.
- [26] CEP, R., KOURIL, K., MRKVICA, I., JANASEK, I., PROCHAZKA, J.: Tests of Kyocera Tools when Discontinuous Cutting Conditions (in Czech). *Strojirenska technologie*, vol. XV, No. 3, 51-58, 2010, ISSN 1211-4162.
- [27] LITVAJ, I., PONISCIAKOVA, O., STANCEKOVA, D., DRBUL, M.: *Knowledge Processes and their Implementation in Small Transport Companies*, 17<sup>th</sup> Intern. Conference Transport Means 2013, Kaunas, 153-156, October 2013, Code 102486, ISSN: 1822-296X
- [28] HOLESOVSKY, F., NAPRSTKOVA, N., NOVAK, M.: GICS for Grinding Process Optimization. *Manufacturing Technology*, XII/12, 22-26, 2012, UJEP: Usti n. Labem, ISSN 1213-2489.
- [29] CEP, R., JANASEK, A., CEPOVA, L., PETRU, J., HLAVATY, I., CAR, Z., HATALA, M.: Experimental Testing of Exchangeable Cutting Inserts Cutting Ability, *Tehnicky Vjesnik* 20 (1), 21-26, ISSN: 1330-3651.
- [30] WHITENTON, E. P., IVESTER, R., et al. in: *Simultaneous Visible and Thermal Imaging of Metals During Machining in Thermosense XXVII*, Orlando, Intern. Society for Optical Engineering, 2005.
- [31] VASILKO, K., PILC, J.: New Technological Knowledge of the Rotary Turning Tool, *J. Manufacturing Technology*, vol. 13, No. 4, 571-575, December 2013, ISSN: 1213-2489.
- [32] KRAJCOVIC, M., BULEJ, V., SAPIETOVA, A., KURIC, I.: Intelligent Manufacturing Systems in Concept of Digital Factory, *Communication - Scientific Letters of the University of Zilina*, No. 2, 2012, ISSN 1335-4205.
- [33] CUBONOVA, N.: Post-processing of CL Data in CAD/CAM system Edgcam using the Constructor of Postprocessors. *Manufacturing Technology: J. for Science, Research and Production*, vol. 13, No. 2, 2013, 158-164. ISSN 1213-2489.

Jerzy Jozwik - Ivan Kuric - Leszek Semotiuk \*

## LASER INTERFEROMETER DIAGNOSTICS OF CNC MACHINE TOOLS

*This paper presents diagnostics of selected CNC machine tools performed with XL80 laser interferometer with XC80 environmental compensation unit, temperature sensors and XR20-W rotary axis calibrator, working together with XL80 laser. Furthermore, the paper includes the methodology and results of conducted linear and angular error measurements, which supplied data for further analysis. The conclusion section presents results of conducted experiment. Measurement results were presented in figures, charts and tables.*

**Keywords:** Manufacturing, CNC machine tools, cutting process diagnostics, diagnostic systems of CNC machine tools, laser interferometer.

### 1. Introduction

Together with the increased demand for high precision of manufactured parts, machine tools and machine tool systems are required to maintain ever-increasing geometric, kinematic, technological and efficiency standards [1 - 5]. There is a particular demand for advancing efficiency together with machining precision and process simulation [6 - 11]. In order to achieve and maintain precision within several micrometres, control and compensation for a variety of errors is imperative; these include, *inter alia*, geometric, kinematic, thermal or cutting force induced errors [12 - 19]. For a 3-axis milling centre, for instance, 21 errors can be distinguished. Major errors that ought to be mentioned are as follows: deviations of the X-axis (position deviation in X-direction (XTX, EXX), straightness deviation in Y direction (XTY, EYX), straightness deviation in Z-direction (XTZ, EZX), roll around X-axis (XRX, EAX), pitch around Y-axis (XRY, EBX), yaw around Z-axis (XRZ, ECX)), deviations of the Y-axis (position deviation in Y-direction (YTY, EYY), straightness deviation in X-direction (YTX, EXY), straightness deviation in Z-direction (YTZ, EZY), roll around Y-axis (YRY, EBY), pitch around X-axis (YRX, EAY), yaw around Z-axis (YRZ, ECY)), deviations of the Z-axis (position deviation in Z-direction (ZTZ, EZZ), straightness deviation in X-direction (ZTX, EXZ), straightness deviation in Y-direction (ZTY, EYZ), roll around Z-axis (ZRZ, ECZ), pitch around X-axis (ZRX, EAZ), yaw around Y-axis (ZRY, EBZ)) and squareness errors (squareness error between X and Y axes (XWY), squareness error between X and Z axes (XWZ), squareness error between Y and Z axes (YWZ)). Although some of these can be significantly reduced, they cannot be completely

eliminated [20 - 23]. Numerically controlled machines (machine tools or robots) respond to motions programmed in the machine coordinate system [24]. The precision of these programmed operations depends on the precision of numerically controlled motions, precise geometry of their positioning and the influence of a technological process realised at a given moment. Above all, supervision over the realisation of programmed motions is required.

Machine tool accuracy measurements are normalised and described by ISO-230. The norm sets requirements and specifications regarding geometric accuracy of machine tools for machining metal and wood, together with requirements and specifications regarding measurements and measuring equipment. Polish Norms describe both general methodology of machine tool measurements and specific methods for error motion determination and limiting conditions associated with tolerances [25].

### 2. Research methodology

The test subjects were three CNC machine tools (Fig. 1), namely, DMU 65 MonoBlock vertical 5-axis machining centre (Fig. 1a), DMC 635 V ECOLINE vertical machining centre (Fig. 1b) and CTX 310 ECOLINE numerical control turning centre (Fig. 1c). The assessment determines positioning error motions in the X, Y, Z axis, particularly, bidirectional accuracy of positioning of a numerically controlled axis A, unidirectional accuracy of positioning of an axis (forward A↑; reverse A↓), unidirectional repeatability of positioning

\* <sup>1</sup>Jerzy Jozwik, <sup>2</sup>Ivan Kuric, <sup>1</sup>Leszek Semotiuk

<sup>1</sup>Department of Production Engineering, Mechanical Engineering Faculty, Lublin University of Technology, Poland

<sup>2</sup>Department of Automation and Production Systems, University of Zilina, Slovakia

E-mail: j.jozwik@pollub.pl



Fig. 1 Analysed machine tools: a) DMU 65 MonoBlock vertical 5-axis machining centre, b) DMC 635 V ECOLINE vertical machining centre, c) CTX 310 ECOLINE numerical control turning centre [26]

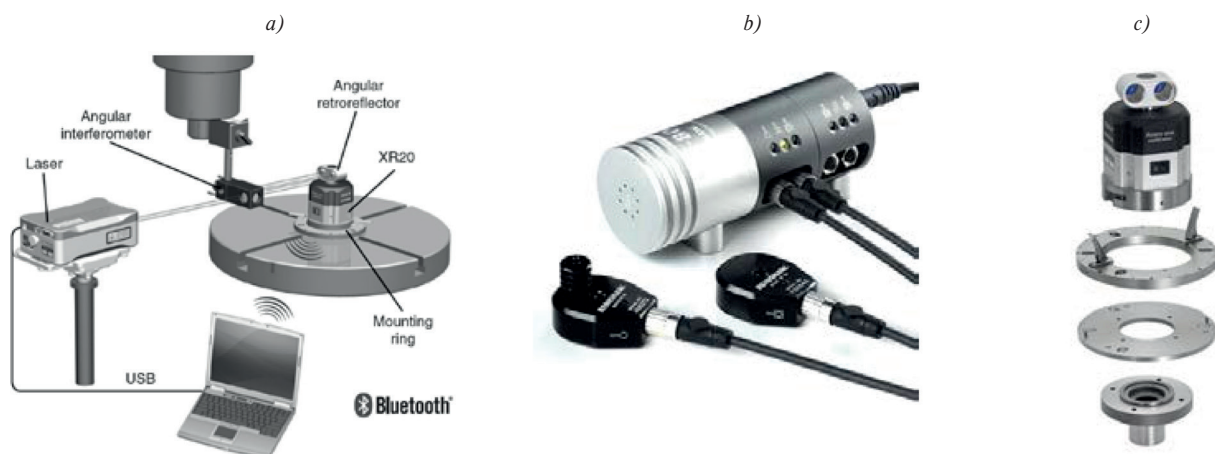


Fig. 2 Renishaw XL80 laser interferometer: a) rotary axis measurement kit, b) XC80 environmental compensation unit with temperature, c) XR20-W calibrator [27]

(forward  $R\uparrow$ ; reverse  $R\downarrow$ ) and reversal value of an axis B. The tolerances for the group of analysed machine tools are as follows:  $A = 22 \mu\text{m}$ ,  $A\uparrow = 16 \mu\text{m}$ ,  $A\downarrow = 16 \mu\text{m}$ ,  $R\uparrow = 6 \mu\text{m}$ ,  $R\downarrow = 6 \mu\text{m}$ ,  $B = 10 \mu\text{m}$ .

Figure 2 presents XL80 laser interferometer with XR20 calibrator and XC80 environmental compensation unit, allowing the measurement and compensation for linear and angular positioning errors.

Laser interferometer has become a worldwide standard and found application at practically all machine tool manufacturing plants. The setting time is relatively short and direct communication of laser software with the machine controller enables immediate measurement configuration and downloading of the data to a compensation table in the machine's controller.

Figure 3 shows measuring stands during setting and measuring of positioning error motion and positioning repeatability of analysed machine tools (DMC 635 V ECOLINE vertical machining centre (Fig. 3a), DMU 65 MonoBlock vertical 5-axis machining centre (Fig. 3b) and CTX 310 ECOLINE numerical control turning centre (Fig. 3c). XR20-W unit used with modern Renishaw XL80 interferometers enables measurements of angle

deviations of the rotary tables of 5-axis machine tools. As in the case of the linear axis, the measurement is notably fast with the accuracy higher than  $1''/\text{turn}$ .

Table 1 presents environmental parameter reading conditions for the DMC 635 V ECOLINE machining tool.

In addition, the instrument enables dynamic measurement (motion and speed as a function of time) and interpretation of the measurement results for various methodologies (Fourier transform). XR20-W calibrator provides time-efficient and uncomplicated wireless testing of CNC machines of various types (e.g. 5-axis centres or measuring machines). Moreover, XR20-W calibrator allows measuring of the positioning accuracy of rotary axes, with an accuracy of 1 arc second. XR20-W calibrator is equipped with a handle adapter – an adapter plate, as well as the mounting ring and the centration aid, together constituting a system applicable to a variety of machines and devices, whose configuration and measurement procedure are controlled with RotaryXL software.

DMC 635 V ecoline vertical machining centre measurement methodology comprised X, Y, Z axes linear positioning measurements. The measuring stand consisted of a DMC

Compensation unit readings describing environmental conditions for DMC 635 V ECOLINE vertical machining centre measurements Table 1

Dane	Axis X		Axis Y		Axis Z	
	Start	End	Start	End	Start	End
Air temperature [°C]	22.99	22.94	23.09	22.86	23.20	22.97
Air pressure [hPa]	1004.80	1004.80	1004.40	1004.40	1004.20	1004.00
Relative humidity [%]	31.19	31.96	32.01	32.34	31.93	32.00
Material temperature [°C]	21.11	21.14	21.20	21.22	21.34	21.32
Environmental parameter	316406.88 $\times 10^{-6}$	316406.75 $\times 10^{-6}$	316406.63 $\times 10^{-6}$	316406.48 $\times 10^{-6}$	316406.16 $\times 10^{-6}$	316406.16 $\times 10^{-6}$

635 V ecoline vertical machining centre, a laser head, a laser interferometer, linear retroreflectors, compensation unit and a computer of specific hardware requirements for the use of XL80 laser (Fig. 3a). Optics accessories were mounted directly on the spindle and the tool table and synchronised with XL80 laser. The measurement consisted in table motion measurement in the following steps: for X-axis by 50 mm (in the range of 0÷600 mm), for Y-axis by 20 mm (in the range of 0÷460 mm) and for Z-axis by 20 mm (in the range of 0÷440 mm) as well as in registering the results at a given measuring point. The measurement was repeated three times for each axis. All measurements were conducted with no load, following proper preheating of the machine and at constant feedrate  $v_f=const$ .

DMU 65 MonoBlock vertical 5-axis machining centre measurements were carried out in workshop conditions, with the application of XL80 laser system with rotary axis calibrator XR20-W (Fig. 3b). The measurement methodology included angular positioning accuracy measurement. XR20-W rotary axis calibrator was mounted in the centre of the machine tool table and configured with XL80 system. The tests consisted in performing a 360° rotation of the table at 30° steps and returning to the starting position of 0°. The system was stopped for 3 seconds at each measuring point for measurement data collection. Each test was repeated three times.

CTX 310 ECOLINE numerical control turning centre measurements were conducted in workshop conditions with the use of XL80 laser system with rotary axis calibrator XR20-W. The measuring stands are presented in Fig. 3c. The methodology consisted of angular positioning of the machine tool measurement. Rotary axis calibrator was mounted in lathe chuck and synchronised with XL80 laser. The measurements procedure consisted in performing a 360° rotation of the lathe chuck at the steps of 20° and returning to the starting position of 0°. The measurement was stopped for 3 seconds at each measuring point for data collection and each procedure was repeated three times.

The process of calibration with XR20-W system is fully automated. XR20-W calibrator is supplied with servocontrolled battery drive, and data capture is synchronised with axis motion. It results in the whole process being automated with no operator intervention required during data capture. Renishaw laser system

is a non-contact reference measurement, characterised by high integrity, operated wirelessly and remotely from the tested axis. All measurements were conducted with no load and with prior preheating of the machine as per manufacturer instructions.

Linear axis measurements not exceeding 2000 mm should consist of minimum five measurements per metre. In set positions measurements are carried out with the adherence to a standard cycle procedure, *i.e.* at least twice in each direction, as per interferometer software specifications.

### 3. Research results and analysis

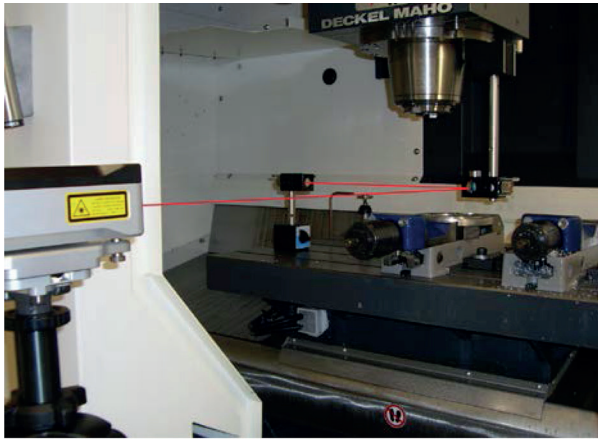
#### 3.1 DMC 635 v ECOLINE vertical machining centre technical condition assessment

Experimental tests provided data of linear positioning errors in X, Y, Z axes in the forward (↑) and reverse (↓) direction. Based on these results the following measurements were carried out: unidirectional and bidirectional accuracy of positioning of axis (A, A↑, A↓), unidirectional repeatability of positioning (forward R↑; reverse R↓) as well as reversal value of an axis (B).

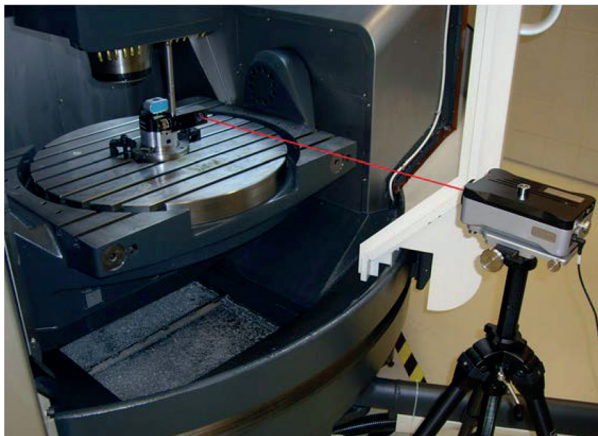
Marked on the horizontal axis there is machine table motion value, whereas on the vertical axis - error motion in micrometres. Figure 4 and its table present measurement results of X-axis. The collated data indicates that bidirectional and unidirectional accuracy of positioning of axis A↑ and A↓, as well as unidirectional repeatability of positioning R↑ and R↓ as well as reversal value of an axis B do not exceed tolerance standards as per the norm.

Figure 5 and incorporated table show linear error motions in the Y-axis. These results present bidirectional accuracy A of positioning of Y-axis, unidirectional accuracy of positioning of axis A↑ and A↓, as well as unidirectional repeatability of positioning R↑ and R↓ as well as reversal value of an axis B. It can be observed that error values increase with the increase of distance from the target and acquire maximum values at the distance of 460 mm. Similarly as in the case of X-axis, all determined parameters are within the tolerance.

a)



b)



c)

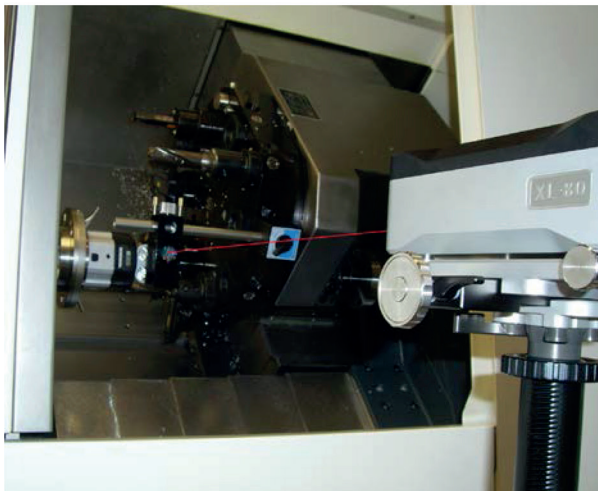


Fig. 3 Setting up and performing positioning error motion and repeatability of:  
 a) DMC 635 V ECOLINE vertical machining centre,  
 b) DMU 65 MonoBlock vertical 5-axis machining centre,  
 c) CTX 310 ECOLINE numerical control turning centre

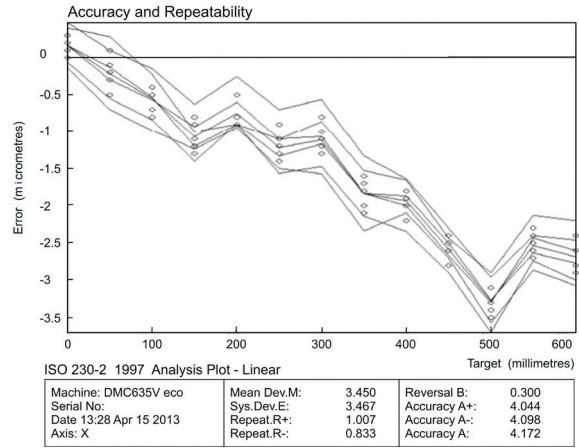


Fig. 4 Linear positioning error motion in the X-axis of DMC 635 V ecoline vertical machining centre

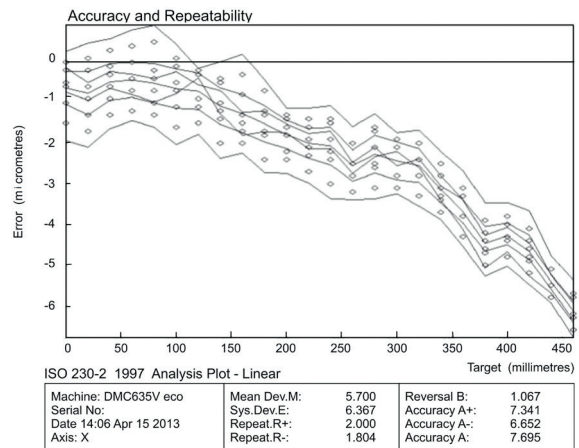


Fig. 5 Linear positioning error motion in the Y-axis of DMC 635 V ecoline vertical machining centre

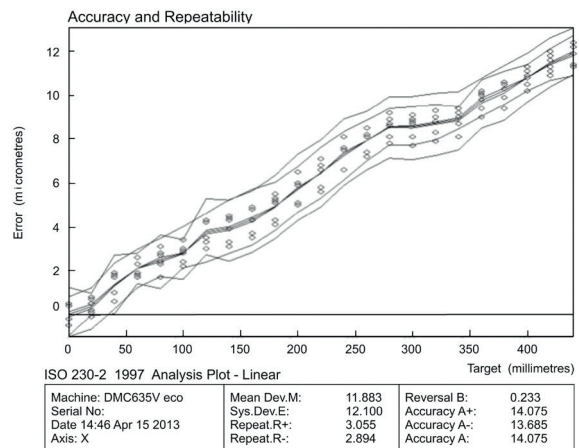


Fig. 6 Linear positioning error motion in the Z-axis of DMC 635 V ecoline vertical machining centre

Analogical results, collected in Fig. 6, were obtained in Z-axis measurements. In comparison with X and Y-axis, where maximum values amount to 6-8 $\mu$ m, the measured error motion values were doubled and within the range of 12-14 $\mu$ m. Nonetheless, all parameters (A, A $\uparrow$ , A $\downarrow$ , R $\uparrow$ , R $\downarrow$ , B) are within the limits of ISO-230 standard.

### 3.2 DMU 65 MonoBlock vertical 5-axis machining centre technical condition assessment

Figure 7 presents mean unidirectional accuracy of positioning of axis in the forward ( $\uparrow$ ) and reverse ( $\downarrow$ ) direction. The analysis of the diagram indicates that the highest error motion value is observed at the angle of 210°.

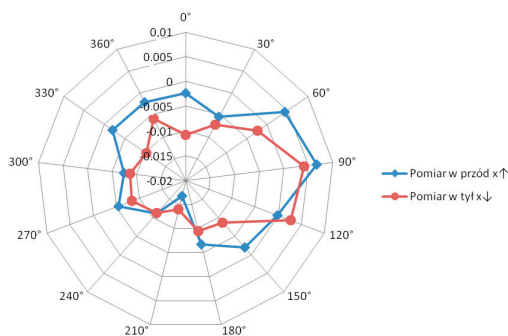


Fig. 7 Mean angular deviation of DMU 65 monoBLOCK

### 3.3 CTX 310 ECOLINE numerical control turning centre technical condition assessment

Figure 8 presents mean unidirectional accuracy of positioning of axis in the forward ( $\uparrow$ ) and reverse ( $\downarrow$ ) direction. The analysis of the diagram indicates that the highest error motion value is observed at the angle of 240°.

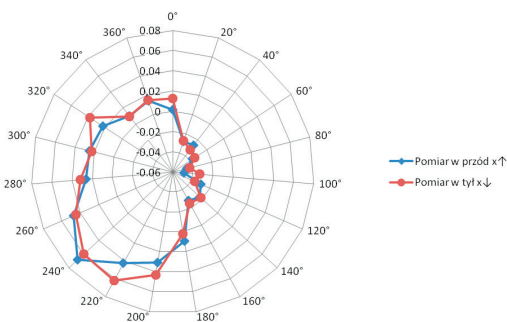


Fig. 8 Mean angular deviation of CTX 310 ECOLINE

Values of axis positioning accuracy (A, A $\uparrow$ , A $\downarrow$ , R $\uparrow$ , R $\downarrow$ , B) derived in tests will provide the basis for future model for error

prognosis, which will apply the methods of Artificial Intelligence. This requires, however, systematic diagnostic measurements with a view to creating geometric accuracy history of a machine tool, based on which such a model could be developed. It does, nonetheless, open the gate for downloading obtained results to the type series of machine tools in service. The goal set by the authors of this paper, *i.e.* creation of models in question is believed to produce notable benefits connected with practical application, which would allow a manufacturer to estimate the future condition of the machine and to take necessary measures to compensate and minimise appearing errors.

## 4. Conclusions

Conducted experimental tests and the analysis of their results lead to the formulation of the following conclusions:

1. Laser interferometer is at present the most precise and universal measuring instrument applied in CNC machine diagnostics. The scope of its applications includes conducting measurements of diverse geometric and kinematic parameters of a machine tool, which is directly reflected in the improvement of the general technical condition of machines through immediate error compensation. Among its most notable features, which must be mentioned is its streamlined operation procedures and intuitive software, generating reports according to current norms.
2. Conducted diagnostics of the analysed machine tool systems proved that none of the determined parameters (A, A $\uparrow$ , A $\downarrow$ , R $\uparrow$ , R $\downarrow$ , B) exceeds the tolerance values described in the Polish Norm PN-ISO-230. It could be, therefore, stated that the machine tool centres in questions are in good technical condition. Nevertheless, frequent systematic diagnostic testing and required regulation of, *e.g.* controllers or drives is of utmost importance.
3. Maximum linear positioning error motion values in the case of DMC 635 V ECOLINE vertical machining centre were observed in extreme positions in each axis of the machine tool. A recommended method for prevention of machining errors which result from the local character of such an error is to avoid machining in the identified workspace of the machine tool.
4. The change of laser optics is obligatory in error motions of axis testing when axis is changed. This solution is, however, inefficient and time-consuming. Furthermore, it leads to the situation when all measurements must be repeatedly conducted for each particular axis, bearing in mind that each laser or optics position change necessitates calibration of the whole system.
5. The selection of a method and a measuring tool should be contingent on: accuracy requirements, the cost of the device, time required for testing and accessibility of the device.

## References

- [1] KURIC, I.: New Methods and Trends in Product Development and Process Planning. *Academic J. of Manufacturing Engineering*. Editura Politehnica: Scientific Papers, vol. 9, No. 1, 2011, 83-88, Cluj-Napoca. ISSN 1583-7904
- [2] CZAN, A., TILLOVA, E., SEMCER, J., PILC, J.: Surface and Subsurface Residual Stresses After Machining and their Analysis by x-ray Diffraction, *Communications - Scientific Letters of the University of Zilina*, No. 2, 2013, 69-76. ISSN 1335-4205
- [3] DUGIN, A., POPOV, A.: Increasing the Accuracy of the Effect of Processing Materials and Cutting Tool Wear on the Ploughing Force Values. *Manufacturing Technology*, vol. 13, No. 2, 2013, 169-173. ISSN 1213-2489
- [4] STANCEKOVA, D., SEMCER, J., DERBAS, M., KURNAVA, T.: Methods of Measuring of Residual Stresses and Evaluation of Residual State of Functional Surfaces by x-ray Diffractometric Methods, *J. Manufacturing Technology*, vol. 13, No. 4, 2013, 547-552, ISSN: 1213-2489.
- [5] VARGA, G.: Effects of Technological Parameters on the Surface Texture of Burnished Surfaces, *Key Engineering Materials, Precision Machining VII*, vol. 581, 2014, 403-408. ISSN 1013-9826, doi:10.4028/www.scientific.net/KEM.581.403
- [6] KUMICAKOVA, D., GORSKI, F., MILECKI, A., GRAJEWSKI, D.: Utilization of Advanced Simulation Methods for Solving of Assembly Processes Automation Partial Tasks. *Manufacturing Technology: J. for Science, Research and Production*, vol. 13, No. 4, 2013, 478-485. ISSN 1213-2489
- [7] NAKAZAWA, H., ITO, K.: Measurement System of Contouring Accuracy on NC Machine Tools. *Bull. Japan Soc. Prec. Eng.*, 12, 4: 189, 1978. Publisher Elsevier
- [8] SAGA M., HANDRIK M., KOPAS P.: Contribution to Computer Simulation of Induction Bending of Large Diameter Pipes. *Metalurgija (Metallurgy) 2010*, vol. 49, No. 2, 498-502, ISSN 0543-5846
- [9] SAGA, M., ZMINDAK, M., DEKYS, V., SAPIETOVA, A., SEGLA, S.: *Selected Methods of Analysis and Synthesis of Mechanical Systems (in Slovak)*. VTS: University of Zilina, 2009, 360 p. ISBN 978-80-89276-17-2
- [10] SAGA, M.: *Development and Application of Selected Algorithms for Finite Element Optimization*. Eds. SAGA, M. et al.: *Advanced Methods in Computational and Experimental Mechanics*. Pearson Education Limited, London, United Kingdom, 2013, 57-112, ISBN 978-1-78434-069-8
- [11] SAPIETOVA, A., SAGA, M., NOVAK, P.: Multi-software Platform for Solving of Multibody Systems Synthesis. *Communication - Scientific Letters of the University of Zilina*, vol. 14, No. 3, 2012, Zilina, pp. 43- 48, ISSN 1335-4205
- [12] HONCZARENKO, J. KWASNIEWICZ, J.: New Measurement Systems for Verifying the Accuracy of CNC Machine Tools (in Polish), *Mechanik*, 12, 2008, 1012-1016. Publisher: Agenda Wydawnicza SIMP. Poland.
- [13] CHEN, J. S., KOU, T. W., CHIOU, S. H.: Geometric Error Calibration of Multi-axis Machines using an Auto-alignment Laser Interferometer. *J. of the Intern. Societies for Precision Engineering and Nanotechnology*, 23, 1999, 243-252. Publisher Elsevier
- [14] IWASAWA, K., IWAMA, A., MITSUI, K.: Development of a Measuring Method for Several Types of Programmed Tool Paths for NC Machine Tools using a Laser Displacement Interferometer and a Rotary Encoder, *Precision Engineering*, 28, 4, 2004, 399-408. Publisher Elsevier
- [15] JOZWIK, J., KURIC, I. SAGA, M., LONKWIC, P.: Diagnostics of CNC Machine Tools in Manufacturing Process with Laser Interferometer Technology. *Manufacturing Technology*, 2014 , vol. 14, No. 1, 23-30, ISSN 1213-2489
- [16] JOZWIK, J., KURIC, I.: *Non-contact Diagnostic Systems of CNC Machine Tools (in Polish)*. 14<sup>th</sup> Intern. Conference Automation in Production Planning and Manufacturing, Zilina, 2013
- [17] JOZWIK, J., LONKWIC, P., SAGA, M., KURIC, I.: R-Test Static Measurement of the 5-Axis CNC Machining Centre Rotary Axis Kinematic Centre Error, accepted to print in *Manufacturing Technology*, vol. 14, No. 2, 2014, ISSN 1213-2489
- [18] KRYNKE, M., SELEJDAK, J., BORKOWSKI, S.: Diagnosis and Damage of Bearings. *Manufacturing Technology*, vol. 12, No. 13, 2012, 140-144. ISSN 1213-2489
- [19] MAYER, K., PEXA, M., PAVLU, J.: Impact of Technical Diagnostics Interval on Machinery Maintenance. *Manufacturing Technology*, vol. 12, No. 12, 2012, 42-46. ISSN 1213-2489
- [20] SHIRINZADEH, B., TEOH, P. L.: Laser Interferometry-based Guidance Methodology for high Precision Positioning of Mechanisms and Robots. *Robotics and Computer-Integrated Manufacturing* 26, 2010, 74-82
- [21] CASTROA, H. F. F., BURDEKINB, M.: Calibration System Based on a Laser Interferometer for Kinematic Accuracy Assessment on Machine Tools. *Inter. J. of Machine Tools & Manufacture*, 46, 2006, 89-97. Publisher Elsevier
- [22] KURIC, I., DURICA, I., MADUDA, M.: Accuracy and Calibration of CNC Machines. *Scientific Bulletin, Series C, Fascicle: Mechanics, Tribology, Machine Manufacturing Technology*, vol. XXIII, 2010, 113-118
- [23] MAJDA, P.: The Influence of Geometric Errors Compensation of a CNC Machine Tool on the Accuracy of Movement with Circular Interpolation. *Advances in Manufacturing Science and Technology*, vol. 36, No. 2, 2012, 59-67. Publisher Elsevier

- [24] CUBONOVA, N.: Postprocessing of CL Data in CAD/CAM System Edgecam using the Constructor of Postprocessors, *Manufacturing Technology: J. for Science, Research and Production*, vol. 13, No. 2, 2013, 158-164. ISSN 1213-2489
- [25] SCHWENKE, H., KNAPP, W., HAITJEMA, H., WECKENMANN, A., SCHMITTE, R., DELBRESSINE, F.: Geometric Error Measurement and Compensation of Machines - An update. *CIRP Annals - Manufacturing Technology*, vol. 57, 2, 2008, 660-675. Publisher Elsevier
- [26] [http://en.dmgmori.com/\(z dn. 01/06/2014r.\)](http://en.dmgmori.com/(z dn. 01/06/2014r.))
- [27] [http://www.renishaw.pl/pl/1030.aspx \(z dn. 01/06/2014r.\)](http://www.renishaw.pl/pl/1030.aspx (z dn. 01/06/2014r.)).

Nadezda Cubonova - Ivan Kuric \*

---

## DATA STRUCTURES IMPLEMENTATION OF THE PROTOCOL STEP-NC AT CNC MACHINES PROGRAMMING

*Standard STEP-NC (ISO 14649) presents a new model for data transmission between CAD/CAM systems and CNC machines. This standard eliminates the shortcomings of the standard G-code and provides new possibilities in their management. At the Department of Automation and Production Systems, Faculty of Mechanical Engineering, University of Zilina in the framework of the research activities was solved a project for the implementation options of STEP-NC format by programming of CNC machines. This paper presents the results of research solutions which focused mainly on the analysis of standard STEP-NC, a methodology on the model data according to the standard STEP-NC using the EXPRESS language as well as the creation of software for the transformation of STEP-NC data - „TERMINAL STEP NC“. The software has been verified in the transmission of STEP-NC data to a particular CNC machine control system. Transfer of STEP-NC data applications gives the possibility of verifying the implementation of the new standard in older types of CNC machines.*

**Keywords:** Standard STEP-NC, data, computer numerical control, CAD/CAM system.

### 1. Introduction

Automation is now a key element of the production process and puts higher demands on the level of mechanization and control of production machines. Therefore, it has resulted in the continuous development of NC and CNC machines. At present, most of the CNC machines are programmed in a language standard ISO 6983 using G and M codes. This 30 years old standard can hardly today describe the high requirements for production of complex parts. Producers of CNC machines extend this standard using various additions and implementations thereby becoming this standard non-universal. Another disadvantage is the lack of portability of data, which prevents the full utilization of all new possibilities of CNC machines and CAD/CAM systems [1]. Therefore, at present, a new standard for transmitting data between CAD/CAM and CNC machine was developed, which eliminates the shortcomings of G-code and provides a new option in the control of CNC machines known as STEP-NC standard. It is the application of STEP methods (Standard for Exchange of Product model) for numerically controlled machines. Contrary to the G-code format, it provides a two-way flow of data between the CNC machine and the CAD/CAM system [2]. It is a new model for data transfer between CAD/CAM systems and CNC machines. The role of STEP-NC programming of CNC machines is the object-oriented way. STEP (ISO 10303) describes the data about the product for

the mechanical parts. Its main advantage is that it allows using the normalized data in all areas of production [3].

Protocol STEP-NC (*Standard for the Exchange of Product data compliant Numerical Control*) is currently being developed as a revolutionary method of controlling and programming of CNC machines. On the basis of this method of controlling and programming opportunities exist for the removing of low-level control of machine tools and allow an open and adaptable architecture for a new generation of control CNC machines. In spite of the short history of the Protocol STEP-NC significant research activities has already been done at the international level. Today, STEP-NC or ISO 14649 is under development in USA, Europe, and Asia. STEP-NC is being developed concurrently under two different subcommittees of *ISO Technical Committee 184* (Industrial automation systems and integration), as two different standards - *ISO 14649* (*Data model for computerized numerical controllers*) and *ISO 10303-238* (*Application interpreted model for computer numeric controllers*). Both of them can be represented in 10303-21 [4].

### 2. STEP-NC structure

The concept of STEP-NC use is simple. It enables a product model database to serve as direct input to a CNC machine tool. No separate files of tool paths. No G&M codes. No

---

\* Nadezda Cubonova, Ivan Kuric

Department of Automation and Production Systems, Faculty of Mechanical Engineering University of Zilina, Slovakia  
E-mail: nadezda.cubonova@fstroj.uniza.sk

postprocessors. This is a radically different approach to CNC programming [5]. Standard STEP-NC generates “workingsteps” which contain information about geometry, tool requirement, and feature definition. With this information, CNC machine tools can receive a file with STEP-NC data, know what it means, and proceed manufacturing the work piece without any more instruction. A comparison between programming with the use of G&M codes and STEP-NC using is described in Fig. 1.

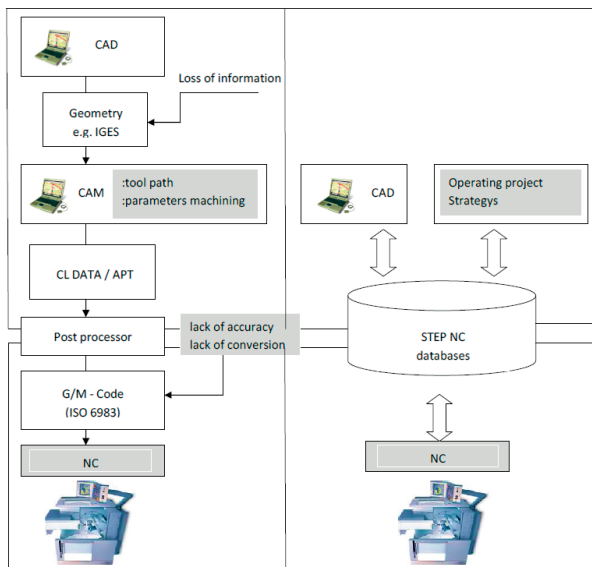


Fig.1 Comparison of the programming process using G&M codes and STEP-NC

Effectively, STEP-NC defines a data input standard for CNC systems. As STEP-NC is an extension of STEP to handling NC processes, it strictly follows the STEP standard. Like other STEP applications, a STEP-NC file also conforms to ISO 10303-21. That is, the file contains two sections marked by the keywords *Header* and *Data* respectively (Fig. 2).

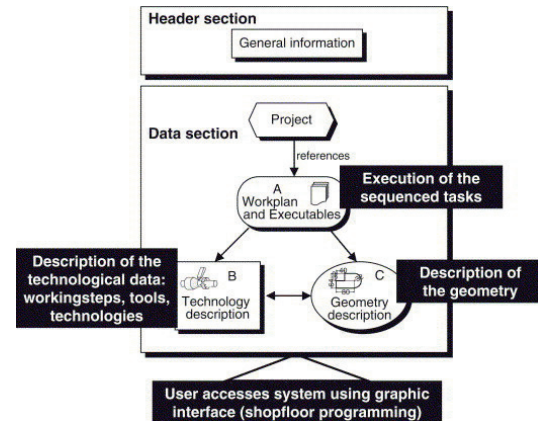


Fig. 2 Structure of the STEP-NC data model [6]

In the *Header* section, some general information and comments concerning the part program are included. These are, for example, filename, author, date and organization. The *Data* section is the main part of the program, containing all the information about manufacturing tasks and geometries. This section also includes a *Project* entity that is an explicit reference for the starting point of the manufacturing tasks. The *Project* entity contains a main *Workplan* that contains sequenced executable manufacturing tasks - *Workingsteps* [3].

Details of each *Workingstep* are given in two parts, Technology description and Geometry description. The *Technology description* contains a detailed and complete definition of all *Workingsteps* in a *Workplan* (Fig. 3).

This may include *tool data* (dimensions, tool type, conditions and usage of the tool), machine functions, machining strategies, other process data and a workpiece definition (surfaces, regions and features of the finished part). The *Geometry description*, which is of ISO 10303 data format, provides the geometrical information for *workpieces*, *set-ups* and *manufacturing features*. At the lowest level, the operations can also contain an explicit and

```

/***** Workpiece definition *****/
#1=WORKPIECE('SIMPLE WORKPIECE',#2,0.010,$,$,$,0);
#2=MATERIAL('DIN EN 10027-1','E 295',(#3));
#3=NUMERIC_PARAMETER('ELASTIC MODULUS',2.E11,'pa');

/***** Manufacturing feature *****/
#10=REVOLVED_FLAT('END FACE',#1,(#20,#21),#70,#80,0.000,#91);
#11=OUTER_DIAMETER('CONE',#1,(#22,#23),#76,#83,#93,#95);
#12=OUTER_DIAMETER('CYLINDER',#1,(#22,#23),#78,#72,#74,$);

/***** Turning operations *****/
#20=FACING_ROUGH($,$,ROUGH END FACE',$,$,#100,#41,#40,#52,#53,#50,0.500);
#21=FACING_FINISH($,$,FINISH END FACE',$,$,#110,#42,#40,#52,#53,#51,0.000);
#22=CONTOURING_ROUGH($,$,ROUGH CONTOUR',$,$,#100,#43,#40,#56,#56,#54,0.500);
#23=CONTOURING_FINISH($,$,FINISH CONTOUR',$,$,#110,#44,#40,#56,#56,#55,0.000);

/***** Project *****/
#29=PROJECT('TURNING EXAMPLE 1',#30,(#1),$,$,$);
#30=WORKPLAN('MAIN WORKPLAN',(#31,#32,#33,#34),$,$,#37,$);
#31=MACHINING_WORKINGSTEP('WS ROUGH END FACE',#63,#10,#20,$);
#32=MACHINING_WORKINGSTEP('WS FINISH END FACE',#63,#10,#21,$);
#33=TURNING_WORKINGSTEP('WS ROUGH CONTOUR',#63,(#11,#12),#22,$);
#34=TURNING_WORKINGSTEP('WS FINISH CONTOUR',#63,(#11,#12),#23,$);
#37=SETUP('SETUP FOR TURNING EXAMPLE 1',$,$,#63,(#38));
#38=WORKPIECE_SETUP(#1,#64,$,$,0);
    
```

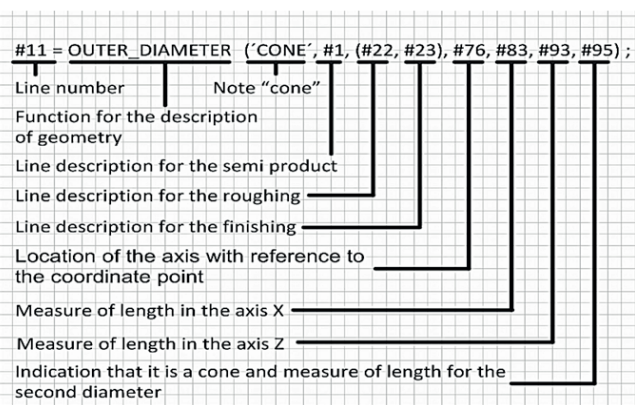


Fig. 3 Sample of STEP-NC program structure

exact description of the tool-path if this is required by a CAM system or an NC controller.

Paper presents the results of research which was focused mainly on the analysis of standard STEP-NC, a methodology on the model data according to the standard STEP-NC using the EXPRESS language as well as the creation of software for the transformation of STEP-NC data - "TERMINAL STEP NC".

### 3. Methodology for the creation of STEP-NC data model

The basic principle of data model is an object-oriented view on programming using the product characteristics instead of the coding of individual sequences of motion axes and functions of tools [7]. Figure 4 shows a general data model which can be specified as a method or philosophy of standard STEP-NC. General data model includes data about geometry, data about production characteristics and data for the manufacturing process. The role of the project solution was to create a data model according to ISO 14649 for turning technology, the selected model was applied for two-axis turning. View of the fact that the Protocol - STEP (area of geometry) is currently already a commercial protocol, in solving of our project was the biggest accent placed on production process and product characteristics. Solving the problem allows

to design and create two methodologies for the creation STEP-NC data model under the standard STEP-NC. The tools used for creating both STEP-NC data models were chosen solely on the platform of *open source softwares*, because nowadays developed softwares for the creation of the STEP-NC data are protected or unaffordable.

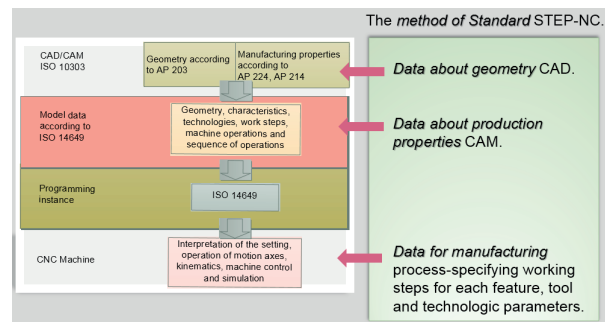


Fig. 4 General STEP-NC data model

The first method of creating the STEP-NC data consisted of modelling the scheme in CASE (Computer Aided Software Engineering) instrument. The first step was to find solution of appropriate software allowing to create in EXPRESS language the STEP NC data model and its graphical design. For the solution of the problem has been selected as the most preferred

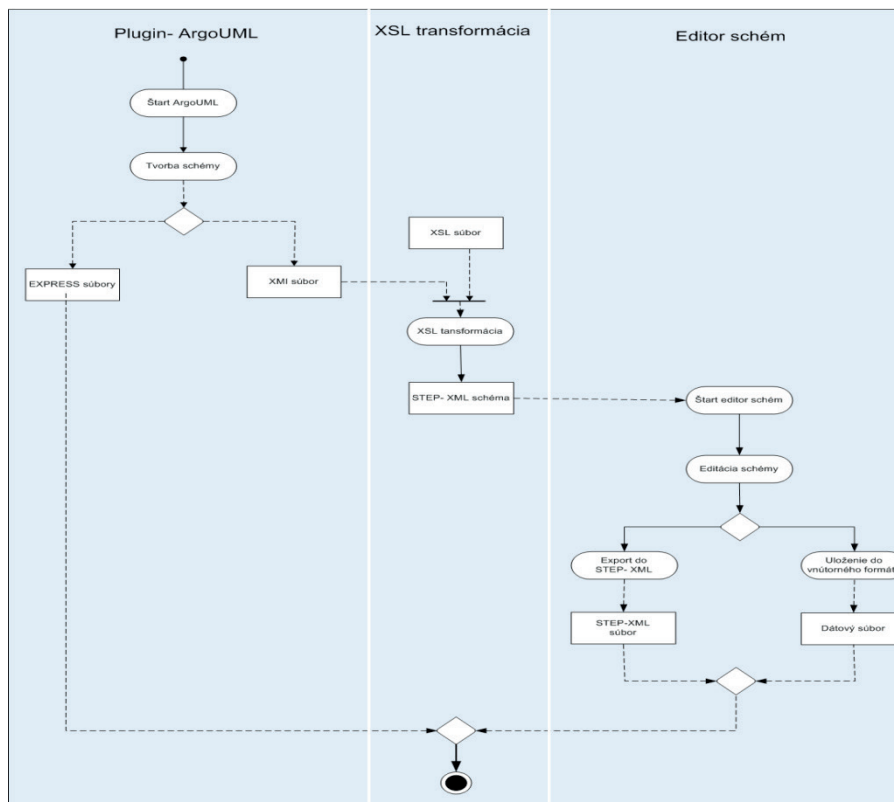


Fig. 5 Sequence activities [8]

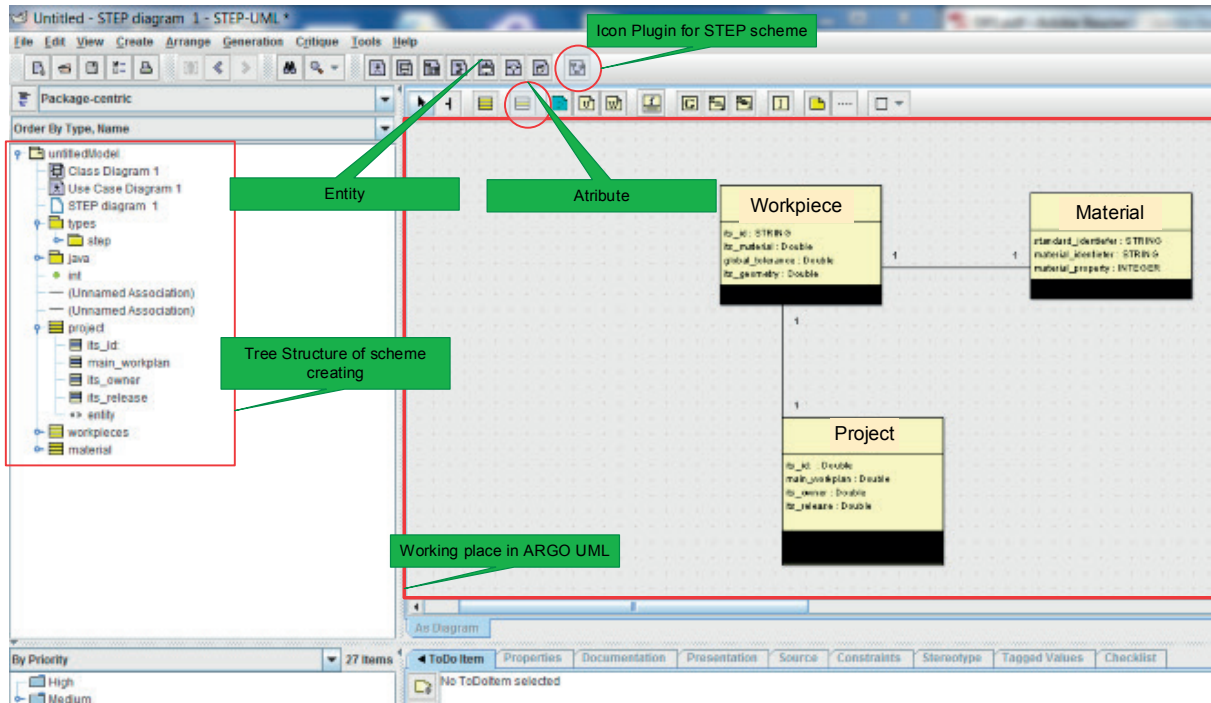


Fig. 6 Work environment in ArgoUML

```

SCHEMA Express_schema;

ENTITY project
  ABSTRACT SUPERTYPE OF(ONEOF (workplan,workpiece));

  main_workplan: workplan;
  its_workpieces: SET [0:?] of workpiece;
END_ENTITY;

ENTITY workplan
  SUBTYPE OF (project);
END_ENTITY;

ENTITY workpiece
  SUBTYPE OF (project);
END_ENTITY;
END_SCHEMA;
    
```

Fig. 7 Partial scheme in language EXPRESS [8]

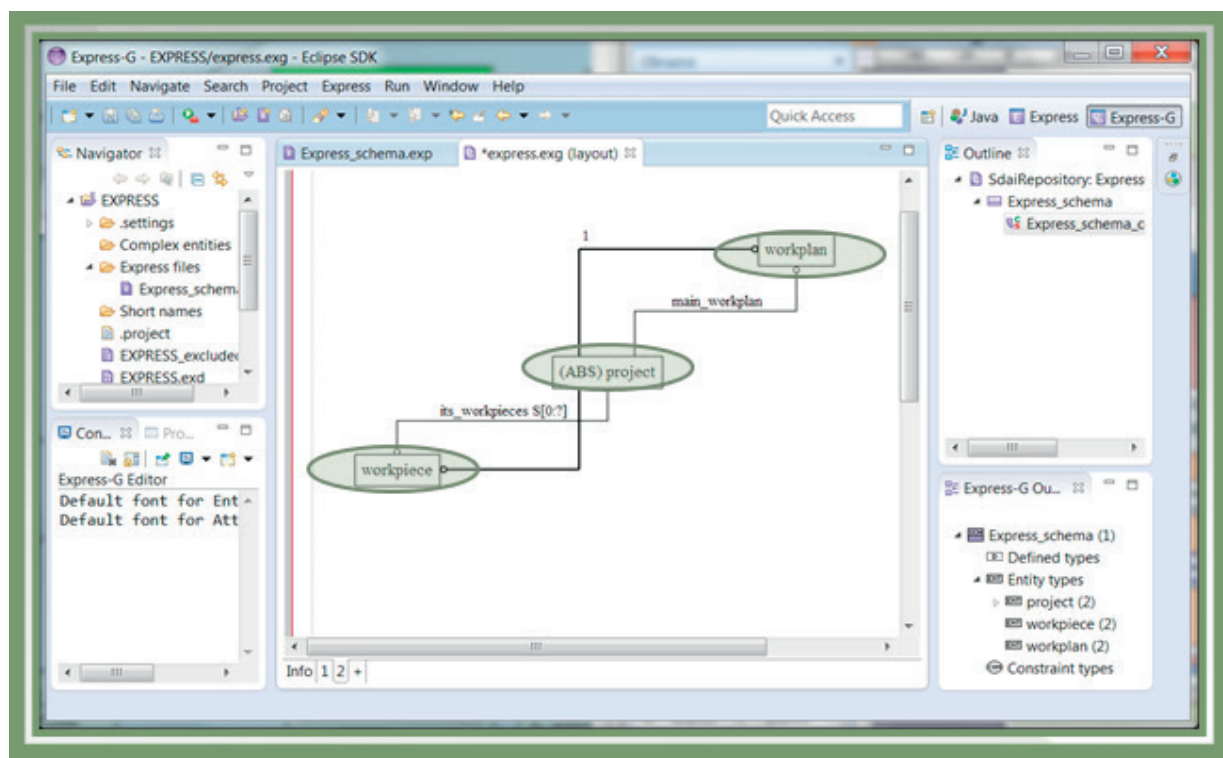


Fig. 8 Partial scheme in EXPRESS- G [8]

ARGO UML software. The scheme was then transformed into the markup language XML which communicates with the editor of schemes. Editor of schemes added instances of entities (schema objects) with ISO14649. The last stage of this methodology was to generate the scheme to STEP Physical File (ISO 10303-21). The activity diagram includes sequence activities for the process of creation of scheme and its subsequent transformation and modification (Fig. 5).

Sequence of steps was divided into three parts; each part belonged to a separate section, they were in different activities. Flow of data first goes through section-plugin ArgoUML which creates XMI file destined to the XSL transformation or generates the code of language Express. Section of *XSL transformations* includes process that receives at its input the XMI file along with the file containing details of transformations. The output of this section is file in STEP-XML format, which is also the entrance to the section of *Schemes editor*, where are performed processes related with editing [8].

The scheme was created by entities “Workpiece, Material, Project” (Fig. 6). Each entity contains the individual attributes that correspond to the entities according to ISO 14649. Data types that is used for drawing of schemes by applied CASE tool - ArgoUML are not included in plugin in sufficient quantity as it is in the language EXPRESS that uses a large number of data types.

The second method of creating STEP-NC data was based on the Java editor which is complemented by a plugin for EXPRESS and EXPRESS-G. The method of creating the STEP-NC data model

using data was performed by direct programming in EXPRESS in which individual entities are in accordance with ISO 14649. The program was written in text form - code (Fig. 7).

This part describes the creation of simple partial scheme at the level of the first three layers (“Project”, “Workplan”, “Workpiece”). Using a graphical interface EXPRESS-G this code can be presented in a graphical form, in the form of scheme (Fig. 8) [8]. The structure of the complex EXPRESS scheme consisted of partial EXPRESS schemes that were sequentially defined under layers and implemented in a comprehensive EXPRESS scheme.

#### 4. Creation of “TERMINAL STEP-NC” software

Within research tasks the software program for the transformation of STEP-NC data *TERMINAL STEP-NC* was created. The software allows processing control STEP-NC program, and based on the proposed communication protocol, sends commands to the motion control lathe controller via the serial interface USB. For creation of software *TERMINAL STEP-NC* was used programming language Visual Basic 6.0. The proposed principle of processing the input file STEP-NC consists of five basic steps and is displayed in Fig. 9. Part - *Decoding of STEP-NC data* is formed by filtration of geometric parameters, by parameterization and by graphical verification [9]. Part - *Communication* is formed by synchronization and by data transmission.

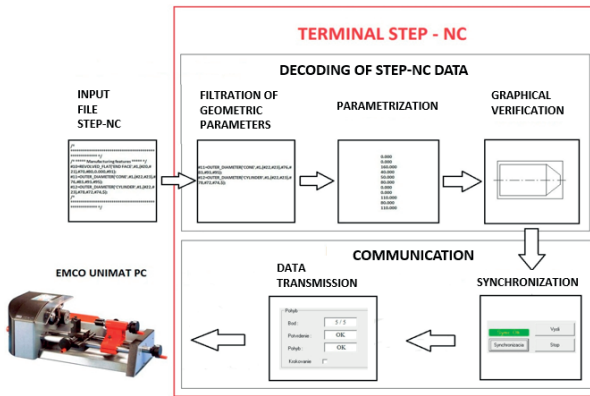


Fig. 9 Working principle of software - TERMINAL STEP-NC

Entry for the program is a text file STEP-NC which is processed by the program so that it can be sent by asynchronous transmission over serial line to the controller lathe Emco Unimat PC (Fig. 10). Software allows visual simulation data transfer. Work environment and the procedure for processing of STEP-NC are displayed in Fig. 11 [10].

TERMINAL STEP-NC was tested on STEP-NC program from Standard - ISO 14649. Verification of functionality, data transmission to the control unit Lathe - Emco Unimat PC is displayed in Fig. 12 [10].

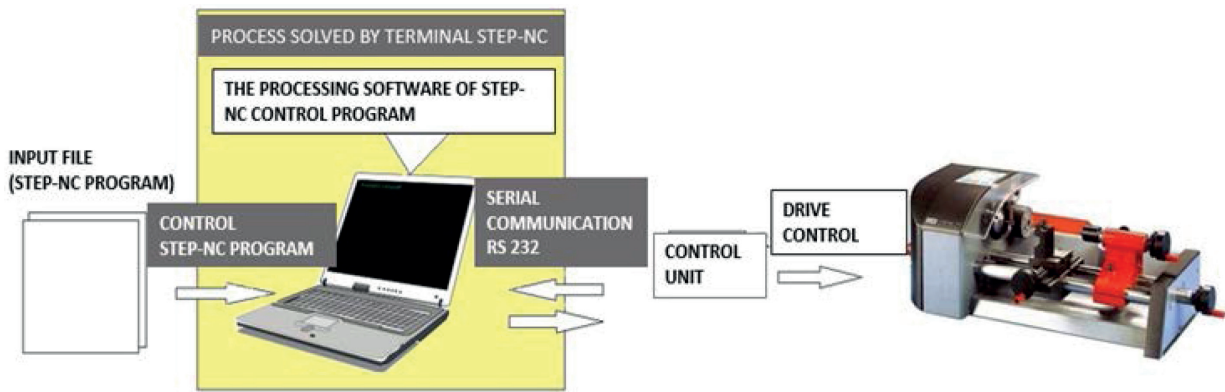
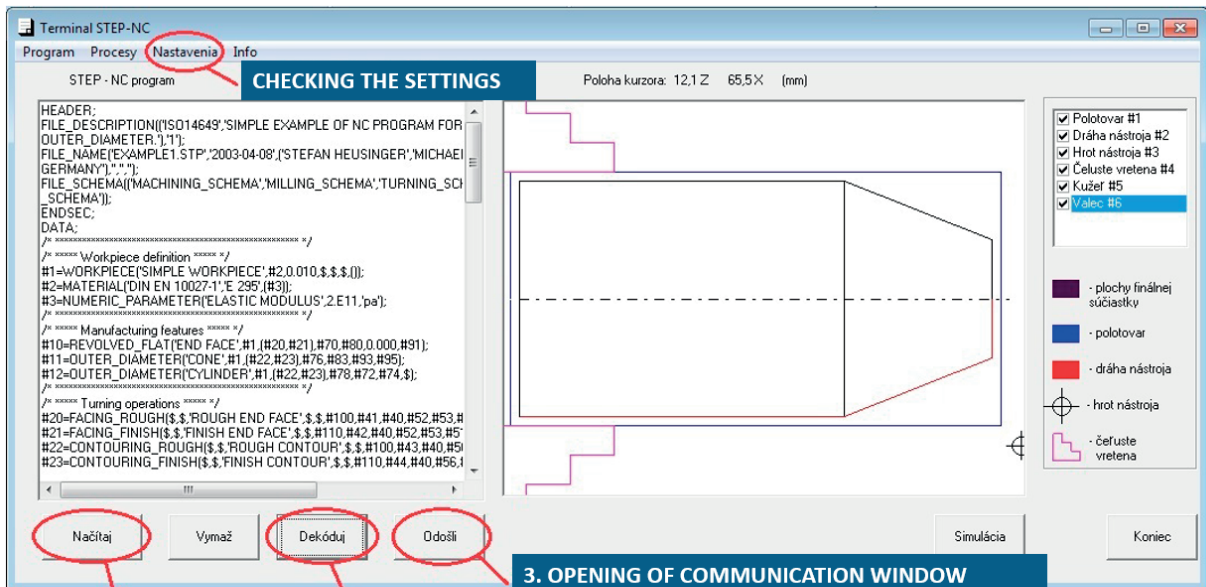


Fig. 10 Process of data transmission to the control unit Lathe - Emco Unimat PC [10]



1. PROGRAM LOADING

2. DECODING AND RENDERING OF COMPONENT

3. OPENING OF COMMUNICATION WINDOW

Fig. 11 Procedure for processing of STEP-NC [10]



Fig. 12 General view of the workplace verification system and use of standard STEP-NC

Presented software program “TERMINAL STEP-NC” can process components with the geometry composed of cylindrical and conical surfaces. Algorithm of software is open so it can be expanded in the future to process other types of surfaces and new features [11]. Communication protocol must be extended by the control unit. Standard STEP-NC allows building a complete database of machining information around it. The database, then, dictates what capabilities must exist in the machine tool controller to cut the part [12].

## 5. Conclusion

The solution of the project allows comparing two different methodologies for data modelling using STEP-NC protocol.

The first methodology is not difficult in terms of programming; the disadvantage is that the plugin was additionally installed in ArgoUML and does not support all data types. It is not possible to create a data model according to the STEP-NC in its fullest extent. Data types, however, can be completed by use of existing or by creation of new plugin. The second method was implemented directly in a programming language EXPRESS. The advantage is that by using APIs interfaces of JSDA and plugins can be modelled the schema in its entirety of STEP-NC (ISO 14649). In solving it is necessary to have experience with EXPRESS language. The complex structure of the EXPRESS schema and also a partial schema cannot be in these solutions generated into the physical file STEP Part 21 because the interface API of JSDA does not contain a plugin that would enable the given generating. To create a plugin that would be able to carry out such an application is, however, practicable. The created software “TERMINAL STEP-NC” verifies the possibility of using ISO 14649 as a new model for data exchange between CAD / CAM systems and CNC machines and also verifies the possibility of implementing a new standard to the older types of CNC machines [13].

## Acknowledgements

The research was supported by the Scientific Grant Agency of Ministry of Education through VEGA grant No. 1/0400/11. The authors thank for support.

## References

- [1] JANDECKA, K., KOZMIN, P.: Aspects of Utilization the New Interpolation Type in NC Machine Programs (in Czech), *Strojirenska technologie*, vol. VIII, No. 4, 2003, ISSN 1211-4162.
- [2] CUBONOVA, N.: Post-processing of CL Data in CAD/CAM System Edgecam Using the Constructor of Post-processors, *Manufacturing Technology: J. for Science, Research and Production*, vol. 13, No. 2, 2013, 158-164. ISSN 1213-2489.
- [3] ISO 14649-1: *Industrial Automation Systems and Integration - Physical device control - Data model for computerized numerical controllers - Part 1: Overview and fundamental principles*, Geneva : Intern. Organization for Standardization, 2003, Retrieved 2008-10-27.
- [4] ISO 10303-21: *Industrial Automation Systems and Integration - Product data representation and exchange - Part 21: Implementation methods: Clear text encoding of the exchange structure*, Geneva, 2002.
- [5] ISO 10303-11: *Industrial Automation Systems and Integration - Product data representation and exchange - Part 11: Description methods: The EXPRESS language reference manual*, Geneva, 2004.
- [6] XU, X. W.: Realization of STEP-NC Enabled Machining. *Robotics and Computer-Integrated Manufacturing*, vol. 22, No. 2, April 2006, 144-153. ISSN: 0736-5845.
- [7] KURIC, I.: New Methods and Trends in Product Development and Process Planning. *Academic J. of Manufacturing Engineering*. Editura Politehnica : Scientific Papers, vol. 9, No. 1, 2011, 83-88, Cluj-Napoca. ISSN 1583-7904.
- [8] KARDOS, J.: *Utilization of Standard STEP NC by the NC Machine Programming (in Slovak)*, Katedra automatizacie a výrobných systemov: EDIS: University of Zilina, 2012.

- [9] KUMICAKOVA, D., GORSKI, F., MILECKI, A., GRAJEWSKI, D.: Utilization of Advanced Simulation Methods for Solving of Assembly Processes Automation Partial Tasks. *Manufacturing Technology : J. for Science, Research and Production*, vol. 13, No. 4, 2013, 478-485. ISSN 1213-2489.
- [10] DURIK, M.: *Proposal and Creation of Software for Transformation of STEP -NC data. (in Slovak)*. MSc. thesis, University of Zilina, 2013.
- [11] SAPIETOVA, A., SAGA, M., NOVAK, P.: Multi-software Platform for Solving of Multibody Systems Synthesis. *Communication - Scientific Letters of the University of Zilina*, vol.14, No. 3, 2012, Zilina, 43-48, ISSN 1335-4205.
- [12] CZAN, A., SAJGALIK, M., HOLUBJAK, J., KOURIL, K.: Studying of Cutting Zone when Finishing Titanium Alloy by Application of Multifunction Measuring System, *Manufacturing Technology*, vol. 13, No. 4, December 2013, 428-431, ISSN: 1213-2489.
- [13] LITVAJ, I., PONISCIAKOVA, O., STANCEKOVA, D., DRBUL, M.: *Knowledge Processes and their Implementation in Small Transport Companies*, 17<sup>th</sup> Intern. Conference Transport Means 2013, Kaunas, October 2013, Code 102486, 153-156. ISSN: 1822-296X.

# TENSION MECHANISM DYNAMIC ANALYSIS

The aim of the presented article is to show how to create a mathematical model of the tension mechanism working by a spring motion generation and contacting a rigid body at the end of the motion.

**Keywords:** Mechanism, analysis, contact force, simulation.

## 1. Introduction

The first step of the above described task solution was the creation of the mechanism mathematical model assembled from three movable parts and the motion generating spring (Fig. 1).

The second step was the analysis of the forces applied on the mechanism during the workflow.

## 2. Mechanism Modeling

The mechanism movement is generated by a spring affecting the sliding joint between the mechanism parts labeled 2 and 3 (Fig. 1).

The main problem of the analysis is the moment when the mechanism reaches its end position and contacts the frame rigid body with the part 1 (Fig. 1) because of the contact properties of the contact point.

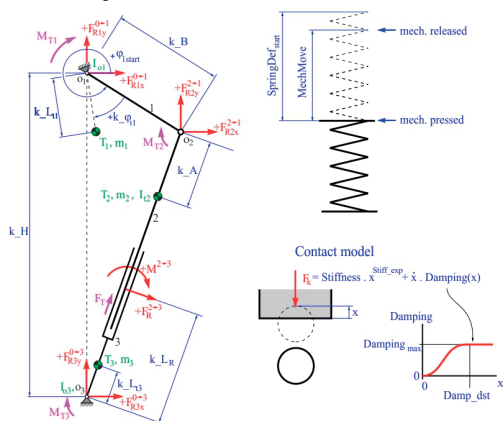


Fig. 1 Model of the mechanism structure including the spring and contact model (Source: authors)

## 2.1 Dimensions and spring parameters

The kinematics of the mechanism parts parameters were defined according to the 3D model and Table 1.

Dimensions and spring parameters of the mechanism Table 1

Name	Label	Value	Unit
Part 1 length	k_B	0.05	m
Part 1 centre of gravity distance	k_L <sub>t1</sub>	0.02	m
Part 1 angle of the centre of gravity	k_φ <sub>t1</sub>	π/4	rad
Part 2 centre of gravity distance	k_A	0.03	m
Part 3 centre of gravity distance	k_L <sub>t3</sub>	0.02	m
Distance of revolution joints O1 and O3	k_H	0.1	m
Spring stiffness	SpringStiffnes	1000	N.m <sup>-1</sup>
Spring working stroke	MechMove	0.03	m
Starting spring deformation	SpringDefstart	0.1	m

The initial values of the mechanism parameters are defined in Table 2.

Initial values of the mechanism parameters Table 2

Name	Label	Value	Unit
Part 1 initial angle of the centre of gravity	φ <sub>1start</sub>	-π/4	rad
Part 2 initial variable distance	k_L <sub>R</sub>	0	m

The angle by the full pressed mechanism is defined as φ<sub>1start</sub>. The reaction force position k\_L<sub>R</sub> influences only the moment value M.

\* <sup>1</sup>Michal Lukac, <sup>1</sup>Frantisek Brumerick, <sup>1</sup>Leszek Krzywonos, <sup>2</sup>Pawel Drozdziel  
<sup>1</sup>Faculty of Mechanical Engineering University of Zilina, Slovakia  
<sup>2</sup>Mechanical Engineering Faculty, Lublin University of technology, Poland  
 E-mail: michal.lukac@fstroj.uniza.sk

The motion generating spring positions are defined in Fig. 2.

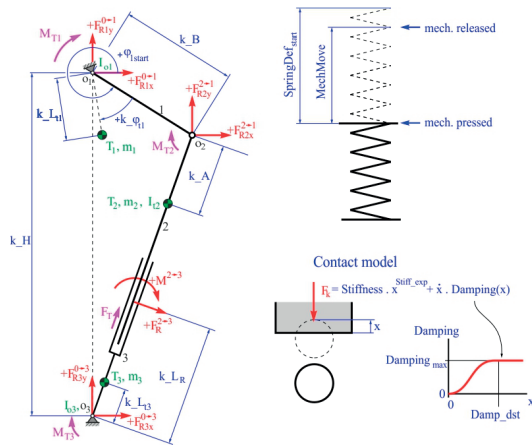


Fig. 2 Spring positions (Source: authors)

### 2.2 Mass properties

The mechanism mass properties are defined according to the 3D model and its calculation model (Fig. 1) in Table 3.

Mass properties parameters of the mechanism Table 3

Name	Label	Value	Unit
Part 1 mass	$m_1$	59.238	kg
Part 1 inertia	$I_{o1}$	$2.843445 \cdot 10^{-2}$	$\text{kg} \cdot \text{m}^2$
Part 2 mass	$m_2$	0.5	kg
Part 2 inertia	$I_{o2}$	0.1	$\text{kg} \cdot \text{m}^2$
Part 3 mass	$m_3$	25.574	kg
Part 3 inertia	$I_{o3}$	$1.13983182 \cdot 10^{-2}$	$\text{kg} \cdot \text{m}^2$

### 2.3 Friction and contact properties

The developed simulation program in the chosen software (Mathcad) allows to activate the friction via the created “Friction” GUI button. Contact properties of the mechanism are defined according to the 3D model in Table 4.

Contact properties parameters of the mechanism Table 4

Name	Label	Value	Unit
Mechanism stiffness	Stiffnes	200000	$\text{N} \cdot \text{m}^{-1}$
Stiffness exponent	Stiff_exp	2 ( $>=1$ )	N.m
Mechanism maximum damping factor	Dampingmax	500	$\text{N} \cdot \text{m}^{-1} \cdot \text{s}$
Distance to max. damping build-up	Damp_dst	0.002	m
Joint O1 friction moment	$M_{T1}$	0.5	N.m
Joint O1 friction factor	$k_{MT1}$	0	-
Joint O2 friction moment	$M_{T2}$	1	N.m
Joint O2 friction factor	$k_{MT2}$	0	-
Joint O3 friction moment	$M_{T3}$	1	N.m
Joint O3 friction factor	$k_{MT3}$	0	-

The  $k_{MT1, 2, 3}$  ( $\text{rad} \cdot \text{s}^{-1}$ ) and  $k_{FT}$  ( $\text{m} \cdot \text{s}^{-1}$ ) values are considered by the friction button turned to ON. The direction of the friction force (moment) depends on the motion direction (from the motion parts relative velocity sign). If the velocity is too slow, its direction can vary and so can also the direction of the friction force. Therefore, the friction force value is defined to rise around zero velocity to maximum [1] and [2].

The described k-value defines the velocity interval of the maximum friction force. The principle of the calculation is similar to the contact model damping calculation (the value is equivalent to the Damp\_dst value). The k-value is different for every friction force because every friction couple velocity varies. The lower is the k-value, the more accurate is the calculation. If the model does not work in the friction mode, the solution is to raise the k-value which is usually  $1 \cdot 10^{-3}$  and lower [3]. The k-value does not affect the calculation without the friction consideration. The start of the simulation has to be done with the zero value and the solver type FIXED (parameters for the Mathcad software).

There is also the fcn\_step function defined because of the smooth transition between two values of the damping coefficient in the contact point. This leads to smooth rise of this coefficient without the step rise to the maximum in the contact moment.

The value of the damping rises during the defined penetration depth Damp\_dst. and then becomes stabilized to “Damping\_max” value (Table 4, Fig. 3).

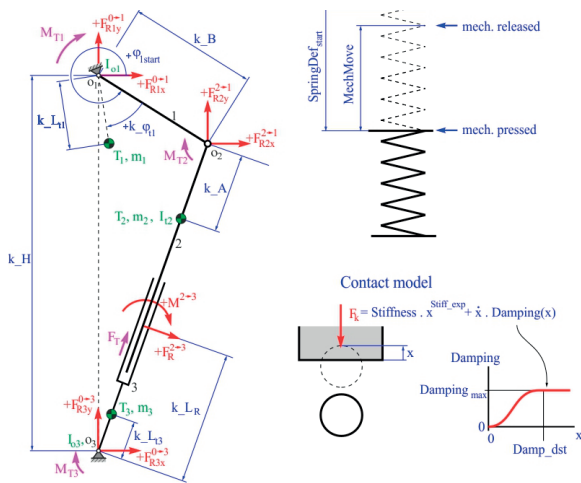


Fig. 3 Contact model (Source: authors)

3. Solver parameters

The solver parameters were defined as follows in Table 5.

Solver parameters Table 5

Name	Label	Value	Unit
Time interval (0 - t <sub>end</sub> )	t <sub>count</sub>	1000	-
Number of the points in the plotted graphs	N <sub>t</sub>	1001	-
End time of the simulation	t <sub>end</sub>	1	S
Friction force	F <sub>T</sub>	10	N
Friction force factor	k <sub>FT</sub>	0	-

The larger is the number of the time interval (0 - t<sub>end</sub>) division during the simulation, the more accurate is the calculation. If the calculation does not converge, new solver has to be used (right button on the odesolve function in the MathCad) [4].

4. Interpolation of bodies coordinates

The bodies coordinates that are interesting for the interpolation during simulation are labeled φ<sub>2</sub> and L<sub>t2</sub> in Fig. 4. The parameters influencing the interpolation are defined in Table 6.

Interpolation influencing parameters Table 6

Name	Label	Value	Unit
Control variable	CTOL	0.00001	-
Control variable	TOL	0.00001	-
Polynomial degree	FitDegree	7	-
Number of points	NuPo	200	-

The Mathcad TOL worksheet variable controls the precision to which integrals and derivatives are evaluated. TOL also controls convergence criteria in Solve Blocks and in the root function. The two most recent estimates of a solution must differ by less than the built-in variable TOL. The CTOL worksheet variable controls how closely a constraint in a Solve Block must be met for a solution to be acceptable. It is used by optimizing functions like: Minimize, Maximize, Find, or Minerr. For example, a constraint such as x < 2 must be satisfied to within CTOL before a solution is returned. If CTOL = 0.001 (the default), this constraint is satisfied if x < 2.001 [5] and [6].

Figure 4 shows the simplified view of the mechanism with all important variables and their first and second derivatives.

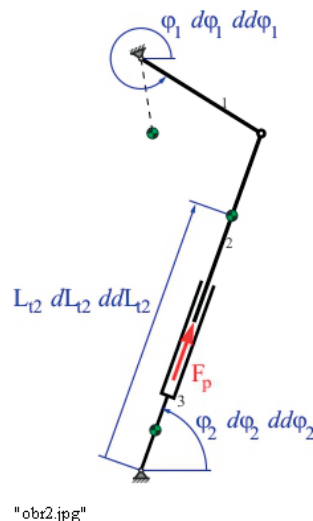


Fig. 4 Simplified view of important mechanism variables (Source: authors)

The calculated mechanism has one degree of freedom (DOF). All forces and masses are reduced to the mechanism part 1 coordinate φ<sub>1</sub>.

It is necessary to define the coordinates L<sub>t2</sub> and φ<sub>2</sub> as a function of the φ<sub>1</sub> coordinate. To make the calculation effective and simple, the coordinates L<sub>t2</sub> and φ<sub>2</sub> are defined as a function of the φ<sub>1</sub> by the interpolation polynomial of the 7-th degree! The FitDegree value has to remain defined to 7 during the calculation because all equations are derived for this polynomial degree [7].

The R\_disp function displays the L<sub>t2</sub> and φ<sub>2</sub> coordinate values depending upon φ<sub>1</sub> for the φ<sub>1</sub> values from -π/2 to π/2. In this interval, the mechanism is resolvable - the values outside the interval will not be calculated correctly.

The number of values labeled NuPo specifies the calculation of the interpolation polynomial coefficients for the φ<sub>2</sub> and L<sub>t2</sub> coordinates. The Disp\_Coeff software feature displays the polynomial coefficients. The angle of the φ<sub>1</sub> coordinate between the threshold limit -π/2 and π/2 is defined as ff1.

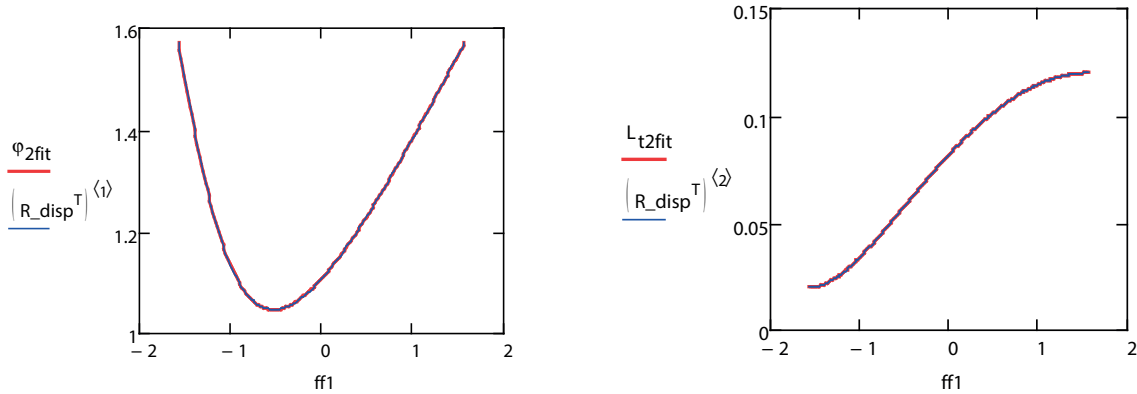


Fig. 5 Interpolated and calculated data match test of the mechanism variables (Source: authors)

The equations representing the relationships between the coordinates are following:

$$\begin{aligned}
 L_{12} \cdot \cos(\varphi_2) + k\_A \cdot \cos(\varphi_2) + k\_B \cdot \cos(\varphi_1 - \pi) &= 0 \\
 L_{12} \cdot \sin(\varphi_2) + k\_A \cdot \sin(\varphi_2) + k\_B \cdot \sin(\varphi_1 - \pi) \\
 -k\_H &= 0
 \end{aligned}
 \tag{1}$$

The comparison between the interpolated data (red) and real data (blue) for the angle  $\varphi_1$  from  $-\pi/2$  to  $\pi/2$  (Fig. 5) attends only for the test of the interpolated and calculated data match. In the case of extreme mechanism dimensions, the values could not match and it would be necessary to rise the interpolation polynomial degree [8] - [10].

The  $\varphi_2$  and  $L_{12}$  coordinates are defined at the start of the simulation (pressed mechanism) for the value  $\varphi_{1start}$ . The initial values for the calculations noted above are shown in Table 7.

Initial values of the mechanism variables Table 7

Name	Label	Value	Unit
Part 2 initial angle of the centre of gravity	$\varphi_{2start}$	61.298	Deg
Part 2 initial variable distance	$L_{12start}$	0.044	M

The spring force labeled as  $fcn\_F_p$ (def) is defined as linear, the output parameter is the  $L_{12}$  value.

### 5. Motion equation calculation

The differential motion equation for the mechanism is defined according to the labels of the parameters defined in the previous text and tables as

$$\begin{aligned}
 I_{red}(x) := I_{o1} + m_2 \cdot & \left[ \begin{aligned} & (7a_{L11} \cdot x^6 + 6a_{L12} \cdot x^5 + 5a_{L13} \cdot x^4 + 4a_{L14} \cdot x^3 + 3a_{L15} \cdot x^2 + 2a_{L16} \cdot x + a_{L17})^2 \dots \\ & + (7a_{\varphi 21} \cdot x^6 + 6a_{\varphi 22} \cdot x^5 + 5a_{\varphi 23} \cdot x^4 + 4a_{\varphi 24} \cdot x^3 + 3a_{\varphi 25} \cdot x^2 + 2a_{\varphi 26} \cdot x + a_{\varphi 27}) \cdot \\ & (a_{L11} \cdot x^7 + a_{L12} \cdot x^6 + a_{L13} \cdot x^5 + a_{L14} \cdot x^4 + a_{L15} \cdot x^3 + a_{L16} \cdot x^2 + a_{L17} \cdot x + a_{L18}) \end{aligned} \right] \\
 + (I_{12} + I_{o3}) \cdot & (7a_{\varphi 21} \cdot x^6 + 6a_{\varphi 22} \cdot x^5 + 5a_{\varphi 23} \cdot x^4 + 4a_{\varphi 24} \cdot x^3 + 3a_{\varphi 25} \cdot x^2 + 2a_{\varphi 26} \cdot x + a_{\varphi 27})^2
 \end{aligned}
 \tag{2}$$

Reduced forces are labeled as  $F_{Pred}$  appertaining the spring,  $F_k$  appertaining the contact and  $F_{TR}$  appertaining the damping.

The motion equation solution leads to the output of the coordinate  $\varphi_1$  - its angular velocity  $d\varphi_1$  and  $\varphi_1$  angle. If the solution failed, it would be necessary to change the solver type (Mathcad "Odesolve" button - ADAMS, FIXED, ...).

The creation of  $N_t$  values for the simulation time 0 - tend ( $\varphi_1$ ,  $d\varphi_1$ ,  $dd\varphi_1$ ) is defined with the help of the tt parameter - the time interval vector from 0 to  $t_{end}$  divided to  $N_t$  values.

### 6. Contact force simulation results

The resulting contact force - the main goal of the complex tension mechanism simulation is shown in Fig. 6. The contact force peak value of 284.14 N was reached in 0.09 s.

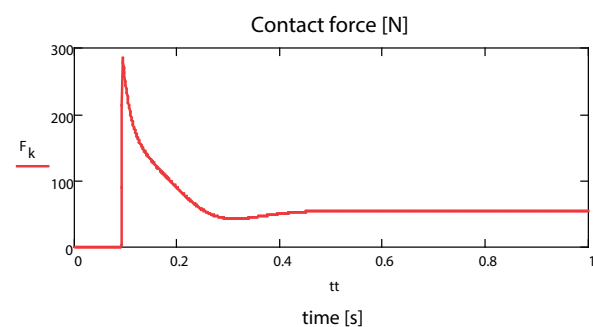


Fig. 6 Tension mechanism contact force calculation result (Source: authors)

## 7. Conclusion

The mathematical model of the tension mechanism working by a spring motion generation and contacting a rigid body at the end of the motion was built considering the main problem of the analysis - the moment when the mechanism reaches its end position and contacts the frame rigid body with one of its

components. It was necessary to use the right model of the friction and contact properties and to calculate the mechanism coordinates via the interpolation polynomial of the 7-th degree. The result of the simulation was the definition of the peak contact force between the mechanism component and the frame rigid body.

## References

- [1] DEKYS, V., BRONCEK, J.: Measuring Strain of the Lattice Towers, *Communications - Scientific Letters of the University of Zilina*, vol. 14, No. 3, 2012, 39-42, ISSN 1335-4205.
- [2] DROZDZIEL, P., KRZYWONOS, L.: The Estimation of the Reliability of the First Daily Diesel Engine Start-up During its Operation in the Vehicle, *Eksplatacja i Niezawodnosc - Maintenance and Reliability* 1(41), 2009, 4-10, ISSN 1507-2711.
- [3] HRCEK, S., KOHAR, R., MEDVECKY, S.: Determination on the Maximum Roller Bearing Load with Regards to Durability there of using FEM Analysis. *Communications - Scientific Letters of the University of Zilina*, vol. 14, No. 3, 2012, 55-61, ISSN 1335-4205.
- [4] HRCEK, S., KRAUS, V., KOHAR, R., MEDVECKY, S., LEHOCKY, P.: Construction of a Bearing Testing Apparatus to Assess Lifetime of Large-scale Bearings. *Communications - Scientific Letters of the University of Zilina*, vol. 11, No. 2, 2009, 57-64, ISSN 1335-4205.
- [5] BRUMERCIK, F., KOCUR, R., PAZICAN, M., LUKAC, M.: Differential Hydro-mechanical Transmissions with Hydrostatic Units. *Communications - Scientific Letters of the University of Zilina*, vol. 7, No. 1, 2005, pp. 49-53, ISSN 1335-4205.
- [6] WU, D., YAO, J., LI, H., QIAN, B.: Control Strategy for Hydro-mechanical Differential Turning System of Tracked Vehicles, *Nongye Gongcheng Xuebao / Transactions of the Chinese Society of Agricultural Engineering*, vol. 28, No. 8, 2012, 78-83, ISSN 1002-6819.
- [7] KOHAR, R., HRCEK, S., MEDVECKY, S.: Usage of Dynamic Analysis to Determine Force Interactions between Components of Rolling Bearings. *Communications - Scientific Letters of the University of Zilina*, vol. 14, No. 3, 2012, 62-67, ISSN 1335-4205.
- [8] KUCERA, L., LUKAC, M., JURAK, L., BRUMERCIK, F.: Hydromechanical Automatic Transmission, *Communications - Scientific Letters of the University of Zilina*, vol. 11, No. 2, 2009, 33-35, ISSN 1335-4205.
- [9] LEHOCKY, P., KOHAR, R., HRCEK, S., PODHORSKY, J., SURMOVA, B., MEDVECKY, S., HRCEKOVA, A.: Automative Unwinding of Waste Paper from Reel Spools. *Communications - Scientific Letters of the University of Zilina*, vol. 9, No. 1, 2007, 60-66, ISSN 1335-4205.
- [10] WANG, G., ZHU, S., SHI, L., TAO, H., VANTHINH, N.: Experimental Optimization on Shift Control of Hydraulic Mechanical Continuously Variable Transmission for Tractor, *Nongye Gongcheng Xuebao / Transactions of the Chinese Society of Agricultural Engineering*, vol. 29, No. 18, 51-59, 2013, ISSN 1002-6819.

Filip Pastorek - Miroslav Omasta – Lenka Bukovinova – Pavel Dolezal – Branislav Hadzima \*

## BIODEGRADATION PROPERTIES OF AZ31 MAGNESIUM ALLOY COATED BY DICALCIUM PHOSPHATE DIHYDRATE

*Biodegradation properties of magnesium and its alloys that can be used for implants are not satisfactory and cause serious problems. These problems can be solved by biodegradable surface coatings. Evaluation of biodegradation process of Mg-3Al-1Zn alloy surfaces after grinding and grinding followed by potential controlled electrodeposition of dicalcium phosphate dihydrate (DCPD) was investigated by electrochemical impedance spectroscopy measurements in this study. The potentiostatic electrodeposition treatment process was performed in water solution of  $\text{Ca}(\text{NO}_3)_2 \cdot 4\text{H}_2\text{O}$ ,  $\text{NH}_4\text{H}_2\text{PO}_4$  and  $\text{H}_2\text{O}_2$ . The corrosion process on treated and nontreated samples after various exposure times was evaluated in 0.9% NaCl solution simulating body fluid environment at 37 °C.*

**Keywords:** Magnesium alloy, electrodeposition, calcium phosphate, electrochemical impedance spectroscopy.

### 1. Introduction

Magnesium is an exceptionally lightweight metal. With a density of 1.74 g/cm<sup>3</sup>, magnesium is 1.6 and 4.5 times less dense than aluminum and steel, respectively [1 - 3]. The fracture toughness of magnesium is greater than ceramic biomaterials such as hydroxyapatite, while the elastic modulus and compressive yield strength of magnesium are closer to those of natural bone than is the case for other commonly used metallic implants made of stainless steel or titanium [4 - 10]. Moreover, magnesium is essential to human metabolism and is naturally found in bone tissue. It is the fourth most abundant cation in the human body, with an estimated 1 mol of magnesium stored in the body of a normal 70 kg adult, with approximately half of the total physiological magnesium stored in bone tissue [11].

The unfortunate complication is that pure magnesium and its alloys can corrode too quickly in the physiological pH (7.4 - 7.6) and high chloride environment of the physiological system, losing mechanical integrity before the tissue has sufficiently healed and producing hydrogen gas in the corrosion process at a rate that is too fast to be dealt with by the host tissue [12]. It is likely that in spite of some early successes with magnesium-based implants [13], the metal was abandoned due to the production of gas during the in vivo corrosion process when stainless steels became available. Several possibilities exist to tailor the corrosion rate of magnesium by using alloying elements and protective coatings, processes that, of course, must lead to a non-toxic, biologically compatible material [4, 12 and 14].

Calcium phosphates have been researched extensively for biomedical applications due to their high biocompatibility and bioactivity [15]. Unfortunately, these ceramic biomaterials do not have the mechanical strength to enable them to succeed in load bearing applications. However, implant materials such as stainless steels and titanium alloys are coated with calcium phosphates [16 - 18].

Compared to conventional preparation methods, such as hot spraying or laser cladding, the structure of Ca-P coatings formed in solution is closer to that of the bone minerals [19]. Moreover, the electrodeposition technique could cost-effectively adjust the morphologies and compositions of Ca-P coatings [20].

The aim of this study is to create calcium phosphate coating on the surface of AZ31 magnesium alloy by potential-controlled electrodeposition and to evaluate the corrosion protection influence of this coating during exposure in electrolyte simulating a human body environment.

### 2. Experimental material and methods

Magnesium alloy AZ31 was chosen as the experimental material. It was continually cast at Brandenburgische Universität in Cottbus, Germany, heat-treated by annealing (420 °C, 6 hours) at TU Clausthal, Germany and its chemical composition was analyzed at the Magnesium innovation centre MagIC GKSS

\* <sup>1,2</sup>Filip Pastorek, <sup>1</sup>Miroslav Omasta, <sup>2</sup>Lenka Bukovinova, <sup>3</sup>Pavel Dolezal, <sup>1,2</sup>Branislav Hadzima

<sup>1</sup>Department of Materials Engineering, Faculty of Mechanical Engineering, University of Zilina, Slovakia

<sup>2</sup>Research centre of the University of Zilina, Slovakia

<sup>3</sup>Institute of Material Science and Engineering, Faculty of Mechanical Engineering, Brno University of Technology, Czech Republic

E-mail: filip.pastorek@fstroj.uniza.sk

Chemical composition of AZ31 alloy

Table 1

Component	Al	Zn	Mn	Si	Cu	Ni	Fe	Mg
wt. %	2.96	0.828	0.433	0.004	0.004	<0.001	0.002	bal.

Geesthacht, Germany. The chemical composition is listed in Table 1.

The microstructure of AZ31 alloy (Fig. 1) was observed by the CARL ZEISS AXIO Imager.A1m light metallographic microscope using AxionVision Rel 4.5 software and AxioCam MRc5 camera in the laboratories of the Department of Materials Engineering, University of Zilina. The microstructure of AZ31 alloy is created by polyedric grains of supersaturated solid solution of aluminum, zinc and other alloying elements in magnesium (solid solution  $\delta$ ). The average grain size is 220  $\mu\text{m}$ .

AZ31 magnesium alloy samples with surface area of 2  $\text{cm}^2$  were ground with 500 and 1000 grit SiC paper to ensure the same surface roughness, then rinsed with demineralized water and ethanol, and dried using a stream of hot air. After described pre-treating the dicalcium phosphate dihydrate (DCPD) was deposited on the samples' surfaces. Treatment electrolyte solution was prepared with 0.1M  $\text{Ca}(\text{NO}_3)_2 \cdot 4\text{H}_2\text{O}$  + 0.06M  $\text{NH}_4\text{H}_2\text{PO}_4$  + 10 ml.l<sup>-1</sup>  $\text{H}_2\text{O}_2$ . A classical three-electrode system consisting of counter electrode (platinum electrode), reference electrode (saturated calomel electrode) and working electrode (sample) was used for electrodeposition process. Electrodeposition was performed with constant potential -1.8 V vs reference electrode potential for 1 hour at room temperature  $22 \pm 2$  °C on a laboratory apparatus VSP (producer BioLogic SAS France).

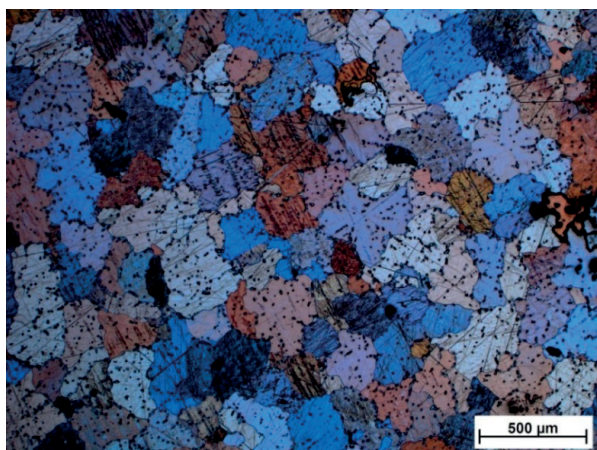


Fig. 1 Microstructure of AZ31 alloy, light microscopy, etch. picric acid + ac. acid + ethanol + water [21]

### 3. Results and discussion

The surface morphology of the treated samples (Fig. 2) was assessed by a stereomicroscope Nikon AZ100 with

a digital camera using NIS Elements software. As can be seen, the continuous layer of DCPD covering the entire surface is composed of irregularly branched units that overlap each other.

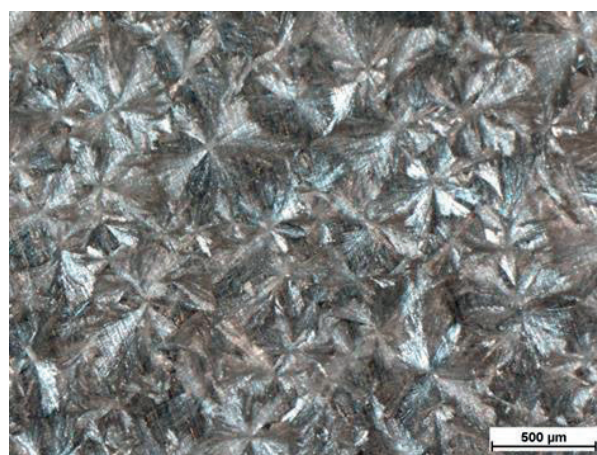
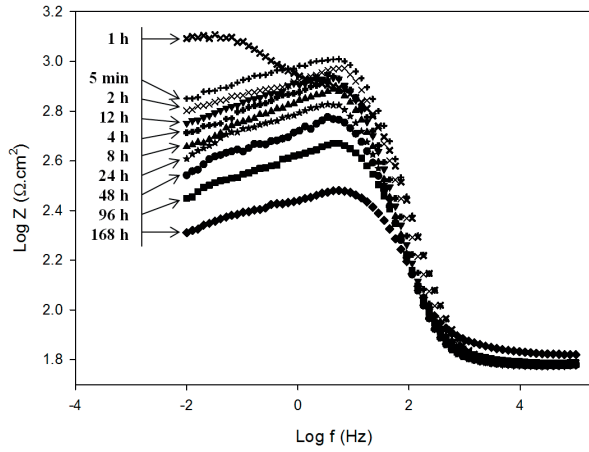


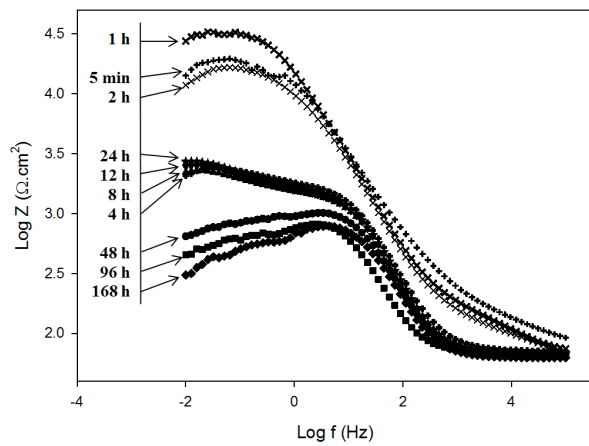
Fig. 2 Morphology of created calcium phosphate, light microscopy

Electrochemical impedance spectroscopy (EIS) was used for the corrosion resistance evaluation of surface layers after exposure times from 5 minutes to 168 hours in 0.9% NaCl solution at  $37 \pm 1$  °C, which represents human body environment conditions. Corrosion electrochemical characteristics were measured and evaluated by a potentiostat/galvanostat/frequency response analyzer VSP from BioLogic SAS France. EIS measurements were performed at open circuit potential with AC voltage amplitude of 15 mV in frequency range from 100 kHz to 10 mHz.

Results from EIS measurements in the form of impedance and phase Bode plots are shown in Fig. 3 and Fig. 4 for AZ31 samples with ground surface and surface coated by DCPD, respectively. Bode plots were analyzed by software EC-Lab V10.12 using equivalent circuits. Fig. 5 expresses the equivalent circuit used for the analysis of Bode plots with one minimum in *phase shift vs log f* interpretation and Fig. 6 the equivalent circuit used for the analysis of Bode plots with two minimums in *phase shift vs log f* interpretation [3]. These equivalent circuits use various elements expressing the character of evaluated surface. In our case,  $R_\Omega$  is resistance of the solution,  $R_{p1}$  and  $R_{p2}$  are polarization resistances of various mechanisms in corrosion model (e.g. charge transfer, film resistance,...),  $R_p$  is mixed polarization resistance or sum of partial polarization resistances ( $R_{p1} + R_{p2}$ ) and  $CPE_1$  and  $CPE_2$  are constant phase elements of mechanisms corresponding with  $R_{p1}$  and  $R_{p2}$ , respectively.  $CPE_1$  in second equivalent circuit is constant phase element of the layer of corrosion products.

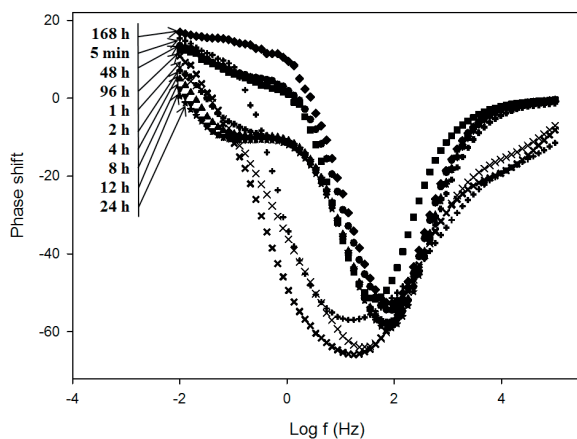


a)

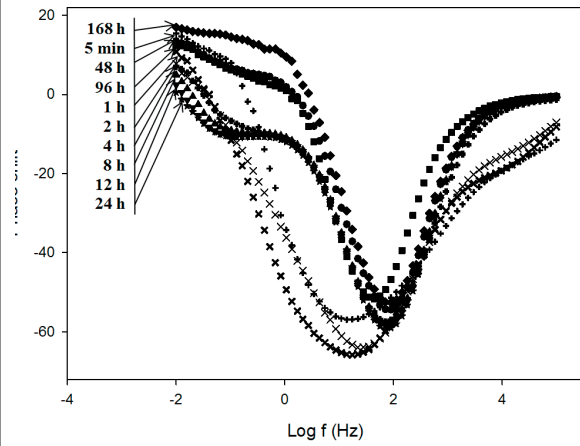


b)

Fig. 3 Impedance Bode plots of AZ31 samples: a) Ground surface, b) Surface with DCPD layer



a)



b)

Fig. 4 Phase Bode plots of AZ31 samples: Ground surface, b) Surface with DCPD layer

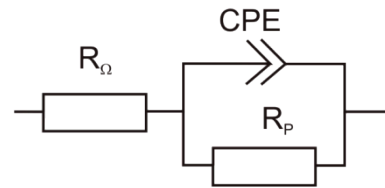


Fig. 5 Equivalent circuit used for the analysis of Bode plots with one minimum in phase shift vs log f interpretation

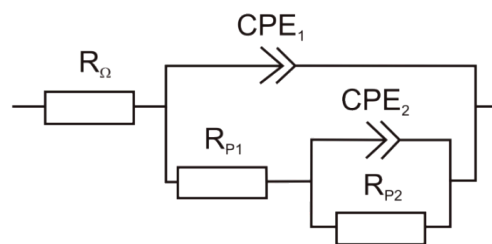


Fig. 6 Equivalent circuit used for the analysis of Bode plots with two minimums in phase shift vs log f interpretation

Based on Bode plots analysis the values of polarization resistance  $R_p$  were obtained. This electrochemical characteristic represents the corrosion resistance of the surface layer (or layers). The values of polarization resistances and other electrochemical characteristics gained after various exposure times on AZ31 magnesium alloy samples without and with DCPD coating are listed in Table 2.

Polarization resistance values of the ground AZ31 samples and ground AZ31 samples with DCPD surface layer after various exposure times (0.9% NaCl)

Table 2

	5min	1 h	2 h	4 h	8 h	12 h	24 h	48 h	96 h	168 h
$R_p (\Omega \cdot \text{cm}^2)$ ground	1059	1239	985	825	729	836	625	539	410	241
$R_p (\Omega \cdot \text{cm}^2)$ ground + DCPD	19047	34972	16868	2421	2236	2664	2729	953	772	730

A formation of the surface layer of corrosion products based on magnesium oxide (MgO) and hydroxide ( $\text{Mg}(\text{OH})_2$ ) was observed in a short time after the immersion of the ground AZ31 sample in 0.9% NaCl at 37 °C. This formation resulted in the increase of polarization resistance  $R_p$  values which is terminated after 1 hour of exposure when the maximum value of  $R_p$  (1239  $\Omega \cdot \text{cm}^2$ ) was reached. By increase of exposure time the gradual decrease of  $R_p$  values is observed up to a minimum 241  $\Omega \cdot \text{cm}^2$  measured after 168 hours of exposure. The decrease of  $R_p$  values can be explained by the degradation of the surface layer formed of corrosion products and by the subsequent local corrosion attack realized by aggressive components of electrolyte.

AZ31 samples with DCPD surface layer showed substantial increase of polarization resistance  $R_p$  values after various exposure times in corrosive environment at 37 °C compared to ground AZ31 samples. The value of  $R_p$  (19047  $\Omega \cdot \text{cm}^2$ ) reached on the surface with DCPD layer after 5 minutes of exposure was 19 - fold higher compared to ground samples at the same exposure. Maximal polarization resistance value  $R_p$  (34972  $\Omega \cdot \text{cm}^2$ ) reached after 1 hour of exposure represented more than 29 times higher value compared to the maximal value of  $R_p$  reached on ground samples. Corrosion process of the samples with DCPD surface layer is different from the corrosion process of ground samples. At the moment of the samples immersion a reaction of DCPD with the corrosive medium (0.9% NaCl, 37 °C) and the formation of corrosion products in places with insufficient DCPD coverage occurred. These two processes resulted in filling imperfections in the DCPD layer thus increasing the polarization resistance  $R_p$ . After 2 hours of exposure there was a decrease in  $R_p$  values (to 16868  $\Omega \cdot \text{cm}^2$ ) caused by a gradual degradation of the surface resulting in local increase of corrosion activity in the weakest DCPD locations. This gradual decrease of  $R_p$  values caused by ongoing DCPD dissolution and more intensive corrosion continued till the end of the immersion test after 168 hours when the minimal value of  $R_p$  was reached (730  $\Omega \cdot \text{cm}^2$ ). Despite of significant loss of DCPD corrosion protection after longer exposure times, the polarization resistance values of the surface with DCPD layer are significantly higher after all exposure times compared to ground surface.

## 5. Conclusions

On the basis of performed experiments, analysis of the results and their interpretations, we came to the following conclusions:

1. Thin calcium phosphate dihydrate (DCPD) coating prepared by potential-controlled electrodeposition process under specified conditions forms the continuous layer composed of irregularly branched flake-like formations of a different size covering the entire surface.
2. The polarization resistance ( $R_p$ ) value of AZ31 samples with DCPD coating (19047  $\Omega \cdot \text{cm}^2$ ) reached after first 5 minutes of exposure in corrosive medium achieves 19-fold higher value compared to that of ground samples (1059  $\Omega \cdot \text{cm}^2$ ) after the same exposure time which represents a relevant improvement of surface layer corrosion protection.
3. Maximum value of  $R_p$  reached on samples with DCPD coating after 1 hour of exposure (34972  $\Omega \cdot \text{cm}^2$ ) is 29 times higher than the maximum  $R_p$  value of the samples with ground surface (1239  $\Omega \cdot \text{cm}^2$ ) recorded also after this exposure time.
4. Prepared DCPD coating provides significant corrosion protection in 0.9% NaCl solution at 37 °C for 4 hours of exposure. Consequently, there is a gradual degradation of the coating and local corrosion processes as evidenced by decrease in polarization resistance values.
5. This surface layer provides higher corrosion resistance of the AZ31 surface layer at all of the selected exposure times when there is still a 3-fold higher value of  $R_p$  measured on samples with DCPD coating compared to ground samples after maximal exposure time 168 hours.

## Acknowledgements

The research is supported by European regional development fund and Slovak state budget by the project: Research centre of the University of Zilina, ITMS 26220220183 and Unique equipment for evaluation of tribological properties of machines parts surfaces, ITMS 26220220048. Authors are grateful for the support of experimental works by project VEGA No. 1/0831/13.

**References**

- [1] DEGARMO, P. E.: *Materials and Processes in Manufacturing*, 5<sup>th</sup> ed., New York: Collin Macmillan, 1979.
- [2] HLAVACOVA, I., PALCEK, P., CHALUPOVA, M., DRESSLEROVA, Z.: *Manufacturing Technology*, 13, 2013, 313-319.
- [3] JANECEK, M., KRAL, R., DOBRON, P., CHMELIK, F., SUPIK, V., HOLLANDER, F.: *Mater. Sci. Eng.: A* 462, 2007, 311-315.
- [4] PASTOREK, F., HADZIMA, B.: *Mater. Eng. - Mater. inz.* 20, 2013, 54-63.
- [5] SARIS, N. E. L.: *Clin. Chim. Acta* 294, 2000, 1-26.
- [6] OKUMA, T.: *Nutrition* 17, 2001, 679-680.
- [7] VORMANN, J.: *Mol. Aspects Med.* 24, 2003, 27-37.
- [8] CZAN, A., SAJGALIK, M., HOLUBJAK, J., KOURIL, K.: *Manufacturing Technology* 13, 2013, 428-431.
- [9] BRONCEK, J., DZIMKO, M., HADZIMA, B., TAKEICHI, Y.: *Acta Metallurgica Slovaca* 20, 2014, 97-104.
- [10] HALAMOVA, M., LIPTAKOVA, T., ALASKARI, A., BOLZONI, F.: *Communications - Scientific Letters of the University of Zilina*, vol. 16, 2014, 78-83.
- [11] HARTWIG, A.: *Mutat Res/Fund Mol Mech Mutagen* 475, 2001, 113-121.
- [12] WITTE, F., KAESE, V., HAFERKAMP, H., SWITZER, E., MEYER-LINDENBERG, A., WIRTH, C. J.: *Biomaterials* 26, 2005, 3557-3563.
- [13] MCBRIDE, E. D.: *J Am Med Assoc* 111, 1938, 2464-2467.
- [14] HADZIMA, B., BUKOVINA, M., DOLEZAL, P.: *Mater. Eng. - Mater. inz.* 17(4), 2010, 14-19.
- [15] BEST, S. M., PORTER, A. E., THIAN, E. S., JUANG, J.: *J. Eur. Ceram. Soc.* 28, 2008, 1319-1327.
- [16] YEN, S. K., KUA, M. C.: *Mater. Sci. Eng. C* 20, 2002, 153-160.
- [17] LIU, D.-M., YANG, Q., TROCZYNSKI, T.: *Biomaterials* 23, 2002, 691-698.
- [18] KANNAN, M. B., WALLIPA, O.: *Mater. Sci. Eng. C* 33, 2013, 675-679.
- [19] ZHANG, J. M., LIN, C. J., FENG, Z. D., TIAN, Z. W.: *J Electroanal Chem* 452, 1998, 235-40.
- [20] SONG, Y., ZHANG, S., LI, J., ZHAO, Ch., ZHANG, X.: *Acta Biomaterialia* 6, 2010, 1736-1742.
- [21] NOVY, F., JANECEK, M., SKORIK, V., MULLER, J., WAGNER, L.: *Int. J. Mater. Res.* 100, 2009, 288-291.

## CORROSION PROPERTIES OF VARIOUS COPPER PIPES JOINTS

*The paper presents the experimental results of various Cu pipes joint corrosion behavior. Joining of copper pipes used for liquid media transport can be made as demountable and fixed joints. The object is to study corrosion resistance of the joints created by soft soldering, hard soldering and fitting. Corrosion properties were investigated by long-term experiment in two identical experimental devices in stagnant and flowing conditions. The experimental environment was water solution of the 3% NaCl, temperature was kept 20° C for 16 hours and 8 hours 80° C per day. In one of the devices for 8 hours the experimental solution was flowing by the input speed 0.27m.s<sup>-1</sup>. In the second one no flow was applied. Evaluation of the joints corrosion attacks was performed visually, by light and scanning electron microscopy.*

**Keywords:** Copper pipes, joints, corrosion, corrosion products.

### 1. Introduction

Copper pipes are mostly used for the distribution of gas and liquid media in a variety of industries. They are used for their excellent corrosion properties and long life [1 - 6]. Due to the differences in device geometry of distribution lines, copper pipes must be bent in certain locations or linked with another circuit. At present mainly three types of joints are used to connect copper pipes. They are the permanent joints made by soft or hard soldering and the demountable joints formed by pressing plastic ring which creates a joint between the copper pipes fixed closed connection (the fitting) [7 and 8]. The joints in copper pipes comprise inhomogeneities which affect, e.g. media flow change, character and sedimentation of corrosion products and thus the degradation process. The main aim of the work was to monitor the synergetic effect of mechanical and chemical stress on corrosion-erosion behavior of the copper pipes joints. The degradation was assessed visually, by light and scanning electron microscopy.

### 2. Experiments

Corrosion behavior of the copper pipes joints was verified by a long-term experiment lasting 11 months. The experimental conditions were chosen to simulate the ones in real distribution. During a day boundary conditions by increasing the temperature and flow of the working medium were set because even their short-term activity can influence the course of corrosion processes.

#### 2.1 Equipment and conditions

For the experiment two identical devices of technical copper (99.5% ± 0.5% Cu) with two types of permanent joints (soft and hard soldering) and one type of demountable molded joint were made. In Fig. 1 the experimental equipment with the marked localities of joints is shown.

Joints were formed under the following conditions:

1. Soft soldering (Fig. 1, area 2, 5, 11) was performed according to DIN 1707 solder L- SnCu3 (DIN EN 29453, S-Sn97Cu3) at 230°C.
2. Hard soldering (Fig. 1, area 4, 6) was performed according to DIN 8513 (EN 1044) using flux and solder CP 203 and L - CuP6 at 730°C.
3. The demountable fitting was created by pressing of Cu pipes with the polymers (Fig. 1, area 3, 9).

Experimental conditions were chosen to simulate operating conditions in practice. The first experimental equipment was filled with the 3% sodium chlorid solution, 16 hours exposed at 20 ± 2 °C without flow of the solution, 8 hours at 80 °C with flow of the solution at the input rate of 0.27 m.s<sup>-1</sup>, caused by an electric motor and observed by a flowmeter. To verify the flow properties in the experimental system the CFD method was used. The method allows quantifying flows and modeling of temperature and flow fields based on Computational Fluid Dynamics - finite volume method [9 - 10]. The second experimental equipment was exposed in the same condition but no flow was applied [11 - 13].

\* <sup>1</sup>Tatiana Liptakova, <sup>1</sup>Monika Halamova, <sup>2</sup>Ayman Alaskari, <sup>1</sup>Martin Lovisek, <sup>3</sup>Maxim Puchnin

<sup>1</sup>Department of Materials Engineering, Faculty of Mechanical Engineering, University of Zilina, Slovakia

<sup>2</sup>Department of Mechanical Production Technology, College of Technological Studies, Shuwaikh, Kuwait

<sup>3</sup>Department of Materials Engineering, Faculty of Mechanical Engineering, Czech Technical University in Prague, Czech Republic

E-mail: tatiana.liptakova@fstroj.uniza.sk

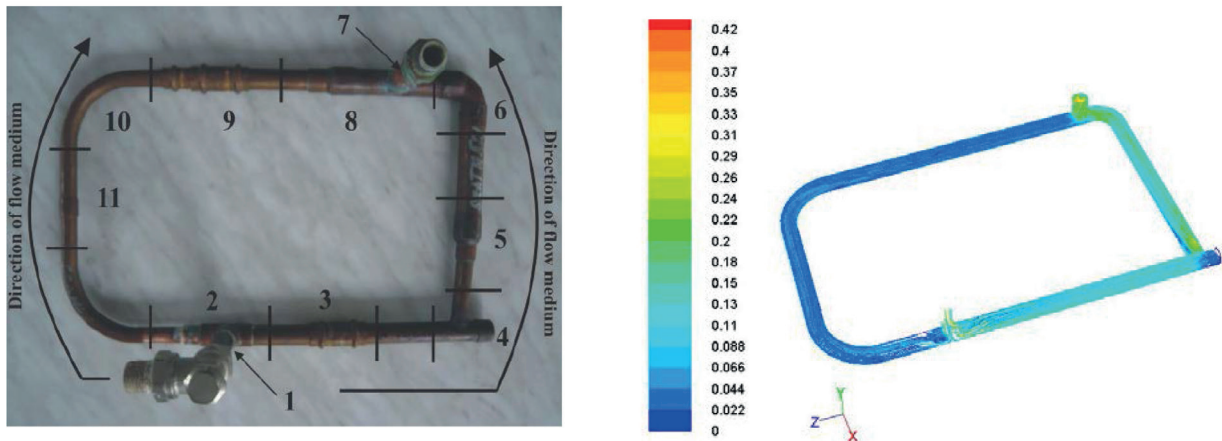


Fig. 1 Experimental equipment and flow conditions

### 3. Results

After 11 months of exposure the samples were taken off, incised to be possible to assess corrosion attack of the monitored joints in stagnant and flow conditions. Assessment of the different joints after exposure was made visually, by light and scan electron microscopy.

#### 3.2 Hard soldering joints

Corrosion attack in the localities of the joint is the same as the one of Cu pipes. In stagnant conditions the corrosion products were black-grey. According to the Pourbaix diagram

corrosion products in aqua environment are (in the potential range from -0.15V to +0.521V) formed by  $\text{CuO}$  ( $\text{Cu}^{2+}$ ) which are black and complex compounds  $\text{CuCl}_2 \cdot 3\text{Cu}(\text{OH})_2$ . Higher temperature ( $80^\circ\text{C}$ ) does not influence the character of corrosion products but their formation is shifted to more acid area (lower value of pH). When the solution is flowing, the character of corrosion products is changed by hydrolysis to greenish color (presence of  $\text{CuCl}$  and  $\text{CuCl}^{(+)}$ ) as shown in Fig. 2. These corrosion products have pure adherence and by flow they are torn off from the metal surface especially on the top of the pipe. No differences of corrosion product character between Cu pipe and the locality of hard soldering joints are observed. In Fig. 2b, the start of intergranular corrosion on the joint and Cu pipe boundary was observed. In flow conditions the surface roughness

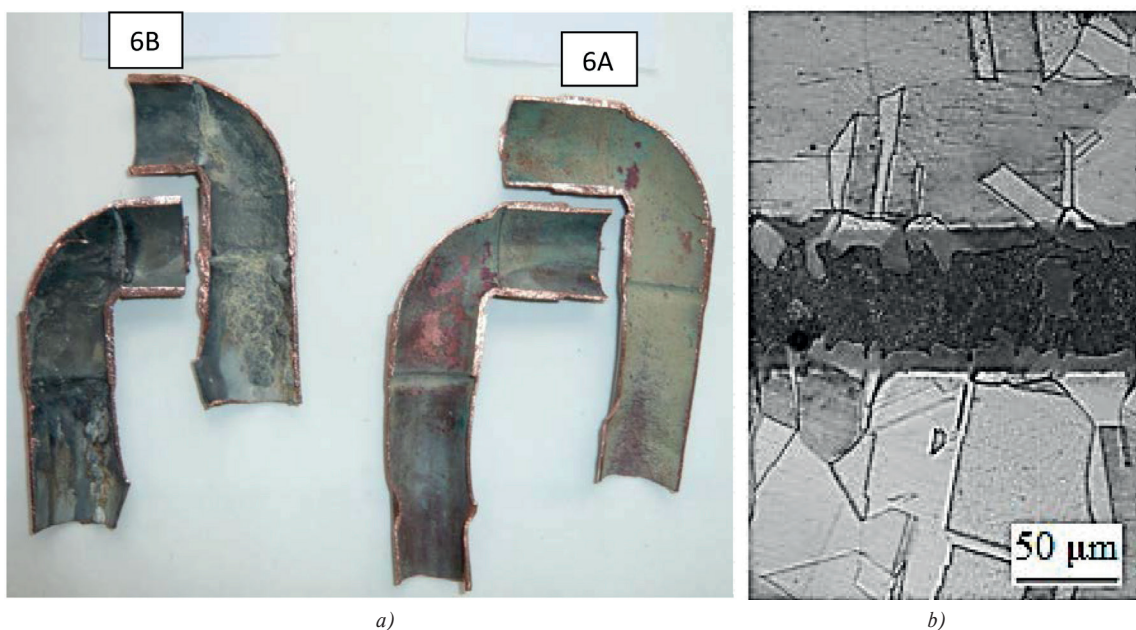


Fig. 2 Character of corrosion in the locality with hard soldering joints 6B - no flow and 6A flow conditions a), and detail joint microstructure b)

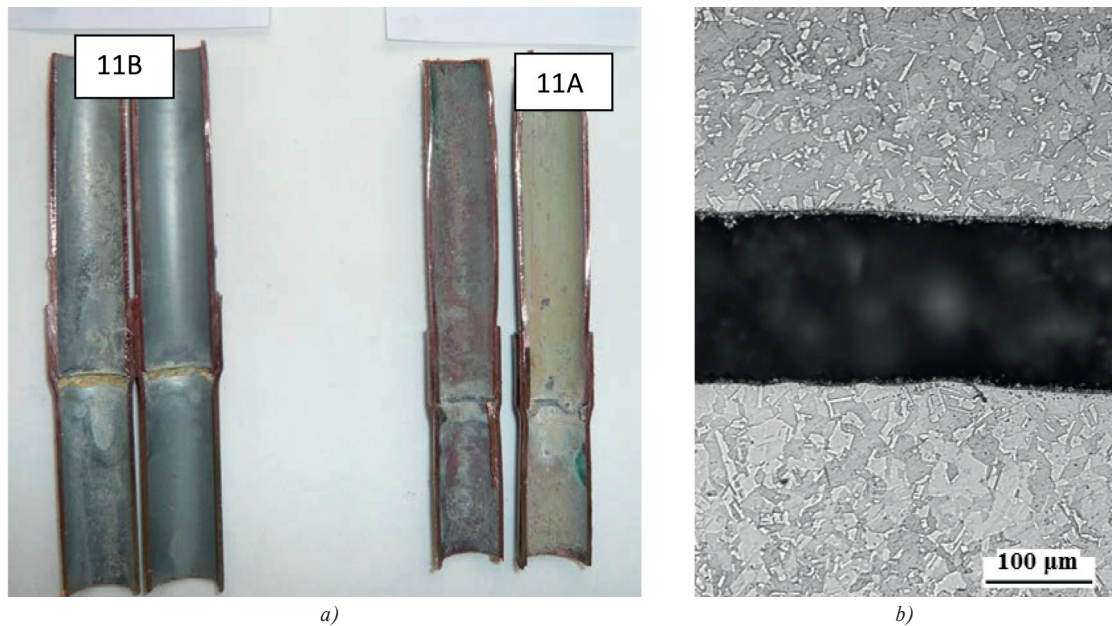


Fig. 3 Character of corrosion in the locality with hard soldering joints 6B - no flow and 6A flow conditions a), and detailed joint microstructure b)

of the joint can change the flow character and increase its effect on damage of Cu pipe system by corrosion-erosion (Fig. 2a, 6A).

### 3.3 Soft soldering joints

The joints created by soft soldering differ from Cu pipe by chemical composition of solder (97% tin Sn). Metallography

of the soldering joint and corrosion attack in flow and no flow conditions is shown in Fig. 3a.

The Sn solder has quite good corrosion resistance. In corrosion environment (scale pH 3.5 - 9) the stable oxides SnO and SnO<sub>2</sub> are created on the surface and feature protection character. The Sn solder creates with Cu pipe a local galvanic cell in the electrolyte and Sn behaves as an anode. After the experiment the local corrosion was determined in the Sn joints in stagnant and flowing conditions. Local corrosion was evoked by

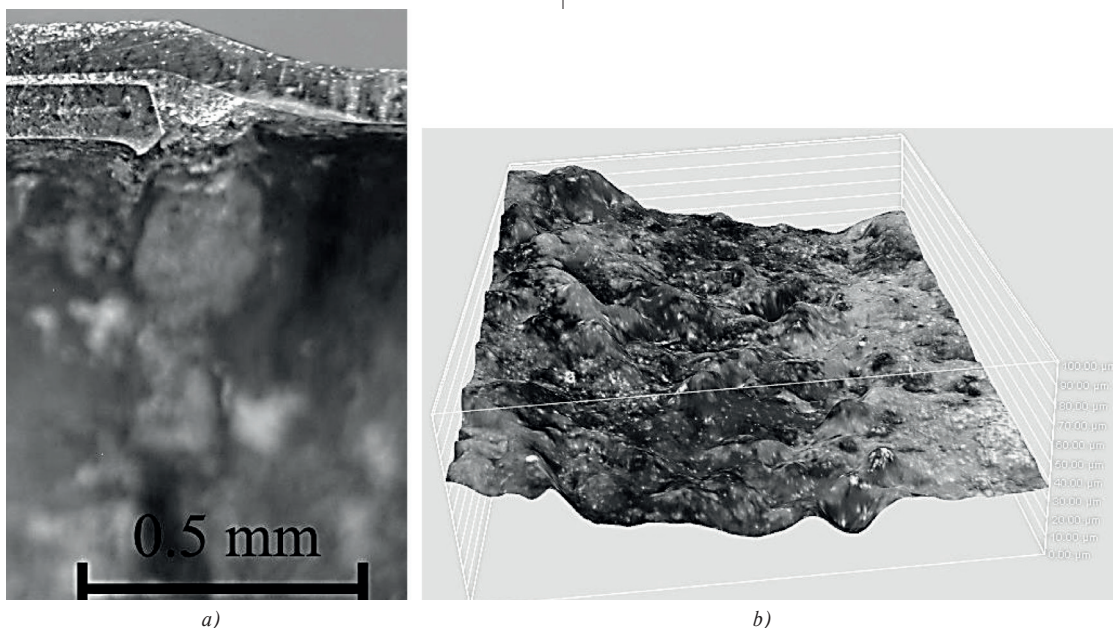


Fig. 4 Corrosion pits on the Sn joint a) and 3-dimensional surface of Sn with visible pits b)

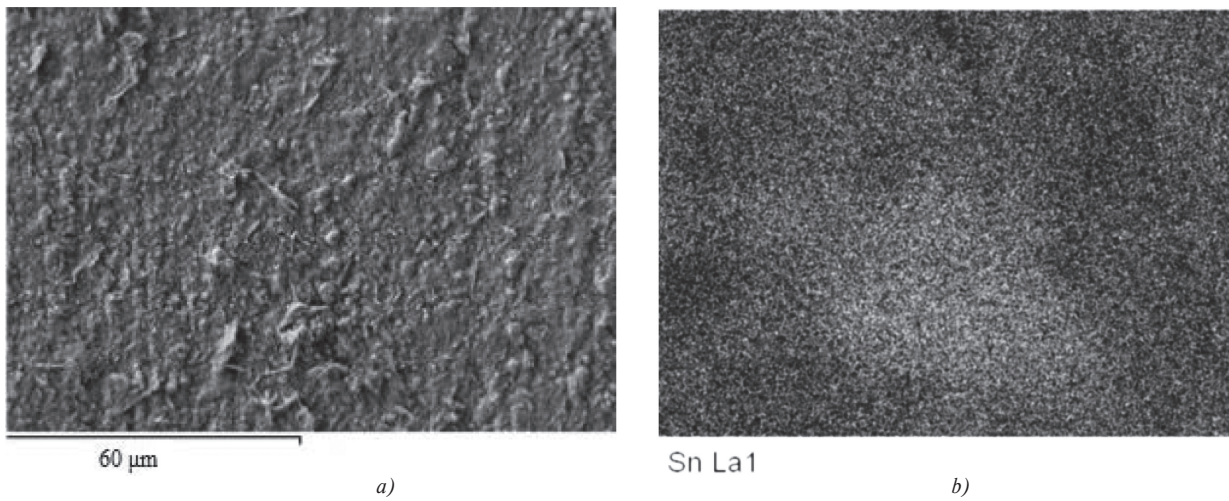


Fig 5. Corrosion products on Cu pipe near Sn joint in stagnant conditions a) and the map of Sn distribution on the surface b)

chloride ions presentation and influenced by higher temperature. Metallography of corrosion attack of the Sn solder and its morphology are in Fig. 4 (a, b).

Intensive corrosion of Sn solder was confirmed by EDX analysis of its corrosion products. The Sn corrosion products diffuse to the electrolyte and they are accumulated in the bottom of Cu pipe. In Fig. 5 the character of corrosion products made by SEM near Sn joint can be seen (a) and a map of Sn distribution (light points) in stagnant solution (b). In Fig 6 the character of corrosion products is compared with Sn distribution from identical place but in flowing solution. Sn corrosion products are more scattered by flow influence and mixed with Cu corrosion products. It is proved by the EDX analysis of corrosion products in no flowing and flowing conditions in the identical places.

In Table 1 chemical composition of corrosion products in stagnant and flow conditions is specified.

Chemical composition of corrosion products in stagnant and flow condition

Table 1

Element	Stagnant conditions		Flow conditions	
	Weight %	Atom. %	Weight %	Atom. %
<b>O</b>	8.7	31.65	65.63	88.87
<b>Cl</b>	0.56	0.91	1.82	1.11
<b>Cu</b>	57.67	49.85	25.74	8.78
<b>Sn</b>	36.03	17.59	6.8	1.24

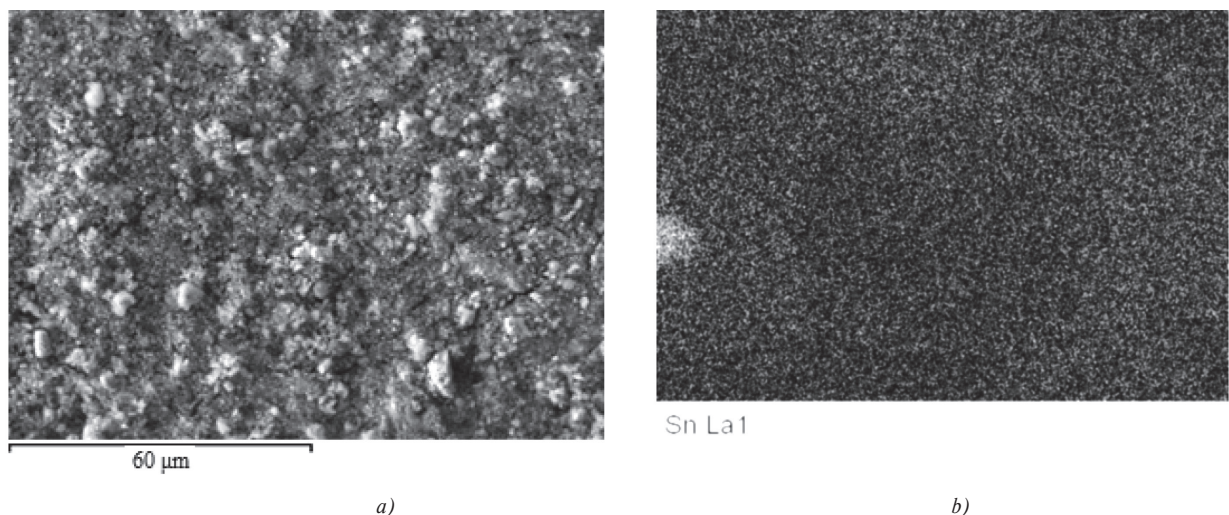


Fig 6. Corrosion products on Cu pipe near Sn joint in flow conditions a) and the map of Sn distribution on the surface b)

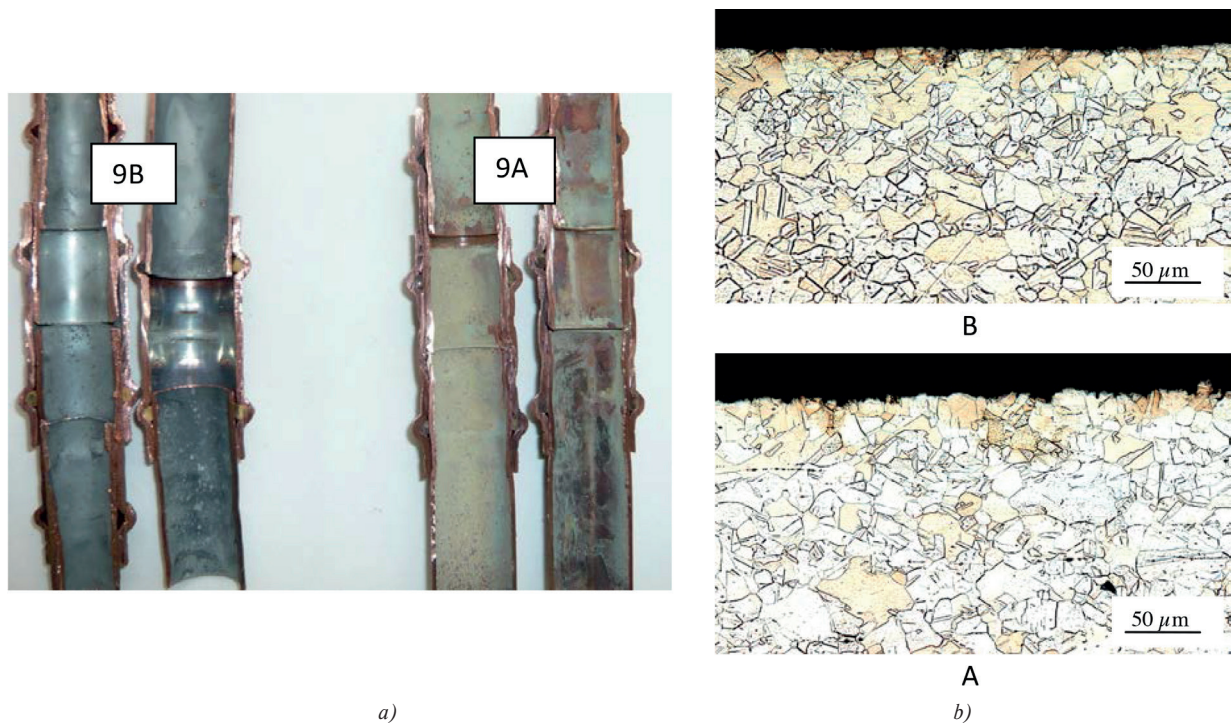


Fig. 7 Localities of fitting in stagnant 9B and flow conditions 9A a) and microstructure of corrosion attack (b)

### 3.4 Fitting

The demountable joint – fitting was constructed at normal room temperature by pressing of Cu pipes with polymer. In this way a very good sealing joint was created without any intermediate film. As it can be seen in Fig. 7a, fitting did not affect character of the Cu corrosion products in stagnant and flow conditions. In the joint locality of Cu pipes no corrosion attack was observed. In moving solution only joint protrusions can slightly change the linear flow. In Fig. 7b the character and intensity of Cu pipe corrosion in stagnant (B) and flow conditions (A) are presented.

### 4. Conclusions

**With regard on the obtained results share can be stated:**

#### Conclusions

- Joints molded by hard soldering were not attacked more intensively than basic material - technical copper. The joint forms in the pipe system crevices and stagnation of operating medium in these crevices creates conditions for corrosion attack. Geometry of crevices can also cause changes in lamellar flowing of operating solution and so it can increase its mechanical effect. The loss of stability of protective cuprous oxide layer due to the hydrolysis and corrosion-

erosion impact is the main cause of faster damage of copper in flow environment.

- Tin joints are attacked by pitting corrosion in medium containing chlorides. The intensity of corrosion damage is not very dangerous for actual dimensions of joint and their stability is not endangered. The empty places originated by inappropriate soldering are more dangerous for safety of the joint. The solid particles of the Sn corrosion products increase the erosion effect in flow conditions.
- Demountable joints formed by pressing plastic rings with polymer material tighten excellently even in aggressive 3% NaCl solution in stagnant and flowing conditions too. The joints create only a little mechanical barrier for flowing medium in Cu pipe system. The hidden areas in the joint locality were in untouched state without any sign of corrosion or in-leak between joined pipes.

#### Acknowledgements

The research was supported by European regional development fund and Slovak state budget by the project “Research center of University of Zilina”, ITMS 26220220183. The authors thank for their support.

**References**

- [1] SRIVASTAVA, A., BALASUBRAMANIAM, R.: Microstructural Characterization of Copper Corrosion in Aqueous and Soil Environments, *Materials Characterization*, vol. 55, No. 2, August 2005, 127-135.
- [2] JANECEK, M., HADZIMA, B., HELLMIG, R.J., ESTRIN, Y.: The Influence of Microstructure on the Corrosion Properties of Cu Polycrystals Prepared by ECAP. *Kovove mater.*, 43 (4), 2005, 258 p.
- [3] HADZIMA, B., JANECEK, M., KUTNYAKOVA, Y., HELLMIG, R. J., ESTRIN, Y.: Microstructure and Corrosion behaviour of Ultrafine-grained Copper, *Mater. Sci. Forum*, vols. 503-504, 2006, 883-888.
- [4] NAVRATILOVA, L., KUNZ, L., NOVY, F., MINTACH, R.: Development of Cyclic Slip Bands in UFG Copper in Gigacycle Fatigue, *Acta Metallurgica Slovaca*, vol. 19, No. 2, 2013, 88-93.
- [5] MERKEL, T. H., GROSS, H. J., WERNER, W., DAHLKE, T., REICHERTER, S., BEUCHLE, G., EBERLE, S. H.: *Water Research*, 36, 2001, 1547-1555.
- [6] SANDBERG, J., ODNEVALL WALLINDER, I., LEYGRAF, C., LE BOZEC, N.: *Corr. Sci.*, 48, 2006, 4316-4338.
- [7] LEZDIK, V., SOBOTA, M., BEZAK, J.: *Welding in Gas Industry (in Slovak)*, EDIS: University of Zilina, 2001.
- [8] BOSCO, N. S., ZOK, F.V.: Strength of Joints Produced by Transient Liquid Phase Bonding in the Cu-Sn System, *Acta Materialia* 53, 2005, 2019-2027.
- [9] LENHARD, R., JAKUBSKY, M., MALCHO, M., JANDACKA, J.: Analysis of Transmission Phenomena in Low-potential Heat Transport by Heat Pipes in the Deep-borehole Simulator, *Communications - Scientific Letters of the University of Zilina*, vol. 14, No. 3, 2012, 10-16.
- [10] KAPJOR, A., MALCHO, M., JANDACKA, J., HUZVAR, J., GRESAK, T.: Optimization of Construction Parameters of a Flow Convector, *Communications - Scientific Letters of the University of Zilina*, vol. 14, No. 4a, 2012, 36-41.
- [11] BABOIAN, R. et al.: *Corrosion Test and Standards: Application and Interpretation*. ASTM Manual Series, Philadelphia: PA 19103, 1995.
- [12] ASM Handbook: *Corrosion*, vol. 13, The Material Information Society, 4<sup>th</sup> Printing, 1992.
- [13] LIPTAKOVA, T., FAJNOR, P., DODEK, A.: Evaluation of the Flow Accelerated Corrosion of Copper Pipes, *Materials Engineering = Materialove inzinierstvo*, vol. 17, No. 4, 2010.

Jaroslav Dubec - Miroslav Neslusan - Anna Micietova - Maria Cillikova \*

## INFLUENCE OF TOOL-WORKPIECE INTERFACE ON SURFACE INTEGRITY AFTER TURNING

*This paper deals with influence of flank wear on decomposition of cutting force in turning roll bearing steel. The decomposition is carried out to evaluate the components of cutting force in the tool-chip as well as tool-workpiece interface. The decomposition enables evaluation of the shear and normal forces in the both interfaces. The results of experiments and the following calculations show that while conditions for chip separation in the tool-chip interface stay nearly untouched due to progressive development of flank wear, mechanical load of machined surface associated with components of cutting forces progressively increases with flank wear. The paper also reports about influence of flank wear on surface integrity expressed in such parameters as residual stresses, surface topography, structure transformation and microhardness.*

**Keywords:** Cutting force, decomposition, flank wear, turning, surface integrity.

### 1. Introduction and theoretical background

Surface integrity can be expressed in a variety of parameters and features. Machined surface is a product of tool-workpiece interface. Due to a certain radius of cutting edge a certain volume of material undergoes the cutting edge. Thickness of the layer undergoing the cutting edge depends mainly on the cutting edge radius and this layer is well known as a minimum chip thickness. This layer can be reported as a minimum cutting depth needed for chip separation [1]. Surface integrity in turning expressed in terms of surface roughness depends mainly on the tool geometry and cutting conditions (mainly feed). On the other hand, surface integrity expressed in such terms as residual stresses, structure and hardness alteration depends mainly on mechanical and thermal load of machined surface in tool-workpiece interface. Flank wear (VB) takes the significant role since it remarkably affects tool-workpiece interface. Flank wear progressively increases within the cutting time and undergoing material is exposed to the high mechanical and thermal load. While mechanical alteration affects mainly the near-surface region, thermal load can penetrate deeply beneath the surface as the flank wear is progressively developed.

Many studies were reported about influence of flank wear on surface integrity expressed in such terms as stress state, microhardness profile and structure [2, 3 and 4]. As it was mentioned, these aspects of surface integrity are affected mainly by mechanical and thermal load. On the other hand, it should be also pointed that heat and temperature are only the different

features associated with the energy consumption derived from forces needed for cutting process. Being so, information about components of cutting force attributed to the pure tool-workpiece interface is essential for analysis of surface integrity. It is well known that decomposition of cutting force can be carried out in a variety of models. Conventional decomposition provided by Merchant [5] ignores existence of cutting edge radius or flank wear. Decomposition of cutting force is associated with pure processes needed for chip separation in the tool-chip interface.

When the cutting edge radius or flank wear are considered, decomposition of cutting force is considered as the decoupling of two basic components. First one is attributed to the tool rake and corresponds with chip separation while the second component is associated with the tool-workpiece interface as Fig. 1 depicts.  $F_\gamma$  component is associated with the energy needed for chip separation in the tool-chip interface while  $F_\alpha$  is component affecting mainly quality of machined surface. Cutting force can be then expressed as follows:

$$\bar{F} = \bar{F}_\gamma + \bar{F}_\alpha \quad (N) \quad (1)$$

Decomposition of cutting force, in relation to tool wear and cutting edge rounding, was discussed by many authors [6 - 8]. It was found that flank wear (VB) affects produced surface integrity expressed in a variety of features such as stress state, surface roughness, microhardness and structure as well as topography of machined surface [3, 4, 9 - 11].

\* Jaroslav Dubec, Miroslav Neslusan, Anna Micietova, Maria Cillikova

Department of Machining and Manufacturing Engineering, University of Zilina, Faculty of Mechanical Engineering, Slovakia

E-mail: jaroslav.dubec@fstroj.uniza.sk

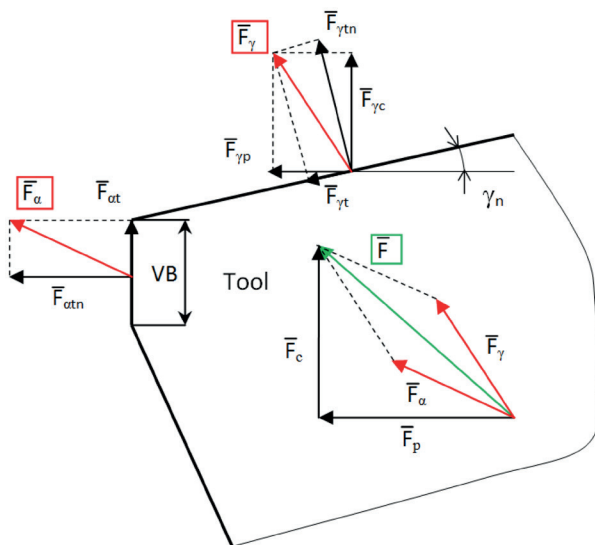


Fig. 1 Decomposition of cutting force in relation to tool wear [1]

For this reason this paper reports about experimental technique for decomposition of cutting force associated with equation (1). The paper is focused on the turning of bearing steel with cutting insert of variable flank wear (see Fig. 2) to discuss why the cutting force is increasing with the progressive flank wear  $VB$  and how the components  $F_y$  and  $F_\alpha$  contribute to cutting force increase.

**2. Experimental conditions**

Experiments were conducted on annealed bearing steel 100Cr6 by the use of cutting insert SNMG 120408E-M ( $\alpha_o = 9^\circ$ ,  $\gamma_o = -6^\circ$ ,  $r_n = 80 \mu\text{m}$ ). Components of cutting force were measured by KISTLER 9265B dynamometer (lathe SUI 40) under the following cutting conditions:

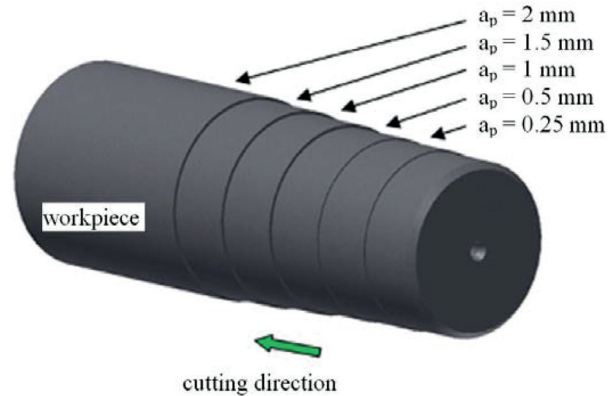


Fig. 3 Workpiece of variable cutting depth adapted for measurement

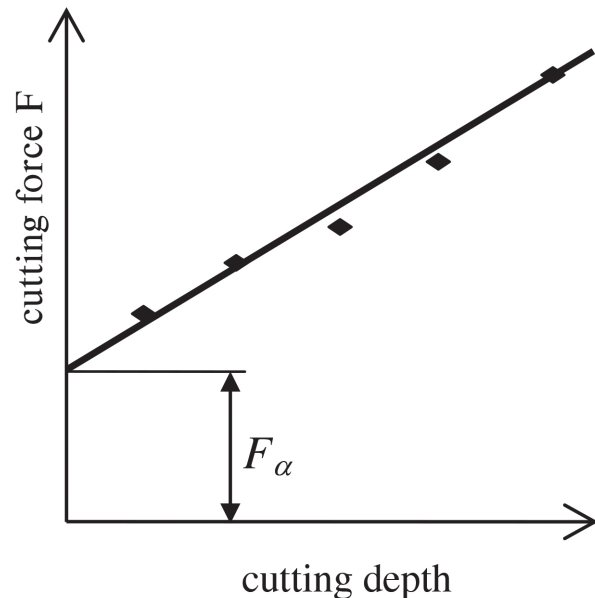


Fig. 4 Graphical illustration of  $F_\alpha$  evaluation

f (mm)	$v_c$ (m.min <sup>-1</sup> )	$a_{p1}$ (mm)	$a_{p2}$ (mm)	$a_{p3}$ (mm)	$a_{p4}$ (mm)	$a_{p5}$ (mm)
0.09	100	0.25	0.5	1	1.5	2
VB <sub>1</sub> = 0.2 mm		VB <sub>2</sub> = 0.5 mm		VB <sub>3</sub> = 0.65 mm		VB <sub>4</sub> = 0.9 mm

Fig. 2 Cutting insert of the different  $VB$  applied for cutting test, microscope AxioCam ER c5c

To analyze the influence of flank wear  $VB$  on  $F_y$  and  $F_a$  components inserts of variable  $VB$  were prepared during the preliminary turning, see Fig. 2. Workpieces illustrated in Fig. 3 were pre-prepared to obtain the variable cutting depth and to analyze relation between the measured components and cutting depth. Separation of  $F_a$  component is based on calculation of trend line as a relationship between measured cutting force components and the corresponding cutting depths.  $F_a$  can be found as a point on the trend line in position where cutting depth is equal to zero, see Fig. 4. Residual stresses were measured by mechanical method based on electrolytic etching of a machined surface (home made system). Vickers microhardness measurement was conducted by Hanneman 300 micro-hardness tester by applying force 300 N for 10 seconds.

### 3. Results of experiments

Figure 5 shows the relationship where  $F_p$  and  $F_c$  are plotted against the different cutting depths and flank wears. Figures 5, 6 and 7 also show that flank wear affects mainly thrust force component  $F_p$  since the thrust force component is mostly attributed to the processes in tool-workpiece interface while only the moderate increase of  $F_c$  component is mostly associated with chip separation in the tool-chip interface.

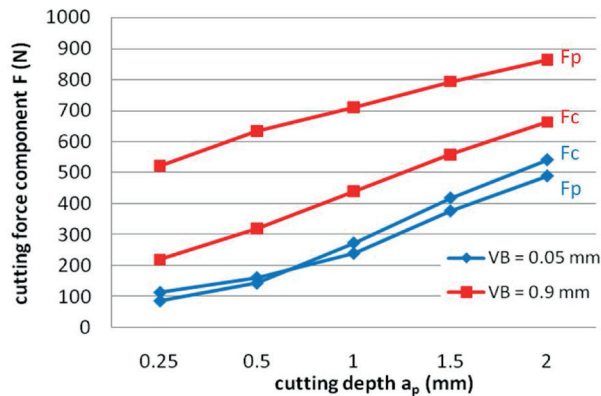


Fig. 5 Influence of  $a_p$  on components of cutting force,  $VB = 0.05\text{ mm}$  - sharp insert,  $VB = 0.9\text{ mm}$

Being so, increasing area of flank wear contributes mainly to the more pronounced increase of thrust force. It should be also mentioned that except for flank wear which is progressively increasing within the cutting time, tool wear in form of a crater is also developed on the rake face of the insert. However, the crater alters mainly the rake angle of the insert when initial negative geometry (negative rake angle for sharp insert) becomes more positive along with increasing flank wear  $VB$ . Results of force measurements indicate that the effect of flank wear dominates

over the effect of crater developed on the rake of the insert since cutting force components progressively increase.

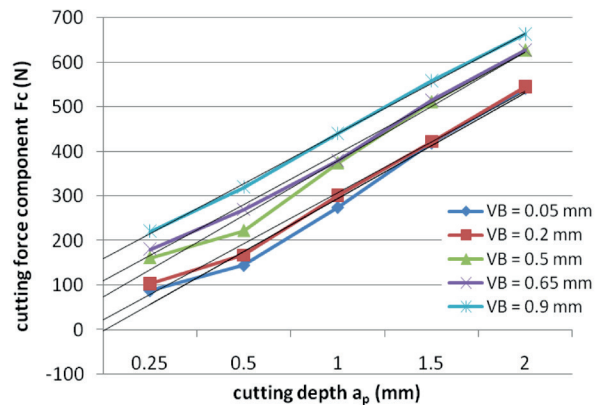


Fig. 6 Influence of cutting depth and flank wear on  $F_c$

Results of decomposition, based on evaluation of intersection points (in position when cutting depth is equal to zero), enable evaluation of components associated with the tool-chip as well as tool-workpiece interface (and the corresponding shear and normal components). Figure 8a depicts that  $F_y$  depends mainly on cutting depth and the corresponding removal rates.

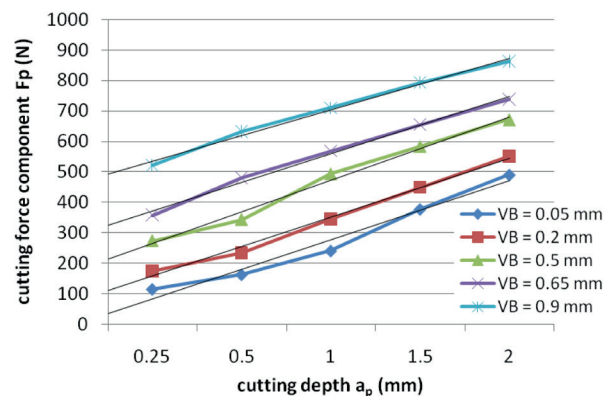


Fig. 7 Influence of cutting depth and flank wear on thrust force  $F_p$

On the other hand, this component stays nearly untouched when flank wear is progressively developed. In other words, flank wear does not contribute to the processes of chip separation in the tool-chip interface and affects mainly mechanical load of surface produced in the tool-workpiece interface. Figure 8b illustrates that  $F_a$  stays nearly untouched at the different cutting depths but abruptly increases with flank wear  $VB$ .

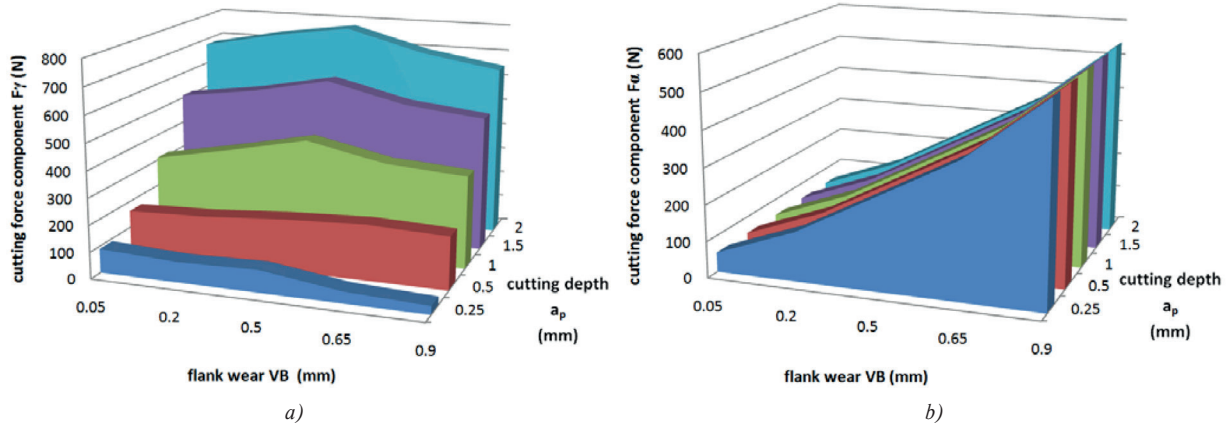


Fig. 8 Influence of tool wear and cutting depth on a)  $F_y$  - face, b)  $F_a$  - flank

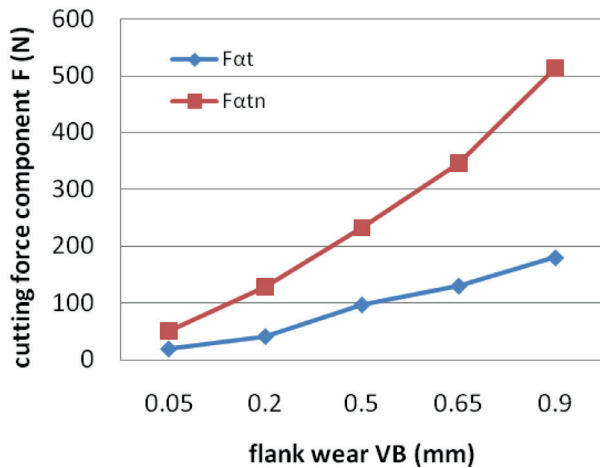


Fig. 9 Influence of flank wear on  $F_{at}$  and  $F_{atn}$  ( $F_{at}$  extracted from Fig. 6 and  $F_{atn}$  extracted from Fig. 7 as the values at zero cutting depth)

Figure 9 shows that normal force component in the tool-workpiece interface dominates over the shear component in correspondence with more pronounced increase of thrust force along with increasing flank wear  $VB$ .

#### 4. Surface integrity

This chapter discusses influence of flank wear on surface integrity expressed in many terms. Tool wear changes dimension and shape of a cutting edge. For this reason, temperature and stress distribution ahead a cutting edge is transformed, which in turns corresponds with variable mechanical and thermal load of a machined surface as well as the appearance of a separated chip. While processes of chip separation are mainly affected by progressive transformations of tool geometry on the tool rake, processes in the tool-workpiece interface affect mainly surface integrity.

It is commonly accepted that mechanical and thermal loads are closely connected since the energy consumption needed for cutting process is converted into heat. Total heat generated in the cutting zone can be expressed as follows:

$$Q = F_c \cdot v_c \quad (\text{J} \cdot \text{min}^{-1}) \quad (2)$$

As it was reported, cutting force can be decoupled as the component needed for chip separation  $F_y$  and the component associated with chip-tool interface  $F_a$ . The average mechanical load of machined surface can be expressed via  $F_{at}$  and  $F_{atn}$  components. On the other hand, a certain idea about thermal load on machined surface can be obtained when the heat generated in the tool-workpiece interface is calculated as follows:

$$Q_j = F_{at} \cdot v_c \quad (\text{J} \cdot \text{min}^{-1}) \quad (3)$$

Thus increasing  $F_{at}$  component directly corresponds with the heat generated in the tool-workpiece interface which in turn corresponds with elevated temperatures when the flank wear  $VB$  is more developed.

It is well known that residual stresses are induced by cutting process. Compressive stresses are obtained when mechanical load dominates whereas elevated temperatures in the tool-workpiece interface cause tensile stresses. It is also well known that machined surface usually undergoes severe plastic deformation as well as intensive thermal load. Being so, when no structure transformation occurs, residual stress state of machined surface is a mixture of both effects. Figure 10 illustrates distribution of residual stresses beneath the surface. Compressive stresses dominate in the near-surface region after turning. This surface layer undergoes the severe plastic deformation due to a certain cutting edge radius as well as flank wear. Figure 10 also shows that the compressive stresses in the near-surface region increases along with flank wear -160 MPa can be found after turning with the sharp cutting insert. When the flank wear  $VB$  becomes more developed the maximum of compressive stresses increases in

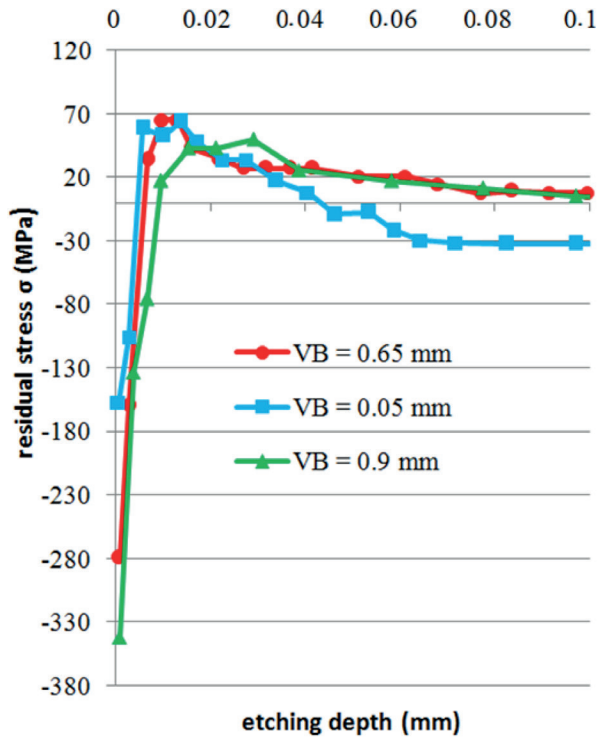
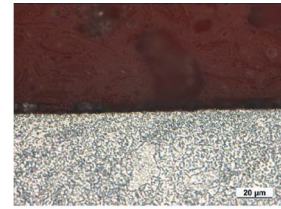


Fig. 10 Depth profile of residual stresses obtained after turning with insert of variable VB

correspondence with increasing  $F_{at}$  and  $F_{atn}$  components (-280 MPa was obtained for  $VB = 0.65$  mm and -345 MPa for  $VB = 0.9$  mm). Figure 10 also shows that thickness of near-surface region containing compressive stresses increases when the flank wear  $VB$  is developed. Furthermore, Fig. 10 illustrates the differences in the stress state in the sub-surface region. Sub-surface layers contain tensile stresses of nearly the same magnitude. On the other hand, tensile stresses extend deeper beneath the surface



a) sharp tool,  $VB = 0.05$  mm



b)  $VB = 0.65$  mm

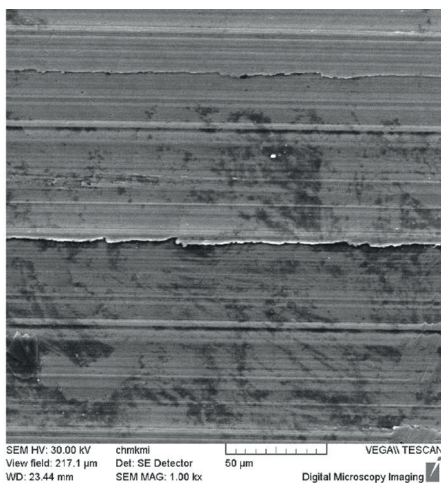


c)  $VB = 0.9$  mm

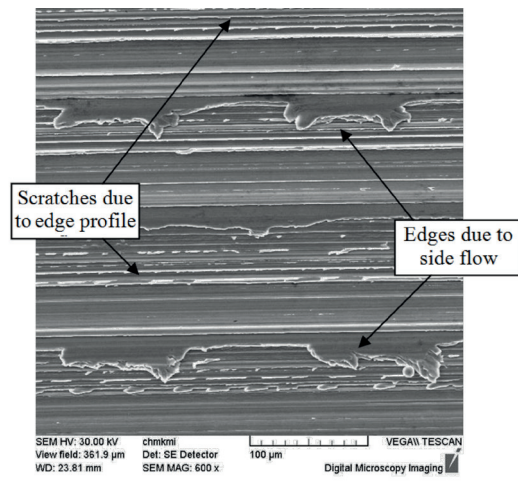
Fig. 11 Micrographs of machined surface, optical microscopy, cross sections

at high flank wear than those obtained for low  $VB$ . Thickness of thermally affected zone for higher  $VB$  (where tensile stresses dominate) exhibits twofold increase in thickness than that produced by sharp insert.

Observation of surfaces obtained for all  $VB$  reveals that structure alterations occur as soon as  $VB$  exceeds 0.5 mm, see Fig. 11. While significant texture with very thin and discontinuous



a) sharp tool,  $VB = 0.05$  mm



b)  $VB = 0.65$  mm

Fig. 12 Micrographs of machined surface, REM

transformed layer can be found on the surface produced with insert of  $VB = 0.65$  mm (Fig. 11b), more pronounced structure transformation occurs when flank wear reaches 0.9 mm (Fig. 11c). Surface texturing is associated with intensification of plastic deformation of undergoing layer together with longer time interval within the produced surface is exposed to severe plastic deformation at elevated temperatures. It was previously discussed [4] that cutting forces and temperature in the cutting zone gradually increase up to the  $VB = 0.65$  mm with a certain fall when visible structure transformations on the produced surface can be observed ( $VB = 0.9$  mm).

Intensity and character of plastic deformation during chip separation can be also evidenced by topography of produced surface as Fig. 12 depicts. Machined surface is quite smooth with the typical pattern produced by turning at low flank wear, see Fig. 12a. On the other hand, intensive side flow during severe plastic deformation in the tool-workpiece interface results in formation of the edges on the machined surface as Fig. 12b illustrates. Moreover, the furrowed profile of abraded cutting edge produces surface with many scratches since a cutting edge profiles copies on machined surface. Thus flank wear strongly affects surface roughness of machined surface.

Hardness of steels is explained in concept of high dislocation density as the carbide precipitation takes minor role. Being so, measured microhardness profiles correlate with microstructure observations and considered density of dislocation cells.

While moderate increase of surface microhardness is attributed to the surfaces without visible structure transformations

(about 400 HVm for near-surface region, bulk microhardness is 300 HVm), steep increase of the near surface hardness (685 HVm) correlates with hardened structure undergoing the severe plastic deformation and containing the high dislocation density.

## 5. Conclusions and final comments

Additional investigations [9] show that deformations after heat treatment depend on surface integrity and the corresponding flank wear  $VB$ . Being so, detailed understanding of these aspects can help us to suppress these deformations and reduce the corresponding stocks, time and cost savings as a significant aspects of improvements in production [12]. Roll bearings are usually heat treated to produce the surface of high hardness and the corresponding wear and fatigue resistance. Despite the surface produced before heat treatment is removed after heat treatment by the following grinding of hard turning, surface integrity expressed in many terms (mainly stress state, microhardness and structure) strongly affects deformation of parts (especially of parts made of thin wall or expressed in other words the parts of high wall thickness to diameter ratios).

## Acknowledgement

This article was edited under the financial support of VEGA project No. 1/0223/11 and 1/0097/12.

## References

- [1] NESLUSAN, M., CILLIKOVA, M.: *Cutting Theory*, EDIS: University of Zilina, 2007
- [2] BRANDT, D.: *Randzonenbeeinflussung beim Hartdrehen*, Dissertation, Hannover, 1995
- [3] WANG, J.Y., LIU, C.R.: *The effect of Tool Flank Wear on the Heat Transfer, Thermal Damage and Cutting Mechanics in Finishing Hard Turning*, CIRP Annals 48/1/1999
- [4] DUBEC, J., NESLUSAN, M.: Multiparametric Analysis of Surface after Turning through Barkhausen Noise in Relation to Tool Wear, *MM Science J.*, July 2012,
- [5] MERCHANT, M. E.: Mechanics of the Metal Cutting Process, *J. of Applied Physics*, 16/1945
- [6] BENO, J.: *Theory of Metal Cutting*, Kosice: Vienala, 1999
- [7] ENDRES, W. J., DEVOOR, R. E., KAPOOR, S. G.: *Dual Mechanism Approach to the Prediction of Machining Forces*. *J. of engineering for industry*, ASME, 1995
- [8] EE, K. C., BALAJI, A. K., LI, P. X., JAWAHIR, I. S.: *Force Decomposition Model for Tool-Wear in Turning with Grooved Cutting Tools*, *Wear*, 249/2001
- [9] DUBEC, J., NESLUSAN, M., CILLIKOVA, M., MICIETOVA, A.: *Magnetic Evaluation of Residual Stresses and Structure Transformations Induced in Soft Steel after Turning*, Nanomaterials and nanotechnology meeting, 1/2013
- [10] KARPUSCHEWSKI, B., SCHMIDT, K., PRILUKOVA, J., BENO, J., MANKOVA, I., HIEU, N. T.: Influence of Tool Edge Preparation on Performance of Ceramic Tool Inserts when Hard Turning, *J. of Materials Processing Technology*, 213, 2013, 1978-1988
- [11] CZAN, A., TILLOVA, E., SEMCER, J., PILC, J.: Surface and Subsurface Residual Stresses after Machining and their Analysis by s-ray Diffraction, *Communications - Scientific Letters of the University of Zilina*, No. 2, 2013, ISSN 1335-4205
- [12] MICIETA, B., STOLLMANN, V.: *Design and Improvement of Production Processes*, DAAAM Intern. Scientific Book 2009, ISSN 1726-9687, ISBN 978-3-901509-69-8.

Luboslav Dulina - Miroslava Bartanusova \*

---

## ERGONOMICS IN PRACTICE AND ITS INFLUENCE ON EMPLOYEES' PERFORMANCE

*The article deals with the human performance and the factors that affect job performance. During the performance of work a person is exposed to risk factors which to some extent adversely affect his health. It is necessary to note that two views of the position of man in the process currently prevail in the company. The first one, promoted by particular employers, puts the emphasis on performance increase of workers and productivity growth. The second one view is supported by employees and emphasizes the need for safety of a man and health at work. The aim of ergonomics is currently referred to harmonise these views.*

**Keywords:** Workload, performance, work performance, performance curve.

### 1. Introduction

Work is an essential and, therefore, the dominant activity in the life of every person. An employer has to create the optimal working conditions for an employee to be able to use their performance-related capacity fully. The results which the keeping of the ergonomic rules in an enterprise brings can be divided into the economic ones, important for the employer and the health keeping ones, important for the employee. A man spends an essential part of their life in a work activity which has formed them during the whole evolution. Therefore, we cannot overlook work activity and its effect on a person because it has progressive importance in human development and it is the factor of mental and physical functions improvement [1 and 2].

More and more difficult combination of the relationship between a man, a working means and an object of work has been culminating recently. Human working activity has been expanding but, at the same time, the working conditions and the demands on a workman have been changing. Nowadays the development of science and technology extends into the structure of productive forces of society. It also influences the relation of a human being to work and their working conditions and thus affects their lifestyle. The demands on development of motor abilities and experience have been decreasing; the importance of sensory experience, theoretical and intellectual knowledge has been increasing. The changes in human behaviour are arising as a consequence. These are the changes of a technical character which influence the working environment as well as the changes

in human behaviour. The changes may occur in positive or negative reactions influencing the satisfaction rate, the level of the spent effort and health risks for workmen while performing [3].

### 2. Current problems in ergonomics

The problems which are related to their influence on the employee emerge simultaneously with the changes of working conditions. Each change in working and technological procedures leads to the changes in work conditions and demands imposed on a person. In most cases we do not pay much attention to these consequences to the employees. We are only interested in them when they have an accident, illness or a negative influence on the employee is visible.

Often there is a conflict of opinions as to the means of production affect humans. On the one hand it can be argued that they facilitate working, on the other hand, may adversely affect the employee performing work [4 and 5]. Also, you can still watch the signs of factors unfavourable for working conditions, such as air pollution, improper spatial solution of workplaces, chemical pollutants, and stressful situations and so on.

It is appropriate to think about the fact that technical progress, which should serve man, often turns against them. The progress of science and technology often facilitates the work of staff outside the work activities but sometimes it is at the cost of human health. It is not only about the damage to health of the employee being influenced by risk factors, such as occupational

---

\* Luboslav Dulina, Miroslava Bartanusova  
Department of Industrial Engineering, Mechanical Faculty, University of Zilina, Slovakia  
E-mail: luboslav.dulina@fstroj.uniza.sk

disease or accidents at work. It may also be the effect of those factors, the importance of which comes to the fore only in a combination with certain conditions of work. They may initially manifest themselves by dissatisfaction, incapacity to work or other forms, which can upset the balance between the claims that are made on the employee and their options to deal with them [6, 7 and 8].

### 3. Workload and work performance

As Skrehot stated [9] the workload is a set of external conditions, requirements and circumstances of the particular job system affecting physiological and psychological state of man. It can therefore be argued that each work activity represents a challenge for the organism. The size of the application of the load depends on several factors [9]: the readiness and capability of the employee to perform the task, from the very nature of the task and the conditions under which the performance of the task takes place. With excessive workload not only the size of physical force, but also the human psyche are worsen.

It can be argued that every individual has a certain performance. Performance is understood as a group of attributes and skills that form the precondition for the proper accomplishment of tasks [5 and 10]. Performance can be characterized as a person's ability to bring power per unit of time. The work output we produce is only a part of the overall performance, which we are able to perform.

Work performance is the result of a purposeful activity that takes place over time under certain conditions [5 and 11]. When we think of how much power is to be submitted during work activities and, for example, in sports, we can perceive a significant difference. During the sport, naturally, we try to give out our maximum and give the best performance. This is not at work. Here, it is particularly important that staff is able to serve the long-term stable performance. We can, therefore, conclude that job performance does not reflect the effort with which the employee performs the activity, or how much of their power reserves has been used. The term work performance can present a concrete result of the work that is done under certain conditions and for a certain time unit.

People bring different power in identical situations. Also, an individual performance in a relatively short time intervals may vary. Due to the mentioned considerations and the fact that every exercise cannot be measured by energy loss per unit time, it is more preferable to consider performance.

As it has already been mentioned a man gives only a certain proportion of their output when working. It is called the performance-related standby where the man leaves the rest (so-called power reserve) mostly to non-work activities [11]. For the activities in the working processes in most cases it is not necessary to use the full performance, with which we dispose, hence the reserve. Natural biological barriers and regulatory

mechanisms prevent it. Exactly these regulate the man's output and for a particular employee they ensure an average and for him the most satisfactory output to be maintained.

### 3.1 The factors influencing work performance

Almost all the operating results are achieved through company employees. Through it, i.e. how they consistently do their jobs, they contribute greatly to the achievements of business objectives, ensuring the competitiveness of the company and increase performance.

As already mentioned, the boundaries of human performance are limited by opportunities and the limitations of power reserve. Subjective factors play an important role here and they represent individual human capacity to use its throughput capacity to complete the required work results [12]. How much a person actually makes the use of the power capacity also depends on the interest to fulfil and achieve the desired performance.

Objective performance conditions include external circumstances in which performance takes place. These are the factors which are extraneous to the employee and the employee cannot affect them either [12]. The mentioned factors (Fig. 1), however, affect their job performance and, therefore, it is necessary to be aware of the degree of their impact on the employee and to examine them in detail.

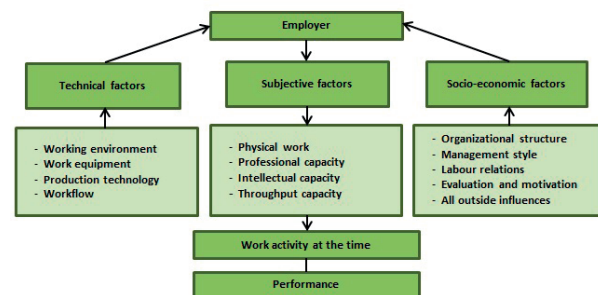


Fig. 1 Factors influencing employee's work performance

Based on the knowledge we have of psychology, physiology, anthropometry, hygiene and other areas that make up the knowledge base of ergonomics, the standardized values of the factors in the working environment have been defined.

According to Gilbertova and Matousek [13] and Kovac [4] the performance capacity of a person is affected by the following factors:

- a) *Sensorimotor capacity* – primarily a function of vision and hearing belong here. Capacity of sight is given by:
  - *Visual acuity* – the ability for the eye to distinguish objects and their details at a distance. It is possible to express it by the angular size (about 5 – 6 minutes of arc) or the so-called acuity is determined, which is the ability of

the eye to identify the two closest points lying as two separate objects. The ability of the sharp perception of the environment by means of vision is determined by the size of the viewing angle which can be measured by perimeter. Optimal field of view in the design is a 20°, normally 60°, 120° and functional up to 220° [14].

- *Spatial vision* - i. e. stereoscopic binocular vision, it is the ability to determine correctly the distance of objects in space, in both horizontal and vertical directions.
- *Eye accommodation* - it is an adaptation of the eye, the change in optical power due to the interest in seeing objects at different distances sharply.
- *Colour vision* - it is the ability to perceive the different colours of light in the visible radiation in the wavelength range 380 - 760 nm. According to studies, healthy human eye is able to distinguish between about 130 to 150 colours in the range 400 - 700 nm. From the point of view of the field of vision, the level of sufficient distinctiveness of colour is in the horizontal plane of the eye 30° - 60° on both sides and 30° above the axis and 70° - 80° below the axis of vision in the vertical plane [13].
- *Adaptation of the eye* - by the eye adapting to the changes of lighting conditions. The requirements for the rapid adaptation of the eye are associated with uniform lighting of workplaces and observing the correct ratio of brightness between the workplace and the environment.
- *Reaction of the hearing to the sound* - it is the ability of the organ of hearing to perceive sound stimuli from the environment. For a man the sound pressure level and frequency of the sound are important. Hearing shows the greatest sensitivity in about 1000 Hz. The time interval for a man needed to realize a sound is 0.1 to 0.15, and its value depends mainly on human attention [4].

b) *Mental capacity* - incorporates psychic abilities (sensorimotor, intellectual, and cognitive), motivation, will and others. Its basis is the intellectual level of a person. The intelligence quotient, which may be obtained by tests and psychological methods, is used to find it out. Unlike sensory capacity, which is determined by the appropriate physiological analyzer and is expressed in physical units, the setting of mental capacity limits is very complicated and the result is only approximate [4].

c) *Human adaptation to working conditions* - it is the ability of humans to adapt to the working conditions and resulting changes. The activity that one must make to overcome the resulting changes is crucial when adapting. It is affected by [4, 14 and 15].

- The type and contents of working activity by which is meant the nature of work tasks and operations, the technology used, machinery, equipment, and material.

- The risks associated with work - harmful working environment, working with hazardous machinery.
- The work and rest - the system of breaks during the shift, unevenly distributed workload and others.
- Social climate in the workplace - interpersonal relationships, level of social support.

### 3.2 Performance curve

Readiness of a man to the work performance during the day varies from person to person. Physiological readiness to bring power is the highest in the morning and decreases gradually during the day. It is, therefore, recommended not to burden a person with strenuous work activity in the afternoon and in the evening (except for Shift-plus operation). For duty cycle control it is necessary to have the basic understanding of the fact that there is a fluctuation in human performance during the workday, 24-hour daily cycle, week, or year [11, 16 and 17].

*Annual fluctuations in performance* - Fig. 2 shows the annual variation of human performance during the year, while the F curve illustrates the physical performance and the P curve the course of mental performance.

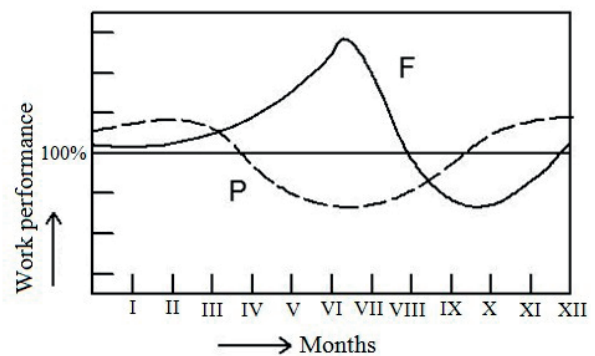


Fig. 2 Annual variation in performance [11]

*Weekly variations in performance* - performance during the week changes (Fig. 3). On Monday the power is the smallest, due to the decrease in dynamic stereotypes and reduced concentration after the weekend. At the end of the week our performance declines, not due to physical fatigue, but due to psychological factors (psychological preparation before the weekend, decreased concentration).

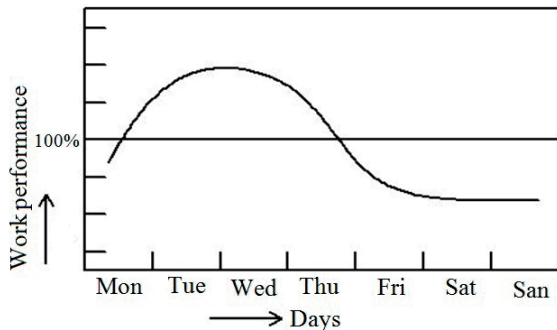


Fig. 3 Weekly variations in performance [11]

Daily fluctuations in performance - the human organism alternately varies during the day and night from the work (power) to the rest (recovery). At the same time physiological functions change (change in blood pressure, body temperature, skin elasticity) as well as mental functions (attention, reaction time). The performance decreases over time in proportion to the intensity and difficulty of work (Fig. 4).

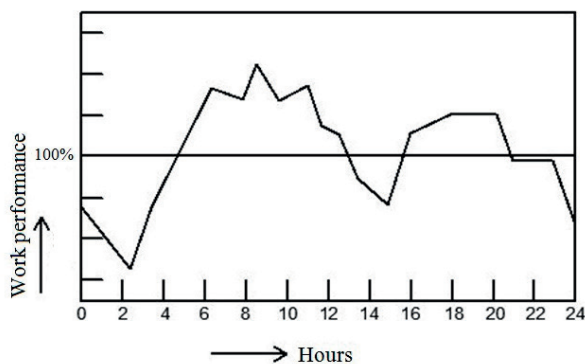


Fig. 4 Daily fluctuations in performance [11]

Fluctuations in performance during the shift - Fig. 5 shows the performance of each hour of a work shift. Due to the type of work and individual abilities of a man the length and the duration of the different phases is different.

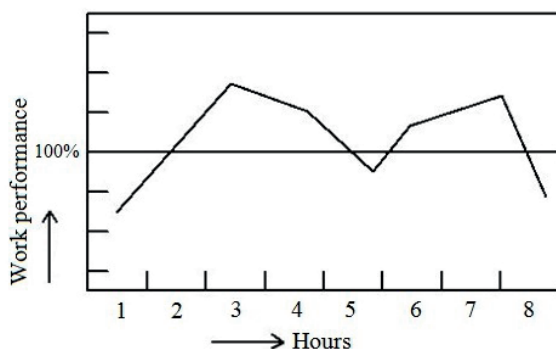


Fig. 5 Variation in performance during the shift [11]

#### 4. Assessment and control of work performance

To assess and evaluate the employee's work performance, i.e. their capability to perform the required work performance, is an important basis for improving the functioning of enterprises, thus increasing their overall efficiency.

Man's work performance can be assessed using the following criteria [12]:

- The length of time needed to carry out the activity.
- The maximum time reserved for that activity.
- The amount of work performed during a certain time.
- The amount of work done regardless of the performance and time.

These criteria are not sufficient to evaluate the job performance and it is needed to supplement them by the additional and more detailed criteria such as performance stability over time, the occurrence and frequency of erroneous decisions, quality of work, accident and more.

Under the conditions that the requirements for a job are met, the employee's performance at work might be regulated as follows:

- *Duration of work* (prolongation or shortening of working hours, alternating time intervals designed to work and relaxation).
- *Speed with which the work is performed and the degree of work pace* (shortening the time appointed for a rest or designated for a work performance).
- *The amount of work done and power expended* (the weight of the load to be handled, the number of manipulated loads).

In case that we would like to regulate the work output it is required from an ergonomic point of view to know the following indicators:

- Thresholds which determine the functional performance values of a healthy organism.
- The interaction of those features that is important for a job performance.
- Factors that may limit the boundaries and hence the performance of the employee.

From my own experience and observation it can be stated that a work performance may not be equally troublesome for different people. The effort you feel as an individual for a specific individual exercise may also vary depending on fatigue, disease, mental status, number of breaks, and many other factors. Between the throughput capacity, which we have and the work performance that has been produced, we also have the already mentioned power reserve. Just the mentioned power reserve helps us cope well with such situations which are considerably of higher demands on our work performance. Despite the reserve which we

have, the increased or decreased performance in the long term can cause significant changes in our bodies.

## 5. Employment impact on humans

At work, which is defined by reserved working conditions, requiring the occupation as such, work environment or work equipment, the fact that human performance is limited comes significantly to the fore. The employer should assess the intensity of work load on the body of the employee. The employer also should focus on how the harmful effects influence the performance and, in particular, their health. The employer is obliged to think of legislation, the task of which is to protect the health of the employee. The factors that affect job performance interact with each other, have a different degree of severity and the degree may, of course, vary depending on the time and the current conditions. It is necessary to note that the factors that affect the performance may be changed in combination with other factors and they may be positive or negative. The employer should be aware of it and in some cases, accept the change of the

employee's performance, thus lower demands may cause more problems for the employee as might be expected.

## 6. Human impact on work activity

With the development of science and technology machine performance has also increased. Businesses are trying to achieve the best results and highest profits. With the advantages that a new technique and technology bring, the employee's performance becomes the weakest link in the production process. Even greater demands are placed on staff in order to utilize their maximum possibilities as well as the maximum use of the machine. From a health perspective, it is possible for a short time, but only if it is followed by a sufficiently long rest. The employer should deal with the contradiction between limited human performance and unlimited possibilities of modern technology.

### Acknowledgement

The article was created within the research project VEGA No. 1/0701/12 Research on the use of low-cost automation and artificial intelligence in the process of stereoscopic recording.

## References

- [1] HLADKY, A.: Ergonomic Increases Motivation and Performance. Ceska ergonomicka spolecnost. *Human Resources Management*, 2007, vol. III., No. 6, 10-12. ISSN 1801-4690
- [2] STEFANIK, A., GRZNAR, P., MICIETA, B.: *Tools for Continual Process Improvement - Simulation and Benchmarking*. Annals of DAAAM for 2003 & Proc. of the 14<sup>th</sup> Intern. DAAAM Symposium: Intelligent manufacturing & automation: Focus on reconstruction and development, 2003, 443-444, ISBN: 978-3-901509-34-6
- [3] GASO, M., MICIETA, B.: *Application of Stereoscopic Records in Ergonomics*. 5<sup>th</sup> Intern. Ergonomics Conference: ERGONOMICS 2013, Zagreb: Croatian Ergonomics Society, 2013, 223-228. ISSN 1848-9699
- [4] KOVAC, J., SZOMBATHYOVA, E.: Impact of Selected Ergonomic Factors on Human Performance at Work. Inovacne centrum automobilovej výroby. *Transfer inovacii*, No. 8, 2005, 76-77, ISBN 80-7093-6
- [5] KUBANI, V.: *Psychology of Work*. PU Presov : FHPV, 2005, 81 p., ISBN 80-8068-331-X
- [6] HATIAR, K.: Modern ergonomics. *Productivity and Innovations*, vol. IX, No. 6, 2008, 22-24, ISSN 1335-5961
- [7] KOVAC, J., SZOMBATHYOVA, E.: *Ergonomics*. TU Kosice: Sjf : Edicia studijnej literatury Kosice, 2010, 122 p., ISBN 978-80-553-0538-7
- [8] VRABLOVA, L., GREGOR, M.: Company in Crisis. *Communications - Scientific Letters of the University of Zilina*, vol. 13, No. 4, 2011, 78-81, ISSN 1335-4205
- [9] SKREHOT, P., MAREK, J.: *Basics of Applied Ergonomics: Safe Company*. Praha: VUBP, 2009, 118 p., ISBN 978-80-86973-58-6
- [10] KRALOVA, Z., KRAJCOVIC, M.: Variance in a Second Language Production Quality. *Communications - Scientific Letters of the University of Zilina*, vol. 11, No. 4, 2009, 15-23, ISSN 1335-4205
- [11] LORKO, M.: *Ergonomics in Manufacturing*. Technicka univerzita, 2001, 105 p., ISBN 80-7099-692-7
- [12] BABELOVA, Z.: *Impact of Employee Performance to Business Performance*. 2004, 323 p., Brno : VUT Juniorstav, ISBN 80-214-2934-8
- [13] GILBERTOVA, S., MATOUSEK, O.: *Ergonomics. Optimization of Human Activity*. Grada Publishing : Praha, 2002, 239 p., ISBN 80-247-0226-6
- [14] CHUNDELA, L.: *Ergonomics*. CVUT Praha, 2000, 55 -57, ISBN 80-01-02301-X

- [15] PALAJOVA, S., GREGOR, M.: Simulation Metamodeling of Manufacturing Processes. *Communications - Scientific Letters of the University of Zilina*, vol. 13, No. 4, 2011, 51- 54, ISSN 1335-4205
- [16] KRAJCOVIC, M., BULEJ, V., SAPIETOVA, A., KURIC, I.: Intelligent Manufacturing Systems in Concept of Digital Factory. *Communications - Scientific Letters of the University of Zilina*, vol. 15, No. 2, 2013. 77-87, ISSN 1335-4205
- [1] GREGOR, M., STEFANIK, A., HROMADA, J.: *Lean Manufacturing Systems Optimisation Supported by Metamodelling*. IFIP Intern. Federation for Information Processing, vol. 257, 2008, ISSN 1571-5736.

**COMMUNICATIONS – Scientific Letters of the University of Zilina  
Writer's Guidelines**

1. Submitted papers must be unpublished and must not be currently under review for any other publication.
2. Submitted manuscripts should not exceed 8 pages including figures and graphs (in Microsoft WORD – format A4, Times Roman size 12, page margins 2.5 cm).
3. Manuscripts written in good English must include abstract and keywords also written in English. The abstract should not exceed 10 lines.
4. Submission should be sent: By e-mail – as an attachment – to one of the following addresses: komunikacie@uniza.sk or holesa@uniza.sk (or on CD to the following address: Zilinska univerzita, OVaV – Komunikacie, Univerzita 1, SK-10 26 Zilina, Slovakia).
5. Uncommon abbreviations must be defined the first time they are used in the text.
6. Figures, graphs and diagrams, if not processed in Microsoft WORD, must be sent in electronic form (as JPG, GIF, TIF, TTF or BMP files) or drawn in high contrast on white paper. Photographs for publication must be either contrastive or on a slide.
7. The numbered reference citation within text should be enclosed in square brackets. The reference list should appear at the end of the article (in compliance with ISO 690).
8. The numbered references (in square brackets), figures, tables and graphs must be also included in text – in numerical order.
9. The author's exact mailing address, full names, E-mail address, telephone or fax number, the name and address of the organization and workplace (also written in English) must be enclosed.
10. The editorial board will assess the submitted paper in its following session. If the manuscript is accepted for publication, it will be sent to peer review and language correction. After reviewing and incorporating the editor's comments, the final draft (before printing) will be sent to authors for final review and minor adjustments
11. Submission deadlines are: September 30, December 31, March 31 and June 30.

COMMUNICATIONS

SCIENTIFIC LETTERS OF THE UNIVERSITY OF ZILINA  
VOLUME 16

**Editor-in-chief:**

Prof. Ing. Otakar Bokuvka, PhD.

**Editorial board:**

Prof. Ing. Jan Bujnak, CSc. – SK  
 Prof. Ing. Otakar Bokuvka, PhD. – SK  
 Prof. RNDr. Peter Bury, CSc. – SK  
 Prof. RNDr. Jan Cerny, DrSc. – CZ  
 Prof. Eduard I. Danilenko, DrSc. – UKR  
 Prof. Ing. Branislav Dobrucky, PhD. – SK  
 Doc. Ing. Pavol Durica, CSc. – SK  
 Prof. Dr.hab Inž. Stefania Grzeszczyk – PL  
 Prof. Ing. Vladimir Hlavna, PhD. – SK  
 Prof. RNDr. Jaroslav Janacek, PhD. – SK  
 Prof. Ing. Hermann Knoflacher – A  
 Doc. Dr. Zdena Kralova, PhD. – SK  
 Doc. Ing. Tomas Lovecek, PhD. – SK  
 Doc. RNDr. Mariana Marcokova, CSc. – SK  
 Prof. Ing. Gianni Nicoletto – I  
 Prof. Ing. Ludovit Parilak, CSc. – SK  
 Prof. Ing. Pavel Polednak, PhD. – SK  
 Prof. Bruno Salgues – F  
 Prof. Andreas Steimel – D  
 Prof. Ing. Miroslav Steiner, DrSc. – CZ  
 Prof. Ing. Marian Sulgan, PhD. – SK  
 Prof. Josu Takala – SU  
 Doc. Ing. Martin Vaculik, PhD. – SK

**Address of the editorial office:**

Zilinská univerzita  
 Office for Science and Research  
 (OVaV)  
 Univerzita 1  
 SK 010 26 Zilina  
 Slovakia

E-mail: komunikacie@uniza.sk

Each paper was reviewed by two reviewers.

Journal is excerpted in Compendex and Scopus.

It is published by the University of Zilina in  
 EDIS – Publishing Institution of Zilina University  
 Registered No: EV 3672/09  
 ISSN 1335-4205

Published quarterly

Single issues of the journal can be found on:  
<http://www.uniza.sk/komunikacie>

ICO 00397 563  
 October 2014